DIRECT LIQUEFACTION: WHERE WE STAND AND WHERE WE ARE SUPPOSED TO GO - AN OVERVIEW

Eneo C. Moroni
U.S. Department of Energy
FE-231 GTN
Washington, D.C. 20545

Keywords: Coal, Liquefaction, Program Planning/Coordination.

INTRODUCTION

The U.S. Department of Energy (DOE) precommercial activities in the 1970's and early 1980's established the commercial viability of direct coal liquefaction from a technical point of view. In the early 1980's, the direct liquefaction program was reoriented toward longer range process research and development activities with the objective of developing improved, lower cost technology.
The DOE development program since then has made substantial and significant improvements in the process technology. Liquid yields have been improved by over 30 percent. On a balanced commercial plant basis, this translates to a production of about 3.3 barrels of liquids per ton of coal for the improved technology compared to 2.5 barrels for the technologies developed in the 1970's.
The quality of the coal-derived distillates produced by the current technology has been substantially improved, but at the expenses of increased consumption of the upgrading catalyst. As a result, the currently produced liquids are of much higher quality than petroleum crudes in general. Other technology improvements include less severe operating conditions which favorably impact construction costs, operability and maintenance; and improved product slate flexibility, which allows greater freedom in producing products for specific market applications.

As a consequence of these improvements in technology, substantial cost reduction has been achieved. Current two-stage technology demonstrated at the Wilsonville, Alabama proof-of-concept (POC) facility gave estimated product costs at about $38-40 per barrel. Because of improved quality, these products would be competitive with crude oil at about $33-35 per barrel.

Supporting and exploratory research made critical contributions in some area of process development, e.g. by providing process analysis data leading to improved process operation and performance. F.Burke and coworkers at the Consolidation Coal R&D Division have done an excellent analytical and process evaluation work in this area. Similarly, D. Gray and the MITRE Corporation team provided valuable process economic information for comparative processes evaluation. To be noted, both activities are crosscutting in that they contribute to all DOE-supported processes under development. In addition, both supporting activities, through many years of experience and close cooperation between them and with the contractors working in process development, have reached a high degree of sophistication in various aspects of process evaluation so that, presently, they are capable of offering valuable research

guidance for the evaluation of novel research activities in coal liquefaction.

For more than a decade DOE has encouraged the generation of an extensive analytical and economic data bank on coal liquefaction processes and on related research activities, with the specific provision that the data and the ensuing process evaluation would be developed by competent sources independently from the actual process developers and from individual researchers.
Presently, we continue to pursue this endeavor by expanding the "teaming arrangement" promoted by Consolidation Coal and MITRE, and to support a similar "teaming" effort by A. Davis at Penn State University to establish an analytical data bank in support of the determination of the mechanisms and the kinetics of the rapid changes occurring in dispersed catalyst composition during the initial stages of liquefaction.

Consequently, we appear on the way to being prepared organizationally for the challenge presented to us in integrating into the current processing schemes the discoveries of present and future research and development studies.

PROGRAM OBJECTIVES/DIRECTION

In line with the current environmental and energy shortage concerns and with the effort to sustain coal as a viable option in competition with other energy sources, the main objective of the DOE's direct coal liquefaction current program is to develop the technology for the production of specification liquid fuels at a cost competitive with crude oil, within the next 5 to 7 years.

More specifically, the program calls for a proof-of concept demonstration, by 1997, of a system capable of producing liquid fuels from coal which complies with environmental requirements at cost of less than $30 per barrel of oil equivalent and with lower greenhouse gas emissions than those from 1980 state-of-the-art coal liquefaction technology, or comparable to petroleum-based systems, and are suitable to be blended with petroleum stocks to produce and, perhaps, enhance the quality of reformulated gasoline, jet fuel and other high quality liquid transportation fuels.

The key issue is the integration of coal-derived liquids into existing petroleum refining systems which would require no major modifications to the fuel distribution and storage infrastructure which currently exists.

In the evaluation and planning of present and future research and development activities, we need to provide answers to two important questions: How should the present activities in the fundamental and applied research at the university and national laboratory level be changed in order that the remaining scientific and technical challenges can be addressed? And, what are the most important feedback information that the process developers and process evaluation teams can provide to the scientific community in order to evidence the most compelling research and development needs to

overcome the current challenges and provide a better understanding of the reactions involved in coal liquefaction?

The first step is the recognition that all of the knowledge in this field does not and cannot reside in a single discipline. We need to support in a substantive way a policy of multi-disciplinary research teamwork and to further encourage cooperative efforts between the fundamental and applied research and bench scale development of integrated process activities.

The excellent study done by a panel group on research needs assessment for coal liquefaction (COLIRN), headed by H.D. Schindler, and sponsored by the DOE Office of Energy Research, Office of Program Analysis, resulted in a publication[1] which provided important recommendations to be implemented by the fundamental and applied researchers in this field. The recommendations were reviewed and approved by the representatives of DOE Office of Fossil Energy, with some reservations about the usefulness of chemical pretreatments in the overall liquefaction processing scheme and the use of novel catalysts prior to gain a better understanding of the mechanism and the kinetics involved in the initial stages of coal liquefaction.

We agree with the conclusion of the COLIRN panel which has challenged the conventional view of the chemistry and the mechanisms of direct liquefaction--that the initial reactions of liquefaction involve thermal homolytic bond cleavage with stabilization of the free radicals formed-- and is being replaced by the recent work on a deeper understanding of bond-breaking and bond-forming processes via hydrogen transfer. This new model of coal depolymerization may explain the cleavage of bonds which are too strong to be broken thermally at liquefaction conditions.

The COLIRN panel agreed that these new understandings of structure and mechanisms are expected to lead to more efficient liquefaction processes, which, eventually, need to be developed before coal liquefaction can be commercialized.

In particular, the panel placed the highest priority on identifying the coal structures responsible for retrograde reactions and the reaction mechanisms and kinetics of these reactions. The panel also placed high priority on developing a coal structure-reactivity relationship, develop kinetic models of liquefaction, and develop intrinsic quantitative rate expressions as a basis for understanding initial reaction paths during coal dissolution.

Among the remaining recommendations the panel scored lower priority for the study on catalytic hydrogenation and cracking functions mechanism to establish their interaction and to determine the effects of thermal reaction on these functions. However, current data from the Wilsonville POC unit[2] indicate that the thermal/catalytic staged liquefaction mode gives substantially higher coal conversion than the catalytic/thermal mode, and this fact is mistfying process evaluators and, as a consequence, a better understanding of the contribution and of the reaction

mechanisms attributed to the thermal and catalytic functions would certainly require a much higher research priority because it is quite evident that our knowledge in this important area is indeed insufficient.

CONCLUSIVE REMARKS

The current advanced research program needs to be reoriented to follow more closely the recommendations of the COLIRN panel and the direction suggested by the process development program, which require a clearer understanding of the initial reaction paths, particularly the reactions involved in the preconversion step and those of the attendant catalyst deactivation mechanism. The acquisition of this knowledge should lead to substantially more efficient liquefaction processes.

According to J. Larsen[3] there are three areas which are crucial to our state of knowledge in coal processing: coal structure, coal as reaction environment, and which reactions are actually occurring in coals.

We agree with J. Larsen that our knowledge in all three areas is sufficiently uncertain to make extrapolation from routine model compound studies to coals quite unreliable. And we need to add that similar extrapolation unreliabilities exist for the current catalyst studies and applications, solvent extraction, alkylation, pyrolysis, chemical pretreatment, water supported reactions and many other approaches fashionable in past and present advanced research activities because they suffer from the same lack of fundamental knowledge of coal structure, reaction mechanisms and kinetics to make them viable for further scaleup consideration.

The process development activities is also at crucial turning point because we are finding that coal derived materials, such as resids and the quality of the solvent, which are used in the recycle stream, exhibit larger beneficial effects in coal liquefaction than the comparison of novel catalyst formulation versus existing commercial catalysts.[2]

Consequently, the commitment of DOE to develop the technology for the production of specification liquid fuels from coal, at a cost competitive with crude oil, within the next 5 to 7 years, will require a reorientation of the advanced research program, increases in both scope and pace of the fundamental and applied research effort, perhaps by teaming arrangements with the process development and process evaluation programs, to produce a timely resolution of the technical issues in order to meet the requirements dictated by the current and perhaps more restrictive future environmental and economic constrains for coal derived liquid fuels.

If a strong and clear message should be given to the participants of this "Symposium on Coal Reaction Mechanism", from the content of this brief overview, it would sound like a mimic of the famous message contained in the inaugural address of the late president of the U.S., J.F. Kennedy:

"Ask not what you can do for coal processing",
"Ask, first, what coal structure/reactions can do for you".

REFERENCES

(1) Coal Liquefaction. A Research Needs Assessment. February 1989. Prepared for U.S. Dept. of Energy, Office of Energy Research, Office of Program Analysis, Contract DE-AC01-87ER30110.

(2) Unpublished current work at the Wilsonville POC unit.

(3) Larsen, J. W., Am.Chem.Soc., Div.Fuel Chem. Preprints, 1990, 35(2), 376.

LIQUEFACTION PATHWAYS OF U.S. COALS

Robert A. Keogh and Burtron H. Davis
Center for Applied Energy Research
University of Kentucky
3572 Iron Works Pike
Lexington, KY 40511

Keywords: coal liquefaction, thermal and catalytic pathways

ABSTRACT

The solubility classes obtained from the thermal liquefaction of 69 high volatile bituminous U.S. coals using a single residence time and three reaction temperatures were combined into the following lumped parameters for examination of the data: (a) oils plus gases, (b) asphaltenes plus preasphaltenes, and (c) IOM (insoluble organic matter). The lumped parameters were plotted on a Wei-Prater diagram and the resulting graph suggested a common liquefaction pathway for these coals. The thermal pathway was verified using a single Western Kentucky #6 coal and a number of residence times and reaction temperatures. The utilization of a number of catalysts and solvents with different hydrogen donor abilities did not change the pathway observed thermally. The effect of coal rank was studied using a Wyodak subbituminous coal. The thermal pathway defined by the liquefaction of the Wyodak coal was substantially different from the pathway defined by the bituminous coals. Addition of a catalyst did not alter the observed pathway defined thermally for this coal.

INTRODUCTION

Historically, lumped parameter kinetic models have been used successfully to describe industrially significant complex processes such as catalytic cracking[1], catalytic reforming[1], addition polymerization[2], and condensation polymerization[3]. Not surprisingly, the same approach has been used in the description of the various liquefaction processes[4,5]. A physically realistic and technically viable lumped parameter kinetic model for liquefaction would be of considerable value in the development of pathways, mechanisms and the scale-up of liquefaction processes.

In this work, the typical solubility classes obtained from the liquefaction products were lumped into the following parameters: (a) oils plus gases (O+G), (b) asphaltenes plus preasphaltenes (A+P), and (c) IOM (insoluble organic matter). The three lumped parameters were plotted on a Wei-Prater diagram (triangle graph) for interpretation. The resulting data suggested a common thermal liquefaction pathway. The effects of catalyst, solvent quality and coal rank are discussed.

EXPERIMENTAL

The description and range of values of the key coal properties of the 69 high volatile bituminous coals used in the initial work are given in Table 1. It should be noted that all of these coals have $\geq$ 80 vol. % vitrinite (dmmf) concentrations. The analyses of the three coals (W.Ky. #6, W.Ky.#9 and Wyodak) which were extensively studied are given in Table 2.

All of the liquefaction experiments were performed in 50 mL batch microautoclaves using a hydrogen atmosphere. Details of the liquefaction procedure and solubility class analysis of the products are given in detail elsewhere[6].

The quantity of catalyst added to the 5g of dry coal were as follows: (a) Shell 324 (1g), (b) molybdenum naphthenate (1g), (c) Fe_2O_3 (.1g), (d) $Fe_2O_3 \cdot SO_4^{=}$ (.1g), (e) $SnCl_2 \cdot 2H_2O$ (.25g), and (f) $ZnCl_2$ (.25g). All of the catalysts, with the exception of Shell 324, were sulfided in-situ by adding twice the stoichiometric amount of dimethyldisulfide required to sulfide the metal to the reactor. The Shell 324 catalyst was presulfided with dimethyldisulfide prior to the addition of coal and liquefaction solvent.

RESULTS AND DISCUSSION

The thermal liquefaction data obtained for the 69 high volatile bituminous coals using a 15 minute residence time and three reaction temperatures (385°C, 427°C, 445°C) are shown in Figure 1. The data suggest a common liquefaction pathway for these coals. A single bituminous coal (W.Ky. #6) was selected to verify the suggested pathway. Liquefaction conditions were selected to produce a series of conversion levels which would define the pathway of the coal from a minimum conversion level to a maximum conversion level. The results of these experiments are shown in Figure 2.

As can be seen in Figure 2, the thermal pathway of the Western Kentucky #6 coal over the entire range of conversions is identical to that suggested in Figure 1 for the diverse set of coals. In the initial stage of dissolution, the primary reaction is the conversion of coal (IOM) to the A+P intermediate. In this region of the pathway, the conversions show a positive linear correlation with the A+P yields. It is also observed in this region of the pathway that the O+G yields remain relatively constant. The pathway changes in the region of maximum conversion (and A+P yield). In this section of the pathway, the primary reaction taking place is in the conversion of the intermediate, A+P, to the final product O+G. During this stage of the liquefaction pathway, conversion remains relatively constant. At the highest reaction temperature (445°C) and long residence times (> 15 min.), the pathway appears to change. In this region, conversion, A+P and O+G yields concurrently decrease, indicating the possibility that retrograde reactions are predominant. The results of these experiments suggest that the high volatile bituminous coals studied in this work have a common thermal liquefaction pathway.

The liquefaction pathway defined by these coals indicates that a maximum in the intermediate yields (A+P) must be achieved prior to an increase in the O+G yields. It is desirable to alter the pathway in such a manner that the O+G yields increases with increase in coal conversion. A number of catalysts were studied to determine if the added catalyst effect the selectivity defined by these reactions and thus change the pathway. The catalytic pathway is compared to the thermal pathway using the Western Kentucky #6 coal and two iron based catalysts in Figure 3. As can be seen, the addition of these catalysts had no effect on the observed thermal pathway. Identical experiments employing a supported catalyst (Shell 324), an oil soluble catalyst precursor (molybdenum naphthenate) and two acid catalysts ($ZnCl_2$ and $SnCl_2 \cdot 2H_2O$) also produced the same pathway that was observed for the thermal experiments. Therefore, the effect of catalyst addition is to increase the rate of production of the intermediate, A+P. The addition of catalysts has no effect on the selectivity defined by the solubility classes.

The effectiveness of a catalyst may be influenced by the quality of the liquefaction solvent[7]. To determine the effect of solvent quality, as measured by hydrogen donor ability, a series of experiments (catalytic and thermal) were conducted using a Western Kentucky #9 coal and a donor (tetralin) and a non-donor (1-methylnaphthalene). The results of these experiments are shown in Figure 4. As can be seen, these data show that no change was observed in the liquefaction pathway. Additional experiments which used a mixture of phenanthrene and hydrogenated phenanthrenes as the liquefaction solvent defined the same pathway described above.

The next task in this investigation was to determine if the catalytic and thermal pathways of low rank coals were the same as that defined by the high volatile bituminous coals. A Wyodak subbituminous coal was chosen for the initial thermal and catalytic (Fe_2O_3, molybdenum naphthenate) experiments. The pathways obtained from the liquefaction of the Wyodak coal are shown in Figure 5. Clearly, the thermal and catalytic pathway are also identical for this coal. However, the pathway for the subbituminous coal is substantially different from the pathway defined by the bituminous coals. Similar to the pathway of the bituminous coal, there are two regions in the pathway of the subbituminous coal. During the initial coal dissolution stage, both the A+P and O+G yield increase with increasing coal conversion. The second region of this pathway is similar to that of the bituminous coal. Here the coal conversion increases minimally and the major reaction is the conversion of A+P to O+G. On the basis of these solubility class data, the subbituminous coal has an improved catalytic and thermal pathway when compared to that of the bituminous coals studied due to the concurrent increase in O+G yields with coal conversion.

CONCLUSIONS

The utilization of lumped solubility class parameters and the Wei-Prater diagram have shown that the bituminous coals studied have a common thermal liquefaction pathway. Attempts to change the observed pathway using a number of catalysts and liquefaction solvents were not successful. The role of the catalyst in this work is to increase the rates of the defined reactions. The catalyst provided no selectivity to the production of the final products, O+G.

The pathway defined by a subbituminous Wyodak coal was substantially different from the pathway of the bituminous coals. The major difference was the parallel increase in A+P and O+G yields with the increase in coal conversion. Similar to the bituminous coal data, addition of catalysts had no effect on the Wyodak thermally defined pathway.

ACKNOWLEDGMENT

This work was supported by the Commonwealth of Kentucky and DOE contract no. DE-FC88PC8806 as part of the Consortium for Fossil Fuel Liquefaction Science (administered by the University of Kentucky).

REFERENCES

1. Weekman, V. W., *AIChE Monograph Series*, No. 11, Vol. **75**, 1979.
2. Platzer, N., *Ind. & Eng. Chem.*, **62** (1), 1970.

3. Flory, P. J., "Principles of Polymer Chemistry", Cornell University Press, New York, NY, 1953.
4. Weller, S., Pelipetz, M. G., and Friedman, S., *Ind. Eng. Chem.*, **43** (7), (1951) 1575.
5. Cronauer, D. C., Shah, Y.T., and Ruberto, R.G., *Ind. Eng. Chem., Process Des. Div.*, **17**, (1978) 281.
6. Keogh, R. A., Chawla, B., Tsai, K. J., and Davis, B. H., *Preprints, Div. Fuel Chem., Am. Chem. Soc.*, **33** (3), (1988).
7. Derbyshire, F. J., *Energy and Fuels*, **3** (3), (1989).

Table 1

Make-up of Sample Set and Range of Key Properties

A. Distribution of Samples by State:

Kentucky	36
Indiana	22
Ohio	10
West Virginia	1

B. Distribution by ASTM Rank Classification:

High volatile bituminous A, B, C

C. Ranges of Key Properties

	Wt.% V.M.(daf)	Wt.% C(daf)	Wt.% Total S.(daf)	Wt.% Org.S.(daf)	Wt.% Pyr.S.(daf)	Vol.% Vitrinite(dmmf)	$R_{o\ max}$
Minimum	34.27	76.04	.70	.55	.03	80.06	.388
Maximum	48.34	86.48	13.78	4.72	8.87	92.70	.984
Mean	43.15	80.67	4.15	2.25	1.70	86.78	.606

Table 2

Coal Analyses

	W.Ky. #6	W.Ky. #9	Wyodak
Ultimate (wt.%, daf)			
Carbon	82.87	76.80	71.02
Hydrogen	5.42	5.41	5.42
Nitrogen	1.72	1.90	1.37
Sulfur	5.15	8.41	1.00
Oxygen[1]	4.84	7.40	21.29
Reflectance ($R_{o\ max}$)	.77	.54	----

1 By difference

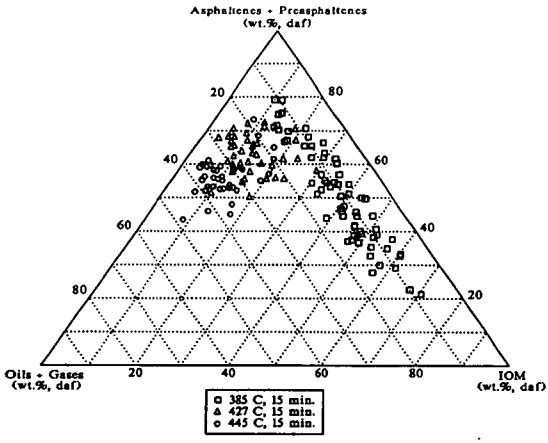

Figure 1. Solubility class distributions of 69 U.S. bituminous Coals

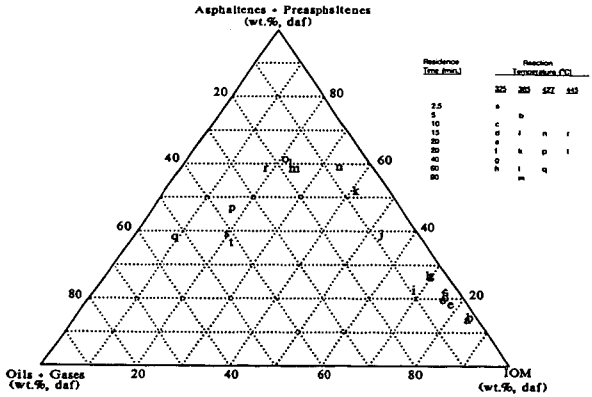

Figure 2. Thermal liquefaction pathway of a W.Ky.#6 bituminous coal.

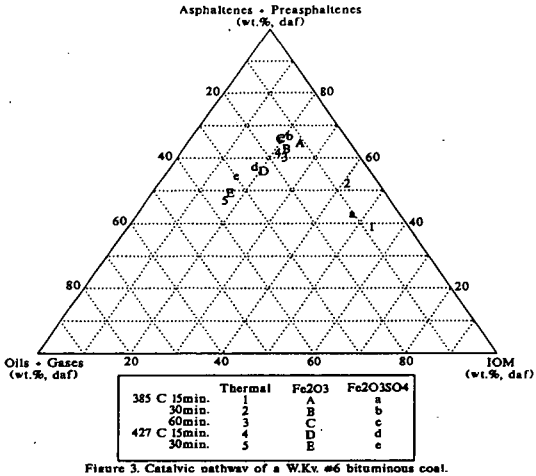

Figure 3. Catalytic pathway of a W.Ky. #6 bituminous coal.

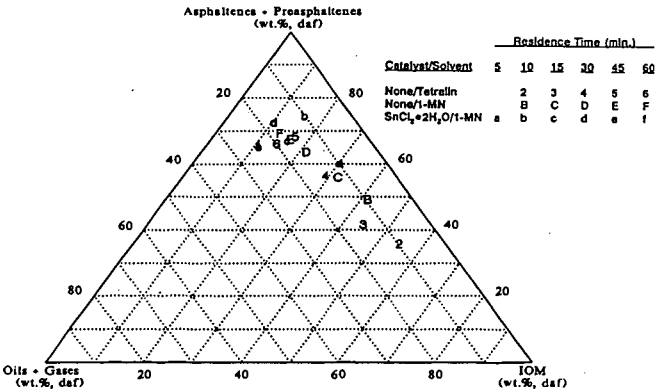

Figure 4. The effect of solvent quality on the pathway of a W.Ky.#9 coal.

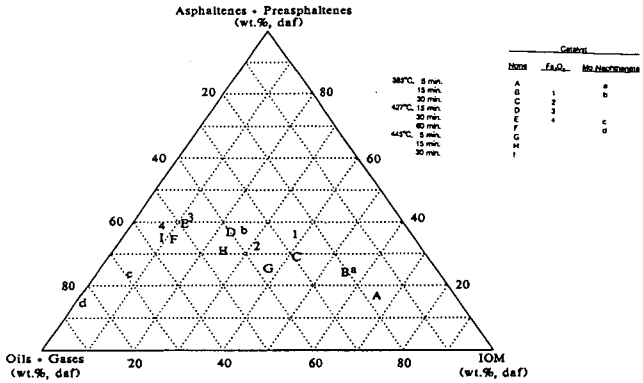

Figure 5. Thermal and catalytic pathway of a Wyodak subbituminous coal.

MICROSCOPIC EVIDENCE OF COMPETING HYDROGENATION AND CONDENSATION REACTIONS DURING COAL LIQUEFACTION

Alan Davis, G.D. Mitchell, F.J. Derbyshire[1], H.H. Schobert, and Rui Lin[2]

Energy and Fuels Research Center
Penn State University
University Park, PA 16802

[1]University of Kentucky, KY, USA
[2]UNOCAL Corp., CA, USA

Keywords: liquefaction, residue microscopy, catalysis

INTRODUCTION

Reflectance characteristics of vitrinite-derived residues from coal liquefaction provide a measure of the response of coals to reaction conditions (1-3). The presence of a low-reflecting primary vitroplast (4,5), an isotropic pitch-like material formed by simple melting of vitrinite, indicates that depolymerization reactions were incomplete. Low-reflecting secondary vitroplast (5), formed by precipitation from the solubilized products, suggests that the coal had been at least partially hydrogenated. High-reflecting vitroplast or vitrinite residue indicates that condensation reactions had predominated. The presence together of the last two of these residue types indicates that hydrogenation and condensation have been locally competing reactions following thermolysis.

This paper discusses the use of residue microscopy in evaluating the influence of a dispersed molybdenum catalyst, of reactor atmosphere, of a pretreatment stage and of coal rank in bench-scale liquefaction experiments.

EXPERIMENTAL

The four coals used in this study (lig, subB, hvC and hvA bituminous) were obtained from the Penn State Coal Sample Bank. Some of their relevant properties are listed in Table 1.

Hydrogenation reactions were performed, mostly without a solvent vehicle (i.e., dry), in batch stainless-steel tube reactors (approx. 25 cm^3 capacity) (6, 7). Approximately 5 g of coal (-60 mesh U.S. sieve size) were charged to the reactor for the dry runs. For hydrogenations conducted with added solvent, 2.5 g of coal and 5 g of solvent were used. If catalyst was present (as 1% sulfided Mo on dmmf coal), a stoichiometric amount of CS_2 was added to ensure that enough available sulfur was present to convert the metal to its sulfide form. The assumption was made that ammonium tetrathiomolybdate (ATM) would convert entirely to MoS_2. The procedure employed for preparing the ATM and dispersing it on the coal, and reference to the metastability of this catalyst precursor are described elsewhere (8, 9).

The loaded reactor was purged of air with nitrogen and then purged three times with the desired gas (hydrogen or nitrogen) before finally being pressurized

to 7 MPa cold pressure. The reactor contents were agitated vertically through 2.5 cm at about 200 cycles per minute by an electrically driven cam system while the reactor was immersed in a preheated, fluidized sandbath. After reaction for the desired time, the reactor was removed from the sandbath and quenched to room temperature by immersion in cold water. First-stage reactions were conducted at 275°C, and the second stage at 425°C, both for 30 min.

In between the steps of the temperature-staged liquefaction experiments, the reactor was quenched and the gaseous products vented. The reactor was then repressurized with 7 MPa hydrogen and reaction was continued at the higher temperature. This procedure was adopted to circumvent the possibility of limiting the hydrogen partial pressure.

Liquefaction experiments were done in duplicate. The products of one of the reactors were used for microscopy. The second reactor was vented and the remaining liquefaction products washed out and extracted with tetrahydrofuran (THF) to determine percent conversion.

RESULTS AND DISCUSSION

Non-Catalytic Reactions

Preceding a coal liquefaction reaction with a low-temperature pretreatment stage has been shown to have a profound effect on conversion and product selectivity, particularly where catalysts are employed in the reaction (1). Consequently, some detailed microscopy was performed on residues that represent pretreatment conditions alone. Three of the coals which had been reacted at 275°C (PSOC-1482, 1401 and 1504) under different atmospheres were evaluated to determine whether there had been any discernible changes in the structure of the reacted coal.

Following pretreatment (first stage) conditions the lignite and subbituminous coals showed almost no microscopic evidence of change in the coal structure other than some separation of coal particles along bedding planes. It is important to note that the vitrinite/huminite macerals showed no rims of low reflectance that would signify that hydrogenation has proceeded via a shell progressive mechanism. Also, there was no evidence of maceral devolatilization or the onset of fluidity that would help to explain the improved conversion and product selectivity that occurs when a low-temperature pretreatment is employed prior to reaction under full liquefaction conditions. Maximum reflectance values were measured for a selection of residues from pretreated coals and are presented in Figure 1. Compared to the reflectance of the feed coal, little change was observed following pretreatment. Only in the case of the subbituminous coal was there a significant increase. These general relationships are consistent whether a hydrogen or a nitrogen atmosphere was employed during the reaction (Table 2).

The same similarity between reflectances of residues from runs in nitrogen and hydrogen was found for the higher temperature and temperature-staged experiments (Table 2). This is somewhat surprising given the fact that the best conversion was observed for the temperature-staged reaction of the bituminous coal in a hydrogen environment. These observations suggest that the reflectance

increase of vitrinite-derived residual material from runs made in the absence of a solvent may be more related to the maximum temperature employed in the reaction than to the reactant gas.

Major changes in the appearance and optical properties of residues were observed following the high-temperature (425°C) and temperature-staged reactions. For the most part the liptinite macerals had been converted and were no longer present in the residues. Huminite/vitrinite remnants and vitroplast were the predominant components found in residues of the lignite (PSOC-1482) and subbituminous (PSOC-1401) coals, whereas vitroplast was the dominant component found in residues from the hvCb (PSOC-1498) and hvAb (PSOC-1504) coals. The maximum reflectances of these residue components were greatly increased over those of the original coal. Fig. 1 compares the trends in reflectance for the different hydrogenation conditions and coals used during this project. For lower coal ranks, temperature-staged residues have a higher reflectance than the single-stage high-temperature liquefaction residues. Reflectance is lower for temperature-staged compared to high-temperature reactions for the hvC and A bituminous coals. If higher reflectance is indicative of a greater degree of molecular condensation, then these data suggest that the lower rank coals have a greater tendency to condense under temperature-staged, dry, non-catalytic liquefaction than the conventional high-temperature liquefaction. The reversal of this tendency, and therefore a lower degree of molecular condensation under temperature-staged conditions, is seen in the residues from the higher rank coals. Finally, the reflectance values measured for both the temperature-staged and high-temperature residues of PSOC-1498 are somewhat low compared to the other coals (Fig. 1). We suspect that the maximum temperature (425°C) used for liquefaction of this hvCb coal may be too low to be optimal. Conversion yield for this coal (PSOC-1498) also supports this conclusion, averaging 21% compared to 34% conversion for the other coals.

Analysis of Extracted Residues to Determine Effects of Molybdenum Sulfide Catalyst

The general relationship in the reflectance of vitrinite-derived residues between non-catalytic and catalytic (1% Mo) temperature-staged hydrogenation experiments is provided in Fig. 2. This figure shows that the residual materials from the catalytic runs generally have higher reflectances than those from non-catalytic runs. The higher volumetric conversion of each coal in the presence of the molybdenum catalyst means that there is much less of the original coal material remaining; therefore, the residues will be of higher molecular weight and more highly condensed than from runs which achieve significantly lower levels of conversion. Another possible contribution to the higher reflectances would result from the catalyst promoting dehydrogenation reactions.

The significance of the foregoing is that a reflectance measurement made on residual material, considered in isolation from all pertinent information, may not be a good indication of the conversion of coal to a soluble product. In particular, low molecular weight products generated as a result of efficient hydrogenation are presumed to have had a relatively low reflectance; however, these materials will have dissolved in the solvent (THF) used to separate the soluble products from the insoluble residues. Because of this problem, a series of experiments was undertaken specifically to study the reflectance distribution

of the whole products (without extraction), as well as the insoluble residues of catalytic and non-catalytic temperature-staged hydrogenation. The results, are summarized in the section entitled "Analyses of Whole Products".

Reflectance analyses also were performed on just the THF-insoluble residues of dry catalytic and non-catalytic, single- and two-staged liquefaction of the subbituminous coal (PSOC-1401) reacted under N_2 and H_2 atmospheres and a combination of the two gases. This series of runs has enabled the influence of atmosphere, catalyst and pretreatment to be evaluated. Table 3 shows that, for both catalytic and non-catalytic runs, vitrinite reflectance values of the residues of pretreatment are low whether generated in a nitrogen or a hydrogen atmosphere. The influence of atmosphere and catalyst becomes more evident as a result of high-temperature and temperature-staged reactions (425°C). The vitrinite was subject to significant changes as shown by a large increase in maximum reflectance and by the qualitative descriptions provided in Table 3. In this table, "reacted" vitrinite (or vitroplast) refers to those vitrinite particles which had undergone thermoplastic deformation and might have developed a granular anisotropy; "unreacted" vitrinite refers to those showing no evidence of thermoplasticity, for the most part retaining their original morphology.

In the presence of the molybdenum catalyst and hydrogen atmosphere, most of the vitrinite particles became plastic in the reactor and were partially subject to condensation leading to the development of a granular anisotropy. In comparison, the other three high-temperature residues processed in a nitrogen atmosphere are composed mainly of "unreacted" vitrinite particles. This demonstrates that the presence of a catalyst and hydrogen gas play an important role in promoting vitrinite reactivity during liquefaction of the subbituminous coal. Although the "unreacted" vitrinite particles may possess a lower reflectance than the "reacted" particles, the latter were associated with a higher volumetric conversion.

During the temperature-staged reactions (275°C + 425°C), the effect of the first stage is negligible when a nitrogen atmosphere was used during the second stage. It was found, for residues of reactions at 425°C, N_2; 275°C, N_2 + 425°C, N_2; and 275°C, H_2 + 425°C, N_2, that the reflectance values were very similar for residues of the catalytic runs and again for those from the non-catalytic runs (Table 3). This suggests that first-stage reactions did not play an important role in liquefaction if an inert atmosphere was used in the second stage. This is further supported by the conversion data for these groups of three reactions (Table 3).

The impact of first-stage reaction became important when a hydrogen atmosphere was employed. In all residues after two-stage reactions with a hydrogen atmosphere, no granular anisotropic carbons were formed from the subbituminous coal (PSOC-1401), whereas this material is present in the residue of the corresponding single, high-temperature stage reaction. Also, the reflectance of the "reacted" vitrinite only is lowest when a hydrogen atmosphere was used in both stages with the catalyst, representing the conditions which gave rise to the highest conversion. This implies that first-stage reaction may have created products or molecular structures which are not as likely to undergo the condensation reactions that would otherwise take place during the second stage.

During the temperature-staged reactions, the presence of the catalyst minimized retrogressive reactions in the subbituminous coal. The reflectance values of the residues from the non-catalytic runs are consistently higher than those of the catalytic ones in the temperature-staged reactions even though there may have been considerably lower conversion (Table 3).

In brief, the influence of different parameters on dry liquefaction are interrelated. The effects of atmosphere and catalysis are manifested during the second stage, whereas they have relatively little apparent effect during the first stage. The presence of a hydrogen gas and catalyst promotes the thermoplastic development of vitrinite in the tubing bomb reactor, in turn favoring liquid conversion as a consequence of enhanced hydrogen transfer and catalyst dispersion.

Analyses of Whole Products, Catalytic and Non-Catalytic

The advantage of performing reflectance analysis upon the whole products of reaction is that a better opportunity is provided for evaluating the efficiency of hydrogenation. As noted above, some of the products of hydrogenation which would be dissolved by the extraction solvent are available for study in addition to undissolved coal and any products of retrogressive condensation reactions. This type of analyses is possible only with the products of dry hydrogenation; when a vehicle solvent is used, the products have a tarry consistency and cannot be formed into a pellet or polished without prior extraction. Published work (2) on the experimental hydrogenation of an hvA bituminous coal has shown that thermal reactions produced only higher reflecting vitrinite-derived materials, but where a dispersed catalyst was employed the reflectance distribution was extended downwards to significantly lower levels. The lower reflecting population, in the latter case, was THF soluble and highly fluorescing under blue-light irradiation. This contrasted with the THF-insoluble and non-fluorescent nature of the higher reflecting population. It was concluded that the low-reflecting material generated under catalytic hydrogenation in these experiments probably was asphaltenic in nature.

Subsequent work (3) showed that although similar reflectance distributions were obtained for the vitrinite-derived materials in the whole products from the hydrogenation of hvA and C bituminous coals, the anisotropic textures of these materials were quite different. A fine-grained anisotropy was apparent in the product of the first of these coals, possibly because of the large size of molecules generated during catalytic liquefaction (the residue of the corresponding thermal run was isotropic). It is supposed that locally, in the absence of hydrogen, the molecular fragments would align and stack to give an anisotropic texture. The same coal catalytically hydrogenated in the presence of a distillate process solvent fraction (220-500°C-boiling H-coal fractionator bottoms from Consolidation Coal Company) produced only negligible anisotropic semicoke; apparently the solvent must aid the dispersal of free radicals so that there is a greater likelihood of hydrogenation. In the case of the hvC bituminous coal, no anisotropic semicoke was produced during the dry hydrogenation under either thermal or catalytic conditions. It was concluded that the aromatic fragments formed during catalytic hydroprocessing of this coal must be less planar than those from the hvA bituminous coal. The reported difference in conversion levels between coals of hvC and A bituminous rank (Figs 1 & 2), and the optical

textures of their respective residues appear to be manifestations of known differences in molecular structure between coals of these ranks. These results, then, illustrate how geochemistry affects coal structure, and the significant effect this can have upon reaction chemistry.

Acknowledgment

The research was conducted with the financial support of a grant from the U.S. Department of Energy (DE-FG22-86PC90910).

REFERENCES

1. Derbyshire, F., Davis, A., Epstein, M. and Stansberry, P., 1986, Fuel, 65, 1233-1239.

2. Derbyshire, F.J., Davis, A. and Lin, R., 1989, Energy & Fuels, 3, 431-437.

3. Davis, A., et al., Optical properties of coals and liquefaction residues as indicators of reactivity, Fuel, in press.

4. Mitchell, G.D., Davis, A. and Spackman, W., in Liquid Fuels from Coal (Ed. R.T. Ellington), Academic Press, 1977, pp. 245-270.

5. Shibaoka, M., 1981, Fuel, 60, 240-246.

6. Yarzab, R.F., Given, P.H., Spackman, W. and Davis, A., 1980, Fuel, 59, 81-92.

7. Szladow, A.J. and Given, P.H., 1981, Ind. Eng. Chem. Proc. Res. Dev., 20, 27.

8. Derbyshire, F., Davis, A., Schobert, H. and Stansberry, P., 1990, American Chemical Society, Division of Fuel Chemistry, Preprints, 35(1), 51-57.

9. Mitchell, G.D., Davis, A. and Derbyshire, F.J., 1989, Proceedings International Coal Science Conference, Tokyo, Japan, International Energy Agency, Vol. II, 751-754.

Table 1. Coal Properties

Penn State Sample Number	PSOC-1482	PSOC-1401	PSOC-1498	PSOC-1504
Seam State ASTM Rank	Hagel North Dakota lig	Lower Wyodak Wyoming subB	Wadge Colorado hvC	Upper Sunnyside Utah hvA
Mean-Maximum Reflectance of Vitrinite (Romax, %)	0.39	0.42	0.60	0.80
Ultimate Analysis (% daf)				
Carbon	72.3	74.3	77.5	82.0
Hydrogen	2.3	5.2	5.5	5.8
Oxygen (by difference)	23.5+	19.3	14.7+	9.7+
Nitrogen	1.0	1.1	1.8	1.8
Organic Sulfur	0.9	0.2	0.6	0.8
Proximate Analysis (a.r.%)				
Moisture	34.7	16.3	9.5	3.4
Volatile Matter	28.1	37.7	38.0	37.5
Fixed Carbon	31.4	41.1	46.1	51.8
Ash	5.9	6.6	6.4	7.3
Petrographic Composition (vol %, mineral-free)				
Vitrinite	88	85	89	87
Liptinite	2	2	2	3
Inertinite	10	13	9	10
Chloroform-soluble extract (% dmmf)	1.76	NA	1.31	1.06

Table 2. Maximum Reflectance Measurements on Vitrinite-Derived THF-Insoluble Residue Material From Dry, Non-catalytic Liquefaction

	Raw	275°C, H_2	275°C, N_2	425°C, H_2	425°C, N_2	275°C, H_2 + 425°C, H_2	275°C, N_2 + 425°C, N_2
PSOC-1482	0.39	0.39	0.38	1.40	1.42	1.43	1.42
PSOC-1401	0.42	0.57	0.56	1.25	1.41	1.41	1.40
PSOC-1504	0.80	0.76	0.73	1.38	1.36	1.35	1.37

Table 3. Maximum Reflectance of Vitrinite-Derived Residue Material (THF insolubles) from Liquefaction of PSOC-1401

	Dry, catalytic (1% MoS_2)			Dry, non-catalytic		
Sample Identification	Reflectance, %	Vitrinite Type	Conversion, %	Reflectance, %	Vitrinite Type	Conversion, %
Raw	0.42	(unreacted)	--	0.42	(unreacted)	--
275°C, N_2	0.62	(unreacted)	4.5	0.56	(unreacted)	7.7
275°C, H_2	0.60	(unreacted)	4.1	0.57	(unreacted)	9.0
425°C, N_2	1.25	(unreacted)	25.9	1.41	(unreacted)	32.0
425°C, H_2	1.58	(reacted)	60.3	1.25	(unreacted)	33.7
275°C, N_2 + 425°C, H_2	1.46	(reacted)	58.7	1.62	(reacted)	41.0
275°C, H_2 + 425°C, N_2	1.24	(unreacted)	25.7	1.43	(unreacted)	32.0
275°C, N_2 + 425°C, N_2	1.19	(unreacted)	24.8	1.40	(unreacted)	32.2
275°C, H_2 + 425°C, H_2	1.40	(reacted)	67.4	1.41	(reacted)	40.4

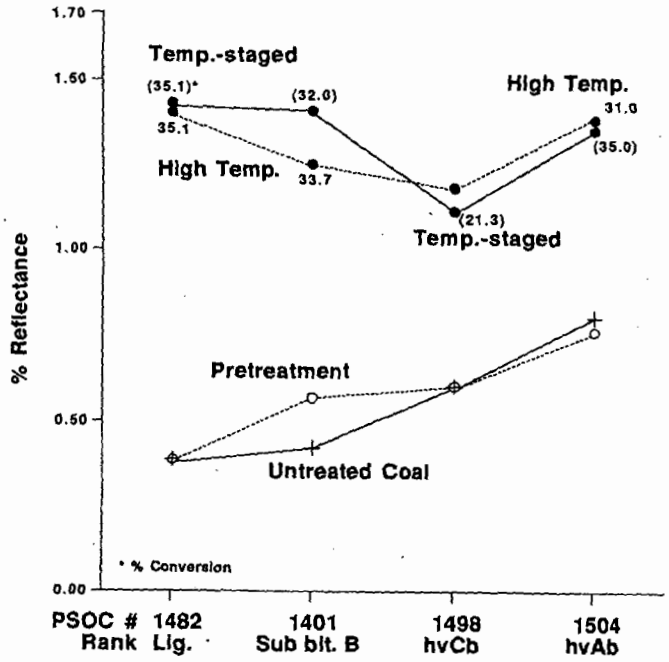

Figure 1. Mean Reflectance of Vitrinite-Derived Materials as a Function of Reaction Conditions; Dry, Non-catalytic Hydrogenation Residues

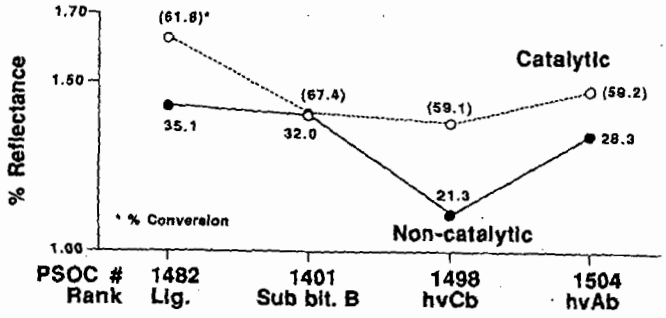

Figure 2. Mean Reflectance of Vitrinite-Derived Materials; Temp.-staged Dry, Catalytic (Mo) and Non-catalytic Hydrogenation Residues

LINKS BETWEEN HYDROGENATION BEHAVIOR OF COALS AND THEIR GIESELER-SOLIDIFICATION

Anna Marzec and Hans-Rolf Schulten*
Institute of Coal Chemistry, Polish Academy of Sciences, 44-100 Gliwice, 1 Maja 62, Poland
*Fachhochschule Fresenius, 6200 Wiesbaden, Dambachtal 20, Germany

INTRODUCTION

The present study aims at better understanding of links that were found between hydrogen acceptor abilities of coals and their solidification temperatures (1) in search for means of prediction of the development of anisotropic texture in coking coal blends (1).

Our approach is based on the four methodological steps applied to a set of twenty coals that represent a wide range of thermoplastic properties. The steps are: (1) determination of hydrogen acceptor abilities of the coals in reaction with tetralin; (2) determination of Gieseler-solidification temperatures of the coals; (3) characterization of the coals by pyrolysis /Py/-field ionization /FI/ mass spectrometry /MS/ of the coals; and (4) multivariate chemometric evaluation of these three data sets. Specific role of Py-FIMS of coals lies in that the technique displays chemical composition of a part of coal material that is able to diffuse and penetrate coal grains on heating during coal processing; it has been found that this movable part influences coal reactivity in reaction with H-donor (2,3) and in low-temperature pyrolysis (4).

The present paper is aimed at search for structural units of coal material that are active in hydrogen transfer and units that are active in reactions resulting in coal solidification on heating. It is believed that the results can contribute to identification of structures active in liquefaction retrogressive reactions.

EXPERIMENTAL

Coal Samples. Twenty carboniferous coals from Poland were studied. Their basic properties (wt.% daf) are: carbon 85-91; hydrogen 4.3-5.3; oxygen 0.8-7.0; sulfur 0.5-3.8. The petrographic composition (wt.% dmmf) is: vitrinite 63-88; exinite 0.-11; inertinite 7-30. Solidification temperatures of the coals (Table 1) are in the 417-490oC range.

Reaction of Coals with Tetralin. The reaction was carried out at 400oC; 60 min; for coal-tetralin mixture 1:2 w/w. The amount of hydrogen transferred from tetralin to coal material /HTr/ was calculated on the basis of GC determination of unreacted tetralin/naphthalene ratio. Other details were reported earlier (3) except for thermal decomposition of tetralin at 400oC. Tetralin was heated in the autoclave at 400oC/60 min and GC analysed . The result of analysis: 97.8 % tetralin; 1.4 % naphthalene; and compounds of lower and higher retention times 0.5 % and 0.3 %, respectively, were used for calculation of corrected HTr values /shown in Table 1/. The same procedure was

applied in determination of HTr for pyridine /Py/- extractables and Py-residues of the coals.

Py-FI MS and Chemometric Techigues. Both have been previously described in details (2-4).

RESULTS

Hydrogen Transfer to Coal Material. The data in Table 1 show that organic material of Py-extractables as well as of Py-residues react with tetralin. Amount of hydrogen transferred to Py-extractables and to the residues is in the same range from 0.4 to 1.0 grams of H / 100 grams of org. material. If one compares HTr values for a coal, its extracted material and residue, one can say, all cases are observed: some coal samples show the highest HTr; in other coals the highest HTr is found for their extractables or for residues.
The correlation coefficient found between HTr values for the coals and their solidification temperatures is very significant / r = 0.87/. Lower r values were found for the products of extraction.
Hydrogen Transfer and FI Difference Mass Spectrum of Selected Coals. Four most reactive coals /HTr in the range from 0.8 to 1.2/ were selected; their FI mass spectra were normalized and summed. Next, four least reactive coals /HTr in 0.1 - 0.4 range/ were chosen and their spectra were normalized and summed. Figure shows the difference spectrum for the two groups of coals. The upper part of Figure shows FI mass signals whose intensities are higher in the high reactive coals. The lower part shows signals whose intensities are higher in the least reactive coals. Hence, it has been concluded that the composition of the volatilized, in the mass spectrometer, material of coals can supply information about components that are active in hydrogen transfer as well as about unreactive species.

FI Mass Signals Correlated with Hydrogen Transfer. Results of correlation analysis carried out for two sets of data: (a) FI mass signals in the range 158-400 a.m.u. and (b) amounts of hydrogen transferred to the samples of coals, are shown in Table 2. Seventy seven FI mass signals were found to be significantly correlated with the HTr values. A vast majority of the coefficients are highly significant ($r > |0.68|$). This indicates that there is a causitive link between structures represented by the correlated signals and reactivity of the coals in hydrogen transfer.
Out of all the correlated signals, forty seven signals are correlated with positive sign /Table 2;upper/ i.e., the higher the intensities of these signals the higher amount of hydrogen is transferred to the coals. All these signals can be found in the upper part of the difference spectrum /Figure/ .
Thirty signals are correlated with negative sign /Table 2; lower/ which means: the higher the intensities of the signals the lower amount of hydrogen is transferred to the coals. All the signals can be found in the lower part of the difference spectrum.

Proposed structures for all correlated signals are shown in Table 3. The structures represent only one of all possible isomers for example, pyrene / m/z 202/ is displayed, although there are three other four-ring aromatic hydrocarbons, all with the same

accurate mass as for pyrene. Isomers not presented in the Table can be found in reference 5.

Structures Active in Hydrogen Transfer /Table 3; upper/. In general, there are two types of compounds that are positively correlated with hydrogen transfer. They are aromatic hydrocarbons and hydroxycompounds. Hydroaromatics seem to be of minor importance for the reactivity of the studied coals, compared with lower rank coals (3,4), since they are represented by a few hydropyrenes.

Aromatic hydrocarbons are represented by 12 classes with respect of number of aromatic rings and mode of their arrangement. They are: 3-aromatic ring hydrocarbon (m/z 190); 4-aromatic ring (m/z 202; 226; 240; 254); 5-aromatic ring (m/z 252; 264; 276; 278); 6-aromatic ring (m/z 302; 328) and 7-aromatic ring hydrocarbon (m/z 300). With respect of alkyl substituents, majority of the hydrocarbons are present as unsubstituted and containing one methyl group. A few hydrocarbons may have C2 and C3 alkyl substituents, for example, accurate masses related to signals m/z 328 and 342 may represent either C2 and C3- coronenes or C0-C1-dibenzochrysenes.

Hydroxycompounds are represented by /OH/- and /OH/2-benzenes;/OH/ and /OH/2-indenes; and /OH/ -naphthalenes, -acenaphthenes, -anthracenes, -fluorenes. No doubt, at least some of the compounds have phenolic OH (m/z 94; 110; 134).

Structures Inactive in Hydrogen Transfer /Table 3; lower/. In contrast to the positively correlated mass signals, the negatively correlated signals represent entirely different structures. None of them can be assigned to unsubstuted aromatic hydrocarbons. Instead of that, the signals represent short alkyl derivatives of naphthalene, fluorene, acenaphthene, anthracene and chrysene, the five classes of aromatic hydrocarbons that are not present at all in the set of active structures. The other aromatics are alkylated, C2-C5, pyrene, perylene, cyclopentachrysene and dibenzopyrene; these aromatics in the positively correlated set are entirely unsubstituted.
A few hydroxycompounds i.e., C4-C7-dihydroxybenzenes were also found to be inactive in hydrogen transfer.

Comparing the present results with results obtained for another set of twenty coals of lower rank (2-4), the major difference is, that in high rank coals much more correlated signals are related to aromatic structures. This refers to the positively as well as negatively correlated signals.

FI Mass Signals and Structures Correlated with Solidification Temperatures. Results of correlation analysis carried out for two sets of data i.e., FI mass signals and temperatures of solidification of coals, Ts, are presented in Table 2. It has been stated that all signals, significantly correlated with Ts, are also significantly correlated with hydrogen transfer, however with opposite sign (Table 2).
This means, the higher the content in a coal of structures shown in upper part of Table 3, the lower is its temperature of solidification and the higher its hydrogen transfer. It clearly indicates a strong link between reactivities of the structures in reactions resulting in solidification and in hydrogen transfer

reactions.
Next, the results of correlation analysis also show: the higher the content in a coal of structures presented in lower part of Table 3, the higher is its temperature of solidification and the lower its hydrogen transfer. Thus, the structures are inactive in solidification as well as hydrogen transfer reactions.

Summing up the results:
- The same structures are reactive in hydrogen transfer from the hydrogen donor and in reactions that result in solidification of coal on its heating. They are: (a) numerous unsubstituted and C1-aromatic hydrocarbons that contain from 3 up to 7 aromatic rings /except for the hydrocarbons quoted in the next para/; a few may have also C2 and C3 alkyls; and (b) C0-C7-alkylated hydroxyaromatic compounds that contain from 1 to 3 aromatic rings.
- Structures that are inactive in hydrogen transfer as well as in solidification reactions, are: alkyl-, up to C3, naphthalenes, fluorenes, acenaphthenes, anthracenes and chrysenes as well as alkyl-, up to C5, aromatic hydrocarbons that have 4 rings (pyrene, perylene, cyclopentachrysene) and 6 rings (dibenzopyrene).

DISCUSSION

The link between H-acceptor capability of coals in reaction with H-donor and their temperature-induced solidification (1) lies in the fact that the same structures that are active in H-transfer from H-donor are also active in thermal reactions resulting in solidification.
Hence, these structures during liquefaction can react via two pathways: they can either react with H-donor or participate in condensation/polymerization reactions. The pathway by which the structure reacts depends on the availability of H-donor molécule or a molecule with which it can condensate or polymerize.

H-transfer activity of the shown aromatic hydrocarbons (Table 3;upper) can be explained on the basis of mechanism worked out by McMillen, Malhotra et al.(6); the aromatics react with hydroaromatic H-donor and give rise to cyclohexadienyl radicals which in turn, lead to cleavage of single bonds in coal material. The mechanism of solidification reactions of the aromatics can be deduced from studies of carbonization at 430-450oC of model aromatic hydrocarbons (7) showing that they undergo condensation reactions. Hence, it is concluded that the shown aromatic hydrocarbons undergo such condensation during liquefaction and that this constitutes a part of retrogressive reactions in liquefaction.

Assuming that the hydroxycompounds (Table 3; upper) are phenolic compounds, one can explain their activity in H-transfer by several hypotheses (8,9). More obscure is mechanism by which they contribute to solidification, except for dihydroxybenzenes (10).It has been stated that they readily polymerize at 400oC; ionic mechanism was suggested (10). Thus, it is concluded that the hydroxycompounds polymerize in liquefaction and give rise to retrogressive reactions in this way, if H-donor is not available on molecular level.

The inactive structures (Table 3; lower) dilute the concentration

of active species. Hence, the higher the content of inactive ones the longer time is needed for solidification. This has been manifested in the Gieseler-plastometer as the increase of solidification temperature.

REFERENCES

(1) S. Iyama, T. Yokono and Y. Sanada, Carbon 1986, 24, 423; and references therein

(2) H-R. Schulten, N. Simmleit and A. Marzec, Fuel 1988, 67,619

(3) A. Marzec, S. Czajkowska, N. Simmleit and H-R. Schulten, Fuel Processing Technology, 1990, 26, 53

(4) H-R. Schulten, A. Marzec, P. Dyla, N. Simmleit and R. Mueller Energy & Fuels 1989, 3, 481

(5) M.L. Lee, V. Novotny and K.D. Bartle, "Analytical Chemistry of Polycyclic Hydrocarbons". Academic Press, 1981, pp.363-386

(6) D.F. McMillen, R. Malhotra, G.P. Hum and S-J. Chang, Energy & Fuels 1987, 1, 193; and references therein

(7) M. Zander, ACS Fuel Chem. Div., Preprints 1989, 34/4/, 1218; and references therein

(8) D.D. Whitehurst, Th.O. Mitchell and M. Farcasiu, "Coal Liquefaction", Academic Press, 1980, Ch. 8 and 9.

(9) L.M. Stock, in: "Chemistry of Coal Conversion", Ed. R.H. Schlosberg. Plenum Press, 1985, pp. 253-313.

(10) F.M. Wang, V.P. Senthilnathan and S.E. Stein, Proceedings of the 1989 Coal Science Conference, Tokyo, vol. 1, p. 165.

ACKNOWLEDGEMENTS. This work was supported by the Deutsche Forschungsgemeinschaft, Bonn-Bad Godesberg /Project Schu 416/15-1/ and by the Polish Academy of Sciences.

Table 1
BASIC CHARACTERISTICS OF THE STUDIED COALS

COAL No	Wt % daf C	Wt % daf O	SOLIDFTN* Ts; oC	HYDROGEN TRANFER, HTr g of H /100 g org.mat. COAL	RESIDUE	EXTRACT
100	85.0	6.9	433	0.78	0.77	0.68
102	87.3	4.6	417	1.06	0.84	0.83
103	85.9	6.6	428	1.20	0.95	0.85
104	85.3	6.9	451	0.71	0.70	0.86
105	85.7	6.9	440	0.68	0.67	0.91
106	85.7	6.6	451	0.76	0.61	1.01
107	86.4	2.8	464	0.74	0.51	0.95
109	88.4	3.8	471	0.63	0.69	0.61
110	88.3	3.6	458	0.55	0.71	0.55
111	86.7	5.2	465	0.42	0.73	0.60
112	90.6	1.9	478	0.49	0.77	0.49
113	91.9	0.8	487	0.32	0.71	0.47
114	89.4	3.2	490	0.12	0.42	0.44
117	84.5	7.5	454	0.76	1.03	0.81
118	85.7	5.3	448	0.61	0.95	0.72
119	89.5	2.7	479	0.27	0.47	0.41
120	84.5	7.7	430	0.83	1.00	0.72
121	91.4	0.8	488	0.41	0.42	0.50
122	88.7	1.7	490	0.36	0.46	0.97
124	85.1	6.8	430	0.73	1.02	0.62
Range	85-91	0.8-7.7	417-490	0.1-1.2	0.4-1.0	0.4-1.0

*/ Gieseler plastometer; standard method PN-62/G-04536.

Table 2
FI MASS SIGNALS CORRELATED WITH HYDROGEN TRANSFER VALUES /HTr/ AND WITH SOLIDIFICATION TEMPERATURES /Ts/ OF THE COALS

m/z	Corrln coeffnt for HTr	Corrln coeffnt for Ts	m/z	Corrln coeffnt for HTr	Corrln coeffnt for Ts
	Upper Part			Upper Part	
158	.85	-.82	374	.67	-.76
160	.59	-.56	376	.80	-.86
162	.81	-.75	378	.88	-.90
164	.82	-.74	380	.59	-.55
172	.85	-.83	388	.74	-.84
174	.69	-.63	390	.87	-.83
176	.76	-.71	392	.84	-.88
188	.79	-.70		Lower Part	
190	.53	-.59			
200	.70	-.67	166	-.70	.70
202	.54	-.60	168	-.58	.70
212	.91	-.85	180	-.80	.87
214	.80	-.83	182	-.71	.80
224	.50	-.60	192	-.78	.85
226	.93	-.91	194	-.83	.85
238	.82	-.88	196	-.62	.55
240	.91	-.94	206	-.91	.90
250	.82	-.81	208	-.71	.77
252	.81	-.84	218	-.72	.74
254	.77	-.75	220	-.80	.59
260	.57	-.64	230	-.86	.90
262	.72	-.75	244	-.90	.90
264	.85	-.90	256	-.69	.74
274	.73	-.73	258	-.90	.85
276	.76	-.76	280	-.75	.85
278	.88	-.79	284	-.74	.71
288	.69	-.70	294	-.86	.91
290	.68	-.55	298	-.72	.71
300	.62	-.65	306	-.75	.79
302	.87	-.85	308	-.87	.84
314	.86	-.86	318	-.81	.85
328	.79	-.83	320	-.88	.95
338	.81	-.77	322	-.59	.62
340	.64	-.48	330	-.57	.70
342	.83	-.77	332	-.83	.87
350	.71	-.72	334	-.87	.79
352	.90	-.92	344	-.83	.79
364	.85	-.88	346	-.87	.85
366	.88	-.83	358	-.72	.68

Table 3
STRUCTURES IN THE CORRELATED FI MASS SIGNALS

Upper: FI signals positively correlated with H-transfer and negatively correlated with solidification temperatures
Lower: FI signals negatively correlated with H-transfer and positively correlated with solidification temperatures

m/z					PROPOSED STRUCTURES
					Upper; ACTIVE STRUCTURES
108	122	136	150	164	C_0 – C_5 -hydroxybenzenes*
110	124	138			C_0 – C_2 -dihydroxybenzenes*
146	160	174	188		C_1 – C_4 -hydroxyindenes *
134	148	162	176	190	C_0, C_1 *, C_2, C_3*-dihydroxyindenes
158	172		200	214	C_1 – C_2 and C_4 – C_5 -hydroxynaphthalenes *
198	212				C_2 – C_3 hydroxyacenaphthenes *
224	238				C_3 – C_4 -hydroxyfluorenes * and
					C_1 – C_2 -octahydropyrenes *
190					4H-cyclopenta[def]phenanthrene *
202					pyrene *
250	and	262			C_3 -hexahydropyrene * and C_4 -tetrahydropyrene *
226	240	254			C_0 – C_2 -benzo[ghi]fluoranthenes *; C_0 – C_1 -cyclo
					penta[def]chrysenes *; C_0 -cyclohexa[def]chrysene *
252					perylene *
260	274	288			$C_n H_{2n} - {}_{20} N_2$ *
264	278				C_0 – C_1 -11H-cyclopenta[ghi]chrysene *; C_0 -picene *;
					C_5 – C_6 -hydroxyanthracenes *
276	290				C_0 – C_1 -anthanthrenes *
302					C_0 -dibenzopyrene *; C_6 – hydroxypyrene *
300	314	328	342		C_0 * , C_1 * , C_2 * , C_3 -coronenes;
					C_0 * – C_1 -dibenzochrysenes
340					C_1 -dibenzocyclopenta[cd]pyrene
350	364	378	392		C_0 – C_3 -benzocoronenes; C_0 – C_1 -tribenzochrysenes
352	366	380			C_0 – C_2 -tribenzopyrenes
374	388	and	376	390	?

Lower: INACTIVE STRUCTURES

142	156			C_1 – C_2 -naphthalenes *
166	180	194	208	C_4 – C_7 -dihydroxybenzenes * a. C_1 – C_3 -fluorenes *
192	206	220		C_1 – C_3 -anthracenes *
218				C_2 – 4H-cyclopenta[def]phenanthrene
168		196		C_1 , C_3 -acenaphthenes * and $C_{13}H_{12}N_2$ *
230	244	258		C_2 – C_4 -pyrenes
256		284	298	C_2 , C_4 *, C_5 -chrysenes
280	294	308	322	C_2 *, C_3 *, C_4 , C_5 -perylenes
306	320	334		C_3 , C_4 , C_5 * -11H-cyclopenta[ghi]chrysenes
304	318	332	346	C_2 – C_5 -anthanthrenes
330	344	358		C_2 *, C_3 , C_4 -dibenzopyrenes

* the assignments have been confirmed by high res. and accurate mass measurements

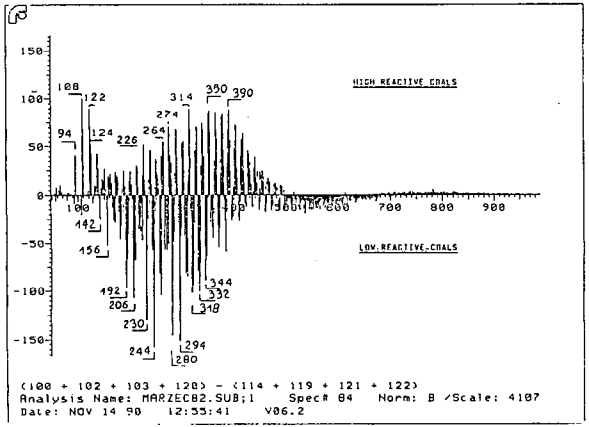

Figure.

FI Difference Mass Spectrum nf Selected Coals showing high and low reactivity towards the H-donor. See Table 1 for coals No. 100, 102, 103, 120 and 114, 119, 121, 122.

EFFECT OF MOLYBDENUM SULFIDE CATALYST ON THE MECHANISM OF COAL LIQUEFACTION

Caroline E. Burgess, Levent Artok, and Harold H. Schobert
Fuel Science Program
Department of Materials Science and Engineering
The Pennsylvania State University
University Park, PA 16802

Keywords: molybdenum sulfide catalyst, liquefaction mechanism, low severity liquefaction

INTRODUCTION

Molybdenum sulfide catalyst has been used to improve liquefaction yield and to refine coal oils for the last 60 to 70 years [1]. It was an important step in coal liquefaction that these catalysts were developed because before that time known catalysts were poisoned by sulfur [1], an element all coals contain. In 1923, M. Pier found selective, oxidic catalysts used in methanol synthesis that were less sensitive to sulfur than the metallic catalyst that was developed from ammonia synthesis [1]. In 1924, M. Pier prepared sulfur resistant coal hydrogenation catalysts: sulfides and oxides of molybdenum, tungsten, and the iron group metals [1].

Weller and Pelipetz [2] used ammonium heptamolybdate (AHM) to liquefy Rock Springs subbituminous B coal (Table 1) and found a remarkable increase in coal conversion when using a catalyst (92.7%) relative to an uncatalyzed reaction (33.7%). Their work shows that both oils and asphaltenes increase in yield. The reaction conditions of 450°C for 1 h at 1000 psig were such that asphaltenes initially produced could easily crack to oils. However, with a change in the oil-to-asphaltene (O/A) ratio from 3.71 for the uncatalyzed reaction to 1.51 for the catalyzed reaction, it appears the catalyst functions mainly to form asphaltenes. With the use of only one coal, there is not enough data to substantiate this trend. Table 2 contains data from Garg and Givens [3] showing AHM catalyst to have virtually no effect on total conversion, but a substantial increase in the O/A ratio from 0.19 to 0.38. At their reaction conditions (825°F for 35 min at 2000 psig), molybdenum catalyst appears to function to hydrogenate asphaltenes to oils. Since these data are in contradiction to those of Weller and Pelipetz, experimental work with more coals is necessary to see how coal rank and structure relate to the mechanism of molybdenum sulfide catalyst behavior in coal liquefaction. If these data are compared to liquefaction work done in our laboratory with molybdenum sulfide catalysts at low severity reaction conditions, the beginning of an understanding of the role molybdenum catalysts play in the coal liquefaction can be developed.

EXPERIMENTAL

Three different catalyst precursors were used. Sulfided ammonium molybdate (SAM) was prepared, as described in several publications [4-6], by bubbling H_2S into a solution of ammonium heptamolybdate. Sulfided tetrahydroquinolinium molybdate (STM) of the chemical formula $(THQH)_6Mo_8S_{22}O_5 \cdot H_2O$ (where THQH represents protonated tetrahydroquinoline) was prepared as described by Burgess and Schobert [7]. Ammonium tetrathiomolybdate (ATM) was prepared in a similar manner to SAM, except the addition of NH_4OH provided sufficient additional ammonium ions to drive the reaction to completion [8].

The coal was impregnated in the same manner as reported previously [4-6]. Coal was slurried with catalyst precursor solutions for 2 hours and vacuum freeze dried to less than 1% moisture. Although several molybdenum sulfide precursors were used, previous data have shown that the predominant active catalyst species is MoS_2 [4-9], and relative comparisons can be made about the effect of molybdenum catalysts on coal liquefaction. However, it should be recognized that the degree of dispersion of the catalyst precursors on coal could be different because three different molybdenum sulfide catalyst precursors were used.

Five coals were used. Data on the elemental composition of each coal are contained in Tables 3-8. All reactions were carried out in 25 ml microautoclave (tubing bomb) reactors, and heating was accomplished in a temperature controlled fluidized sandbath. The catalyst loading was 1% expressed as weight of molybdenum (not of molybdenum compound) on a daf basis. The reactor was flushed three times with hydrogen, with the final addition pressurized to 6.9 MPa (cold). The reactor was vertically oscillated 2.5 cm at 200 cycles per minute. Two subbituminous B coals and a hvA bituminous coal used a single stage reaction at 425°C for 10 min and a temperature-staged reaction (350°C for 1 h followed by 425°C for 10 min). The solvent used was naphthalene at a 2/1 solvent-to-coal ratio, and the mass of the coal reacted was 2.5g. A Texas lignite and a hvB bituminous coal used the following reaction conditions: a phenanthrene solvent at a 1/1 solvent-to-coal ratio, with the coal mass 5g, and the reaction temperature was 275°C for 30 min.

For the first three coals (PSOC 1266, 1401, and 1488), the cooled reactor was vented into a glass expansion bulb, and the contents were analyzed by gas chromatography using a Varian model 3700. The contents of the reactor were then rinsed with tetrahydrofuran (THF) into a dried Soxhlet thimble and extracted for about 12 h under nitrogen. The THF was removed by rotary evaporation. The solid residue was dried at 100°C for 12 h before weighing. Conversion was calculated by subtracting the weight of the residue from the weight of the coal and dividing by the dmmf weight of the coal. Liquids were further separated into asphaltenes and oils by adding hexane to the THF-soluble portion. This mixture was refluxed for 12 h under nitrogen, followed by filtration into hexane-solubles and insolubles. The hexane was removed by rotary evaporation, and the samples were dried at 100°C for 1 h before weighing. The oil (hexane-soluble) yield was calculated by difference from the conversion percentages of the gas yield, THF solubles, and the THF insolubles.

For the last two coals (DECS-1 and DECS-6), the work-up procedure was changed slightly. Gas percentages were not determined, so the calculated difference for the oils includes the gas yield as well. Once the pressure was vented from the reactor, the contents of the tubing bomb were rinsed with toluene into a dried, weighed ceramic thimble and Soxhlet extracted for about 12 h under nitrogen. The toluene was removed from the extract by rotary evaporation. Toluene-solubles were further separated into asphaltenes and oils by adding about 400 ml of hexane to the extract. The mixture was stirred for 1 h and asphaltenes were allowed to settle overnight, with solids separated by vacuum filtration. The toluene-insoluble residue was then Soxhlet extracted with THF to separate preasphaltenes from the residue. THF was removed from the extract by rotary evaporation. Preasphaltenes, asphaltenes, and residue were dried overnight under vacuum at 110°C. Conversion was calculated by subtracting the weight of the residue from the weight of the coal and dividing by the daf weight of the coal.

RESULTS AND DISCUSSION

Conversion data for coals PSOC 1266 and 1401 at 425°C for 10 min are contained in Table 3, and conversion data for these two coals at 350°C for 1h followed by 425°C for 10 min are contained in Table 4. These data were obtained by M. Epstein [2]. For the single stage at 425°C, the bituminous coal (PSOC 1266) and the subbituminous coal (PSOC 1401) reacted in a similar manner. When comparing catalyzed experiments to uncatalyzed experiments, the change in total conversion was ~25% for both coals, with oil yields decreasing and asphaltene yields increasing substantially. The O/A for PSOC 1266 was 0.32 for the uncatalyzed experiment and 0.07 for the catalyzed experiment. A similar trend was noticed with PSOC 1401 with an O/A 6.1 for the uncatalyzed experiment and 0.42 for the catalyzed experiment.

Temperature-staging had a substantial effect on conversion of both coals. For PSOC 1266, when comparing catalyzed experiments to uncatalyzed experiments, the change in total conversion was about the same, ~28%, but the increase was substantial for the oil yield, while the asphaltene yield decreased. The O/A changed from 0.22 for the uncatalyzed experiment to 1.33 for the catalyzed experiment. However, for the subbituminous coal PSOC 1401, when comparing catalyzed experiments to uncatalyzed experiments, the conversion increased ~50%, with increases in both oil and asphaltene yields. The greatest increase occurred in the asphaltene yield, with O/A for the uncatalyzed experiments 1.46 and for the catalyzed experiments 0.60.

PSOC 1488 liquefaction data using two different molybdenum sulfide catalyst precursors are located in Tables 5-7. Table 5 contains data at 425°C for 10 min, Table 6 contains data at 350°C for 1 h followed by 425°C for 10 min, and Table 7 contains data for 350°C for 1h. At 425°C for 10 min, total conversion for the uncatalyzed experiment is low, at 25%. The experiment using SAM has a total conversion of 66%. There is little change in the oil yield (~14%), but there is a large increase in asphaltene production, from 10% for no catalyst to 46% for the SAM-catalyzed experiment. At this temperature, STM-catalyzed experiments showed poor yields, with oil yield about the same (14%) and asphaltene yield at 20%. The O/A ratio reflects this behavior by decreasing from 1.25 for the uncatalyzed experiment to 0.73 for the STM-catalyzed experiment and 0.29 for the SAM-catalyzed experiment.

Temperature-staging also had a significant effect on the catalyzed experiments. When using no catalyst, total conversion was 31%, with low oil yield (12%) and low asphaltene yield (14%). However, when comparing experiments using SAM and STM, total conversion increased to ~80%. The predominant increase for both catalytic experiments was in asphaltene yield, from 14% to 58% for SAM-catalyzed experiments and 50% for STM-catalyzed experiments. Although the STM experiment showed a lower asphaltene yield, a high oil yield (~25%) was observed compared to SAM-catalyzed experiments (~16%). STM seems to be more effective for hydrogenating asphaltenes to oils, as discussed elsewhere [9]. The O/A of the uncatalyzed experiment is 0.84, and similar to the 425°C experiments, the O/A decreased for the STM-catalyzed experiment to 0.52 and to 0.28 for the SAM-catalyzed experiment.

Data for experiments at 350°C for 1 h are located in Table 7. However, although the yields are lower than the temperature-staged experiments, the catalytic experiments showed an increase primarily in the asphaltene yields compared to uncatalyzed experiments, as in the previous results for PSOC 1488. At low severity, an indication of the coal's liquefaction ability can be readily seen, although the liquid yields are not high. The next set of data to be discussed is at even lower severity reaction conditions, but can be used to indicate a trend in how the coal will liquefy at higher reaction conditions.

Liquefaction data at 275°C for 30 min for a Texas subbituminous C coal (DECS-1) and a hvB bituminous coal (DECS-6) are located in Table 8. Conversion for DECS-1 is low at 275°C, but when comparing catalyzed experiments to uncatalyzed experiments, the predominant increase occurs in the preasphaltenes and asphaltenes and not in the oil fraction. The O/A (here A represents the sum of preasphaltenes and asphaltenes) changes from 0.32 for the uncatalyzed experiments to 0.2 for ATM-catalyzed experiments. The bituminous coal has a higher initial conversion (18% versus 6% for uncatalyzed). Although the total conversion increases in the ATM-catalyzed experiments (25%) compared to uncatalyzed experiments for DECS-6, the O/A remains constant at 0.38.

Despite the facts that different reaction conditions and different molybdenum catalyst precursors were used, there are some trends that can be seen in this whole body of work [2-9]. In the Penn State experimental work, two bituminous coals were reacted. PSOC 1266 (temperature-staged reaction) liquefaction yields (Tables 4) increased when comparing catalyzed experiments to uncatalyzed experiments, with the increased conversion being predominantly oils. DECS-6 liquefaction yields (Table 8) increased when comparing catalyzed experiments to uncatalyzed experiments, where liquefaction yield increases were equal between oils and asphaltenes. DECS-6 was reacted at very low severity reaction conditions (275°C), however, and cracking asphaltenes to oils at 275°C may be difficult. If these data are compared to Garg and Given's data (Table 2) [3], in which they used a hvC bituminous coal, a similar trend is noticed. They obtained a very high liquefaction conversion without catalyst (85%), and although in the catalytic experiment the total conversion did not increase much (87%), the O/A increased from 0.19 to 0.38. The molybdenum catalyst appears to function predominantly to hydrogenate asphaltenes to oils because, in all of these cases, initial conversion to asphaltenes even without catalyst is usually high. There was one exception with PSOC 1266 for the 425°C/10 min experiment (Table 3). The O/A ratio decreased when comparing the catalyzed experiment to the uncatalyzed experiment from 0.32 to 0.07. This phenomenon may be because the reaction conditions do not allow enough time for asphaltenes to be hydrogenated to oils. PSOC 1488, a subbituminous coal, (Table 5) at 425°C/10 min shows a similar occurrence. However, for

experiments using STM, reaction yields are very low, and may be due to poisoning of MoS_2 by products of THQ decomposition [9].

Three subbituminous coals were reacted. Liquefaction yields for all three (Tables 3-8) were substantially increased by the use of catalyst. For PSOC 1401, for the temperature-staged experiment, total conversion (Table 4) increased from 42% to 91%, where the increase in conversion was predominantly in the asphaltenes. The O/A ratio changed from 1.46 for the uncatalyzed experiment to 0.60 for the SAM-catalyzed experiment. For PSOC 1488, for all reaction conditions and both catalyst precursors (Tables 5-7), the catalytic experiments showed an increase in total conversion compared to uncatalyzed experiments, where the predominant increase was in the asphaltenes. DECS-1 (Table 8) showed a similar trend. Weller and Pelipetz [2] also show a similar trend (Table 1). The catalyst appears to first function to break apart the macromolecular network, and then, function to hydrogenate some of the asphaltenes to oils if conditions are conducive to do so. So why is the molybdenum catalyst functioning differently in bituminous and subbituminous coals?

Subbituminous coals contain more oxygen and are thought to be more highly crosslinked than bituminous coals. Hirsch describes low-rank coals with an open structure where there are many crosslinks (heteroatoms and hydrocarbon chains) connected to small aromatic systems (3 rings or less) [10]. Bituminous coals (85-91% C) tend to have a liquid structure, where there are fewer crosslinks, larger aromatic systems, and overall more order in structure [10]. Without catalyst or hydrogen donor solvent, little atomic hydrogen is available externally because hydrogen radicals generated from H_2 tend to react with each other before being able to react with radicals as the crosslinks break apart. Since ether, thioether, and some carbon-carbon bonds are relatively weak [11-13], if catalyst provides atomic hydrogen at the milder reaction conditions ($\leq 350°C$ or temperature-staging), radicals can be generated more slowly and capped more efficiently to form asphaltenes. Since subbituminous coals in general contain more crosslinks to break apart, the catalyst functions mainly to provide hydrogen for capping generated radicals. Hence the large asphaltene yields and relatively large conversions for subbituminous coals when using molybdenum catalyst. Bituminous coals contain fewer crosslinks, so the requirement for radical capping with hydrogen supplied via the catalyst is lower relative to subbituminous coals. Therefore, molybdenum catalyst can function to hydrogenate generated asphaltenes to oils.

CONCLUSIONS

When coal liquefies, there are competing reaction mechanisms of coal depolymerization to asphaltenes, repolymerization of generated radicals to char, and the formation of oils from asphaltenes. It appears that molybdenum sulfide catalyst, during temperature-staging and low severity conditions, primarily intervenes in liquefaction for subbituminous coals to provide atomic hydrogen to cap depolymerized coal fragments that form asphaltenes. This is because subbituminous coal contain a relatively high crosslink density compared to higher ranks of coals, and the catalyst remains very busy generating asphaltenes. For bituminous coals, conversions without catalyst tend to be relatively high, so molybdenum catalyst primarily intervenes to provide atomic hydrogen to help crack asphaltenes to oils. Because the crosslink density in bituminous coal is lower than in subbituminous coal, the catalyst is not as involved in capping radicals and can be effective as a hydrogenation vehicle to generate oils. Repolymerization is reduced as the activity in the other processes increases, therefore, less char is produced. For the coals DECS-1,6, work is still in progress to include temperature-staging and to evaluate various methods of dispersing catalyst. These results will be reported at future meetings. Since the sample set is coals is quite small, similar experiments on a larger set of coals would provide more insight into the role rank plays with molybdenum catalyst and low severity coal liquefaction.

ACKNOWLEDGEMENTS

Various portions of this work have been supported by the U.S. Department of Energy, The Pennsylvania Research Corporation, and The Pennsylvania State University Mining and Mineral Resources Research Institute. The authors are pleased to acknowledge this support.

REFERENCES

1. Donath, E.E and Hoering, M. *Fuel Proc. Tech.*, **1**, (1), 3, 1977.
2. Weller, S. and Pelipetz, M.G. *Ind. Eng. Chem.*, **43**, (5), 1243, 1951.
3. Garg, D. and Givens, E. *Preprints, Amer. Chem. Soc., Div. Fuel Chem*, **28**, (5), 200, 1983.
4. Epstein, M.J. M.S. Thesis, The Pennsylvania State University, 1987.
5. Derbyshire, F.J., Davis, A., Lin, R., Stansberry, P.G., and Terrer, M-T. *Fuel Proc. Tech.*, **12**, (7), 127, 1986.
6. Garcia, A.B. and Schobert, H.H. *Fuel*, **68**, 1613, 1989.
7. Burgess, C.E. and Schobert, H.H. *Preprints, Amer. Chem. Soc., Div. Fuel Chem*, **35**, (1), 31, 1990.
8. Davis, A., Schobert, H.H., Mitchell, G.D., and Artok, L. "Catalyst Dispersion and Activity Under Conditions of Temperature-Staged Liquefaction", DOE-PC-89877-1,2,3, Progress Reports, 1989-1990.
9. Burgess, C.E. and Schobert, H.H. *Fuel* (Special Edition from Coal Structure and Reactivity Conference Sept. 1990). Accepted for publication Nov 1990.
10. Hirsch, P.B. *Proc. Roy. Soc., (London)*, **A 226**, 143, 1954.
11. Stock, L.M., in *Coal Science* (Eds. M.L. Gorbaty, J.W. Larsen, and I. Wender) Academic Press, N.Y., 248, 1982.
12. Mastral, A.M. and Rubio, B. *Fuel*, **68**, 80, 1989.
13. Calkins, W.H. *Energy and Fuels*, **1**, 59, 1987.

Table 1: Liquefaction Conversion Data Comparing the Use of Molybdenum Catalyst to Using No Catalyst - Data from Weller and Pelipetz [7]

Authors	Weller and Pelipetz [7]		
Coal	Rock Springs - Sub B - C-73.9, H-5.0, N-1.5, S-0.8, O-13.6		
Conditions	450°C, 1 hr, 1000 psi H_2		
Conversion		**No Catalyst**	**AHM[c]**
Tot Conv (Benzene Insolubles)[a]		33.7	92.7
Oils (Hexane Solubles)		10.4	41.1
Asphaltenes (Benzene Sol/Hexane Insol)		2.8	27.2
O/A[b]		3.71	1.51

a) Total conversion.
b) Oil to asphaltene ratio.
c) Catalyst is ammonium heptamolybdate.

Table 2: Liquefaction Conversion Data Comparing the Use of Molybdenum Catalyst to Using No Catalyst - Data from Garg and Givens [8]

Authors	Garg and Givens [8]		
Coal	Kentucky Elkhorn #2 -hvCb C-77.8 H-5.2, N-1.8, S-1.1, O-7.2		
Conditions	825°F, 35 min, 2000 psig, H_2 18.9 MCF/T		
Conversion		**No Catalyst**	**AHM[c]**
Tot Conv (THF Insolubles)[a]		85.3	86.8
Oils (Hexane Solubles)		12.2	21.7
Asphaltenes (THF Sol/Hexane Insol)		65.4	57.9
O/A[b]		0.187	0.375

a) Total conversion.
b) Oil to asphaltene ratio.
c) Catalyst is ammonium heptamolybdate.

Table 3: Liquefaction Conversion Data Comparing the Use of Molybdenum Catalyst to Using No Catalyst - Epstein [2]

Author	Epstein [2]			
Coals	PSOC 1266-dmmf- hvAb - C-83.2, H-5.0, N-2.1, S-0.5, O-8.6			
	PSOC 1401-dmmf-Sub B - C-74.3 H-5.2, N-1.1, S-0.2, O-19.3			
Conditions	425°C, 10 min, 1000 psi H_2			
Coal	**PSOC 1266**		**PSOC 1401**	
Conversion	**No Cat[d]**	**SAM[e]**	**No Cat**	**SAM**
Tot Conv (THF Insol)[a]	58.1	72.6	42.5	66.7
Oils (Hex Sol)	13.7	4.8	28.8	17.6
Asph (THF. Sol/Hexane Insol)[b]	42.8	66.7	4.7	41.8
Gas	1.6	1.1	9.0	7.3
O/A [c]	0.32	0.07	6.1	0.42

a) Total conversion.
b) Asphaltenes.
c) Oil to asphaltene ratio.
d) No catalyst.
e) Catalyst is sulfided ammonium molybdate.

Table 4: Liquefaction Conversion Data Comparing the Use of Molybdenum Catalyst to Using No Catalyst - Epstein [2]

Author	Epstein [2]			
Coals	PSOC 1266-dmmf- hvAb - C-83.2, H-5.0, N-2.1, S-0.5, O-8.6			
	PSOC 1401-dmmf-Sub B - C-74.3 H-5.2, N-1.1, S-0.2, O-19.3			
Conditions	350°C, 1 h/425°C, 10 min, 1000 psi H_2			
Coal	**PSOC 1266**		**PSOC 1401**	
Conversion	**No Cat[d]**	**SAM[e]**	**No Cat**	**SAM**
Tot Conv (THF Insol)[a]	59.0	77.3	41.9	90.7
Oils (Hex Sol)	10.2	48.8	14.5 [g]	28.2 [g]
Asph (THF. Sol/Hexane Insol)[b]	47.3	36.8	9.9	46.7
Gas[f]	2.5	2.4	17.5	15.8
O/A [c]	0.22	1.33	1.46	0.60

a) Total conversion.
b) Asphaltenes.
c) Oil to asphaltene ratio.
d) No catalyst.
e) Catalyst is sulfided ammonium molybdate.
f) Gas a total of both stages.
g) Corrected data.

Table 5: Liquefaction Conversion Data Comparing the Use of Molybdenum Catalyst to Using No Catalyst - Burgess and Schobert [5,9]

Author	Burgess and Schobert [5,9]		
Coals	PSOC 1488-dmmf-Sub B - C-76.6, H-5.2, N-1.0, S-0.5, O-17.2		
Conditions	425°C, 10 min, 1000 psi H_2		
Coal	**PSOC 1488**		
Conversion	**No Cat[d]**	**SAM[e]**	**STM[f]**
Tot Conv (THF Insol)[a]	25.4	65.7	42.7
Oils (Hex Sol)	12.0	13.1	14.6
Asph (THF. Sol/Hexane Insol)[b]	9.6	45.8	20.0
Gas	3.9	6.8	8.1
O/A [c]	1.25	0.29	0.73

a) Total conversion.
b) Asphaltenes.
c) Oil to asphaltene ratio.
d) No catalyst.
e) Catalyst is sulfided ammonium molybdate.
f) Catalyst is sulfided tetrahydroquinolinium molybdate.

Table 6: Liquefaction Conversion Data Comparing the Use of Molybdenum Catalyst to Using No Catalyst - Burgess and Schobert [5,9]

Author	Burgess and Schobert [5,9]		
Coals	PSOC 1488-dmmf-Sub B - C-76.6, H-5.2, N-1.0, S-0.5, O-17.2		
Conditions	350°C, 1h/425°C, 10 min, 1000 psi H_2		
Coal	**PSOC 1488**		
Conversion	**No Cat[d]**	**SAM[e]**	**STM[f]**
Tot Conv (THF Insol)[a]	30.8	78.5	80.1
Oils (Hex Sol)	11.7	16.2	25.2
Asph (THF. Sol/Hexane Insol)[b]	13.9	57.7	49.5
Gas	5.2	5.5	5.5
O/A [c]	0.84	0.28	0.52

a) Total conversion.
b) Asphaltenes.
c) Oil to asphaltene ratio.
d) No catalyst.
e) Catalyst is sulfided ammonium molybdate.
f) Catalyst is sulfided tetrahydroquinolinium molybdate.

Table 7: Liquefaction Conversion Data Comparing the Use of Molybdenum Catalyst to Using No Catalyst - Burgess and Schobert [5,9]

Author	Burgess and Schobert [5,9]		
Coals	PSOC 1488-dmmf-Sub B - C-76.6, H-5.2, N-1.0, S-0.5, O-17.2		
Conditions	350°C, 1h 1000 psi H_2		
Coal	**PSOC 1488**		
Conversion	**No Cat[d]**	**SAM[e]**	**STM[f]**
Tot Conv (THF Insol)[a]	18.3	47.8	48.5
Oils (Hex Sol)	6.8	10.2	11.1
Asph (THF. Sol/Hexane Insol)[b]	7.1	33.9	33.8
Gas	4.4	3.8	3.6
O/A [c]	0.96	0.30	0.33

a) Total conversion.
b) Asphaltenes.
c) Oil to asphaltene ratio.
d) No catalyst.
e) Catalyst is sulfided ammonium molybdate.
f) Catalyst is sulfided tetrahydroquinolinium molybdate.

Table 8: Liquefaction Conversion Data Comparing the Use of Molybdenum Catalyst to Using No Catalyst - Data from Davis et al. [6]

Authors	Davis, Schobert, Mitchell, and Artok [6]			
Coals	DECS 1-dmmf - Sub C - C-76.1, H-5.5, N-1.5, S-1.1, O-15.8			
	DECS 6 -dmmf - hvB b - C-80.8, H-6.1, N-1.6, S-0.5, O-11.0			
Conditions	275°C, 30 min, 1000 psi H_2			
Coal	**DECS - 1**		**DECS - 6**	
Conversion	**No Cat[e]**	**ATM[f]**	**No Cat**	**ATM**
Tot Conv (THF Insol)[a]	6.6	9.0	17.7	25.0
Oils (Hex Sol) + Gas	1.6	1.5	4.9	6.9
Asph (Tol. Sol/Hexane Insol)[b]	2.2	3.6	2.1	3.0
Preasph.(THF Insol/Tol. Sol)[c]	2.8	3.9	10.7	15.1
O/A (where A=Asph+Preasph)[d]	0.32	0.2	0.38	0.38

a) Total conversion.
b) Asphaltenes.
c) Preasphaltenes.
d) Oil to asphaltene ratio.
e) No catalyst.
f) Catalyst is ammonium tetrathiomolybdate.

CHARACTERIZATION OF MARTIN LAKE LIGNITE AND ITS RESIDUES AFTER LIQUEFACTION

S. M. Fatemi-Badi, A. J. Swanson, N. K. Sethi and R. T. Roginski

Amoco Corporation and Amoco Oil Company
Amoco Research Center, P. O. Box 3011, Naperville, Illinois 60566

Keywords: coal liquefaction, coal/residue characterization, coal conversion

ABSTRACT

Martin Lake, Texas lignite typically gives 90-93% conversion in two-stage thermal/catalytic (T/C) liquefaction and 85-90% conversion in two-stage catalytic/catalytic liquefaction (C/C), as demonstrated at Amoco and at the Advanced Coal Liquefaction Facility in Wilsonville, Alabama. To identify the chemical and physical phenomena that underlie this low conversion, Martin Lake lignite and two of its residues, from C/C runs at Amoco, were analyzed by several analytical methods.

The atomic H/C ratio in the solids went through a minimum from 0.86, to 0.78, to 0.90 as conversion increased from 0%, to 64%, and 89%, respectively. Oxygen (wt.%, dry) was lowest in the high-conversion residue, giving 21.2%, 14.3%, and 11.4% at 0%, 64%, and 89% conversion, respectively. X-ray photoelectron spectroscopy (XPS) showed a similar trend of more carbon-oxygen bonds on the surface of unconverted lignite particles. XPS also showed surface enrichment of Ca and Mg with increase in conversion, whereas bulk Ca and Mg remained a constant fraction of the mineral matter. Carbonyl, aliphatic, and aromatic phenol/ether carbons were converted more rapidly than protonated aromatic, substituted aromatic, or bridgehead aromatic carbons, as shown by ^{13}C NMR. Volatile matter remained quite high, 26% (dry), in the high-conversion residue. Petrographic analysis showed a decrease in vitrinites, near-depletion of liptinites, and a sharp increase in the ratio of fusinite to semi-fusinite as conversion increased.

Overall, Martin Lake lignite showed a decrease in the most reactive components as conversion increased, which may explain why conversion slows down at 85-90%. The remaining residue is not totally unreactive, however, suggesting that higher conversion may be possible with the proper process or pretreatment.

INTRODUCTION

Work at Amoco and at the direct coal liquefaction pilot plant facility, operated by the Southern Company Services for the U.S. Department of Energy in Wilsonville, Alabama, has shown that typical conversion for Martin Lake, Texas lignite is in the range of 90-93% for two-stage liquefaction when the first stage reactor is opearated at about 825 °F. However, when supported hydrogention catalyst is used in the first stage, temperatures are kept below 810 °F to preserve catalyst activity. In these cases, coal conversion is only 85-90%. To identify the chemical and physical phenomena that underlie this low conversion, Martin Lake lignite and two of its residues, from runs at Amoco, were characterized using several analytical methods. Our main objective was to investigate the chemical and physical differences between the unreacted, unconverted Martin Lake lignite and converted residue samples after liquefaction. The specific objectives of this work were to find some reasonable answers to the questions of "what are the chemical functionalities involved in the liquefaction of low rank coals" and "why does conversion of low rank coals stop at 85-90% during catalytic/catalytic (C/C) liquefaction."

Three samples were used in this investigation, an unconverted Martin Lake lignite (0% conversion), a residue product from the low conversion process (64% conversion) and a residue product from the high conversion process (89% conversion). The samples were analyzed for elemental analysis (C, H, N, S, and O), proximate analysis (moisture, ash, volatile matter and fixed carbon), bulk

metals by Inductively Coupled Plasma (ICP) spectroscopy, surface minerals by X-ray Photoelectron Spectroscopy (XPS), Scanning Electron Microscopy (SEM), solid state ^{13}C NMR, and IR spectroscopy. Petrographic analysis was also performed.

EXPERIMENTAL

The two Martin Lake lignite residues were obtained from Amoco's AU-51L pilot plant and were the products of the two stage catalytic/catalytic (C/C) liquefaction process with Amocat-1C™ catalyst. Stage 1 and stage 2 process temperatures for low conversion residue were 100 and 740 °F and for the high conversion residue were 790 and 740 °F, respectively. Both residues and unconverted Martin Lake Lignite samples were washed with 40 volumes of THF prior to the analytical work.

The organic carbon, hydrogen and nitrogen content of the samples were measured by a Leco CHN-600 elemental analyzer. Total sulfur and oxygen content of the samples were determined using a Leco SC-132 sulfur analyzer and a Leco RO-478 oxygen determinator, respectively. The values for moisture, ash, volatile matter and fixed carbon of the samples were determined using a Perkin Elmer TGA 7 thermogravimetric analyzer.

The NMR data were obtained on a Chemagnetic M100 solid state NMR spectrometer operating at ^{13}C resonance frequency of 25.15 MHz. Cross-Polarization/Magic Angle Spinning (CP/MAS) technique was used to obtain solid state ^{13}C NMR spectrum. Based upon our previous studies of similar systems, cross-polarization contact time of 1 msec with 1 sec recycle delay were chosen as the best experimental parameters to obtain a quantitative ^{13}C spectrum. Dipolar Dephasing/Magic Angle Spinning (DD/MAS) technique was used to provide quantitative differentiation between quaternary and tertiary aromatic carbons. For the DD/MAS technique a period of 40 μsec was inserted between the end of the cross-polarization sequence and the beginning of the data acquisition, during which the high power proton decoupling field was turned off. In order to avoid linear phase distortions in the spectrum, rotational synchronized spin-echo procedure was used for both CP/MAS and DD/MAS techniques.

Diffused reflectance technique was used to obtain the IR data. Samples for diffuse reflectance infrared spectra were prepared by weighing 0.020 g sample and 0.980 g of KBr into a metal vial and shaking them for one minute on a Wig-L-Bug apparatus. The samples were transferred to the sample holder of a Harrick "Praying Mantis" diffuse reflectance apparatus. Spectra were obtained at 8 cm^{-1} resolution on a Mattson Cygnus 100 spectrometer using an MCT-A detector. A total of 1000 scans were co-added to obtain the final spectra.

A Perkin Elmer model 5400 Small Spot X-ray Photoelectron Spectrometer was used for XPS data collection. The data were obtained using an unmonochromatized radiation source from Mg K_α at 1253.6 ev on about 600 μm analysis area. The samples were pressed into pellets before analysis. The SEM data were obtained on a JEOL 840 A Scanning Electron Microscope equipped with a secondary and a Back Scatter Electron (BSE) detector. In addition, a TRACOR NORTHERN 5500 Energy Dispersive X-ray (EDX) system was used to obtain elemental composition of elements with atomic number of 11 or greater. The samples were prepared for SEM analysis by sprinkling them onto a sticky covered SEM stub and then coating them with AU/Pd (60/40) in vacuum evaporator. To expose cross sectional areas of the particles for detailed analysis, the samples were also embedded in a crystal bond compound and then grounded and polished before examination. SEM micrographs were obtained at 100, 500, and 5000 magnification. For microscopic examination of petrographic constituents, the samples were pelletized and polished according to the ASTM D 2797 procedure. The microscopic examinations were carried out at a magnification of 500 diameters, under oil immersion in reflected light illumination.

RESULTS AND DISCUSSION

Process conditions, percent conversion and product quality of Martin Lake lignite after liquefaction are shown in Table 1. Increasing the temperature of the first stage of the process from 100 to 740 °F, the lignite conversion (wt.%) was increased by more than 39% (from 64 to 89%). Most of this increase was in the lighter products such as C1-C3 and C4-360 °F distillate, which increased by 250%, and 360-640 °F distillate, which increased by more than 59%. The amount of product in the 650-975 °F range did not change significantly, and resid (975+ °F) was nearly eliminated.

Proximate analysis (wt.%, dry) and elemental analyses (wt.%, dry-ash-free) of the Martin Lake lignite and its two residues are shown in Table 2. As conversion of the lignite increased, a significant increase was observed in the ash content. This was followed by substantial decreases in the volatile matter (VM) and fixed carbon. Although oxygen content, determined by direct analysis, did not show a significant decrease with increasing lignite conversion, a considerable decrease was observed in the oxygen content calculated by difference, Table 2. The high values for direct oxygen of the residues reported here are believed to be distorted by the oxygen from the water present as moisture in these samples. In any case, the elemental oxygen data suggests a reduction in the oxygenated components during the process. As expected, the atomic H/C ratio was lower for the residue from the 64% converted sample (0.78) compared to the unconverted lignite (0.86). The atomic H/C ratio of the residue from the 89% converted sample, however, did not follow the same trend and increased (0.90). Although it is difficult to explain the increase in atomic H/C ratio, one explanation could be that some solvent is trapped in the residue from high conversion.

Solid state ^{13}C NMR data are shown in Table 3. The structural parameters, assuming 100 carbons per cluster, were derived by using combined CP/MAS and DD/MAS data following the method of Solum et. al[1]. In this procedure, linear integration over selected chemical shift ranges of the CP/MAS spectrum provides the relative concentration of different carbon types. Magic angle spinning generates high and low field spinning sidebands from SP^2 carbons. Sideband intensity is appropriately distributed for all SP^2 carbon types. The use of DD/MAS technique permits quantitative differentiation of protonated and bridgehead aromatic carbons. In the 40 µsec time period, for which the proton decoupling field is turned off, all the signal from protonated aromatic carbons is lost while quaternary aromatics lose only about 10% of their signal.[2] Thus, from the difference in aromatic band intensity between CP/MAS and DD/MAS spectra and accounting for 10% loss in intensity of quaternary carbons, relative concentration of protonated aromatic is calculated. Finally, simple mass balance provides the relative concentration of bridgehead aromatic carbons.

In general, solid state ^{13}C NMR data, in Table 3, indicate that as the lignite conversion increased, the carbon aromaticity increased and the carboxyl groups decreased. The size of condensed aromatic clusters is directly related to the ratio of bridgehead aromatic to ring aromatic carbons, i.e., the fraction of aromatic carbons in the bridgehead position.[1, 3] As an example, for the original lignite (0% conversion), the ratio of bridgehead carbons (12.7) to total ring carbons (54.9) is 0.23, which corresponds to an aromatic cluster slightly bigger than naphthalene. The same ratios for 64% and 89% conversion residues are 0.25 and 0.27, respectively, which corresponds to an aromatic cluster slightly smaller than anthracene. NMR data also indicated an increase in total SP^2 carbons, aromatic carbons, protonated and bridgehead carbons with increasing conversion. Although the data did not show any significant changes in substituted aromatic carbons with increasing conversion, there was a significant decrease in oxygenated functional groups. This clearly suggests that decarboxylation and reduction of phenols/ethers had taken place in the liquefaction process. It should be mentioned that the decrease in oxygenated functional groups was also seen in the data obtained from elemental analysis, IR and XPS spectroscopies.

The carbonyl and C-H stretch regions were analyzed using diffused reflectance IR spectroscopy. IR spectra for the original lignite (0% conversion) and the low conversion (64%) residue are shown in Figure 1. The specific band assignments are based on spectral information compiled by Painter

et al.[4-7] A comparison of spectra clearly shows that, while there is very little change in the C-H stretch region with treatment, there is clearly a loss in intensity for the bands in the 1740-1690 cm^{-1} region corresponding to oxygen-containing functional groups. Second derivative analysis of the spectra also indicates an intensity loss in the 1650-1560 cm^{-1} region, this loss is not obvious from the untreated spectra. While the bands near 1740 cm^{-1} and 1720-1690 cm^{-1} region may be attributed to an ester, ketone, aldehyde or carboxyl functional group, the bands in the 1650-1630 and ~1600 cm^{-1} are due to the highly conjugated C=O and highly conjugated hydrogen bonded C=O. The band at ~1600 cm^{-1} could also be attributed to aromatic ring breathing. The band in the 1590-1560 cm^{-1} is due to the carboxyl group in salt form (COO^-). Figure 2 compares the spectra for the original lignite (0% conversion) and the high conversion (89%) residue. In this case, a change in intensity of the C-H stretch band was seen. Of particular note are the relative decreases in intensity of the aliphatic CH_3 asymmetric stretch near 2960 cm^{-1} and aliphatic CH_2 and CH_3 symmetric stretch near 2850 cm^{-1}; and the increases in the intensity of aliphatic CH_2 and CH_3 asymmetric stretch near 2925 cm^{-1} and aromatic C-H stretch in the region of 3100-2990 cm^{-1}. Here again, the loss in the intensity of the bands corresponding to the loss of oxygen-containing functional groups can also be observed.

Surface composition (wt.%, relative) obtained by XPS and bulk metal composition obtained by ICP analyses are shown in Tables 4 and 5, respectively. The bulk analysis of the samples by ICP indicated that the major elements in the samples were Si, Fe, Al, Ca, Mg, Na, K and Ti. As was expected, the concentration of these elements increased as the lignite conversion increased. Two important pieces of information were obtained from XPS surface analysis. First, while the relative surface concentration (wt.%) for most of the elements (C, Si, Al, S, N, and Fe) did not change with increasing lignite conversion, the relative surface concentration of two elements (Ca and Mg) increased significantly with increasing conversion. There is some evidence in the literature that cations like Na^+, K^+ and Ca^{++} are inhibitors in coal pyrolysis[8, 9], but are promoter catalysts in coal steam gasification[10, 11]. Therefore, in coal liquefaction, it is possible that the increase in Ca and Mg at the surface of the reacting lignite particles slows down significantly, or stops, conversion at 85-90%. Second, the electron binding energies obtained from XPS show significant loss of oxygen-containing functional groups during the liquefaction process supporting the data from NMR and IR spectroscopy. Therfore, as the lignite conversion approaches 90%, the remaining residue is a highly aromatic material, hence the conversion slows down considerably.

Maceral compositions obtained from petrographic analysis are shown in Table 6. The data are presented on a mineral-matter-free basis to allow the comparison between the maceral groups vitrinite, inertinite and liptinite. The inertinite maceral group can be subdivided into fusinite, semifusinite, micrinite, macrinite and sclerotinite and the liptinite maceral group can be subdivided into sporinite, resinite and cutinite. Vitrinites and liptinites are considered to be the potentially most reactive macerals. Inertinites, on the other hand, are considered to be unreactive macerals with the exception of semifusinite which may be partially reactive. As expected, the vitrinite macerals (wt.%, mmf) decreased from 58.2 to 51.4 and then to 41.2 as the lignite conversion increased from 0% to 64% and to 89%, respectively. Liptinite macerals also showed the same trend, dropping from 10.0 for the original lignite to 3.5 for the 64% conversion residue and almost to zero (0.4%) for the high conversion residue. Decreases in vitrinite and liptinite macerals were offset by increases in inertinites. However, for the high conversion (89%) residue the relative increase in fusinite was much higher than the increase in semifusinite. This could mean that some of the semifusinite had reacted at high conversion conditions. Petrographic analysis indicated a significant increase in the mineral matter (13.9, 26.4, 52.4%) with increasing lignite conversion. This was expected, due to the disappearance of the reactive macerals with increasing conversion.

SEM also showed changes in morphology of the samples with increasing conversion. The sample from high conversion (85%) is composed of smaller and more porous particles than unconverted

or low conversion (64%) samples. Also, the unconverted and low conversion samples consisted of large organic particles decorated with mineral particles. Large organic particles are not seen in the high conversion sample; mineral and organic phases are intimately mixed.

SUMMARY AND CONCLUSIONS

The NMR data clearly suggests that the main structural transformations during liquefaction of Martin Lake lignite are aliphatic sidechain cracking, decarboxylation, and deoxygenation. Some of the NMR data from Table 3 are shown graphically in Figure 3 to suggest answers for the two questions asked earlier; "what are the chemical functionalities involved in the liquefaction of low rank coals" and "why does conversion of low rank coals stop at 85-90% during catalytic/catalytic (C/C) liquefaction." As the lignite conversion approaches 90%, aliphatic and carbonyl functional groups are depleted. The remaining residue is a highly aromatic material, therefore, the conversion slows down considerably. IR data confirmed the increase in aromatic C-H groups and decrease in aliphatic C-H functional groups. IR also indicated a significant loss of reactive carbonyl functional groups, which may cause slow conversion. Data from XPS analysis indicated that the relative surface concentration of two elements (Ca and Mg) increased significantly with increasing conversion, which could also decrease the reaction rate, and hence, reduce the conversion. The electron binding energies from XPS also showed a decrease in C-O and C=O functional groups during the liquefaction process. Petrographic analysis showed a significant decrease in the reactive macerals (vitrinites and liptinites), sharp increase in the unreactive macerals (inertinites) and partial conversion of semifusinite as conversion increased.

Overall, Martin Lake lignite showed a decrease in the most reactive components as conversion increased, which may explain why conversion slows down at 85-90%. The remaining residue is not totally unreactive, however, suggesting that higher conversion may be possible with the proper process or pretreatment.

REFERENCES

1. Solum. M. S., Pugmire, R. J., and Grant, D. M., Energy and Fuels, 3, 1989, 187.
2. Alemany, L. B., Grant, D. M., Pugmire, R. J., Alger, T. D., and Zilm, K. W., J. Am. Chem. Soc., 105, 1983, 2142.
3. Sethi, N. K., Facelli, J. C., Pugmire, R. J., and Grant, D. M., Analytical Chemistry, 60, 1988, 1574.
4. Painter, P. C., Coleman, M. M., Jenkins, R. G., and Walker, P. L., Jr., Fuel, 57, 1978, 125.
5. Painter, P. C., Coleman, M. M., Jenkins, R. G., Whang, P. W., and Walker, P. L., Jr., Fuel, 57, 1978, 337.
6. Painter, P. C., Snyder, R. W., Starsinic, M., Coleman, M. M., Kuehn, D. W., and Davis, A., Applied Spectroscopy, 35, 1981, 475.
7. Painter, P. C., Starsinic, M., and Coleman, M. M., "Determination of Functional Group in Coal by Fourier Transform Interferometry" in Fourier Transform Infrared Spectroscopy, Ferraro, J. R. andBasile, L. J., eds, vol. 4, 1985, Academic Press, N. Y.
8. Tyler, R. J., Fuel, 58, 1979, 680.
9. Tyler, R. J., and Schafer H. N., Fuel, 59, 1980, 487.
10. Hengel, T. D., and Walker, P. L., Jr., Fuel, 63, 1984, 1214.
11. Linares-Solano, A., Hippo, E. J., and Walker, P. L., Jr., Fuel, 65, 1986, 776.

ACKNOWLEDGEMENTS

The authors would like to thank Dr. K. Kuehn of Western Kentucky University for the petrographic analysis and interpretation of the petrographic data. We also would like to thank J. Schreiner and P. Hruskoci of Analytical Research and Services at Amoco Corporation for the XPS and SEM analyses. We are grateful to R. Lumpkin and J. Joseph for their helpful comments in reviewing this work. The contribution of D. Maciejewski and E. Hauber to this work are also greatly appreciated.

Table 1.

Process Conditions and Product Quality Data for Martin Lake Lignite

Conditions and Products	Lignite Conversion 0	64	89
Stage 1 Temperature, °F	Unreacted	100	790
Stage 2 Temperature, °F	Lignite	740	740
C1-C3, wt.%		3.4	10.1
C4-360 °F, wt.,%		3.9	13.7
360-650 °F, wt.%		24.4	38.8
650-975 °F, wt,%		8.8	9.5
975+ °F, wt.%		9.8	1.0
H_2 Consumption, wt.%		7.8	8.6

Table 2.

Proximate and Elemental Analyses Data Obtained for Martin Lake Lignite and the Converted Residues

	Lignite Conversion 0	64	89
Proximate Analysis (wt.%, dry)			
Moisture[a]	2.35	3.59	1.52
Ash	13.35	25.93	43.57
Volatile Matter	42.89	32.57	26.13
Fixed Carbon	43.76	41.50	30.30
Elemental Analysis (wt.%, dry-ash-free)			
Carbon	70.90	76.55	76.12
Hydrogen	5.11	5.03	5.76
Nitrogen	1.22	1.62	1.46
Sulfur	1.60	2.52	5.22
Oxygen (by difference)	21.17	14.28	11.44
Oxygen (direct)	21.76	18.20	17.98
H/C (atomic ratio)	0.86	0.78	0.90

[a]Moisture values are on as-recieved basis.

Table 3.

Solid State ^{13}C NMR Data for Martin Lake Lignite and the Converted Residues

Structural Parameters	Lignite Conversion 0	64	89
Carbon Types (total = 100)			
Total SP^2	64.1	73.3	80.3
-- Carbonyl	9.0	6.0	6.0
-- Ring Aromatic	54.9	66.7	73.8
* Phenolic/Ethers	9.7	9.4	8.9
* Protonated	19.8	25.9	29.1
* Substituted	12.8	14.9	15.9
* Bridgehead	12.7	16.6	19.9
Total SP^3	35.9	26.7	19.7
# Bridgehead / # Rings	0.23	0.25	0.27
# Carbons / Cluster	10	11	12

Table 4.

Surface Composition (wt.%, Relative) Data from XPS Analysis of Martin Lake Lignite and the Converted Residues

Lignite Conversion	O	C	Si	Al	S	N	Fe	Ca	Mg
0	30.4	52.0	8.1	5.6	0.4	0.9	1.0	0.7	0.9
64	24.0	57.1	8.2	4.7	0.1	1.2	0.8	1.9	1.7
89	24.7	55.8	7.3	5.2	0.4	1.0	1.0	2.5	1.8

Table 5.

Metal Composition (Wt.%) Data from ICP Analysis of Martin Lake Lignite and the Converted Residues

Lignite Conversion	Mg	Ca	Al	Si	Fe	Na	K	Ti	Sr
0	0.26	1.08	1.16	2.91	1.23	0.07	0.06	0.08	0.03
64	0.51	2.34	2.43	5.40	2.70	0.13	0.11	0.15	0.07
89	0.71	3.80	3.81	7.60	4.70	0.19	0.18	0.22	0.10

Table 6.

Maceral Composition Obtained from Petrographic Analysis of Martin Lake Lignite and the Converted Residues

Macerals (wt.%, mineral-matter-free)	Lignite Conversion 0	64	89
Vitrinites	58.2	51.4	41.2
Inertinites	29.2	44.3	58.4
* Fusinite	2.3	3.8	16.7
* Semifusinite	22.7	36.4	32.8
* Micrinite	2.6	3.3	7.6
* Macrinite	1.4	0.8	1.3
* Sclerotinite	0.2	0.0	0.0
Liptinite	12.6	4.3	0.4
* Sporinite	10.0	3.5	0.4
* Resinite	2.1	0.8	0.0
* Cutinite	0.5	0.0	0.0

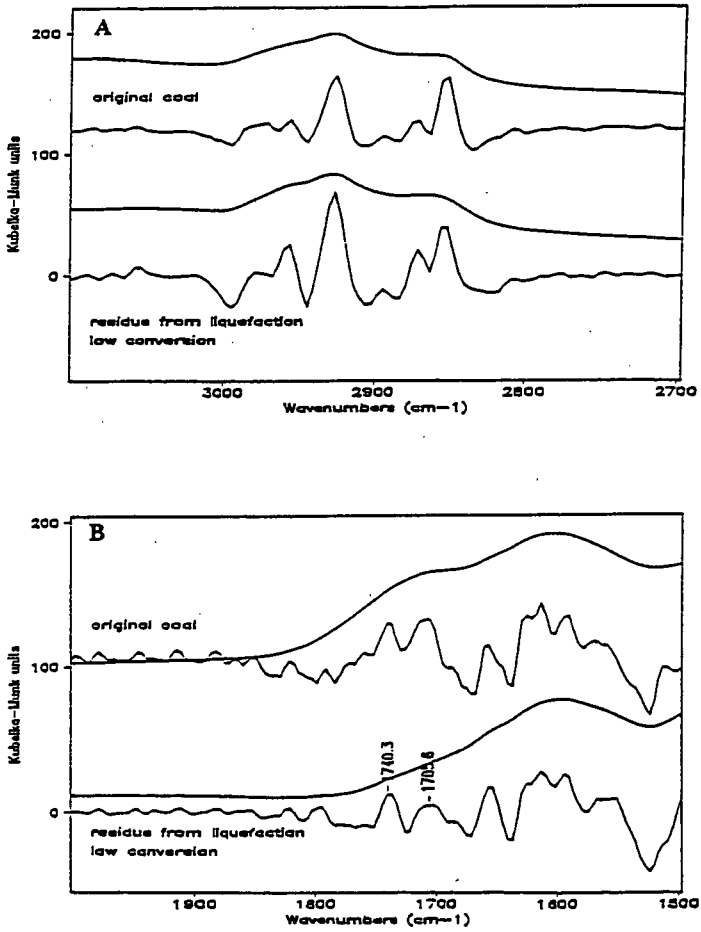

Figure 1. Infrared Spectrum for Martin Lake Lignite Coal and Low Conversion Residue. A) C-H Stretch; B) C=O Stretch.

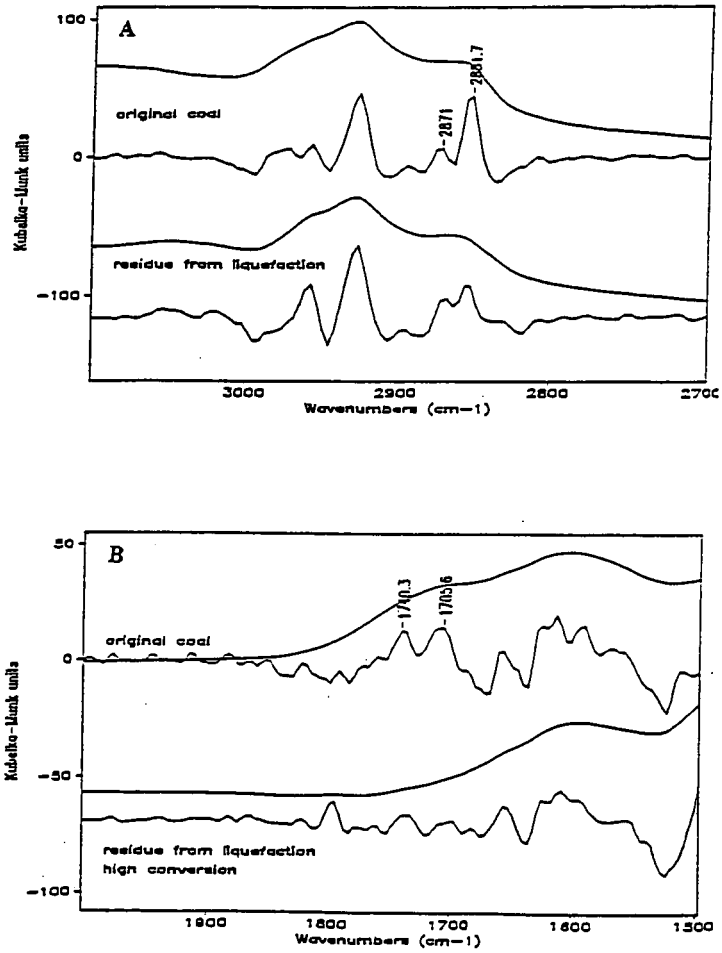

Figure 2. Infrared Spectrum for Martin Lake Lignite Coal and High Conversion Residue. A) C-H Stretch; B) C=O Stretch.

Figure 3. Carbon Types in Unconverted Martin Lake Lignite by C^{13} NMR

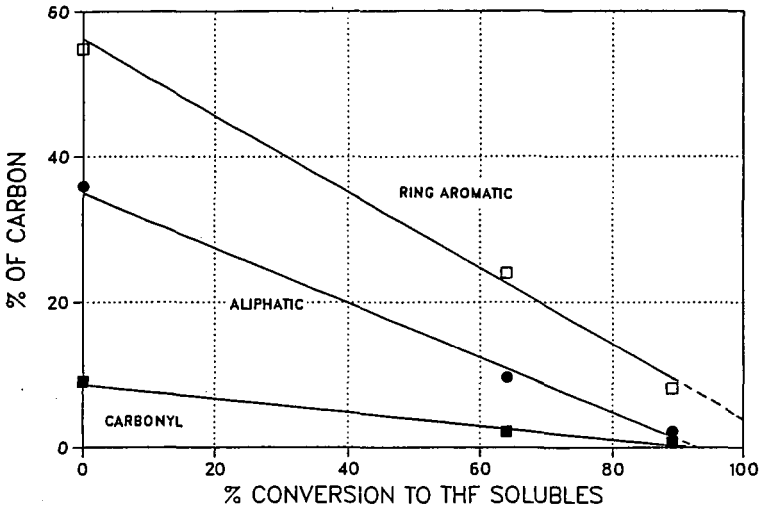

SOLUBILIZATION OF HIGH RANK POCAHONTAS NO. 3 COAL

Kuntal Chatterjee and Leon M. Stock
Chemistry Division
Argonne National Laboratory
9700 South Cass Avenue
Argonne, Illinois 60439.

INTRODUCTION

Reductive and non-reductive alkylation reactions are efficient methods of coal solubilization (**1**). C-Alkylation reactions using the strongly basic mixture of *n*-butyllithium and potassium *tert*-butoxide (called Lochmann's base) were successful for the near quantitative solubilization of Lower Kittanning coal (**2**). This contribution concerns the use of this reagent to promote C-alkylation of a high rank coal, Pocahontas No. 3, from the Premium Sample Program of Argonne National Laboratory. Evidence will also be presented to show that, apart from promoting C-alkylation, the basic reagent can alter the coal macromolecular structure by forming smaller fragments through hydrocarbon β-elimination reactions.

EXPERIMENTAL SECTION.

Materials. Pocahontas No. 3 coal, APCSP 5, was supplied by the Premium Sample Program of the Argonne National Laboratory (Anal. C, 91.1; H, 4.4;

N, 1.3; S, 0.5; O (by difference) 2.7; ash 4.7). The coal samples were dried at 110 °C under vacuum for 48 h prior to use.

n-Heptane (Aldrich) was shaken with concentrated sulfuric acid and subsequently distilled. The purified solvent was stored in the presence of molecular sieve 5A. Pyridine was purified by distillation over barium oxide. The alkyl iodides were obtained from Aldrich and were dried over molecular sieve 5A. The other chemicals such as *n*-butyllithium (1.6 M solution in hexane), potassium *tert*-butoxide, ammonium chloride and methanol were used as received from Aldrich Chemical Company.

Reaction Procedure for the Coal Sample. The C-alkylation reactions of the coal sample were carried out as reported earlier (**2,3**). *n*-Heptane (170 mL), potassium *tert*-butoxide (5.01g, 45 mmol) and *n*-butyllithium (30 mL, 1.6 M solution in hexane, 48 mmol) were added to a flame dried flask. The mixture was stirred at room temperature for 15 min, the coal sample (1g) was added, and the solution was refluxed for 6 h. The initial black solution turned brown when refluxing began. The alkyl iodide (55 to 60 mmol) was added dropwise to this coal anion suspension, after cooling the flask at 0 °C. The mixture was stirred for 48 h at room temperature to ensure complete alkylation of the coal anions. The residual base was quenched by adding ammonium chloride and methanol. The solvents were removed by a rotary evaporator. The product was carefully collected and washed with an acidic solution of water and methanol (3:1 by volume), aqueous methanol (3:1, 20 L) and *n*-hexane (4L). The product was dried to constant weight at 110 °C under vacuum for 48 h. A portion of each of the product was subjected to Soxhlet extraction with pyridine.

In order to investigate bond cleavage reactions with bases, the coal anions were quenched with dilute acids instead of alkyl halides. The products thus obtained were washed and dried as usual and were subjected to pyridine extractions. In order to establish the optimum conditions for solubilization, the reaction conditions, the nature of base used, and the length of the alkyl group in the alkyl iodide were varied. The results are presented in the Tables.

RESULTS

The C-alkylation reaction of Pocahontas No. 3 coal (APCSP 5) with sodium amide in liquid ammonia was studied first. Previous work in our laboratory using sodium amide in liquid ammonia with another high rank coal, *Lower Kittanning* coal, PSOC 1197, gave significantly soluble alkylated products (4). As shown in Table I, the solubilty of the products increased with an increase in length of the alkyl group. With 45 mmol of the base per gram of coal, the octylated product was about 38% soluble in pyridine. It should be mentioned that the raw coal is only 5% soluble in pyridine.

The solubility of the products increased when the base concentration was increased. With 15 mmol of sodium amide, the butylated product was only 13% soluble whereas with 200 mmol of the base, the butylated product was 46% soluble.

When a stronger base was used to alkylate this coal, better results were obtained. The results of Lochmann's base promoted C-alkylations of Pocahontas No. 3 are summarized in Table II.

When the coal was treated with Lochmann's base in refluxing heptane for 6 h and quenched with methyl iodide, the product was 45% soluble in pyridine (compared to only 12% with sodium amide). However, when the coal was butylated with *n*-butyl iodide, the solubilty of the product remained at 45%. In addition, when the coal was refluxed with the base for 18 h instead of 6 h, a 10% increase in solubilty was observed. Once again both the butylated and octylated products gave the same solubility (55%).

We next probed for the occurrence of carbon - carbon bond cleavage reactions with very strong bases. The results are shown in Table III. Use of sodium amide in liquid ammonia at -75 °C, *n*-butyllithium at 98 °C, potassium *tert*-butoxide at 98 °C and Lochmann's base at 98 °C show that only Lochmann's base provides any evidence for C-C bond cleavage.

DISCUSSION

Non-reductive C-alkylation reactions of Pocahontas No. 3 coal with sodium amide in liquid ammonia convert the 5% soluble coal to a material which is 46% soluble. The increase in solubility with the increase in the size of alkyl group is in agreement with our previous results (4). The larger groups can disrupt the intermolecular polarization forces thereby enhancing solubilty. However, the fact that a higher concentration of the base enhances the solubilty to a greater extent suggested that other factors are also important.

Lochmann's base appears to be a superior reagent for the conversion of the coal into soluble materials. The extent of solubilization is

virtually independent of the size of the alkyl group, and the methylated and butylated products are equally soluble. When the coal was treated with the base for 18 rather than 6 hours, there was a modest enhancement in the solubilty of the product.

The results in Table III suggested that a prominant reason for the high solubilty of the products obtained after Lochmann's base are due to carbon - carbon bond cleavage. When the coal sample was treated with Lochmann's base in refluxing heptane and quenched with dilute acid, the solubilty of the coal increased from 5% to about 35% depending on the time of reaction. Thus base treatment alone can convert the coal to soluble materials. We infer that the strong base forms carbanions that can fragment via β-elimination as previously proposed (**1(B), 5**).

CONCLUSION

The Lochmann's base system is more effective than any other base system for the C-alkylation and solubilization of high rank Pocahontas No. 3 coal. Our results suggest that coal carbanions undergo fragmentation to reduce the molecular dimensions. The solubilty realized by these fragmentation reactions is enhanced by C-alkylation reactions.

ACKNOWLEDGEMENT

We acknowledge the support of this work from the Office of Basic Energy Sciences, Division of Chemical Sciences, U. S. Department of Energy.

REFERENCES

1. (A) Davidson, R. M. *Coal Sci.*, 1982, **1**, 84-160; (B) Stock, L. M. *Coal Sci.*, 1982, **1**, 161-282.

2. Chatterjee, K.; Miyake, M.; and Stock, L. M. *Energy & Fuels*, 1990, **4**, 242-248.

3. Chatterjee, K.; Miyake, M.; and Stock, L. M. *Prep. pap. Am. Chem. Soc., Div. Fuel Chem.*, 1990, **35(1)**, 46-50.

4. Miyake, M. and Stock, L. M. *Energy & Fuels*, 1988, **2**, 815-818.

5. Chatterjee, K., Ph.D. Dissertation, The University of Chicago, 1990.

Table I. The C-alkylation of Pocahontas No. 3 coal with sodium amide in liquid ammonia.

reaction conditions: base, solvent, temperature, time	electrophile	solubility, wt% in pyridine
raw coal	-	5
coal ; $NaNH_2$ (45 mmol / g), $NH_3(l)$, -75 °C, 6 h	CH_3I	12
coal ; $NaNH_2$ (45 mmol / g), $NH_3(l)$, -75 °C, 6 h	n-C_4H_9I	21
coal ; $NaNH_2$ (45 mmol / g), $NH_3(l)$, -75 °C, 6 h	n-$C_8H_{17}I$	38
coal ; $NaNH_2$ (15 mmol / g), $NH_3(l)$, -75 °C, 6 h	n-C_4H_9I	13
coal ; $NaNH_2$ (100 mmol / g), $NH_3(l)$, -75 °C, 6 h	n-C_4H_9I	31
coal ; $NaNH_2$ (200 mmol / g), $NH_3(l)$, -75 °C, 6 h	n-C_4H_9I	46

Table II. The C-alkylation of Pocahontas No. 3 coal with Lochmann's base.

reaction conditions: base, solvent, temperature, time	electrophile	solubility, wt% in pyridine
raw coal	-	5
coal; *n*-BuLi + K*t*-OBu (1:1), heptane, 98 °C, 6 h	CH_3I	45
coal; *n*-BuLi + K*t*-OBu (1:1), heptane, 98 °C, 6 h	*n*-C_4H_9I	45
coal; *n*-BuLi + K*t*-OBu (1:1), heptane, 98 °C, 18 h	*n*-C_4H_9I	55
coal; *n*-BuLi + K*t*-OBu (1:1), heptane, 98 °C, 18 h	*n*-$C_8H_{17}I$	55

Table III. Base promoted solubilization reactions of Pocahontas No. 3 coal.

reaction conditions	product recovered, %	solubility, wt% in pyridine
raw coal	-	5
coal ; $NaNH_2$ (45 mmol / g), NH_3(l), -75 °C, 6 h, protonation	92	5
coal ; $NaNH_2$ (100 mmol / g), NH_3(l), -75 °C, 6 h, protonation	99	9
coal ; *n*-BuLi (45 mmol / g), heptane, 98 °C, 6 h, protonation	89	8
coal ; K*t*-OBu (45 mmol / g), heptane, 98 °C, 6 h, protonation	91	10
coal ; Lochmann's base (45 mmol / g), heptane, 98 °C, 6 h, protonation	88	32
coal; Lochmann's base (45 mmol /g) heptane, 98 °C, 18 h, protonation	105	39

COAL LIQUEFACTION WITH MODEL SOLVENTS CONTAINING HYDROPHENANTHRENS AND/OR HYDROPYRENES

Kevin Bate* and Graham Harrison

Department of Applied Sciences,
Staffordshire Polytechnic,
College Road,
Stoke-on-Trent,
ST4 2DE UK.

***now at Point of Ayr, Coal Liquefaction Project,**
Flynnongroew, Clwyd, North Wales, CH8 9JJ

Keywords: H-donors, hydrophenanthrenes, hydropyrenes.

INTRODUCTION

The importance of the quality of the solvent in coal liquefaction is well known. Model solvent studies have helped to characterise and elucidate reactions occurring during coal liquefaction, particularly coal dissolution but have been limited in that the model solvents chosen have not been very representative of actual process solvents. Tetralin, the model solvent often used, is unlikely to be present in a significant concentration in recycle solvents which tend to contain mainly three and four ring compounds. Studies using hydroaromatic compounds with three and four rings are more representative but again hardly represent the complex nature of recycle solvents. Consequently, there is a need to undertake studies using more complex model solvents, particularly to evaluate the contribution from individual hydrogen donors to coal dissolution.

EXPERIMENTAL

Samples of hydrogenated phenanthrene and hydrogenated pyrene were obtained by hydrogenating the parent aromatic compound using a CoMo catalyst under a high hydrogen overpressure at elevated temperatures. Some variation in reaction conditions did apply but typical conditions were: 200 bar H_2 at 400°C for 2h, 100g of aromatic and 5g of 3% Co/15% Mo catalyst. All hydrogenations were conducted in a spinning/falling basket autoclave with the catalyst contained in a squat wire mesh basket as described previously (1).

Coal dissolution experiments were also carried out in the spinning/falling basket autoclave. The experiments used 300g of solvent and 150 g of air dried Point of Ayr coal (supplied by CRE), mainly at 420°C with variation in run times from 1 to 6h. The proximate (mass %, air dried) and ultimate (mass%, dmmf) analyses of the coal sample were: proximate - ash 15.9, moisture 3.5 and volatites 27.8%; and ultimate - carbon 84.6, hydrogen 4.6, nitrogen 1.3, sulphur 1.3 and oxygen (by difference) 8.2%. The solvents used were denoted as follows: solvent A - hydrogenated phenanthrene; solvent B - 50 mass % hydrogenated phenanthrene plus 50 mass% phenanthrene; solvent C - 50 mass %, hydrogenated phenanthrene plus 50 mass % pyrene; solvent D - hydrogenated pyrene; and solvent E - 50 mass % hydrogenated pyrene plus 50 mass % hydrogenated phenanthrene.

After the dissolutions, undissolved material was removed by elevated pressure filtration (2 bar N_2 at 200°C) through a special unit described elsewhere(2). The filter cakes were washed with dichloromethane (DCM) to remove entrained solvent at a DCM cake ratio of 5 :1; the solvent was removed by vacuum filtration and the cake was washed with further portions of

DCM until the washings were colourless. Samples of dried washed filter cakes were analysed for their ash contents using a Leco Proximate Analyser.

The filtered coal liquid was separated by solvent fractionation into toluene-insoluble, toluene-soluble/hexane insoluble and hexane-soluble materials. The hexane-soluble materials were analysed by gc using an OV101 capillary column contained in a Perkin-Elmer Sigma 3B Chromatograph equipped with 'on-column' injection. Similar gc analysis was carried out on the starting solvents dissolved in hexane.

RESULTS AND DISCUSSION

Analysis of Solvents

The results of the quantitative gc analysis of the five model solvents are shown in table 1. The contents of the various hydroaromatics of phenanthrene and pyrene, including the separate geometric isomers as well as peaks characterised as products from cracking reactions during the hydrogenations (butyltetralin and biphenyl) have been quantified. Characterisation of the chromatograms made use of marker compounds and gc.ms information supplied by CRE. Unfortunately the peaks for the two geometric isomers of H_6Py and $H_{10}Py$ could not be attributed to the specific isomers and are referred to as H_6Py^1, H_6Py^2, $H_{10}Py^1$ and $H_{10}Py^2$

In figure 1, the chromatogram of the most complex of the solvents (solvent E) is compared with that of a batch of recycle solvent (supplied by CRE). Although there was a difference in the ramp rates for the temperature programme for the two chromatograms (5°C min^{-1} for the recycle solvent, 8°C min^{-1} for solvent E), it is apparent that many of the peaks for the recycle solvent chromatogram were in common with those for the solvent E chromatogram, showing that solvent E would be very representative of an actual process solvent.

Coal Dissolution - Comparison of Solvent Performances

The solvents were compared in a series of coal dissolution experiments conducted at 420°C for different times. The results for solvents A,B, D and E are illustrated graphically in figure 2. For solvent C only 2h duplicate experiments were conducted, giving dissolutions (calculated by ash balance and expressed on 'daf' basis) of 69.2 and 69.4%; duplicate experiments were also carried out the solvent A for the 2h run and gave identical dissolutions of 72.4%. In spite of the excellent repeatability of the results, it is considered that the value for solvent D at 2h was abnormally high.

The total hydrogen donor contents of the starting solvents were evaluated from their gas chromatograms. For the recycle solvents fractions after dissolution, it was assumed that the hexane-soluble material contained the recycle solvent only and hence their hydrogen donor contents were determined from the chromatograms of the hexane-soluble fractions see (figure 3). This assumption was reasonable since the starting solvents were soluble in hexane (>99.5%) but most of the coal fragments produced during dissolution would not be and mass balance calculation on the solubility results indicated that the proportion extracted by hexane corresponded well with the mass of solvent in the dissolution.

After one hour, solvent A (hydrophenanthrenes) dissolved 62.4% of 'daf' coal and its H-donor content was reduced from 2.3 to 1.4% i.e. by 39%. For solvent D after one hour, the H-donor content was reduced by 61% from 1.8 to 0.7% for a dissolution of 72.4%. After 4h dissolution with solvent A, dissolution increased to 72.4% but donor depletion was only 57%. Hence hydropyrenes induced a higher dissolution after 1h but used more of their H-donor content to produce the same dissolution, probably as a result of producing wasteful hydrogen gas through dehydrogentation without utilising the hydrogen for capping radicals.

Solvent E, which contained both hdrophenanthrenes and hydropyrenes, effected about the same dissolution as solvent D after 1h (71.9 vs.72.4%) but utilised less of its H-donor content (49 vs 61%). Solvent B, which only has an initial H-donor content of 1.15%, showed the lowest dissolution (57.3% after 2h) whereas solvent C with the same initial H-donor content provided a dissolution of 69.2% after 2h. Therefore the addition of pyrenes to hydrophenanthrenes induces a greater dissolution than the addition of phenanthrene, probable

because pyrene is more able to promote H-shuttling. The improved dissolution with solvent C was at the expense of a higher H-donor depletion (61 vs. 52%).

Coal Dissolution - Depletion of Individual Donors.

The variation of the contents of hydrophenanthrenes and phenanthrene with time is depicted in Figure 4 for solvents A and E Figure 5 shows similar plots for the hydropyrenes and pyrene for solvents E and D. The general trends in figure 3 are: a gradual rise on the phenanthrene content becoming linear after the first hour; a rapid fall on the H_2P and s- H_8P contents, particularly over the first hour, an initial rise in the content of H_4P (due to it being produced from the dehydrogenation of s-H_8P more rapidly than it being lost by dehydrogenation to H_2P) followed by a gradual fall; an an almost constant (solvent E) or small decrease (solvent A) in the content of a-H_8P. The initial rapid decrease in the contents of s-H_8P and H_2P corresponded with the initial increase in the phenanthrene contents and the decrease was more rapid for solvent A because of the absence of hydropyrenes which appear to have a larger contribution then hydropyrenes in the early stages of dissolution.

The general trends in figure 4 are: a rapid increase in the pyrene content over the first hour after which the pyrene content seemed to approach a constant value; a rapid decrease in the contents of H_4Py, the two H_6Py isomers and the two $H_{10}Py$ isomers; and an initial decrease in the content of H_2Py after which there was a tendency to approach a constant value, mirroring the Py content and suggesting that an equilbrium ratio of H_2Py: Py was being approached.

Table 2 shows the percentage relative depletions of the various hydrogen donors for solvent E over 1h. It can be seen that, apart from H_2Py, the hydropyrenes were depleted by similar extents and to much larger extents than the hydrophendathrenes. Therefore most of the hydropyrene contents in the recycle solvent fraction will be lost more readily than the hydrophenanthrene contents and, after the early stages of dissolution, the only hydropyrene remaining in a significant amount will by H_2Py. For the hydrophenanthrenes, the H_2P and s-H_8P contents despite being reduced quite quickly will still be in sufficient quantities to provide a supply of donor hydrogen after most of the hydropyrene content has been used. The concentration of a-H_8P was not reduced, indicating it has a higher stability towards dehydrogenation. However, its content might become important in the later stages of dissolution when its rate of dehydrogentation might be sufficiently fast to provide hydrogen for capping the radicals produced from cleavage of the more stable bonds bridging aromatic centres.

In a two-stage liquefaction process, bridging bonds surviving dissolution will be mainly catalytically cracked and stabilisation of the carbocations produces should come from the hydrogen held as hydrides at the catalyst surface not demanding any solvent H-donation. However, the second stage is often operated at higher temperatures and some thermally promoted cracking might take place in the bulk phase in which case the likely presence of the donors H_2Py and a-H_8P could become important for further radical stabilisation.

CONCLUSIONS

The rate of coal dissolution is improved by the presence of hydropyrenes but these hydroaromatic compounds utilise more of their hydrogen donor contents than do hydrophenanthrenes for the same level of dissolution. The best solvent is one containing both hydrophenanthrenes and hydropyrenes and generally the contents of these compounds in actual process recycle solvent are high. Most of the coal is dissolved in the early stages and thereafter further dissolution becomes expensive in terms of consumption of hydrogen donors i.e. most of the donors are dehydrogenating at a much faster than the production of free radicals resulting in the generation of wasteful hydrogen gas. Therefore it might be economic to sacrifice some coal dissolution in order to maintain a better solvent quality.

Certain donors will be depleted more rapidly than others and, if dissolution starts to decrease with solvent recycle, it could be that the contents of the 'faster donors' are not being properly made up during solvent rehydrogenation in the second stage rather than overhydrogenation of the solvent to saturates. Consequently it is important not only to monitor the total hydrogen donor content of the solvent but also to analyse the solvent for its content of the various

hydropyrenes and hydrophenanthrenes, a task that should be possible by gc analysis of the solvent. Based on these assessments it should be possible to control the second stage conditions to ensure the current balance between hydrogenation and hydrocracking.

References

1. Doughty, P.W., PhD Thesis, Staffordshire Polytechnic (CNAA), April 1988
2. Bate, R., PhD Thesis, Staffordshire Polytechnic (CNAA), September 1990.

Compound	Composition (mass %)				
	A	B	C	D	E
P	23.0	61.5	11.5		11.7
H_2P	2.2	1.1	1.1		1.1
H_4P	17.8	8.9	8.9		9.0
s-H_8P	27.9	14.0	14.0	2.1	14.8
a-H_8P	11.6	5.8	5.8		5.8
iso-H_8P	2.8	1.4	1.4		1.6
$H_{14}P$	3.6	1.8	1.8		2.0
Py			50.0	29.3	14.9
H_2Py				18.6	9.5
H_4Py				3.6	1.9
H_6Py^1				18.7	9.5
H_6Py^2				13.4	7.0
$H_{10}Py^1$				7.1	3.7
$H_{10}Py^2$				3.9	1.9
BT	2.8		1.4		1.3
BP	1.3		0.6		0.6
T	0.2		1.1		

Table 1. Composition of Model Solvents by G.C

P - phenanthrene, H_2P - dihydrophenanthrene, H_4P - tetrahydrophenanthrene
s - H_8P - sym - octahydrophenanthrene, a - H_8P - antisym - octahydrophenanthrene
iso-H_8P - isomerised octahydrophenanthrene, $H_{14}P$ - perhydrophenanthrene
Py-pyrene, H_2Py - dihydropyrene, H_4Py - tetrahydropyrene, H_6Py^1, H_6Py^2 - hexahydropyrene, $H_{10}Py^2$ - decahydropyrene, BT - butyltetralin, BP - biphenyl, T - tetralin.

Relative Depletion (%)

Hydrophenanthrenes				Hydropyrenes					
H_2P,	H_4P,	s - H_8P,	a - H_8P	H_2Py,	H_4Py,	H_6Py^1,	H_6Py^2,	$H_{10}Py^1$,	$H_{10}Py^2$
54.5	-3.3	50.0	0	51.6	89.5	85.3	88.7	89.2	89.5

Table 2 Percentage Relative Depletions of Individual H-donors for Solvent E Over One Hour

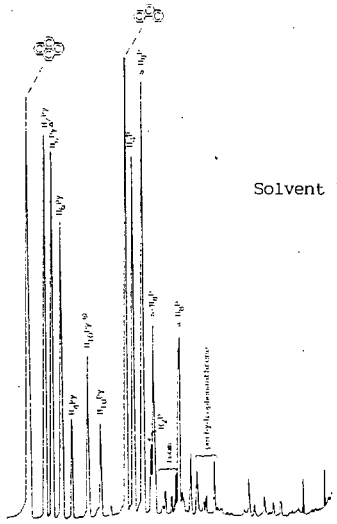

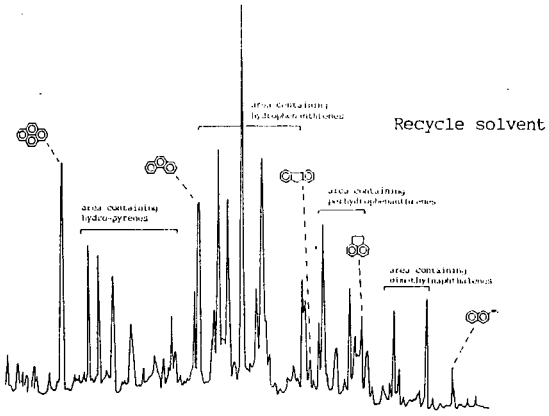

Figure 1. Gas chromatogram for solvent E (ramp rate 8°C min^{-1}) and a recycle solvent (ramp rate 5°C min^{-1})

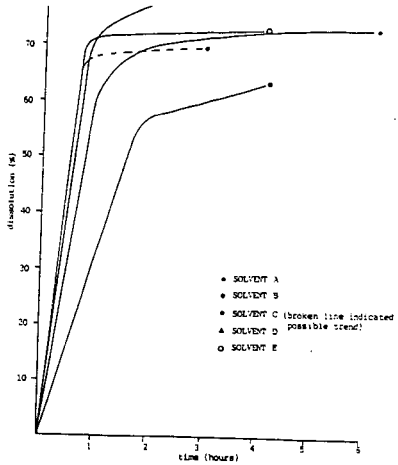

Figure 2. Plots of percentage dissolution vs time for the five model solvents A-E

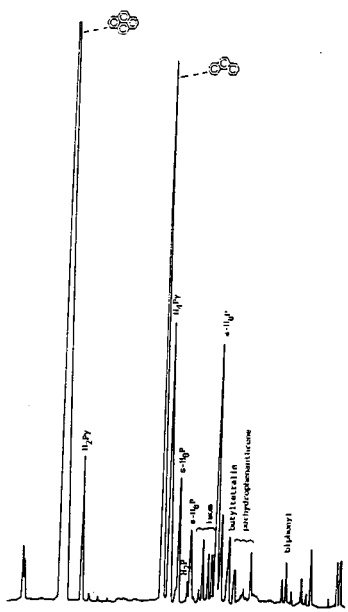

Figure 3. Gas chromatogram of a hexane-soluble material fraction of a coal liquid

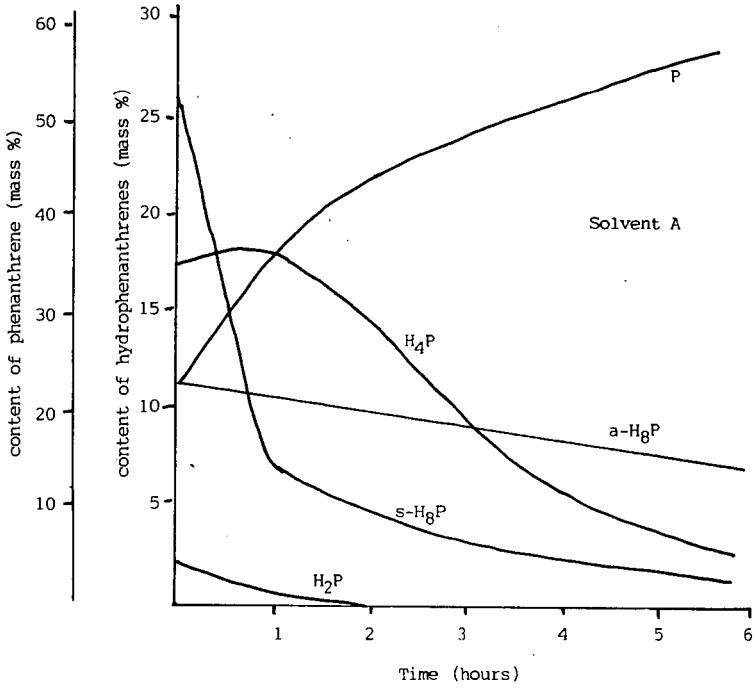

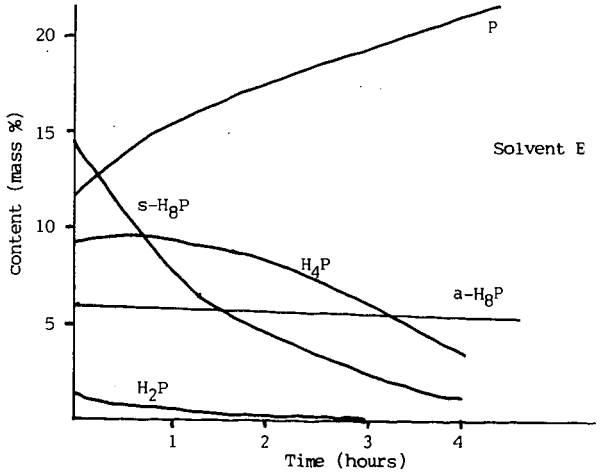

Figure 4. Variation of contents of phenanthrene and hydrophenanthrenes with dissolution time for solvents E (bottom) and A (top)

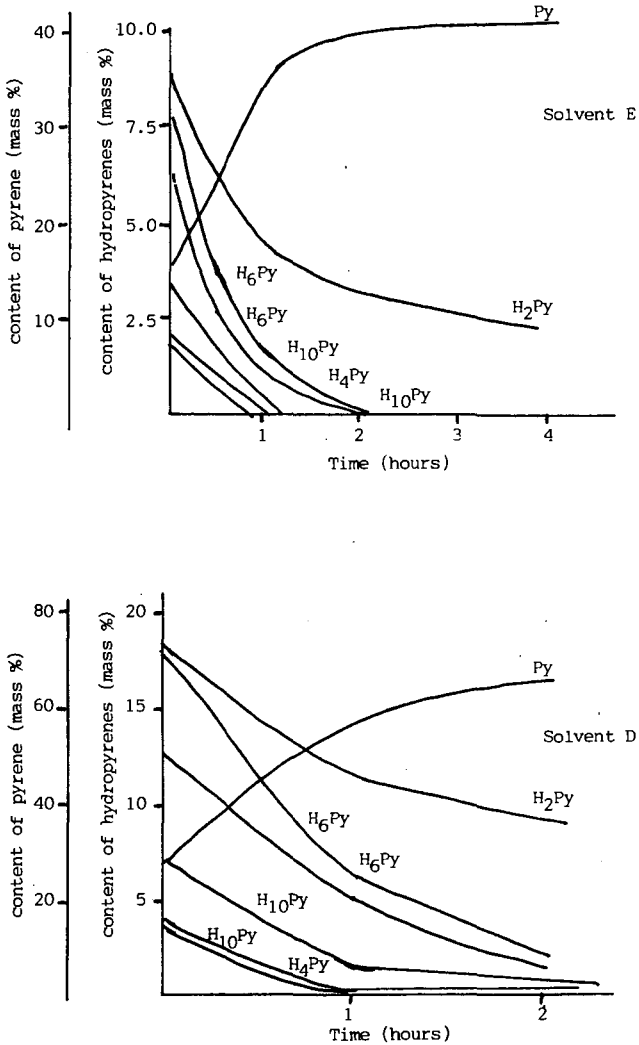

Figure 5. Variation of contents of pyrene and hydropyrenes with dissolution time for solvents D (bottom) and E (top)

CLEAVAGE OF BENZYLAROMATICS AND THEIR RELEVANCE TO COAL CONVERSION

D. F. McMillen, R. Malhotra, and D. S. Tse
Chemical Kinetics Department, SRI International, Menlo Park, California 94025.

KEYWORDS: Mechanism, Liquefaction, Hydrogen-transfer, RHT, Bond-Cleavage.

INTRODUCTION

The modes by which bonds are cleaved during coal liquefaction continues to be a subject of controversy, not only because the nature of the "critical" linkages in coals are not known with any certainty, but also because the detailed nature of some of the hydrogen-transfer reactions that lead to cleavage is still not fully understood. It is now fairly well agreed that ipso hydrogen displacement not involving free H-atoms can result in the cleavage of some coal-like structures under liquefaction conditions (1-8). However, it is still a matter of debate whether such cleavage is (a) general for linkages to aromatic rings, (b) significant for coal liquefaction, and (c) takes place by the radical hydrogen-transfer (RHT) process, as has been claimed (1). In this paper we present data that indicate that cleavage not involving free H-atoms (i.e., a solvent-mediated hydrogenolysis) is general for linkages to aromatic rings (though at rates which vary widely with the nature of the ring system). We also discuss, in the light of this recent data, some previously reported results that suggest such cleavages are indeed significant in coal liquefaction. Finally, we discuss those mechanistic alternatives to an actual RHT process that have not been eliminated by previous results. We defer all discussion of RHT itself or its specific mechanistic alternatives until the questions of generality of solvent mediated hydrogenolysis and its relevance to coal liquefaction have first been considered.

RESULTS AND DISCUSSION

Cleavage of Benzylaromatics. Figure 1 shows the measured rates of ipso-displacement of benzyl groups from arenes containing one to four aromatic rings in a 1:1 mixture of anthracene and 9,10-dihydroanthracene at 400°C. These experiments were performed in sealed fused-silica ampoules containing 10 wt% substrate in a 1:1 anthracene/dihydroanthracene mixture, and were analyzed by GC-MS. The measured rates are expressed as defined first-order rate constants. Displacement was observed in all cases, with the reaction becoming progressively more facile as the $\Delta H°$ for H-atom addition to the aromatics becomes more negative. While this cleavage is indeed extremely facile for alkyl-anthracenes and -pyrenes, as has recently been noted by several authors (4,6,7,11), it is clear from the data in Figure 1 that it is general for substituted aromatics, rather than unique to pyrene and anthracene type structures as has been suggested (6).

The defined first-order rate constants increase by almost four orders of magnitude (a factor of 6×10^3) in going from diphenylmethane to 1-benzylpyrene. This sensitivity is very similar to that observed by Futamura and coworkers (7) for reaction of diarylmethanes in tetralin, and is far greater than would result from addition of highly reactive free H-atoms to the respective arenes to give the cyclohexadienyl radical cleavage intermediates. Reported H-atom addition rates (9) give an Evans-Polanyi factor less than 0.2 and an anticipated rate increase of less than a factor of ten for free H-atom addition to benzylaromatics in this series. Thus, there is little doubt that some active H-donor other than H-atom itself is transferring hydrogen to the closed-shell reactants to generate the necessary cyclohexadienyl radical intermediate.

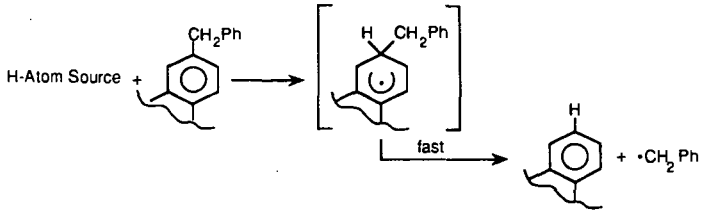

Scheme 1. Cleavage of Benzylaromatics by H-Atom Transfer.

Transfer of an H-atom directly from a dihydroaromatic (i.e., an RRD process) would certainly exhibit high selectivity (higher even than RHT). However, the rough similarity of cleavage rate constants observed in solvents having vastly different C-H bond strengths, such as dihydroanthracene and dihydrophenanthrene (1,2,11,22), and even tetralin (7), have already demonstrated that RRD cannot, in all cases, constitute the stoichiometric and rate-determining H-transfer step.

Significance for Coal Liquefaction. An explicit determination of the importance of cleavage by ipso-desubstitution in coal liquefaction, as noted above, is not possible at the present time, since the nature of the critical linkages broken during liquefaction cannot be determined with any certainty. However, as we have previously pointed out, (a) the ability of hydroaromatics to engender hydrogenolysis even in the absence of hydrogen pressures and catalysts, (b) the effectiveness of these known hydrogenolysis agents in coal liquefaction, and (c) the ineffectiveness of pure "scavengers", such as toluene, ethylbenzene and indane, together strongly suggest that hydrogenolytic cleavage of strong bonds is important in coal liquefaction (1,11,12-15). In addition to this descriptive evidence, we have shown several instances where the incorporation of strong-bond cleavage into the liquefaction mechanism pictures enables one to rationalize, and in some cases (15) even predict, coal liquefaction behavior that defies interpretation if one is limited to the traditional weak-bond scission picture of liquefaction. Studies by Zabransky and Stock (16) on coals with various structures grafted onto them very clearly showed that scission of strong bonds induced by the system was competitive with scission of the weak bonds.

The importance of hydrodealkylation has been questioned on the grounds that it is generally a very slow reaction and that other reactions, most notably H-abstraction--β-scission, can also result in cleavage of strong bonds. Recently, Ceylan and Stock (17) have reported that demethylation of 1,3-dimethylnaphthalene in tetralin/coal mixtures occurs only to a minor extent (~1-4%) in two hours at 400°C, and is much slower than the H-abstraction--β-scission cleavage of 1,3-diphenylpropane (~35% at 400°C in 30 min.). We do not disagree with these results. Indeed, we find the rates reported by Ceylan and Stock for demethylation of 1,3-dinaphthylmethane to be in good agreement with those we had reported for the decomposition of 1,2'-dinaphthylmethane (1,12).

However, in trying to judge whether hydrodealkylation is a significant bond cleavage mode in liquefaction, we must remember that the H-abstraction--β-scission chain decompositions cannot be the **critical** bond cleavages that occur during coal liquefaction. H-abstraction--β-scission cleavages are recognized (5) to be very facile at 400°C, even under neat conditions, and are known not to benefit significantly from tetralin or other hydrogen donors. This type of bond cleavage makes the **aliphatic** portions of crude petroleums easy to thermally crack even in the absence of H-donors, but it does not lead to substantially increased distillate production rates in the presence of donors or other added sources of hydrogen (18,19). This behavior is of course in stark contrast to that of coals, whose liquefaction benefits enormously from "donor" solvents. Thus, while bond cleavages of the H-abstraction--β-scission type may indeed be more facile than the typical hydrodealkylation reaction, they are not necessarily **the** important category of cleavage. By the very fact that ispo desubstitutions sometimes occur only at modest rates and primarily in the presence of favorable reagents, they might properly be judged to be more "critical" than those cleavages which are more facile, and occur anyway.

Furthermore, the rates of hydrodealkylation reactions are highly dependent on the nature of the aromatic ring system to which the linkage is connected, as shown in Figure 1. In addition to the effect of ring size, illustrated by the data in Figure 1, there are the steric and electronic effects of other substituents, notably alkyl and hydroxyl groups. In previous work involving hydroquinone-promoted dealkylation (20), we had observed that in dihydroanthracene the demethylation of 2-methyl-1-naphthol is ~10 times faster than that of 2-methylnaphthalene. Given the degree of phenolic substitution on aromatic ring systems in bituminous and lower rank coals, the cleavage of alkyl linkages to any given naphthalene ring system in a coal is very likely to be significantly higher than that of methylnaphthalene. For instance, had Ceylan and Stock used a methylnaphthol as their probe molecule, we anticipate they would have observed 20 to 30% demethylation in two hours at 400°C in their tetralin-coal-resid mixtures.

Finally, the cleavage rates for low molecular-weight model compounds are not necessarily indicative of how that same bond type will behave in a polymeric matrix such as coal. We have recently described (13) the "liquefaction" of a bibenzyl-type polymer, poly(1,4-dimethylenenaphthalene), in which the bond scission by hydrodealkylation was observed to be much faster than we had anticipated on the basis of monomeric model compound measurements. Furthermore, the net rate of spontaneous scission (homolysis) of the weak central bond was found to be much slower than one would anticipate from non-polymeric model compound measurements. We rationalized this latter observation by suggesting that the polymeric matrix provides an effective cage in which recombination of spontaneously produced benzylic radicals is drastically reduced. In contrast, bond scission by hydrodealkylation is a process not so easily reversed (since reversal involves an activated radical addition process to produce a highly unstable cyclohexadienyl radical). In fact, it appears that strong bond scission is enhanced in the polymeric system. Most likely, this is because every act of scavenging of polymer fragments by the donor dihydrophenanthrene produces a 9-hydrophenanthryl radical, which is capable of engendering hydrodealkylation, in the vicinity of the polymer. Regardless of the correctness of these explanations, the experimental result was that a hydrodealkylation expected to be some 300 times slower than a weak-bond homolysis had become, in the polymeric system, roughly as fast (13).

For all of the reasons cited in the above paragraphs, we assert that the fact that non-polymeric, unhydroxylated, two-ring probe molecules cleave at the rate of only a few percent per hour does not constitute convincing evidence that cleavages by ipso-substitution are unimportant in coal liquefaction. On the contrary, the other evidence retierated above warrants the acceptance, at least as a working hypothesis, of the proposition that ipso-diplacement by hydrogen constitutes an important part of coal conversion under liquefaction and coprocessing conditions. Given this conclusion, it becomes more than a mere academic exercise to determine in greater detail how the hydrogen transfer which induces this cleavage is taking place.

The Mechanism of Solvent-Mediated Hydrogenolysis. In the purely radical realm, several pathways for transfer of hydrogen leading to strong-bond cleavage have been considered (1,2,4,6,21,22). These pathways include radical hydrogen-transfer (RHT), reverse radical-disproportionation (RRD), also called "molecule-induced homolysis," concerted transfer of H_2, and a multi-step process in which the hydrogen atom source is the same cyclohexadienyl radical carrier species that would be the hydrogen atom donor in RHT itself. Another alternative that cannot be categorically excluded is an electron-transfer--proton-transfer sequence. Although we have been unable to find definitive evidence that would rule out this possibility, we consider it unlikely in systems where both the donor and acceptor are hydrocarbons.

Reverse radical-disproportionation has in some cases (i.e., those with 9,10-dihydroanthracene as the donor and high concentrations of substituted anthracenes as the acceptor) been shown (22) to constitute the stoichiometric hydrogen-transfer step, but with other common donor components, such as 9,10-dihydrophenanthrene and 4,5-dihydropyrene, RRD has been shown (1,2) not to be a major contributor. Similarly, thermodynamic requirements make a concerted transfer of H_2 much slower than sequential transfer in most cases of interest here (1,23). We have also previously presented evidence that a three-step indirect transfer process, such as that depicted in Scheme 2, is not responsible for the observed cleavage (1). However, recent experiments and calculations (6,8) have also raised additional questions (at least in the experimentally and computationally accessible systems) about the specific direct transfer route we

had previously invoked (RHT). Therefore, in the paragraphs below, we reexamine the principal remaining possibility, namely the indirect route.

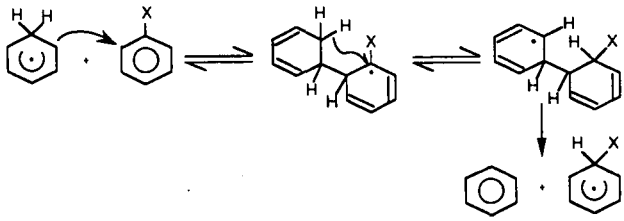

Scheme 2. Three-Step H-Transfer Mechanism

H-transfer by a Multi-Step Process. This route is comprised of three known elementary reactions: radical addition, intramolecular H-atom abstraction, and β-scission. Because this was a reasonable alternative to the invoking of a new reaction in RHT, and because it had been previously suggested as a likely alternative (21), we discussed this possibility in detail in an earlier paper (1). At that time we ruled it out on the basis of two principal considerations. First, ipso H-transfer by an indirect route requires initial radical-addition at some position other than ipso, usually ortho or para to the ipso position, depending on whether the donor radical is of the 9-hydrophenanthryl type or the 9-hydroanthryl type. In some cases this addition would be extremely electronically unfavorable, because ortho or para is a fused ring position. Second, because reversal of the initial addition is expected to be many orders of magnitude faster than intramolecular H-abstraction (1), we would anticipate many initial additions to different sites (i.e., not just those o- or p- to the substituent), including ipso attack. Ipso attack should then lead to radical displacement products, which were often not observed. Since the recent experimental and theoretical work of Autrey and Franz (8), and of Freund et al.(6), have raised additional questions about the viabilitiy of the RHT pathway itself, we felt it was desirable to provide additional experimental evidence on the matter.

The most convincing evidence against the indirect route comes in fact from the displacement of 1-substituted pyrene derivatives -- ironically the same system whose reactions have caused Freund et al. (6) to invoke the indirect route. A feature of all indirect routes that commence with a radical addition is that subsequent intramolecular H-abstraction provides a set of linked aromatic systems in which the original donor framework again bears the free radical and the substrate portion has become a dihydro derivative. In other words, transfer of a single H-atom requires formation, as an intermediate, of a dihydro species. In the case of ultimate transfer of a hydrogen to the 1-position of pyrene, this intermediate would be a 1,2- or a 1,5-dihydropyrene. Both of these species are highly unstable (relative to the 4,5-dihydro species), since their formation requires destruction of the aromaticity of two of the rings of pyrene. Although there are no measured heats of formation available for these unstable dihydropyrenes, we can reliably estimate that the required intramolecular H-abstraction reactions would be more than three orders of magnitude slower for reaction of pyrene derivatives than for reaction of naphthalene derivatives (Table 1).

In contrast with these estimates, experimental results show that cleavage of pyrene derivatives is actually about two orders of magnitude **faster** than that of naphthalene derivatives. There is now not merely a quantitative mismatch between estimated and observed relative rates, but a qualitative inconsistency: those reactions which would have to be much slower, are actually much faster. Thus the increased susceptibility of pyrene linkages to ipso displacement that has been recently discussed (4,6) cannot be the result of a multi-step sequence of free radical reactions that has the same net result as the one-step RHT process.

CONCLUSIONS

The experimental evidence now makes it clear that cleavage induced by H-transfer is general for benzyl and alkyl linkages to aromatic ring systems. The substrate and positional selectivities of this cleavage show that it cannot simply result from displacement by free H-atoms, and relative rates in different solvent systems show it cannot result merely from reverse radical-disproportionation. Comparison of the response of coal liquefaction on the one hand and H-abstraction--β-scission on the other to the presence of donor solvents is a strong indicator that the latter type of strong-bond cleavage, while probably important in resid conversion, does not constitute the "critical" cleavage that distinguishes between better and poorer liquefaction systems. Finally, a multi-step radical process for hydrogen transfer is ruled out by the sensitivity of linkages to the 1-position of pyrene, coupled with the marked instability of the 1,2- and 1,5-dihydropyrene intermediates that would be necessary in a multi-step process.

REFERENCES

1. McMillen, D. F.; Malhotra, R.; Chang, S. -J.; Fleming, R. H.; Ogier, W. C.; Nigenda, S. E. *Fuel* **1987**, *66*, 1611.

2. Bilmers, R.; Brown, R. L.; Stein, S. E. *Int. J. Chem. Kinetics* **1989**, *21*, 375.

3. Bockrath, B. C.; Schroeder, K. T.; Smith, M. R. *Energy and Fuels* **1989**, *3*, 268.

4. Smith, C. M.; Savage, P. E., "Reactions of Polycyclic Alkylaromatics, Part 1: Pathways, Kinetics, and Mechanisms for 1-Dodecylpyrene," *Ind. Eng. Chem. Res.* **1991**, *31*, XXX.

5. Poutsma, M. L. *Energy and Fuels*, **1990**, *4*, 114.

6. Freund, H.; Matturro, M. G.; Olmstead, W. N.; Reynolds, R. P.; Upton, T. H. *Am. Chem. Soc., Div. Fuel Chem. Preprints* **1990**, *35*(2), 496.

7. Futamura, S.; Koyanagi, S.; Kamiya, Y. *Fuel* **1988**, *67*, 1436

8. Autrey, T.; Franz, J. A. *Am. Chem. Soc., Div. Fuel Chem. Preprints* **1990**, *35*(2), 382

9. a. Tsang, W. *J. Amer. Chem. Soc.* **1985**, *107*, 2872.
   b. Tsang, W. *J. Phys. Chem.* **1986**, *90*, 1152.

10. Bockrath, B. C.; Bittner, E.; McGrew, J. *J. Am. Chem. Soc.* **1984**, *106*, 135.

11. Malhotra, R.; McMillen, D. F. *Energy and Fuels* **1990**, *4*, 184.

12. McMillen, D. F.; Malhotra, R.; Hum, G. P.; Chang, S. -J. *Energy and Fuels* **1987**, *1*, 193.

13. Malhotra, R.; McMillen, D. F.; Tse, D. S.; St.John, G. A. *Am. Chem. Soc.* **1989**, *3*, 465.

14. McMillen, D. F.; Malhotra, R.; Nigenda, S. E. *Fuel* **1989**, *68*, 380.

15. McMillen, D. F.; Malhotra, R.; Tse, D. S., *Energy and Fuels* **1991**, *5*, XXX.

16. Rose, G. R.; Zabransky, R. F.; Stock, L. M.; Huang, C.-B.; Srinivas, V. R.; Tse, K.-T. *Fuel* **1984**, *63*, 1339.

17. Ceylan, K.; Stock, L. M. *Fuel* **1990**, *69*, 1386.

18. Savage, P. E.; Klein, M. T.; Kukes, S. G. *Energy and Fuels* **1988**, *2*, 619.

19. Khorasheh, F.; Rangwala, H. A.; Gray, M. G.; Lana, I. G. D. *Energy and Fuels* **1989**, *3*, 716.

20. McMillen, D. F.; Chang, S. -J.; Fleming, R. H.; Laine, R. M.; Malhotra, R.; Nigenda, E.; Ogier, W., "Effect of of Amine Solvents and Oxygen Functionalities on Coal Liquefaction," *EPRI Research Project 2147-5* , **1985**.

21. Stein, S. E, "Free Radicals in Coal Conversion," in *Chemistry of Coal Conversion*, Schlosberg, R. H., Ed.; Plenum Press: N.Y., **1985**, 13.

22. Billmers, R.; Griffith, L. L.; Stein, S. E., *J. Phys. Chem.* **1986**, *90*, 517.

22. King, H.-H.; Stock, L. M. *Fuel* **1981**, *60*, 748.

23. Benson, S. W., *Therochemical Kinetics*, 2nd ed; John Wiley and Sons: New York, **1976**.

24. Pedley, J. B.; Naylor, R. D.; Kirby, S. P., *Thermodynamics of Organic Compounds*, Chapman and Hall: New York, **1986**.

TABLE 1.

Comparison of Measured Rates of Cleavage with Estimated Rates of Multi-Step Components for Naphthalene and Pyrene Derivatives.

Benzylaromatic	exptl $k_{cleavage}, s^{-1}$	Estimated Rate Constants[a] for Reaction of Three-Step Intermediate, s^{-1}		$\Delta H°$ Intramol H-Abs[b]
		Reversal	Intramol H-Abs	kcal/mol
1-Benzylnaphthalene	3×10^{-6}	5×10^{-8}	6×10^{-6}	~-1
1-Benzylpyrene	5.4×10^{-4}	5×10^{-8}	$<4 \times 10^{-3}$	>+14

a. Rate constants estimated according to the regimen and data sources given in reference 11.
b. Estimated by group additivity procedures as described in reference 23, and by comparison with measured heats of formation for closest available analogs, as given in reference 24.

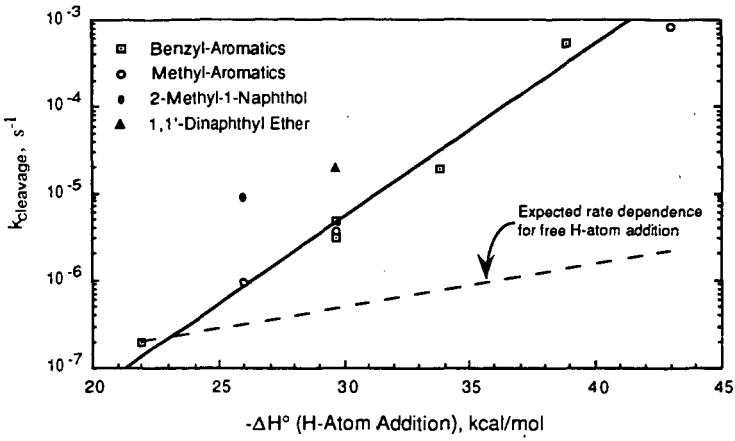

Figure 1 Measured rates of cleavage of benzyl- and methyl- aromatics in anthracene/ dihydroanthracene at 400°C, as a function of the exothermicity of free H-atom addition.

Measured and estimated ΔH° (addition) are taken from reference 11. They are, in kcal/mol: phenyl, -22; 2-naphthyl, -26; 1-naphthyl, -27.9; 9-phenanthryl, -33.8; 1-pyrenyl, -38.9; and 9-anthryl, -43.

REACTIVITIES OF HYDROGENATED DI(1-NAPHTHYL)METHANES TOWARD THERMAL DECOMPOSITION AND HYDROCRACKING

Xian-Yong Wei, Eisuke Ogata, Shigeru Futamura, Yoshio Kamiya, and Etsuo Niki
Department of Reaction Chemistry, Faculty of Engineering, The University of Tokyo, 7-3-1, Hongo, Bunkyo-Ku, Tokyo, 113 Japan

Keywords: Hydrogenated Di(1-naphthyl)methanes, Thermal Decomposition, Hydrocracking

INTRODUCTION

The decomposition mechanism of diarylmethanes has been extensively investigated [1-5], and it is generally accepted that the decomposition occurs via the ipso-addition of a hydrogen atom transferred from hydrogen donating solvent or gaseous hydrogen. It is noteworthy that the feasibility of the hydrogen transfer to the ipso-positions of diarylmethanes depends not only on the species of hydrogen donating solvent, hydrogen pressure and catalyst, but on aromatic ring sizes [4,5].

In the hydrogenolysis of di(1-naphthyl)methane(DNM) [5,6], hydrogenated di(1-naphthyl)methanes(H-DNMs) were formed in addition to naphthalene(Np) and 1-methylnaphthalene(1-MN). We previously reported that at low temperatures, the selectivities of H-DNMs were dependent upon the catalyst used to a large extent [7]. It is of significance to know how the reactivities of H-DNMs toward thermal decomposition or hydrocracking change with the degree of hydrogenation of H-DNMs.

EXPERIMENTAL

Materials

DNM was synthesized according to the methods described in the previous paper [5] and 1,2-di(1-naphthyl)ethane(DNE) according to the method of Buu-Hoï [8]. H-DNMs were prepared by hydrogenating DNM with Ni-Mo-S/Al_2O_3, stabilized nickel or ultra fine metallic iron catalyst, respectively, as shown in Table 1. DNM and H-DNMs prepared were identified by GC-MS. Table 2 shows the structures of these compounds. The other substrates such as diphenylmethane (DPM) and 1,2-diphenylethane(DPE), and solvent dodecane were purchased commercially and further purified if necessary by conventional methods.

Thermal decomposition and hydrocracking of the substrates

7.5 mmol of a substrate, 30 ml of dodecane were put into a 90 ml stainless steel, magnetically stirred autoclave. After being pressurized by hydrogen or nitrogen to 10 MPa, the autoclave was heated to a reaction temperature and kept for a prescribed period of time. Then, the autoclave was immediately cooled to room temperature in an ice-water bath. Thermal decomposition was usually carried out under nitrogen at 400°C, and hydrocracking in the presence of 0.5 g of FeS_2 catalyst with 0.05 g of sulfur under hydrogen at 300°C.

The products were identified by GC-MS and quantified by GC.

RESULTS AND DISCUSSION

Reactivities of DNM and H-DNMs toward thermal decomposition

Figure 1(a) shows the reactivities of DNM and H-DNMs mixture (MIX) toward thermal decomposition under nitrogen in the tempera-ture range 300-430°C. At 300°C, the thermal decomposition does not proceed for any substrate. Ditetralylmethanes(8H-DNM and 8H'-DNM) slightly decompose at 350°C. At above 400°C, 4H-DNM begins to decompose with concurrent increase in the DNM concentration, suggesting the occurrence of dehydrogenation of H-DNMs. Figure 1 (a) shows that the reactivities of H-DNMs toward thermal decompo-sition decrease in the order: 8H'-DNM > 8H-DNM > 4H-DNM. Although the thermal decomposition of DNM and 4H-DNM were promoted under hydrogen(Fig.2(b)), the order of the reactivities did not change.

8H-DNMs(1) was thermally decomposed. Figure 2 shows that in spite of low initial concentration of 8H'-DNM, the molar ratio of 8H'-DNM to 8H-DNMs decreases steadily as the reaction proceeds, indicating that 8H'-DNM decomposes faster than 8H-DNM. As the reaction proceeds, the selectivities of the dehydrogenated products such as 4H-DNM and DNM, and that of a hydrogenated product, 14H-DNM increased, while those of the decomposed products such as tetralin(THN) and 5-methyltetralin(5-MT) decreased. These facts suggest that the disproportionation reaction concurs. The time profile of the product distribution for the thermal decomposition of 8H-DNMs(2) is illustrated in Fig.3. These results given in Fig.3 show that 8H-DNM is as reactive as 14H-DNM, but much lower than 8H'-DNM in reactivity.

To clarify the different reactivities of 8H-DNM and 8H'-DNM, the thermal decomposition of DPM and DPE were separately carried out under the conditions similar to those for 8H-DNMs. As shown in Table 3, in comparison with ca. 6% of conversion for DPE, DPM does not decompose at all. The bond dissociation energies of some diaryl hydrocarbons lised in Table 4 indicate that the aliphatic C-C bonds in DPE and DNE are thermally cleaved much more readily than the C_{ar}-C_{alk} in DPM. By analogy of structural similarity between these compounds and octahydro-derivatives of DNM, the discrepancy in the reactivities of 8H-DNM and 8H'-DNM may be due to the different labilities of their breaking C-C bonds.

On the other hand, compared to 8H-DNM and 8H'-DNM, DPM and DPE are much less reactive, respectively. The difference should be attributed to the hydrogen donating effect of tetralyl groups in ditetralylmethanes. Table 3 indicates that DNM and DNE decompose more readily than DPM and DPE, respectively, but they are less reactive than 8H-DNM and 8H'-DNM, respectively. Because neither gaseous hydrogen nor hydrogen donating solvent was used, the hydrogen consumed in the thermal decomposition of DNM and DNE should result from dodecane used as a solvent. In decalin solvent, DNM does not decompose at all, but DNE decomposes much the same as in dodecane solvent. Two blank tests show that under the same reaction conditions(400°C, 10 MPa of N_2, 1 h), ca. 1% of dodecane decomposes, but that decalin does not. These results indicate that the hydrogenolysis of DNM occurs in dodecane solvent. 20H-DNM derived from the complete hydrogenation of DNM shows even lower reactivitiy toward thermal decomposition than DNM. Compari-

son of the reactivities of the substrates listed in Table 3 suggests that the intramolecular hydrogen transfer plays a significant role in the cleavage of $R-CH_2-R'$, where the R and R' denote aromatic or hydroaromatic rings. It could be also said that the thermal decomposition of H-DNMs, except for 20H-DNM , includes hydrogenolysis primarily induced by the intramolecular hydrogen transfer. The reactivities of DNM and H-DNMs toward thermal decomposition decrease in the order: 8H'-DNM > 8H-DNM > 4H-DNM > DNM > 20H-DNM.

Reactivities of DNM and H-DNMs toward hydrocracking catalyzed by FeS_2

The hydrocracking of a mixture of DNM and H-DNMs was carried out at 300°C in the presence of FeS_2 catalyst. Figure 4 shows that the reactivities of DNM and H-DNMs toward hydrocracking decrease in the order: DNM > 4H-DNM > 8H-DNM > 8H'-DNM, which is the reverse of that toward thermal decomposition(see above). The slight increase in the concentration of 8H'-DNM with the course of the reaction was observed, which may be due to the hydrogenation of DNM and 4H-DNM.

Fig.5 shows the results of the hydrocracking of 8H-DNMs(1). In contrast to the relatively rapid hydrocracking of 8H-DNM, 8H'-DNM is hardly hydrocracked, partially because of its low concentration. Fig.6 shows that in the hydrocracking of 8H-DNMs(2), the rate for the hydrocracking of 8H-DNM is above tenfold greater than that of 8H'-DNM. As is consistent with the low reactivity of 8H'-DNM toward hydrocracking, the yield of 1-methyltetralin(1-MT) is only small. As the hydrocracking of DNM and H-DNMs results principally from the ipso-addition of a hydrogen atom to an aromatic ring under the reaction conditions, the different reactivities of 8H-DNM and 8H'-DNM can be illustrated in Fig.7. In the hydrocracking of 8H-DNM, the ipso-position of both tetralin rings can be attacked by H-atoms, and as an intermediate produced after the hydrocraking, tetralyl-5-methyl radical is much more stable than tetralyl-1-methyl radical. Hence, 8H-DNM is expected to decompose much more readily than 8H'-DNM after the ipso-addition of a hydrogen atom.

Table 5 shows the different reactivities of DPM and DPE, and those of DNM and DNE. DNE is mainly hydrogenated rather than decomposed. In general, hydrogen donating solvent scarcely shows its donating ability at a temperature as low as 300°C, especially in the presence of both gaseous hydrogen and an active catalyst [12-14]. Thus, the difference in the hydrocracking reactivities between 8H-DNM and DPM, and those between 8H'-DNM and DPE should be primarily due to the ring size effect. Under the same reaction conditions, 20H-DNM does not decompose at all. The order of the hydrocracking reactivities decreases: DNM > 4H-DNM > 8H-DNM > 8H'-DNM > 20H-DNM. The results may be explained on the basis of the hydrogen-accepting ability and adsorption ability [13,14] on the surface of catalyst used. They decrease in the order: naphthalene > tetralin > decalin. Because the hydrocracking proceeds mainly on the surface of FeS_2 catalyst via the attack(involving ipso-addition) on the substrates by H-atoms dissociated, the synergistic effect can be expected in the hydrocracking of DNM and H-DNMs.

Whitehurst et al. [15] have proposed that coal reactivity in liquefaction reactions is affected by its chemical structure. Takegami et al. [16] and Maekawa et al. [17] suggested that coal liquefaction proceeds through cleavage of ether and methylene bridges connecting relatively small structure units, such as polycyclic aromatic and hydroaromatic rings. According to our results, therefore, the severe hydrogenation of aromatic moieties in coal structure is likely to decrease the reactivity of the coal hydrogenated in the catalyzed hydroliquefaction, but the partial hydrogenation of aromatic moieties in coal structure forms precursors which are labile to thermal decomposition.

CONCLUSION

1. Mono- and di-tetralylmethanes, which are afforded in the partial hydrogenation of DNM, are more reactive than DNM toward thermal decomposition. This fact suggests that the intramolecular hydrogen donation plays a significant role in the thermal decomposition of hydrogenated dinaphthylmethanes.
2. In hydrocracking with FeS_2, di(1-naphthyl)methane decomposes rapidly, and the more fully it is hydrogenated, the more slowly its hydro-derivatives decompose.

REFERENCES

1 McMillen, D.F., Ogier, W.C., and Ross, D.S. J. Org. Chem., 46, 3322(1981)
2 McMillen, D.F., Ogier, W.C., Chang, S.-J., Fleming, R.H. and Malhotra, R., Proc., Int. Conf. on Coal Sci., Pittsburgh, p. 199 (1983)
3 McMillen, D.F., Malhotra, R. Chang, S.-J., Ogier, W.C., Nigenda, S.E., and Fleming, R.H. Fuel, 66, 1611 (1987)
4 Kamiya, Y., Futamura, S., Mizuki, T., Kajioka, M. and Koshi, K. Fuel Process. Technol., 14, 79 (1986)
5 Futamura, S., Koyanagi, S. and Kamiya, Y. Fuel, 67, 1436(1988)
6 Sakurai, A., Harada, Y., Oda, H. and Yokokawa, C. Proc., 24th Coal Sci. Conf. Jpn, Soc. Fuel, Tokyo, p. 2 (1987)
7 Ogata, E., Wei, X.-Y., Fukasawa, T. and Kamiya, Y. Proc., Int. Conf. on Coal Sci., Tokyo, pp. 879-882
8 Buu-Hoi, Ng.Ph. and Hoan, Ng. J. Org. Chem., 46, 1023 (1949)
9 Vernon, L.W. Fuel, 59, 102 (1979)
10 Hei, R.D., Sweeny, P.G. and Stenberg, V.I. Fuel, 65, 577(1986)
11 Malhotra, R., McMillen, D.F., Tse, D.S. and John G.A.S. Energy & Fuels, 3, 465 (1989)
12 Ohe, S., Itoh, H., Makabe, M. and Ouchi, K. Fuel, 64, 902-1111 (1985)
13 Ouchi, K. and Makabe, M. Fuel, 67, 1536 (1988)
14 Ogata, E., Tamura, T. and Kamiya, Y. Proc., Int. Conf. on Coal Sci., Maastricht, p. 243 (1987)
15 Whitehurst, D.D., Mitchell, T.O. and Farcasiu, M. In: Coal Liquefaction, "The Chemistry and Technology of Thermal Processes", Academic Press, 1980, chap. 5
16 Takegami, Y., Kajiyama, S. and Yokokawa, C. Fuel, 42, 291 (1963)
17 Maekawa, Y., Shimokawa, K., shii, T. and Takeya, J. Fuel Soc. Jpn., 46, 927 (1967)

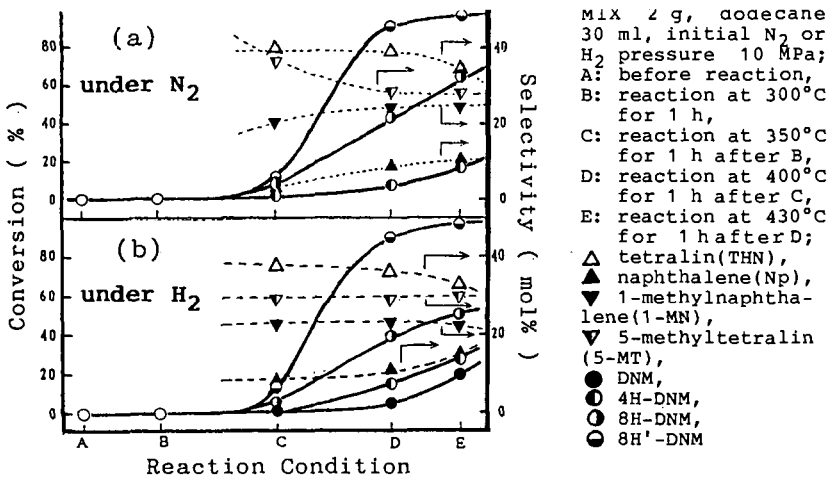

Fig. 1. Thermal decomposition of DNM and H-DNMs mixture(MIX)

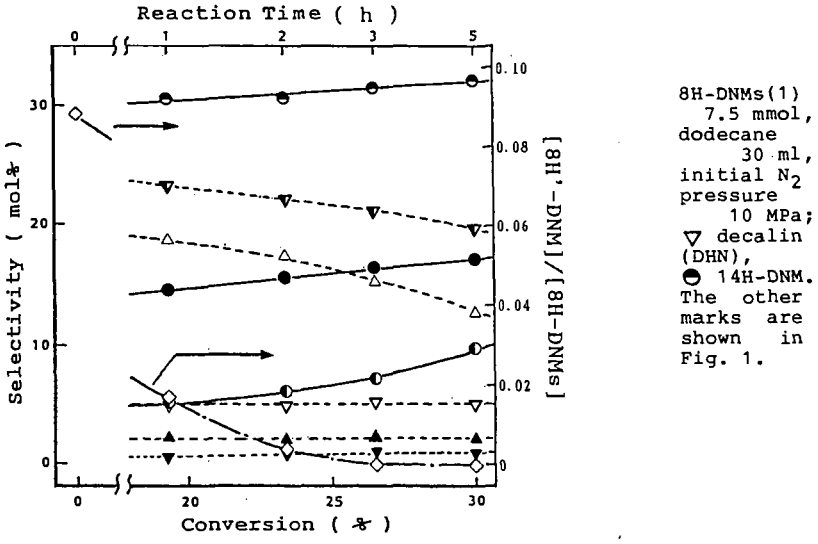

Fig. 2. Thermal decomposition of 8H-DNMs(1) at 400°C

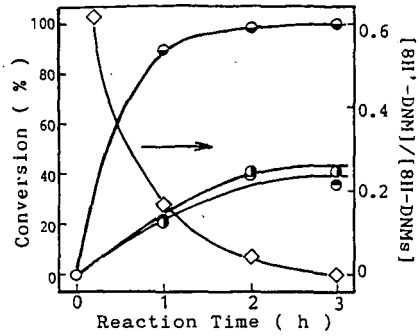

Fig. 3. Thermal decomposition of 8H-DNMs(2) at 400°C

8H-DNMs(2) 7.5 mmol, dodecane 30 ml, initial N_2 pressure 10 MPa. The marks are shown in Figs. 1 and 2.

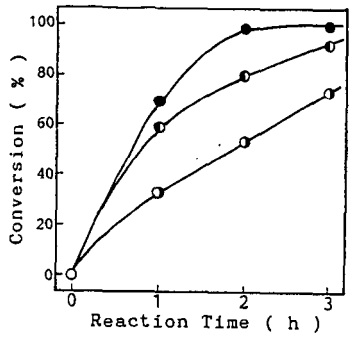

Fig. 4. Hydrocracking of MIX with FeS_2 catalyst at 300°C

MIX 2 g, dodecane 30 ml, FeS_2 0.5 g, sulfur 0.05 g, initial H_2 pressure 10MPa. The marks are shown in Fig. 1.

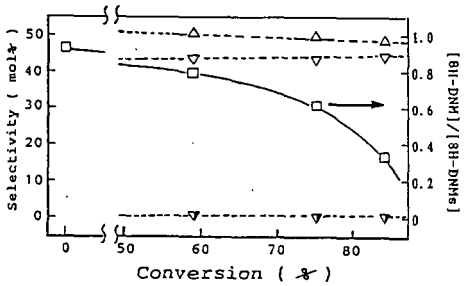

Fig. 5. Hydrocracking of 8H-DNMs(1) with FeS_2 catalyst at 300°C

8H-DNMs(1) 7.5 mmol, dodecane 30 ml, FeS_2 0.5 g, sulfur 0.05 g, initial H_2 pressure 10 MPa,
▽ 1-methyltetralin (1-MT). The other marks are shown in Figs. 1 and 2.

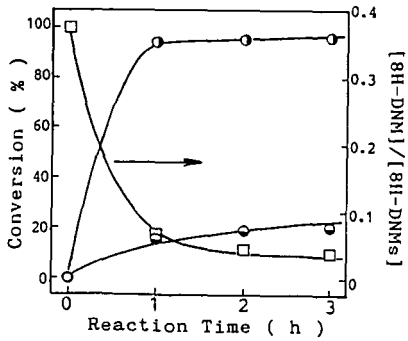

Fig. 6. Hydrocracking of 8H-DNMs(2) with FeS_2 catalyst at 300°C

8H-DNMs(2) 7.5 mmol, dodecane 30 ml, FeS_2 0.5 g, sulfur 0.05 g, initial H_2 pressure 10 MPa.
The marks are shown in Fig. 1.

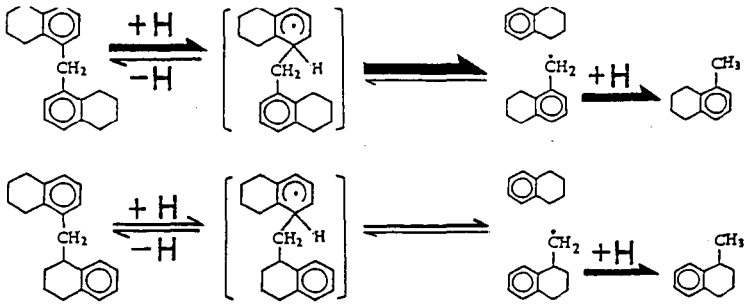

Fig. 7. Scheme for the hydrocracking of 8H-DNM and 8H'-DNM with FeS_2 catalyst

Table 1 Preparation conditions and compositions of H-DNMs

Run	Prearation conditions[a]					H-DNMs abbrev.[b]	Product distribution (mol%)						
	DNM (g)	DHN (ml)	cat. (g)	temp. (°C)	time (h)		DNM	4H-	8H-	8H'-	14-	20H-	Others
1	9.5	30	0.2[c]	250	24	MIX	12.6	33.5	32.0	10.6	0	0	11.3
2	4.2	15	1.0[d]	45	10	8H-(1)	0	0	88.7	8.6	1.0	0	1.7
3[e]	5.0	15	0.5[f]	300	1	8H-(2)	0	0.9	29.6	48.6	14.8	0.5	5.6
4	4.5	15	1.0[d]	150	4	20H-	0	0	0	0	0	93.1	6.9

[a]·initial H_2 pressure 13 MPa; [b]·yields were ca. 90% for 8H-DNMs(2), 95% for MIX and nearly 100% for 8H-DNMs(1) and 20H-DNM; [c]·Ni-Mo-S/Al_2O_3; [d]·stabilized nickel(Nikki,N-103); [e]·After reaction for 1 h, the reaction was carried out for ca. 10 min with 0.05 g of sulfur to decrease the concentration of 8H-DNM; [f]·ultrafine of Fe^0(ca. 200 Å). 4H-: 4H-DNM, 8H-: 8H-DNM, 8H'-: 8H'-DNM, 14-: 14H-DNM, 20-: 20H-DNM, Others: unidentified products.

Table 2 Molecular structure of DNM and H-DNMs identified by GC-MS analysis

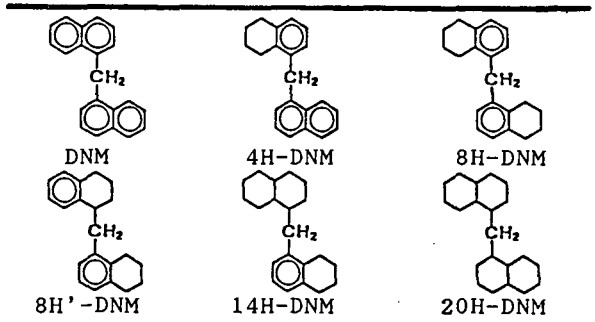

Table 3 Thermal decomposition of H-DNMs and diarylalkanes at 400 °C for 1 h

Substrate	Conv. (%)	Selectivity (mol%)							
		DHN	THN	Np	5-MT	1-MN	1-EN	Tol	Others
DNM	8.3[a]	0	0	50	0	50	-	-	0
DNE	46.8	0	0	0.7	1.3	86.9	0.6	-	10.5
8H-DNMs(1)	19.3[b] 84.7[c]	5.1	18.6	2.2	23.1	0.6	-	-	50.4
8H-DNMs(2)	22.6[b] 89.5[c]	3.0	28.9	4.2	45.5	4.1	-	-	14.3
20H-DNM	~ 4	>90	-	-	-	-	-	-	-
DPM	0	-	-	-	-	-	-	0	-
DPE	6.0	-	-	-	-	-	-	15.9	84.10

substrate(s) 7.5 mmol, dodecane 30 ml, initial N_2 pressure 10 MPa; Tol: toluene, 1-EN: 1-ethylnaphthalene, [a]·In decalin at 400 °C, DNM does not decompose; [b]·conversion of 8H-DNM; [c]·conversion of 8H'-DNM; Others: including hydro- and dehydro-derivatives for DNE, 8H-DNMs(1), 8H-DNMs(2), and other alkylbenzenes for DPE.

Table 4 Bond dissociation energies(BDE) of some hydrocarbons

Bond	BDE(kcal/mol)	Reference
Ph-Ph	100	9
$PhCH_2$-Ph	84,89	9, 1
$PhCH_2CH_2$-Ph	97	10
$PhCH_2$-CH_2Ph	56,62	9, 1
$NpCH_2$-CH_2Np	50,55	9, 11

Np denotes naphthyl group.

Table 5 Hydrocracking of H-DNMs and diarylalkanes at 300 °C for 1

Substrate	Conv. (%)	Selectivity (mol%)								
		THN	Np	5-MT	1-MN	1-EN	H-DNMs	H-DNEs	Bz	Tol
DNM	87.4	2.3	48.1	1.8	42.3	-	2.9	-	-	-
DNE	49.1	tr.	0.9	1.4	1.2	0.2	-	86.1	-	-
8H-DNMs(1)	59.1[a]	50.2	0.5	48.0	0	-	0.2	-	-	-
20H-DNM	0	0	0	0	0	-	-	-	-	-
DPM	6.1	-	-	-	-	-	-	-	28.0	35.0
DPE	0	-	-	-	-	-	-	-	0	0

substrate(s) 7.5 mmol, dodecane 30 ml, FeS_2 0.5 g, sulfur 0.05 g, initial H_2 pressure 10 MPa; Bz: benzene; H-DNMs: hydro-derivatives of DNE. The other abbreviations are defined in Figs 1, 2 and Table 3. [a]·conversion of 8H-DNM. In the case of DNE, 8H-DNMs(1) and DPM, some unidentified products were obtained.

MECHANISMS FOR NONCATALYTIC AND CATALYTIC HYDROGEN TRANSFER PROCESSES UNDER COAL LIQUEFACTION CONDITIONS

Shigeru FUTAMURA, Seiya KOYANAGI, and Yoshio KAMIYA
Department of Reaction Chemistry, Faculty of Engineering, The University of Tokyo, Hongo, Bunkyo-ku, Tokyo, 113 Japan

Keywords: hydrogen transfer, solvents, iron catalysts

INTRODUCTION

Recent progress in the chemistry of coal liquefaction has enabled us to envisage that radical-induced monohydrogen transfer is one of the key processes in the hydrogenolysis of strong bonds bridging aromatic units in coal[1-4]. We have succeeded in verifying that radical mechanism operates in the noncatalytic and Fe-catalyzed hydrogenolyses of reporter molecules such as trans-stilbene [5] and 9-benzylphenanthrene [6].

This paper intended to discuss 1) hydrogen transfer mechanisms for hydrogenolyses of the above compounds, 2) selectivities of benzylic radicals toward addition to aromatic nucleus and hydrogen abstraction in hydroaromatic hydrocarbon solvents, 3) catalysis of Fe compounds in solvent-mediated hydrogen transfer processes, and 4) reactant dependent catalytic activities of Fe compounds such as Fe_2O_3, α-Fe, and $Fe_{1-x}S$.

EXPERIMENTAL

Materials

9-Benzylphenanthrene (9-BP) and di(1-naphthyl)methane (DNM) were synthesized according to the method described in the previous paper [4]. trans-Stilbene and the solvents were commercially purchased and purified if necessary by conventional methods. α-Fe was prepared by reducing Fe_2O_3 in hydrogen streams at 450°C for 20 h. Its BET surface area was 14.2 m^2g^{-1} (Shimadzu 2200). $Fe_{1-x}S$ was prepared by reacting α-Fe with a small excess of elemental sulfur in tetralin under nitrogen at 380°C for 30 min. Its BET surface area was 10.4 m^2g^{-1}. The above catalysts were identified by X-ray diffraction analysis (Rigaku Denki RU-200A). After preparation, they were immediately immersed in 1-methylnaphthalene (1-MN) or in tetralin in a dry box under nitrogen and kept until use.

Batch experiments

A reaction solution consisting of a model compound and a hydrocarbon solvent with or without an Fe catalyst was put into a 90 ml SUS 316, magnetically stirred autoclave, pressurized by hydrogen or nitrogen. It was heated up to a reaction temperature and was kept there for 30 min. After the reaction, the autoclave was cooled by an electric fan to room temperature.

Product analysis

Benzyl(1-methyl)naphthalene (BMN), 1-benzylnaphthalene (1-BN), and octahydrobinaphthalenes were identified by GC-MS (JEOL JMS-

DX300, equipped with a glass column (4mm diameter, 1m length) of 5 % OV-1 on Chromosorb W). 6-Benzyl-1,2,3,4-tetrahydronaphthalene (BTHN) and 6-(1,2-diphenylethyl)-1,2,3,4-tetrahydronaphthalene (DETN) were isolated by column chromatography and vacuum distillation, and they were identified by MS, ^{1}H-NMR (Varian EM 360A (60 MHz)), and ^{13}C-NMR (JEOL JMN-GX-400 (400 MHz)).

The reaction products collected with tetrahydrofuran were analyzed quantitatively by GC (Shimadzu GC-4C, equipped with a stainless column (4 mm diameter, 4 m length) of 10 % OV-17 on Chromosorb W (DMCS)).

RESULTS AND DISCUSSION

Reaction products

The spectral data of the reaction products obtained in the hydrogenolyses of trans-stilbene and 9-BP are as follows.
BMN m/z: 232 (100, M^+), 217 (68), 115 (13).
1-BN m/z: 218 (100, M^+), 217 (55), 141 (17).
BTHN m/z: 222 (62, M^+), 131 (100), 91 (36). ^{1}H-NMR δ in CCl_4 (ppm) 1.69 (4H, m), 2.62 (4H, m), 3.77 (2H, s), 6.80 (3H, bs), 7.09 (5H, bs). ^{13}C-NMR δ in $CDCl_3$ (ppm) 23.24, 23.30, 29.01, 29.39, 41.59, 125.89, 126.06, 128.36, 128.85, 129.17, 129.48, 134.74, 137.06, 138.10, 141.44.
DETN m/z: 312 (2.3, M^+), 221 (100), 91 (17). ^{1}H-NMR δ in CCl_4 (ppm) 1.39-2.12 (4H, m), 2.32-3.04 (4H, m), 3.21 (2H, d, J=7.6 Hz), 4.05 (1H, dd, J=7.6Hz), 6.56-7.48 (13H, m). ^{13}C-NMR δ in $CDCl_3$ (ppm) 23.22, 23.24, 28.96, 29.44, 42.18, 52.75, 127.91, 128.06, 128.12, 128.30, 128.34, 128.49, 128.64, 128.92, 129.12, 134.82, 136.85, 140.46, 141.62, 144.63.
The regiospecific formation of DETN and BTHN was described in the previous paper [5].
1,1',2,2',3,3',4,4'-Octahydrobinaphthalenes m/z: 262 (22, M^+), 131 (100), 130 (68), 91 (32). 1,2,3,4,5',6',7',8'-Octahydrobinaphthalenes m/z: 262 (50, M^+), 130 (100), 104 (84).

Hydrogen transfer mechanism for the hydrogenolysis of trans-stilbene

trans-Stilbene can be a pertinent probe in order to verify hydrogen transfer mechanism and to characterize hydrogen donating abilities of solvents and activities of catalysts because the degree of stilbene isomerization can be a measure for mechanism determination, and dibenzyl cannot be dehydrogenated to trans-stilbene at 380°C.

Figure 1 shows the plot of the cis-stilbene content against the stilbene conversion. A fairly good linear correlation suggests that the stilbene isomerization cannot be ascribed to thermochemical equilibration of trans- and cis-stilbenes, supporting radical mechanism. A possible intermediate could be 1,2-diphenylethyl radical because the step from 1,2-diphenylethyl cation to dibenzyl is unlikely. In fact, the adduct of this radical to tetralin (DETN) was obtained in the hydrogenolysis of trans-stilbene in the presence of α-Fe. These findings may suggest that 1,2-diphenylethyl radical is an intermediate in the

hydrogenation of trans-stilbene. Since the acidity of α-Fe is negligible [7], 1,2-diphenylethyl radical stabilized on the surface of α-Fe could be trapped by tetralin solvent.

Selectivities of benzylic radicals toward addition and hydrogen abstraction

Table 1 summarizes some data on selectivities of benzylic radicals toward addition and hydrogen abstraction, which are relevant to radical-induced monohydrogen transfer from solvents. Dibenzyl added in the system of DNM and a solvent (Reaction 1) thermally decomposes to selectively give benzyl radicals. Their relative reactivity of addition to hydrogen abstraction is 0.015 in tetralin and 0.033 in 1-MN. These findings are the first example of ipso-substitution by benzyl radicals, i.e., alkyl-dealkylation [8].

This type of benzyl radical addition to the aromatic nucleus is promoted by α-Fe in the hydrogenolysis of 9-BP (Reaction 2), where only a low concentration of the benzyl radical is present.

As described above, addition of 1,2-diphenylethyl radical to tetralin can be observed only in the presence of α-Fe, and the relative ratios of addition to hydrogen abstraction are around 0.2 at initial hydrogen pressure of 1.0 to 6.0 MPa (Reaction 3). On the other hand, $Fe_{1-x}S$ promoted further hydrogenation to give dibenzyl in higher selectivities. When tetralin was used as solvent, trace amounts of octahydrobinaphthalenes were obtained only in the presence of α-Fe.

In a binary solvent system of 9,10-dihydrophenanthrene (DHP) and 1-MN, only dibenzyl was obtained from stilbenes with no formation of 1,2-diphenylethylphenanthrene or benzylphenanthrene. This fact can be ascribed to the rapid capping of 1,2-diphenylethyl radical by DHP, which is a superior hydrogen donor.

The chemical behavior of 1,2-diphenylethyl radical could be affected by hydrogen donating ability of solvent and stability of solvent adduct itself.

These data confirm that monohydrogen transfer predominates from hydroaromatic radicals such as tetralyl and hydrophenanthryl.

Catalysis of Fe compounds in solvent-mediated hydrogenolysis of trans-stilbene

Table 2 shows the effects of Fe catalysts and hydrogen pressure on the hydrogenation of trans-stilbene in 1-MN. Comparison of Runs 1 and 3 shows that catalytic hydrogen transfer from 1-MN to trans-stilbene is negligible, and only about 2 % of 1-MN is consumed in these cases. Direct hydrogenation of trans-stilbene by molecular hydrogen is rather slow in the absence of α-Fe in 1-MN (see Runs 2 and 4). $Fe_{1-x}S$ showed a comparable catalytic activity, but it was more effective as hydrogenation catalyst than α-Fe. The differences in the trans-stilbene conversions and in the dibenzyl yields between Runs 1, 4, and 5 give the baseline increments caused by the α-Fe-catalyzed hydrogenation of trans-

stilbene, and comparison of Runs 1, 7, and 8 gives the corresponding increments for the $Fe_{1-x}S$-catalyzed reactions.

Comparison of Runs 9, 11, and 14 (Table 3) clearly shows that intermolecular hydrogen transfer from tetralin to trans-stilbene is greatly promoted by α-Fe and $Fe_{1-x}S$. Dibenzyl yield increments at 6.0 MPa of hydrogen in the presence of α-Fe and $Fe_{1-x}S$ were 45 and 63%, respectively. The expected increment caused by catalytic incorporation of molecular hydrogen is not more than 25% for α-Fe (compare Runs 2 and 5) and 26% for $Fe_{1-x}S$ (compare Runs 2 and 8). Thus, in the system of H_2-tetralin-Fe catalyst, trans-stilbene could be hydrogenated predominantly on the catalytic cycle.

Ogawa and coworkers have shown that the catalytic activity of $Fe_{1-x}S$ highly depends on H_2S pressure in the hydrocracking of diphenylmethane without solvent at 450°C[9]. At low pressures of H_2S, $Fe_{1-x}S$ is converted to FeS which is less active than $Fe_{1-x}S$. However, our results clearly show that both of α-Fe and $Fe_{1-x}S$ promote tetralin-mediated hydrogen transfer from gaseous hydrogen. Since dry coal liquefaction is not so feasible, catalyzed solvent-mediated hydrogen transfer could be a key reaction in coal liquefaction.

Reactant dependent catalytic activities of Fe compounds

As Table 4 shows, the catalytic activities of Fe compounds in the hydrogenolysis of 9-BP decreased in the order: α-Fe > $Fe_{1-x}S$ > Fe_2O_3. The apparent catalytic activity of Fe_2O_3 can be ascribed to that of α-Fe partly produced in the deoxygenative reduction of Fe_2O_3 during the course of the reaction. The above order is different from that for the hydrogenolysis of trans-stilbene at 380°C. Almost the same product distributions with α-Fe and $Fe_{1-x}S$, and negligible surface area changes of both the catalysts suggest the catalyst dependent adsorption behavior of 9-BP, i.e., 9-BP is selectively adsorbed at its 9,10-position on α-Fe, while 9-BP is competitively adsorbed at its 1,2-, 3,4-, 5,6-, 7,8-, 9,10- positions on $Fe_{1-x}S$ [10]. For radical **A** in Scheme 1, a benzyl radical release is energetically more favorable than that of a hydrogen atom, promoting the hydrogenolysis of 9-BP. On the other hand, reversible hydrogen atom elimination predominates over subsequent hydrogenation for radicals **B** ∿ **F**, which decreases the apparent conversion of 9-BP.

These data suggest that the regioselectivity of 9-BP adsorption is lost on $Fe_{1-x}S$ compared to α-Fe, and that radicals **B** ∿ **F** are competitively formed against radical **A**.

The lack of such catalyst dependence of trans-stilbene hydrogenolysis can be ascribed to the stronger adsorbing ability of the olefinic moiety in trans-stilbene.

Figure 2 shows the relationship between the 9-BP conversion and the yield of naphthalene derived from tetralin. A good linear correlation suggests that the bimolecular hydrogen transfer from tetralin to 9-BP is promoted by α-Fe and $Fe_{1-x}S$.

CONCLUSION

We have shown that in the noncatalytic and Fe-catalyzed hydrogenolyses of trans-stilbene and 9-benzylphenanthrene, radical mechanism operates, and that bimolecular hydrogen transfer from solvents is promoted by α-Fe and $Fe_{1-x}S$ without overhydrogenation of aromatic nuclei.

REFERENCES

1. Y. Kamiya, S. Futamura, T. Mizuki, M. Kajioka, and K. Koshi, Fuel Proc. Technol., 14, 79 (1986).
2. Y. Kamiya, E. Ogata, K. Goto, and T. Nomi, Fuel, 65, 586 (1986).
3. D. F. McMillen, R. Malhotra, S.-J. Chang, W. C. Ogier, S. E. Nigenda, and R. H. Fleming, Fuel, 66, 1611 (1987).
4. S. Futamura, S. Koyanagi, and Y. Kamiya, Fuel, 67, 1436 (1988).
5. S. Futamura, K. Fujimoto, and Y. Kamiya, Bull. Chem. Soc. Jpn., 63, 2564 (1990).
6. S. Futamura, S. Koyanagi, and Y. Kamiya, J. Fuel Soc. Jpn., in press.
7. K. Tanabe and H. Hattori, Sekiyu Gakkaishi, 29, 280 (1986).
8. M. Tiecco and L. Testaferri in 'Reactive Intermediates', Vol. 3 (Ed. R. A. Abramovitch), Plenum Press, New York, 1983, p. 88.
9. T. Ogawa, V. I. Stenberg, and P. A. Montano, Fuel, 63, 1660 (1984).
10. M. Minabe and K. Nakada, Bull. Chem. Soc. Jpn., 58, 1962 (1985).

Table 1 Selectivities of Benzylic Radicals toward Addition and Hydrogen Abstraction.

Reaction	Solvent	Catalyst	Radical	Addition/H abstraction
1	Tetralin	None	Benzyl	0.015 [b]
1	1-MN	None	Benzyl	0.033 [b]
2	Tetralin	Fe_2O_3	Benzyl	∿0
2	Tetralin	α-Fe	Benzyl	0.057 [c]
2	Tetralin	$Fe_{1-x}S$	Benzyl	∿0
2	1-MN	Fe_2O_3	Benzyl	∿0
2	1-MN	α-Fe	Benzyl	0.14 [d]
2	1-MN	$Fe_{1-x}S$	Benzyl	∿0
3	Tetralin	None	[a]	∿0
3	Tetralin	α-Fe	[a]	0.21 [e]
3	Tetralin	$Fe_{1-x}S$	[a]	∿0

Reaction 1: hydrogenolysis of DNM in the presence of dibenzyl (0.5-1.0 mol equiv.) under hydrogen (2.0 MPa) at 460°C.
Reaction 2: hydrogenolysis of 9-BP in the presence of Fe catalyst (0.5 mol equiv.) under hydrogen (6.0 MPa) at 450°C.
Reaction 3: hydrogenolysis of trans-stilbene in the presence of Fe catalyst under hydrogen (1.0 MPa) at 380°C.
a: 1,2-Diphenylethyl. b: [1-BN]/[toluene]; c: [BTHN]/[toluene]; d: [BMN]/[toluene]; e: ([DETN]+[BTHN])/[dibenzyl].

Table 2 Fe-Catalyzed Hydrogenolysis of trans-Stilbene in 1-MN.

Run	Gas phase (MPa)	Cat.	t-ST conv. (mol%)	Products(Selectivity/mol%) c-ST	Dibenzyl	Toluene
1	N_2(1.0)	None	6.9	43	44	tr.
2	H_2(1.0)	None	10	38	50	—
3	N_2(1.0)	α-Fe	7.4	53	36	3.6
4	H_2(1.0)	α-Fe	26	13	62	3.8
5	H_2(6.0)	α-Fe	44	6.6	68	3.0
6	N_2(1.0)	$Fe_{1-x}S$	7.9	48	37	3.8
7	H_2(1.0)	$Fe_{1-x}S$	21	18	71	3.3
8	H_2(6.0)	$Fe_{1-x}S$	40	7.7	78	2.9

trans-Stilbene 3 g (16.7 mmol), 1-MN 15 g (106 mmol), Fe catalyst 3.75 mmol of Fe, reaction temperature 380°C, reaction time 30 min.
c- and t-ST = cis- and trans-Stilbenes. tr.=trace.

Table 3 Fe-Catalyzed Hydrogenolysis of trans-Stilbene in Tetralin.

Run	Gas phase (MPa)	Cat.	t-ST conv. (mol%)	Products(Selectivity/mol%) c-ST	Dibenzyl	Toluene	BTHN	DETN
9	N_2(1.0)	None	24	18	39	—	—	—
10	H_2(1.0)	None	27	15	41	—	—	—
11	N_2(1.0)	α-Fe	41	8.3	51	5.6	4.1	5.6
12	H_2(1.0)	α-Fe	64	4.2	59	6.1	3.9	5.5
13	H_2(6.0)	α-Fe	95	—	71	9.5	7.8	6.4
14	N_2(1.0)	$Fe_{1-x}S$	51	6.7	69	—	—	—
15	H_2(1.0)	$Fe_{1-x}S$	61	4.6	70	2.1	—	—
16	H_2(6.0)	$Fe_{1-x}S$	91	—	81	1.6	—	—

trans-Stilbene 3 g (16.7 mmol), tetralin 15 ml (110 mmol), Fe catalyst 3.75 mmol of Fe, reaction temperature 380°C, reaction time 30 min.
c- and t-ST = cis- and trans-Stilbenes.

Table 4 Additive Effect of Fe Catalysts on the Hydrogenolysis of 9-BP in Tetralin (Tet).

Catalyst	Conv. of 9-BP	Selectivities of Tol	BTHN	Phen	DHP
None	4%	100%	nd.	80%	3%
Fe_2O_3	20	90	tr.	83	10
α-Fe	72	87	5%	92	8
$Fe_{1-x}S$	39	87	tr.	82	10

9-BP 7.5 mmol, Tet 75 mmol, Fe catalyst 3.75 mmol of Fe, initial hydrogen pressure 6.0 MPa, 450°C, 30 min.
Tol=Toluene, Phen=Phenanthrene.
Nd. and tr. denote 'not detected' and 'traces', respectively.

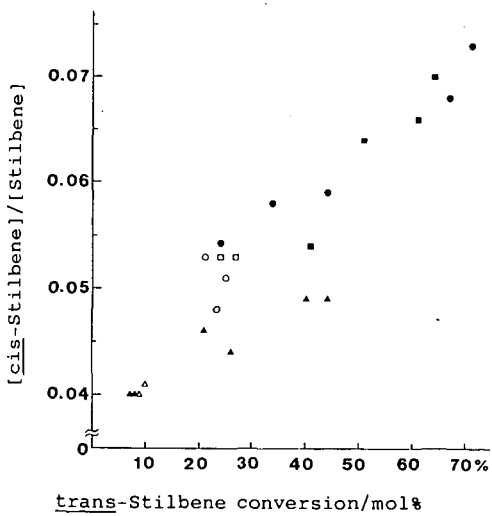

Fig. 1 Correlation of the trans-Stilbene Conversion and the cis-Stilbene Content in the Hydrogenolysis of trans-Stilbene at 380°C. ● DHP-1-MN, Fe cat. ○ DHP-1-MN, no cat. ■ Tetralin, Fe cat. □ Tetralin, no cat. ▲ 1-MN, Fe cat. △ 1-MN, no cat.

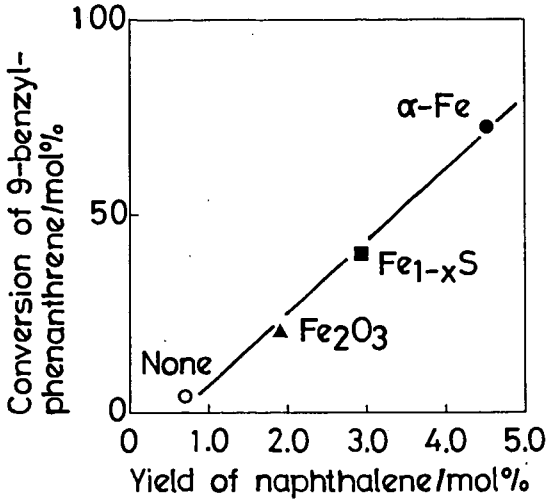

Fig. 2 Relationship between the 9-BP Conversion and the Naphthalene Yield in the Hydrogenolysis of 9-BP in Tetralin. 9-BP 7.5 mmol, tetralin 75 mmol, initial hydrogen pressure 6.0 MPa, 450°C, 30 min.

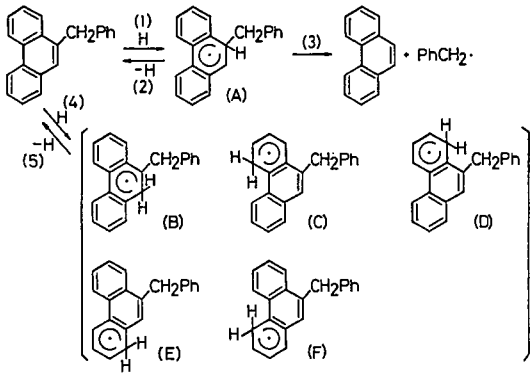

Scheme 1 Mechanism for the Hydrogenolysis of 9-BP.

A THEORETICAL AND EXPERIMENTAL STUDY OF UNIMOLECULAR AND BIMOLECULAR RADICAL HYDROGEN TRANSFER REACTIONS

Tom Autrey, Gerald J. Gleicher, Donald M. Camaioni, Kim F. Ferris and James A. Franz

Pacific Northwest Laboratory[a]
P. O. Box 999 Richland, WA 99352

Keywords: Radical Hydrogen Transfer, RHT, AM1, Semiempirical Quantum Chemical Calculations

INTRODUCTION

The bimolecular transfer of hydrogen atom from an organic radical to an olefin or aromatic system, known as the radical hydrogen transfer (RHT) reaction, has been proposed as an important pathway for hydrogen transfer in liquid phase pyrolysis reactions and as an important pathway for selective bond cleavage in coal liquefaction.[1-5]

Experimental observation of the RHT reaction was apparently first reported by Metzger,[6] followed almost simultaneously by a study of Billmers et al.[7] In Metzger's work, the radical addition of cyclohexane to dimethylfumarate and methyl cinnamate at 250 to 400 °C was examined:

$$\underset{\mathbf{1}}{R^1\text{-}CH{=}CH\text{-}R^2} + \underset{\mathbf{2}}{c\text{-}C_6H_{12}} \;\text{---->}\; \underset{\mathbf{3}}{R^1\text{-}CH_2CH(C_6H_{11})R^2} + \underset{\mathbf{4}}{R^1CH(C_6H_{11})CH_2R^2} + \underset{\mathbf{5}}{\text{Cyclohexene}} + \underset{\mathbf{6}}{R^1\text{-}CH_2CH_2\text{-}R^2} \qquad (1)$$

(a) $R^1 = R^2 = COOCH_3$ (b) $R^1 = Ph$, $R^2 = COOCH_3$

The reaction, which exhibits a chain length of 100, is initiated by hydrogen transfer from cyclohexane to **1**. Reversible addition of cyclohexyl radical to **1** followed by abstraction from **2** leads to **3** and **4**. The formation of reduced product **6** is suggested to occur via the RHT reaction of cyclohexyl radical with **1**:

$$c\text{-}C_6H_{11}(\cdot) + \mathbf{1} \;\text{---->}\; \mathbf{5} + \underset{\mathbf{7}}{R^1\text{-}CH_2CH(\cdot)\text{-}R^2} \qquad (2)$$

(a) Operated for the U. S. Department of Energy by Battelle Memorial Institute.

Chain propagation occurs by reaction of **7** with cyclohexane to produce the RHT product, **6**:

$$\mathbf{7} + c\text{-}C_6H_{12} \longrightarrow \mathbf{6} + c\text{-}C_6H_{11}(\cdot) \qquad (3)$$

Chain propagation also occurs by abstraction of hydrogen atom from cyclohexane by the adducts of cyclohexyl radical to 1. An alternate mechanism for formation of 6, the scission of hydrogen atom from cyclohexyl radical and addition of the H atom to 1, leading to **6**, was ruled out, based on the observed first order dependence on 1 for the formation of 6. Unfortunately, hydrogen (H_2), which would have revealed the production of H•, was not analyzed in the reaction mixture. From the chain length of the reaction, the yield of 6 produced in the initiation step was suggested to be insignificant.

Metzger's results[6] are indeed surprising, since they imply a very low barrier for the RHT reaction. The rate of β-scission of hydrogen from cyclohexyl radical is given by $k_\beta = 5 \times 10^{13} \exp(-36000/RT)$, or $k_\beta = 1.2 \times 10^2$ $\underline{M}^{-1}s^{-1}$ at 400 °C. For RHT transfer of hydrogen to the olefin, to occur 10 times faster than β-scission of free hydrogen at the 5×10^{-3} $\underline{M}$ concentrations of 1 employed, an RHT barrier of only 9.7 kcal/mole would be required. For RHT to occur 100 times faster than free hydrogen atom production requires an RHT barrier of only 6.6 kcal/mole. This assumes a typical bimolecular A-factor of $10^{8.5}$ $\underline{M}^{-1}s^{-1}$ for RHT.

The study of Billmers et al.,[7] examined the transfer of hydrogen from 9,10-dihydroanthracene (ANH2) to 2-ethylanthracene (EAN) to form 9,10-dihydro-2-ethylanthracene (EAH2) and anthracene (AN). The kinetic order of the non-chain reaction and the observed Arrhenius dependence were consistent with a mechanism involving rate-determining reverse radical disproportionation (RRD) (eq. 4). Other key steps include production of EANH(•) by RHT, eq 5, and formation of the product EANH2 is by disproportionation (eq. 8) or abstraction (eq. 9).

$$\mathrm{ANH2} + \mathrm{EAN} \rightleftharpoons \mathrm{ANH}(\cdot) + \mathrm{EANH}(\cdot) \qquad (4)$$

$$\mathrm{ANH}(\cdot) + \mathrm{EAN} \longrightarrow \mathrm{AN} + \mathrm{EANH}(\cdot) \qquad (5)$$

$$\mathrm{ANH}(\cdot) + \mathrm{EANH}(\cdot) \longrightarrow \mathrm{AN} + \mathrm{EANH2} \qquad (6)$$

$$2\ \mathrm{ANH}(\cdot) \longrightarrow \mathrm{ANH2} + \mathrm{AN} \qquad (7)$$

$$2\ \mathrm{EANH}(\cdot) \longrightarrow \mathrm{EAN} + \mathrm{EANH2} \qquad (8)$$

$$\mathrm{EANH}(\cdot) + \mathrm{ANH2} \longrightarrow \mathrm{EANH2} + \mathrm{ANH}(\cdot) \qquad (9)$$

Billmers et al.[7] found that the rate of formation of EANH2 was decreased by increasing the ratio AN/ANH2 at fixed concentrations of ANH2 and EAN in the initial reaction mixture. This is presumed to be due to the reverse of eq. 5. From an analysis of the reduction of the rate of production of EANH2 with increasing AN/ANH2, k_{-5} was estimated to be 120 $\underline{M}^{-1}s^{-1}$ at 350°C, or E_{-5} = 18.3 kcal/mole.

In a related study of hydrogen transfer between 9,10-dihydrophenanthrene and anthracene,[8] computer modeling of the observed kinetics led to an "RHT" rate constant $k = 7.5 \times 10^3\ \underline{M}^{-1}s^{-1}$ at 350 °C, corresponding to $E_a = 13.3$ kcal/mole. If correct, this is a surprisingly low activation barrier, since the barrier was lowered fully as much as the enthalpy change for the reaction compared to the thermoneutral transfer between anthracenes, -5 kcal/mole. This corresponds to an Evans-Polanyi factor of ca. 1 for the reaction, whereas hydrogen atom metathesis reactions usually exhibit Evans-Polanyi factors of 0.5 or less. The authors point out that the reaction kinetics are suggested to be equally well represented by a 3-step sequence of addition of hydrophenanthrenyl radical to anthracene, intramolecular hydrogen atom transfer, and radical scission to give phenanthrene and 9-hydroanthracenyl radical, without postulating the unconventional RHT reaction.

In recent work,[9] we examined the intramolecular RHT reaction of the 2-(2-phenylethyl)cyclohexadienyl radical, **8**, (eq. 10). Intramolecular hydrogen shift from the cyclohexadienyl ring to the <u>ipso</u> position of the phenyl ring, followed by β-scission would have given benzene and ethylbenzene as products.

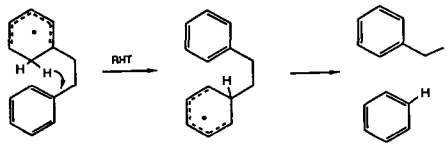

(10)

8

Competing with this reaction is β-scission to give benzyl radical and isotoluene, or hydrogen loss to give bibenzyl. No detectable RHT occurred at 235 °C for this near-thermoneutral reaction. The ratio of H• loss (or the isoenergetic β-scission) to RHT, determined by product detection limits, was greater than 100:1. The predicted A-factor for intramolecular RHT, $A_1 = 10^{10.8}$ $\underline{M}^{-1}s^{-1}$, and the predicted rate constant for H atom loss, $7.7 \times 10^2\ \underline{M}^{-1}s^{-1}$, results in a minimum barrier for the intramolecular RHT reaction of 23 kcal/mole for the slightly endergonic hydrogen transfer ($\Delta H° = 0.5$ kcal/mole). In research currently under way, we are preparing exothermic analogues of intramolecular RHT to attempt to unambiguously observe, in a stereochemically restricted system, a "true" RHT reaction with no possibility of free H atom involvement.

In summary, studies to date suggest a barrier for thermoneutral hydrogen transfer in the RHT reaction between aromatic systems of ca. 18 kcal/mole. None of the studies of RHT or equivalent mechanisms have attempted to directly observe H_2, and direct determination of Arrhenius parameters and a detailed examination of the pathway of the hydrogen transfer process remains to be carried out.

To better understand the structural and energetic aspects of RHT, we have carried out a semiempirical molecular orbital study of bimolecular and intramolecular RHT reactions for a variety of aromatic systems. We also examined in detail the energetics of hydrogen transfer between ethyl radical

and ethylene via RHT, an addition/metathesis/scission pathway, and a hybrid "concerted" pathway.

RESULTS AND DISCUSSION

AM1/RHF[10] transition states were located for hydrogen transfer reactions from the cyclohexadienyl radical to benzene, the ipso position of toluene, the 1-position of naphthalene, and the 9-position of anthracene. In addition, RHT transition states were located for thermoneutral hydrogen transfer between naphthalenes (1-positions) and anthracenes (9-positions), and the thermoneutral RHT reaction between ethyl radical and ethylene was examined. In each case, the hydrogen is caused to migrate to the olefinic or aromatic carbon.

Table I lists activation barriers for thermoneutral transfer of hydrogen between pairs of benzene, naphthalene, and anthracene rings. AM1 calculations often result in barriers that are higher than experimental values for reactions involving stretched bonds in open-shell systems. However, hydrogen abstraction barriers predicted by AM1 are often in good agreement with experimental values. For example, AM1/RHF predicts a barrier of 18 kcal/mole for the symmetric hydrogen abstraction reaction from cyclohexadiene by the cyclohexadienyl radical, in good agreement with thermoneutral abstraction reactions of alkyl radicals from alkanes, which, in the absence of steric effects, exhibit barriers of ca. 14 kcal/mole.[11] Thus, it was surprising to find that the nominally similar RHT reactions gave substantially higher barriers. Table II presents results for transfer of hydrogen from cyclohexadienyl to aromatic systems. For purposes of comparison, Table III gives calculated and experimental values of C-H bond dissociation energies and activation barriers for hydrogen loss from hydroaryl and ethyl radicals. Although a totally satisfactory calibration of the AM1 method for the present category of reactions is not possible, the overestimations of C-H bond dissociation energies for hydroaryl radicals suggest that the calculated AM1/RHF RHT barriers are 25 to 50% higher than the actual values. Finally, in Table IV, barriers for intramolecular RHT reactions are presented for 2, 3, and 4-carbon bridging linkages.

Although the AM1 method has obvious limitations, some interesting observations are possible: (1) RHT barriers for thermoneutral hydrogen transfer reactions are predicted to be closely spaced, with a slight increase in barrier going from benzene to anthracene. Thus, the hydroaryl radicals that have the strongest C-H bonds correspond to the aromatic systems best able to stabilize the liberated hydrogen atoms. (2) The predicted barriers drop dramatically as the hydrogen transfer reactions become more exothermic, such that the barrier for transfer between cyclohexadienyl and anthracene is low enough for the reaction to be observable at moderate (< ca. 250°C) temperatures. The dramatic drop is reminiscent of the drop in barrier for hydrophenanthrenyl H_2 transfer to anthracene vs. thermoneutral transfer between anthracenes.[7] (3) In every case, the activation barrier for RHT is below that of free hydrogen atom production. Finally, (4) intramolecular RHT with 2-, 3- and 4-carbon bridges between the two benzenoid aromatic systems results in closely spaced activation barriers, higher by 2 to 4 kcal/mole than thermoneutral intermolecular RHT reactions. The question becomes whether RHT

will compete with free H• reaction or with the more conventional addition/ transfer/scission pathway for hydrogen transfer.

The Addition/Transfer/Scission Pathway

The AM1/RHF barrier for the RHT reaction between ethyl radical and ethylene, 40.0 kcal/mole, is found to be less than the barrier for hydrogen scission, 52 kcal/mole, but remains a high energy pathway. To examine an alternative pathway to RHT, that of addition, metathesis, and scission, we examined the reaction of ethyl + ethylene. The results of a map of several possible surfaces is depicted in Figure 1. Throughout the calculation, the C4-C3 and C1-C2 bonds were constrained to be planar. The lower path shows the energy profile for addition of ethyl to ethylene to yield an eclipsed butyl radical (the trans conformer is calculated to be 5 kcal/mole more stable). The upper surface in Figure 1 shows the energy as a function of the C2-C3 distance, with equal C1-H-C4 distances at the position of maximum energy, corresponding to the energy barrier for hydrogen migration from C1 to C4. The energy gap labeled A shows the barrier for 1,4-hydrogen transfer, which is less than that of β-scission. The energy gap B corresponds to RHT via a cyclic transition state structure. It is calculated to be 1 kcal/mole lower than the acyclic transition state structure in which C2 and C3 do not interact. The energy gap C corresponds to H atom elimination. It is energetically the least favored reaction path. This calculation suggests that conventional addition/ transfer/scission pathways may be favored by enthalpy over the direct RHT path, and that the RHT barrier is reduced (B in Figure 1) by the interaction of the two pi systems. Also, the position of the upper curve between 1.5 to 1.8 Å below the β-scission transition state energy raises the possibility that the addition/transfer/scission pathway might become concerted at suitably high temperatures. Further work to examine similar effects with RHT between aromatic systems is underway.

Finally, the lower predicted barriers for addition/metathesis/scission in this system may mean that intramolecular RHT reactions that are stereochemically precluded from the addition/metathesis pathways (and are true "RHT" reactions) may actually be significantly higher energy pathways. We are currently synthesizing model intramolecular RHT systems to observe exothermic RHT reactions to attempt to unambiguously observe and characterize RHT reactions.

REFERENCES

1) D. F. McMillen, W. C. Ogier, S.-J. Chang, R. H. Fleming and R. Malhotra, Proc. Intl. Conf. on Coal Science, Pittsburgh, PA 15-19 August, 1983, p. 199.

2) D. F. McMillen, R. Malhotra, S.-J. Chang, and S. E. Nigenda, Am. Chem. Soc., Div. Fuel Chem Preprints, 1985, 30(4), 297.

3) D. F. McMillen and R. Malhotra, Proc. 1987 Intl Conf. Coal Science, Maastricht, The Netherlands, 26-30 October, 1987.

4) D. F. McMillen, R. Malhotra, S.-J. Chang, W. C. Ogier, E. Nigenda and R. H. Fleming, Fuel, 1987, 66, 1611.

5) D. F. McMillen, R. Malhotra, G. P. Hum, and S.-J. Chang, Energy & Fuels, 1987, 1(2), 193.

6) J. O. Metzger, Angew. Chem. Int. Ed. Engl. 1986, 25, 80.

7) R. Billmers, L. L. Griffith and S. E. Stein, J. Phys. Chem. 1986, 90, 517.

8) R. Billmers, R. L. Brown, and S. E. Stein, Int. J. Chem. Kinetics, 1989, 21, 375.

9) Tom Autrey and James A. Franz "A Search for the Radical Hydrogen Transfer Pathway in Coal Liquefaction," Prepr. Fuel Div. Am. Chem. Soc. 1990, 35(2), 381.

10) MOPAC Molecular Orbital Program, Quantum Chemistry Program Exchange, Program No. 455, version 5.0, Quantum Chemistry Program Exchange, Department of Chemistry, Indiana University.

11) J. A. Franz, M. S. Alnajjar, R. D. Barrows, D. A. Kaisaki, D. M. Camaioni, and N. K. Suleman, J. Org. Chem. 1986, 51, 1446.

ACKNOWLEDGEMENT

The authors thank Dr. J. O. Metzger for useful discussions. This work was supported by the Office of Basic Energy Sciences, U. S. Department of Energy, under contract DE-AC06-76RLO 1830.

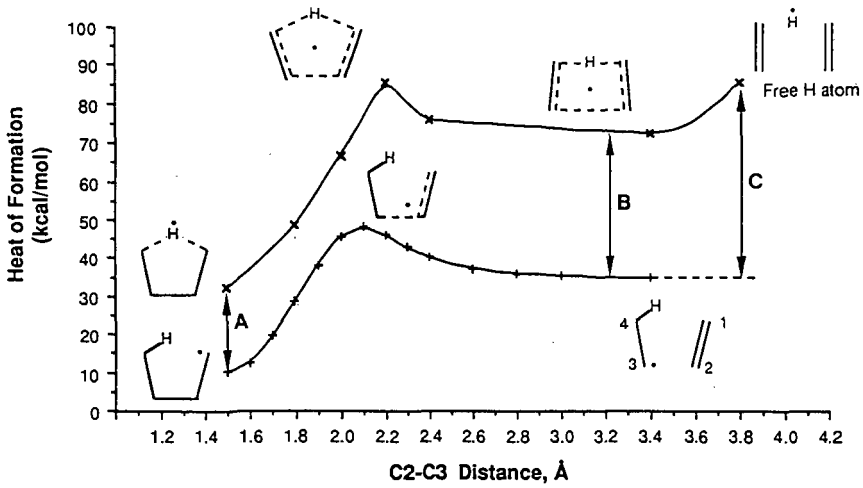

Figure 1. Reaction paths for ethyl radical + ethylene calculated with AM1/RHF. A: Barrier for 1,4-hydrogen atom shift from eclipsed butyl radical (trans-butyl radical conformation is 5 kcal/mole lower in energy). B: Barrier for radical hydrogen transfer (RHT). The Z-shaped or alicyclic TS structure with non-interacting termini is calculated to be 1 kcal/mole higher in energy. C: Barrier for H• atom elimination-addition reaction.

Table I. AM1/RHF Barriers for Thermoneutral Hydrogen Transfer From Hydroaryl Radicals to Aromatic Rings and the Ethyl + Ethylene Reaction

Reaction	$\Delta H^{\ddagger}$, kcal/mole
Cyclohexadienyl + Benzene	32.7
1-Hydronaphthyl + Naphthalene	34.5
9-Hydroanthracenyl + Anthracene	36.6
Ethyl + Ethylene	40.0

Table II. AM1/RHF Barriers for Hydrogen Transfer From Cyclohexadienyl Radical to Aromatic Rings

Reaction	$\Delta H^{\ddagger}$, kcal/mole[a]	$\Delta H°$, kcal/mole[b]
Cyclohexadienyl + Toluene (*ipso* position)	36.4	0.4
Cyclohexadienyl + Benzene	32.7	0.0
Cyclohexadienyl + Naphthalene	25.6	-7.5
Cyclohexadienyl + Anthracene	16.4	-18.8

[a]AM1/RHF calculation
[b]Experimental heat of reaction for the hydrogen atom transfer reaction

Table III. Hydrogen Atom Scission from Hydroaryl and Ethyl Radicals

Reaction	$\Delta H^{\ddagger}$, kcal/mole[a]		$\Delta H°$, kcal/mole[b]	
	expt	calc	expt	calc
Cyclohexadienyl ---> benzene + H	28.7	44	25.7	34.8
1-Hydronaphthyl ---> naphthalene + H	37	--	35	39.9
9-Hydroanthracenyl ---> Anthracene + H	45	58	43	50.3
Ethyl ---> Ethylene + H	38	52	35.6	49.4

[a]AM1/RHF calculation
[b]Experimental heat of reaction for the hydrogen atom transfer reaction

Table IV. AM1/RHF Barriers for Intramolecular RHT Reactions[a]

Ground State Radical	$\Delta H^{\ddagger}$, kcal/mole
2-(2-phenylethyl)cyclohexadienyl, 8	38.2
2-(2-phenylpropyl)cyclohexadienyl	40.8
2-(2-phenylbutyl)cyclohexadienyl	39.4

[a]The hydrogen is transferred to the *ipso* position of the appended ring. See, e.g., eq. 10

THERMOLYSIS OF SURFACE-IMMOBILIZED PHENETHYL PHENYL ETHER

P. F. Britt, A. C. Buchanan, III, and V. M. Hitsman
Chemistry Division
Oak Ridge National Laboratory
P. O. Box 2008
Oak Ridge, TN 37831-6197

ABSTRACT

Our research has focused on modeling the constraints on free-radical reactions that might be imposed in coal as a consequence of its cross-linked macromolecular structure by covalently bonding diphenylalkanes to an inert silica surface. A surface-immobilized phenethyl phenyl ether (≈$PhCH_2CH_2OPh$, or ≈PPE-3) has been prepared as a model for ether linkages in lignin by the condensation of *p*-$HOPhCH_2CH_2OPh$ with the surface hydroxyls of a high purity fumed silica. Thermolysis of ≈PPE-3 at saturation surface coverage at 375 °C produces ≈$PhCH{=}CH_2$ and PhOH as the major products which are consistent with the proposed free-radical chain mechanism for the decomposition of fluid-phase phenethyl phenyl ether. However, significant quantities of ≈$PhCH_3$ and PhCHO (ca. 18% of the products) are produced indicating the emergence of a new reaction pathway on the surface. The mechanism for the decomposition of ≈PPE-3 will be discussed in light of this new information.

Keywords: thermolysis, model compounds, mechanisms, restricted diffusion

INTRODUCTION

Attempts to probe the fundamental chemical reactions responsible for the thermal conversion of coal into liquid products has been hampered by the complex heterogeneous macromolecular structure of coal. Our efforts have focused on modelling the impact of restricted diffusional mobility on the thermal reactivity of coal by covalently bonding model compounds representing structural features in coal to an inert silica surface. Thus far, our research has focused on the thermally induced free radical decomposition of α, ω–diphenylalkanes ($Ph(CH_2)_nPh$ where n=0-4) at 345-400 °C.[1-5] The results have shown that significant perturbations can occur in free radical reaction mechanisms which can alter reaction rates and product selectivities compared to the corresponding fluid phase behavior. We now have initiated a study on the the effects of restricted mass transport on the thermal decomposition of ether bridges which are prevalent in low rank coals and lignites. Although ether linkages are more thermally labile than the corresponding carbon analogues, it has been observed that

under liquefaction conditions optimized for bituminous coals, low rank coals and lignites afford low liquefaction yields. [6] It has been proposed that cross-linking reactions associated with oxygen functional groups (-OH, $-OCH_3$, and -COOH) are responsible for the low yields.[6,7] In order to better understand the chemical reactions leading to retrograde processes, the effects of restricted diffusion of the thermolysis of surface-attached phenethyl phenyl ether (≈$PhCH_2CH_2OPh$, ≈PPE-3) has been studied. Although the thermal decomposition of phenethyl phenyl ether (PPE) has been previously studied in the gas phase,[8,9a] liquid phase,[9a] and in the presence of tetralin,[8,10] hydrogen,[10,11] and metal catalysts,[11] our results show that a previously undetected free radical decomposition pathway is available for the thermal cracking of ≈PPE.

EXPERIMENTAL

Surface-immobilized phenethyl phenyl ether (≈PPE-3) was prepared at saturation surface coverage by the condensation of p-$HOC_6H_4CH_2CH_2OPh$ (2.25 equiv) with the surface hydroxyl groups of a high purity fumed amorphous silica (Cab-O-Sil, grade M-5, Cabot Corp., 200 $m^2\ g^{-1}$, ca. 4.5 OH nm^{-2}) at 222 °C for 30 min as previously described.[1-3] The excess phenol was sublimed from the sample by heating for 70 min at 254 °C under vacuum (3×10^{-3} Torr). The surface-attached PPE was liberated from the silica as the phenol by a base hydrolysis procedure, silylated to the trimethylsilyl ether, and analyzed by GC and GC/MS. The surface coverage was 0.562 mmol of ≈PPE-3 per gram of derivatized silica with the purity of recovered phenol >99.9% by GC. The starting phenol, p-$HOC_6H_4CH_2CH_2OPh$, was prepared in four steps from p-$HOC_6H_4CH_2CH_2OH$ by selective benzylation of the phenol with K_2CO_3 and $PhCH_2Br$ in dimethyl formamide, conversion of the alcohol to the tosylate with tosyl chloride in pyridine, base catalyzed alkylation of phenol with the tosylate using K_2CO_3 and PhOH in dimethyl formamide, and debenzylation by catalytic hydrogenolysis using Pd/C in HOAc with 10 % H_2SO_4. Repeated crystallizations from benzene/hexanes afforded p-$HOC_6H_4CH_2CH_2OPh$ in >99.9% purity by GC.

Thermolysis of ≈PPE-3 was preformed at 375 ± 1 °C in T-shaped tubes sealed under high vacuum (ca. 10^{-6} Torr). The volatile products were collected as they formed in a cold trap (77 K), analyzed by GC and GC/MS, and quantitated by the use of internal standards with measured GC detector response factors. The surface-attached products were removed from the silica as the corresponding phenols by a base hydrolysis procedure, silylated to the trimethylsilyl ethers, and analyzed as above. All products were identified by the mass spectra and whenever possible, by comparison with an authentic sample.

RESULTS AND DISCUSSION

Thermolysis of ≈PPE-3 at 375 °C has been studied at saturation coverage from ca. 1-17 % conversion. At low conversion, ≈PPE-3 cracks to from approximately equal amounts of phenol plus surface-attached styrene (≈PhCH=CH_2) as the major products (ca. 81 mol %) and benzaldehyde plus surface-attached toluene (≈$PhCH_3$) as minor products (ca. 18 mol %). A trace amount of surface-attached ethylbenzene (≈$PhCH_2CH_3$, ca. 1.5 mol %) was also detected. The conversion dependence of the products is shown in Figure 1.

$$\approx PhCH_2CH_2OPh \rightarrow \approx PhCH{=}CH_2 + PhOH + \approx PhCH_2CH_3 \qquad (1)$$

$$\approx PhCH_3 + PhCHO$$

Thermolysis of phenethyl phenyl ether (PPE) in the gas or liquid phase at low conversions at 325-400 °C has been reported to yield PhOH and PhCH=CH_2 as

$$PhCH_2CH_2OPh \rightarrow PhCH{=}CH_2 + PhOH \qquad (2)$$

the major products (eq 2).[8,9] Although minor amounts of $PhCH_3$ and $PhCH_2CH_3$ have been detected, they were attributed to secondary decomposition of PhCH=CH_2.[8] However, benzaldehyde has not been reported from the thermal decomposition of PPE in the gas, liquid phase, or in the presence of hydrogen donors. In the thermolysis of ≈PPE-3, ≈$PhCH_3$ does not appear to be a secondary product formed at the expense of the surface-attached styrene as shown in Figure 1. The rate of decomposition of PPE in the liquid phase at 350-390 °C is similar to that of the carbon analogue 1,3-diphenylpropane ($Ph(CH_2)_3Ph$, DPP)[9] and can be accelerated by the addition of benzyl phenyl ether. Likewise, the rate of decomposition of ≈PPE-3 at 375 °C (8.3 % h^{-1}) is similar to that of surface-attached $Ph(CH_2)_3Ph$ (≈DPP) at saturation coverage (7-9 % h^{-1}).[2] Since the rates of conversion of DPP and ≈DPP are similar, surface-attachment does not perturb the initial reaction behavior in the decomposition of ≈PPE-3.

The cracking of PPE is proposed to proceed by a free radical chain decomposition reaction, although a minor contribution from a concerted retro-ene reaction can not be completely ruled out.[8] The decomposition reaction is initiated by homolysis of the weak C-O bond (bond dissociation energy estimated as ca. 63 kcal mol^{-1})[12] to form 2-phenylethyl and phenoxy radicals. The radical chain propagation steps are show in eq 3 and 4.

$$PhO^{\bullet} + PhCH_2CH_2OPh \rightarrow PhOH + Ph\dot{C}HCH_2OPh \qquad (3)$$

$$\mathrm{Ph\dot{C}HCH_2OPh} \rightarrow \mathrm{PhCH{=}CH_2} + \mathrm{PhO^{\bullet}} \qquad (4)$$

In the thermolysis of ≈PPE-3, a similar free radical decomposition reaction can be written to explain the formation of the products (eq 5-12). The reaction is initiated by the homolysis of the weak C-O bond. The resulting radicals can abstract hydrogen from ≈PPE-3 to form a surface-attached 1-phenoxy-2-phenyl-2-ethyl radical (**1**) which can undergo β-scission to yield surface-attached styrene and the chain carrying phenoxy radical.

$$\approx\mathrm{PhCH_2CH_2OPh} \rightarrow \approx\mathrm{PhCH_2CH_2^{\bullet}} + \mathrm{PhO^{\bullet}} \qquad (5)$$

$$\approx\mathrm{PhCH_2CH_2^{\bullet}} + \approx\mathrm{PhCH_2CH_2OPh} \rightarrow \approx\mathrm{PhCH_2CH_3} + \underset{\mathbf{1}}{\approx\mathrm{Ph\dot{C}HCH_2OPh}} \qquad (6)$$

$$\mathrm{PhO^{\bullet}} + \approx\mathrm{PhCH_2CH_2OPh} \rightarrow \mathrm{PhOH} + \mathbf{1} \qquad (7)$$

$$\mathbf{1} \rightarrow \approx\mathrm{PhCH{=}CH_2} + \mathrm{PhO^{\bullet}} \qquad (8)$$

Surface-attached $PhCH_3$ and gas phase PhCHO can be formed by a free radical chain process shown in steps 9-12. Hydrogen abstraction at the aliphatic site forms 1-phenoxy-2-phenyl-1-ethyl radical (**2**). Although radical **1** is estimated to be more stable than **2** by ca. 7 kcal mol^{-1},[12] there is precedence for the competitive formation of products from the thermodynamically less stable radical of tetralin (2-tetralyl radical)[13] and 1,4-diphenylbutane (1,4-diphenyl-2-butyl radical)[14] at these temperatures.

$$\mathrm{PhO^{\bullet}} + \approx\mathrm{PhCH_2CH_2OPh} \rightarrow \mathrm{PhOH} + \underset{\mathbf{2}}{\approx\mathrm{PhCH_2\dot{C}HOPh}} \qquad (9)$$

$$\approx\mathrm{PhCH_2\dot{C}HOPh} \rightarrow \approx\mathrm{PhCH_2\underset{Ph}{C}HO^{\bullet}} \qquad (10)$$

$$\approx\mathrm{PhCH_2\underset{Ph}{C}HO^{\bullet}} \rightarrow \approx\mathrm{PhCH_2^{\bullet}} + \mathrm{PhCHO} \qquad (11)$$

$$\approx\mathrm{PhCH_2^{\bullet}} + \approx\mathrm{PhCH_2CH_2OPh} \rightarrow \begin{cases} \approx\mathrm{PhCH_3} + \mathbf{1} & (12a) \\ \approx\mathrm{PhCH_3} + \mathbf{2} & (12b) \end{cases}$$

Radical **2** can undergo a 1,2-phenyl shift from oxygen to carbon (eq 10). Analogous intramolecular 1,2-phenyl shifts have been reported in the thermal decomposition of phenetole ($PhOCH_2CH_3$)[15] and anisole at 400 °C.[16] β-scission of the rearranged radical affords benzaldehyde and the chain carrying surface-attached benzyl radical. Formation of $\approx PhCH_3$ from C-C homolysis of ≈PPE, producing $\approx PhCH_2^{\bullet}$ and $PhOCH_2^{\bullet}$, is predicted to be small

since the C-C bond is estimated to be ca. 7 kcal mol^{-1} stronger than the corresponding C-O bond in PPE.[12] Furthermore, no anisole (from hydrogen abstraction by $PhOCH_2^{\bullet}$) or benzyl alcohol (from 1,2-phenyl shift and hydrogen abstraction by $PhCH_2O^{\bullet}$) was detected. Additional evidence for this previously undetected free radical pathway for the thermal degradation of PPE is found in the thermolysis of the $\approx PhOCH_2CH_2Ph$ (≈PPE-1) at 375 °C in which ≈PhOH and $PhCH{=}CH_2$ are formed as the major products (ca. 80 mol %) and ≈PhCHO and $PhCH_3$ are formed as the minor products (ca. 20 mol %) indicating a similar free radical chain mechanism as described in steps 5-12 is occurring.[17]

At this point, it is unclear whether the additional mechanistic steps (eq 9-12) required to rationalize the product distribution from the thermolysis of ≈PPE are a consequence of restricted diffusion, or an undetected reaction pathway in the thermolysis of liquid phase PPE. However, these reactions may explain the formation of toluene at low conversions and the formation of 1,2-diphenylethane and benzyl phenyl ether at higher conversions (termination reactions of $PhCH_2^{\bullet}$) which are reported for the thermal decomposition of PPE.[8] These steps may also be participating in the thermal decomposition of the homopolymers of 4-allylphenol and eugenol, which contain β-ether types linkages.[18,19] The previous mechanism for the decomposition of PPE (steps 3 and 4)[9] could not explain the formation of C_1-phenol and catechol (cresol, *m/e* 108 and 2-methoxy-4-methylphenol, *m/e* 138). However, by inclusion of reactions analogous to those in steps 9-12, a reasonable free radical chain pathway is available for formation of these products.

CONCLUSIONS

Covalent attachment of organic compounds to an inert silica surface has proven useful in modeling the effects of restricted substrate diffusion on free radical decomposition reactions which may occur in coal as a consequence of its cross-linked macromolecular structure. Thermolysis of surface-attached phenethyl phenyl ether, as a model for ether linkages in lignin, has shown a previously undetected pathway for the free radical chain decomposition of PPE which affords surface-attached toluene and gas phase benzaldehyde. Additional studies into the role of the radical rearrangements and the origin of this new decomposition pathway in the thermal decomposition of ≈PPE are currently under way.

ACKNOWLEDGEMENTS

This research was sponsored by the Division of Chemical Sciences, Office of Basic Energy Sciences, U. S. Department of Energy under contract DE-AC05-

840R21400 with Martin Marietta Energy Systems, Inc. VMH was supported by Oak Ridge Associated Universities Undergraduate Research Participation Program.

REFERENCES

1. Buchanan, III, A. C.; Dunstan, T. D. J.; Douglas, E. C.; Poutsma, M. L. *J. Am. Chem. Soc.* **1986**, *108*, 7703.
2. Buchanan, III, A. C.; Biggs, C. A. *J. Org. Chem.* **1989**, *54*, 517.
3. (a) Britt, P. F.; Buchanan, III, A. C.; Biggs, C. A. *Prep. Pap. -Am. Chem. Soc., Div. Fuel Chem.* **1989**, *34(2)*, 567. (b) Britt, P. F.; Buchanan, III, A. C., submitted for publication.
4. (a) Buchanan, III, A. C.; Britt, P. F.; Biggs, C. A. *Energy & Fuels* **1990**, *4*, 415. (b) Buchanan, III, A. C.; Britt, P. F.; Biggs, C. A. *Prep. Pap. -Am. Chem. Soc., Div. Fuel Chem.* **1989**, *34(4)*, 1317.
5. Buchanan, III, A. C.; Britt, P. F.; Poutsma, M. L. *Prep. Pap. -Am. Chem. Soc., Div. Fuel Chem.* **1990**, *35(1)*, 217.
6. Solomon, P. R.; Serio, M. A.; Deshpande, G. V.; Kroo, E.; Schobert, H.; Burgess, C. *Prep. Pap. -Am. Chem. Soc., Div. Fuel Chem.* **1989**, *34(3)*, 803.
7. Suuberg, E. M.; Lee, D.; Larsen, J. W. *Fuel* **1985**, *64*, 1668.
8. Klein, M. T.; Virk, P. S. *Ind. Eng. Chem. Fundam.* **1983**, *22*, 35.
9. (a) Gilbert, K. E.; Gajewski, J. J. *J. Org. Chem.* **1982**, *47*, 4899. (b) Gilbert, K. E. *J. Org. Chem.* **1984**, *49*, 6.
10. Korobkov, V. Y.; Grigorieva, E. N.; Bykov, V. I.; Senko, O. V.; Kalechitz, I. V. *Fuel* **1988**, *67*, 657.
11. Cassidy, P. J.; Jackson, W. R.; Larkins, F. P. *Fuel* **1983**, *62*, 1404.
12. (a) Benson, S. W. *Thermochemical Kinetics*, 2nd ed.; Wiley-Interscience: New York, 1976. (b) McMillen, D. F.; Golden, D. M. *Annu. Rev. Phys. Chem.* **1982**, *33*, 493.
13. (a) Franz, J. A.; Camaioni, D. M. *J. Org. Chem.* **1980**, *45*, 5247. (b) Benjamin, B. M.; Hagaman, E. W.; Raaen, V. F.; Collins, C. J. *Fuel* **1979**, *58*, 386.
14. Poutsma, M. L.; Dyer, C. W. *J. Org. Chem.* **1982**, *47*, 4903.
15. Collins, C. J.; Roark, W. H.; Raaen, V. F.; Benjamin, B. M. *J. Am. Chem. Soc.* **1979**, *101*, 1877.
16. Afifi, A. I.; Hindermann, J. P.; Chornet, E.; Overend, R. P. *Fuel* **1989**, *68*, 498.
17. Britt, P. F.; Fox, Jr., J. B., unpublished results.
18. McMillen, D. F.; Malhotra, R.; Serio, M. A. *Prep. Pap. -Am. Chem. Soc., Div. Fuel Chem.* **1990**, *35(2)*, 430.
19. These polymers presumable contain the analogous C-C-O linkage; However, conclusive evidence for the structures of the polymers is not currently available.

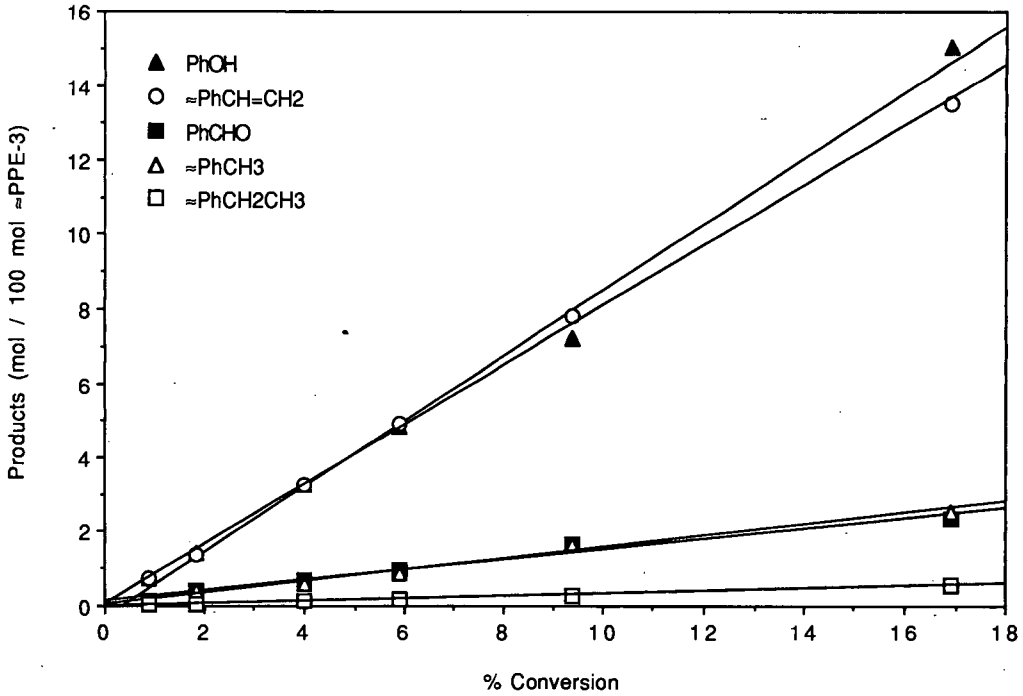

Figure 1. Product selectivities as a function of conversion for thermolysis of ≈PPE-3 at 375 °C at saturation coverage.

ACID-CATALYZED CRACKING OF SURFACE-IMMOBILIZED 1,3-DIPHENYLPROPANE IN DISPERSED SOLIDS

A. C. Buchanan, III, P. F. Britt, and C. A. Biggs
Chemistry Division
Oak Ridge National Laboratory
P.O. Box 2008
Oak Ridge, Tennessee 37831-6197

Keywords: acid catalysis, surface-immobilization, reaction mechanisms

ABSTRACT

We previously examined the impact of restricted mass transport on thermally induced, free-radical reaction pathways through the study of diarylalkanes covalently linked to an inert silica surface. We have now dispersed surface-attached 1,3-diphenylpropane (≈DPP) with a low acidity SiO_2-1% Al_2O_3 (surface area of 170 m^2/g) by solvent removal from a colloidal suspension of the components. Thermolysis studies at 310-375 °C under vacuum reveal a surprisingly efficient and selective acid-catalyzed cracking reaction for ≈DPP in the solid state. Even at 375 °C, acid-catalyzed aromatic dealkylation of ≈DPP dominates over the normal free-radical decomposition path. The results indicate that significant solid-state interactions between catalyst and substrate can occur, which has significant implications for the use of dispersed catalysts in coal liquefaction and hydropyrolysis.

INTRODUCTION

There has been considerable recent interest in the development of unsupported, highly dispersed catalysts for improving the conversion and product selectivity in coal liquefaction[1,2] and hydropyrolysis.[3] This includes the study of sulfate-promoted metal oxide catalysts, which are reported to have strong surface acidity.[2b] One potential advantage of such dispersed catalysts is the improved contact between the coal, solvent vehicle if present, hydrogen gas and the catalyst surface, particularly when catalysts with very small particle sizes can be generated. A significant mechanistic question still to be addressed is if, in the early stages of coal dissolution, significant activation of <u>solid</u> coal particles by <u>solid</u> catalyst can occur. In this paper we report initial results from model systems that begin to address this issue.

The cross-linked, network structure of coal may impose constraints on conventional reaction mechanisms as a consequence of restricted mass transport. We have examined this phenomenon for thermal reactions through the study of model compounds that are covalently anchored to an inert silica surface.[4-7] In our current study, we employ surface-immobilized 1,3-diphenylpropane (≈DPP) as the model compound. Thermolysis of ≈DPP has been studied in detail both by itself[5] and in the presence of co-attached aromatics.[6] The free-radical chain decomposition reaction that occurs for ≈DPP can be considered prototypical for

trimethylene (and longer) aliphatic groups that connect aromatic clusters in coal. In this study we examine the reactivity of solid ≈DPP dispersed in solid SiO_2-1% Al_2O_3 at 310-375 °C. Products that may be generated from potential acid-catalyzed reactions of ≈DPP will be easily distinguished from products of the thermal, free-radical reaction.

EXPERIMENTAL

Two-batches of ≈DPP were prepared with surface coverages of 0.532 and 0.320 mmol/g according to published procedures[5] by the reaction of p-$HOC_6H_4(CH_2)_3C_6H_5$ with the surface hydroxyls of a fumed silica (Cabosil M-5, Cabot Corp., 200 ± 25 m^2/g). The solid diluents, Aerosil 200 silica or Aerosil MOX 170 silica-alumina (Degussa Corp.), were dried in air at 200 °C for 4 h prior to use. The Aerosil 200 is an amorphous, fumed silica (200 ± 25 m^2/g; average primary particle size of 12 nm), while the Aerosil Mox 170 is a co-fumed oxide containing ca. 1% Al_2O_3 (170 ± 30 m^2/g; average primary particle size of 15 nm).[8] Solid mixtures were prepared by making dilute slurries of ≈DPP and diluent in dry benzene, followed by solvent removal at 70 °C under vacuum. Analysis of aliquots of the diluted ≈DPP by standard procedures[5] gave the expected amounts of ≈DPP within ±5%.

Reactions were performed at 310-375 °C (±1 °C) under vacuum (ca. 5 x 10^{-6} torr) in a controlled temperature tube furnace as previously described.[4,5] Vapor-phase products migrated from the heated zone into a liquid nitrogen cold trap, and were analyzed by GC and GC-MS with the use of internal standards. Products on the surface were detached by digestion of the solid in aqueous base and, following workup, were analyzed by GC and GC-MS as phenols or the corresponding trimethylsilyl ethers.

RESULTS AND DISCUSSION

Thermolysis of ≈DPP (0.532 mmol/g) alone occurs readily at 375 °C by a free-radical chain pathway to afford the simple product mixture shown in Fig. 1a and Table 1. The origins of selectivity in product formation including the dependence on surface coverage and co-attached aromatics have been discussed.[5,6] When ≈DPP is diluted with the Aerosil 200 silica (wt ratio of 1:2.8), the thermolysis products are the same but, as shown in Table 1, the rate of conversion of ≈DPP is reduced by a factor of four.

On the other hand, dilution of ≈DPP with the silica-alumina leads to a substantial rate acceleration as well as a remarkably different set of reaction products as shown in Table 1. Even at 375 °C, the products obtained are principally derived from aromatic dealkylation chemistry, which is characteristic of acid-catalyzed reactions over aluminosilicates involving carbocation intermediates.[9] Another indicator of acid-catalyzed chemistry is the fact that the $\approx PhCH_3$ and $\approx PhC_2H_5$ products (isolated as the corresponding phenols) are isomerized to a mixture of ortho-, meta- and para- isomers with the meta-isomers formed in the largest amounts. Although numerous other products were detected in very small quantities, the acid-catalyzed cracking of ≈DPP is reasonably selective leading principally to surface-attached benzene (≈PhH) and vapor-phase indan as the major products (Fig. 1b). Over the temperature range of 375-310 °C, these two products account for 67-74% of the total products (mass balances were ≥95%).

Large quantities of catalyst are not required to drive this reaction. Thermolysis of ≈DPP (surface coverage of 0.320 mmol/g) at 375 °C for 60 min with weight ratios of silica-alumina:≈DPP of 0, 0.20, and 2.80 gave ≈DPP conversions of 5.5, 11.6, and 18.2%, respectively. Again, in the absence of the silica-alumina only thermally derived products are detected. However, even in the presence of the small quantity of catalyst, the product distribution is dominated by acid-catalyzed products and is similar to the distribution obtained when excess catalyst is employed.

The mechanism of acid-catalyzed cracking of liquid or vapor-phase organics over aluminosilicates is generally accepted to occur through the generation of carbocation intermediates at Broensted and/or Lewis acid sites.[8-11] Although diarylalkanes have received little attention, alkylbenzenes exhibit products resulting from competition between cracking, transalkylation, and various isomerization reactions. Acid-catalyzed cracking of alkanes over aluminosilicates appears to proceed through a chain reaction involving hydride transfer from reactant molecules to chemically transformed (isomerized, cracked, etc.) carbocations.[9-11] For cracking of alkylbenzenes, a pathway is generally invoked involving protonation at the ipso position on the benzene ring followed by cleavage of the alkyl group as a carbocation, which generally leads to formation of an alkene.[9] A similar path has been used to explain the hydrocracking at 350 °C of bibenzyl (to benzene and ethylbenzene) with zinc chloride supported on silica gel.[12] On the other hand, fluid-phase DPP has been shown to undergo selective acid-catalyzed cracking to benzene and indan at 100-130 °C in $SbCl_3$ and $SbCl_3$-$AlCl_3$ melts by a benzylic cation/hydride transfer chain mechanism.[13] In the current study, cracking of ≈DPP to ≈PhH and indan (Fig. 1b) can be accomodated by either an ipso protonation path or a benzylic cation/hydride transfer chain path. Additional studies will be required to probe the involvement of these processes on the catalytic cracking of ≈DPP in dispersed solids.

It is interesting that the aluminosilicate employed in this study has a Si/Al atomic ratio of ca. 84, which indicates that a much smaller density of acidic sites is present than for typical amorphous aluminosilicate cracking catalysts whose corresponding ratio is 3-8.[9] Furthermore, the substrate is a solid and the DPP moieties are subject to diffusional constraints as a result of surface attachment. Yet, the acid-catalyzed cracking of ≈DPP in this solid mixture is quite efficient. The small particle size of the fumed silica-alumina employed and the highly dispersed nature of the catalyst may be key factors in the observed efficiency of acid-catalyzed cracking of ≈DPP.

CONCLUSIONS

We have used surface-immobilized 1,3-diphenylpropane (≈DPP) as a model system to investigate the potential role of acid-catalyzed cracking in dispersed solids. Initial results employing a small particle size, low aluminum content amorphous aluminosilicate demonstrate that efficient catalysis can occur in the dispersed solids at 310-375 °C. The product distribution is distinctly different from that obtained from a thermal free-radical process, and is consistent with the intermediacy of carbocations. The results indicate that significant interactions between the catalyst and substrate occur in the solid state. Hence, these results suggest that small particle size, highly dispersed catalysts may interact significantly with solid coal particles in the early stages of coal liquefaction/hydropyrolysis.

ACKNOWLEDGEMENT

This research was sponsored by the Division of Chemical Sciences, Office of Basic Energy Sciences, U.S. Department of Energy under contract DE-AC05-84OR21400 with Martin Marietta Energy Systems, Inc.

REFERENCES

1. (a) Utz, B. R.; Cugini, A. V.; Frommell, E. A. *ACS Symp. Ser.* 1990, *437*, 289. (b) Dosch, R. G.; Stohl, F. V.; Richardson, J. T. *Ibid.* 1990, *437*, 279.

2. (a) Herrick, D. E.; Tierney, J. W.; Wender, I.; Huffman, G. P.; Huggins, F. E. *Energy and Fuels*, 1990, *4*, 231. (b) Pradhan, V.; Tierney, J. W.; Wender, I. *Prepr. Pap.-Am. Chem. Soc., Div. Fuel Chem.* 1990, *35(3)*, 793.

3. Snape, C. E.; Bolton, C.; Dosch, R. G.; Stephens, H. P. *Prepr. Pap.-Am. Chem. Soc., Div. Fuel Chem.* 1988, *33(3)*, 351.

4. Buchanan, III, A. C.; Dunstan, T. D. J.; Douglas, E. C.; Poutsma, M. L. *J. Am. Chem. Soc.* 1986, *108*, 7703.

5. Buchanan, III, A. C.; Biggs, C. A. *J. Org. Chem.* 1989, *54*, 517.

6. Buchanan, III, A. C.; Britt, P. F.; Biggs, C. A. *Energy and Fuels* 1990, *4*, 415.

7. Britt, P. F.; Buchanan, III, A. C.; Biggs, C. A. *Prepr. Pap.-Am. Chem. Soc., Div. Fuel Chem.* 1989, *34(2)*, 567.

8. Degussa Corporation, Technical Bulletin.

9. (a) Pines, H. "The Chemistry of Catalytic Hydrocarbon Conversions"; Academic Press: New York, 1981; Chapter 1. (b) Corma, A.; Wojciechowski, B. W. *Catal. Rev.* 1985, *27*, 29.

10. Guisnet, M. R. *Accts. Chem. Res.* 1990, *23*, 392.

11. Rabo, J. A.; Gajda, G. J. *Catal. Rev.* 1990, *31*, 385.

12. Sharma, R. K.; Diehl, J. W.; Olson, E. S. *Prepr. Pap.-Am. Chem. Soc., Div. Fuel Chem.* 1990, *35(2)*, 414.

13. Buchanan, III, A. C.; Dworkin, A. S.; Smith, G. P. *J. Am. Chem. Soc.* 1983, *105*, 2843.

Table 1. Effect of Dispersed Solids on Thermolysis of ≈DPP (0.532 mmol/g)

Diluent[a]	None	A	B	B	B	B
≈DPP (mmol)	0.255	0.0692	0.0644	0.0675	0.0437	0.0413
Temp (°C)	375	375	375	375	345	310
Time (min)	60	60	60	10	10	10
≈DPP Conversion(%)[b]	10.3	2.6	23.5	17.4	11.8	4.8
Products (mol/100 mol ≈DPP)						
$PhCH_3$	4.45	1.26	0.27	0.13	0.06	c
$\approx PhCH_3$[e]	5.85	1.34	2.61[e]	1.60[e]	1.00[e]	0.36[e]
$PhCH{=}CH_2$	5.85	1.28	0.18	0.09	c	c
$\approx PhCH{=}CH_2$	4.38	1.36	c	c	c	c
PhC_2H_5	c	c	1.79	1.25	0.65	0.20
$\approx PhC_2H_5$[e]	c	c	0.88	0.70	0.44	0.24
PhH	d	d	5.17	3.47	1.95	0.73
≈PhH	d	d	15.13	11.07	8.07	3.21
Indan	d	d	16.24	12.76	9.17	3.70
≈Indan[f]	d	d	0.87	1.15	0.84	0.36
Indene	d	d	2.57	1.42	0.87	0.54
PhC_3H_7	d	d	0.76	0.48	0.21	c
$PhCH{=}CHCH_3$	d	d	0.30	0.14	c	c

[a]A=Aerosil 200 SiO_2; B=Aerosil MOX-170 SiO_2-1%Al_2O_3; wt diluent:≈DPP=2.80.
[b]Mass balances ≥ 95%.
[c]<0.05.
[d]Not detected.
[e]Mixture of ortho-, meta-, and para- isomers in runs with silica-alumina.
[f]Mixture of two isomers.

Figure 1. Principal products from the reactions of surface–attached 1,3–diphenylpropane

(a) Thermolysis at 345–400 °C

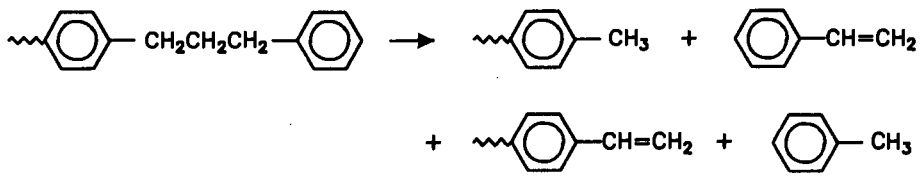

(b) Acid–catalyzed cracking at 310–375 °C

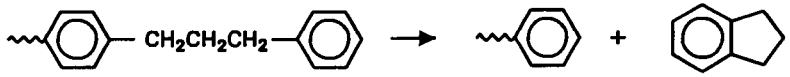

EFFECT OF PORE STRUCTURE OF Ni-Mo CATALYSTS ON HYDROCRACKING OF ASPHALTENE AND PREASPHALTENE AND HETEROATOM REMOVAL

Chunshan SONG+*, Toshihiko NIHONMATSU†, Kouji HANAOKA† and Masakatsu NOMURA†

+Fuel Science Program, Department of Materials Science and Engineering
The Pennsylvania State University, University Park, PA 16802, USA
†Department of Applied Chemistry, Faculty of Engineering, Osaka University
Yamada-oka 2-1, Suita, Osaka 565, Japan

Keywords: Catalyst pore size; Asphaltene conversion; Heteroatom removal

INTRODUCTION

Catalytic upgrading of coal liquids is an important step in two-stage coal liquefaction. This process is still confronted with the problem of achieving high catalyst performance for efficient conversion of heavy materials. A number of previous works showed the importance of catalyst pore structure in coal liquefaction (1-3) and in hydroprocessing of petroleum residues due to diffusional limitations (4-7). Several reports on hydrotreating of coal liquids (8-10) suggested that large pore catalysts are effective in converting 450°C+ fractions. Our preliminary results showed that the pore size of Mo catalysts supported on silica or alumina affects the conversion of asphaltene and preasphaltene (11-13).

The major purpose in upgrading primary coal liquids is to convert the heavy materials such as asphaltene and preasphaltene into oils (hexane solubles) with low heteroatom content, which can be used as feed for further refining by conventional petroleum processing technology. The knowledge on the catalyst pore size effect for converting coal-derived asphaltene and preasphaltene is still very limited. This work aimed at clarifying the effects of pore size of Ni-Mo catalysts on their performance in converting the heavy materials and in heteroatom removal. The results and mechanistic considerations are reported in this paper.

EXPERIMENTAL

The catalyst supports were cylindrical gamma-alumina extrudate prepared from boehmite gel (Table 1), which were provided by Sumitomo Metal Mining Co. (S-1), the Catalyst Society of Japan (S-2), and Chiyoda Chemical Engineering and Construction Co.(S-3 and S-4). The catalysts were prepared by co-impregnation of ammonium heptamolybdate and nickel nitrate from their aqueous solution, in which 25% aqueous ammonia was added to give a homogeneous solution, followed by evaporation under reduced pressure. The impregnated extrudates were then dried at 250°C for 2 h in a tube furnace (to remove adsorbed water) and calcined at 500°C for 5 h in an air flow. The catalysts were sulfided (11) and kept in hexane before use. Table 1 gives the physical properties, and Figure 1 shows the pore size distribution of the four Ni-Mo/Al_2O_3 catalysts prepared by using the same procedure. The pore size distribution was measured by using a Shimadzu AutoPore-9200 mercury porosimeter. A commercial KF-153S sulfided Ni-Mo/Al_2O_3 (14) catalyst (Cat-C) was also used in some experiments. The prepared catalysts have the same contents of Ni and Mo to those of the commercial Cat-C (NiO: 2.9, MoO_3: 15.8 wt%). The size of the available extrudates was 1.5 mm (d) for Cat-1, Cat-2 and Cat-C, and 0.8 mm for Cat-3 and Cat-4. In practice, the lowest catalyst sizes permitted in industrial fixed-bed operations are 0.8-1.6 mm.

Table 2 gives the sources and properties of the feed samples, in which Wan-SRC and Aka-SRC were produced from Wandoan subbituminous coal (at 440°C) and Akabira bituminous coal (at 420°C) in a coal liquefaction plant at Sumitomo Coal Mining Co. (11). The coal-derived asphaltenes, Aka-Asp and Wan-Asp (hexane-insoluble benzene solubles) and preasphaltene (Wan-Preasp) were separated from the corresponding SRC. The bitumen asphaltene (Aosb-Asp) was separated from Athabasca oil sand bitumen (12). The original asphaltenes were analyzed by using gel permeation chromatography, GPC (14-15) and ^1H NMR (16-17). The hydrocracking was carried out in a 60 ml rocking autoclave at 425°C for 1 h with 4.9 MPa H_2 (cold). Tetralin was used as solvent unless otherwise mentioned (5g feed/0.5g cylindrical catalyst/5g solvent). The products were separated into gases, oils (hexane solubles), asphaltene, and benzene insolubles, BI (15). The gases were analyzed by GC(Shimadzu 9A). The H_2S in gases were analyzed by using H_2S indicator tube (Kitagawa Indicator) at room temperature.

RESULTS AND DISCUSSION

Asphaltene Structure and Reactivity

Structure of Asphaltene. Table 3 gives the NMR results. As can be seen from Tables 2-3, the coal-derived asphaltenes, Aka-Asp and Wan-Asp have higher C, O and N contents, higher aromaticity and lower H/C atomic ratios, while the bitumen asphaltene (Aosb-Asp) has higher H and S contents, higher H/C ratio and lower aromaticity. Aka-Asp and Wan-Asp contain more aromatic hydrogens (Har), whereas Aosb-Asp is rich in aliphatic hydrogens present in long alkyl side-chains and naphthenic groups (Table 3). The size distribution of the asphaltenes was evaluated by GPC. Figure 2 shows the GPC results, in which the molecular size decreases with increase in elution (retention) time. The broad GPC curves of Aka-Asp and Wan-Asp show that they consist of various components ranging from relatively small to large molecules. The peak sizes correspond to a molecular weight (MW) range of about 200-1000. On the other hand, Aosb-Asp shows a sharp GPC peak in the range of much larger molecular sizes, corresponding to peak MW values of at least over 1000. The average MW values are in the range of 400-600 for Aka-Asp, Wan-Asp and other coal-derived asphaltenes (12,18), and 3000-6000 for Aosb-Asp and other bitumen and petroleum asphaltenes (12,19). These results showed that most coal-derived asphaltene molecules have smaller size and lower MW than bitumen and petroleum asphaltenes.

Reactivity of Asphaltene. Table 4 presents the data on asphaltene reactivity. The thermal run of coal-derived Aka-Asp in H2-tetralin gave similar conversion to that of the bitumen asphaltene Aosb-Asp. However, the oil yield was lower, and the amount of BI formed from retrogressive reactions was higher with Aka-Asp. The run of Wan-Asp was also accompanied by considerable BI formation. The effect of tetralin in suppressing retrogressive reactions was evaluated by the runs using decalin. The BI from Aka-Asp increased from 9.7 to 12.2% when the solvent changed from H-donor tetralin to decalin, whereas there was little change in BI from Aosb-Asp (1.8 vs. 1.9%). These results showed that coal-derived asphaltenes have high thermal reactivity which also leads to remarkable retrogressive reactions to form BI. Probably the BI formation involved the crosslinking and condensation of reactive radicals and some unstable compounds, especially hydroxy compounds which are rich in coal-derived asphaltenes (18,20) and tend to undergo coupling reactions to form more refractory materials (21-22). As shown in Table 4, H2S was also formed in the thermal runs, and considerable amounts of H2S were produced from Aosb-Asp both in tetralin and in decalin. From these results, it seems that thermal decomposition of the bitumen asphaltene involved the cleavage of weak C-C and aliphatic C-S bonds (23), and the resulting radicals were readily stabilized in H2-solvent systems to form oils, C1-C4 and H2S.

Catalytic Conversion of Asphaltene and Preasphaltene

Catalyst Properties. With an attempt to examine the effects of catalyst pore size on an unified basis, we prepared four Ni-Mo catalysts using pure gamma-alumina supports. As can be seen from Figure 1 and Table 1, each of the four prepared Ni-Mo catalysts exhibits an unimodal distribution of pore sizes within a specific range. The median pore diameter (MPD) increases in the order of Cat-1 (120 Å) < Cat-2 (150 Å) < Cat-3 (290 Å) < Cat-4 (730 Å). The surface area, however, decreases as pore size increases. The unimodal pore structure and the significantly different pore sizes of Cat-1 through Cat-4 prepared by using the same procedure, enabled us to evaluate the pore size effects.

Asphaltene Hydrocracking. Figure 3 shows the distribution of products from hydrocracking of a coal-derived asphaltene, Aka-Asp. The catalysts significantly promoted Aka-Asp conversion and increased oil yields from 50.7% to more than 69%, without increase in gas yields. The catalysts also reduced BI from 9.7% to less than 3%. Figure 4 shows the conversions and product yields as a function of catalyst pore size (MPD). It is clear from Figure 4 that the conversions of Aka-Asp and oil yields increased remarkably with increase in catalyst MPD up to 290 Å, in spite of the decrease in catalyst surface area with increasing MPD. On the other hand, further increase in MPD from 290 to 730 Å did not offer any advantage. We also examined the solvent effect in the catalytic runs of Aka-Asp with Cat-1 and Cat-3. Using decalin instead of tetralin resulted in 1-2% more BI and slightly higher H2 consumption. The amounts of BI formed in both cases were lower with large pore Cat-3 than with small pore Cat-1.

Figure 5 presents the results for hydrocracking of Aosb-Asp. The conversions and yields of oils plus gases increased with MPD up to 290 Å, while further increasing MPD to 730 Å decreased the conversion. In this case, catalysts also enhanced the formation of BI and gases. The amounts of H2S formed in gas phase changed remarkably with different catalysts. The detected H2S (ml at 25°C under ambient pressure) amounts were as follows: none (26.9) < Cat-1 (45.5) < Cat-2 (52.5) < Cat-3 (77.8) > Cat-4 (34.4). Because of the low S content of Aka-Asp (0.5%) as compared to that of Aosb-Asp (8.3%), the amounts of detected H2S were much smaller, within 2-4 ml (Cat-1: 3.7; Cat-2: 2.0; Cat-3: 1.8; Cat-4: 1.9).

Since the sizes of the bitumen asphaltene molecules are very large (Figure 2), it might be expected that their conversion might be more sensitive to catalyst pore size. Nevertheless, the increasing extents of oil yields and conversions with MPD were higher with the coal-derived Aka-Asp (Figure 4). Moreover, the highest oil yield from Aosb-Asp with the largest-pore Cat-4 (69.4%) was still lower by 11% than that from Aka-Asp with Cat-3 (80.4%). This comparison suggests that the conversion of coal-derived asphaltenes is sensitive to catalyst pore size although their molecular sizes are, on average, much smaller than bitumen and petroleum asphaltenes. In addition, the catalytic runs of Aka-Asp consumed slightly more H2 (2.1-2.3wt%) than the corresponding runs of Aosb-Asp (1.9-2.2wt% based on asphaltene). In both cases, H2 consumptions with large pore Cat-3 were slightly higher than with small pore Cat-1.

Preasphaltene Hydrocracking. Preasphaltene is also a major fraction in primary coal liquids. Figure 6 presents the results for a coal-derived preasphaltene, Wan-Preasp using Cat-1, Cat-3 and Cat-4. The yields of asphaltenes and recovered benzene insolubles were 24.8 and 41.2% with Cat-1, 30.1 and 34.4% with Cat-3, and 33.1 and 29.5% with Cat-4. Apparently, asphaltene yields increased with increasing catalyst MPD from 120 Å (Cat-1) up to 730 Å (Cat-4), rather than a decreasing trend as would be anticipated from the results with the asphaltene fraction as feed (Figure 4). These results suggest that the effect of catalyst pore size on product distribution also depends on the feed used.

SRC Hydroprocessing. Figure 7 presents the results for the unfractionated Wan-SRC, which contained each of the following fractions: oils (35.7%), asphaltene (33.1%) and preasphaltene (31.2%). In this case, we also used a sulfided commercial KF-153S Ni-Mo catalyst (Cat-C, Table 1), which has a MPD value similar to that of the well known Shell 324M Ni-Mo (90 vs. 86 Å). It should be noted that Cat-1 though Cat-4 is alumina-supported catalyst, while Cat-C contains 4.5wt% SiO2. Figure 8 shows the results for Aka-SRC which contained more preasphaltene (41.5%) and less asphaltene (27.0%) and oils (31.5%) as compared to Wan-SRC. As can be seen from Figures 7 and 8, the yields of preasphaltene decreased with increasing MPD. The oil yields from both SRC increased with MPD up to 290 Å. The gas yields were nearly constant in the runs of Wan-SRC (3.6-4.6%) and Aka-SRC (4.3-5.0%).

Figure 9 shows the effect of catalyst pore size on the net conversion of the heavy materials during SRC hydroprocessing. For runs of both Wan-SRC and Aka-SRC, increasing catalyst pore size significantly promoted preasphaltene conversion. This is consistent with the results shown in Figure 6 for runs of the isolated preasphaltene fraction. It is interesting to note that increasing MPD above certain sizes caused decrease in asphaltene conversion during the runs of the whole SRC (Figure 9). This is considerably different from the trend observed in the runs of isolated asphaltene fraction, where increasing MPD remarkably promoted asphaltene conversion and oil yields (Figure 4). The net conversion of the heavy fractions, especially asphaltene, also appeared to be lower in the runs of unfractionated SRC.

Combination of the results in Figures 3-4 and in Figures 6-9 revealed that in SRC upgrading, when the catalyst pores exceeded certain sizes, more preasphaltene molecules which have larger sizes than asphaltenes will diffuse into pores and react on catalyst surface, producing more asphaltene. There is no doubt that increasing pore size also facilitates the diffusion and reaction of asphaltene fractions (Figures 3-5), but the first step of catalytic conversion is adsorption. As the pore sizes become large enough to allow the diffusion of larger molecules, preasphaltene tend to adsorb on the catalyst surface in preference to asphaltene, probably because of the higher aromaticity and higher polarity of the former. The present results were obtained with cylindrical extrudate catalysts. Previous works showed that the change in the extrudate size within the range of 1.6 to 0.8 mm does not have any significant effect on initial activity, while the <100 mesh fine particles generally afford higher conversions than extrudates (24), which is another indication of the diffusional limitations occurring during SRC hydroprocessing.

Heteroatom Removal

Relative to the thermal runs, the Ni-Mo catalysts increased H contents and H/C ratios, and decreased heteroatom contents; the oils from coal-derived materials have lower H/C ratios (1.01-1.05) than those (1.36-1.39) from the bitumen asphaltene (24). Using the catalysts with different pore sizes caused considerable differences in O contents of the products from coal-derived materials and the recovered asphaltenes from Aosb-Asp, and in S contents of both oils and asphaltenes from Aosb-Asp, indicating the importance of catalyst pore size in hydrodeoxygenation (HDO) and hydrodesulfurization (HDS).

Figure 10 shows the O contents of products from Aka-Asp and Wan-SRC and those of recovered asphaltenes from Aosb-Asp as a function of catalyst MPD. There is little or no literature information relating to the effect of catalyst pore size on HDO of coal liquids and bitumen or petroleum. In this work, the analytical results for Aka-Asp and Aosb-Asp were confirmed by repeated analyses of samples from duplicated runs. The maximum HDO degree of given products corresponds to the lowest O contents. As can be seen from Figure 10, the MPD values of 120 Å (Cat-1) and 150 Å (Cat-2) correspond to higher HDO degree of oils, while the latter was superior (to the former) for HDO of asphaltenes where a maximum HDO was achieved in the cases of both Aka-Asp and Aosb-Asp. When SRC was the feed (Wan-SRC), the MPD range corresponding to higher HDO degrees of asphaltenes appeared to become wider or larger. Combining the results in Figures 1 and 10 suggests that 80-160 Å pores with a peak around 120 Å are effective for HDO of oils, while 100-200 Å (MPD: 150 Å) pores are preferable for HDO of asphaltenes.

In Figure 11 the S contents of oils and asphaltenes as well as the amounts of H_2S formed from the sulfur-rich Aosb-Asp were plotted against the catalyst MPD. Unlike HDO of Aosb-Asp, its HDS degree reached a maximum at catalyst MPD of 290 Å (Cat-3), which corresponds to the lowest S contents of products and the highest H_2S amount in gas. Sulfur is also the major heteroatom in petroleum, and there are many reports on HDS of petroleum crudes and heavy oils including the effect of pore size (4-7). In the catalytic runs of the coal-derived sulfur-less Aka-Asp, no difference in HDS was apparent, because all the catalysts completely removed sulfur from the products (24). Bertolacini et al.(1) showed that in the liquefaction of a high-sulfur coal using Co-Mo catalysts (60-100 mesh), the higher activities for HDS and coal conversion correspond to MPD of 100-120 Å and about 200 Å, respectively.

The HDO and HDS results can be explained in terms of relation between pore size and surface area, and competitive adsorption and reaction on catalyst surface. It is considered that there are two main paths for heteroatom removal: simultaneous asphaltene conversion and heteroatom removal, and HDO/HDS of formed or originally present oils and asphaltenes. By applying the molecular size distribution concept as suggested by GPC (Figure 2), one anticipates that the smaller pores contribute to HDS and HDO of small molecules, and larger pores promote the reactions of large molecules. Large pores facilitate the diffusion of large molecules, whereas the large pore catalysts possess lower surface area which lower the activity on catalyst weight basis. The results for runs of coal-derived materials (Figures 4,6,9) suggest that pore size change also affects the competition between adsorption of different compounds/fractions, and heavier molecules such as those in preasphaltene tend to adsorb in preference, which partially inhibit the conversion of less heavier asphaltene molecules. As long as the molecules can diffuse fast enough into the interior of the pores and can adsorb on the active sites, the degrees of HDO and HDS are then determined mainly by the area and intrinsic activity of the catalysts. Therefore, the existence of different ranges of preferable pore sizes for different reactions and for different feed materials is due to the interdependence between pore size, surface area, and competitive adsorption/reaction.

It is expected that there is difference in catalyst dispersion. With the chemically identical supports, the catalyst dispersion should increase with surface area. One can hardly see any effect in the observed trends with Cat-1, Cat-2 and Cat-3 that might be attributed to different dispersion. However, the generally lower HDS and HDO activities of the largest pore Cat-4 may be due in part to its lowest surface area, and poor dispersion of Ni-Mo active phase. On the other hand, there was little decrease in N content of products, probably because of the mild conditions (low H_2 pressure, 4.9 MPa). Stiegel et al.(8) reported that higher metal loadings and larger pores appear to yield some improvement in HDN. In addition, HDN over conventional Ni-Mo and Co-Mo catalysts is known to be more difficult than HDO and HDS, and requires extensive hydrogenation. Shabtai et al. (25) and Hirschon et al. (26) have found that adding Ru to alumina-supported Mo catalysts can improve HDN selectivity.

CONCLUSIONS

1. The performance of unimodal Ni-Mo catalysts for asphaltene and preasphaltene conversion and for oxygen and sulfur removal at 425°C with 4.9 MPa H2 appeared to depend on their pore size distribution.
2. In the runs of isolated heavy fractions, the conversions increased with catalyst MPD up to 290 Å, and further MPD increase to 730 Å did not offer apparent advantage for converting coal- and oil sand bitumen-derived asphaltenes, but had positive effect in the runs of coal-derived preasphaltene.
3. Relative to the bitumen asphaltene, the sizes of most coal derived asphaltenes are much smaller, but their conversions are sensitive to catalyst pore size. The thermal conversion of coal-derived asphaltenes is accompanied by remarkable retrogressive reactions, even in the presence of H-donor solvent. When the large pore catalyst (MPD: 290 Å) was used, these materials can be converted into oils in high yields under mild conditions, while the oils have lower H/C ratios than those from the bitumen asphaltene.
4. In the hydroprocessing of unfractionated primary coal liquids which contain preasphaltene in addition to asphaltene and oils (SRC), increasing catalyst pore size significantly promoted preasphaltene conversion, producing more asphaltene. In this case, the use of large pore catalysts seems to decrease the net conversion of asphaltene fraction.
5. The preferable pore size ranges, which may not be the optimum, appeared to be 80-160 Å with a peak MPD around 120 Å for HDO (oxygen removal) of oils, and 100-200 Å with a peak MPD around 150 Å for HDO of asphaltenes. Maximum HDS (sulfur removal) of the sulfur-rich bitumen asphaltene was observed at MPD of 290 Å which corresponds to a pore size range of 200-400 Å.

REFERENCES

1. Bertolacini, R.J.; Gutberlet, L.C.; Kim, D.K.; Robinson, K.K. *ACS Fuel Chem. Prepr.* 1978, 23 , 1-10.
2. Ho, P.N.; Weller, S.W. *Fuel Processing. Technol.* 1981, 4, 21-29.
3. Shimada, H.; Kurita, M.; Sato, T.; Yoshimura, Y.; Kawakami, T.; Yoshitomi, S.; Nishijima, A. *Bull. Chem. Soc. Japan* 1984, 57, 2000-2004.
4. Ohtsuka, T. *Catal. Rev.-Sci. Eng.* 1977, 16, 291-325.
5. Green, D.C.; Broderick, D.H. *Chem. Eng. Prog.* 1981, 77, 33-39.
6. Takeuchi, C. *Kagaku Kogaku* 1986, 50, 598-603.
7. Onuma, K. *Shokubai* 1989, 31, 182-187.
8. Stiegel, G.J.; Tischer, R.E.; Polinski, L.M. *I & EC Prod. Res. Dev.* 1983, 22, 411-420.
9. Tischer, R.; Narain, N.K.; Stiegel, G.J.; Cillo, D.L. *J. Catal.* 1985, 95, 406-413.
10. Yoshimura, Y.; Sato, T.; Shimada, H.; Nishijima, A. *Fuel Sci. Technol. Int'L* 1986, 4, 621-642.
11. Hanaoka, K.; Song, C.; Nomura, M. *Proc. 24th Japan Coal Sci. Conf.* , Tokyo, 1988, 222-225.
12. Song, C.; Nihonmatsu, T.; Nomura, M. *Proc. 24th Japan Coal Sci. Conf.* , Tokyo, 1988, 226-228.
13. Song, C.; Hanoka, K. Nihonmatsu, T.; Nomura, M. *Proc. 1989 Int. Conf. Coal Sci.* , Tokyo, 1989, 226-228. The catalyst pore size reported in this paper refers to the pore radius, not diameter.
14. Song, C.; Hanoka, K. ; Ono, T.; Nomura, M. *Bull. Chem. Soc. Japan* 1988, 61, 3788-3790.
15. Song, C.; Hanoka, K. ; Nomura, M. *Fuel* 1989, 68, 287-292.
16. Song, C.; Nomura, M. *Bull. Chem. Soc. Japan* 1986, 59, 3643-3648.
17. Song, C.; Hanoka, K. ; Nomura, M. *Energy & Fuels* 1988, 2, 639-644.
18. Schwager, I.; Yen, T.F. *Fuel* 1979, 58, 219-227.
19. Nakamura, M.; Shiroto, Y.; Takahashi, H. *Nippon Kagaku Kaishi* 1980, 1037- 1046.
20. Hertan, P.A.; Jackson, W.R.; Larkins, F.P. *Fuel* 1986, 65, 368-372.
21. McMillen, D.F.; Chang, S.-J. Nigenda, S.E.; Malhotra, R. *ACS Fuel Chem. Prepr.* 1985, 30, 414-426.
22. Derbyshire, F.J.; Davis, A.; Lin, R. *Energy & Fuels* 1989, 3, 431-437.
23. Strausz, O.P. *ACS Petr. Chem. Prepr.* 1989, 34, 395-400.
24. Song, C.; Hanaoka, K.; Nihonmatsu, T.; Nomura, M. , unpublished results.
25. Shabtai, J.; Guohe, Q.; Balsuami, K.; Nag, N.K.; Massoth, F.E. *J. Catal.* 1988, 113, 206-219.
26. Hirschon, A.S.; Wilson Jr., R.B.; Laine, R.M. *Appl. Catal.* 1987, 34, 311-316.

Table 1. Properties of Supports and Sulfided Ni-Mo Catalysts

Properties	Al_2O_3 supports[a]				Ni-Mo/Al_2O_3 catalysts[b]				
	S-1	S-2	S-3	S-4	Cat-1	Cat-2	Cat-3	Cat-4	Cat-C[c]
Median pore diam., Å	115	120	280	750	120	150	290	730	90
Surface area, m^2/g	203	174			152	128	126	80	255
Pore volume, ml/g	0.79	0.65	1.05	1.49	0.49	0.45	0.84	1.01	0.56

a) Data received; b) Measured for prepared catalysts; c) Commercial KF-153S-1.5E Ni-Mo/Al_2O_3; Metal loading in Cat-1 to Cat-4 and Cat-C, MoO_3: 15.8, NiO: 2.9 wt%.

Table 2. Elemental Analysis of Coal- and Bitumen-Derived Asphaltene and SRC

Asphaltene & SRC	Elemental (wt%)					Atomic H/C	Source and content		
	C	H	N	S	O[a]		Origin	Source	wt%
Aka-Asp	83.8	6.1	2.0	0.5	7.6	0.87	Akabira Coal	SRC	27.1
Wan-Asp	84.3	6.0	1.6	0	8.1	0.86	Wandoan Coal	SRC	33.1
Aosb-Asp	80.1	8.0	1.2	8.3	2.4	1.20	Ath. Oil Sand	Bitumen	15.0
Wan-Preasp	83.0	5.0	2.0	0	10.0	0.72	Wandoan Coal	SRC	31.2
Wan-SRC	85.7	6.1	1.5	0	6.7	0.85	Wandoan Coal	SRC	100.0
Aka-SRC	84.9	6.2	1.8	0.3	6.8	0.87	Akabira Coal	SRC	100.0

a) By difference.

Table 3. ^1H NMR Analysis of Coal- and Bitumen-Derived Asphaltenes

Asphaltene	H distribution per 100 C atoms[a]							Aromaticity
	H_{ar}	H_{n-CH2}[b]	$H_{\alpha CH2}$	$H_{\alpha CH3}$	$H_{\beta CH2}$	$H_{\beta CH3}$[c]	H_r[d]	f_a
Aka-Asp	28.0	6.0	17.2	7.2	7.9	14.0	6.7	0.74
Wan-Asp	30.6	5.1	14.8	6.9	7.1	15.6	5.9	0.77
Aosb-Asp	9.6	5.5	15.1	7.3	11.9	41.1	28.6	0.58

a) Based on ^1H NMR and elemental analysis; b) Methylene H α to two aromatic rings; c) Includes β-CH_3 and methylene H γ or further from an aromatic ring; d) Methyl H γ or further from an aromatic ring.

Table 4. Reactivity of Asphaltenes in Non-Catalytic Hydrocracking

Solvent	Tetralin			Decalin	
Asphaltene	Aka-Asp	Wan-Asp	Aosb-Asp	Aka-Asp	Aosb-Asp
Products (wt%)					
Gas	5.7	4.8	4.2	4.9	6.5
Oil	50.7	49.0	59.4	50.6	58.2
Asphaltene	33.9	37.7	34.6	32.3	33.4
BI	9.7	8.5	1.8	12.2	1.9
H_2S in gas (ml	2.7	1.1	26.9	1.0	20.1
Conversion (wt%)	66.1	62.3	65.4	67.7	66.6
H_2 consumption (wt%)	0.5	0.6	0.9	0.9	1.1

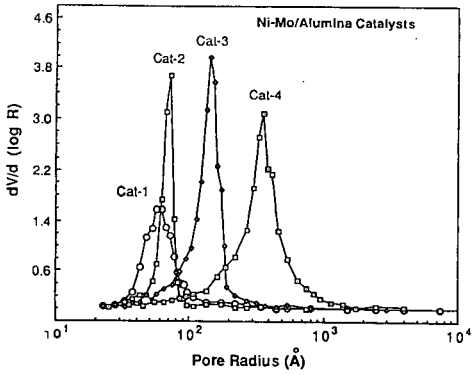

Figure 1. Pore size distribution of prepared Ni-Mo/Al_2O_3 catalysts

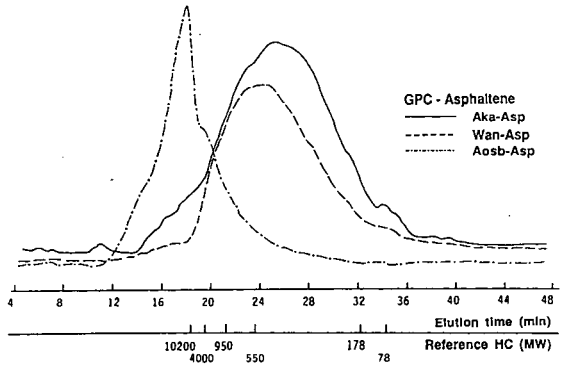

Figure 2. Gel permeation chromatograms of asphaltenes using $CHCl_3$ as mobile phase

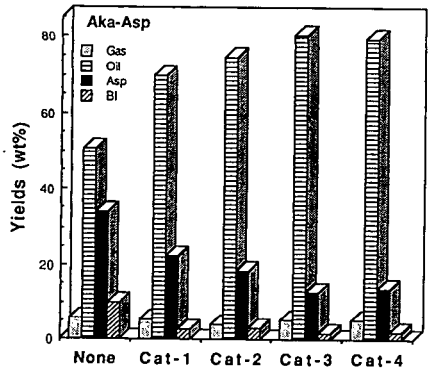

Figure 3. Effect of Ni-Mo catalysts in Aka-Asp hydrocracking

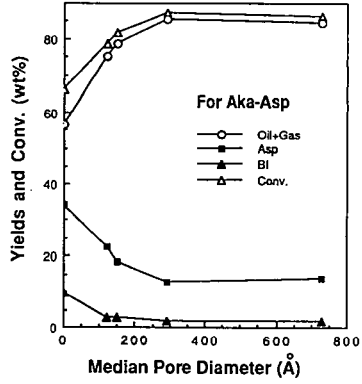

Figure 4. Effect of catalyst pore size on hydrocracking of coal-derived asphaltene

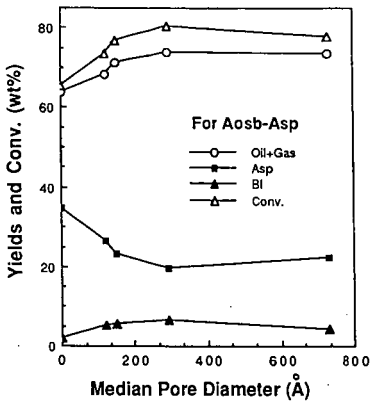

Figure 5. Effect of catalyst pore size on hydrocracking of oil sand bitumen-derived asphaltene

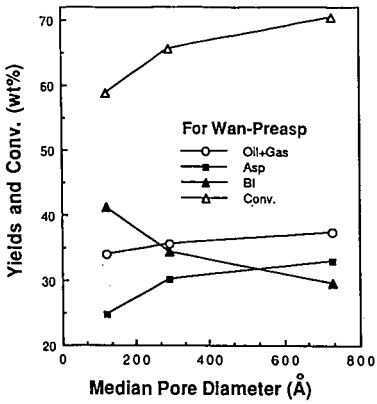

Figure 6. Effect of catalyst pore size on hydrocracking of coal-derived preasphaltene

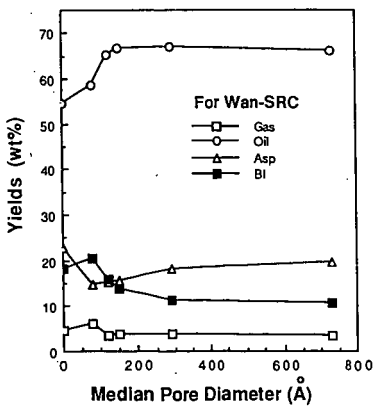

Figure 7. Effect of catalyst pore size on hydroprocessing of unfractionated SRC (Wan-SRC)

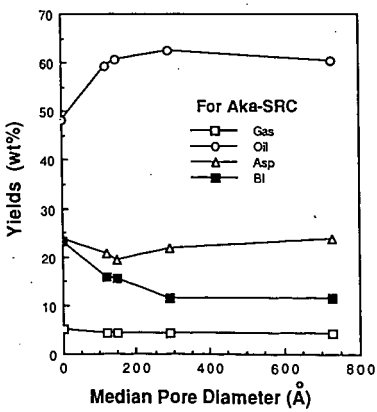

Figure 8. Effect of catalyst pore size on hydroprocessing of unfractionated SRC (Aka-SRC)

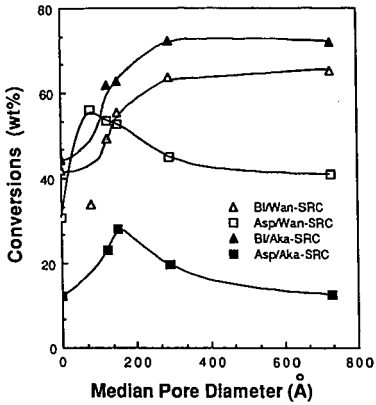

Figure 9. Effect of catalyst pore size on net conversion of asphaltene and preasphaltene in SRC hydroprocessing

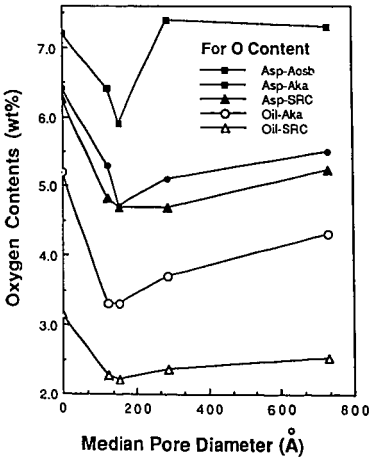

Figure 10. Effect of catalyst pore size on oxygen removal

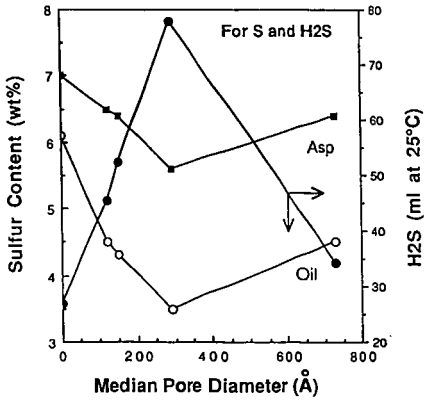

Figure 11. Effect of catalyst pore size on the removal of sulfur from the bitumen asphaltene

Ultrafine Iron Catalysts for Coal Dissolution

P.C. Eklund*, J.M. Stencel, Xiang-Xin Bi*,
R.A. Keogh and F.J. Derbyshire
University of Kentucky,
Center for Applied Energy Research,
3572 Iron Works Pike,
Lexington, KY 40511-8433
* Department of Physics and Astronomy

Keywords: Iron Catalysts, Ultrafine particles, Coal dissolution

Introduction

Over the last several years, developments in coal liquefaction technology have significantly lowered the estimated cost of producing coal liquids (1-3). Among the notable improvements and innovations have been the introduction of the ebullated bed reactor, the adoption of two-stage processing with the additional use of catalyst in the first as well as second stage, and the recycling of residual products to extinction with the production of higher yields of distillate liquids. Progress can be measured in terms of increased selectivity to distillates, improved hydrogen utilization and reduced operating severity.

At this time it is considered that further cost reductions could be realized through a combination of incremental measures rather than any single radical one (although there is always hope that this type of statement will prove to be hopelessly incorrect). One example of a physical process step which can benefit liquefaction economics is to use a cleaned coal feed (4). This would reduce the inventory of inert material in the reactor system, allowing a reduction in reactor size, decreased wear on engineering components and reducing the loss of valuable product with the rejection of these solids. Relatedly, more efficient methods for solid separation would be advantageous.

With regard to the chemistry of coal liquefaction, positive gains could be made by the development of supported catalysts with improved activity, selectivity and life. However, it is considered that a more fruitful approach lies in trying to achieve a greater degree of control over the initial

dissolution reactions through the use of highly dispersed catalysts (5). The specific objectives of research into the development and application of slurry phase catalysts are to increase the rate of conversion and to produce a solubilized product which can be upgraded with greater facility in the second stage. The anticipated outcome of successful research would be to alleviate the problems encountered by the supported catalysts in the second stage, increase throughput, and further improve selectivity to distillates. Moreover, the effective use of slurry phase catalysts can provide the means to liquefy efficiently low-rank coals. Subbituminous coals from the western US are much cheaper feedstocks than eastern bituminous coals. It has been shown that they can produce lower boiling and higher quality liquids (6-8), and that they cause less rapid deactivation of the second stage catalyst (2). The main problem is their lower rate and extent of conversion which causes inefficient use of reactor space and the loss of additional product on solids separation. If, as supposed, this is related to an imbalance between the rates of bond cleavage and hydrogenation, then it is possible that the situation can be redressed by the use of appropriate catalysts.

Molybdenum and iron are the most commonly investigated catalyst metals and both form an active sulfide under liquefaction conditions, or can be introduced after presulfiding. Although iron catalysts are less active, they are preferred for reasons of economy. A great deal of research has been spent in attempting to understand the chemistry of liquefaction in the presence of iron catalysts and the composition of the active phase. It has also been demonstrated that the use of powdered iron catalysts has allowed the liquefaction of subbituminous coals which could not otherwise be processed (see 8). Nevertheless, the activity of these catalysts is still much less than desired and means to enhance their activity are under investigation.

The catalyst activity is determined principally by its composition and the extent of its dispersion and intimate contact with the coal-solvent slurry. While it is generally considered that the active phase of Fe and Mo is a sulfide form, recent studies by Oyama and co-workers have shown that supported and unsupported Mo carbides and nitrides exhibit high activity for hydrodenitrogenation and hydrodesulfurization reactions (9-12), raising the possibility that the carbides and nitrides of Mo and other metals may be active liquefaction catalysts.

The catalyst dispersion is dependent upon the form and mode of addition of

the catalyst precursor. High activities are reportedly favored by catalysts introduced as oil-soluble organometallic precursors such as naphthenates and carbonyls (13-15). The results of some studies, however, indicate that even with these precursors, quite large crystallites or agglomerates can be formed during liquefaction and hence the potentially high dispersion is not maintained. There is some evidence to indicate that, if introduced as particulates, there is less tendency for agglomeration. Fine iron particles (50 nm mean diameter) synthesized by a flame pyrolysis technique appeared to have retained their particle size and shape during presulfiding and coal liquefaction (16,17). Other work has shown that FeS is more active as a colloid than in powder form (18).

The increase in catalytic activity that is expected with decreasing particle size may be due to a combination of effects: an increase in exterior surface and an associated enhancement of sulfiding kinetics; a radical departure from bulk properties, especially with regard to surface energetics as the particle size is reduced below about 10 nm. The synthesis of ultrafine catalyst particles could therefore provide a means to enhance the activity of dispersed iron (or other metal) catalysts.

To examine this proposition, a program of research has been initiated to synthesize ultrafine iron-based particles by a laser pyrolysis technique and to relate their composition, structure and other properties to their behavior as liquefaction catalysts. Later it is intended to investigate effect of the modifying their composition by the addition of promoters during synthesis. This paper describes some of the early findings of this research.

Experimental

Particle Synthesis

The technique for synthesizing ultrafine particles by laser pyrolysis appears to have first been performed by Haggerty and co-workers (19) whose interest was the preparation of silicon-containing ceramics. The method was utilized by researchers at Exxon to produce transition metal carbide particles for use as catalysts for synthesis gas reactions (20,21). One of the examples in the patents involved the synthesis of Fe_3C particles by the laser pyrolysis of vapor mixtures of $Fe(CO)_5$ and ethylene. This has been the starting point for the present program and the primary aim in the initial studies has been to produce reproducibly iron carbide particles of nanometer

size.

The apparatus used for synthesis has been described previously (22). The reaction cell is shown schematically in Figure 1.

The cell was fabricated from a six-way cross made from 3.8 mm diameter stainless steel tubing. The reactant gases ($Fe(CO)_5$ and C_2H_4) flow vertically out of the tip of a ~ 1mm dia. stainless tube and intersect the horizontal beam from a tunable cw CO_2 laser. The reactant gas mixture is heated in a small volume above the reactant gas nozzle by tuning the laser frequency to a strong rotational-vibrational band of C_2H_4 at ~ 940 cm^{-1}. Thermal decomposition of $Fe(CO)_5$ to Fe and CO occurs and the Fe reacts with the ethylene to produce ultrafine spherical particles which drift in a well-collimated stream vertically out of the cell. The particles are collected in a teflon membrane filter with average pore size 200 nm.

The reactant gases are confined near the vertical axis of the cross via a coaxial flow of argon which passes through a larger tube (~15 mm diameter) concentric with the much smaller reactant gas tube. Pre-heating the Ar flowing into the coaxial sheath to temperatures T ~ 150°C, raised the pyrolysis temperature. Argon is also passed over the inside of NaCl windows to prevent the deposition of stray particles on the windows. Mass flow controllers were used to establish steady flows of Ar to the windows (~70 sccm) and coaxial sheath (~70 sccm). Another mass flow controller was used to regulate the flow of C_2H_4 (~ 4-8 sccm) through a pyrex bubbler containing liquid $Fe(CO)_5$. The relative concentrations of $Fe(CO)_5$ and C_2H_4 in the reactant gas stream were determined from the cell pressure (measured by a capacitance manometer) and the equilibrium vapor pressure of the $Fe(CO)_5$. Cell pressure was controlled by adjustment of a needle valve located between a rotary vacuum pump and the cross. To control the laser power density and the size of the"pyrolysis zone", a ZnSe lens was used to position the laser beam waist either directly above the reactant gas nozzle for maximum power density, or to one side of the nozzle or the other to reduce the power density. Approximately ~5% of the power was absorbed in the reactant gas mixture.

Liquefaction

The liquefaction experiments were conducted in 50 mL batch autoclaves using a reaction temperature of 658 K, a 15 minute residence time, tetralin

as the solvent and a hydrogen atmosphere (5.5 MPa, ambient). The reactor was charged with 5g of dry coal and 7.5 g of tetralin. Catalyst precursors, including Fe $(CO)_5$, $Fe(C_5O_2H_7)_3$ and molybdenum naphthenate, were added to the reactor in concentrations required to produce equal amounts of metal sulfide during the liquefaction experiment. Two ultrafine, iron-containing catalyst preparations (referred as Fe1 and Fe2) produced by laser pyrolysis were added in 0.1g quantities. Dimethyldisulfide was added for all tests as the sulfiding agent. Coal conversion was obtained by determining the amount of pyridine insolubles (daf) after soxhlet extraction of the reactor products.

The coals used were a Western Kentucky #6 (bituminous) and a Wyodak coal (subbitumnous). The analytical data for the two coals are given in Table 1.

Results and Discussion

Two preparations of spherical iron carbide particles were produced with diameters in the range 3 to 13 nm, both exhibiting the cementite (Fe_3C) structure as indicated by X-ray and electron diffraction. The two preparations are referred to as Fe1 and Fe2. They were prepared at laser power densities of about 1200 and 500 $W.cm^{-2}$, respectively. The particles differed in that Fe1 was stable in air whereas Fe2 was not and spontaneously ignited. To allow their removal from the system for further study, the Fe2 particles were first slowly passivated in the reaction cell with an Ar/O_2 mixture (99%/1%). It is presently believed that Fe2 has a cementite core and a monolayer coating of Fe.

Examination by high resolution transmission electron microscopy showed that the particles were almost spherical in shape and confirmed their small particle size. Analyses of Fe1 particles by XPS, after exposure to air, were consistent with a surface stoichiometry of Fe:C:O of 1:1:2. Hence a significant amount of oxygen is attached to the surface of these particles. The XPS spectra indicated that the surface iron was predominantly as Fe^{3+} in oxide form with about 10% as the carbide.

The conversions obtained in coal liquefaction experiments in the presence of the different additives are summarized in Table 2.

All of the catalysts enhanced the coal conversion over that obtained in the thermal case. For the bituminous coal, the highest conversions were obtained with Fe2 and molybdenum naphthenate. The other iron catalyst precursors

were significantly less effective.

For the subbituminous coal, the conversions tended to be lower. The highest was produced in the presence of molybdenum naphthenate and the iron catalysts all behaved similarly. In view of the high activity displayed by Fe2 with the bituminous coal, the low conversion obtained with the lower rank coal is unexpected. The findings are preliminary and will be confirmed in future work.

At this point at least it may be concluded that the synthesis technique can satisfactorily produce nanometer size particles and that there are some indications that these iron carbides may possess moderate to high activity for coal conversion. Whether they also influence the product distribution and composition is yet to be determined.

Current work continues to focus on catalyst synthesis and on investigations of the catalyst phase after sulfiding and after liquefaction, and studies are being initiated of the catalyst functions through the use of model compounds.

References

1. Lumpkin R E, 1988, Science; **239**; 873-877

2. El Sawy A, Gray D, Talib A, Tomlinson G, 1986, Report SAND86-7103, Albuquerque, NM, USA, Sandia National Laboratories, 198pp.

3. Gray D, Tomlinson G, 1988, Report SAND87-7147, Albuquerque, NM, USA, Sandia National Laboratories.

4. Gray D, Tomlinson G. Wan, E, Moran D, Karlson F, Parsons T "Integrating Coal Cleaning and Pyrolysis with Two-Stage Direct Coal Liquefaction: Assessment of Technical and Economic Potential", presented at DOE Direct Liquefaction Contractors' Meeting, Pittsburgh, Pa, September, 1990.

5. Derbyshire F J, 1988, Catalysis in Coal Liquefaction, IEACR/08, London, UK, IEA Coal Research, 69pp.

6. Wu W R K, Storch H H, 1968, Hydrogenation of Coal and Tar. Bulletin 633, Washington, DC, USA, US Department of the Interior, Bureau of Mines, 195pp.

7. Derbyshire F J, Stansberry P G, 1987, Fuel; **66**; 1741-2
8. Tomlinson G C, Gray D, Neuworth M B, Talib A, Report SAND85-7238, Albuquerque, NM, USA, Sandia National Laboratories, 105pp.

9. Lee J S, Oyama S T, Boudart M, 1987, J. Catalysis; **106**; 125-133

10. Oyama S T, Schlatter J C, Metcalfe J E, Lambert J M, 1988, I & EC Research; **27**; 1639-1648

11. Schlatter J C, Oyama S T, Metcalfe J E, Lambert J M, 1988, I & EC Research; **27**; 1648-1653

12. Sajkowski D J, Oyama S T, American Chemical Society, Div. Petroleum Chemistry, Preprints, 35(2), 233-236, 1990

13. Hawk C O, Hiteshue R W, 1965, Hydrogenation of Coal in the Batch Autoclave. Bulletin 6322 Washington, DC, USA, US Department of the Interior, Bureau of Mines, 42pp.

14. Watanabe Y, Yamada O, Fujita K, Takegami Y, Suzuki T, 1984, Fuel; **63**; 752-755

15. Suzuki T, Yamada O, Then J H, Ando T, Watanabe Y, 1985. Proceedings - 1985 ICCS, Sydney, NSW, Australia, Pergamon Press, pp 205-8

16. Andres M, Charcosset H, Chiche P, Davignon L, Djega-Mariadassou G, Joly J-P, Pregermain S, 1983, Fuel; **62**; 69-72

17. Andres M, Charcosset H, Chiche P, Djega-Mariadassou G, Joly J-P, Pregermain S, 1983, Preparation of catalysts III (Eds. G Poncelet and P Grange), Elsevier, pp675-682

18. Nakao Y, Yokoyama S, Maekawa Y, Kaeriyama K, 1984, Fuel; **63**; 721

19. Haggerty J S, Cannon W R, 1981, in Laser-Induced Chemical Processes (Ed. J I Steinfeld), Plenum Press, New York, NY, USA

20. Fiato R A et al, 1987, US pat. 4,637,753

21. Rice G W et al, 1987, US pat. 4,659, 681

22. Bi X-X, Eklund P C, Stencel J M, Gonzalez R E, Srinivasan R, Derbyshire F J, Proceedings Materials Research Society Meeting, Boston, MA, 26th Nov - 1 Dec, 1990, pp. 167-170.

Table 1
Coal Properties

	C(daf)	H(daf)	N(daf)	TS(daf)	O(daf)1	VM(daf)
W.Ky.#6	82.87	5.42	1.72	5.15	4.8	43.10
Wyodak	71.02	5.42	1.37	1.00	21.2	59.92

1 By difference

Table 2
Coal Conversion Data

Wt. Conversion (daf)

Coal	None	Molybdenum Naphthenate	$Fe(C_5H_7O_2)_3$	$Fe(CO)_5$	Fe1	Fe2
Bituminous (W.Ky.#6	47.1	80.3	62.7	70.4	n.d.1	80.9
Subbituminous (Wyodak)	45.0	73.7	64.6	66.5	61.5	65.0

1 Not determined

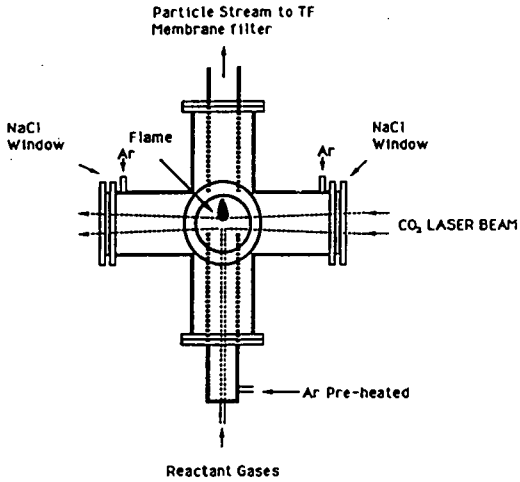

Fig. 1. Schematic Laser Pyrolysis Cell.

STRUCTURE AND DISPERSION OF IRON-BASED DIRECT COAL LIQUEFACTION CATALYSTS

G. P. Huffman, Bhaswati Ganguly, Mehdi Taghiei, F. E. Huggins and Naresh Shah
CFFLS, 233 Mining & Mineral Resources Bldg., University of Kentucky, Lexington, KY 40506-0107

Keywords: liquefaction, catalyst, iron, Mössbauer, XAFS.

Abstract

Mössbauer spectroscopy and X-ray absorption fine structure (XAFS) spectroscopy have been used to characterize the atomic structure and size dispersion of iron-based direct coal liquefaction (DCL) catalysts synthesized by a variety of methods. Samples investigated included a sulfated Fe_2O_3 catalyst, iron added to several coals by chemical impregnation, and iron added to lignite by cation exchange. In the as-dispersed state, all of these catalysts were in the form of superparamagnetic ferric oxides or oxyhydroxides. Size distributions were determined by measuring the percentages of iron contributing to magnetic hyperfine Mössbauer spectra at several temperatures between liquid helium and room temperature, and relating each temperature to a critical particle volume. Size information was also obtained from third and fourth nearest neighbor (nn) iron shell peak amplitudes in radial structure functions derived from the XAFS spectra.

Introduction

There has been much interest in recent years in the use of highly dispersed iron-based DCL catalysts. Several groups have developed methods of preparing such catalysts in very highly dispersed forms.[1-14] It is clearly of interest to develop methods for determining the structure and size of such catalysts. ^{57}Fe Mössbauer spectroscopy has been used by a number of researchers to characterize DCL catalysts.[3,13-20] Yamashita et al.[20] have conducted complementary Mössbauer and XAFS spectroscopy studies on iron-based catalysts in coal.

In the current study, Mössbauer and XAFS spectroscopies have been used to characterize highly dispersed iron-based DCL catalysts prepared by several different research groups. The samples studied included Fe_2O_3 dispersed on carbon black,[21] iron incorporated into coal by chemical impregnation with $FeCl_3$,[5-7] a sulfated Fe_2O_3 catalyst,[9,10] and iron added to lignite by cation exchange.

Experimental Procedure

Catalyst preparation and the efficacy of the various catalysts in DCL have been discussed elsewhere.[1-14] The iron cation-exchanged lignites were prepared in our own laboratory using procedures outlined by Walker and coworkers.[22-24] A lignite from the Penn State sample bank (PSU 1482, Hagel seam) was used.

A standard constant acceleration Mössbauer spectrometer was used. Experimental and least squares analysis procedures are discussed elsewhere.[25,26] Sample temperatures were varied between 12 and 295 K using a Displex cryogenic system.

The XAFS measurements were conducted on beamline X-19A at the National Synchrotron Light Source (NSLS) and beamline IV-1 at the Stanford Synchrotron

Radiation Laboratory (SSRL). X-ray energy was varied using Si(111) double crystal monochromators. All experiments were conducted in the fluorescent mode as described elsewhere.[27]

Results and Discussion

Typical Mössbauer spectra are shown in Figures 1 and 2, which show the spectra obtained at room temperature and 12K from a Wyodak coal impregnated with Fe from an $FeCl_3$ solution[5-7] and from an Fe_2O_3 on carbon black catalyst.[21] All spectra were typical of superparamagnetic ferric oxides. As discussed in more detail elsewhere,[28] the spectra were least squares fitted a series of Lorentzian peaks constrained as quadrupole doublets or magnetic sextets. For most samples, the quadrupole doublet component of the spectrum was dominant at room temperature and exhibited Mössbauer parameters typical of a ferric oxide or oxyhydroxide (isomer shift ≈ 0.34 to 0.39 mm/s, quadrupole splitting ≈ 0.60 to 0.70 mm/s), while the magnetic component became dominant at low temperature and exhibited ferric isomer shifts (0.45 to 0.50 mm/s) and a range of magnetic hyperfine fields (450 to 540 kilogauss). For the samples prepared by Shabtai et al.[5-7] and the cation-exchanged lignites, the Mössbauer parameters were consistent with a superparamagnetic iron oxyhydroxide, while those observed for the Fe_2O_3/SO_4^{-2} and Fe_2O_3 on carbon black were consistent with very fine particle hematite.

As discussed elsewhere,[29-31] when a magnetically ordered particle is small enough, thermal vibrations may cause the ordered spins of the particle to flip over the magnetic anisotropy energy barrier to a new orientation. To a first approximation, the frequency of spin flipping is given by

$$f = f_o \exp\left(\frac{-K_a V}{kT}\right) \tag{1}$$

where K_a is the magnetic anisotropy constant, V is the volume of the particle, k is the Boltzman constant and T is the temperature. The frequency factor f_o is given by Kundig et al.[29] as

$$f = K_a A / \rho N_L h \tag{2}$$

where A is the molecular weight, ρ is the density, N_L is Avogadro's number, and h is the Planck constant. For the magnetic anisotropy constants, we have used the values give by van der Kraan;[31] $K_a = 0.55 \times 10^5$ joule/m^3 for hematite, and $K_a = 1.67 \times 10^5$ joule/m^3 for goethite. Eq. (2) then gives $f_o = 4.2 \times 10^9$ sec^{-1} for hematite and $f_o = 8.7 \times 10^9$ sec^{-1} for goethite. When f is small compared to the nuclear Larmor precession frequency of the ^{57}Fe nuclear magnetic moment ($f_L = 5 \times 10^7$ sec^{-1}), the particle will exhibit a well-resolved six line magnetic hyperfine spectrum. However, when f becomes comparable to or exceeds f_L, the magnetic spectrum collapses to a two peak quadrupole doublet. Putting f equal to f_L and rewriting Eq. (1), we obtain

$$V_c = \frac{kT}{K_a} \ln\left(\frac{f_o}{f_L}\right) \tag{3}$$

Eq. (3) can be viewed as defining a critical volume, V_c, for temperature T. At temperature T, to a first approximation, particles of volume > V_c will give rise to a six-line magnetic hyperfine spectrum, while particles of volume < V_c will exhibit a

paramagnetic quadrupole doublet.

The temperature variation of the magnetic and paramagnetic (quadrupole) percentages is then used with Eq. 3 to generate size distributions. The results are summarized in Figure 3 for all of the as synthesized catalysts investigated by size histograms that show the percentage of iron contained in ferric oxide particles as a function of particle diameter. Spherical particles are assumed in order to derive diameters from the volumes given by Equ. (3). The resolution of these size distributions depends, of course, on the number of temperatures at which spectra are obtained. As discussed in more detail elsewwhere, [28] the error in the diameters indicated in these histograms is approximately ± 5 - 10 Å, while the error in the iron percentages is about ± 5%.

It is seen that most of the catalyst particles in all of the catalysts examined are smaller than approximately 65 - 85 Å in diameter, with from 10 to 70% of the iron contained in particles less than 20-30 Å in diameter. Moreover, many of the particles in the smallest size bin may be of molecular dimensions. It is also seen that the samples prepared by the Shabtai $FeCl_3$ impregnation method[5-7] exhibit the smallest size distributions. During the mild hydrotreatment (290°C, 1500 psig H_2 hot, 2 hours) used by Shabtai and coworkers,[5-7] the iron remains in the form of a ferric oxide or oxyhydroxide and the particle sizes increase somewhat, as seen in Figure 5.

Fourier transformation of the extended X-ray absorption fine structure (EXAFS) of the XAFS spectrum produces a radial structure function (RSF) that is similar to a radial distribution function. Some typical RSFs from the current samples are shown in Figures 4-5. As discussed in detail elsewhere,[32] each peak represents a shell of atoms surrounding the central iron atom. The peak positions on the distance axis are shifted slightly downward by about 0.5 Å relative to the true interatomic distances because of phase shifts, and the peak amplitudes are proportional to several factors, one of which is the shell coordination number.

In Figure 5, the radial structure function (RSF) of α-Fe_2O_3 is compared to that of the Fe_2O_3/SO_4^{-2} catalyst. It is seen that the amplitudes of the peaks arising from the third and fourth nearest neighbor (nn) iron shells in the catalyst are significantly reduced relative to those of the same shells in bulk α-Fe_2O_3. For the cation-exchanged samples and for all of the Shabtai samples, before and after hydrotreatment, the RSFs are similar to that of goethite, but in most cases the third and fourth nn Fe shells are nearly undetectable. This is illustrated by Figure 4.

One explanation of the decreased amplitudes of the third and fourth nn iron shell peaks is that the iron atoms at or near the surfaces of these very small catalyst particles do not have their full complement of third and fourth iron nn. Since it may reasonably be expected that the first nn oxygen coordination of these iron atoms is unchanged, a convenient measure of the decrease in the average number of iron atoms in the third and fourth nn shells is the ratio of those peak heights in the RSF to that of the oxygen first nn shell. These peak height ratios are summarized for all catalyst samples and for the appropriate standard compounds in Table 1. Assuming that these ratios are proportional to the ratios of the coordination numbers, we can deduce the average iron coordination numbers for the catalysts by comparing their peak height ratios to those of the standard compounds for which the coordination numbers are known. These results are also indicated in Table 1. It is of interest to note that the third and fourth nn shell peaks are essentially absent from the RSFs of several of the Shabtai and cation-exchanged samples. However, because of the noise level of the RSFs, the lowest peak height ratio that can be reliably determined from the current data is approximately 0.2. Therefore, we can only put a lower limit on coordination numbers for these samples.

Table 1. Summary of peak height information from RSFs. H/H_{OX} is the ratio of the height of the peak from the iron shell to that of the oxygen nn shell.

Sample	Peak No.	Shell type	Distance (Å)	H/H_{OX} (±0.1)	Coord. No. (±1)
Magnetite, Fe_3O_4	3	Fe	2.97	1.65	8
	4	Fe	3.49	1.69	12
PSOC 1482, ion ex.	3	Fe		1.00	4.8
0.5M $Fe(OOCCH_3)_2$	4	Fe		1.07	7.6
Hematite, 2-Fe_2O_3	3	Fe	2.88, 2.97 } <2.95>	1.74	1, 3 } 4
	4	Fe*	3.70	1.27	6
Fe_2O_3/SO_4^{-2}	3	Fe		0.91	2.1
	4	Fe*		0.70	3.3
Fe_2O_3 on carbon black	3	Fe		1.03	2.4
	4	Fe*		0.58	2.7
Goethite, α-FeOOH	3	Fe	3.01, 3.21, 3.42 } <3.28>	0.80	2, 2, 4 } 8
PSOC 1482, ion ex., 0.02 M Fe $(OOCCH_3)_2$	3	Fe		0.43	4.3
PSOC 1482, ion ex., $FeCL_2$	3	Fe		<0.2	<2
Blind Canyon [$FeCl_3$ treated - Shabtai]	3	Fe		<0.2	<2

*Oxygen neighbor shells also contribute to this peak.

Summary and Conclusions

A variety of iron-based liquefaction catalysts have been investigated by Mössbauer and XAFS spectroscopy. Samples investigated included coals subjected to an $FeCl_3$ impregnation treatment described by Shabtai and coworkers,[5-7] a highly dispersed Fe_2O_3 on carbon black catalyst,[21] iron dispersed in a lignite by cation exchange, and a sulfated hematite catalyst (Fe_2O_3/SO_4^{-2}) prepared by Wender and coworkers,[9,10]. The results may be summarized briefly as follows:

1. Both Mössbauer and XAFS spectroscopies can determine the structure of the catalysts and provide information on their size. The Mössbauer technique is more accurate but is also a much slower measurement, typically requiring 10-20 hours, while the XAFS measurement normally requires about 30-60 minutes.
2. In all cases, the initial as-dispersed or as-prepared catalyst is in the form of a highly dispersed ferric oxide or oxyhydroxide.
3. Because of superparamagnetic relaxation effects, the Mössbauer spectra exhibit a

significant increase in the percentage of iron contributing to magnetic hyperfine patterns as the sample temperature is lowered. These magnetic hyperfine percentages may be converted into particle size distributions which indicate that the size of the as-dispersed ferric oxyhydroxides and oxides range from molecular to particles ~20 - 100 Å in diameter.

A more detailed discussion of these results will be given elsewhere.[28]

Acknowledgement

This research was sponsored by the U.S. Department of Energy under DOE Contract No. DE-FC22-90PC90029. The NSLS and SSRL facilities are also sponsored by the U.S. DOE. We are grateful to Dr. Joseph Shabtai of the University of Utah, Dr. Irving Wender of the University of Pittsburgh and Dr. Malvina Farcasiu of the U.S. DOE Pittsburgh Energy Technology Center for providing us with samples.

References

1. Suzuki, T.; Yamada, O.; Takehaski, Y.; Watanabe, Y. *Fuel Process. Technol.*, **1985**, *10*, 33-43.
2. Watanabe, Y.; Yamada, O.; Fujita, K.; Takegami, Y.; Suzuki, T. *Fuel* **1984**, *63*, 752-755.
3. Herrick, D. E.; Tierney, J. W.; Wender, I.; Huffman, G. P.; and Huggins, *Energy and Fuels*, 1990, *4*, 231-236.
4. Herrick, D. E., Ph.D. Thesis, University of Pittsburgh, **1990**.
5. Shabtai, J. S.; Saito, I.; U.S. Patent, 4,728,418 (1988).
6. Shabtai, J. S.; Zhang, Y. *Proc. 1989 Internat. Confer. Coal Science*, Tokyo **1989**, Vol. II, 807-810.
7. Shabtai, J. S., Skulthai, T. *Proc. 1987 Internat. Conference Coal Science* Maastricht, The Netherlands, Elsevier, 761-764.
8. Marriadassou, D. G.; Charcosset, H.; Andres, M; Chiche, P.; *Fuel*, **1986**, Vol. 62, pp. 69-72.
9. Pradhan, V. R. ; Tierney, J. W.; Wender, I.;' Preprints, Div. of Fuel Chem., *American Chemical Society*, August **1990**, vol. 35, No. 3, p. 793.
10. Pradhan, V. R.; Tierney, J. W.; Wender, I.; and Huffman, G. P.; **1991**, submitted to *Energy & Fuels*.
11. Tanabe, K.; Yamaguchi, T.; Hattori, H.; Sanada, Y.; Yuokoyama, S.; *Fuel Processing Technology*, **1984**, Vol. 14, pp. 247-260.
12. Tanabe, K.; Tamaguchi, T.; Hattori, H.; Matsuhashi, H.; Kimura, A.; *Fuel Processing Technology*, **1986**, Vol. 8, pp. 117-122.
13. Cook, P. S. and Cashion, J. D.; *Fuel*, **1987**, *66*, 661-668.
14. Cook, P. S. and Cashion, J. D.; *Fuel*, **1987**, *66*, 669-677.
15. Montano, P. A. and Granoff, F., *Fuel*, **1980**, *59*, 214.
16. Montano, P. A.; Bommannavar, A. S.; and Shah, V.; *Fuel*, **1981**, *60*, 703.
17. Bommannavar, A. S. and Montano, P. A.; *Fuel*, **1982**, *61*, 523.
18. Ogawa, T.; Stenberg, V. I.; and Montano, P. A.; *Fuel*, **1984**, *63*, 1660-1663.
19. Montano, P. A.; Stenberg, V. I.; and Sweeny, P.; *J. Phys. Chem.*, **1986**, *90*, 156-159.
20. Yamashita, H.; Oktsuka, Y.; Yoshida, S.; and Tomita, A.; *Energy & Fuels*, **1989**, *3*, 686.
21. Sample provided by Malvina Farcasiu, U. S. DOE Pittsburgh Energy Technology Center.
22. Walker, Jr., P. S.; Matsumoto, S.; Hanzawa, T.; Murira, T.; Ismail, I. M. K.; *Fuel*, **1983**, *62*, 140-149.
23. Jenkins, R. G.; Nandi, S. P.; and Walker, P. L.; *Fuel*, **1973**, *52*, 288.

24. Mahajan, O. P.; Yarzab, R; and Walker, P. L.; *Fuel*, **1978**, *57*, 643.
25. Huffman, G. P.; Huggins, F. E.; *Fuel* **1978**, *47*, 592-604.
26. Huggins, F. E.; Huffman, G. P. Mössbauer Analysis of the Iron-Bearing Phases in Coal, Coke, and Ash. *Analytical Methods for Coal and Coal Products*; Karr, Jr., C., Ed.; Academic Press: New York, 1979; Vol. III p. 371-423.
27. Lytle, F. W.; Greegor, R. B.; Sandstrom, D. R.; Marques, E. C.; Wong, Joe; Sprio, C. L.; Huffman, G. P.; and Huggins, F. E.; *Nucl. Instrum & Methods*, **1984**, *226*, 542-548.
28. Huffman, G. P.; Huggins, F. E.; Ganguly, B.; Taghiei, M.; and Shah, N., "Structure and Dispersion of Iron-Based DCL Catalysts," submitted to *Energy & Fuels*.
29. Kundig, W.; Bömmel, Constabaris, G.; Lindquist, R. H.; *Phys. Rev.*, **1966**, *142*, 327.
30. Wickman, H. H.; "Mössbauer Paramagnetic Hyperfine Structure," pp. 39-66, *Mössbauer Effect Methodology*, Ed. I. J. Gruverman, Plenum Press, NY, 1966.
31. van der Kraan, A. M.; *Phys. Stat. Sol.* **1973**, (a) *18*, 215.
32. Lee, P. A.; Citrin, P. H.; Eisenberger,; and Kincaid, B. M.; *Rev. Mod. Phys.*, **1981**, *53*, 769-806.

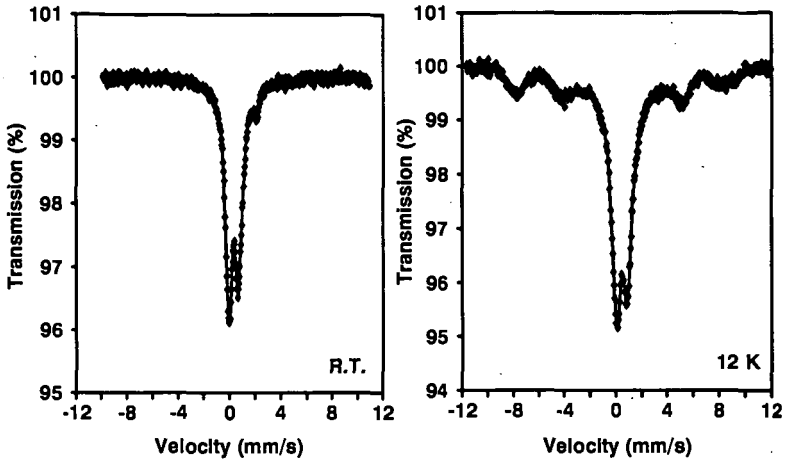

Figure 1- Room temperature and 12 K Mössbauer spectra of a Wyodak coal impregnated with iron by the Shabtai treatment.

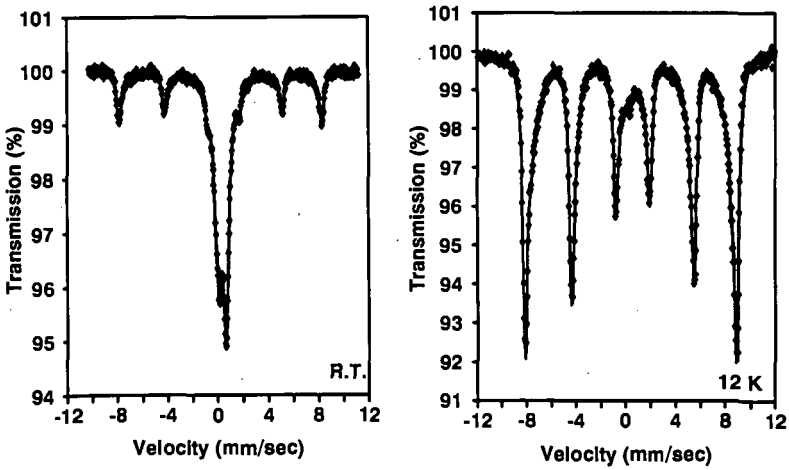

Figure 2- Room temperature and 12K Mössbauer spectra of an Fe_2O_3 on carbon black catalyst.

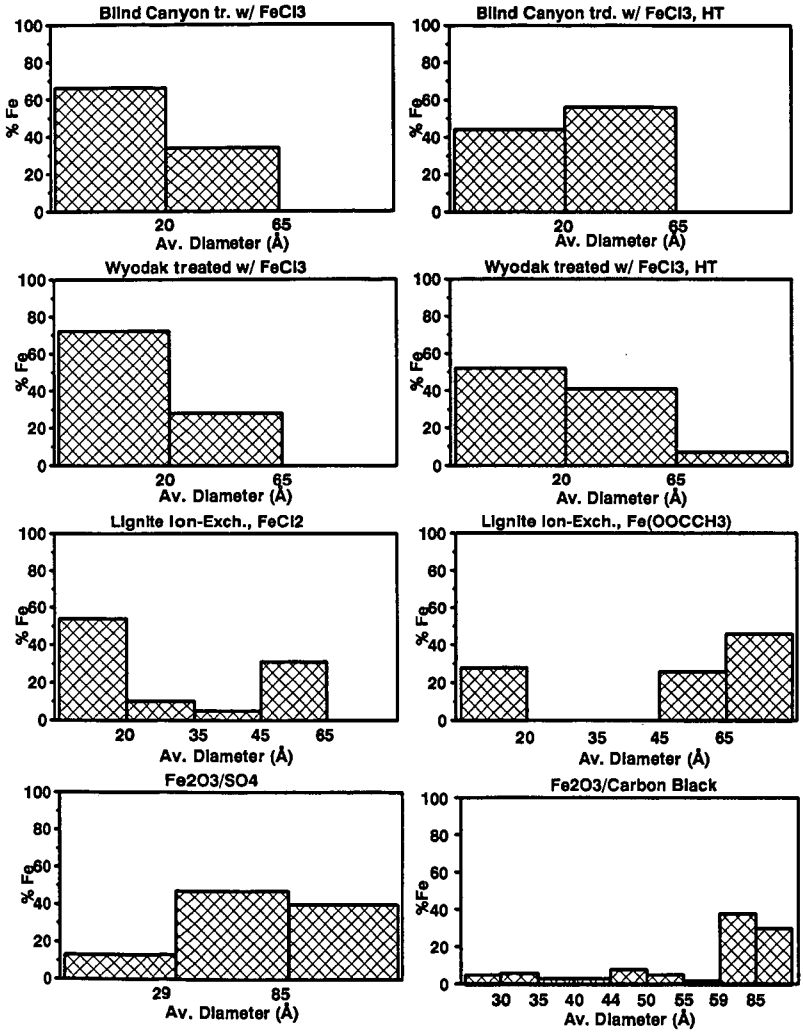

Figure 3- Size distribution for various as-dispersed iron DCL catalysts derived from Mössbauer data.

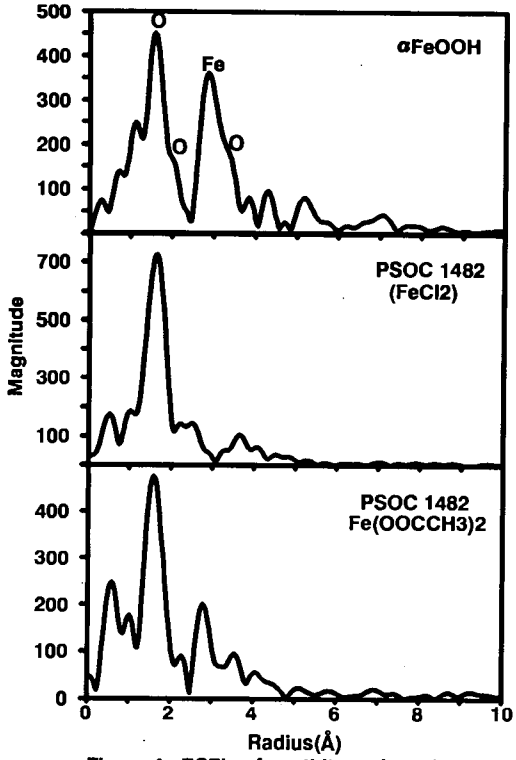

Figure 4. RSF's of goethite and two iron cation-exchanged lignites.

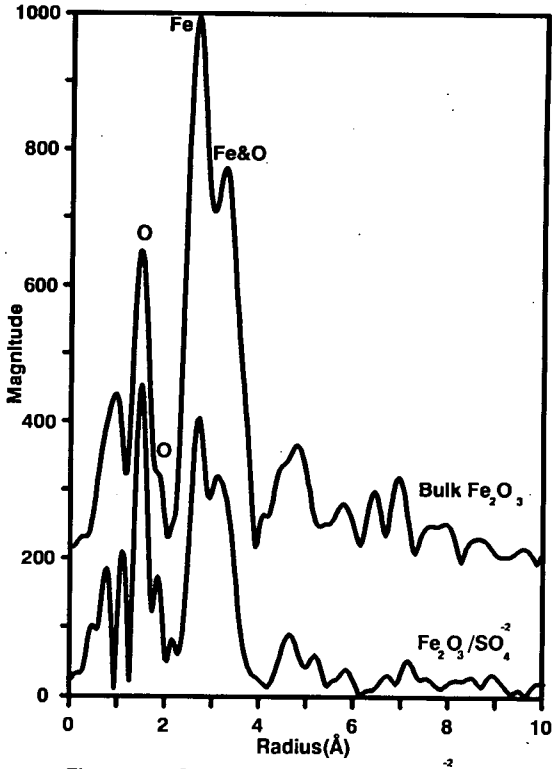

Figure 5. RSF's of hematite and Fe_2O_3/SO_4^{-2} catalyst.

HYDROTALCITE CATALYSIS OF HYDROTREATING REACTIONS

Ramesh K. Sharma, Daniel C. Stanley, Paul L. Holm,
and Edwin S. Olson,
University of North Dakota Energy and Environmental Research Center
Box 8213, University Station, Grand Forks, ND 58202

Key Words: Hydrotalcite, pillared, hydrotreating

Magnesium-aluminum hydrotalcites have been tested for hydrotreating coal liquids. To understand the mechanism of the reactions that are catalyzed by the hydrotalcites, model compounds have been reacted with various potential hydrogen donors in the presence of several forms of the hydrotalcites. Aryl-heteroatom bonds are easily cleaved by hydrogen at temperatures below 350°C, not only with terephthalate-pillared hydrotalcite, but also with hydrotalcite carbonate. Evidence favors a Lewis acid catalysis mechanism for this process. Although molecular hydrogen is required for heteroatom cleavage, no activation of molecular hydrogen or any hydrogen donor molecule occurs on the hydrotalcite. Thiomolybdate-exchanged pillared hydrotalcite is converted to an active hydrogenation catalyst at these temperatures. However, higher temperatures are required for hydrocracking activity.

INTRODUCTION

Novel supports for metallic sulfide catalysts have been under investigation for their potential use in coal liquefaction. Conventional supported hydrogenation catalysts have encountered difficulties in coal liquefaction due to deactivation and coking (1-4). New catalysts may require more dispersed forms of catalytic sites or greater micropore dimensions to improve accessibility to catalytic sites. Hydrotalcites have been utilized in catalytic processing of various types (5-10), and recently, pillared hydrotalcites with large micropores were utilized in oxidation reactions (11).

This paper describes recent efforts to understand the effects of the hydrotalcite structure during hydrotreatment processing. Model compounds were treated with hydrogen and hydrogen donors in the presence of various pillared and nonpillared hydrotalcites.

EXPERIMENTAL

The following reagents: bibenzyl, cumene, 1-methylnaphthalene, diphenyl sulfide, 9,10-dihydroanthracene, and neopentylbenzene were obtained from Aldrich Chemicals, Co., Milwaukee, Wisconsin.

Preparation of Catalysts:

Hydrotalcites and molybdenum-exchanged hydrotalcites were prepared as described earlier (11,12). Instead of ammonium molybdate, ammonium tetrathiomolybdate was used for exchange into hydrotalcite. For the preparation of formate-pillared hydrotalcite, 160 mL of carbon dioxide-free distilled water were placed in a three-necked round-bottomed flask fitted with nitrogen inlet and outlet tubes and a dropping funnel. The system was purged with nitrogen for 30 minutes. Sodium formate (21.77 g) and sodium hydroxide (57.66 g) were placed into the reaction flask and stirred. When the dissolution of sodium formate was complete, a solution of 41.04 g of magnesium nitrate hexahydrate and 30.0 g of aluminum nitrate nonahydrate in 128 mL of carbon dioxide-free water was added dropwise into

the flask. The addition was completed after about one hour. A gel-like white precipitate was formed. The dropping funnel was then replaced by a reflux condenser and the reaction mixture heated to 75-85°C and allowed to stir overnight. After 9 hours had elapsed, about one third of the water had escaped from the container, so additional carbon dioxide-free water was added to bring the volume back to its original level and the reaction stirred for 9 more hours. The crude product was isolated by vacuum filtration and purified by resuspending in carbon dioxide-free water and centrifuging. The pasty white material was dried by heating in vacuum at 65°C until all the moisture had been driven off. The infrared spectum of the formate-hydrotalcite showed strong absorptions at 1593 and 1379-1406 cm^{-1} which are consistent with bands expected for the antisymmetrical and symmetrical vibrations of the COO^- structure (13).

Infrared spectra were obtained in KBr on either a Perkin Elmer Model 283 spectrometer or a Nicolet 20SXB FTIR spectrometer, equipped with a mercury cadmium telluride (MCTA) detector, and a Nicolet 1280 computer with a fast Fourier transform coprocessor. Quantitative GC/FID analyses were performed with a Hewlett Packard 5880A gas chromatograph equipped with Pectrocol column. Isooctane and n-octadecane were the internal standards. GC/MS was performed on a Finnigan 800 ITD ion trap detector with a HP 5890A gas chromatograph and a J&W 30-m x 0.32-mm (ID), 1.0-micron film of DB-5. A 15-m x 0.25-mm (ID), 0.25-micron DB-5 film capillary column was used for the analysis of high-boiling components. A Dupont Model 951 thermogravimetric analyzer module interfaced with a Dupont Model 1090 thermal analyzer was used to determine the thermal decomposition of the catalysts.

Hydrotreating Reactions:

In a typical run, 0.5 g of substrate and 0.25 g of catalyst were placed in a tubing bomb reactor. The reactor was sealed and pressurized with 68 atm of hydrogen or deuterium if needed, placed in a rocking autoclave heated to desired temperature, and heated for three hours. The reactor was cooled in dry ice-acetone slurry, degassed, and opened. The contents of the reactor were mixed with an appropriate internal standard and transferred into a centrifugation tube by washing with dichloromethane. The solid was separated by centrifugation. The liquid sample was analyzed by quantitative GC and GC/FTIR/MS. The solid was dried in vacuum at 110°C for 3 hours. The analytical data are given in Table 1.

RESULTS AND DISCUSSION

A thermogravimetric method was used to determine the thermal decomposition of hydrotalcite and supported-hydrotalcite catalysts. Heating terephthalate-pillared hydrotalcite to 100°C resulted in 3.8% weight loss. This can be assumed to be the loss of interstitial water. For the tetrathiomolybdate-exchanged terephthalate-pillared hydrotalcite, the weight loss continued to 240°C. The additional loss may be due to the removal of sulfur from MoS_4 moieties. In the 240-300°C range, rapid loss was observed, which could be due to further loss of sulfur to form MoS_2 moieties. When the temperature was increased further, the weight loss was more or less continuous until 466°C. A 25% weight loss occurred in this temperature regime, which may be attributed to the decomposition of terephthalate. The weight loss is not consistent with that expected for decomposition of the hydrotalcite layer structure. Thus the hydrotalcite layer structure is stable at temperatures used for hydrotreating reactions.

In order to identify the selectivity and reactivity of hydrotalcite catalysts, the reactions of model compounds such as bibenzyl, 1-methylnaphthalene, cumene, neopentylbenzene, and dipheny sulfide were carried out with hydrotalcite, pillared

hydrotalcite, and molybdenum sulfide supported on hydrotalcite catalysts. Diphenyl sulfide was used as a test compound to investigate the catalytic activity of hydrotalcite catalysts for aryl-sulfur bond cleavages. The reaction of diphenyl sulfide with terephthalate-pillared hydrotalcite at 300°C for 3 hours in the presence of 68 atm of hydrogen gave 86.4% conversion of the substrate into products (Table 1). Reaction products were mainly benzene and H_2S, along with a small amount of benzenethiol. When the same reaction was carried out in the absence of catalyst, the conversion was very small (1%). A trace amount of benzene was the only product. The reaction of diphenyl sulfide with tetrathiomolybdate-exchanged terephthalate-pillared hydrotalcite at 300°C for 3 hours in the presence of 68 atm of hydrogen gave a high conversion (88.9%) of diphenyl sulfide. The major product from this reaction was benzene. Small amounts of cyclohexane, thiophenol, cyclohexanethiol were also formed. Nonpillared hydrotalcite (carbonate) gave conversion and product distributions

TABLE 1. CATALYTIC HYDROTREATING OF DIPHENYL SULFIDE (DPS)

Reaction Temp. = 300°C, Reaction Time = 3 hrs
Catalyst wt./Substrate wt. = 0.5, H_2 = 68 atm

Catalyst (g)	Substrate (mmol)	Conv. (%)	Major Products (mmol)
None	DPS (2.68)	1	Benzene (trace)
Mg-Al-HT (0.25)	DPS (2.73)	81.7	Benzene (4.5) Benzenethiol (0.13)
Zn-Cr-HT (0.25)	DPS (2.64)	60	Benzene (2.9) Benzenethiol (tr.)
PH-HT (0.25)	DPS (2.95)	86.4	Benzene (4.4) Benzenethiol (0.12)
F-HT (0.25)	DPS (2.71)	83.4	Benzene (4.0) Benzenethiol (0.2)
MgO (0.25)	DPS (2.67)	2	Benzene (trace)
Calcined Mg-Al-HT (0.25)	DPS (2.74)	40	Benzene (1.9) Benzenethiol (0.15)
Mo-PH-HT (0.25)	DPS (2.79)	88.9	Benzene (4.5) Cyclohexane (0.1)

Mg-Al-HT = Magnesium aluminum hydrotalcite carbonate
Zn-Cr-HT = Zinc chromium hydrotalcite nitrate
PH-HT = Terephthalate-pillared hydrotalcite
F-HT = Formate-exchanged hydrotalcite
Mo-PH-HT = Molybdenum-exchanged terephthalate-pillared hydrotalcite

similar to the terephthalate-pillared hydrotalcite described above. Thus neither the molybdenum (sulfide) nor the pillared structure are required for carbon-sulfur bond cleavage; the hydrotalcite itself is sufficient for catalysis of hydrogenolysis of these bonds. The active sites for this catalysis were hypothesized to be electron deficient aluminum sites in the hydrotalcite layer. The hydrotalcite-carbonate was calcined at 450°C to dehydrate and decompose carbonate. The hydrotalcite layer structure is significantly altered at higher temperatures. The calcined hydrotalcite was then used to catalyze the hydrogenolysis reaction of diphenyl sulfide. The conversion was low, but activity was not totally lost. Magnesium oxide was, however, completely inactive as a catalyst for diphenyl sulfide hydrogenation. These oxides are, of course, basic, but the calcined hydrotalcite may still contain active Lewis acid sites corresponding to trigonal Al atoms.

With zinc-chromium hydrotalcite (nitrate) as the catalyst, the conversion was significantly lower (60%). The product distribution was the same as that with magnesium-aluminum hydrotalcite carbonate. The conversion and product distributions from the reaction of formate-exchanged hydrotalcite were also comparable with that of terephthalate-pillared hydrotalcite. Unlike reactions with solid acid catalysts, no coking, oligomeric products, or dibenzothiin were observed in any of the reactions (14).

Reactions of diphenyl sulfide with terephthalate-pillared hydrotalcite (no molybdenum) in the absence of hydrogen gas indicated a very small conversion (3%) of diphenyl sulfide into products. A trace amount of benzene was the only product from this reaction (Table 2). Thus molecular hydrogen is required for carbon-sulfur bond cleavage in the hydrotalcite reactions. This was not the case in the reactions of various model compounds with strong acid catalysts, where products such as benzene were observed even when molecular hydrogen was not present. These products could be derived from proton addition to the ipso position of the benzene ring (Brönsted-acid mechanism) followed by cleavage of the substituent groups and probably hydride donation from Scholl intermediates. No condensation to oligomeric or polymeric material or coke was observed for any of the hydrotalcite reactions carried out in the absence of molecular hydrogen. This fact and the requirement for molecular hydrogen are inconsistent with a Brönsted acid mechanism for the hydrotalcite reaction.

When hydrogen was replaced by deuterium, the conversion of diphenyl sulfide was considerably smaller. The decreased conversion could be attributed to isotope effects. The majority of the benzene product was singly labeled, but multiple labeling was also observed. No deuterium was incorporated into the recovered diphenyl sulfide.

The reaction of molecular hydrogen with 1-methylnaphthalene was investigated with the hydrotalcite to determine if the hydrotalcite structure can catalyze the addition of hydrogen. The conversion of 1-methylnaphthalene was only 9% with the phthalate-pillared hydrotalcite, whereas the tetrathiomolybdate-exchanged phthalate-pillared hydrotalcite gave 95% conversion. Only a small amount of cracking to naphthalene occurred in either reaction. It is clear that the tetrathiomolybdate in the interstitial layer was converted to a form that was highly active for catalyzing the addition of molecular hydrogen to aromatics. It is not yet known what the form of molybdenum is: MoS_2 microcrystals, MoS cluster, or some monomeric form.

TABLE 2. REACTIONS OF DIPHENYL SUFIDE

Reaction Temp. = 300°C, Reaction Time = 3 hrs
Catalyst wt./Substrate wt. = 0.5

Catalyst (g)	Substrate (mmol)	Reduc. (psi/g)	Conv. (%)	Major Products (mmol)
PH-HT (0.25)	DPS (2.77)	None	3.0	Benzene (tr.)
PH-HT (0.25)	DPS (2.95)	Hydrogen 68 atm	86.4	Benzene (4.4) Benzenethiol (0.12)
PH-HT (0.25)	DPS (2.67)	Deuterium 68 atm	21.1	Benzene (0.4) Benzenethiol (tr.)
PH-HT (0.25)	DPS (2.75)	CO/H_2O 68 atm 0.22 g	10.2	Benzene (0.3) Benzenethiol (tr.)
PH-HT (0.25)	DPS (2.77)	DHA 1.00 g	9.0	Benzene (0.3) Benzenethiol (tr.)
PH-HT 0.25	DPS (2.83)	Methanol 1.00 g	7.1	Benzene (0.2)
F-HT (0.25)	DPS (2.79)	None	4.0	Benzene (tr.) Benzenethiol (tr.)

Thus, the hydrotalcite structure itself (no molybdenum) possesses significant capability for hydrodesulfurization. Since only minimal hydrogenation was observed with 1-methylnaphthalene, we conclude that hydrotalcite does not activate hydrogen, but hydrogen is required for the conversion of diphenyl sulfide with hydrotalcite. The question of how the C-S bonds are cleaved in the presence of hydrogen is very interesting and deserves further study. Since molecular hydrogen is evidently not activated directly by the hydrotalcite catalyst for addition to aromatics, the use of hydrogen sources other than molecular hydrogen was examined to determine whether the hydrotalcite catalyst could catalyze the transfer of hydrogen from these hydrogen sources to a sulfur-containing species, thereby catalyzing reductive cleavage of the C-S bond. The interlayer space of hydrotalcite contains basic species that could be involved in the formation of hydride-donor intermediates that would affect the reduction. Since carbon monoxide and water generate potential hydride donor species in the presence of a base, the reaction of diphenyl sulfide in this system was investigated (no molecular hydrogen added). Conversion was very small (10%). Hydrotalcite (formate) gave a similar poor conversion in the absence of hydrogen. Methanol has been shown to be an effective reductant in basic conditions, but it also gave a poor conversion of diphenyl sulfide in the reaction with hydrotalcite. A radical hydrogen transfer mechanism is another route for reduction of the C-S bond. The reaction of diphenyl sulfide was carried out in the presence of 9,10-dihydroanthracene. If the mechanism involved homolytic cleavage of the C-S bond to give a radical intermediate, this radical intermediate should be able to abstract hydrogen from dihydroanthracene. However, the conversion in the experiment was,

again, very poor (9%). Since the conversions in these experiments are a bit higher than in the case with no hydrogen or no reductant, there may have been some small amount of hydrogen generated in the experiments as a result of a water-gas reaction or dihydroanthracene decomposition to hydrogen.

No evidence for phenol was found in any reaction. The formation of phenol would have indicated that the basic species directly attacked the C-S bond. Catalysis of the C-S bond cleavage appears to be associated with the hydrotalcite layers, rather than basic species. Because of the aluminum atoms in the layer structure, many electron deficient sites (Lewis acids) are available for catalysis. The reactions observed with hydrotalcites are significantly different from reactions with other solid acid catalysts, however, since condensations and formation of dibenzodithiin were not found.

The hydrocracking activity of hydrotalcite and molybdenum supported on hydrotalcite was investigated by reacting bibenzyl, cumene, and neopentylbenzene with this catalyst. The reaction of bibenzyl with molybdenum supported on hydrotalcite at 300°C for 3 hours and in the presence of 68 atm of hydrogen gave a small percent conversion. Traces of benzene and toluene were the only products. Increasing the temperature (350 and 400°C) resulted in an increase in the percent conversion of bibenzyl (25 and 40%, respectively). Benzene, toluene, and ethylbenzene were major products of this reaction. Previous studies with solid acid catalysts gave mostly benzene and ethylbenzene via the Brönsted acid-ipso cleavage mechanism. The large amount of toluene formed from bibenzyl indicates that a major pathway for hydrocracking in the HT-catalyzed reaction is cleavage of the bond adjacent to the ring (α-β cleavage). A similar cleavage was observed for the reaction of cumene with HT catalyst, which gave ethylbenzene as the major product. Other products resulted from Lewis acid-catalyzed rearrangement and alkyl addition reactions of the cumene. Neopentylbenzene exhibited similar α-β cleavage to give toluene.

A mechanism involving the Lewis acid HT sites is shown in Figure 1. Al in the figure represents an electron deficient Lewis acid site that bonds to the aryl ring.

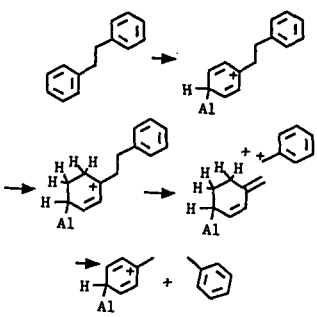

Figure 1. Hydrotalcite-catalyzed mechanism.

TABLE 3. CATALYTIC HYDROTREATMENT OF MODEL COMPOUNDS

Reaction Time = 3 hrs, Hydrogen = 68 atm
Catalyst wt./Substrate wt. = 0.5

Catalyst (g)	Substrate (mmol)	Temp. (°C)	Conv. (%)	Major Products (mmol)
PH-HT (0.25)	1-MENP (3.66)	350	9	Methyltetralins (0.1) Naphthalene (0.06)
MO-PH-HT (0.25)	(1-MENP) (3.67)	350	94.6	Methyltetralins (2.8) Decalin (0.2) Naphthalene (0.06) Tetralin (0.12)
PH-HT (0.25)	BB (2.69)	300	8	Benzene (tr.) Toluene (tr.)
Mo-PH-HT (0.25)	BB (2.76)	350	25	Benzene (0.04) Toluene (0.1) Ethylbenzene (0.2)
MO-PH-HT (0.25)	BB (2.75)	400	40	Benzene (0.2) Toluene (0.4) Ethylbenzene (0.2)
PH-HT (0.25)	Cumene (4.10)	400	14	Ethylbenzene (0.3) Benzene (0.1) n-Propylbenzene (0.1)
PH-HT (0.25)	NPB (3.40)	400	23.8	Benzene (0.13) Toluene (0.5)

PH-HT = Molybdenum-exchanged terephthalate-pillared hydrotalcite
DPS = Diphenyl sulfide
BB = Bibenzyl
NPB = Neopentylbenzene

CONCLUSIONS

Thiomolybdate-exchanged terephthalate-pillared hydrotalcite is converted to active hydrogenation catalyst during heating with the substrates. Effective hydrodesulfurization activity resides with the hydrotalcite portion of the catalyst. At higher temperatures, hydrocracking activity is also observed.

ACKNOWLEDGMENTS

This research was supported by contract No. DOE-FC21-86MC10637 from the U.S. Department of Energy. References herein to any specific commercial product by trade name or manufacturer does not necessarily constitute or imply its endorsement, recommendation, or favoring by the United States Government or any agency thereof.

REFERENCES

1. Derbyshire, F. ACS Div. of Fuel Chem. Preprints 1988, 33, (3), 188.

2. Garg, D.; Givens, E.N. Fuel Proc. Technol. 1984, 9, 29.

3. Kovach, S.M.; Castle, L.J.; Bennett, J.V.; Svrodt, J.T. Ind. Eng.Chem. Prod. Res. Dev. 1978, 17, 62.

4. Mills, G.A.; Beodeker, E.R.; Oblad, A.G. J. Am. Chem. Soc. 1950, 72 1554.

5. Reichle, W.T.; Warren, N.J. U.S. Patent 4 458 026, 1984.

6. Reichle, W.T. J. of Catalysis 1985, 4, 547.

7. Reichle, W.T.; Kang, S.Y.; Everhardt, D.S. J. of Catalysis 1986, 101, 352.

8. Rameswaren, M.; Dimotakus, E.; Pinnavaia, T.J. ACS Div. of Fuel Chem. Preprints 1988, 33, (4), 942.

9. Kohjiya, S.; Sato, T.; Nakayama, T.; Yamashita, S. Makromol. Chem., Rapid Commun. 1981, 2, 231.

10. Nakatsuka, T.; Kawasaki, H.; Yamashita, S.; Kohjiya, S. Bull. Chem. Soc. Japan 1979, 52, 2449.

11. Drezdon, M.A. U.S. Patent 4 774 212, 1988.

12. Olson, E.S. "Quarterly Technical Progress Report for the Period July to September 1989," EERC.

13. Bellamy, L.J. The Infrared Spectra of Complex Molecules; 3rd Ed., John Wiley & Sons, Inc.: New York, 1975, 199.

14. Sharma, R.K.; Diehl, J.W.; Olson, E.S. ACS Div. of Fuel Chem. Preprints 1990, 35, (2), 414.

MECHANISM OF HYDROTREATING REACTIONS: SOLID ACID CATALYSIS

University of North Dakota, Grand Forks, ND 58201
Energy and Environmental Research Center
by
Edwin S. Olson, John W. Diehl, and Ramesh K. Sharma

ABSTRACT

Acid catalysis of coal liquefaction has been extensively studied with both solid and liquid forms of catalysts. Zinc chloride has been utilized in the molten state, complexed with methanol, and supported on silica gel and other materials. This paper addresses the differences between the mechanistic pathways occurring in these various states. Thermal studies of the silica gel-supported zinc chloride demonstrate a change from Lewis to Bronsted acidity with increasing temperature. The major pathway for silica gel-supported zinc chloride is Bronsted acid catalysis, but some Lewis acid activity is found. Since hydrogen does not add directly to the primary carbonium ion intermediates involved in hydrodealkylation of alkylarenes, the role of hydrogen in driving the reaction to the cracked products rather than condensation is being investigated.

Key Words: Brönsted acidity, solid acid catalyst, oligomer

INTRODUCTION

Conversion of coal to a liquid product with an acid catalyst has been extensively investigated in the last quarter century. A liquefaction process which utilized molten zinc chloride as an acid catalyst was developed by consolidation Coal Company (1). Fundamental studies of the chemistry of zinc chloride-catalyzed liquefaction were pursued at Berkeley and other laboratories. Zinc chloride is a mild Lewis acid, and under anhydrous conditions was not able to effectively catalyze the cleavage of aryl-alkyl bonds at moderate temperatures (325°C) unless the rings were highly activated (2). Complexation of zinc chloride with methanol, water, or hydrogen halide gave catalysts with proton-donating potential (Bronsted acidity) that were able to catalyze hydrocracking more effectively (3). Reactions with dibenzylether at 325°C gave products that could have resulted from Lewis acid catalysis of cleavage of C-O bond (4); however, hydrogen chloride, which formed as a reaction product from the ether caused rapid cleavage of the ether when combined with the zinc chloride.

We have recently developed effective catalysts for coal hydrotreatment in which zinc chloride is complexed to solid supports. Zinc chloride bonded to silica gel or clay supports have been found to effectively catalyze cleavage reactions and remove heteroatoms from model compounds (5,6) as well as coal liquids (7,8).

This paper reports our work on the characterization of acidic sites of the silica gel-supported zinc chloride catalysts. Reactions with model compounds confirmed the mechanistic implications of these studies.

EXPERIMENTAL

Catalyst Preparation

Silica gel-supported zinc chloride catalysts, SZC-50 (50 wt.% zinc chloride-loaded silica gel) and SZC-16 (16 wt.% zinc chloride-loaded silica gel) were prepared as described earlier (5).

Characterization of Solid Acid Catalysts

Acidity Measurements

Surface acidity of the solid acid catalysts was determined by pyridine adsorption and desorption using infrared and thermogravimetric analyses.

Infrared Method

A small amount of sample (100 mg) was placed in a glass chamber attached to a vacuum pump, gas inlet, and a gas outlet. The chamber was evacuated, and argon saturated with pyridine was introduced into the chamber until the weight increase ceased. At this stage, the chamber was evacuated until the physisorbed pyridine was removed as indicated by the constant weight of the base absorbed sample. The infrared spectra of the pyridine-absorbed catalyst was obtained in KBr on a Nicolet 20SXB FTIR spectrometer with diffused reflectance cell, equipped with a mercury cadmium telluride (MCTA) detector, and a Nicolet 1280 computer with a fast Fourier transform coprocessor. The pyridine-absorbed catalyst was heated in vacuo at several temperatures, and infrared spectrum was recorded for the residue formed at each temperature.

Thermogravimetric Method

Approximately 20 mg of catalyst were placed on the sample pan of the DuPont 951 thermogravimetric balance module which was interfaced with a DuPont 1090 thermoanalyzer (controller and data station). The sample was purged at ambient temperature with argon until constant weight was achieved (several minutes). The argon flow was then stopped, and the sample chamber was evacuated. The vacuum pump continued to hold the partial vacuum until constant weight was once again achieved. The pump was then turned off, and a flow of pyridine-saturated argon at ambient temperature was introduced into the sample chamber. The pyridine-argon flow continued for 180 minutes at which time the weight gained by the sample had nearly ceased. The chamber was again evacuated, still at ambient temperature, and held under partial vacuum for 40 minutes. When constant weight was achieved, the temperature was increased at 20°C/min to 105°C where it was held for 30 minutes. The temperature was then increased at 2°C/min to 202°C and held there for 30 minutes, followed by a temperature increase at 20°C/min to 300°C where it was held for 60 minutes. Upon reaching constant weight, the experiment was terminated.

Hydrotreating Reactions

The details of experimental procedures used for the hydrotreating reactions are available in the reports published in the literature (5-9). The method of Vogel (10) was used for chlorine analysis.

RESULTS AND DISCUSSION

Elemental analyses of the zinc (II) chloride mixtures with silica gel obtained from the reaction in carbon tetrachloride and THF indicated that a small amount of chloride loss occurred during the heating procedure. Most of the salt (98%) was present, and only a small amount of chlorine was present as Si-O-ZnCl. The catalyst was a mixture of zinc chloride, zinc chloride complexed with silica gel, and oxyzinc salt.

Previous results from Hammett acidity studies at ambient temperature for SZC-50 indicated that highly acidic sites are present in this catalyst (6). Coordination of zinc chloride to surface silica hydroxyls on the silica gel-supported catalyst will be expected to generate new acidic sites of both Lewis and Brönsted types. The nature of these sites in the SZC-50 and SZC-16 catalysts at both ambient and higher temperatures is elucidated by the present study.

Infrared spectroscopy of the pyridine complex was used to determine the relative proportion of Lewis and Brönsted acid sites in the silica gel-zinc chloride catalysts. In the infrared spectrum of the pyridine-absorbed catalyst, the bands around 1440 and 1536 cm^{-1} are assigned to the pyridine-Lewis acid coordination bond and the pyridine-Brönsted acid bond respectively. The relative intensities of these bands were converted to the concentration ratio by using the respective extinction coefficients. In the SZC-16 catalyst, very few Brönsted acid sites were present at ambient temperature. However, on heating the pyridine complex of SZC-16 at several temperatures (25-200°C) for 1 hour, the intensity of the band due to the pyridine-Brönsted acid bond increased (Table 1). The increase in the intensity of the Brönsted band must be due to creation of new strong Brönsted acid sites as the temperature increases. This process is accompanied by the loss of pyridine from that portion of the Lewis sites that are weakly acidic. Thus, there is a continuing decrease in the Lewis band, and corresponding decrease in the ratio of the concentration of Lewis sites to Brönsted sites with temperature. Table 1 also gives the calculated ratios from the absorbance data from the SZC-16 sample and extinction coefficients for the bands.

At ambient temperature, the ratio of the concentration of Lewis sites to Bronsted sites for the SZC-50 was 3.4. This lower ratio of Lewis/Brönsted acid sites in the SZC-50, which corresponds to a larger concentration of Brönsted sites, is likely due to increased electron-withdrawing effects of the greater number of zinc chloride moieties coordinated with the silica hydroxyls.

TABLE 1

INFRARED ABSORBANCE OF PYRIDINE-ADSORBED SZC-16

Temp (°C)	Absorbance		Lewis/BrönstedSites
	1440 cm^{-1} Band (L-P Band)	1536 cm^{-1} Band (B-P Band)	
25	0.181	0.01	12.46
100	0.184	0.022	8.52
150	0.129	0.027	4.78
200	0.043	0.018	2.39

A thermogravimetric technique was also used to determine the total acid sites and stability of the catalyst. In the TGA experiment, the weight of the catalyst increased by 41.62 and 12.13 wt% for SZC-50 and SZC-16 catalysts respectively, upon pyridine absorption followed by evacuation at ambient temperature. The weight increase is due to the chemical reaction of the pyridine at both Lewis and Brönsted acid sites and, therefore, is a measure of the total acidity of the catalyst. The total acidity for SZC-50 and SZC-16 is 5.04 and 1.75 meq/g catalyst respectively.

Upon slowly heating the catalyst (2°C/min) to 300°C, all of the adsorbed pyridine could be removed. Heating above 300°C resulted in the loss of chlorine due to decomposition and or sublimation of zinc chloride from the catalyst surface.

Catalytic Hydrotreating of Model Compounds:

Reactions of model compounds such as bibenzyl, diphenyl sulfide, dibenzothiophene, cumene, 1-phenyldecane, n-hexadecane, and p-cresol with supported zinc chloride catalysts gave products indicative of a carbonium ion mechanism (5,6). The formation/conversion of acidic sites on the SZC catalyst to Bronsted acids at higher temperatures such as those useful in hydrotreating reactions has not yet been studied. However, we may speculate that at higher temperatures, significant numbers of Bronsted sites are present, and these sites are responsible for the majority of catalytic effects in cleavage of alkylarenes at temperatures between 300 and 400°C. Several experiments were carried out to identify whether Lewis or Bronsted catalysis is predominant at these temperatures with various related materials.

The reaction of bibenzyl in molten zinc chloride (ZC-melt) was carried out under conditions similar to those used for SZC catalysts, and a poor conversion was obtained (Table 2). This result is consistent with the earlier study of Bell (2), that demonstrated the poor catalytic ability of zinc chloride for hydrocracking when restricted to only Lewis acidity (no added hydroxy compound). A reaction conducted with silica gel (SG, no zinc chloride) gave a very poor conversion, consistent with the weak acidity of the silica hydroxyls. When the reaction was carried out with silica gel-zinc chloride (50% zinc chloride) catalyst, 85% of bibenzyl was converted into products. The major products were benzene, ethylbenzene and a small amount of toluene. The ratio of benzene to ethylbenzene was 3. In addition, 18% of the starting material was converted into oligomers. No coke formation occurred under these conditions. The conversion and product distribution from the reaction of bibenzyl with SZC-16 was comparable with that obtained from SZC (50% zinc chloride loaded silica gel). These results suggest that 16% zinc chloride loading on silica gel may be adequate for optimum catalytic activity.

The most likely mechanism for the reaction of bibenzyl with the SZC catalyst is the same as that proposed for the zinc chloride-hydroxyl or zinc chloride-hydrogen chloride complex suggested earlier (2) to account for the formation of ethylbenzene and benzene at temperatures in the 300°C regime. This mechanism proceeds via ipso protonation followed by cleavage of the aryl-alkyl bond to form the phenylethyl carbonium ion intermediate. The carbonium ion is then reduced to the alkyl group. Ethylbenzene is further cracked to benzene via the same steps, the extent depending on the activity of the catalyst.

The effect of molecular hydrogen on the conversion of bibenzyl and the product distribution was investigated by carrying out reactions both in the presence and absence of hydrogen. The percent conversion measured as the disappearance of the substrate was almost the same in both these reactions. However, the product distribution was significantly affected by the presence of hydrogen (Table 2). The reaction with no hydrogen produced 7% of coke which is formed due to retrograde condensation reactions. Also the amount of condensation products (substituted bibenzyls) increased from 18% to 27% in the absence of hydrogen. In the presence of hydrogen the amount of benzene was only slightly higher, but the amount of ethylbenzene increased considerably. In the reaction mechanism postulated above, the phenylethyl carbonium ion can undergo a variety of reactions (Figure 1) to give

TABLE 2

CATALYTIC HYDROCRACKING OF BIBENZYL

Reaction Temp. = 350°C, Reaction Time = 3 Hrs, 5.49 mmols Bibenzyl

Catalyst (g)	Hydrogen (psig)	Conversion (%)	Major Products (mmols)
SG (0.25)	Hydrogen 1000	2	Benzene (tr.) Ethylbenzene (tr.) Toluene (tr.)
ZC-melt (0.25)	Hydrogen 1000	13	Benzene (0.08) Ethylbenzene (0.04) Toluene (0.02)
SZC-50 (0.5)	Hydrogen 1000	85	Benzene (3.54) Ethylbenzene (1.35) Toluene (0.15) Cond. Prod. (18%) Coke (0%)
SZC-50 (0.5)	None	83	Benzene (3.2) Ethylbenzene (0.8) Toluene (0.2) Cond. Prod. (27%) Coke (7%)
SZC-50 (0.5)	Deuterium 1000	64	Benzene (2.6) Ethylbenzene (1.1) Toluene (0.1) Cond. Prod. (24%) Coke (0%)
SZC-16 (0.5)	Hydrogen 1000	75	Benzene (3.12) Ethylbenzene (0.9) Toluene (0.2)

ethylbenzene product. The fact that ethylbenzene forms even in the absence of molecular hydrogen indicates that hydride transfer from Scholl intermediates or hydroaromatic condensation products is the major mechanism for formation of ethylbenzene. Hydrogen may be indirectly involved through reductions of these condensation products.

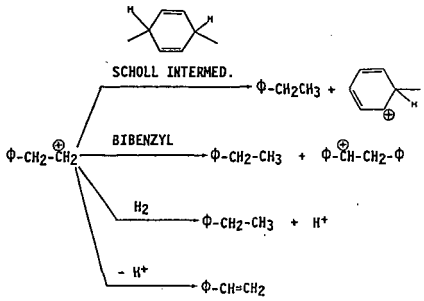

Figure 1. Reactions of Phenylethyl Carbonium Ion

When hydrogen was replaced with deuterium, the conversion was somewhat lower. This is very likely the result of an isotope effect that reduces the rate of hydrogenation of the Scholl intermediates or the rate of transfer of hydrogens from the hydrogenated Scholl intermediates to the carbonium ion intermediates.

1,3-Diphenylpropane (DPP) and neopentylbenzene (NPB) were also used to investigate the catalysis mechanism of silica gel-zinc chloride. The reactions were carried out at 350°C for 3 hours in the presence of 1000 psig of hydrogen. Major products and the percent conversion for these reactions are presented in Table 3. 1,3-diphenylpropane gave benzene and indan as the major products. The formation of these products requires no hydrogen or reduction, only the Brönsted acid catalyst. Ipso protonation of the aromatic ring, followed by aryl-methylene bond cleavage gives the phenylpropyl carbonium ion, that undergoes cyclization to give indan as the second major product. The minor products from this reaction were C_1-C_3 benzenes. These products probably result from other mechanism involving Lewis acid catalysis.

The conversion of neopentylbenzene was much lower than that of diphenylpropane, and a variety of products were obtained. The major product from this reaction was benzene, which again is formed by the ipso protonation of the aromatic ring followed by aryl-methylene bond cleavage. Neopentyl carbonium ion rearranged to produce 2-methylbutane (Figure 2). Toluene and 2-methylpropane may have been formed from the Lewis acid-catalyzed cracking of neopentylbenzene.

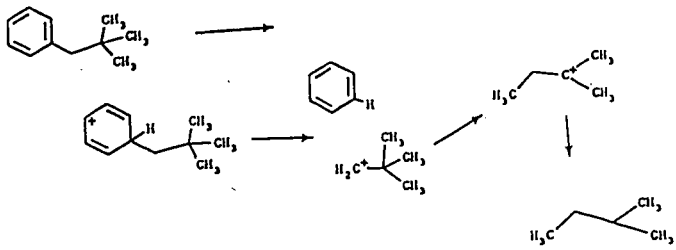

Figure 2. Brönsted Acid-Catalyzed Mechanism

TABLE 3

CATALYTIC HYDROCRACKING OF 1,3-DIPHENYLPROPANE AND NEOPENTYL BENZENE

Reaction Temp. = 350°C, Reaction Time = 3 HRS
Catalyst wt./substrate wt. = 0.5, H_2 = 1000 psig

Catalyst (g)	Substrate (mmols)	Conv. (%)	Major Products (mmols)
SZC-50 (0.25	DPP (2.6)	76	Indan (1.39) Propylbenzene (0.08) Ethylbenzene (0.06) Toluene (0.05) Benzene (2.43) Cond. Prod. (0%) Coke (0)%
SZC-50 (0.25	NPB (3.5)	26	Benzene (0.29) 2-Methylbutane (0.08) 2,2-Dimethylpropane (0.003) Toluene (0.06) 2-Methylpropane (0.04) Butane (0.003) Pentane (0.001) Ethylbenzene (0.03)

CONCLUSIONS

SZC catalysts contain fewer Brönsted acid sites at ambient temperature, but these sites increase at higher temperatures. At the hydrotreating temperatures, the cleavages of aryl-alkyl bonds are Brönsted acid-catalyzed. Hydrogen is not required for hydrocracking reactions, but prevents coking reactions.

ACKNOWLEDGEMENT

This research was supported by Contract No. DOE-FC21-86MC10637 from the U.S. Department of Energy. References herein to any specific commercial product by trade name or manufacturer does not necessarily constitute or imply its endorsement, recommendation, or favoring by the United States Government or any agency thereof. The assistance of Daniel Stanley is greatly appreciated.

REFERENCES

1. Zielke, C.W.; Struck, R.T.; Evans, J.M.; Costanza, C.P.; Gorin, E. Ind. Eng. Chem. Proc. Res. Dev., 1966, 5, 158-164.

2. Taylor, N.D.; Bell, A.T. Fuel, 1980, 59, 499-506.

3. Frederick, T.J.; Bell, A.T. J of Catalysis, 1984, 87, 196-204.

4. Frederick, T.J.; Bell, A.T. J. of Catalysis, 1984, 87, 226-237.

5. Sharma, R.K.; Diehl, J.W.; Olson, E.S. Processing and Utilization of High-Sulfur Coals III, Elsevier Science Publishers B.V., Amsterdam, 1990, 735-743.

6. Sharma, R.K.; Diehl, J.W.; Olson, E.S. ACS Div. of Fuel Chem. Preprints, 1990, 35 (2), 414-422.

7. Olson, E.S.; Diehl, J.W.; Sharma, R.K. ACS Div. of Fuel Chem. Preprints, 1990, 35 (2), 563-569.

8. Sharma, R.K.; Diehl, J.W.; Olson, E.S. ACS Div. of Fuel Chem. Preprints, 1990, 35 (3), pp.

9. Olson, E.S.; Diehl, J.W. Anal. Chem. 1987, 443-448.

10. Vogel, A. Textbook of Quantitative Inorganic Analysis, 4th edn., Longman Sci. and Tech. Group Essex, Eng., 1978, 434.

CATALYSIS OF MULTI-COMPONENT LEWIS ACIDS FOR COAL HYDROLIQUEFACTION AND MODEL REACTIONS

Chunshan SONG+*, Masakatsu NOMURA†, and Tomohiro ONO†

+Fuel Science Program, Department of Materials Science and Engineering
The Pennsylvania State University, University Park, PA 16802, USA
†Department of Applied Chemistry, Faculty of Engineering, Osaka University
Yamada-oka 2-1, Suita, Osaka 565, Japan

Keywords: Lewis acids, Multi-component catalysts, Coal liquefaction

INTRODUCTION

Development of new catalysts is a promising approach to more efficient coal liquefaction. It has been recognized that dispersed catalysts are superior to supported catalysts for primary liquefaction, because the control of coal depolymerization or dissolution requires intimate contact between the catalyst and coal. The dispersed catalysts can be divided into metals and their oxides and sulfides (e.g. MoS_2), and acid catalysts such as $ZnCl_2$. An excellent review of coal liquefaction catalysts has been published recently by Derbyshire (1), which also incorporated many previous works on the catalytic effects of Lewis acids. In particular, the process development research conducted by Zielke and co-workers (2-4) at the Consolidation Coal Co. demonstrated the potential of using massive $ZnCl_2$ catalyst to liquefy coals. The fundamental studies on model reactions by Bell and co-workers (5-8) at the University of California contributed to a mechanistic understanding of the catalytic effects of $ZnCl_2$ for coal liquefaction.

While $ZnCl_2$ and $SnCl_2$ have always been considered attractive because of their high activity and low cost, a considerable body of research at Osaka university has demonstrated that $ZnCl_2$ and $SnCl_2$ doped with alkali metal chlorides or transition metal chlorides are more effective for liquefaction of many bituminous, subbituminous and brown coals (9-13). One of the important observations from these works is that the addition of alkali metal chlorides to $ZnCl_2$ increases the yields of oils (hexane solubles) and decreases the gas yields and reduces H_2 consumption. This is desirable because hydrogen consumption is a major cost of coal liquefaction plant. With an attempt to develop new catalysts, we examined the catalytic effects of MCln-LiCl-NaCl-KCl and MCln-LiCl-KCl (MCln = $CoCl_2$, $NiCl_2$, $MoCl_3$, $SnCl_2$, $ZnCl_2$) for coal liquefaction. The results showed that $NiCl_2$- and $MoCl_3$-LiCl-KCl ternary salts are promising catalysts in view of high oil yields and coal conversions and lower heteroatom contents of oils (14-17), and they appeared to be superior to $ZnCl_2$-, $SnCl_2$- and $CoCl_2$-containing and other $NiCl_2$- and $MoCl_3$-containing salts (14,18). Little is known about the reaction chemistry, more specifically, the hydrogenation and cracking of polyaromatics and the cleavage of bridge structures during coal liquefaction using the $NiCl_2$- and $MoCl_3$-based catalysts. The purpose of this paper is to evaluate the catalysis of these two new catalysts based on coal liquefaction, pyrolysis, and model compound studies.

EXPERIMENTAL

The salts used are synthesized $MoCl_3$ (14), reagent grade $NiCl_2$, LiCl and KCl. The molar compositions of $NiCl_2$- and $MoCl_3$-LiCl-KCl and LiCl-KCl were 14:50:36,12:51:37 and 58:42, respectively, unless otherwise mentioned. The catalysts were impregnated on to coals from their methanol solution or suspension. The coals used are Morwell (C: 67%, daf basis) brown, Taiheiyo (C: 76%), Wandoan (C: 78%) and Yilan (C: 79%) subbituminous, and Akabira (C: 83%) bituminous coals (14-17). The temperature-programmed pyrolysis was conducted by using TGA in a nitrogen flow (14,19). The solvent-free coal liquefaction was carried out in a 200 ml shaking autoclave at 400°C for 1 hour with 9.8 MPa H_2 (14-15). The liquefaction in the presence of tetralin was conducted in 70 ml rocking autoclaves at 400°C for 1 h with 4.9 MPa H_2 (17). The products were separated into gases, oils (hexane solubles), asphaltene (hexane-insoluble benzene solubles), preasphaltene (benzene-insoluble pyridine or THF solubles), and residue (16). The gases were analyzed by GC for C1-C4, CO and CO_2; the oils and asphaltene were subjected to ^1H NMR (15,17) and elemental analyses. The model compounds tested are anthracene, phenanthrene, naphthalene, dibenzyl, benzylphenylether, and dibenzylether. Their reactions were performed in the 70 ml autoclaves under different conditions. The products were analyzed by GC, and GC-MS (20).

RESULTS

Temperature-Programmed Pyrolysis. The non-catalytic pyrolysis of the five coals in N_2 was conducted using two temperature programs: r.t. to 600°C at 5°C/min; and r.t. to 400°C at 5°C/min and then held at 400°C for 60 min. The second program was also used in catalytic pyrolysis in accordance with the temperature/time conditions in liquefaction (14). Figure 1 shows the pyrolysis results of the five coals up to 600°C. The yields of volatile products were calculated from the weight loss determined by TGA. The weight loss below 200°C is mainly due to adsorbed water and was not accounted as volatile materials. The amounts of volatile materials formed below 450°C decreased with increasing rank, daf C% of the coals. Figure 2 presents the results of catalytic pyrolysis of Akabira coal in N_2. Figure 3 shows the temperature-pressure profiles during heat-up and holding at 400°C for solvent-free liquefaction of Akabira coal with 9.8 MPa H_2. The $NiCl_2$- and $MoCl_3$-LiCl-KCl catalysts began to exert a measurable effect in enhancing coal pyrolysis in N_2 at the temperatures above 300°C (Figure 2). During the heat-up of the coal impregnated with these catalysts under pressurized H_2, the H_2 uptake became apparent at the same temperature region, indicating the onset of the catalytic reactions at the temperatures as low as about 300°C (Figure 3). The same trends were observed in the pyrolysis (14, 19) and t-p profiles in liquefaction of other coals. The t-p profiles for liquefaction of Akabira coal in the presence of tetralin were similar to those for the solvent-free runs, except that the evaporation of tetralin caused the pressure increase (below 300°C).

Solvent-free Liquefaction. In general, acids are used in massive amounts (1-9) as catalysts and reaction medium. In this work, the concentration of Lewis acids in temary salts for liquefaction were below 15 mol%. Figure 4 shows the results of solvent-free liquefaction of Australian Wandoan subbituminous coal (400°C, 1 h, 9.8 MPa H_2) using various MCl_n-LiCl-NaCl-KCl and MCl_n-LiCl-KCl (MCl_n: 12-14 mol%, salts to coal: 1, wt ratio), where the yields of products are plotted against H_2 consumptions. It is clear from the product distribution that $NiCl_2$- and $MoCl_3$-LiCl-KCl afforded over 60% (daf coal basis) oils and showed higher selectivity to oils without remarkable increase in gas-make. The previous results for Wandoan coal (3 h runs, other conditions were the same) using $ZnCl_2$ and $ZnCl_2$-KCl (60:40, mol%) are also shown in Figure 4. Relative to $ZnCl_2$, $ZnCl_2$-KCl gave higher oil yield and lower gas yield with lower H_2 consumption, as has been observed for many other coals (9-11). Although the catalysts and reaction time were different, the results in Figure 4 showed that higher oil yields can be obtained with relatively lower H_2 consumption.

In order to examine the general effectiveness of the new catalysts, we conducted the solvent-free liquefaction of Australian Morwell coal, Japanese Taiheiyo and Akabira coals under the same conditions (400°C, 1 h, 9.8 MPa H_2). The results are summarized in Figure 5. Relative to the thermal runs, both $NiCl_2$- and $MoCl_3$-LiCl-KCl catalysts significantly enhanced coal conversion. More importantly, the oil yields of all the catalytic runs are almost three times that of non-catalytic runs of the bituminous, subbituminous and brown coals. These results established the general applicability of these two catalysts for liquefaction of coals, especially subbituminous coals (oil yields: $\geq$ 56%). ^1H NMR and elemental analyses revealed that the catalysts increased the contents of naphthenic CH_2 hydrogens (hydroaromatics) and decreased the O and N contents of oils.

Liquefaction in the Presence of H-Donor. In a previous work, addition of tetralin was found to further increase the conversion of coal, although this effect was substantially smaller in the catalytic runs than in the non-catalytic run (16). The $NiCl_2$- and $MoCl_3$-based catalysts played a key role in promoting oil production, while adding tetralin appeared to enhance the selectivity of the catalytic reactions, in view of increased conversion and decreased total hydrogen consumption. Based on these observations, we examined the catalyst performance at different loading levels for liquefaction of Chinese Yilan coal in the presence of tetralin under low H_2 pressure (400°C, 1 h, 4.9 MPa H_2; tetralin/coal: 5g/5g; metal to coal: Ni, 1.2-12 wt%; Mo, 1.7-17 wt%). Figures 6 and 7 show the effect of catalyst loading on the product distribution and hydrogen transfer, respectively. The loading of $NiCl_2$-LiCl-KCl to coal up to 20wt% (2.4wt% Ni to coal) significantly increased oil yields, coal conversions, enhanced gas-phase H_2 consumptions but decreased the net hydrogen-transfer from tetralin (Figure 6B). Further increase in its loading resulted in a little decrease in gas-phase H_2 and total hydrogen consumptions, in spite of the increase in oil yield. In the case of $MoCl_3$-LiCl-KCl, increase in its loading progressively increased oil yields and gas-phase H_2 consumptions and decreased the net hydrogen-transfer from tetralin (Figure 6A). In contrast to these trends, the use of LiCl-KCl, even at low loading, considerably suppressed the gas-phase H_2 consumption without any negative impact on the product distribution (Figure 6C).

Figure 7 shows the effect of catalyst loading on H-distribution of oils per 100 C atoms, as determined from NMR (17). The HCH_3 values indicate the contents of alpha-, beta- and gamma-CH_3 hydrogens and gamma-CH_2 hydrogens; the HCH_2 refers to the alpha- and beta-CH_2 hydrogens. As shown in Figure 7, the HCH_2 values increased, but HCH_3 decreased with catalyst loading, reflecting that loading the catalysts increased the contents of naphthenic CH_2 hydrogens present in hydroaromatic rings. These trends were also observed in the ^1H NMR analysis of oils from solvent-free liquefaction of the other four coals (15-16).

Model Compounds Studies. To gain a better understanding of the catalytic functions, the model reactions were undertaken using NiCl2, MoCl3, LiCl-KCl, and their combinations. Tables 1 and 2 present the results for anthracene and phenanthrene (400°C, 1 h, 9.8 MPa H2), respectively, with constant molar ratio (0.3) of NiCl2 or MoCl3 to the reactant (3 g, 16.85 mmol). As shown in Table 1, both NiCl2- and MoCl3-LiCl-KCl considerably promoted the hydrogenation of anthracene to form tetra- and octahydroanthracene. In the runs of phenanthrene, which is known to have lower reactivity (20), the catalysts enhanced the formation of di- and tetrahydrophenanthrene. In the runs of naphthalene, these catalysts promoted hydrogenation to produce tetralin, but the conversions were within 15%. As shown in Tables 1-2, the use of LiCl-KCl gave nearly identical results to the thermal runs. However, adding LiCl-KCl to NiCl2 and MoCl3, especially to MoCl3 which exhibited very high cracking activity, significantly suppressed the extensive hydrogenation and ring-openning cracking. Figure 8 shows the effect of MCln content in the runs of anthracene. The yields of hydroaromatics and cracking products appeared to depend on the contents of Lewis acids MCln, especially in the case of MoCl3.

Table 3 is a summary of the bond dissociation energy of a number of C-O and C-C linkages. Various connecting linkages between aromatic rings are believed to be present in coals. We conducted model reactions of C-O linkage structures using benzylphenylether and dibenzylether at 350°C for 1 h with 4.9 MPa H2. As shown in Table 4, the presence of the salts significantly affected the reactions of the ethers. The use of NiCl2- and MoCl3-LiCl-KCl decreased the yields of simple products such as toluene, and increased the yields of the products from rearrangement and coupling reactions such as PhCH2PhOH and PhCH2(PhCH3)CH2Ph. The considerable formation of these products indicates that these catalysts promoted the C-O bond cleavage through acidic actions to produce benzyl cation, which underwent two main reactions: stabilization by hydrogenation; attacking other species to cause rearrangement or condensation. Table 5 shows the results for dibenzyl (C-C linkage) at 400-425°C for 1 h with 9.8 MPa H2. The NiCl2- and MoCl3-LiCl-KCl catalysts showed essentially no effect at 400°C for breaking this type of C-C linkage. It is to be noted that the use of LiCl-KCl has neither positive nor negative effect on hydrogenation of polyaromatics such as anthracene, phenanthrene (Tables 1-2) and dibenzyl, but it showed pronounced effect in the runs of the ethers especially dibenzylether. For comparison of catalytic functions, we also conducted the model reactions using a commercial Ni-Mo/Al2O3 catalyst (Table 6), because it has high activity for hydrogenation of polyaromatics (20).

DISCUSSION

Catalytic Functions. In the earlier stage of this work, we inferred based on the high liquid yields in pyrolysis and in liquefaction of Wandoan coal that the NiCl2- and MoCl3-LiCl-KCl catalysts have higher hydrocracking ability (14). However, the model reactions using polyaromatics clearly showed that while they have hydrogenating ability, they do not possess high hydrocracking ability (Tables 1-2). In fact, their cracking ability is much lower than MoCl3 or ZnCl2, and their hydrogenating ability is much lower than sulfided Ni-Mo commercial catalyst (20). The **key question** that arise is what are the key functions of the catalysts leading to high oil yields and coal conversions? The motivation of the later works on the pyrolysis, and model reactions presented in this paper comes from the desire to answer this question.

Analytical pyrolysis in N2 is an useful technique for evaluating the coal reactivity and the effect of catalyst on the cleavage of bridge bonds.The pyrolysis showed that the NiCl2- and MoCl3-LiCl-KCl catalysts enhanced the formation of volatile materials from bituminous (Figure 2), subbituminous and brown coals in N2 at the temperatures above 300°C (14,19). In fact, the yields of volatiles from non-catalytic pyrolysis up to 600°C can be obtained by the catalytic pyrolysis at 400°C (Figures 1-2). The fact that the temperatures for the appearance of catalytic enhancement in pyrolysis in N2 correspond to the onset of H2 uptake in the liquefaction of Akabira coal (Figures 2-3) and other coals indicates that the interactions between catalyst and coal and the participation of molecular H2 begin to occur at the temperatures as low as about 300°C.

From the above results, it becomes clear that the $NiCl_2$- and $MoCl_3$-LiCl-KCl catalysts can promote the cleavage of connecting linkages in coal at low temperatures, followed by stabilization of the reactive fragments by transferable hydrogens in the internal (coal and its products) and external (H_2) hydrogen sources. The model reactions using the bridge-type compounds showed that they can promote the cleavage of C-O bond in ethers at low temperatures (Table 4). While the cleavage of C-C linkage in dibenzyl was not affected by the catalysts at 400°C (Table 5), there is a possibility that these catalysts can promote the C-C bond cleavage for the dinaphthylethane type C-C linkage, because the bond strength of the latter is lower than the former (210-235 vs. 255-258 KJ/mol, Table 3), and the latter is closer to that of bezylphenylether (221 KJ/mol, Table 3).

The liquefaction results showed that $NiCl_2$- and $MoCl_3$-LiCl-KCl significantly promote the production of oils without any significant increase in gas-make. The observed relationship between hydrogen consumptions and products distribution (Figures 4,6) suggests that the molecular H_2 was consumed mainly in producing oils in the catalytic runs.The results of model reactions in Tables 1-2 showed that adding LiCl-KCl to $MoCl_3$ and $NiCl_2$ suppressed extensive hydrocracking of polyaromatics, but retained their hydrogenation activity to produce partially hydrogenated species from 3- and 2-ring aromatics without remarkable ring-openning cracking. These results also confirmed the observation from ^1H NMR that the $NiCl_2$- and $MoCl_3$-based catalysts gave more hydroaromatic products in oils from both solvent-free (15,16) and tetralin-mediated coal liquefaction (Figure 7). The partially hydrogenated polyaromatics are also H-donors, which could be more effective than tetralin in terms of H-donation rate in coal liquefaction (17).

The cracking ability of the Lewis acid catalysts is determined mainly by their acid strength. When $ZnCl_2$ is used in coal liquefaction, it always increases the C_1-C_4 gas yield and the ratio of iso-C_4 to n-C_4, which has been taken as an acidity measure (2-3, 10). $NiCl_2$- and $MoCl_3$-LiCl-KCl do not remarkably enhance C_1-C_4 yields and the iso-C_4/n-C_4 ratio, because the ring-openning cracking and dealkylation were very limited. However, it is worthy while noting that *sym*-octahydrophenanthrene was also produced from anthracene in the catalytic runs (Table 1). Its yields increased with increasing MCl_n content, as shown in Figure 9. This is considered to be a result of acid-catalyzed isomerization of *sym*-octahydroanthracene. The extent of the isomerization shown in Figure 9 suggests that the acid strength of MCl_n-LiCl-KCl decreases with increasing LiCl-KCl content. We also observed some interesting trends in the case of $ZnCl_2$. It was found that adding KCl to $ZnCl_2$ enhanced H-D exchange in H_2-D_2 model reactions, which is indicative of the enhanced ability for activating molecular H_2 upon KCl doping. On the other hand, $ZnCl_2$-KCl afforded higher oil yield and coal conversion and lower gas yield with lower consumption of molecular H_2, indicating the lower cracking ability and higher oil selectivity of $ZnCl_2$-KCl relative to $ZnCl_2$ alone. This is a general trend in the solvent-free runs of many coals (9-11) including Wandoan coal (Figure 4).

The side reactions such as condensation (via benzyl cation) observed in model reactions (Table 4) seem to suggest that the hydrogenating ability of the $NiCl_2$- and $MoCl_3$-based catalysts is not sufficiently high. This trend is similar to that observed by Bell and co-workers for the reactions of ether compounds using $ZnCl_2$ (7-8), where the condensation reactions were more remarkable even at lower temperatures, 193-225°C. It should be noted that unsulfided and sulfided Ni-Mo/Al_2O_3 catalysts exhibited relatively similar activity in hydrogenating anthracene, phenanthrene (20) and dibenzyl, whereas the former also caused remarkable condensation in the reactions of the ethers (Table 6). On the other hand, the side reactions may be inhibited by H-donation during coal liquefaction. Apparently, the reactions of the bridge-type model compounds are far from the real situation, and the resulting data should not be over-emphasized.

The general implications from the above results are as follows: 1) To obtain high oil yields with catalysts, the extensive hydrocracking reactions such as those over $MoCl_3$ or $ZnCl_2$ are not necessarily required; such reactions will decrease oil yields and coal conversion and increase gas yields and H_2 consumptions; 2) It is critical to suppress the acidic cracking ability of the acid catalysts to achieve a better balance of hydrogenating ability with the cracking ability; 3) Selective reactions over dispersed catalysts, which begin to occur at low temperatures, can be more efficient in controlling coal depolymerization and promoting oil production. The target in primary liquefaction using multi-component catalysts is to obtain the products containing more oils and less asphaltene and preasphaltene with relatively lower H_2 consumption. The products should be derived under less-severe conditions and retain moderate reactivity for subsequent upgrading using supported catalysts.

Role of Catalyst Components and Retrogressive Reactions. The catalyst physical state and dispersion are also important factors, which have physical and/or chemical effect. Unlike $ZnCl_2$ or $SnCl_2$ which becomes molten salt at 313°C or 255°C, $NiCl_2$ and $MoCl_3$ do not melt even at 600°C. However, from DTA analysis of various salts (18), we found that they become molten when a mixture of 58%LiCl:42%KCl was added. The DTA suggested the melting points of the two catalysts to be 360°C and 387°C, respectively (14). The test using an electric furnace showed that at 400°C, $NiCl_2$-LiCl-KCl is a homogeneous liquid, and $MoCl_3$-LiCl-KCl exists in a semi-molten state. While the catalytic effects become measurable below their melting points (Figures 2-3), the molten state provides much better catalyst dispersion and more intimate contact with coal, which offers an advantage in controlling the depolymerization of solid coal. The addition of LiCl-KCl to $NiCl_2$ and $MoCl_3$ also causes the formation of some complex ions such as $NiCl_4^{2-}$ and $MoCl_6^{3-}$ at low and/or high temperatures (21). The decrease in the acid strength is probably associated with the formation of such complex ions. In addition, our preliminary tests showed that $NiCl_2$ can be reduced by H_2 at 400°C; $MoCl_3$ is not readily reducible even by using K (molten potassium) but it disproportionates at the temperatures above 420-450°C. They appeared to become stable upon the addition of LiCl-KCl at the reaction temperatures.

Figure 10 shows a H-transfer network model modified from previous reports (16-17), and Figure 11 presents a general reaction model (22). Recent research has revealed that coal reactivity is higher than had been thought previously, and the liquefaction of coals under conventional process conditions involves considerable retrogressive reactions, as illustrated in Figure 11 (PRIOM formation), especially in the cases of subbituminous coals and lignites (22-24). The use of $NiCl_2$- and $MoCl_3$-LiCl-KCl has been found to be especially effective for liquefying subbituminous coals. While the relative effectiveness of these two catalysts changes with the coals used, it appears that they can significantly stabilize the coal-derived fragments by interaction, direct and indirect hydrogenation (Figure 10) to suppress their retrogressive reactions (Figure 11). Although the model reactions using ethers did not provide positive support, this consideration is strongly supported by the fact that very high oil yields (56-65%, daf) were obtained from the subbituminous coals by using these catalysts in the absence of any solvent (Figure 5) , and the fairly high conversions (82-92%) are also an convincing evidence. In the runs of Akabira bituminous coals (16), the addition of tetralin was found to further increase coal conversions in the catalytic runs (84-86% to 91-94%), indicating that the use of H-donor solvent is also beneficial. However, such a effect in the catalytic runs was much smaller than in the non-catalytic runs (46 to 92%). It is likely that in the catalytic runs both H_2 gas and the hydroaromatic products (Figures 6-7) contributed to H-transfer (Figure 10), in addition to the H-donation from solvent and from coal itself. In the non-catalytic runs at 400°C (16,22), the effect of tetralin addition appeared to be smaller for converting subbituminous coals such as Wandoan coal (49 to 61%) than for bituminous coals. It is to be noted that McMillen, Malhotra and co-workers (27-28) proposed that hydroaromatics can induce the cleavage of some strong bonds through radical hydrogen transfer.

CONCLUSIONS

The liquefaction of five coals established the general effectiveness of the two new ternary catalysts, $NiCl_2$- and $MoCl_3$-LiCl-KCl both in solvent-free runs and in the runs with added tetralin. The catalysts begin to interact with coal and exert measurable effects on coal pyrolysis in N_2 and the participation of molecular H_2 in coal liquefaction at the temperatures as low as about 300°C. The desirable features of these catalysts in coal liquefaction are characterized by the high oil yields and high conversions , and that molecular H_2 is mainly consumed in producing oils without remarkable increase in gas-make. The active components in the ternary catalysts are $NiCl_2$ and $MoCl_3$, in which the LiCl-KCl acts to adjust (decrease) the acidity and to suppress the cracking ability, which contributes to balancing the catalytic functions. At the temperature of 400°C, $NiCl_2$ and $MoCl_3$ are solubilized and stabilized by LiCl-KCl, producing a chemically more stable, but mobile catalyst phase which is important for controlling coal depolymerization. LiCl-KCl binary salts are inactive for pure hydrocarbons but can interact with some heteroatom-containing structures such as ethers. In the presence of tetralin solvent, $NiCl_2$- and $MoCl_3$-LiCl-KCl increase the gas-phase H_2 consumption but decrease the net hydrogen transfer from tetralin; the use of LiCl-KCl remarkably reduces the H_2 consumption without any negative impact on product yields. The $NiCl_2$- and $MoCl_3$-based catalysts play a key role in promoting oil production from the coals, increasing the the contents of hydroaromatics and decreasing O and N contents of oils, probably by enhancing the cleavage of some connecting linkages and selectively promoting the hydrogenation of polyaromatics (to create in-situ H-donors).

FUTURE RESEARCH

The present research contributes to an improved understanding of the key factors for developing novel multi-component, dual-functional catalysts. The catalysts examined and the conditions used, however, are not considered to be the best.Temperature-programmed pyrolysis and t-p profiles for liquefaction of coals suggest that coals can be liquefied at the temperatures below 400°C. The future work on the acid catalysts should be directed toward the low-severity liquefaction. Efforts should be made to minimize the catalyst loading, and achieve better balance of catalytic functions.(suppressing the acid strength and/or increasing hydrogenating ability) by exploring novel formulations. For the effects of various catalysts, more attention should be given to liquefying low-rank coals, and to increasing oil yields (rather than the conversions toTHF solubles). The coal pretreatment followed by low-severity liquefaction using novel acidic dispersed catalyst should be tested in the future work. An interesting two-stage coal depolymerization procedure involving the use of Lewis acid such as $FeCl_3$ (3-20 wt% on coal) in the first stage and a base in the second stage at the temperatures of 250-310°C has been proposed by Shabatai and co-workers (27-28). Their results and our results suggest that selective reactions of coals at low temperatures in the presence of specific acid catalysts can be very effective in promoting coal depolymerization and oil production. If more effective dispersed catalysts for primary liquefaction and the supported catalysts with proper pore structure (29) for upgrading coal liquids, can be developed and applied, further reduction in severity of the current two-stage liquefaction processes (400-460°C, 17-20 MPa) is practically possible.

REFERENCES

1. Derbyshire, F.J. *Catalysis in Coal Liquefaction,* IEA Coal Research: London, 1988, 69 pp.
2. Zielke, C.W.; Struck, R.T.; Evans,J.M.; Costanza, C.P.; Gorin, E. *I & EC Process. Res. Dev.* 1966, 5, 151.
3. Zielke, C.W.; Struck, R.T.; Evans,J.M.; Costanza, C.P.; Gorin, E. *I & EC Process. Res. Dev.* 1966, 5, 158.
4. Struck, R.T.; Zielke, C.W. *Industrial Conversion of Coal and Carbon to Gase, Liquid and High-Value Products,* Society for Chemical Industry: London, 1981.
5. Salim, S.S.; Bell, A.T. *Fuel* 1982, 61, 745.
6. Salim, S.S.; Bell, A.T. *Fuel* 1984, 63, 469.
7. Frederick, T.J.; Bell, A.T. *J. Catal.* 1984, 87, 210.
8. Frederick, T.J.; Bell, A.T. *J. Catal.* 1984, 87, 226.
9. Nomura, M.; Miyake, M. *J. High Temper. Soc.* 1982, 8, 138.
10. Nomura, M.; Kimura, K.; Kikkawa, S. *Fuel* 1982, 61, 1119.
11. Nomura, M.; Yoshida, T.; Morida, Z. *I & EC Prod. Res. Dev.* 1984, 23, 215.
12. Nomura, M.; Sakashita, H.; Miyake, M.; Kikkawa, S. *Fuel* 1983, 62, 73.
13. Nakatsuji, Kubo, T.; Nomura, M.; Kikkawa, S. *Bull. Chem. Soc. Japan* 1978, 51, 618.
14. Song, C.; Nomura, M. *Fuel* 1986, 65, 922.
15. Song, C.; Nomura, M. *Bull. Chem. Soc. Japan* 1986, 59, 3643.
16. Song, C.; Nomura, M. *Fuel* 1987, 66, 1225.
17. Song, C.; Hanoka, K. ; Nomura, M. *Energy & Fuels* 1988, 2, 639.
18. Song, C.; Nomura, M. *Prepr. 50th Chem. Soc. Japan Ann. Meet.* , Tokyo, 1985, p.775.
19. Song, C.; Nomura, M. *Proc. 17th Japan Petr. Chem. Sym.* , Fukuoka, 1987, p.122.
20. Song, C.; Hanaoka, K.; Ono, T.; Nomura, M. *Bull. Chem. Soc. Japan* 1988, 61, 3788.
21. Song, C.; Ono, T.; Nomura, M. *Bull. Chem. Soc. Japan* 1989, 62, 630.
22. Song, C.; Hanoka, K. ; Nomura, M. *Fuel* 1989, 68, 287.
23. US DOE COLIRN Panel, *Coal Liquefaction,* Final Report, DOE/ER-0400, 1989, p.3-10.
24. Derbyshire, F.J.; Davis, A.; Lin, R. *Energy & Fuels* 1989, 3, 431.
25. McMillen, D.F.; Malhotra, R.; Chang, S.-J. *Proc. 1987 Int. Conf. Coal Sci.* , Maastricht, 1987, p.197.
26. McMillen, D.F.; Malhotra, R.; Hum, G.P.; Chang, S.-J. *Energy & Fuels,* 1987, 1, 193.
27. Shabatai, J.; Skulthai, T. *Proc. 1987 Int. Conf. Coal Sci.* , Maastricht, 1987, p.761.
28. Shabatai, J.; Znang, Y. *Proc. 1989 Int. Conf. Coal Sci.* , Tokyo, 1989, p.807.
29. Song, C.; Nihonmatsu, T.; Hanaoka, K.; Nomura, M. *ACS Fuel Chem. Prepr.,* paper in this issue.

Table 1. Hydrogenation and Cracking of Anthracene

Run No.	1	2	3[a)]	4[b)]	5	6
Catalyst	None	LiCl-KCl	$MoCl_3$-LiCl-KCl	$NiCl_2$-LiCl-KCl	$MoCl_3$	$NiCl_2$
Products[c)] (wt%)						
C_1-C_4	0.1	0.2	0.9	0.2	2.6	0.2
C_5-C_9	-	-	0.1	-	2.1	0.7
R_1-⬡-R_2	-	-	0.9	-	1.1	-
R_1-⬡⬡-R_2 + ⬡⬡-R	0.1	0.1	3.0	0.8	40.2	1.6
R_1-⬡⬡-R_2	0.2	0.1	0.6	0.1	1.8	0.1
⬡⬡⬡[d)] + ⬡⬡⬡-R	0.3	0.1	7.7	4.3	15.6	11.4
⬡⬡⬡[e)]	-	-	10.4	8.0	9.7	15.8
⬡⬡⬡	14.9	15.8	44.9	41.0	6.4	37.3
⬡⬡⬡	69.3	66.4	19.9	30.2	-	21.0
⬡⬡⬡	14.4	13.8	6.4	12.1	2.4	7.6
⬡⬡⬡[f)]	-	-	2.1	1.6	8.7	4.0
Conversion	85.6	86.2	93.6	87.9	97.6	92.4

a-b) Molar contents of $MoCl_3$ (a) and $NiCl_2$ (b) are 12% and 14%, respectively; c) R, R_1 and R_2 mean alkyl groups or hydrogen; d) *unsym*-Octahydroanthracene; e) *sym*-Octahydroanthracene; f) *sym*-Octahydrophenanthrene

Table 2. Hydrogenation and Cracking of Phenanthrene

Run No.	9	10	11	12	13	14
Catalyst	None	LiCl-KCl	$MoCl_3$-LiCl-KCl	$NiCl_2$-LiCl-KCl	$MoCl_3$	$NiCl_2$
Products[a)] (wt%)						
C_1-C_4	-	0.1	0.1	0.2	3.4	0.1
C_5-C_9	0.2	-	-	0.1	10.4	0.3
R_1-⬡-R_2[b)]	0.1	-	0.5	-	10.1	0.1
R_1-⬡⬡-R_2 + ⬡⬡-R	0.4	-	-	0.1	27.1	0.2
R_1-⬡⬡-R_2	-	-	-	-	1.1	0.1
⬡⬡[c)] + ⬡⬡-R	-	-	0.1	0.1	10.2	0.9
⬡⬡[d)]	-	-	-	0.8	5.3	1.6
⬡⬡-R	0.7	1.0	0.3	-	2.1	0.1
⬡⬡	0.8	0.9	1.5	6.0	4.6	9.7
⬡⬡	1.3	1.4	6.3	8.2	9.7	12.0
⬡⬡	96.3	95.4	90.9	83.4	13.9	74.1
Conversion	3.7	4.6	9.1	16.6	86.1	25.9

a) R, R_1 and R_2 mean alkyl groups or hydrogen; b) Including cyclohexyl phenyl ethane; c) *unsym*- and d) *sym*-octahydrophenanthrene.

Table 3. Dissociation Energy of C-O and C-C Bonds (Ph: Phenyl, Np: Naphthyl, An: Anthryl)

Structure	BDE, KJ/mol	Ref.	Structure	BDE, KJ/mol	Ref.
C—O linkage			C—C Linkage		
PhO—CH_2Ph	221	a	$PhCH_2$—CH_2Ph	258, 255	b,e
PhO—PhOH	318+12	b	$NpCH_2$—CH_2Np*	235	e
PhO—Ph	327+8	b	$NpCH_2$—CH_2Np**	210	f
C_2H_5—OC_2H_5	331	c	$PhCH_2$—CH_2CH_2Ph	288	d
CH_3—OCH_3	335	c	$PhCH_2CH_2$—CH_2CH_2Ph	343	d
			CH_3—CH_3	349	f
C-C Bond			$PhCH_2$—PhOH	350+13	b
$AnCH_2$—CH_3	251	d	$PhCH_2$—Ph	372+13, 350,	b,f
$NpCH_2$—CH_3	285	d	$PhCH_2CH_2$—Ph	405	g
$PhCH_2$—CH_3	301, 364	d,f	Ph—Ph	486, 480, 419	d,f,c
Ph—CH_3	382	d			

a) P.J. Cassidy et al., Fuel 1983, 62, 1404; b) D.F. McMilen et al., J. Org. Chem. 1981, 46, 3322; c) Y. Kamiya, J. Fuel Soc. Japan 1977, 56, 320; d) D.S. Ross et al., ACS Sym. Ser. 1980, 139, 301; e) Y. Sato, Fuel 1979, 58, 318; f) H. Juntgen, Fuel 1984, 63, 731; g) R.D. Hei et al., Fuel 1986, 65, No.4;
*: alpha-dinaphthylethane; **: beta-dinaphthylethane.

Table 4. Conversion of Ethers at 350°C for 1 h with 4.9 MPa H_2

Reactant	Benzylphenylether				Dibenzylether			
Catalyst	None	LiCl-KCl	$NiCl_2$-LiCl-KCl	$MoCl_3$-LiCl-KCl	None	LiCl-KCl	$NiCl_2$-LiCl-KCl	$MoCl_3$-LiCl-KCl
Products (wt%)								
Benzene	0.1	0.3	1.3	7.6	0.3	0.2	0.3	tr.
Toluene	25.2	19.9	3.8	5.8	65.6	34.3	23.2	26.3
Phenol	42.3	33.7	30.2	43.8				
Cresol	-	-	1.0	6.2				
PhCH=O					6.8	5.3	-	-
$PhCH_2OH$					6.2	16.8	-	-
$PhCH_2OPh$	2.9	1.1	-	-				
$PhCH_2OCH_2Ph$					6.1	45.3	-	-
$PhCH_2Ph$	1.0	8.4	3.5	8.5	-	-	3.7	3.6
$PhCH_2PhOH$	15.0	14.2	39.8	21.3				
$PhCH_2CH_2Ph$	4.2	1.6	tr.	1.0	8.8	2.1	tr.	12.3
$PhCH_2PhCH_3$					0.8	0.7	11.6	7.6
$PhCH_2(PhOH)CH_2Ph$	3.0	3.2	13.7	3.3				
$PhCH_2(PhCH_3)CH_2Ph$[a]					2.5	0.2	25.8	20.1
Conv. (wt%)	97.1	98.9	100.0	100.0	93.9	54.7	100.0	100.0

a) Including some $PhCH_2PhCH_2Ph$.

Table 5. Reaction of Dibenzyl at 400-425°C for 1 h with 9.8 MPa H_2

Temperature	400°C				425°C			
Catalyst	None	LiCl-KCl	$NiCl_2$-LiCl-KCl	$MoCl_3$-LiCl-KCl	None	LiCl-KCl	$NiCl_2$-LiCl-KCl	$MoCl_3$-LiCl-KCl
Products (wt%)								
Benzene	0.2	0.3	0.4	1.1	2.5	1.9	3.2	3.3
Toluene	0.8	1.1	1.5	1.6	6.7	6.5	8.3	8.7
Ethylbenzene	1.1	1.4	1.1	1.3	5.7	6.2	6.7	6.0
Dibenzyl	97.9	97.3	96.2	95.5	83.4	83.3	78.6	79.6
Conv. (wt%)	2.1	2.7	3.8	4.5	16.6	16.7	21.5	20.4

Table 6. Conversion of Bridge-Type Compounds over Ni-Mo/Al_2O_3 Catalyst

Reactant	Dibenzyl[a]			Benzylphenylether[b]			Dibenzylether[b]		
Catalyst[c]	None	Ni-Mo	S-NiMo	None	Ni-Mo	S-NiMo	None	Ni-Mo	S-NiMo
Products[d] (wt%)									
Cyclohexane	-	0.2	0.3	-	tr.	2.0			
C_1-cyclohexane	-	0.5	0.6	-	-	tr.	-	-	0.5
C_2-cyclohexane	-	tr.	0.4						
Benzene	0.2	0.4	0.6	0.1	0.6	1.2	0.3	0.2	-
Toluene	0.8	1.4	2.2	25.2	2.7	35.2	65.6	43.0	91.1
C_2-benzene[e]	1.1	1.7	3.2						
Phenol				42.3	20.6	27.5			
Cresol				-	0.2	-			
PhCH=O							6.8	1.1	-
$PhCH_2OH$							6.2	-	-
$ChCH_2Ph$				-	0.7	7.5			
$ChCH_2CH_2Ph$/Ch	-	42.8	43.6						
$PhCH_2OPh$				2.9	3.8	0.5			
$PhCH_2OCH_2Ph$							6.1	-	-
$PhCH_2Ph$				1.0	1.1	2.2	-	2.2	-
$PhCH_2CH_2Ph$	97.9	53.0	49.1	4.2	-	-	8.8	14.2	2.2
$PhCH_2PhOH$				15.0	43.8	15.9			
$PhCH_2(PhOH)CH_2Ph$				3.0	22.6	3.1			
$PhCH_2(PhCH_3)CH_2Ph$							2.5	16.8	0.1
Conv. (wt%)	2.1	47.0	50.9	97.1	96.2	99.5	93.9	100.0	100.0

a) Runs at 400°C for 1 h with 9.8 MPa H_2; b) Runs at 350°C for 1 h with 4.9 MPa H_2; c) Comercial (KF-153S) sulfided (S-NiMo) and unsulfided (Ni-Mo) catalysts; d) Ch: Cyclohexyl; Ph: Phenyl; e) Including ethyl and dimethylbenzenes.

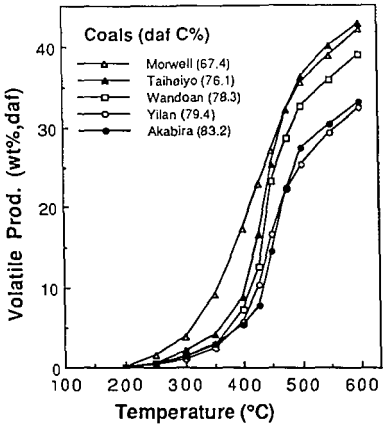

Figure 1. Coal pyrolysis in N_2 up to 600°C.

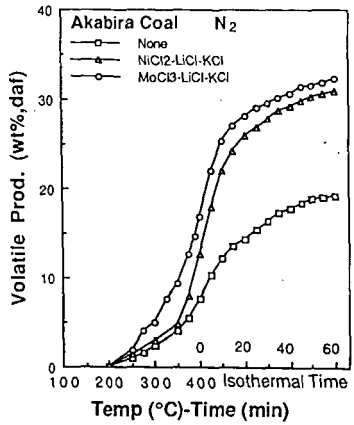

Figure 2. Pyrolysis of Akabira coal in N_2.

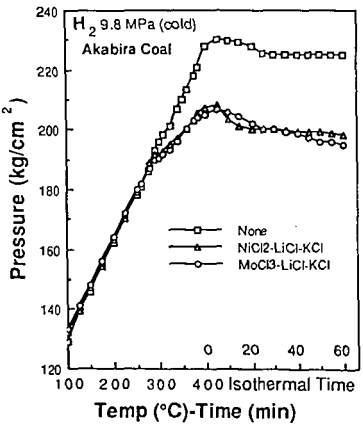

Figure 3. Reactor **t-p** profiles for liquefaction.

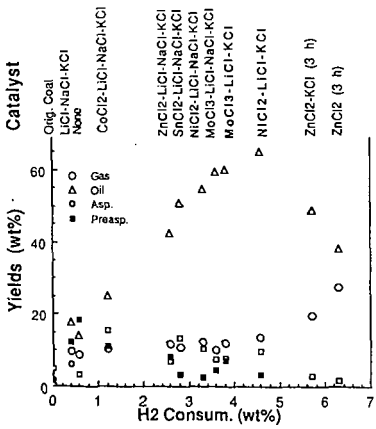

Figure 4. Dry liquefaction of Wandoan coal.

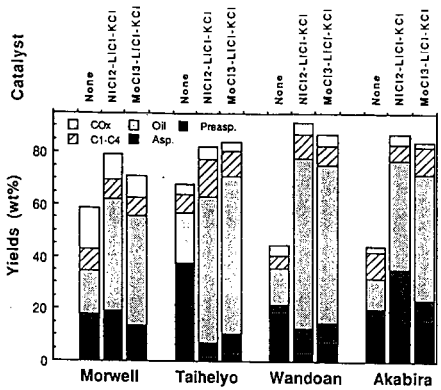

Figure 5. Dry liquefaction of coals.

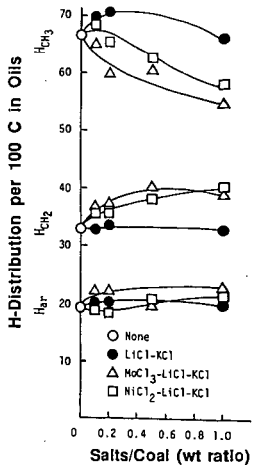

Figure 7. H-distribution of oils

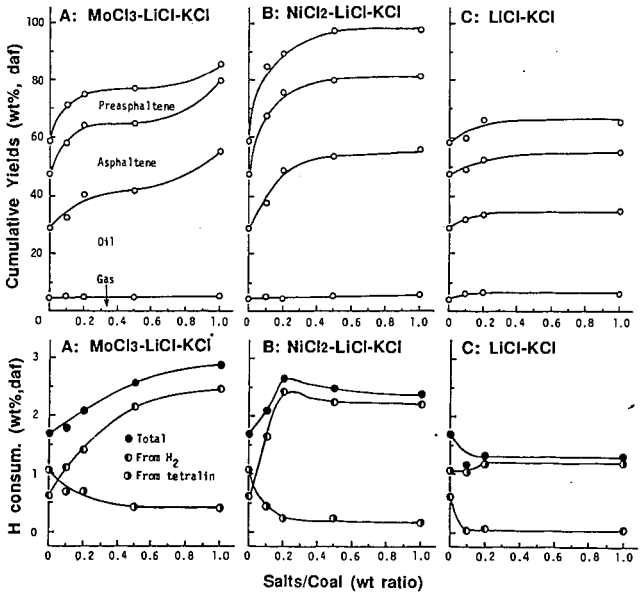

Figure 6. Effect of salt loading on coal conversion and H-transfer under low H_2 pressure

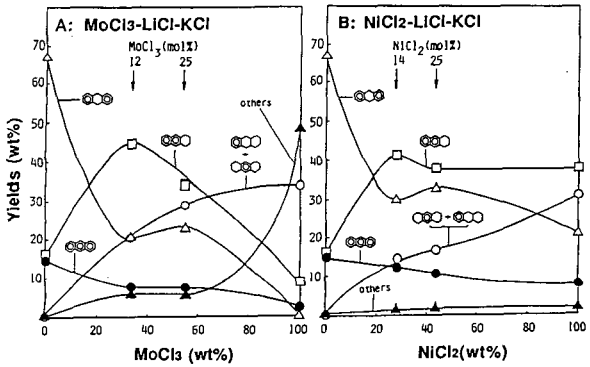

Figure 8. Effect of MCln content on hydrogenation of anthracene

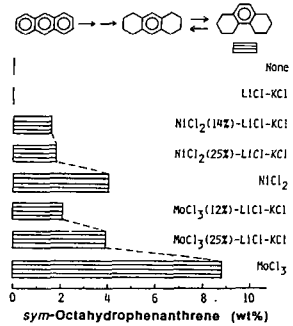

Figure 9. *sym*-octahydrophenanthrene from anthracene

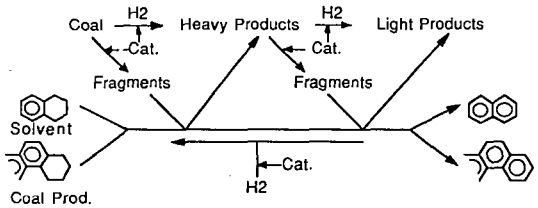

Figure 10. Hydrogen-transfer network in liquefaction

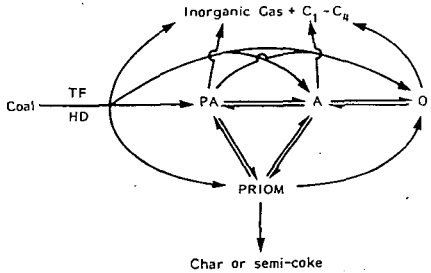

Figure 11. A reaction model for coal liquefaction
TF: Thermal fragmentation; HD: Hydrogen donation by H in coal itself, vehicle and gas; PRIOM: Promptly repolymerized or re-crosslinked insoluble organic materials; A: Asphaltene; PA: Preasphaltene; O: Oils including light distillate.

SULFATED METAL OXIDES AS CATALYSTS FOR COAL-OIL COPROCESSING

Vivek Pradhan, J. W. Tierney and Irving Wender
Department of Chemical and Petroleum Engineering
University of Pittsburgh, Pittsburgh, PA 15261

ABSTRACT

We recently reported on the investigation of the catalytic activities of iron and tin oxides treated with varying amounts of sulfate for the direct liquefaction of Argonne coals.[1,2] This paper deals with the use of the same catalysts in addition to novel bifunctional, bimetallic catalysts such as $Mo/Fe_2O_3.SO_4^{2-}$ containing about 0.5 to 2 wt% of Mo on the sulfate-promoted oxide (20-100 ppm Mo with respect to coal) for coprocessing of Argonne Illinois No.6 coal with Maya (650°F) ATB oil (20% coal+80% oil). The properties of these sulfate-promoted iron oxides before reaction and the types of active phases formed under liquefaction conditions (determined by XRD, electron microscopy, and Mossbauer spectroscopy) are correlated with their apparent activities for coprocessing carried out at 400°C. The sulfated bifunctional catalysts containing about 3500 ppm Fe and 50 ppm Mo with respect to coal are highly active for coprocessing, giving 80+% total coal conversion and 70 % yield of lighter oils with Illinois No. 6 coal and Maya ATB. These conversion values are higher than those obtained with ferric sulfate or carbonyl precursors such as $Fe(CO)_5$ and $Mo(CO)_6$. High catalyst dispersion and surface acidity are major factors that contribute to increased activity of these catalysts; Mo contributes a good hydrogenation function.

INTRODUCTION

The effects of catalytic activities of sulfate-treated iron and tin oxides and their relation to their catalytic activities in direct coal liquefaction have been reported.[1,2,3] The high activity of these unsupported catalysts have been attributed mainly to their highly dispersed forms (available surface area per gm of catalyst) and to their enhanced surface acidity.

It is important to note that these sulfated oxides $[M_XO_Y/SO_4^{2-}]$ do not have real stochiometric formulas but are a symbol for oxides which contain chemically attached surface species usually constituting a few percent of the total oxide. With Fe_2O_3/SO_4^{2-}, for instance, this could be considered as SO_3 chemisorbed on the Fe_2O_3 surface. We have found[4] that the presence of a very small amount of moisture in the catalyst system helps maintain high acidic activity, likely due to transformation of the catalyst to its Bronsted acid form, responsible for generating carbocations.

The effects of various anions such as Cl^-, PO_4^{3-}, and SO_4^{2-} in the form of dopants added to metal oxides to decrease their particle size has been the topic of considerable interest in material science since the early eighties. It is known[5] that the sulfate anion prevents sintering of ceramic oxide powders during calcination, thereby reducing the degree of crystallinity and

lowering the average crystallite size of these oxides. It has been shown that[1] the superacid Fe_2O_3/SO_4^{2-} forms a highly dispersed catalyst in the form of particles of about 30-100 A° units in diameter. It is this very property that also makes sulfated iron oxides good sensors for combustible gases.[5]

Addition of molybdenum to the sulfated iron oxide provides an excellent hydrogenation function to contribute to the catalytic action of the highly dispersed, superacidic Fe_2O_3/SO_4^{2-}.

EXPERIMENTAL

Catalyst Preparation and Characterization: The Fe_2O_3/SO_4^{2-} and $Mo/Fe_2O_3/SO_4^{2-}$ catalysts consisting of varying amounts of molybdenum were prepared using homogeneous coprecipitation followed by an incipient wetness technique. Ammonium heptamolybdate was used as a starting salt for molybdenum impregnation. Conditions for the preparation of these catalysts are given in Table 1. The catalysts were characterized by BET-surface area analysis, sulfur analysis, thermal stability measurements, X-ray diffraction, and electron microscopy. A Phillips X-ray Diffractometer using Cu-Kα radiation at 30 kV and 25 mA was used to obtain the powder diffraction patterns of the catalysts.

Average crystallite sizes of these catalysts were calculated from line broadening of the peaks, corrected for instrumental broadening. Transmission electron microscopy (TEM) and scanning electron microscopy (SEM) were carried out for structural investigation of the catalysts using JEOL 35 CX SEM and JEOL 200 CX TEM models. The residues of coal liquefaction experiments were also analyzed using X-ray diffraction and a JEOL 2000 FX STEM (100 kV beam) with an energy dispersive X-ray spectrometer (EDX) to determine composition and dispersion information about the catalytic phases formed under liquefaction conditions.

Reaction Studies: Coprocessing experiments were conducted in a 300ml stainless steel autoclave (Autoclave Engineers) agitated by a turbine impeller and heated by a tube furnace. Coal (10.0g), 40.0g Maya ATB residuum, and the desired catalyst precursors/sulfated catalysts were placed into the reactor, which was flushed with helium and stirred at 50°C for two hours to ensure mixing of the catalyst precursor in the viscous residuum. The reactor was pressurized with hydrogen to 6.9 MPa, heated to reaction temperature (400 or 425°C) in 30 minutes, and held there for 60 minutes while stirring at 1400 rpm. The reactor was then cooled to below 300°C in about five minutes. Soxhlet extraction with methylene chloride was used to determine conversion. Soluble products were recovered by rotary evaporation at 45°C under vacuum. Pentane solubles were determined by adding 40 volumes of n-pentane to the methylene chloride (CH_2Cl_2) solubles and then using Soxhlet extraction with n-pentane. Transmission electron microscopy was carried out using a JEOL 2000FX STEM (100kV beam) with an energy dispersive X-ray spectrometer.

RESULTS AND DISCUSSION

Catalyst Characterization: The iron and tin oxides treated with different amounts of sulfate were characterized by DTA/TGA to determine their thermal stability. For sulfated iron oxides promoted with small amounts of molybdenum, $Mo/Fe_2O_3/SO_4^{2-}$, decomposition of the sulfate group was found to occur above 600°C under an N_2 atmosphere. The effects of sulfate anion on reduction of grain sizes were published earlier.[3] The average crystallite size

of the oxide particles had decreased upon treatment with 2 to 6 wt % of sulfate anion; this was accompanied by a corresponding increase in the specific surface area of these oxides, observed when liquid nitrogen physisorption was carried out using the BET method. A linear relationship was observed between the concentration of sulfuric acid used for sulfate treatment and the final amounts of SO_4^{2-} groups on the iron oxides up to about 8 wt% sulfate loading. From X-ray diffraction studies of the sulfated iron oxides, α- and γ-Fe_2O_3 were found to be the most abundant crystalline phases, while for tin oxides, the most abundant phase was crystalline SnO_2. Catalyst characterization results are listed in Table 2. For $Mo/Fe_2O_3/SO_4^{2-}$ containing 20-100 ppm of Mo with respect to coal, no molybdenum was detected by X-ray diffraction; this could be due to the very fine dispersion of Mo apart from its small concentration on the Fe_2O_3/SO_4^{2-} catalyst. Temperatures of the onset of liquefaction of Illinois No.6 coal using different sulfate-treated oxides as catalysts are listed in Table 2. These temperatures were determined using a high pressure, high temperature polarizing optical microscope with flowing H_2 at 300 psig pressure. $Mo/Fe_2O_3/SO_4^{2-}$ catalysts were also characterized by electron microscopy and found to have a grain size of about 10-15 nm. The amounts of Mo in the catalysts were determined by inductively coupled plasma analysis.

Reaction Studies: Initially a thermal (no added catalyst) run was carried out to determine the catalytic activities of the mineral matter (especially pyrite) inherent in coal. The coal conversion values listed in this paper are calculated based on weight of the final residue.

(I) Activities of the Sulfated Oxides

The sulfated iron and tin oxides were used in small concentrations for coprocessing of Illinois No. 6 with Maya ATB. Use of the Fe_2O_3/SO_4^{2-} catalyst containing about 3.4 wt% of sulfate group, resulted in a coal conversion of 70 wt % with 72 wt % selectivity to oils at 400°C with about 3500 ppm iron with respect to the coal-oil mixture. When SnO_2/SO_4^{2-} (3.9 wt% sulfate) was used as the catalyst with 3500 ppm of tin at 400°C, about 62 wt% conversion was obtained with about 76 wt% selectivity to oils. A reaction was carried out with a molybdenum containing catalyst precursor, $Mo(CO)_6$, for comparison, using about 100 ppm Mo with respect to the mixture of coal and oil. This resulted in a 71 wt% coal conversion with 70 wt% selectivity to lighter oils. Use of a bimetallic, bifunctional catalyst, $Mo/Fe_2O_3/SO_4^{2-}$, consisting of 50 ppm Mo and 3500 ppm Fe with respect to the coal-oil mixture gave a coal conversion of 80 wt% with 80 wt% selectivity to lighter oils. The higher activity of this catalyst is attributed to the hydrogenation ability of Mo and, possibly, to the acid sites of the sulfated catalyst. Results of these catalyst activity comparisons and those obtained in the coprocessing reaction employing a bimetallic sulfated oxide of iron and tin, $SnO_2/Fe_2O_3/SO_4^{2-}$, (with 1750 ppm of each iron and tin) are shown in Figure 1(A).

Enhancement in total conversions as well as conversions to oils obtained with sulfated oxides are attributed mainly to enhanced "dispersions" (surface area/gm) with a possible contribution from the high surface acidity of these oxides upon sulfate treatment. It is likely that, with increase in the specific surface area and decrease in the average particle size of the oxides upon addition of small amounts of the sulfate group, conversion of the oxides to active catalytic sulfide phases, especially non-stoichiometric sulfides of iron, is facilitated.[6] More of the active catalyst surface of these sulfides becomes available for reaction.

(II) Activity of $Mo/Fe_2O_3/SO_4^{2-}$ Catalysts at 400 and 425°C

Addition of small amounts of Mo to 0.5 to 2 wt% of the sulfated iron oxides (about 20-100 ppm Mo concentration with respect to the coal-oil mixture) resulted in substantial improvement in the selectivity to oils. A series of experiments were carried out to determine the coprocessing conversion of Illinois No. 6 with Maya ATB at two different reaction temperatures (400 and 425°C) and for different amounts of Mo loadings on Fe_2O_3/SO_4^{2-}. The results of experiments carried out at 400 and 425°C are shown in Figure 1(B).

Total coal conversions, as well as selectivities to lighter oils, increased for both temperatures with the amount of molybdenum in the sulfated iron oxide catalyst (0-100 ppm Mo with respect to the coal-oil mixture). Conversions as high as 84 wt% (maf coal) with selectivity values of higher than 80 wt% were obtained at about 100 ppm Mo + 3500 ppm Fe added in the form of $Mo/Fe_2O_3/SO_4^{2-}$. Surprisingly, we obtained slightly lower values for both coal conversion and selectivity to oils in almost all the reactions carried out at 425°C as compared to those at 400°C. This apparent decrease in coprocessing conversion is likely due to the extensive coking reactions occurring because of the presence of an acidic functionality in the catalyst. The coal liquefaction residues obtained in this case (425°C) had a rock-like appearance.

All of the aforementioned reactions were carried out without adding any external sulfur compound since Illinois No. 6 coal and the heavy oil (Maya ATB) together have enough sulfur to sulfide the added metals during reaction. Nevertheless, a run was made with addition of elemental sulfur (10% in excess of that required for complete sulfidation of both the Fe and Mo in the catalyst) to the coal-oil mixture prior to reaction at 400°C with 3500 ppm of iron and 100 ppm of Mo . No effect of the added sulfur was observed on either overall coal conversion (86 wt%) or the selectivity to lighter oils (82 wt%).

Product Characterization:

(i)Elemental Analyses of Methylene Chloride-Soluble Products

The methylene chloride solubles of the coprocessing product from using the Fe-Mo precursor were analyzed for C,H,N, and S contents. As seen from Table 3, an improvement in the H/C atomic ratios is obtained for the soluble products for the sulfated iron oxides containing small amounts of molybdenum as catalysts. At the same time, a significant degree of sulfur and nitrogen removal (75 to 80 % HDN and HDS) is obtained. With the $Mo/Fe_2O_3/SO_4^{2-}$ catalysts, this could be attributed to the enhanced acidic strength and high dispersions of the catalysts and the hydrogenative function contributed by Mo.

(ii) X-Ray Diffraction and Electron Microscopy of Residues

X-ray diffraction (XRD) was performed on the methylene chloride-insoluble fraction of the coprocessing runs carried out with Illinois #6 coal with added iron catalysts. Transmission electron microscopy was employed to determine the size range of the iron- and molybdenum-containing particles produced from $Fe(CO)_5$ and $Mo(CO)_6$ precursors. To eliminate interference of the iron and other mineral matter in the coal, a model system was used which consisted of activated carbon with molybdenum or Fe-Mo deposited on it. This mixture was produced by heating a mixture of activated carbon (with a very low iron content), toluene (solvent), and $Mo(CO)_6$ with or without $Fe(CO)_5$ in an autoclave to decompose the precursor into small particles, some of which would end up on the carbon support. Similarly, for the electron microscopic studies, a $Mo/Fe_2O_3/SO_4^{2-}$ catalyst was deposited on an activated carbon matrix using tetralin as dispersion medium. These TEM images show the catalyst particles containing Fe and mo on active carbon with sizes ranging from 10-30 nm.

CONCLUSIONS

Sulfated iron and tin oxide catalysts were found to be active for the coprocessing of Argonne Illinois No.6 coal with Maya ATB (20:80 coal:oil) both at 400 and 425°C. For a bimetallic catalyst, $Mo/Fe_2O_3/SO_4^{2-}$, consisting of 50 ppm Mo and 3500 ppm iron, a 78 % coal conversion of Illinois No. 6 was obtained with an oil- selectivity of 80 % at 400°C. The sulfated iron oxide catalysts with small amounts of Mo(20-100 ppm) were more active than the soluble precursors of the same metals at 400°C. Significant HDN (~75 %) and HDS(~80%) were obtained with Mo-promoted sulfated iron oxide catalysts. We attribute the higher activity of the sulfated oxides to their fine grain size (30-100 A°) with increased catalyst dispersion and to increase in their acid strength. The comparison between the activities of sulfated oxides and the soluble precursors shows that finely divided solid catalysts could be as active as the catalysts produced from the soluble precursors of iron and molybdenum. Thus, the catalytic activity of the sulfated oxides are the result of several factors: the fine grain size is probably of the greatest importance, the superacidity of the starting catalysts may play a part during the initial phases of the reaction. In the case of $Mo/Fe_2O_3/SO_4^{2-}$, the hydrogenation ability of Mo certainly plays a part. However, there is still much to be learned about the mechanisms involved in these types of reactions. With these superacidic sulfated metal oxides as catalysts, the chemistry of the reactions in coal liquefaction could be different from what is known so far (such as possible involvement of radical ion intermediates). These finely divided solid catalyst-precursors therefore show great promise for application in hydroprocessing reactions

ACKNOWLEDGMENTS

The authors gratefully acknowledge the contributions of the Argonne coal sample bank for providing the coal samples, C. van Ormer and J.R. Blachere for the transmission electron microscopy, the donation of Maya crude by CITGO, and funding support from the U.S. Department of Energy under grant number DE-FC22-88PC8806.

References

1. Pradhan, V. R., Tierney, J. W., Wender, I., Preprints, Div. of Fuel Chem., *American Chemical Society*, August, **1990**, Vol. 35, No. 3, p. 793

2. Pradhan, V. R., Tierney, J. W., Wender, I., Paper Presented at the 'Direct Liquefaction Contractors' Review Meeting (DOE)' Pittsburgh, **1990**

3. Pradhan, V. R., Huffman, G.P., Tierney, J. W., Wender, I., *submitted to Energy and Fuels for Publication*

4. Wen, M. Y., Wender, I., Tiemey, J., *Energy and Fuels*, Vol.4, **1990**, pp.392-397

5. Nakatani, Y., Sakai, M., Matsuoka, M., *J. of Appl. Physics*, Vol. 21, **1982**, pp. L758

6. Montano, P.A., Bommannavar, A. S., Shah, V., *Fuel*, **1981**, Vol. 60, P. 703

Table 1. Preparation Conditions of Sulfated Iron and Tin Oxides

Catalyst	Catalyst Designation	Starting Salts	Norm. H_2SO_4	Calcination, T°C
Fe_2O_3/SO_4^{2-}	I	Fe Alum[a]	--	500
$Mo/Fe_2O_3/SO_4^{2-}$	II	Fe Alum[a]	--	500
$Mo/Fe_2O_3/SO_4^{2-}$	III	Fe Alum[a]	--	500
$Mo/Fe_2O_3/SO_4^{2-}$	IV	Fe Alum[a]	--	500
SnO_2/SO_4^{2-}	V	$SnCl_4/5H_2O$	6.0	600
$SnO_2/Fe_2O_3/SO_4^{2-}$	VI	Chloride Salts[b]	6.0	500

[a] Urea was used as the precipitating agent whereas ammonium heptamolybdate was used to impregnate small amounts of Mo on sulfated iron oxide before calcination.

[b] The ferric and tin chloride salts were used here with 28 % ammonia water as a precipitation agent.

Table 2. Physicochemical Properties of the Sulfated Oxide Catalysts

Catalyst	Wt % Mo	S_g, m^2/g	XRD: $D_{avg.}$	TEM :$D_{avg.}$	Onset T°C[a]
Catalyst I	0.0	81.72	16 nm	20-25 nm	410
Catalyst II	0.4	81.50	12 nm	20-30 nm	nd
Catalyst III	1.0	88.00	9 nm	15-20 nm	400
Catalyst IV	2.0	92.21	9 nm	10-15 nm	400
Catalyst V	--	146.23	5 nm	10-15 nm	385
Catalyst VI[b]	--	320.00	5 nm	5-10 nm	nd

[a] Onset coal liquefaction temperature for a non-catalytic liquefaction run for Argonne Illinois No.6 coal was 450°C as determined using a high temperature, high pressure polarizing microscope.

[b] This catalyst consisted of equal weight percents of SnO_2 and Fe_2O_3.

Table 3. Elemental Analysis of CH_2Cl_2 Solubles Obtained from Coprocessing of Illinois No.6 and Maya with Different Catalysts

Amount of Catalysts vs. Analysis : Wt %							
Catalyst	ppm Mo	ppm Fe	% C	% H	% N	% S	(H/C)atom
None	--	--	83.00	10.30	0.25	3.18	1.49
Catalyst III	50	3500	47.58	5.83	0.55	2.01	1.47
Catalyst IV	100	3500	66.99	8.52	0.72	2.13	1.53
$Fe(CO)_5$	--	5000	83.83	10.45	0.33	3.01	1.50
Carbonyls	500	5000	82.53	10.79	0.43	2.94	1.57
Mo-naph.[b]	500	5000	83.07	10.50	0.40	2.89	1.52

[a] All runs were made with Illinois No.6, 425°C, 1000 psig cold H_2, 60 minutes, 20 wt% coal/80 wt% Maya ATB.

[b] $Fe(CO)_5$ was used in this run with Mo-naphthenate.

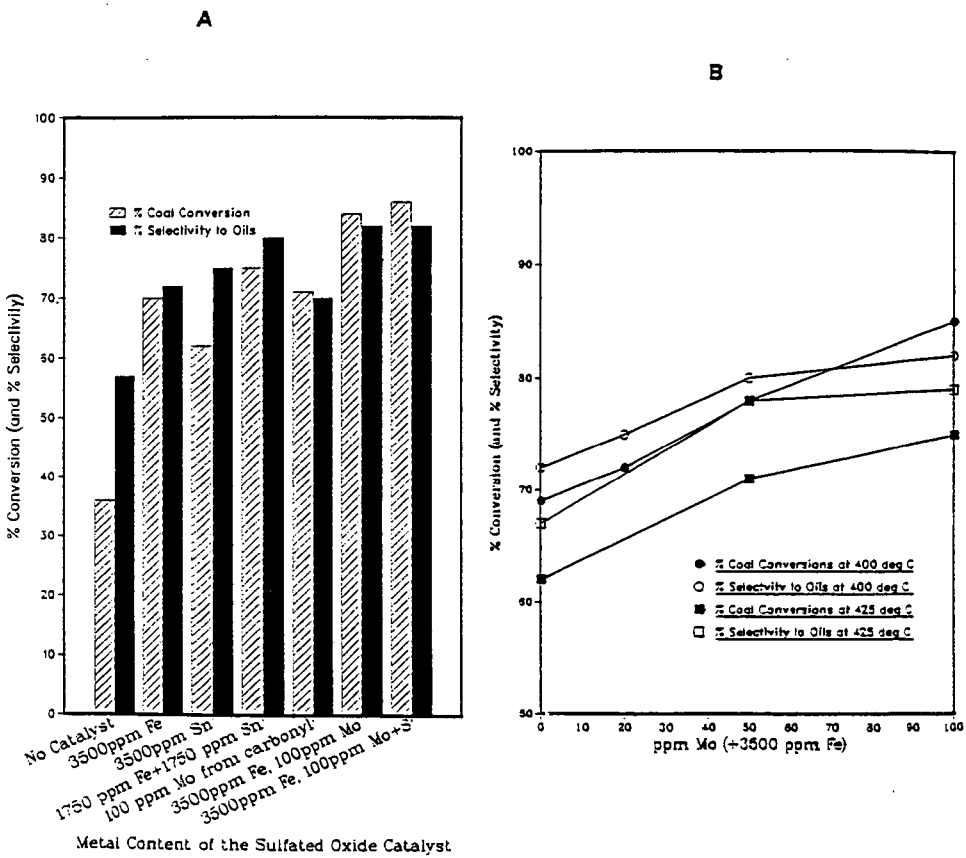

Figure 1. (A) Activity of Sulfated Metal Oxides for Coprocessing of Illinois No.6 Coal at 400°C, 1000 psig cold H_2, 1h and (B) Activity of $Mo/Fe_2O_3/SO_4^{2-}$ Catalysts for Coprocessing at 400 and 425°C, 1000 psig cold H_2, 1h

DIHYDROQUINONE FOR ENHANCING COAL LIQUEFACTION YIELDS

J. H. Penn*, Y.-Q. Liu, and P. Yassini
Department of Chemistry
West Virginia University
Morgantown, WV 26506

Keywords: Dihydroquinone, Coal Liquefaction, THF extractables

Abstract

Finding reagents and/or catalysts to enhance liquefaction of coal continues to be an area of active interest. During our studies directed towards the use of PI-acceptor induced bond cleavage reactions, we have found that 1,4-dihydroquinone enhances the yield of THF-extractables for a series of coals ranging from low rank sub-bituminous to high volatile bituminous. In certain cases, benzoquinone can also enhance the yields of THF extractables from coal. These reactions take place at surprisingly low temperatures (*i.e.*, 200°C).

Introduction

As part of our on-going effort to develop new ways to cleave bonds (1) through the use of electron transfer chemistry, we have been particularly interested in the reactions of quinones and their ability to cleave ether bonds (2). Representative of our work to date is the reaction of benzyl ether (**BE**) with 2,3-dichloro-5,6-dicyano-1,4-quinone (**DDQ**) which yields benzaldehyde and benzyl alcohol when heated together at 200°C in acetonitrile (CH_3CN) (2) as shown in eq (1).

(1)

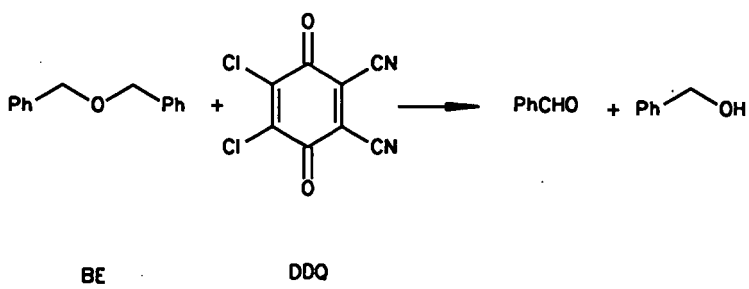

Although the use of quinones proved to be useful to bond

cleavage in model compounds, quinones proved to have only a small effect on enhancing liquid yields liquids from coal under similar conditions to those used in model compound studies. Interestingly, small quantities of quinones did appear to have a small positive effect on achieving greater quantities of THF-extractables. One rationale for this lack of enhancement arises from the oxidizing nature of these compounds. Since the major goal for liquefaction seems to involve the addition of hydrogen to the molecular framework of the coal polymer as it unravels, we reasoned that dihydroquinones, as the redox couples of quinones (note eq (2)), might prove effect in increasing liquid yields. Although dihydroquinones have been used as part of a complex mixture for enhancing coal liquefaction, we report here that **DHQ** by itself is sufficient to enhance the amount of THF-extractable material from a number of coals.

(2)

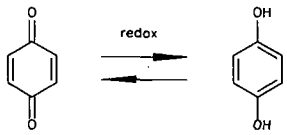

Experimental

Samples of coal were obtained from the Argonne Premium Coal Sample Bank. Bakerstown coal and Sewell coal were obtained from the West Virginia Coal Sample Bank.

A given weight of coal and a given weight of the added reagent were added to 5 mL of acetonitrile (CH_3CN, freshly distilled from NaH) in a 10 mm glass tube. Oxygen was removed from the solution *via* 3 freeze-pump-thaw degassing cycles and the sample tube was then sealed *in vacuo*. The sample tube was placed in a tubing bomb reactor to which excess CH_3CN was added to equalize the pressure on the outside and inside of the glass. The tube was then placed in an oil bath at the indicated temperature for the indicated length of time. After removal from the oil bath, the contents of the glass tube are placed in a Soxhlett extractor and refluxed with THF for 24 h. After evaporation of the THF *in vacuo*, the weight of the extract and the weight of the insolubles were determined.

Results and Discussion

In order to evaluate the effect of a reagent on liquefaction of coal, control experiments were performed with no added reagent to establish the amount of extractables without reagent. In all

cases, the coal was heated at 200°C for 48 h in the indicated solvent. Not surprisingly, the choice of solvent does have an effect upon the amount of THF-extractables obtained in these experiments. The results of these experiments are given in Table I. As expected, there is a solvent dependence on the amount of THF-extractability as evidenced by the effects shown on the Bakerstown coal. These experiments were mandated by the high mass balances afforded by acetonitrile (CH_3CN). Since all other solvents yielded mass balances less than 100%, we conclude that incorporation of CH_3CN into the insolubles and into the THF extractables occurs similarly in all experiments.

The results of adding a 1:1 weight ratio of dihydroquinone (**DHQ**) to the coal are shown in Table II. In these experiments, the coal and the **DHQ** have been heated together in the indicated solvent for 48 h at 200°C. In this table, the effects of the reagent are given by a Liquefaction Enhancement (L.E.) which has been defined by eq (3). In this equation, THF_{coal} and THF_{DHQ} are the amounts of extractables when either the coal or DHQ are treated alone. Normalization to the starting amount of coal is performed to enable comparison of one coal to another coal.

$$L.E. = \frac{(Total\ THF\ extract) - (THF_{coal} + THF_{DHQ})}{starting\ weight\ coal} \times 100\% \qquad (3)$$

As can be seen in Table II, reasonable enhancements in the liquid yields are obtained. These results are made more remarkable when one considers that these LEs were obtained for temperatures as low as 200°C. A solvent dependence is noted for this effect, with only CH_3CN and cyclohexane (C_6H_{12}) showing positive enhancements.

Although these results are still preliminary in nature, we speculate that **DHQ** serves primarily as a hydrogen donor. In support of this hypothesis, **DHQ** gives a greater LE than tetralin (L.E.=-12%) for Bakerstown coal under similar conditions. Since a limited amount of 1,4-benzoquinone (**BQ**) shows a small positive L.E., the use of **DHQ** offers the possibility that a catalytic cycle may be opened up, making the product(s) of **DHQ** (*i.e.*, **BQ**) effective for more liquefaction activity.

References

1. (a) Penn, J.H.; Lin, Z.; Deng, D.-L. *J. Am. Chem. Soc.*, **1991**, in press. (b) Penn, J.H.; Lin, Z.; Deng, D.-L. *Tetrahedron Lett.*, **1988**, *29*, 3635.

2. (a) Penn, J.H.; Lin, Z. *J. Org. Chem.*, **1990**, *55*, 1554. (b) Penn, J.H.; Deng, D.-L.; Aleshire, S.K. *J. Org. Chem.*, **1988**, *53*, 3572. (c) Penn, J.H.; Smith, R.S. *Tetrahedron Lett.*, **1986**, *27*, 3475.

Table I
Coal Extractability Without Added Reagent

Coal	Coal Rank	Solvent	%THF Extractable
Bakerstown		CH_3CN	19.9
		THF	25.9
		C_6H_6	21.7
		C_6H_{12}	4.8
Sewell		CH_3CN	19.5
Pittsburgh #8	HV Bituminous	CH_3CN	34.4
Blind Canyon	HV Bituminous	CH_3CN	26.4
Upper Freeport		CH_3CN	12.7
Beulah-Zap	Lignite	CH_3CN	5.4

Table II
Enhancements Using **DHQ** as a Co-reagent

Coal	Coal Rank	Solvent	L.E.
Bakerstown		CH_3CN	20.5
		THF	1.0
		C_6H_6	2.3
		C_6H_{12}	10.0
Sewell		CH_3CN	-1.9
Pittsburgh #8	HV Bituminous	CH_3CN	41.7
Blind Canyon	HV Bituminous	CH_3CN	7.8
Upper Freeport		CH_3CN	3.4
Beulah Zap	Lignite	CH_3CN	45.4

EVALUATION OF CATALYTIC ROLE OF VANADIUM IN COAL-OIL PROCESSING USING MODEL SYSTEMS

H. Kim and C. W. Curtis
Department of Chemical Engineering
Auburn University, AL 36849

Keywords: vanadium, coal-oil processing, model systems

ABSTRACT

The catalytic activity of vanadium for hydrogenation and heteroatom removal reactions occurring in coal-oil processing was evaluated using model systems. Two-ring aromatics, hydroaromatics and heteroatomic species containing S, N and O were selected as the models representing typical species in coal and oil. Vanadium catalysts generated *in situ* from organic vanadium complexes, such as vanadium acetylacetonate and vanadylacetylacetonate, were activated in the presence of sulfur. Their activity increased as the amount of sulfur present increased. The vanadium catalysts were active for partial saturation of two-ring aromatics to hydroaromatics but far less active for the further saturation to alicyclic compounds. The vanadium catalysts were severely poisoned by organic nitrogen compounds, showing lower activity for N removal than for S and O removal and achieving low amounts of hydrogenation and heteroatom removal of other reactants when nitrogen compounds were present.

INTRODUCTION

Vanadium (V) is one of the most abundant trace metals in petroleum and is more concentrated in the petroleum residuum than in the crude.(1) V sulfides, which are generated from their organic precursors such as V naphthenate, octoate or acetylacetonate in the presence of sulfur, have been used as hydrodesulfurization catalysts in petroleum refining.(2-5) The V indigenous to residuum may form V sulfide and be catalytic under coal-oil processing conditions. These species may influence the reaction pathways and product slates involved in the processing.

The objective of this study is to evaluate the catalytic activity of V sulfide for hydrogenation and heteroatom removal reactions occurring in coprocessing. The activity and selectivity of *in situ* generated V sulfide were evaluated by reacting model hydrocarbon and heteroatomic systems with V precursors, vanadium acetylacetonate and vanadylacetylacetonate, and excess sulfur under coal-oil processing conditions. The activity and selectivity of *in situ* generated V sulfide for the reactions of model compounds were also compared to those of a Mo sulfide catalyst generated *in situ* from Mo naphthenate and sulfur.

EXPERIMENTAL

Chemicals

The model reactants used were naphthalene (99%), indan (97%), indene (99%), benzothiophene (97%), o-cresol (99%), benzofuran (99.5%), quinoline (99%) and indole (99%). n-Hexadecane (99%) was used as a solvent. All of these chemicals were obtained from Aldrich. The V precursors were vanadium(III) acetylacetonate (VAcAc) and vanadyl(IV)acetylacetonate (VOAcAc). VAcAc was obtained from Shepherd Chemical and Aldrich, and VOAcAc was obtained from Aldrich.

Reactions and Analyses

Hydrogenation reactions were conducted in 20 cm^3 batch tubing bomb microreactors. Four grams of hexadecane solution containing 2 wt% naphthalene and/or 1 wt% of

each of other reactants were charged to the reactor. The V precursor was introduced at a level of 2850 to 2950 ppm V while always keeping a constant weight ratio of V to reactant. Excess elemental sulfur, 0.034 g S which was three times the stoichiometric amount of sulfur to form V_2S_3 from V precursors, was added to the reaction. Prior to the reaction, 1250 psig H_2 was introduced at ambient temperature. The reactions were conducted at 380°C for 30 minutes with horizontal agitation at 550 cpm. The liquid products were analyzed by gas chromatography using a 30 m fused silica DB-5 column (J & W Scientific) and FID detection with p-xylene as the internal standard. Some of the reaction products were identified by GC/MS equipped with a VG 70EHF mass spectrometer and a Varian 3700 gas chromatograph.

RESULTS AND DISCUSSION

The catalytic activity of V generated *in situ* from VAcAc and VOAcAc was investigated in hydrogenation reactions of hydrocarbons and heteroatomic species individually or in combination under coprocessing conditions. In addition, the effect of sulfur on the activity of V species was determined.

The degree to which hydrogenation and heteroatom removal occurred in each reaction is reported in terms of percent hydrogenation (% HYD), percent hydrodesulfurization (% HDS), percent hydrodeoxygenation (% HDO), and percent hydrodenitrogenation (% HDN). The % HYD is defined as the number of moles of hydrogen used to achieve the final liquid product distribution as a percentage of the moles of hydrogen required to achieve the most hydrogenated liquid product. The % HDS, % HDN and % HDO are the summations of the mole percents of products not containing sulfur, nitrogen and oxygen, respectively. In the calculation of % HYD, the most hydrogenated liquid products defined for the systems used were decalin for naphthalene and tetralin; cyclohexane for indan, indene, benzothiophene, o-cresol, benzofuran, and indole; and n-propylcyclohexane and n-butylcyclopentane for quinoline.

Catalytic Activity of V for Aromatic Ring Saturation

The activity of V generated *in situ* from VAcAc and VOAcAc in the presence of excess sulfur was evaluated for hydrogenation of aromatics and alkylaromatics: naphthalene, tetralin, n-butylbenzene, n-propylbenzene, ethylbenzene and toluene. The result was compared to the activity of *in situ* generated Mo sulfide at the same metal loading level for the same systems. The V species from both precursors showed high activity for partially saturating two-ring aromatics to hydroaromatics, but low activity for fully saturating the two-ring aromatics or single-ring alkylaromatics to alicyclics and alkylalicyclics as did the Mo sulfide; only 2-5% of aromatic ring in alkylaromatics was saturated to alkylalicyclics with VAcAc, and only 3-9% was saturated with VOAcAC. However, the V sulfide catalysts showed a slightly higher activity for both the aromatic ring saturation and the ring hydrogenolysis than the Mo sulfide catalyst.

Activity and Selectivity of V Catalyst for Hydrogenation and Heteroatom Removal

The catalytic activity and selectivity of *in situ* generated V for reactions involving hydrogenation, hydrogenolysis and heteroatom removal were evaluated by using individual model systems. The major products and the degree of hydrogenation and heteroatom removal achieved with V catalysts were compared to those from comparable systems reacted with *in situ* generated Mo sulfide at equivalent reaction conditions (Tables 1).

Naphthalene and Tetralin. With V sulfide, both naphthalene and tetralin produced a partially saturated hydroaromatic, tetralin, as the primary product, as the same product with Mo sulfide. V sulfide, especially from VOAcAc, produced more decalin from both reactants, hence achieving higher % HYDs, than did Mo sulfide.

The V sulfide also produced various hydrogenolyzed products.

Indan and Indene. V sulfides showed low activity for saturating the aromatic ring of indan as did Mo sulfide. Indene was completely converted to indan with V catalysts, but only less than 12% of indan was converted further to fully saturated hexahydroindan, predominantly to *cis*-hexahydroindan. Compared to Mo sulfide, V catalysts were relatively more active for saturating the aromatic ring and for hydrogenolyzing the five-membered ring, showing a higher % HYD.

Benzothiophene. VAcAc and VOAcAc without sulfur was nearly inactive for hydrogenation of benzothiophene. But in the presence of excess sulfur, both V precursors almost completely hydrodesulfurized benzothiophene, producing ethylbenzene and ethylcyclohexane as the primary and secondary products, respectively. When compared to Mo sulfide, V sulfides were more active for producing ethylcyclohexane; the mole ratio of ethylcyclohexane to ethylbenzene produced was 6:90 with MoNaph, 23:72 with VAcAc and 23:66 with VOAcAc. Hence, V sulfides yielded higher % HYD than Mo sulfide.

o-Cresol. In the absence of sulfur, VAcAc and VOAcAc did not catalyze the deoxygenation of o-cresol. But, in the presence of excess sulfur, o-cresol was completely deoxygenated with both precursors. When compared to Mo sulfide, V sulfides removed more oxygen and produced more alkylalicyclics, such as methylcyclohexane, ethylcyclopentane and their isomers, and less alkylaromatics such as toluene, hence yielding higher % HYD.

Benzofuran. With VAcAc and VOAcAc in the absence of sulfur, no oxygen was removed from benzofuran. But in the presence of excess sulfur, both VAcAc and VOAcAc completely converted benzofuran and achieved a high level of oxygen removal, producing ethylcyclohexane and ethylbenzene as the primary and the secondary products, respectively. V catalysts were more active for hydrogenolyzing the five-membered ring and removing oxygen from benzofuran than Mo sulfide.

Quinoline. VAcAc and VOAcAc in the presence of excess sulfur showed a relatively low activity for the hydrodenitrogenation of quinoline. With the *in situ* generated Mo sulfide, quinoline was completely converted, achieving 90% HDN. Propylcyclohexane and butylcyclopentane were the major products. By contrast, only 31% HDN and 36% HDN were achieved with VAcAc and VOAcAc, respectively, and 1,2,3,4-tetrahydroquinoline was the major product. The low activity for nitrogen removal and, thus, the low % HYD achieved suggested that the V sulfides, which were highly active for hydrogenation of aromatics and removal of S and O, might be severely poisoned by organic nitrogen compounds. In the absence of sulfur, V precursors were nearly inactive for quinoline denitrogenation.

Indole. With VAcAc and VOAcAc in the presence of excess sulfur, indole was completely converted, yielding o-ethylaniline as the primary product and ethylcyclohexane as the secondary product. V sulfides were less active for nitrogen removal compared to Mo sulfide,. This low activity for indole denitrogenation again suggested that the activity of V catalysts might be severely inhibited b y organic nitrogen compounds. Without sulfur, VOAcAc did not catalyze the nitrogen removal from indole.

Reaction Pathway of Heteroatom Removal. Because V sulfides did not actively catalyze the direct hydrogenation of ethylbenzene to ethylcyclohexane (only up to 3-4%) and toluene to methylcyclohexane (5-9%), the large amounts of ethylcyclohexane produced from the hydrogenation of benzothiophene (23% with VAcAc and VOAcAc), benzofuran (66% with VAcAc, 58% with VOAcAc) and indole (26% with VAcAc, 32% with VOAcAc) and methylcyclohexane from o-cresol hydrogenation (60% with VAcAc, 55% with VOAcAc) appeared to be produced from heteroatom-

containing intermediates: octahydrobenzothiophene and 2-ethylcyclohexanethiol for benzothiophene, octahydrobenzofuran and 2-ethylcyclohexanol for benzofuran, perhydroindoline and 2-ethylcyclohexylamine for indole, and methylcyclohexanol for o-cresol. Therefore, heteroatom removal with V sulfides was simultaneously achieved through two different pathways as with Mo sulfide.(6) For removal of the heteroatom from benzothiophene, benzofuran and indole, one pathway proceeded through the hydrogenation to dihydro-products, followed by heteroatom removal, producing ethylbenzene, and the other pathway proceeded through the aromatic ring saturation, thereby producing the heteroatom-containing saturated intermediates that later released heteroatoms, producing ethylcyclohexane. For o-cresol, one pathway proceeded through direct oxygen removal from o-cresol, producing toluene, and the other proceeded through aromatic ring saturation, producing methylcyclohexanol, and then followed by oxygen removal, producing methylcyclohexane. When compared to Mo sulfide, V sulfides catalyzed the heteroatom removal principally through the second pathway, which utilized the heteroatom-containing saturated intermediates to produce alkylalicyclics. Hence, the % HYD achieved with V sulfides was higher than that with Mo sulfide in all cases except for the systems containing nitrogen compounds.

Effect of Combined Reactants

The effect of additional hydrocarbon and heteroatomic species on the hydrogenation of other reactants was tested with VOAcAc in the presence of excess sulfur (Table 2). In this experiment, two compounds of naphthalene, indan, benzothiophene, o-cresol, benzofuran, quinoline, indole or pyridine were mixed.

Effect on Naphthalene Hydrogenation. The activity of V sulfide for naphthalene hydrogenation was not affected much by other hydrocarbons, sulfur-compounds or oxygen-compounds. The slightly reduced % HYD of naphthalene was because of possible competitive reactions occurring on the same active sites of the catalyst. When nitrogen-containing compounds were mixed, the activity of V sulfide was tremendously reduced, indicating that organic nitrogen compounds inhibited the activity of V sulfide for hydrogenation of aromatics.

Effect on Benzothiophene Hydrodesulfurization. Nitrogen-containing reactants and products severely inhibited the activity of VOAcAc for sulfur removal from benzothiophene, while hydrocarbons and oxygen-compounds reduced % HYD in a small amount by competitive reactions on the same catalyst.

Effect on the Hydrodeoxygenation of o-Cresol and Benzofuran. The extent of hydrodeoxygenation catalyzed by V sulfides was slightly reduced by additional sulfur-compounds, while not being greatly affected by other hydrocarbons and oxygen-compounds. When quinoline was added, the activity of the V sulfide catalyst for HDO was severely inhibited. Therefore, nitrogen compounds appeared to be the most detrimental to V sulfide catalysts not only for the hydrodenitrogenation of nitrogen-containing reactants but also for other hydrogenation and heteroatom removal reactions.

Effect of Sulfur Amount on the Activity of V Catalyst

The activity of V species was generated in the presence of sulfur. The effect of the amount of sulfur on the activity of *in situ* generated V species was examined using naphthalene hydrogenation (Table 3). Without sulfur, neither V precursors showed any activity for naphthalene conversion. When sulfur was added, catalytic activity of the V species was observed. Addition of more sulfur induced higher conversion of naphthalene to decalin, indicating that the activity of the *in situ* generated V catalyst strongly depended on the amount of sulfur present.

The effect of sulfur amount on the activity of V catalysts for hydrogenation of aromatics and heteroatom removal was also tested by introducing more sulfur in combined reactions (Table 4). Two different levels of sulfur, three times and

nine times the stoichiometric amount of sulfur required to form V_2S_3 (0.034 g and 0.102 g S, respectively), were added in each reaction set. In the hydrogenation of combined sets of naphthalene-indan, naphthalene-benzothiophene and naphthalene-indole, the higher sulfur amount achieved higher % HYDs of all reactants and also markedly increased the extent of nitrogen removal from indole. However, in the combined reaction of naphthalene and o-cresol, more sulfur increased naphthalene hydrogenation, but it decreased o-cresol deoxygenation and thereby decreased o-cresol hydrogenation. These results indicated that the addition of more sulfur could enhance the activity of V sulfide for aromatic hydrogenation, sulfur removal and nitrogen removal, but that excessive sulfur might reduce the activity of V sulfide for oxygen removal.

SUMMARY

The activity of V sulfide generated *in situ* from VAcAc and VOAcAc was strongly dependent upon the amount of sulfur present. The characteristics of V sulfides in the model hydrogenation and heteroatom removal reactions were somewhat similar to those observed with the *in situ* generated Mo sulfide. In the hydrogenation of aromatics and alkylaromatics, V sulfide was active for the partial saturation of an aromatic ring in multiring aromatics but far less active for the further saturation to alicyclics and for the saturation of single-ring alkylaromatics. The heteroatom removal with V sulfide simultaneously occurred through two pathways as did with Mo sulfide: one pathway for heteroatom removal prior to saturation of the aromatic ring, producing alkylaromatics and the other for heteroatom removal following the saturation of the aromatic ring, producing alkylalicyclics. When compared to Mo sulfide, the V sulfide was more active for the hydrogenation of aromatic rings adjacent to the heteroatom before the heteroatom was removed, producing more heteroatom-containing alkylalicyclics as the intermediates and thus more alkylalicyclics in the final product slates. Therefore, V sulfide achieved higher % HYDs in the hydrogenation of oxygen and sulfur-containing compounds than did Mo sulfide. V sulfide was more active for O removal but less active for N removal than Mo sulfide.

In combined reactions, the activity of V sulfide for hydrogenation and heteroatom removal was only slightly affected by other aromatics, hydroaromatics, organic sulfur compounds, and organic oxygen compounds, but it was severely inhibited by organic nitrogen compounds. A higher content of sulfur enhanced the activity of V sulfide for the hydrogenation of aromatics, hydroaromatics and sulfur- and nitrogen-containing compounds and for the removal of S and N. However, this excessive sulfur slightly inhibited the activity of V sulfide for O removal.

Because coprocessing feed materials contain several percents of indigenous sulfur, the V indigenous to residuum may be converted to V sulfide *in situ* and show a catalytic activity for the aromatic hydrogenation and heteroatom removal reactions involved in coprocessing. However, because the activity of V sulfide can be inhibited by organic nitrogen components indigenous to the feed materials, V sulfide can be far less catalytic in coprocessing than that shown in the model hydrogenation reactions.

REFERENCES

1. Speight, J.G. "The Desulfurization of Heavy Oil and Residua"; Marcel Dekker: New York, 1981; Chapters 1 and 2.
2. Herbstman, S. U.S. Patent 4,125,455, 1978.
3. Gleim, W.K.T.; Lake, I.; Gatsis, J.G.; Plaines, D, III. U.S. Patents (a) 3,165,463, 1965, (b) 3,161,585, 1965, and (c) 3,252,895, 1966.
4. Hutchings, L.R.E. U.S.Patent 4,139,453, 1979.
5. Gatsis, J.G. U.S. Patent 3,915,842, 1975.
6. Kim, H; Curtis, C.W. Energy Fuels 1990, 4, 206-14.

Table 1. Comparison of the Hydrogenation Activity of <u>In Situ</u> Generated V Sulfide from VAcAc and VOAcAc and Mo sulfide from MoNaph in Model Systems[a]

Reactant	Hetero atom (X)	Major Products		% HYD[b]			% HDX[c]		
		V sulfide	Mo sulfide	V sulfide VAcAc	V sulfide VOAcAc	Mo sulfide MoNaph	V sulfide VAcAc	V sulfide VOAcAc	Mo sulfide MoNaph
Naphthalene	-	tetralin	tetralin	42.9±0.8	50.8±3.0	42.6±0.4	-	-	-
Tetralin	-	tetralin	tetralin	15.3±0.3	26.9±0.8	4.7±0.3	-	-	-
Indene	-	indan	indan	17.2±1.3	18.0±0.6	16.0±0.3	-	-	-
Indan	-	indan	indan	3.6	6.8±0.2	3.4±0.3	-	-	-
Benzothiophene	S	ethylbenzene	ethylbenzene	47.6±1.4	50.3±0.6	40.7±0.7	99.6±0.8	100.0±0.0	100.0±0.0
o-Cresol	O	methylcyclohexane	toluene	74.2±0.4	71.6±0.2	36.2±0.2	100.0±0.0	100.0±0.0	86.7±0.4
Benzofuran	O	ethylcyclohexane	ethylbenzene	67.4±0.6	69.1±0.2	46.3±0.7	92.4±0.8	98.6±0.1	79.3±2.1
Quinoline	N	1,2,3,4-THQ[d]	propylcyclohexane	51.9±1.8	54.9±0.1	90.6±1.5	31.0±2.4	36.2±0.3	89.7±2.2
Indole	N	o-ethylaniline	ethylcyclohexane	38.8±0.3	43.8±0.0	70.4±2.2	33.8±0.7	41.0±0.9	96.2±4.5

[a] The reactions were conducted at 380°C for 30 minutes with 3000 ppm metal loading in the presence of excess sulfur, three times the stoichiometric sulfur to form V_2S_3 and MoS_2 (0.034 g for V, 0.024 g for Mo). Most reactions were at least duplicated, and the amount of hydrogenation and heteroatom removal was summarized as the average value and standard deviation of $X \pm \sigma_n$.

[b] The most hydrogenated liquid products used in calculating % HYD were: decalin for naphthalene and tetralin, and cyclohexane for indan, indene, benzothiophene, benzofuran and o-cresol.

[c] % HDX: percent heteroatom removal of S, N and O.

[d] 1,2,3,4-Tetrahydroquinoline.

Table 2. Effect of Multiple Compounds on the V Sulfide-Catalyzed Hydrogenation of Naphthalene, Benzothiophene, o-Cresol and Benzofuran[a]

(A) Naphthalene

Additional Compound[b]	Naphthalene % HYD
None	50.8±3.0
Indan	43.5±1.2
Benzothiophene	50.1
Benzofuran	49.0±2.5
o-Cresol	48.8±3.9
Quinoline	5.7±0.6
Indole	9.1±0.1
Pyridine	14.4±1.6

(B) Benzothiophene

Additional Compound[b]	Benzothiophene % HYD	% HDS
None	50.3±0.6	100.0±0.0
Naphthalene	48.2	100.0
o-Cresol	46.7±0.5	100.0±0.0
Quinoline	19.8±0.5	32.3±1.4

(C) o-Cresol and Benzofuran

Additional Compound[b]	Reactant			
	o-Cresol		Benzofuran	
	% HYD	% HDO	% HYD	% HDO
None	71.6±0.2	100.0±0.0	69.1±0.2	98.6±0.1
Naphthalene	69.3±2.3	97.1±2.9	67.4±1.9	95.5±3.5
Benzothiophene	66.0±0.7	92.5±1.2	-	-
Benzofuran	72.7	100.0	-	-
o-Cresol	-	-	69.9	100.0
Quinoline	7.3±0.3	12.8±0.6	26.0±0.1	5.2±0.2

[a] Most of the reactions were performed two or three times with VOAcAc and 0.034 g S and the % HYD, % HDS and % HDO were expressed as an average value and a standard deviation in the form of $X \pm \sigma_n$. In calculating % HYD, the most hydrogenated liquid products determined were decalin for naphthalene and cyclohexane for benzothiophene, o-cresol and benzofuran.

[b] Each reactant except for naphthalene (2 wt%) was added at 1 wt% level in the hexadecane solution.

Table 3. Effect of Sulfur Amount on the Activity of *In Situ* Generated Vanadium Catalysts in Hydrogenation of Naphthalene

Product, mole %	Sulfur Amount[a]					
	0	1	2	3	5	10
VAcAc						
% HYD[b]	0.9	5.3±1.5	35.7±1.4	42.9±0.8	50.2±0.8	61.3
t-D/c-D Ratio[c]	-	-	-	1.09±0.08	1.14±0.03	1.37
VOAcAc						
% HYD[b]	0.7	21.2	40.4	50.8±3.0	57.3±1.1	NP[d]
t-D/c-D Ratio[c]	-	-	-	1.10±0.02	1.13±0.01	

[a] Multiples of the stoichiometric amount of sulfur required to form V_2S_3.
[b] % HYD calculated using decalin as the most hydrogenated liquid product.
[c] Approximate ratio of trans- to cis-decalin.
[d] NP: not performed.

Table 4. Effect of Sulfur Amount on the V Sulfide-Catalyzed Hydrogenation of Model Compounds[a]

Sulfur Amount[b]	Reactants[c]		
Naphthalene/Indan	Naphthalene % HYD	Indan % HYD	
3	43.5±1.2	3.0±0.5	
9	55.8±0.3	10.0±0.2	
Naphthalene/Benzothiophene	Naphthalene % HYD	Benzothiophene % HYD	% HDS
3	50.1	48.2	100.0
9	54.8±0.5	53.9±0.1	100.0±0.0
Naphthalene/o-Cresol	Naphthalene % HYD	o-Cresol % HYD	% HDO
3	48.8±3.9	69.3±2.3	97.1±2.9
9	52.4±3.2	63.7±2.5	89.7±2.9
Naphthalene/Indole	Naphthalene % HYD	Indole % HYD	% HDN
3	9.1±0.1	41.9±0.1	37.1±0.3
9	15.7±0.3	55.3±0.6	58.0±3.6

[a] Combined reactions of 2 wt% naphthalene and 1 wt% of other compounds were performed with VOAcAc.
[b] The sulfur amount was expressed as multiple times the sulfur required to form V_2S_3.
[c] In calculating % HYD, the most hydrogenated liquid products used were decalin for naphthalene and cyclohexane for the other reactants.

RETROGRESSIVE REACTIONS IN COAL/PETROLEUM CO-PROCESSING

Jasna Tomic and Harold H.Schobert
Fuel Science Program,
Department of Materials Science and Engineering,
The Pennsylvania State University,
University Park, PA 16802

Key words: co-processing, model compounds, retrogressive reactions

INTRODUCTION

Co-processing is the simultaneous reaction of coal and petroleum resids to produce distillable liquids. It can be viewed as a new approach to direct liquefaction where the petroleum resid takes the role of the traditional liquefaction solvent [1]. The co-processing system is somewhat more complex from a chemical standpoint because of the predominantly aromatic character of the coal and mainly aliphatic nature of the petroleum products. The variety of hydrocarbons present in such a system determine the chemical reactions. One of the major undesirable reaction products is coke (or semi-coke) which causes problems in the co-processing technology.The formation of coke diverts carbon into unwanted by-products, reducing yields of the more desired products, and can upset heat and mass transfer processes in the reactor.

The intention of this study is to examine the chemical interactions and process conditions that contribute to retrogressive reactions during co-processing. We studied only thermal reactions (that is, reactions without added catalyst) since the aim is to focus on the retrogressive reaction chemistry that takes place between the different organic components of the system, and not to optimize the system for maximum liquids yields. The main objectives of this project are : 1) to determine the groups of chemical components originating from the coal and the petroleum that are responsible for initiating coke formation; 2) to identify the optimum reaction conditions that decrease the amount of insoluble coke; and 3) to rank pairs of coal/petroleum feedstock that minimize the amount of coke formed during co-processing reactions.

EXPERIMENTAL

Five coal samples from the Penn State Coal Sample Bank were used in this project, ranging in rank from subbituminous B through high volatile A bituminous. Data on the elemental composition on these coals is given in Table 1. The selected coal samples were first reacted with five model compounds representative of petroleum resids: eicosane, 1-phenyldodecane, 1,4-diisopropylbenzene, durene, and pyrene. The model compounds were obtained from Aldrich and were used as received. These model compounds were chosen on basis of their aromaticity and H/C ratios, to provide a set of compounds having a reasonably wide range of both properties. Real co-processing reactions were conducted with three vacuum feed resids. Analyses of the petroleum feedstock are presented in Table 2. Two of the petroleum feedstock were obtained from Amoco Co. (West Texas FHC-470 and Blend FHC-571) and one from Unocal (Hondo).

All of the reactions were conducted in a 20ml stainless steel vertical tubing bomb (microautoclave) reactor. Each reaction was conducted with 2.5g of coal and 5g of model compound or resid. The coal was dried to a 1% moisture under vacuum and was stored under a nitrogen blanket. The starting pressure (cold) was 3.5MPa (500 psi) of nitrogen or hydrogen. The reaction temperatures were 350° C, 400° C, 450° C and the time was fixed at 30 min.

The contents of the reactor were rinsed with tetrahydrofuran (THF) and the products were separated to THF-solubles and THF-insolubles. The Soxhlet thimble containing the insoluble matter was then extracted under a nitrogen atmosphere for 24 h. Excess THF was removed by rotary evaporation and the solid residue was dried under vacuum for 12 h before weighting. The degree of

retrogressive reactions occuring was defined by the yield of tetrahydrofuran insolubles which was calculated on a percent basis dividing the weight of the THF-insolubles by the weight of the coal (daf).

In order to assess the influence and contribution of the model compounds to the formation of solid residue during these reactions, blank runs of the model compounds (in the absence of coal) were performed. Similarly coal was reacted alone under the same reaction conditions in order to obtain the information on the products resulting directly from the coal itself and baseline data for thermal stability of the resids was obtained.

Solid state ^{13}C NMR and Fourier transform (DRIFT) spectroscopy was performed on the unreacted coal. These spectra were used as a baseline to be later compared with the spectra obtained on the THF-insoluble residue in order to examine the structural changes occuring during the reactions. Some of the solid products were analyzed by elemental analysis in order to determine the H/C ratios which in a very crude way can give indications about the aromaticity.

RESULTS AND DISCUSSION

Some results from the reactions of the five coals with the five model compounds under nitrogen and hydrogen are presented in Table 3. The most obvious observation is that the yield of THF-insolubles is the lowest in the reactions with pyrene. Also the values obtained for reactions with coal/eicosane and coal/1-phenyldodecane are very close to each other, as well as are the ones for coal in reaction with 1,4-diisopropylbenzene and durene. This was also verified when the H/C atomic ratios of the solid residue were plotted as a function of reaction temperature. Figure 1 shows that coal reacts with eicosane and 1-phenyldodecane in a similar fashion and that coal also reacts similarly in the presence of 1,4-diisopropylbenzene and durene. Pyrene reacts in a way notably different than the other four model compounds.

Eicosane and 1-phenyldodecane have in common the long paraffin chain. Thermal cracking of eicosane will lead to the production of 1° radicals by C-C bond cleavage, as for example:

$$R - CH_2 - CH_2 - R \longrightarrow 2\ R - CH_2\ ^{\bullet}$$

A similar reaction path for alkylated benzene compounds (1-phenyldodecane) is supported by a collateral study in our laboratory [2] where it was shown that n-butylbenzene decomposes to:

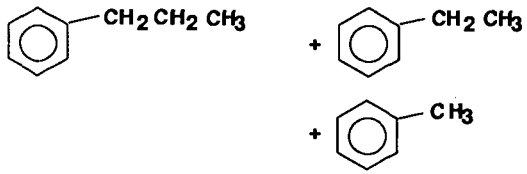

In other words, the alkylated benzene compound tends to crack at every possible position along the chain. This process also gives rise to primary radicals via:

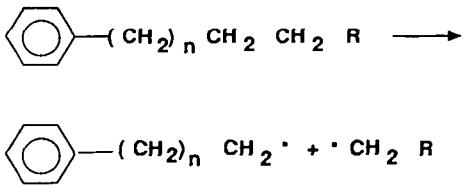

Therefore, 1-phenyldodecane will form similar radicals to eicosane because most probably the cracking of bonds will take place along the dodecyl chain.

On the other hand, cracking of durene and 1,4-diisopropylbenzene will lead to benzyl radicals like the one shown below:

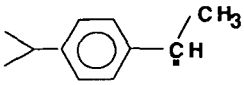

Pyrene, being a polyaromatic hydrocarbon, is very stable and does not easily form radicals by thermal cracking. In the literature pyrene has been described as a good "hydrogen shuttler" [3]. While transferring the hydrogen the pyrene most likely transforms to a hydroaromatic structure. Therefore, the similar chemistry of eicosane and 1-phenyldodecane arise from the fact that both crack to 1° radicals, and the similar behavior of durene and 1,4-diisopropylbenzene arises from the formation of the benzylic radicals from the two compounds. Pyrene would do neither. The expected thermal behavior of the 1° radical-forming compounds, benzylic radical-forming compounds, and pyrene is reflected both in the relative yields of THF-insolubles from a given coal and the variation of H/C ratio (Figure 1) as a function of temperature.

The reactions were performed under a nitrogen and hydrogen atmosphere. Under the given conditions of these experiments, namely 3.5MPa overpressure, the differences in degree of coal conversion calculated on basis of THF-insoluble are not significant. Comparisons of coal conversions under a nitrogen and hydrogen atmosphere at a given temperature are shown in Figure 3. Although it might be expected that the conversions would increase in the presence of hydrogen gas under the given reaction conditions the effect of the chemical nature of the coal and model compound (or petroleum resid) override the effects of the gas atmosphere. Furthermore, it should be recalled that these reactions are conducted without a hydrogenation catalyst being present.

Three temperatures of reaction were used in these experiments; 350°, 400°, and 450° C. Overall, the lowest yield of insoluble matter was recorded at 400° C. The lowest temperature is probably not enough for significant radical generation by fragmentation to take place while at 450° extensive cracking of the model compounds (and resids) takes place. In cases of severe cracking reactions it was not possible to maintain a good material balance. The effect of the reaction temperature is dependent on the rank of coal. For the two lower rank coals used , subbituminous B (PSOC 1488) and hvC bituminous (PSOC 1498) the coal conversion increases with increasing temperature of reaction. The three remaining project coals (hvB and hvA bituminous) achieve their highest conversion to THF-solubles at 400° C. Alternatively, it can be said that retrogressive reactions are at a minimum at 400° C. These optimum temperatures seem to coincide with the maximum fluidity temperatures of the coals. The three higher rank coals have temperatures of maximum fluidity above 400° C while the two lower rank coals do not pass through a fluid phase (with FSI's of 0 and 0.5). The temperature dependance of the coal conversion for the five project coals is shown on Figure 2.

Thermal stability tests on the petroleum resids (that is in the absence of coal) showed that considerable insoluble matter was formed only at the highest reaction temperature of 450° C. For West Texas FHC-470 the maximum insoluble is 17% of the total weight, for Blend FHC-571 the maximum is 3.73%, and for Hondo resid 5.77%.

The resids were reacted with the five project coals under the identical conditions as the model compound reactions. The yield of THF-insolubles was the lowest at 400° C. This agrees with the results reported by Moschopedis et al. [4]. When the temperature is increased to 450° C a drastic increase in solid residue is observed. This is attributed to extensive cracking taking place at higher reaction temperatures, with the high population of radicals thus increasing opportunities for retrogressive reactions. This observation is consistent with the results from the reactions with some of the model compounds, namely the ones containing the long side chains. When the coal conversion for the reactions with the model compounds and with the petroleum resids are compared (Figure 4), it is found that conversion in the presence of the resids is comparable to that achieved in the presence of pyrene. For reaction temperatures less than 450° C, the petroleum resids are as good a solvent for coal particles as pyrene. At higher reaction temperatures the interactions between the coal particles and petroleum resids seem to favour retrogressive reactions and the formation of insoluble matter.

CONCLUSIONS

The coal/model compound reactions showed that the reactivity of the vehicle is based on radical generation: eicosane-like, durene-like, and pyrene-like. The yield of THF-insolubles, therefore the degree of retrogressive reactions, is the lowest in the presence of pyrene. Coal/ resid co-processing reactions at 400°C give coal conversions comparable to those in the presence of pyrene. The optimum temperature for minimizing retrogressive reactions in co-processing reactions is around 400° C. In addition, the maximum fluidity temperature of the coal defines the optimum temperature for coal conversion under co-processing reaction conditions.

ACKNOWLEDGMENT

The authors are pleased to acknowledge the financial support for this research provided by the U.S.Department of Energy. We are also grateful for the assistance of Dr. O.P. Mahajan of Amoco Corporation and Dr. G.E. Dolbear of Unocal in obtaining the resid samples. We have also enjoyed useful discussions with; Drs. Bruce Utz and Karl Schroder of the Pittsburgh Energy Technology Center (DOE).

REFERENCES

[1] Curtis, C.W., and R.A. Winschel. in "Coal Liquefaction: A Research Needs Assessment Technical Background" DOE/ER-0400 UC-108, Final Report, Vol II, February 1989.

[2] Eser, S., C. Song, H.H. Schobert and, P.G. Hatcher. "Compositional Factors Affecting the Thermal Degradation of Jet Fuels", U.S.D.O.E. Report, No. 42-3462-TPR-Annual, 1990.

[3] Derbyshire, F.J. and, D.D. Whitehurst, *Fuel*, 60, p.655, 1981.

[4] Moschopedis, S.E., R.W. Hawkins, and J.G.Speight, *Fuel Processing Technology*, p.213, 1982.

Table 1. Analyses of Project Coals.

Coal (rank)	PSOC-1488 subB	PSOC-1498 hvCb	PSOC-1501 hvBb	PSOC-1504 hvAb	PSOC-1448 hvAb
%C (dmmf)	76.56	78.24	81.17	82.88	85.20
%H	5.27	5.50	5.32	5.86	6.12
%N	0.95	1.83	1.56	1.77	1.86
%O	17.22	14.43	11.95	9.49	6.81
FSI	0.0	0.5	2.0	5.5	8.0
max fluid.T,°C	n/a	n/a	421	433	438

Table 2. Analyses of Petroleum Feedstock.

	Hondo	W. Texas FHC-470	Blend FHC-571
Oils (wt.%)	43.9	39.4	21.4
Resins	40.2	59.1	62.8
Asphaltenes	15.9	0.5	14.8
%C	83.40	86.39	83.91
%H	11.80	11.23	10.26

Table 3. Yields of THF-insolubles for PSOC 1488 with model compounds at three different temperatures under hydrogen.

	Yield THF-insoluble, %		
	PSOC 1488 (350° C, H_2)	PSOC 1488 (400° C, H_2)	PSOC 1488 (450° C, H_2)
Eicosane	94.41	84.06	80.12
1-Phen	94.13	82.32	79.42
1,4-Diiso	95.90	81.77	81.68
Durene	96.07	85.01	84.30
Pyrene	83.25	73.47	74.24

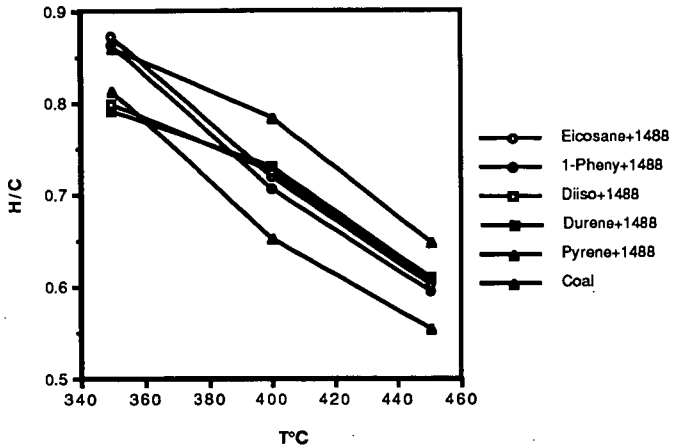

Figure 1: H/C atomic ratios of the THF-insolubles as a function of reaction temperature for different feed combinations for PSOC 1488

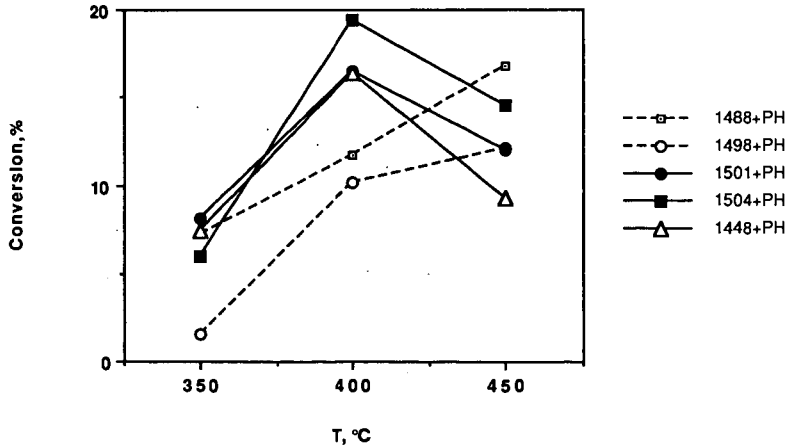

Figure 2: Temperature dependence of coal conversion for the five project coals.

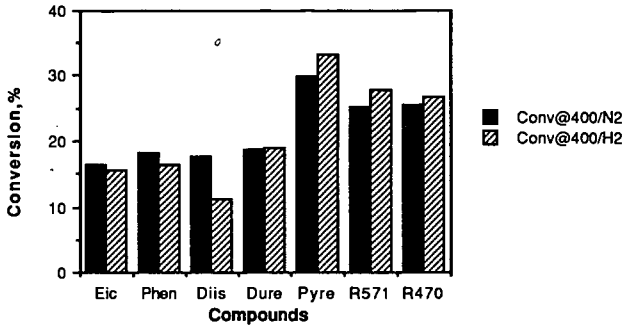

Figure 3: Conversion for PSOC 1501 at 400° C under N_2 and H_2.

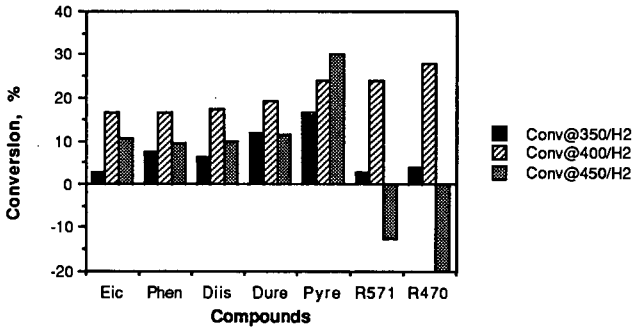

Figure 4: Conversion for PSOC 1448 at three reaction temperatures under H_2.

RETROGRESSIVE ARYL-ALKYL BOND FORMING REACTIONS FACILITATED BY REACTIONS OF SULFUR-CENTERED FREE RADICALS

Mikhail S. Alnajjar and James A. Franz

Pacific Northwest Laboratory
Battelle Memorial Institute
P. O. Box 999, Richland, WA 99352

Keywords: Sulfur, C-C Bond Cleavage, Rearrangements

INTRODUCTION

It is well known that additives such as elemental sulfur, pyritic minerals and thiols play a significant role in structural reorganization during the thermal degradation of coals.[1-4] Studies have shown that the rates for hydrogen atom transfer reactions between benzylic positions of model compounds and coals are increased significantly with higher sulfur content.[5,6] Displacement reactions of aromatic substituents by thiyl radicals and abstraction reactions by sulfur-centered radicals have long been recognized,[7-10] and are thought to be important in coal liquefaction. However, the mechanistic aspects of C-C and C-S bond formation and the rearrangement of organic structure in coal facilitated by thiyl radicals is less well understood.

Recently, we have demonstrated the importance of thiyl radicals in the enhancement of the cleavage of strong C-C bonds and in the formation of inert thiophene structures (eq. 1).[11,12] Products from the pyrolysis of bibenzyl in the presence of PhSSPh are shown in eq. 1. Diphenylmethane is formed in

$$PhCH_2CH_2Ph \xrightarrow{PhSSPh} PhCH_3 + Ph_2CH_2 + \text{2,3-diphenylbenzothiophene} + \text{other products} \quad (1)$$

a sequence of reactions involving the key step of phenyl migration from sulfur to the carbon-centered radical (eq. 2)[13]. Thus, at coal

$$PhCH(\cdot)SPh \xrightarrow{k_2} Ph_2CHS\cdot \longrightarrow \longrightarrow Ph_2CH_2 \quad (2)$$

liquefaction temperatures (450°C), reaction (2) proceeds very rapidly and the rate constant of the phenyl migration (k_2) approaches $1.5 \times 10^4\ s^{-1}$.[13]

In this paper, we present preliminary results of high-temperature reactions of elemental sulfur with diphenylmethane and triphenylmethane. These results demonstrate the complete reversibility of reaction (2) and provide direct evidence of thiyl radical participation in the cleavage of strong carbon-carbon bonds through a series of abstraction and migration reactions.

RESULTS AND DISCUSSION

Pyrolysis of diphenylmethane in the presence of excess elemental sulfur at 380 ± 3 °C gave toluene, thiophenol and triphenylmethane as the major products along with lesser amounts of $PhCH_2SPh$, PhSPh, PhSSPh and higher molecular weight products (Table I). The near unity ratio of toluene to thiophenol demonstrates the elementary free radical reactions in eqs. 3-10.

$$S_8 \xrightarrow{\Delta} \cdot SS_6S\cdot \longrightarrow SS\cdot \tag{3}$$

$$S_8 \longrightarrow \cdot SS_6S\cdot \tag{4}$$

$$Ph_2CH_2 + \cdot SS_6S\cdot \longrightarrow \underset{\underline{A}}{Ph_2CH(\cdot)} + HS_6SS\cdot \tag{5}$$

$$\underline{A} + S_8 \longrightarrow \longrightarrow \underset{\underline{B}}{Ph_2CHS(\cdot)} \tag{6}$$

DH (hydrogen donor)

$$\underline{B} \xrightarrow{\Delta} PhCH(\cdot)SPh \longrightarrow \underset{\underline{C}}{PhCH_2SPh} \tag{7}$$

$$\underline{C} \longrightarrow \underset{\underline{D}}{PhCH_2(\cdot)} + \underset{\underline{E}}{PhS(\cdot)} \tag{8}$$

$$\underline{D} + DH \longrightarrow PhCH_3 \tag{9}$$

$$\underline{E} + DH \longrightarrow PhSH \tag{10}$$

Triphenylmethane is formed via the termination reaction of diphenylmethyl and thiophenoxyl radicals followed by hydrogen atom abstraction and phenyl migration reactions (eqs. 11-13). The formation of

$$Ph_2CH(\cdot) + PhS(\cdot) \longrightarrow \underset{\underline{F}}{Ph_2CHSPh} \quad (11)$$

$$\underline{F} + RS(\cdot) \longrightarrow \underset{\underline{G}}{Ph_2C(\cdot)SPh} \quad (12)$$

$$\underline{G} \longrightarrow Ph_3CS(\cdot) \longrightarrow \longrightarrow \longrightarrow Ph_3CH \quad (13)$$

The minor products show the origin of termination, displacement, abstraction, and oxidation reactions.[12]

As noted in Table I (compare entries 4 and 2), triphenylmethane was more abundant at low sulfur concentration. Rapid phenyl migration in eq. 13 and the low concentration of thiol donors provide an explanation for the observed result.

Table II gives the product distributions of the pyrolysis reaction of triphenylmethane with elemental sulfur at 380°C ± 3. The formation of thiophenol and diphenylmethane is a consequence of phenyl migration from carbon to a sulfur-centered radical, eqs. 14-19. The production

$$Ph_3CH + \cdot SS_6S\cdot \longrightarrow \underset{\underline{H}}{Ph_3C(\cdot)} + \cdot SS_6SH \quad (14)$$

$$\underline{H} + S_8 \longrightarrow \longrightarrow \underset{\underline{I}}{Ph_3CS(\cdot)} \quad (15)$$

$$\underline{I} \longrightarrow \underset{\underline{J}}{Ph_2C(\cdot)SPh} \quad (16)$$

$$\underline{J} \longrightarrow \longrightarrow Ph_2CH(\cdot) + PhS(\cdot) \quad (17)$$

$$Ph_2CH(\cdot) \xrightarrow{DH} Ph_2CH_2 \quad (18)$$

$$PhS(\cdot) \xrightarrow{DH} PhSH \quad (19)$$

of toluene and diphenyldisulfide is the result of further reactions of diphenylmethane with sulfur and the termination of thiophenoxyl radical respectively. A similar interpretation explains the high yield of Ph_2CH_2 in the presence of low concentration of sulfur (Table II, entry 4). Rapid phenyl

migration, eq. 16, followed by abstraction and further reduction produced the desired product.

SUMMARY

These observations show that the cleavage of strong alkyl-aromatic carbon-carbon bonds can become completely reversible under the influence of thiyl radicals, via a rapid sequence of 1,2-phenyl migration, or neophyl-like rearrangements of thiyl radicals.[12,13]

EXPERIMENTAL

General. Diphenylmethane, triphenylmethane, and sulfur were purchased from the Aldrich Chemical Co. and used as received. Products were identified by gas chromatography by coinjection with authentic samples. Gas chromatography was carried out using a Hewlett-Packard Model 5890A equipped with an on-column injector and flame-ionization detection. Analyses were performed on a 25-m, 0.32 mm i.d. J&W Scientific DB-5 capillary column.

General procedure for Thermolysis Reactions. To a 0.01-0.05g of diphenylmethane or triphenylmethane was added an appropriate amount of sulfur. The mixture was mixed, freeze-thaw degassed in liquid nitrogen, and sealed under high vacuum. The tubes were introduced to a fluidized sand bath at 380°C $\pm$ 3 for intervals of 5 and 20 minutes, cooled immediately in tap water, open under nitrogen, and transferred to a degassed solution of CH_2Cl_2 containing naphthalene as an internal G.C. standard.

ACKNOWLEDGEMENT

This work was supported by the Office of Basic Energy Sciences, U. S. Department of Energy, under contract DE-AC06-76RLO 1830. Pacific Northwest Laboratory is operated for the U. S. Department of Energy by Battelle Memorial Institute.

REFERENCES

1) A. Attar, Fuel 1978, 57, 201.
2) R. F. Yarzab, P. H. Given, W. Spackman, and A. Davis, Fuel 1980, 59, 81.
3) H. H. King and L. M. Stock, Fuel 1980, 59, 447.

4) P. A. Montano, Y. C. Lee, A. YeYe-Odu, and C. H. Chien, "Iron Sulfide Catalysis in Coal Liquefaction" in Mineral Matter in Coal, Ed. K. Vorres, American Chemical Society Symposium, Series 301 (1986), 416.
5) C. B. Huang, and L. M. Stock, Prepr., Div. Fuel. Chem., Am. Chem. Soc. 1982, 27(3-4) 28.
6) J. A. Franz, and D. M. Camaioni, Fuel 1984, 63, 990.
7) C. Walling, "Free Radicals in Solution", Wiley-Interscience, New York, NY, 1957.
8) M. L. Poutsma, "Free Radicals", (Ed. Kochi, J.), Wiley, New York, NY, Vol. II, 1973.
9) H. B. Glass and D. E. Reid J. Am. Chem. Soc., 1929, 51, 3428.
10) S. Oae and S. Kawamura, Bull. Chem. Soc. Jap. 1963, 36, 163.
11) M. S. Alnajjar, and J. A. Franz, Am. Chem. Soc., Prepr., Div. Fuel. Chem., Am. Chem. Soc. 1986, 31, 287.
12. M. S. Alnajjar and J. A. Franz, Proceedings International Conference Coal Chemistry. Eds. J. A. Moulin, K. A. Nater, and H. A. J. Chermin, Elsevier Science Publisher, Amsterdam, The Netherlands, 1987, 273.
13. M. S. Alnajjar, J. A. Franz, Proceedings International Conference on Coal Science, Tokyo, 1990, Vol. I, p. 181.

Table I

Effect of Sulfur on Product Distributions from Diphenylmethane Thermolysis at 380 ± 3 °C.[a,b,c]

$[Ph_2CH_2]/[S]$[d]	Time (min)	$PhCH_3$[e] ($\times 10^{-3}$)	PhSH[e] ($\times 10^{-3}$)	Ph_3CH[e] ($\times 10^{-4}$)
0.55	5	0.86	0.68	1.32
0.55	20	1.42	1.40	1.80
0.22	20	0.82	1.10	0.80
10.0[f]	20	1.60	1.75	8.9

a) In the control experiment, the absence of sulfur, Ph_2CH_2 produced trace amounts of $PhCH_3$, $PhCH_2CH_2Ph$, Ph_3CH and tetraphenylethane under the reaction conditions. b) % Conversion of Ph_2CH_2 = 10-20%. c) $PhCH_2SPh$, PhSSPh, PhSPh and higher molecular weight materials were also produced in small amounts. d) Ratio of diphenylmethane to sulfur. e) In mmoles. f) $PhCH_2CH_2Ph$ and Stilbene were also produced.

Table II

Effect of Sulfur on Product Distributions from Triphenylmethane Thermolysis at 380 ± 3 °C.[a,b,c]

$[Ph_3CH]/[S]$[d]	Time (min)	$PhCH_3$[e] ($\times 10^{-4}$)	PhSH[e] ($\times 10^{-3}$)	Ph_2CH_2[e] ($\times 10^{-3}$)	PhSSPh[e] ($\times 10^{-3}$)
0.55	5	0.30	1.0	3.63	0.45
0.55	20	9.7	3.38	6.55	1.2
0.22	20	7.15	2.20	4.03	0.20
10.0	20	3.0	3.20	17.7	1.75

a) In a control experiment in the absence of sulfur, Ph_3CH produced no detectable products. b) % conversion of Ph_3CH = 10-20%. c) Higher molecular weight materials were also produced. d) Ratio of triphenylmethane to sulfur. e) In mmoles.

REACTION PATHWAYS DURING COPROCESSING. THE REACTION OF ILLINOIS NO. 6 COAL WITH LLOYDMINSTER RESID UNDER MILD CONDITIONS

Kadim Ceylan and Leon M. Stock*
Department of Chemistry
The University of Chicago
Chicago, Illinois 60637

Keywords: Coprocessing, Hydrogen Transfer

INTRODUCTION

Over the past few years a number of processes have been developed for the direct liquefaction of coal. Typically, these processes involve thermal degradation of the macromolecular structure of coal, and are followed by hydrogenation to stabilize the degraded material and to increase the hydrogen-to-carbon ratio of the distillable products. In conventional coal liquefaction, a hydrogenated coal derived solvent is used as a vehicle for the transfer of hydrogen to the coal components. Coprocessing of coal with petroleum resid is an alternative technology in which the petroleum resid replaces the donor solvent. Coprocessing of petroleum resid with coal is a bridge between coal liquefaction and hydrocracking that simultaneously upgrades coal and resid. Consequently, coprocessing may offer some special advantages.

It has been observed that a better understanding of the chemistry of coprocessing might yield improvements in the technology (1). Therefore, coprocessing has received recent attention and new effort has been directed to elucidate the reaction pathways (2-6). The coprocessing of Illinois No. 6 and Wyodak coals with Lloydminster and Hondo resid has been thoroughly investigated (7,8), and other studies have discussed the hydrogen atom exchange, hydrogen atom transfer, and carbon-carbon bond cleavage reactions that may occur during coprocessing (9-14).

It seemed appropriate to establish more securely the relationship between the basic work and the reaction pathways that are involved in coprocessing. Accordingly, we have studied the coprocessing reactions of Illinois No. 6 coal with Lloydminster resid under the same reaction conditions that were used to investigate the influence of these fossil materials on hydrogen atom transfer and carbon-carbon cleavage reactions.

EXPERIMENTAL

Materials and equipment. The coals, resids, and the reference catalyst were supplied by John G. Gatsis of the Allied Research Center.

Illinois No. 6 coal was prepared by the Kentucky Center for Energy Research (KCER) and used as received (Anal. %C, 68.60; %H, 4.51; %N, 1.39; %S, 3.04; %O, 9.65; %H_2O, 3.15; %Ash, 9.65). Wyodak Coal was obtained from the Pennsylvania State University program and was prepared by KCER, and was dried prior to use (Anal. %C, 63.01; %H, 4.50; %N, 0.90; %S, 1.08; %O, 16.73; %H_2O, 1.78; %Ash, 12.00). Lloydminster Resid (Anal. %C, 83.6; %H, 11.5; %S, 4.77) and Hondo Resid (Anal. %C, 82.3; %H, 10.3; %S, 6.08; %N, 1.24) were obtained by UOP Research Center and used as is. The catalyst was a UOP proprietary material. The other chemicals were available commercially and they were purified as necessary.

The reactions were carried out in a SBL-2 fluidized sand bath equipped with Techne TC-8D temperature control unit. Three types of reactors were used. The glass capillary reactors were 2.4 mm (i.d.) × 20 cm, the glass tubular reactors were 5 mm (i.d.) × 20 cm, and the stainless steel (SS) reactors had an internal volume of 4.5 ml.

Nuclear magnetic resonance spectroscopy for ^1H was performed with the University of Chicago 500 MHz system and ^2H analysis was performed with a Varian XL-400 system. Infrared spectra were recorded with a Nicolet 20 SX spectrometer.

Procedures. The procedures for coprocessing were closely parallel to the procedures that were used in the previous study (11). The total quantity of material in the reactors were approximately 75 mg for the glass capillary, 500 mg for the glass tubular reactors, and 1.2 g for the stainless steel reactors. A mixture of the fossil fuel material, in which the resid and coal were combined in a 2:1 ratio (maf basis), was placed into the reactor, and it was carefully sealed under an atmospheric pressure of argon or pressurized with argon or dideuterium. The starting cold argon or dideuterium gas pressure in the stainless steel reactors was approximately 500 psig. The reaction vessels were then immersed into the sand bath which had been preheated at 400 °C. The reactor was vigorously shaken during the reaction. At an appropriate time, the reactor was removed from the sand bath and cooled immediately by immersing it in water. The glass reactors were cut and the stainless steel reactors were carefully vented to the atmosphere and then opened. The reactor contents were extracted into tetrahydrofuran, filtered, and the residue was Soxhlet extracted with tetrahydrofuran. The soluble product was fractionated into asphaltenes (n-heptane insoluble), resins (n-hepane soluble, n-pentane insoluble), and oils (n-pentane soluble) by successive extractions with n-heptane and n-pentane, according to the procedure suggested by Speight and co-workers (15).

RESULTS AND DISCUSSION

Illinois No. 6 coal was coprocessed with Lloydminster resid. The earlier coprocessing work with these materials was carried out at 420 °C in 2 hrs with a high pressure of dihydrogen, 3000 psi (7,8). Under these conditions, Gatsis and his co-workers achieved very high conversions of the coals into tetrahydrofuran soluble products. We elected to examine the same fossil materials under much milder conditions so that the conversion of the coal would be less complete, and the influences of selected reaction parameters on the product yield and distribution could be investigated. Accordingly, the reaction temperature was decreased to 400 °C, and the reaction time was decreased to 1 hr. Dideuterium was used in some experiments, but at 500 psi. The results are summarized in Table I.

Coal conversion was the principal parameter that we used to evaluate the results. The conversion values were calculated on the basis of the transformation of the insoluble coal into tetrahydrofuran soluble materials. As expected, the conversions that are presented in Table I are considerably less than the conversions that were reported by Gatsis and co-workers (7,8).

The reaction time is an important variable. An increase in the reaction time for the coprocessing of Illinois No. 6 coal and Lloydminster resid from 60 to 90 min in an inert atmosphere increased the conversion from 44 to 54%. Similarly, an increase in the reaction time for the coprocessing of the same substances from 15 to 60 min in a dideuterium atmosphere increased the conversion from 28 to 52%. These findings are in accord with the results and conclusions of Gatsis and his co-workers who also pointed out that the incremental increase diminished after the first 60 min (7,8). The observations for Illinois No. 6 coal and Lloydminster resid indicate that the use of dideuterium increases the conversion from 44 to 52%, the use of a catalyst increases the conversion from 44 to 50% and the incorporation of both a catalyst and dideuterium increases the conversion to 53%. The oil yields are not impacted in the same way. The addition of the catalyst in the absence of dideuterium actually reduces the oil yield from 27 to 22%. Indeed, the highest oil yield was observed when the reaction was carried out with dideuterium but in the absence of the catalyst.

Additional experiments were carried out with Wyodak coal and Hondo resid. It was found that coprocessing of these fossil fuels without the catalyst at 400 °C for 1 hr produced the following reactivity patterns.

For Coal Conversion and Oil Yield

Wyodak Lloydminster > Wyodak Hondo > Illinois No. 6 Lloydminster > Illinois No. 6 Hondo

The order of reactivity for coprocessing without a catalyst is exactly inverse to the order of reactivity of the same pairs of fossil materials in the exchange of hydrogen atoms with tetralin-d_{12} under the same experimental conditions (11).

For Exchange of Hydrogen with Tetralin-d_{12} at 400 °C

Wyodak Lloydminster	<	Wyodak Hondo	<	Illinois No. 6 Lloydminster	<	Illinois No. 6 Hondo

The order of reactivity in the molybdenum-promoted coprocessing reaction is also essentially inverse to the reactivity pattern for exchange with tetralin-d_{12}.

Previous work with 1,3-diphenylpropane suggested that Illinois No. 6 coal was the most effective initiator as well as the most effective hydrogen atom donor among the four fossil materials and that Lloydminster resid was the least effective initiator as well as the least effective hydrogen atom donor. Although it is difficult to provide a comprehensive interpretation of the observations for the complex coprocessing system, it is relevant to consider the chemistry of the thermolytic reactions of the coals and resids. Success in coprocessing depends upon facile initiation reactions and the occurrence of uninterrupted chain propagation sequences that redistribute hydrogen atoms, fragment the large coal and resid molecules, and enhance the solubility through adduction. Parallel heteroatom removal reactions are also essential.

Free radical decomposition reactions of the coal macromolecule must proceed in order to initiate the free radical propagation reactions that are necessary to convert it and the resid into lower molecular weight fragments and eventually into n-pentane soluble products. The resids that we have examined are much less effective initiators than the coals. They are also less effective hydrogen atom donors than the coals. Indeed, the observations for the coprocessing of the resid with Illinois No. 6 coal, which is simultaneously the best initiator and best hydrogen donor, suggest that its donor properties interfere with its successful coprocessing because hydrogen donation terminates the essential chain reactions and simultaneously increases the aromatic character of the coal macromolecules. The observations also suggest that blends of coals and resids may offer opportunities for enhanced conversion.

Dihydrogen addition clearly plays a major role in the liquefaction of coals (15,16). Evidence concerning the utilization of dihydrogen in coprocessing is more limited, but Curtis and Cassel have reported that the addition of hydrogen atom donors to the reaction system decreases the dihydrogen gas consumption (5). Their observations also imply that the hydrogen donor capacity of the collection of the fossil materials in the liquid phase can interfere with the desirable addition of dihydrogen to the initially highly aromatic coal molecules. We examined selected spectroscopic properties of the reaction products to gain further perspective on the course of the reaction. Representative nuclear magnetic resonance spectra are shown in Figure 1. Dideuterium was used to probe the role of dihydrogen in the reaction. Although the influence of the gas on the conversion and oil yields was modest, the spectroscopic information clearly establish that deuterium atoms were incorporated into the products. Weak absorptions near 2100 cm^{-1} were observed in the infrared spectra of most products. Our preliminary results suggest that more deuterium is incorporated in the oil than in the other fractions, and the representative ^2H NMR spectra indicate that the deuterium is abundantly incorporated into aliphatic structural elements with resonances between 1 and 2 ppm. Lesser amounts of deuterium appear in benzylic and aromatic positions. We estimate that 0.1 to 0.2 mmol of dideuterium is incorporated per gram of the reactants in these reactions at 400 °C and 500 psi dideuterium. These results prompted further study of the distribution of dideuterium among the reactions products. The work is discussed in the next paper.

CONCLUSION

The experimental results strongly suggest that hydrogen transfer processes occur very rapidly among all the constituents, and that dideuterium is added to the reaction products in the presence and absence of the molybdenum catalyst. The reactivity pattern for the four fossil materials suggest that the

hydrogen atom transfer reactions have a significant influence on the course of the reaction. In particular, the hydrogen donor properties of Illinois No. 6 coal appear to interfere with its conversion.

Acknowledgement. We are indebted to the Office of Fossil Energy of the U. S. Department of Energy for their support of this investigation and to John Gatsis for his very able assistance in the preparation and characterization of the fossil fuels.

REFERENCES

1. Cugini, A. V.; Lett, R. G.; Wender, I. Energy Fuels 1989, 3, 120.
2. Curtis, C. W.; Chung, W. J. Energy Fuels 1989, 3, 148.
3. Fouda, S. A.; Kelly, J. F.; Rahimi, P. M. Energy Fuels 1989, 3, 154.
4. Ohuchi, T.; Steer, J.; Muehlenbachs, K.; Carson, D. Fuel Process Techn 1988, 15, 429.
5. Curtis, C. W.; Cassel, F. N. Energy Fuels 1988, 2, 1.
6. Miller, R. L.; Giacomelli, G. F.; McHugh, K. J.; Baldwin, R. M. Energy Fuels 1989, 3, 127.
7. Gatsis, J. G.; Nelson, B. J.; Lea, C. L.; Nafsis, D. A.; Humbach, M. J.; Davis, S. P. "Continuous Bench-Scale Single Stage Catalyzed Coprocessing", Contractor's Review Meeting, Pittsburgh, October 6-8, 1987.
8. Nafsis, D. A.; Humach, M. J.; Gatsis, J. G. "Coal Liquefaction, Co-Processing", Final Report, DOE/PC/70002-TE, 1988.
9. McMillan, D. F.; Malhotra, R.; Hum, G. P.; Chang, S. J. energy Fuels 1987, 1, 193.
10. Bockrath, B. C.; Schroeder, K. T.; Smith, M. R. Energy Fuels 1989, 3, 268.
11. Ceylan, K.; Stock, L.M. Fuel 1990, 69, 1386.
12. Stock, L. M. "Hydrogen Transfer Reactions" in "The Chemistry of Coal Conversion", Schlosberg, R., Ed., Plenum Publishing Co., 1985, Chapter 6.
13. King, H. H., Stock, L. M. Fuel 1984, 63, 810.
14. King, H. H.; Stock, L. M. Fuel 1982, 61, 257.
15. Speight, J. S.; Long, R. B.; Trowbridge, T. D. Fuel 1984, 63, 616.
16. Hayatsu, R. Unpublished research.

Table I. Coprocessing Reactions of Fossil Fuels[a]

Entry	Coal and Resid	Reactor	Gas	Cat,%[b]	conv wt%	soluble product composition asph	resin	oil
1	Illinois No. 6 + Lloydminster	tubular	Ar	-	44.2	28.7	9.7	61.6
2	Illinois No. 6 + Lloydminster	tubular	Ar	-	53.9	21.7	11.2	67.1[c]
3	Illinois No. 6 + Lloydminster	SS	D_2	-	27.8	27.6	12.1	60.1[d]
4	Illinois No. 6 + Lloydminster	SS	D_2	-	51.5	33.5	3.3	63.2
5	Illinois No. 6 + Lloydminster	SS	Ar	1%	50.0	50.0	7.0	43.1
6	Illinois No. 6 + Lloydminster	SS	D_2	1%	53.0	33.1	7.1	59.1
7	Illinois No. 6 + Lloydminster	capillary	Ar	-	40.8	22.0	-	78.0[e]

[a]The reactions were carried out at 400 °C for 1 hr. The coal conversion is based upon the quantity of insoluble residue. [b]The wt% catalyst concentration was calculated from 100 (molybdenum/coal (maf)). [c]This reaction was carried out for 90 min. [d]This reaction was carried out for 15 min. [e]The yield of n-heptane soluble material is reported.

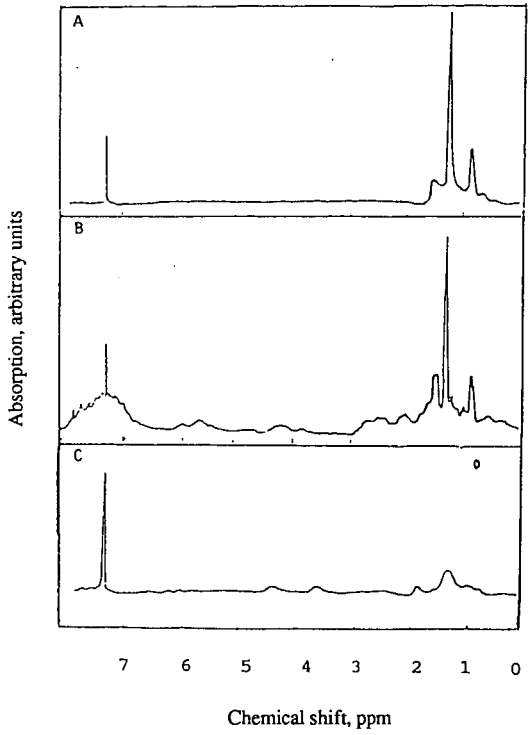

Figure 1. A. The ^{1}H NMR spectrum of the oil fraction of Lloydminster resid.
B. The ^{1}H NMR spectrum of the oil produced in experiment 4.
C. The ^{2}H NMR spectrum of the asphatene produced in experiment 4.

DETERMINATION OF DIDEUTERIUM UPTAKE IN COAL PETROLEUM RESID COPROCESSING

Michael D. Ettinger and Leon M. Stock
Department of Chemistry, University of Chicago, Chicago, Illinois 60637

John G. Gatsis, UOP Research Center, Des Plaines, Illinois 60017

Keywords: Coprocessing, NMR, Liquefaction

INTRODUCTION

Coal petroleum resid coprocessing is a novel application of direct coal liquefaction which has potential for practical applications. Several lines of argument suggest that a better understanding of the chemistry of the coprocessing reaction would lead to improvements in coprocessing technology. In order to gain insight into this problem, batch autoclave studies were carried out by using Illinois No. 6 coal with Lloydminster resid under a dideuterium atmosphere to study the deuterium incorporation in the products. Quantitative deuterium nuclear magnetic resonance methods were used to analyze the liquid products, and gas chromatography-mass spectrometry was used to analyze the gas products.

EXPERIMENTAL

Materials. The materials used were the same as those described in the accompanying article.

Coprocessing Reaction Procedure. Weighed amounts of Lloydminster resid and Illinois No. 6 in a two-to-one ratio (resid/MAF coal) and the catalyst (.02% wt) were added to an 1800 cc rocking autoclave. The autoclave was sealed and pressurized first with hydrogen sulfide and then with dihydrogen or dideuterium to give a 10 vol% hydrogen sulfide and 90 vol% dideuterium blend at 1470 psi. The autoclave was heated to 420 °C for a residence time of 2 hrs. At the reaction conditions, dideuterium was added automatically so that the desired reaction pressure (3000 psi at temperature) was maintained. After the desired time-at-temperature, the autoclave was cooled to room temperature, and then depressurized with the gas passing through a foam trap, caustic scrubbers, metering system, and then a sample was collected for analysis. To remove additional gas from the remaining reaction mixture, the material in the autoclave was stripped with dinitrogen.

This gas was also passed through the foam trap, caustic scrubber, metering system, and analyzed. Any slurry product in the foam trap was recovered with toluene and added to the toluene rinse solution. The slurry product from the autoclave was poured off. The material remaining in the autoclave was removed by rinsing the vessel with toluene until the autoclave was clean. The combined slurry product was solvent separated into four fractions according to the flow chart shown in Figure 1.

Deuterium spectra were obtained on a Varian XL 400 MHz spectrometer. One hundred to 200 scans were acquired using a 90° pulse and a 30-sec delay between pulses. Triphenylmethane-d_1 was used as a quantitative internal standard. Proton spectra were obtained similarly on the University of Chicago 500 MHz spectrometer by using tetrakis(trimethylsilyl)silane as a quantitative internal standard.

RESULTS

The autoclave reaction using a combination of Illinois No. 6 coal with Lloydminster resid mixed with a molybdenum based UOP proprietary catalyst was carried out at 420 °C for two hours under a dideuterium atmosphere at a constant pressure of 3000 psi. The results of the solvent separation of

the products are summarized in Table I. The oil, resin, asphaltene, and insoluble yields are based upon the starting amount of MAF coal and resid. As can be seen from Table I, approximately 23% of the starting material is unaccounted for. This portion represents the gas yield and the loss of a small amount of light material in the work-up procedure. The asphaltene conversion is calculated as the amount of asphaltene and unconverted coal (insolubles) in the autoclave product divided by the amount of starting MAF coal and asphaltene fraction of the starting resid. An asphaltene yield of 74% was obtained with Illinois No. 6 coal and Lloydminster resid. Coal conversion is calculated as the amount of starting MAF coal minus unconverted MAF coal (insolubles) divided by the starting amount of MAF coal. A coal conversion of 93% is obtained with Lloydminster resid and Illinois No. 6 coal. The elemental analysis of the oil, resin, asphaltene, and insoluble fractions are shown in Table II along with the fractional analyses of the starting resid. In all of the product fractions, the sulfur content significantly decreased even though hydrogen sulfide gas was present.

The deuterium incorporation into the different molecular fragments defines the paths of hydrogen transfer. In this first analysis of the results, the assignments are made according to the following chemical shift ranges. Deuterium resonances in the range of 6.3-10 ppm are assigned to aromatic deuterium atoms, while those found in the range of 4.2-0 ppm are assigned to aliphatic types. A further breakdown of the resonances in the ranges 4.2-2.0 ppm, 2.0-1.0 ppm, and 1.0-0 ppm was made by assigning resonances in those ranges to deuterium atoms alpha to aromatic rings, deuterium atoms beta to aromatic rings and in methylene and methine positions not alpha to aromatic rings, and deuterium atoms in methyl groups gamma or further from aromatic rings, respectively. Proton NMR characterization was also carried out to complement the results for deuterium. The proton NMR experiments use tetrakis(trimethylsilyl)silane as an internal standard. The NMR data from the coprocessing reaction products of Illinois No. 6 coal with Lloydminster resid are shown in Tables III and IV. In addition to the actual amount of deuterium incorporated into the products, Table III also shows the hydrogen content in each of the products. Thus, the percent deuteration of the aromatic and aliphatic regions was determined.

A relatively large amount of deuterium, 24.1 mmol g^{-1}, was incorporated into the aliphatic component of the oil. While the absolute amounts of deuterium uptake at the different structural positions vary from 2.9 mmol g^{-1} to 24.1 mmol g^{-1}, the relative percentages of deuteration are high and not quite so varied indicating that significant exchange had taken place at all positions. These percentages are close to the initial deuterium to total hydrogen ratio of (H/H+D) = 0.25 at the start of the reaction. Some selectivity of the catalyst was observed between the solvent separated fractions with the extent of deuteration decreasing in the order asphaltene > resin > oil. In addition, aliphatic positions were slightly preferred in the asphaltene and resin fractions while the smallest amount and smallest percentage of deuterium incorporation occurred at the aromatic sites in the oil fraction.

CONCLUSIONS

Analysis of the deuterium NMR results clearly shows that the level of deuterium atom incorporation was significant at all positions. All components of the system are undergoing hydrogen transfer chemistry, and there are plentiful opportunities for fragmentation and adduction reactions. The deuterium contents of the reaction products, (D/H+D), are only moderately different than the values expected for complete equilibration. The modest differences that do exist are compatible with the view that the weaker carbon-hydrogen bonds such as the alpha aliphatic group undergo reaction selectively even in the presence of the effective catalyst. The high deuterium incorporation at the other sites such as the methyl and methylene groups in paraffinic components, when coupled with the fact that the catalyst is essential for high conversions, suggests that the modest selectivity that is observed arises more from the differences in the way in which the organic molecules bind to the catalyst than to inherent differences in their thermal chemistry.

Acknowledgement. We are indebted to the Office of Fossil Energy of the U. S. Department of Energy for their support of this investigation.

Table I. Solvent Separation of Coprocessed Lloydminster Resid and Illinois No. 6 Coal with Dideuterium

Sample	Wt % MAF
Oil	62.32
Resin	3.91
Asphaltene	8.50
Insoluble	2.40
Coal Conversion	92.78
Asphaltene Conversion	74.08

Table II. Analysis of Original Resid Components and Solvent Separated Product

	Starting Material	Products
Oil fraction		
Wt.% MAF	73.50	62.32
Carbon, wt.%	82.86	84.88
Hydrogen, wt.%	10.82	13.67
Sulfur, wt.%	4.30	1.24
Resin fraction		
Wt.% MAF	10.41	3.91
Carbon, wt.%	82.68	86.16
Hydrogen, wt.%	8.76	8.66
Sulfur, wt %	7.44	1.73
Asphaltene fraction		
Wt.% MAF	16.09	8.50
Carbon, wt.%	82.82	87.70
Hydrogen, wt.%	8.51	7.09
Sulfur, wt.%	7.85	1.68
Insoluble fractions		
Wt.% MAF	-	2.40
Carbon, wt.%	-	24.03
Hydrogen, wt.%	-	1.71
Sulfur, wt.%	-	6.51

Table III. Hydrogen and Deuterium Content of Solvent Separated Coprocessing Products

	Hydrogen (mmol g^{-1})		Deuterium (mmol g^{-1})		% Deuteration	
	Aromatic (6.3-10 ppm)	Aliphatic (4.2-.5 ppm)	Aromatic (6.3-10 ppm)	Aliphatic (4.2-0 ppm)	Aromatic (6.3-10 ppm)	Aliphatic (4.2-0 ppm)
Oil	14.5	86.8	2.9	24.1	16.7	21.7
Resin	16.7	45.6	5.3	14.6	24.1	24.3
Asphaltene	14.5	31.7	5.0	11.9	25.6	27.3

Table IV. Aliphatic Deuterium Content in Solvent Separated Coprocessing Products

Solvent separated fraction	Alpha-D 2.0-4.2 ppm (mmol g^{-1})	Beta-D 1.0-2.0 ppm (mmol g^{-1})	Gamma-D 0.0-1.0 ppm (mmol g^{-1})	% Alpha deuteration
Oil	6.2	15.6	2.3	31.6
Resin	7.5	6.0	1.1	29.1
Asphaltene	5.9	4.8	1.2	29.4

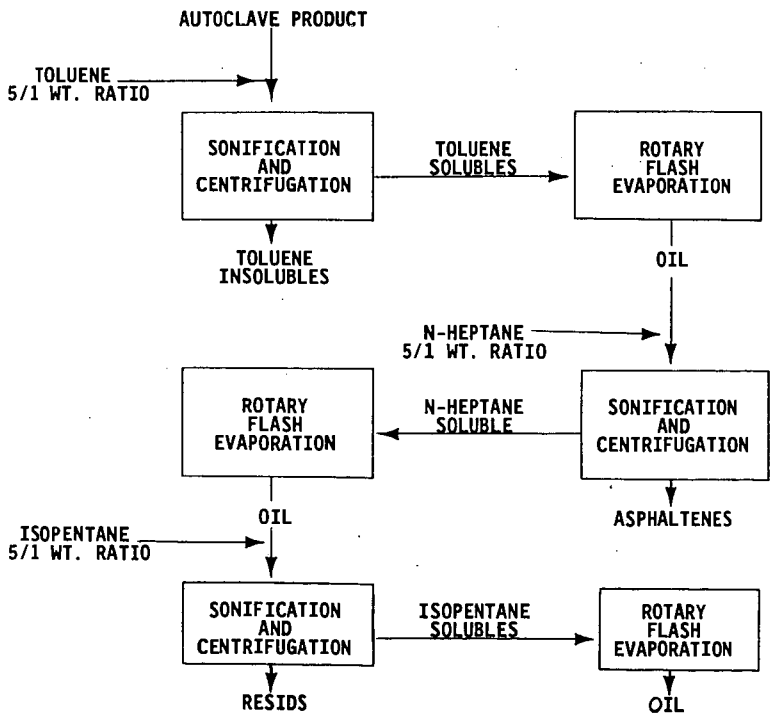

Figure 1. Solvent Separation of Coprocessing Product

A Complete Thermal Processing System for Fuels and Polymer Analysis

J.W. Washall, T.P. Wampler and W.A. Bowe,
Autoclave Engineers - Oxford/CDS Instruments 7000 Limestone Rd, Oxford, PA 19363

Thermal Characterization of fuel sources is essential in geochemical exploration. Determining the maturity of source rock and coal beds aids in the processing of these fuel sources. Quantitative assessment of the migratory hydrocarbons (P_1), kerogen (P_2) and fixed gases (P_3) provide vital information about the fuel generating capability of the sample.

Total thermal processing of samples, both geochemical and polymeric, can occur with temperatures up to 1400°C. The system used in this evaluation makes use of both furnace and filament pyrolysis. Samples analyzed included oil shales, polymers and composite materials.

Pyrolysis equipment in general is composed of three major components. First and foremost, a filament, wire or furnace in which the sample is deposited for pyrolysis. The second component is a heated chamber which prevents the pyrolysate from condensing and not reaching the injection port. The final component is a modification or add-on to the injection port of the gas chromatograph [1-3]. Egsgaard and Carlsen describe a low pressure continuous flow inletting system for Curie Point pyrolysis into a mass spectrometer [4]. In their work they describe three separate inletting systems depending on sample matrix: gas, liquid or solid. Many mass spectrometers, however, can accommodate direct insertion probes for pyrolysis in the source [5,6]. This technique, although valuable for many applications, tends to produce highly complex spectra because there is no chromatographic separation. Cold trapping prior to injecting the pyrolysate onto the GC will improve resolution, however, highly volatile components may tend to breakthrough and go undetected.

The impetus of his work was to provide an analytical system which would provide a full range of thermal processing capabilities, including dynamic headspace, furnace pyrolysis and filament pyrolysis. Previously, thermal treatment of samples involved Curie Point, furnace or filament pyrolysis. Each of these pyrolysis techniques has advantages and limitations.

The system in this study makes use of a programmable furnace pyrolyzer for temperatures up to 600°C and a filament pyrolyzer capable of reaching temperatures up to 1400°C. A major benefit of this system is the programmable furnace in combination with a series of adsorbent traps which enable fractions to be collected prior to chromatographic analysis.

All heated zones in the system are controlled via the systems computer terminal which can accommodate 20 separate methods. As the sample is heated, sample flow passes over the sample and sweeps the volatiles through an adjustable split valve. Part of the sample then moves to a monitor flame ionization detector (FID), the rest of the sample is carried to an absorbent trap. At that point a second temperature fraction can be collected in the same manner. A molecular sieve trap can also collect any fixed gases which may be evolved from the sample. These gases are then analyzed by a self contained packed column GC with a thermal conductivity detector. This is the first analytical system to employ furnace pyrolysis, filament pyrolysis and trapping capabilities. Heating rate capabilities range form 0.01°C/minute to a maximum rate to 20,000°C/second.

Experimental Section

The system described in this paper makes use of existing elements of analytical instrumentation in a unique combination. A CDS Instruments Model 920 Thermal Processing System was used in these experiments. Dynamic headspace/purge and trap, furnace pyrolysis and filament pyrolysis can all be performed during a single experiment.

The thermal processing unit consists of a thermal desorption/furnace pyrolysis chamber mounted on the side of the instrument. For dynamic headspace and/or furnace pyrolysis the chamber has a maximum temperature of 600°C. The heating rate of the furnace is up to 60°C/minute. If higher temperatures or heating rates are required, the Pyroprobe 2000 can be used to heat the sample to a maximum temperature to 1400°C at rates from 0.01°C/minute to 20,000°C/second. As the sample is heated, carrier flow directs the volatiles to the three on-line traps. These traps contain Tenax TA to retain organic fractions or molecular sieve 5A for trapping fixed gases.

Figure 1 shows a flow diagram for this system, which contains three traps, a monitor FID, packed column GC with a TCD and a capillary column GC with an FID. In terms of geochemical analysis, the furnace heats the sample to 300°C, while the migratory hydrocarbons are trapped onto trap A. At the same time part of this fraction goes on to a monitor FID to determine the total P_1 concentration. The sample is then heated to 600°C. The cracked kerogen passes to a split valve where part of the sample is collected onto trap B and the remainder passes on to the monitor FID for P_2 evaluation. After collection of the fixed gases on the molecular sieve trap, the fixed gases are analyzed with a packed column GC and a thermal conductivity detector. After this, the trap containing the migratory hydrocarbons (P_1) is backflushed through a heated transfer line to a capillary GC with a 50M X 0.25mm SE-54 capillary column. After this analysis, trap B containing the cracked kerogen components is backflushed and analyzed by the capillary GC.

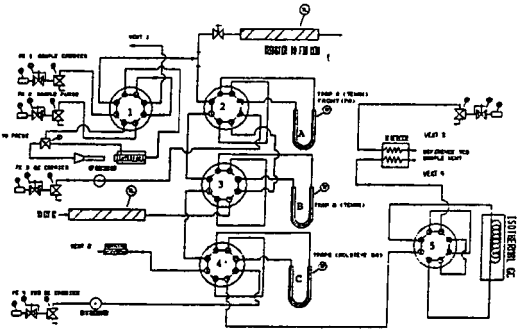

Figure 1: Flow schematic of thermal processing system.

Due to the flexibility and programming capability of this system, any number of thermal treatments can be performed depending on analytical needs.

Results

Two geochemical samples were compared in this study. The first sample was an Alaskan oil shale, the second sample was from the Green River. The samples were heated to 300°C and then to 600°C using the furnace pyrolyzer. Figure 2 shows the monitor FID composite results of the Alaskan oil shale sample along with the temperature profile. The P_1 composite fraction elutes at approximately 138°C and P_2 elutes at a sample temperature of 530°C. The area ratio of P_1/P_2 was measured to be 0.084.

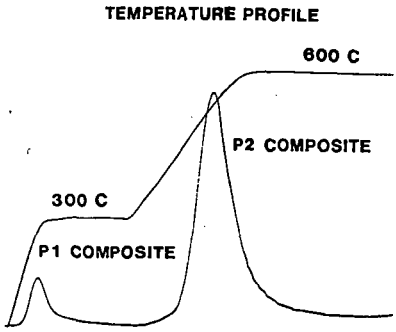

Figure 2: Temperature profile, P_1 and P_2 fractions of an Alaskan oil shale.

Figures 3 and 4 respectively, show the capillary column chromatograms of these two fractions. The P_1 fraction shows the migratory hydrocarbons from pentane to tetradecane. The larger fraction, P_2 displays the cracked kerogen geopolymer. Compounds generated by thermal treatment up to 600°C produces hydrocarbons up to C_{30}.

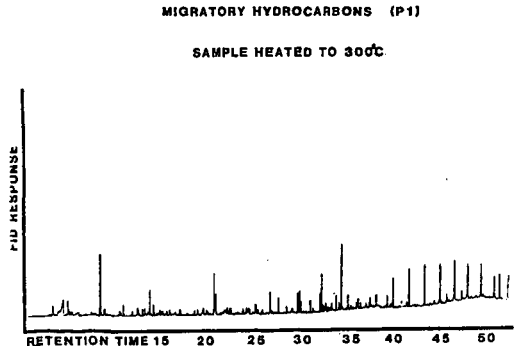

Figure 3: Alaskan oil shale heated to 300 C.

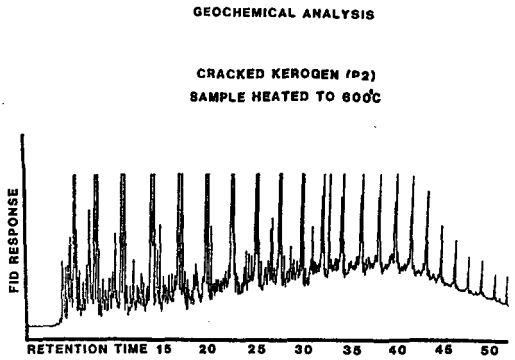

Figure 4: Alaskan oil shale heated to 600 C.

A second application of this instrument is in the field of synthetic polymer analysis. Residual solvent analysis, polymer identification and structural determinations are all possibilities. Figure 5 displays a 10 mg. sample of polystyrene which was heated to 300°C. The chromatogram shows primarily solvents used in the processing of this polymer and especially residual styrene monomer.

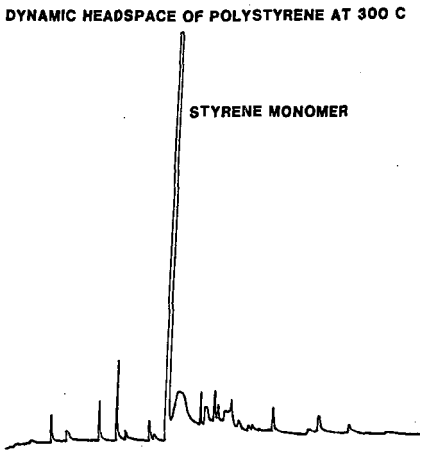

Figure 5: Polystyrene heated to 300 C for 10 minutes.

After residual solvent analysis, a portion of the residue (approximately 500 micrograms) was pyrolyzed at 750°C for 10 seconds. Figure 6 shows the results of this procedure. Styrene monomer, dimer and trimer are all products of this thermal treatment.

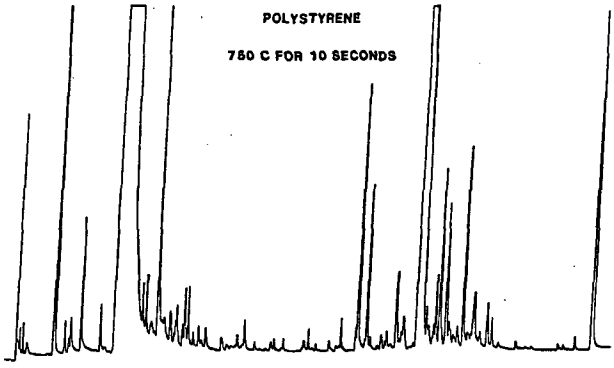

Figure 6: Pyrolysis/GC analysis of polystyrene at 750 C.

Finally, the most complex type of analysis involves composite materials which contain many components of varying volatilities. Cosmetics are a group of materials which fit ideally into this category. Mascara samples frequently contain solvents, pigments, polymers and inorganics which can hinder the analysis. A mascara sample was heated to 300°C and then pyrolyzed at 700°C for 10 seconds. The solvent analysis of the mascara sample is shown in figure 7. This chromatogram reveals solvents and the black pigments used in this commercial product. Subsequent pyrolysis of the residue, figure 8, shows the presence of an acrylate polymer which was identified as polymethylmethacrylate.

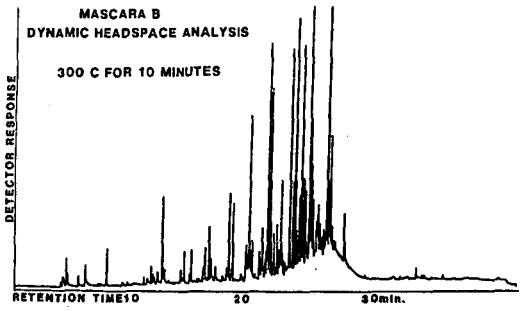

Figure 7: Dynamic headspace of mascara at 300 C.

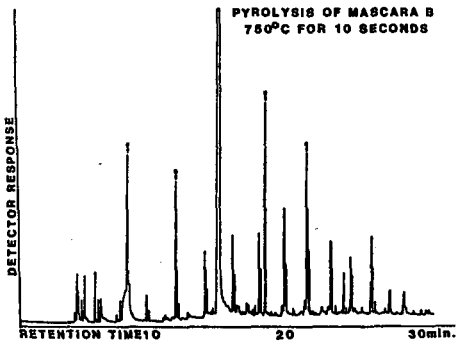

Figure 8: Pyrolysis/GC analysis of mascara residue.

Conclusions

The analytical system described in this paper proves to be versatile instrument for the thermal processing of a diverse range of samples. Due to the trapping capabilities of the system, several temperature dependent fractions can be collected an subsequently analyzed by GC, GC/MS or GC/FT-IR.

References

(1) Hickman, D.S.; Jane, I., Analyst, 1979, 104, 334

(2) Ohtani, H.; Nagaya, T.; Sugimura, Y, Tsuge, S. J. Anal. Appl. Pyrol., 1982, 4, 117.

(3) Washall, J.W.; Wampler, T.P. J. Chromatogr. Sci. 1989, 27, 144.

(4) Egsgaard, H.; Carlsen, L. J. Anal. Appl. Pyrol. 1984, 7, 1.

(5) Westall, W.A.; Ridduck, A.J. J. Anal. Appl. Pyrol. 1987, 11, 3.

(6) Montaudo, G. J. Anal. Appl. Pyrol. 1988, 13, 1.

(7) Whiton, A.S.; Morgan, S.L. Anal. Chem. 1985, 57, 778.

Thermal Degradation of Polyarylethersulfones
1. Review of Underlying Chemistry

C. Libanati, C. LaMarca, M. T. Klein*, S. M. Andrews[1], and R. J. Cotter[1]

Center for Catalytic Science and Technology
Department of Chemical Engineering
University of Delaware
Newark, DE 19716

KEYWORDS: polymer, pyrolysis, mechanisms.

The development of composite materials and the appearance of new applications in the aerospace and automotive industries have revived interest in high performance organic polymers, identified as possible matrices for fiber/polymers composites. Polyarylethers, which were some of the first commercialized plastics, are among the polymers being considered. They form a class of polymers that are tough, have a high softening temperature and maintain their mechanical properties for extended periods of time at temperatures over 150°C [1,2,3].

Sulfone-containing polyarylethers generally include one or more aromatic rings linked together by ether and sulfone groups. One class of these polymers also contains isopropylidene linkages. The nature and proportions of the different linkages determine the physical properties of each polymer. Herein we focus attention on polymers with phenyl ether (Ph-O-Ph) and phenyl sulfone (Ph-SO_2-Ph) bonds; we will consider polymers containing the propylidene linkage in a follow-up paper.

The thermoplastic behavior of polyarylethersulfones makes them very attractive for injection molding, forming, pultrusion and other manufacturing techniques in which the raw material is softened by heating in order to be processed. Due to their high softening temperature (glass transition temperature > 195°C), these polymers require processing temperatures of 350 to 400°C. At these temperatures, the chemical bonds within the macromolecules are thermally labile, which can lead to changes in the structure of the polymer. Structural changes can also occur when the polymers are maintained at high operational temperatures (150 to 200°C) for an extended period of time.

The foregoing manufacturing and operational issues have motivated studies of the thermal behavior of the polyarylethersulfones since the early stages of development, and elucidation of the mechanism of degradation has been pursued. The literature in this area is largely experimental and suggests that the thermal decomposition chemistry can cause topological changes leading to altered polymer properties, such as the formation of a gel from a linear polymer. This literature motivated the present work aimed at the development of a molecular model of polymer reaction and diffusion using our recently formulated Monte Carlo approach to the simulation of the reaction of macromolecules.

Most of the experimental work on thermal and radiolytic stability has recently been reviewed by Verma [1]. As is evident in the literature, there is no objective measure of the thermal stability of polyarylethersulfones. If the maximum decomposition temperature is the important parameter, polymers align in the order of increasing stability in one way [5,6,7]. On the other hand, if gel formation is to be avoided (e.g. during injection molding), then stability is ordered in another way [6]. Thus, thermal or radiative stability must be considered in relation to one or more of the polymer's properties when exposed to heat or radiation.

The properties of interest are directly linked to the applications for which the polymers are intended. Polymers may have good stability for certain applications while performing poorly in others. For example, a polymer with a high degradation temperature may exhibit rapid gel formation at processing temperature. The following have been used as a measure of thermal stability: lowest degradation temperature and weight percent loss in vacuum or in air obtained from TGA analysis [5,6,7;10,11,16,17], gel and gas formation [6,7,8,10,11,12,13,18], intrinsic and limiting viscosity of the sol fraction [8,9,10,18,12,13,15], modulus [9], tensile flexural strength [9,13,15] and molecular weight distribution of sol fraction [14,20,21]. Some properties studied in the literature have no direct link to properties necessary for use or manufacturing, but provide clues towards the determination of the underlying phenomena. They include optical density [19], infrared and nmr spectra [6,10,17,18,20] and bond scission and crosslinking rates [8,9].

---

[1] Amoco Performance Products, Inc., Research & Development Center, 4500 McGinnis Ferry Rd., Alpharetta, GA 30202-3944.

The behavior of the polymer depends not only on its chemical composition but on the physical structure as well. Only one recent publication by Nakron and coworkers [19] addresses the influence of initial molecular weight distributions on the thermal reaction of polyarylethersulfones. They show marked differences in the optical densities and oxygen uptake in the degradation of different molecular weight fractions of the chemically identical polyarylethersulfones. Also, Brown et al. [13] have shown large differences in the gel formation during radiolitic degradation of polyarylethersulfones when the reaction temperature is above and below the glass transition temperature.

This explicit relationship between reactivity and structure has prompted the development of the present molecular model of polymer degradation. This model, which incorporates fundamental information concerning the reaction of the polymers' reactive moieties and mobility of the polymer segment, explicitly links the structure of the system to its reactivity and reaction path. The model consists of a Monte Carlo simulation, within a percolation grid, of reaction and segmental mobility of polymer chains.

The framework for this model is the underlying basic chemistry on which it rests. We present the development of the model in two parts. Part 1, the present manuscript, delineates the controlling elementary steps of pyrolysis. These are assembled into a prediction of the reactivity of a model polysulfone in Part 2, when the mechanics of the Monte Carlo simulation of structure, reaction, and diffusion are presented.

Thus our present focus is on basic chemistry. What follows is a result of a thorough review of not only the polyarylethersulfone literature but also the physical and organic chemistry literature of the reactions of polyarylethersulfone-related moieties. Our objective was to discern reaction pathways and kinetics parameters. The former would provide Monte Carlo allowable "transitions" while the latter would provide transition probabilities.

THE THERMAL CHEMISTRY OF POLYETHERSULFONE SYSTEMS

The thermal degradation of polyarylethersulfones was postulated in the original study by Hale et al.[7] to be free radical in nature. This has been probed since in numerous thermal and radiative degradation studies with different formulations of related polyarylethersulfones [4,6,8,10,21]. An important publication by Lyons et al. [22] on the radiative effects on polyarylethersulfones and related model compounds confirmed such an assumption by identifying the presence of several free radicals during ESR monitoring of the reaction.

Although they formulated the main hypothesis behind the degradation process, namely that the "weaker" link breaks and generates radicals, Hale et al. [7] did not account for crosslinking reactions. Their study reports thermal gravimetric experiments that mask the extent of the structural changes occurring in the melt. Their proposed mechanism includes only bond breaking through initiation and bond forming through termination.

Davis [8] was the first to obtain explicit evidence of crosslinking reactions by measuring the gel fraction in the reaction products as a function of time. The experimental curve was similar to the gelation results obtained during copolymerization of polyfunctional monomers [44]. He concluded that crosslinking must occur by addition of polymer radicals to other polymer chains, but did not advance a mechanism for such a process.

A mechanism for crosslinking, involving cyclohexadienyl-type radicals observed by Lyons et al. [22], was later proposed by Danilina et al. [6]. It involves the addition of phenyl radicals, produced by initiation, to the benzene rings in the polymer chains, followed by elimination of hydrogen atoms. More recent publications by Narkon et al. [18] and Kuroda et al. [21] calculate crosslinking and bond scission rates from experimental results, using the Charlesby method for the former and their own novel method for the latter. Their calculations, however, do not take into account the nature of the crosslinking process and only schematic mechanisms of reaction are presented.

It is clear from the literature that structurally significant reactions involved in the radical chains include not only initiation and termination reactions, but also addition steps that can lead to crosslinking. Herein, we reduce the enormous complexity of these types of reactions via their organization into reaction families. Reactions involving radicals are classified into three main groups :

- Initiation reactions, which create radicals from stable molecules;
- Propagation reactions, in which the number of radicals is conserved;
- Termination reactions, which consume radicals.

INITIATION REACTIONS

Hale [7] first proposed that the scission of the "weaker" bonds were responsible for the generation of radicals. Bond dissociation energies identify the carbon-sulfur bond (66 kcal/mole) in the sulfone group.

Although the nature of the initiation has been widely accepted, the mechanism remains a subject of discussion. The dominant view, proposed by Hale et al. [7], consist of a two step initiation mechanism, where the carbon-sulfur bond breaks to produce a phenyl radical and a sulfonyl radical. The Ph-SO_2• radical can further decompose to Ph• and SO_2 or react with other molecules. This view is shared by Lyons et al. in their radiation damage studied, but no conclusive evidence has been provided in the literature [22].

Ayscough [23] proposed a concerted mechanism in which simultaneous cleavage of adjacent carbon-sulfur bonds occurs.

The fission to Ph• and Ph-SO_2• described above occurs with $\log_{10}A_1$ (s^{-1}) = 15 and an activation energy equal to the dissociation energy of the carbon-sulfur bond, E_1 = 65 kcal/Mole. For reaction of Ph-SO_2• to Ph• and SO_2, $\log_{10}A_2$ (s^{-1}) = 15 and E_2= 45 kcal/Mole is equal to the enthalpy of reaction, for the unimolecular decomposition†.

The phenyl radicals produced in the initiation steps can either terminate or react with other molecules generating new radicals, which propagate a pseudo kinetic chain. The list of possible radicals participating in radical-molecule reactions is limited to H• , Ph•, R-O•, R-SO_2•, Cyclohexadienyl radicals, cyclohexenyl radicals and cyclohexyl radicals.

PROPAGATION REACTIONS

Three types of propagation reactions are present in the degradation mechanism: Addition of a radical to benzene rings and double bonds; elimination or β-scission; and hydrogen abstraction by a radical from a stable molecule. We consider each in turn.

Addition Reactions

The work of Danilina et al. [6] suggest that addition reactions to the polymer's benzene ring is the vehicle for crosslinking. Radicals can add to a substituted benzene ring to yield a substituted cyclohexadienyl radical.

These reactions are very fast when the attacking radical is a phenyl radical [24,27,29,30,31,32,34,35,36,39] or a hydrogen atom [25,26,28,37,38]. In the case of phenyl radicals, at 450°C the addition to a benzene ring is 40 times faster that abstraction of hydrogen by the radical from benzene.

Rate constants for addition of hydrogen atoms and phenyl radicals to substituted benzenes have been reported in the synthetic organic chemistry literature[24–39]. Jansen [27] provides a value of 7.8×10^4 M^{-1} s^{-1} for the rate constant of addition of phenyl radicals to benzene. Pryor [25] estimated the rate constant for addition of hydrogen to benzene at 10^9 M^{-1} s-1 at 35°C. The activation energy for the latter reaction is known to be 3.8 kcal/mole [24,26,37], which implies a $\log_{10}A$ (M^{-1} s^{-1}) = 11.7. Modelling the transition state for the addition of phenyl radicals provides an estimate of $\log_{10}A$(M^{-1} s^{-1}) = 7.7. Combined with the reported rate constant, the activation energy is calculated at E*= 3.83 kcal/moles. This value is very close to the hydrogen value and is consistent with the energetics of the reaction; the estimated enthalpy of reaction for hydrogen and phenyl additions are essentially equal at ΔH_R^o = -24.9 kcal/moles and 25.1 kcal/mole respectively [25,26].

For all other radicals, the rate constant for addition, in its Arrhenius form, has been estimated from an Evans-Polanyi relationship relating activation energies to heats of reaction. The Evans-Polanyi relationship was used to estimate activation energies ($E^* = E^*_0 + \alpha\, \Delta H_R^o$ for exothermic reactions and $E^* = E^*_0 + (1-\alpha)\, \Delta H_R^o$ for endothermic reactions).

ΔH_R^o is the enthalpy of reaction, E^*_0 = 16.3 kcal M^{-1} , and α = 0.56. ΔH_R is calculated from the heat of formation of reactant and products determined from literature information or group additivity [41]. Estimated heats of formation are summarized in Table 1. The parameters E^*_0 and α were determined from the values of the activation energies for the addition of phenyl radicals and the addition of cyclohexadienyl radicals [27,42]. This procedure is described in detail elsewhere.

The pre-exponential factors are assumed to be 5×10^7 M^{-1} s^{-1}, equal to the one for phenyl radical addition.

The rate constant for addition can also be affected by electronic effects due to the presence of substituents on the reactant molecules. This is particularly true for addition at different positions in substituted benzenes. According to the extensive literature on radical addition to substituted benzene rings [25–39], neutral radicals, such as phenyl radicals, preferentially add to the benzene ring at non-substituted positions. The reasons for such behavior are unclear. A possible ex-

† The heat of formation of the sulfonyl radical was calculated from the heat of formation of diphenyl sulfone, ΔH_f = -30.98 Kcal/Mole, and the bond dissociation energy of the C-S bond. Substituent effects, generated by the ether linkages at the para position to the sulfone linkage, have been neglected here.

planation is that for large radicals, the substituent may present an important steric hindrance to ipso-substitution reactions. Because of their size, small hydrogen atoms are assumed to be an exception and are allowed in our reaction scheme to substitute at occupied positions on a benzene ring. For any of the electro-neutral radicals that participate in the reaction mechanism, including the hydrogen atom, the preferred position for addition is ortho to a substituent, followed by the para position and, finally, the usually much less reactive meta position [24,29]. The relative selectivity toward each position is influenced by the electronic characteristics (electron donating or electron withdrawing) of the substituent and the attacking radical [24,29,31].

As an example, the rate constant for addition of a phenyl radical at an ortho position from an NO_2 group is 9 times greater than the rate of addition of the same radical on an unsubstituted benzene [24]. Values of the estimated relative activation energy and rate constant for addition of phenyl radicals, at 425°C, at every position of a substituted benzene to the rate constant of addition to any position in an unsubstituted benzene are summarized in Table 2 for all the possible substituents in the polymer systems considered in this work. Similar studies with other radicals show qualitatively the same results, for electro-neutral radicals [24,29,39]. Quantitatively, the values reported show a stronger influence of the substituents present on the neutral molecule rather than of the nature of the attacking radical. Consequently, the ratios reported in Table 2 are assumed to be the same for all other radicals present during polysulfone degradation.

An analogous reaction is the addition of radicals to the double bonds of cyclohexadiene and cyclohexene, which are not present in the original polymer but can be formed during reaction. Additions to double bonds are similar in nature to the addition to benzenes and consequently the same Evans-Polanyi relation was used to estimate activation energies.

Elimination Reactions.

The reverse reaction to additions are eliminations reactions. They are β-scission reactions in which hydrogen or a substituent are eliminated. The pre-exponential factors for these reactions were estimated at $5x10^{13}$ when hydrogen is eliminated and $5x10^{12}$ for elimination of a bulkier substituent. The activation energy, E^*_β, can be calculated from E^*_A, the activation energy of the reverse addition reaction (from section IV.2.2.1), and the heat of reaction ΔH_R, $E^*_\beta = E^*_A - \Delta H_R$, already determined from Table 1.

Hydrogen Abstraction

The last family of radical-molecule reactions is hydrogen abstraction from a stable molecule by any of the radicals. There is very little easily extractable hydrogen in the initial polymer. When the benzyl hydrogen is the one exchanged in this reaction, the rate for the fastest abstraction (by phenyl radicals or H•) is already several orders of magnitude slower then that for addition to the benzene ring. The only easily abstractable hydrogen in the initial polyethersulfone systems is the phenoxy-H. As the reaction progresses, however, more-saturated cyclohexadienes, cyclohexenes and cyclohexene, as well as a higher number of hydroxy and possible $-SO_2H$ groups form and bring an extra source of abstractable hydrogen.

The pre-exponential factor for these reactions was estimated from modelling the transition state at 10^{10} M^{-1} s^{-1} when R• = H• and 10^8 $M^{-1}s^{-1}$ otherwise. It is comparable with literature values [43]. The activation energy was calculated using the Evans-Polanyi relation.

In this case, $\Delta H_R = d^o_{R-H} - d^o_{R'-H}$. The bond energies d^o_{R-H} and $d^o_{R'-H}$ were found in the literature [(56)] or estimated from group contribution methods. They are summarized in Table 3.

TERMINATION REACTIONS

Radical-radical reactions consume two radical chain carriers. These very fast reactions are responsible for the termination of the kinetic chain. They have kinetics implications, because they eliminate the chain carriers from the reaction mixture, and also structural implications, because they can create bonds.

Recombination Reactions

Recombination of two radicals is the simplest case of termination. Recombination is assumed to be non-activated and with $\log_{10}A$ (M^{-1} s^{-1}) = 10 when R_1 or R_2 are hydrogen atoms and $\log_{10}A$ (M^{-1} s^{-1}) = 9 M^{-1} s^{-1} otherwise.

Recombination reactions produce an increase in molecular weight but can only be responsible for crosslinking when one of the terminating radicals is a central radical in the polymer chain, such as a phenyl or cyclohexadienyl radical linked to two other benzene rings.

Disproportionation Reactions

Disproportionation reactions can occur, in competition with recombination, when one of the radicals has a donatable hydrogen at the α position. This is the case for cyclohexadienyl, cyclohexenyl or cyclohexyl radicals. From product yields reported in literature [24,26], the rate constant for disproportionation appears to be 3 times smaller than the one for recombination.

SUMMARY

The observed chemistry is the combination of these simultaneous reactions. Their quantitative contributions to the degradation process is a function of their relative rates and their structural significance in the complex mechanism of reaction. The model developed in the following sections incorporates the complete set of elementary steps into a quantitative molecular representation of the polymeric melt. We conclude here with a more quantitative description of the kinetically and structurally significant chemistry.

The thermal reaction begins by fission of the weak Ph-SO_2-Ph bond. The net result is the formation of SO_2 gas and two polymeric phenyl radicals.

The phenyl radicals begin the propagation steps. Phenyl radical addition to a benzene ring affords a substituted cyclohexadienyl (CHD) radical, the key intermediate in the overall chemistry. The CHD radical can add to a neighboring benzene ring, creating a crosslink and a different CHD radical. The CHD radical can also revert to the original phenyl radical and benzene ring, or eliminate a substituent as a radical that can continue the propagation cycle. The CHD radical can also terminate which, when by recombination, will generally lead to another crosslink.

The complexity of this system is that at least seven (7) different radicals can participate in this chemistry. Moreover, the importance of a given reaction depends on whether the radical is at the terminus, or interior of a linear chain, a free low molecular weight radical, or part of a crosslinked polymeric arm. This motivates the use of structure-explicit computer models to track the reaction rates and structural significance. This is the topic of our companion paper to follow.

REFERENCES

1. Rose, J. B., *Polymer*, **15**, 456, 1974.
2. Gotham, K. V. and S. Turner. *Polymer*, **15**, 1974.
3. Johnson, R. N., A. G. Farnham, R. A. Clendinning, W. F. Hale, and C. N. Marriam. *J. Polym. Sci.: Part A-1*, **5**, pp. 2375-2398, 1967.
4. Verma, A. K. *Prog. Polym. Sci.*, **12**, pp. 219-228, 1986.
5. Crossland, B., G. J. Knight, and W. W. Wright. *Brit. Polymer J.* **18**, p. 3, 1986.
6. Danilina, L. I., E. N. Teleshov, and A. N. Pravednikov. *Vysokomol. soyed.*, **A16(3)**, pp. 581-587, 1974.
7. Hale, W. F., A. G. Farnham, R. N. Johnson, and R. A. Clendinning. *J. Polym. Sci.: Part A-1*, **5**, pp. 2399-2414, 1967.
8. Davis, A. *Die Makromolekulare Chemie*, **128**, pp. 242-251, 1969.
9. Davis, A., M. H. Gleaves, J. H. Golden, and M. B. Huglin. *Die Makromolekulare Chemie*, **129**, pp. 62-72, 1969.
10. Levantovskaya, I. I., G. V. Dralyuk, O. A. Mochalova, I. A. Yurkova, M. S. Akutin, and B. M. Kovarskaya. *Vysokomol. soyed*, **A13(1)**, pp. 8-15, 1971.
11. Davis, A. *Die Makromolekulare Chemie*, **132**, pp. 23-33, 1970.
12. *Polymer Letters*, **8**, pp. 121-126, 1970.
13. Brown, J. R. and J. H. O'Donnell. *J. Appl. Polm. Sci.*, **23**, pp. 2763-2775, 1979.
14. Levantovskaya, I. I., A. L. Narkon, O. V. Yershov, V. V. Gur'yanova, L. I. Reitburd, M. P. Radetskaya (dec.), L. M. Bolotina, A. B. Blyumenfel'd, A. V. Pavlov, and M. A. Morotina. *Polymer Science U.S.S.R.*, **27(2)**, pp. 404-411, 1985.
15. Brown, J. R. and J. H. O'Donnell. *J. Appl. Polym. Sci.*, **19**, pp. 405-417, 1975.
16. Mikitayev, A. K., G. B. Shustov, A. M. Kharayev, V. V. Korshak, B. I. Kunizhev, and V. T. Dorofeyev. *Polym. Sci. U.S.S.R.*, **26(1)**, pp. 83-87, 1984.
17. Wu, Z., R. Yokota, M. Kochi, and H. Kambe. *Kobunski Ronbunshu*, **38(7)**, pp. 479-484, 1981.

18. Narkon, A. L., I. I. Levantovskaya, Y. L. Kotov, B. Y. Konovalvova, L. I. Reitburd, L. M. Bolotina, and A. B. Blyumenfel'd. *Polymer Science U.S.S.R.*, **26(8)**, pp. 1917-1923, 1984.
19. Narkon, A. L., I. I. Levantovskaya, V. V. Gur'yanova, L. I. Reitburd, O. V. Yershov, G. V. Dralyuk, M. A. Motorina, Y. I. Metelkina, L. M. Bolotina, A. B. Blyumenfel'd, and A. V. Pavlov. *Polm. Sci. U.S.S.R.*, **28(3)**, pp. 562-567, 1986.
20. Coulter, D. R., M. V. Smith, F.-D. Tsay, and A. Gupta. *J. Appl. Polym. Sci.*, **30**, pp. 1753-1765.
21. Kuroda, S.-I, K. Terauchi, K. Nogami, and I. Mita. *Eur. Polym. J.*, **25(1)**, pp. 1-7, 1989.
22. Lyons, A. R., M. C. R. Symons, and J. K. Yandell. *Die Makromolekulare Chemie*, **157**, pp. 103-109, 1972.
23. Ayscough, P. B., K. J. Ivin, J. H. O'Donnell. *Trans. Faraday Soc*, **61**, 1110, 1965.
24. Kochi, J. K., Free Radicals, VII, Vol I. Wiley-Interscience, 1973.
25. Henderson, R. W., Pryor W. A., *J. Am. Chem. Soc.*, **97:26**, December 24, 1975.
26. James, D. G. L.,R. D. Suart. 2735-2751, 1966.
27. Janzen, E. G., C. A. Evans. *J. Am. Chem. Soc.*, **97:1**, January 8, 1975.
28. Benson, S. W., R. Sherv. *J. Am. Chem. Soc.* **89:21**, October 11, 1967.
29. Hey, D. H. *Adv. Free Radical Chem.*V2, 1967.
30. Ito, R., T. Migita, N. Morikawa, O. Simamura. *Tetrsheohon*, **21**, 955-961, 1965.
31. Tiecro, M. *Accounts of Chemical Research*, **13**, 1980.
32. Hey, D. H., M. J. Perkins, Gareth, H. Williams. *J. Chem. Soc.*, 3412-3418, 1969.
33. Gill, G. B., Gareth. *J. Chem. Soc.*, 995-1002, 1965.
34. Detar, D. F., R. A. J. Long, J. Rendleman, J. Bradley, P. Duncan. *J. Am. Chem. Soc.*, **89:16**, August 2, 1967.
35. Detar, D. F. *J. Am. Chem. Soc.* **89:16**, Aug 2, 1967.
36. Pryor, W. A., J. T. Echols, K. Smith. *J. Am. Chem. Soc.* **88:6**, March 20, 1968.
37. James, D. G. L., R. D. Suart. 2752-2769, 1966.
38. Brett, C.L., V. Gold. *Chemical Communications.*, 1971.
39. Pryor, W. A., F. Y. Tony, R. H. Tony, D. F. Chuch. *J. Am. Chem. Soc.*, **104**, 2885-2891, 1982.
40. Bevington, J. C. and J. Toole. *J. Polymer Science*, **Vol. XXVIII**, 413-410, 1958).
41. McMillen, D. F. and D. M. Golden. *Am. Rev. Phys. Chem.*, **33**, 493-532, 1982.
42. Shelton, J. R., C. W. Uzelmeier. *J. Am. Chem. Soc.*, **88:22**, Nov. 20, 1966.
43. Sundarrom, K. M., G. F. Froment. *Ind. Eng. Chem. Fundm.*, **17:3**, 179-180, 1978.
44. Flory, P. J. *Principles of Polymer Chemistry*, Cornell University Press, Ithaca and London, 1953.

Table 2. Substituent Effects for Phenyl Radical Addition to Substituted Benzenes

Substituents	Ortho	Meta	Para
- SO2 -†	2.3	1.0	2.1
- O -††	1.2	1.0	1.1
Others†††	1.0	1.0	1.0

† Reactivity towards $-SO_2-$ substituted benzenes was estimated from values for NO_2 substituted benzenes.
†† Reactivity towards -O- substituted benzenes was estimated from values from $-O-CH_3$ substituted benzenes.
††† Estimated from the values for saturated hydrocarbon.

Table 1. Heat of Formation of Molecules and Radicals [kcal/mol]

H_2	0	H•	52.1
	19.8		78.6
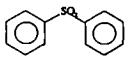	−30.98		43.9
Ph–O–Ph	8.2		80.4
Ph–Ph	42.92		0.65
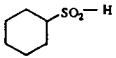	−97.27		
	26		43.24
	−0.8		30

	−29.3		40.4
			13
SO_2	−70.9		47
	−40.9	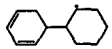	45.33
Ph–O•	12.1	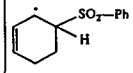	−23.12
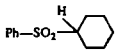	−38.16	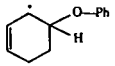	12.99
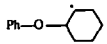	3.35		53.17
	38.98	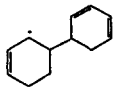	58.94
	45.33		24.42

Table 1. Heat of Formation of Molecules and Radicals [kcal/mol]

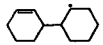	18.52
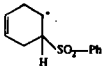	−10.76
	40.4
	−69.37
	−40.24
	3.39

Table 3. Bond Dissociation Energies [kcal/mol]

H—H	104.2
	110.9
	86.5
	−66
Ph-SO_2-Ph	66
Ph-O-Ph	86
	73±5
	95.5
C_2H_5-H	98.2±1
iC_3H_7-H	95.1±1
C_6H_5-CH_2-H	88±1
C = C-C-H	86.3±1.5
	82.5±1.3
C=C-C=C-C-H	83.±3
CH_3-O-H	104.4±1
nC_3H_7-O-H	103.4±1
nC_4H_4-O-H	102.4±1
iC_3H_7-O-H	104.7±1
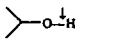	104.7
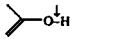	86
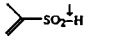	65
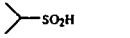	80

Thermal Degradation of Poly(arylether sulfones)
2. Monte Carlo Simulation of Polymer Structure, Reaction, and Diffusion

C. Libanati, C. LaMarca, M. T. Klein*, S. M. Andrews[1], and R. J. Cotter[1]

Center for Catalytic Science and Technology
Department of Chemical Engineering
University of Delaware
Newark, DE 19716

keywords: polymer, pyrolysis, modelling

INTRODUCTION

Sulfone-containing polyarylethers generally include one or more aromatic rings linked together by ether and sulfone groups. One class of these polymers also contains isopropylidene linkages. They form a class of polymers that are tough, have a high softening temperature, and maintain their desirable properties for extended periods of time.

The neat poly(arylether sulfones) are softened by heating for processing. The literature [38] suggests that some of the challenges to this processing are engendered by the valuable properties of the polymers themselves. The same desirable high temperature softening point for end-use applications is also high enough that some thermal degradation can occur during front-end processing. This can lead to gas evolution and viscosity increase, the latter presumably owing to the formation of a gel.

These literature reports motivated the present work aimed at applying our previously developed reaction modelling technique using Monte Carlo simulation to the reactions of poly(arylether sulfones). The particular appeal was that the literature suggested the thermal reactions have structural implications (e.g., gel formation), and our Monte Carlo technique is structurally explicit. There thus appeared to be a good match.

Our model therefore sought an explicit link among polymer structure, reactivity and properties. The link between polymer structure and reactivity was formed by basing the reaction pathways and kinetics on model compound chemistry. Part 1 of this series described the elementary steps modelled to control the thermal degradation of poly(arylether sulfones). The link between the thus-changing polymer structure and properties was established by phrasing the model in terms of a three-dimensional lattice, on which lattice sites represented monomer units and lattice site connections represented bonds. Polymer diffusion on this lattice was described by the movement of monomers to adjacent empty lattice sites. Polymer reaction was described by the destruction or formation of bonds between lattice sites, the nature and probabilities of which being described by model compound pathways and kinetics.

This percolation model of gelation allowed determination of gel, sol and gas fractions as a function of reaction time. Other relationships or models linking properties of the material to its structure (e.g., viscosity from molecular weight distribution or modulus from number of crosslinks and degree of polymerization between crosslinks) can be used to determine the adequacy of the polymer to the application for which it is intended.

The input to the model consists of the chemical and physical structure of the polymer of interest, an assumed mechanism of segmental mobility and associated transport constants, and the postulated mechanism of thermal reaction and its associated rate constants. The output is a prediction of the structure and chemical identity of the system as a function of time. Because the model describes the system at the molecular level, at which all polymers share structure and chemistry, the simulation parameters, such as reaction and transport time constants, are independent of the system modelled, and can be determined from other sources such as experiments with model compounds. Thus this model is envisioned as a tool for the understanding of the underlying fundamentals and for the determination and design of optimal systems.

Although models have been frequently used to improve qualitative understanding, any significant quantitative use of a model's prediction is achieved through comparison with laboratory experimental results. However, the lack of precise characterization of the starting material renders difficult quantitative comparisons between experimental studies and simulation results, especially when the polymers studied were synthesized for a particular study. In particular, a frequent omission in the studies reported in the literature is the molecular weight distribution of the original polymers studied. For the purpose of obtaining pertinent experimental data, we have developed our own experimental procedure which will be reported upon in a follow-up paper. Herein we focus on only the development and operation of the Monte

1 Amoco Performance Products,Inc., 4500 McGinnis Ferry Rd., Alpharetta, GA 30202-3944.

Carlo simulation of polymer degradation. We begin by considering the basic issue of gelation, which controls the present structure-property link sought.

GELATION AND PERCOLATION.

Part 1 described the basic chemistry of poly(arylether sulfone) degradation. Occurring in the polymer, these elementary steps have structural significance. We need to account for more than just the net bond formation/bond breaking; we need to account for crosslinking and longer-range connectivity. This requires a model of the gelation process. Gelation involves the formation of indefinitely large polymer structure, which will extend through the volume of the polymer sample and, on the molecular scale, may be considered essentially infinite.

Gelation is always the result of crosslinking. Its main characteristic is the existence of a gelation point or threshold. This point is akin to the critical point in thermodynamics. As conversion increases during the polymerization of a system containing multi-functional monomers, a point is reached where the system suddenly changes from a viscous homogeneous fluid to a two-phase system, containing an insoluble cluster, the gel, and a soluble portion, the sol [1-8,11, 12,20]. The existence of a gelation point has also been demonstrated in systems where initial constituents are not monomers but linear polymers [1,9-16].

Models of gelation address the connectivity of the system. An early analytical model was developed by Flory and Stockmayer [1,11,12]. Their approach is based on three main assumptions: functional groups react independently of one another; identical functional groups have the same reactivity; no intramolecular reactions occur. Also, any functional group can react with any other functional group, independent of position, and excluded volume effects are neglected.

Based on these assumptions, the system can be represented as a Bethe lattice [5] of functionality equal to the functionality of the monomers. A statistical analysis on this network provides information on the size of the clusters and the connectivity of the monomers as a function of conversion, ρ being defined as the number of bonds formed over the total number of possible bonds. This approach correctly describes the gelation transition and the critical conversion value ρ_c for the existence of an infinite cluster, calculated as $\rho_c = 1/(f-1)$, for monomer of functionality f [1]. The same approach has also been used to describe the crosslinking of linear polymer chains in the vulcanization of rubber [9,10,13-16].

The assumptions stated earlier limit the quantitative use of the analytical approach to but a handful of simple systems. For instance, neglecting intramolecular reaction is probably unreasonable when the initial condition is a set of large linear molecules rather than a collection of monomers. Also, excluded volume effects become important as the reaction proceeds, generating isolated sites, and the equal accessibility rule breaks down in strongly transport-limited systems. Percolation models of gelation are considered to account for the deficiencies of the analytical approach.

The central concept in percolation is the discrete description of space. Space is spanned by a lattice of dimensionality N. The lattice sites can be occupied by monomers, and are connected to neighboring sites by a certain number f of bonds, corresponding to the functionality of the monomers. It can be noted here that the Flory-Stockmayer approach is equivalent to a percolation of infinite dimensionality.

Percolation models are usually implemented numerically and grids of finite size are used to describe a representative fraction of the system. The boundaries of the grid are then considered to be periodic. In these instances, gelation is attained when percolation occurs. In other words, a cluster becomes infinite when it spans the length of the lattice. Based on the state of the lattice a slate of statistical quantities, regarding the composition of the system, can be calculated. The reaction network and kinetics determine the rules by which bonds are formed, linking ρ to reaction time.

In the case of poly(arylether sulfone) degradation, crosslinking occurs as a consequence of breaking and forming linkages within an initially linear polymeric system. The grid percolation models offer the advantage, over the analytical model, of describing the physical and chemical environment of a reactant. A reactive intermediate has a certain number of nearest neighbors with which it can react. Therefore, reactions can be considered at the elementary step level, where bond breaking and bond forming occur. These were presented in Part 1 and can be organized, from a topological point of view, into three main classes:

Bond-breaking reactions:	Initiations and eliminations from cyclohexadienyl, cyclohexyl or cyclohexenyl radicals.
Bond-forming reactions:	Additions and terminations.
"Bond-neutral" reactions :	Hydrogen abstractions and disproportionations.

In the next section, the Monte Carlo simulation of poly(arylether sulfone) degradation is presented, using a three-dimensional square-grid percolation model that incorporates the entire set of elementary steps described earlier.

MONTE CARLO MODEL DEVELOPMENT.

The Monte Carlo simulation of degradation of poly(arylether sulfones) is summarized in terms of major modules of the overall simulation scheme. The initial polymer configuration is constructed from structural information. Once an original configuration is determined, radicals are generated within the grid using an event-space algorithm. The time t_i and nature of the initiating event (initiation reaction or diffusion into the lattice) are calculated. The new state of the system is determined, and time is updated (time =time + t_i). Once radicals are present in the lattice, polymer segments are moved, and all radicals present are tested for reaction with their environment during a fixed time interval

Δt. If, after that time interval, radicals are still present in the lattice, the total time is updated (time = time + Δt), and the previous step is repeated. If, on the contrary, all radicals have disappeared from the lattice (via termination or by diffusing out through a grid boundary), new radicals are generated within the lattice. Then time is updated and the same movement/reaction process described above is repeated. Results are stored at desired reaction times. Once the final reaction time is reached, a new initial configuration is generated for each subsequent run. The results of all runs are averaged to yield statistically significant quantities.

The following subsections present in detail the features of each unit of the overall simulation, starting with the simulation of structure, including the initial configuration and the dynamic simulation of structure, followed by simulation of initiation and propagation reactions. The mechanics of the program developed are detailed elsewhere [39].

SIMULATION OF STRUCTURE

The polymeric melt is represented by a three dimensional square grid of dimension N x N x N. Polymer chains are represented by monomers occupying grid sites connected by bonds. Each grid site has six nearest neighbors with which to interact through linkages or reaction. This representation of the system allows the description of the chemical environment of each site, as well as the global connectivity of the system. It also allows for spatial movement of the monomers, from site to site according to specified rules, to account for diffusion.

In poly(arylether sulfone) systems, the grid sites represent substituted benzene rings, and the bonds represent the linkages between aromatic units. For the system considered here, these bonds are sulfonyl linkages, ether linkages or carbon-carbon bonds (arising from thermal reaction).

Initial configuration

The initial configuration of the system is determined by randomly placing molecules in the grid. Polymer molecules are initially linear. They are represented by self-avoiding random walks in the cubic lattice [1,20,17-19,21]. The degree of polymerization (chain length) of each molecule is randomly chosen from the initial degree of polymerization distribution. The molecule is then placed in the percolation grid, by placing monomers one by one, until the pre-determined length is attained. Where structure is concerned, the boundaries of the grid are periodic. This means that a polymer chain that exits the grid through one face reenters it through the opposite face. This procedure is repeated with new polymer chains until a fraction of the lattice, corresponding to the polymer's density, is filled.

In order to calculate the occupied fraction of the grid, the Van der Waals volume of the polymer, estimated by optimizing the structure of the polymer's building blocks (in this case diphenylsulfone and diphenyl ether), was compared with the total volume of the lattice, assumed to be the total volume occupied by the polymer. The estimation of the polymer molecular volume was achieved by optimizing structure using extended Hückel molecular orbital calculations. The occupied fraction was obtained by dividing the molar Van der Waals volume of the polymer's building block by the molar density of the polymer. In the case of poly(arylether sulfone), the density is 1.06 g/cc, and an average volume of diphenylsulfone and diphenylether was estimated at 130 $Å^3$. The occupied fraction in this case is 75%.

The initial polymer configuration gives the complete connectivity of the polymeric melt, the free volume that will allow polymer movement and the chemical identity of each lattice site and bond. Reaction and movement of polymer units can then be explicitly addressed at the molecular level.

Dynamic structure simulation.

The transport characteristics of the medium in which radical reactions occur have a strong influence on pathways and kinetics. The radical reactions involved in the degradation mechanism are very fast. Fast reactions have been shown to be affected by the ability of the reactant to move [22-24,28,30,32-36]. The time scale of these reactions is often comparable to that for molecular movement, especially in restricted systems like polymer melts. Also, the connectivity of the network can affect or be affected by transport limitations, as is apparent in the work of Brown in the radiolitic degradation of poly(arylether sulfone) at temperatures above and below the glass transition temperature [22]. It is therefore important to introduce mechanisms that account for the movement of the monomers.

The approach taken follows the idea that a polymer molecule diffuses through the movement of its smaller segments, in a wormlike fashion [39]. In simulation, a number of movements, equal to the number of monomers present in the medium, are attempted in a time step Δt. Since the CPU requirement to move every possible segment in the system becomes prohibitively large with grid size, only polymer segments within three lattice sites of a given radical were moved in one step. This local diffusion model captured the environment about a reactive site while still allowing reasonable computational demand. The model has been described in detail elsewhere [39].

Simulation of Reaction

Reactions are simulated according to the stochastic algorithm described elsewhere [39]. Two classes of events are distinguished: The initiation events, creating active centers (radicals) within the lattice, and propagation events, carrying the radical chain reactions.

Initiation Events. Radicals responsible for the degradation of poly(arylether sulfone) are formed in initiation reactions. The sulfonyl linkages break to give two radicals, a phenyl radical and a sulfonyl radical. These radicals can propagate the reaction by interacting with stable monomers, or they can terminate.

An event-space algorithm is used to generate radicals. The initiation possibilities include the breaking of any of the N_{SO_2} sulfonyl linkages present in the lattice. Each one of them represents an event that can happen with rate constant k_{init}. However, due to the finite size of the grid, an extra initiation event was included: radicals generated elsewhere in the melt and outside of the lattice were allowed to diffuse into the grid. The necessity for such an event was prompted by the relative values of initiation and termination rate constants. Rate constants for initiation are usually orders of magnitude smaller than those for propagation reactions and up to 10^{15} times smaller than termination rate constants. Concentrations of radicals in this system are of the order of 10^{-8}–10^{-10} times the concentration of initiating linkages. Memory availability and CPU requirement limit grid sizes to values well below the 10^8 sites necessary to simulate a representative sample of polymer melt. This means that periodic boundary conditions cannot be applied regarding the movement of radical intermediates. If a radical moves out of the percolation grid, it disappears. Having it reenter the grid through the opposing face would artificially increase the concentration of radicals. Including this second (transport) component to the "initiation" or generation of radicals involved the evaluation of the rate of "diffusion" of radicals into the lattice. This was accomplished by calculating the number of radicals that will cross the lattice boundaries inwards per unit time. A radical will move a distance equal to one lattice unit in an average time $\tau = \pi l^2 / 16 D$, where D is the effective diffusion coefficient and l is the size of a lattice unit. There are 6 neighboring sites to which the radical can move. If a radical is positioned one lattice site outside the lattice boundary, only one of its neighboring sites is part of the lattice. Thus, on average, 1/6 of the radicals in those positions will move into the lattice. The number of radicals diffusing into the lattice per unit time is then $n_{rad} = C_{rad} \times V / 6\tau$, where C_{rad} is the global concentration of radicals in the melt and $V = 6 (N l)^2$ is the volume represented by a slab one-lattice-site thick around the outside of the lattice boundaries. Estimations of C_{rad} and D were required in order to calculate n_{rad}.

The effective diffusion coefficient of radicals is a result of the combined effect of the mobility of polymer chains and segments and the reaction of radicals with occupied neighboring sites. The diffusing species is the radical reactive center and can move from molecule to molecule by reaction. This means that a radical center can "diffuse" even when the molecules bearing it are fixed.

The effective diffusion coefficient was therefore related not only to the physical characteristics of the system, through its transport properties (i.e. viscosity, molecular weight, crosslinks) but to its chemical structure as well. It was evaluated by placing a radical in the center of the reactive lattice and performing the simulation disabling initiation and termination chemistry. The average distance travelled, $\bar{d}$, by the radicals in a time t = 1 second was recorded, and the diffusion coefficient was calculated by assuming the radical performed a random walk. In such a case, $D = \pi \bar{d}^2 / 16 t$ or $\overline{d^2} / 6 t$.

Finally, the evaluation of the rate of radicals diffusing into the lattice requires the knowledge of C_{rad}, the global concentration of radicals in the melt. The theory of reactions in solution as well as the pseudo-steady state approximation were applied to evaluate C_{rad} *a priori*, as described in detail elsewhere [39].

The final result is shown in Eq. 1, where $[SO_2]$ is the concentration of unreacted SO_2 linkages.

$$C_{rad} = \left(\frac{k_{init} k_d}{k_c k_{term}} [\text{-}SO_2\text{-}] \right)^{1/2} \qquad (1)$$

The rate of diffusion of radicals into the lattice was thereby determined as a function of the physical and chemical characteristics of the real system and of the simulation parameters (i.e. grid size).

An event-space simulation is performed to calculate the time and nature of the next initiation event. The list of possible events includes the scission of any of the N_{SO_2} sulfonyl linkages and the diffusion of a radical into the lattice. The total rate constant for radical generation is then $k_{rg} = N_{SO_2} k_{init} + n_{rad}$. The time interval between the present time and the next event, τ, is determined according to the algorithm described elsewhere [36]. A random number, RN, is then drawn to determine which event occurred. If $RN < N_{SO_2} k_{init} / k_{rg}$, a sulfonyl linkage, chosen at random, breaks, generating two radicals. Otherwise, an occupied position selected at random on the lattice boundary is modified to become a radical (i.e. if the occupied position is a benzene ring, it is changed to a phenyl radical or a cyclohexadienyl radical, or to a phenoxy radical if it has phenoxy substituents), to represent the generation of an active center via diffusion. The reaction time was at this point updated by adding τ to the current time.

Once reactive intermediates appeared in the lattice they could undergo a series of faster radical-molecule, radical-radical or β-scission reactions.

Propagation reactions. Propagation reactions can be strongly affected by segmental mobility. A fixed time step approach [37, 39] was used to simulate the reactions of radicals with their environment. A radical can react with any of its nearest neighbors to which it is not connected.

In the general case n reactions will be possible for a given radical. The probability for reaction i to occur is given by Equation (2):

$$P_i = \frac{k_j}{\sum_1^n k_j}\left(1 - \exp\left(-\sum_1^n k_j \Delta t\right)\right) \quad (2)$$

The possible transitions and their associated probabilities are computed according to the environment of the radical and the energetics of elementary steps listed in Part 1. However, for bimolecular reactions, the reactants must come within one lattice unit of each other before they can react. Following the "reactions in solution" formalism, it is justified to say that they must form an encountered pair of reactant, A:B*, for them to react. Chemical transformation of this pair is best described by a first-order process, the disappearance of the species identified as "an encountered pair of reactants". In short, the rate constants of Part 1 and the "reactions in solution" formalism [23,25,28] were reconciled [39] to determine the transition probability for this first order process. The final result is $k_{\text{first Order}} = vpe^{-E/RT} = \frac{4}{3}\pi \rho^3 L\, A_{\text{Second Order}}\, e^{-E^*/RT}$, where the second order reaction and that of the encountered pair have the same activation energy.

To implement the simulation, the occurrence and nature of a reaction was determined through the algorithm for parallel reactions [37,39]. A random number, RN_1^i, was compared to the probability $P_i = \left(1 - \exp\left(-\sum_1^n k_j \Delta t\right)\right)$ that a radical i reacts. If reaction occurs a second random number determines its nature. The state of the lattice is then updated, and the random number RN_1, the rate constant of the reaction that did occur and $\sum_1^n k_j$ are kept in memory. The same procedure is applied to all the radicals present in the lattice. The formalism of reactions in series [37,39] was used to account for the fact that several reactions in series can occur in Δt. If radical i reacts in the time interval to yield another radical (it does not terminate or "escape" from the grid), the new radical is tested for reaction. This procedure is repeated until no further reaction occurs.

Once all radicals have been checked for reaction in Δt, the reaction time is updated by adding Δt to the current time. A new time step is allowed to pass or new radicals are generated in the lattice depending on the status of the lattice. When the reaction time reaches predetermined output times, the status of the grid is recorded. Results of several Markov Chains are averaged to yield statistically significant numbers.

OUTPUT OF THE SIMULATION

The simulation results are recorded to allow for comparison with laboratory kinetics experiments. The computer "experiment" is the average of the results of N Markov Chains, for which results were recorded after 0–30 minutes of simulated reaction time.

The output of the simulation summarizes the detailed chemical structure and connectivity of the polymeric system as a function of reaction time. The attributes of the system are described in fractions (sol fraction, gel fraction, fraction of crosslinked monomers), averages (average molecular weight, average number of OH groups per monomer) or distributions (sol fraction molecular weight distribution, distribution of number of linkages per monomer).

The choice of attributes is often determined by the desired comparison with laboratory experiments, as is the case for the gel, sol and gas fractions. However, attributes unavailable from laboratory experiments may present considerable importance in the understanding of the underlying fundamentals. For example, the fraction of crosslinked monomers can be used to evaluate the validity of the Flory-Stockmayer model assumptions.

The quantities recorded for the present simulations were: distribution of monomer types (benzene rings, cyclohexadienes, cyclohexenes, cyclohexanes); total number of linkages; fraction of sulfonyl, ether and biphenyl linkages; fraction of monomers with one, two, three, and four linkages; gas, sol and gel fractions; number-average and weight-average molecular weight and degree of polymerization of the sol fraction; sol fraction molecular weight distribution; gas fraction composition; number of OH groups per monomer; number of chain ends; number of SO_2H groups per monomer; total number of radicals generated in the lattice.

Most of the foregoing quantities are determined by simple inspection of the lattice. Determination of gel, sol and gas fractions from the simulated pyrolysis requires more attention. Experimentally, these fractions are related to the solubility protocol used: the gas fraction is the portion of the mixture that is volatile at room temperature and one atmosphere total pressure; the gel fraction is the portion insoluble in a suitable solvent or any molecule unable to pass through a 5 μ micro-fiberglass filter; the sol fraction is the rest of material. The determination of the gel fraction was by making the conceptual link that the gel fraction corresponded to the portion of polymer that is insoluble in a solvent that dissolves linear polymers of same chemical compositions. The existence of a gel implies, according to Flory [1], the presence of an infinite network of crosslinked material.

SIMULATION RESULTS

Model predictions are presented in terms of temporal variation of average structural parameters and the yields of solubility-based product fractions from simulated poly(arylether sulfone) pyrolyses. The results presented here are the output of the simulation performed on a three-dimensional square grid of dimension 40 x 40 x 40.

PRODUCT FRACTIONS

The determination of products belonging to the gel fraction, the sol fraction or the gas fraction was made according to the rules described above. Calculating the weight of each monomer and its associated linkages, summing these for the gel and sol fractions, and dividing by the total weight of all particles in these two fractions enabled prediction of the weight yield of the sol and gel fractions from simulated pyrolyses.

Figure 1 presents the temporal variations of the sol and gel product fractions for simulated pyrolysis at 425°C. The gel fraction shows a general increase with time, and the sol fraction shows the complementary decrease with time. A small fraction of gel is formed at times < 500 s, but a dramatic increase occurs at 500 s, where the gel fraction increases sharply to slightly greater than 20%. This can be qualitatively likened to the existence of a gelation point which has been reported during experimental polymer pyrolyses. The small fluctuations in the gel fraction prior to the dramatic increase can be attributed to computational factors. The simulation allows for bond-breaking initiations at all time steps. Chains already considered to be a part of the gel fraction can undergo chain scission at later reaction stages and therefore may no longer satisfy the percolation and crosslinking requirements for gelation. The frequency of this occurring is very small, however, and, in any event, dampens as the number of Markov Chains increases.

The yields of sulfur-containing product gases, H_2S and SO_2, from the simulated pyrolysis are shown in Figure 2. The percent yield is based on the amount of sulfone linkages contained in the reactant poly(arylether sulfone). The yield of SO_2 increases linearly with time and reaches an ultimate value of 4% after 1100 s of simulated reaction time. The percentage of H_2S formed is much lower and achieves a value of only 0.1% after 1100 s of reaction time. The balance of the sulfur would remain in the gel or sol fraction as SO_2 linkages between monomers.

STRUCTURAL PARAMETERS

The model explicitly monitored the length of each chain (number of monomeric units) and the type and number of links for each of the monomers. This information could be assembled to specify values of average structural parameters for the entire polymer or any of its product fractions.

The number average degree of polymerization, $\overline{x_n}$, for the sol product fraction as a function of time is presented in Figure 3. The value of $\overline{x_n}$ is defined in the simulation as:

$$\overline{x_n} = \frac{\sum_i \text{number of chains of degree of polymerization } i \times i}{\text{total number of chains}}$$

where i=1 would represent one unit in the polymer chain where a unit is taken to be a single benzene-derived ring or, in simulation terms, one grid point. Note that the value of $\overline{x_n}$ continually decreases, exhibiting a value of 108 at the initial time and decreasing to an ultimate value of 20 at 1100 s. Chain scission and crosslinking have opposing effects on the value of $\overline{x_n}$. However, $\overline{x_n}$ is particularly sensitive to the proportion, by number, of shorter chain lengths, and therefore exhibits the generally decreasing trend.

In the region of 500 s, there is a marked decrease in the value of $\overline{x_n}$. This is the point when a significant portion of gel fraction forms and the large, crosslinked chains no longer contribute to the value of $\overline{x_n}$ for the sol fraction. The time at which this occurs is simultaneous with the point considered to be the gelation point in the gel fraction versus time curve presented above.

The temporal variation of the weight average degree of polymerization, $\overline{x_w}$, is shown in Figure 4. The definition of $\overline{x_w}$ used in the simulation is :

$$\overline{x_w} = \frac{\sum_i \text{number of chains of degree of polymerization } i \times i^2}{\sum_i \text{number of chains of degree of polymerization } i \times i}$$

The value of $\overline{x_w}$, in contrast with the value of $\overline{x_n}$, increases with time in the initial stages of reaction. The weight average degree of polymerization is particularly sensitive to the presence of larger chain lengths, and therefore, the effect of crosslinking dominates over chain scission. The sharpest rise occurs in the region of 450 s followed by a sharp decline. This corresponds to the region, identified earlier as a gelation point. Here the infinite chains in the gel no longer contribute to any parameters measured in the sol fraction. In the later stages of reaction, more of the material is contained in the gel fractions, and the sol fraction is composed of small chains which gives rise to a small ultimate value of $\overline{x_w}$.

All of the results presented are for the reaction at 425°C of a poly(arylether sulfone) with a single initial degree of polymerization. We are just beginning to use the model to explore other polymers and conditions. The object of this report was to describe and record the approach and methodologies used. The agreement between model predictions and experimentally observed temporal variations of the yields of product fractions and the values of structural parameters will be assessed quantitatively in a follow-up communication.

CONCLUSIONS

1. Poly(arylether sulfone) structure, reactions, and diffusion can be described quantitatively in terms of a dynamic reaction lattice.
2. Model compound kinetics provide a basis for modelling the bond-breaking and bond-forming reactions of poly(arylether sulfones).
3. Gelation was associated with the attainment of a spanning cluster on the lattice. The gel fraction was sensitive to the fraction of bonds formed, as in polymerization.
4. The model represents a flexible computer experiment for testing the influence of processing conditions.

REFERENCES

1. Flory, P.S., *Principles of Polymer Chemistry*, Cornell University Press, Ithaca and London, 1953.
2. de Gennes, P. G., Phys. Lett. A, **38**, pp. 339-42, 1972.
3. de Gennes, P. G., J. Physique, **36**, pp. 1049-54, 1975.
4. Stauffer, D., J. Chem. Soc. Faraday Trans II, **72**, pp. 1354-64, 1976.
5. Stauffer, D., *Introduction to Percolation Theory*, Taylor and Francis, London and Philadelphia, 1985.
6. Coniglio, A., Starly, H. E., Klein, W., Phys. Rev. Let., **42**, pp. 518-22, 1979.
7. Earnoux, B., Ann. Phys. Paris 1, pp. 73-141, 1976.
8. Lubensky, T. C. and Isaacson, S., Phys. Rev. Lett., **41**, pp. 829-32, 1978.
9. Coniglio, A., Daout, M., J. Phys. A: Meth. Gen., Vol. 12, No. 10, 1979.
10. Gonzalez, A.E., Daout, M., J. Phys. A: Meth Gen, **14**, pp. 2441-2457, 1981.
11. Stockmeyer, W. H., J. Chem. Phys., **11**, 45, 1943.
12. Stockmeyer, W. H., J. Chem. Phys., **12**, 125, 1944.
13. Gordon, M., Proc. R. Soc. A., **268**, 240, 1962.
14. Gordon, M. and Malcolm, G. N., Proc. R. Soc. A., **295**, 29, 1966.
15. Gordon, M. and Ross-Murrphy, S. B., Pure and Appl. Chem. **43**, 1, 1975.
16. Gordon, M. and Scontlelnry, G. R., Proc. R. Soc., **292**, 380, 1966.
17. Weiss, G. H. and Rubin, R. J., "Random Walks: Theory and Applications," Advances in Chemical Physics, **52**, 1983.
18. Domb, C., Adv. Chem. Phys., **15**, 229, 1969.
19. McKenzie, Phys. Rep., **27C**, 35, 1976.
20. de Gennes, P. G., *Scaling Concepts in Polymer Physics*, Cornell University Press, Ithaca, N.Y., 1979.
21. Rudnick, J. and Graspari, G., Science, **237**, 1987.
22. Brown, J. R. and O'Donnell, J. H., "Effects of Gamma Radiation on Two Aromatic Polysulfones. II. A Comparison of Irradiation at Various Temperatures in Air-Vacuum Environments," J. Appl. Polym. Sci., **23**, pp. 2763-2775, 1979.
23. Moore, J. W. and Pearson, R. G., *Kinetics and Mechanics*, John Wiley and Sons, New York, 1981.
24. Troe, J., J. Phys. Chem., Vol. **90**, no. 30, 1980.
25. Rabinowitch, E., Trans Faraday Soc., **32**, 1381, 1936.
26. Fowler, R. H. and Slatev, N. B., Trans Faraday Soc., **33**, 1185, 1937.
27. North, A. M., *The Collision Theory of Chemical Reactions in Liquids*, Methuen, London, 1964.
28. Smoluchowski, M. V., Phys. Z., **17**, 1917.
29. Moeliogn-Hughes, E. A., *The Kinetics of Reactions in Solutions*, The Clerendon Press, Oxford, 2nd ed., 1947.
30. Noyes, R. M., J. Am. Chem. Soc., **86**, 4529, 1964.
31. Noyes, R. M., Prog. React. Kinet., **1**, 129, 1961.
32. Caldin, E. F. and Hasinoff, B. B., J. Chem. Soc., Faraday Trans. I, **71**, 515, 1975.
33. Trommsdorff, E., Kohle, H., Lagelly, P., Makromolec. Chem. **1**, 169, 1948.
34. Tulig, T. J. and Tinell, M., Macrom. **15**, 459, 1982.
35. Tulig, T. J. and Tinell, M., Macrom. **14**, 1501, 1981.
36. Rohr, D. and Klein, M. T., I&EC Research, **29**, 1210, 1990.
37. McDermott, J. B., Libanati, C., LaMarca, C. and Klein, M. T., I&EC Research, **29**, p. 22, 1990.
38. Rose, J. B., "Preparation and Properties of polylarylene ether sulphones," Polymer **15**, pp. 456-465, 1974.
39. Libanati, C., Ph.D. Thesis, University of Delaware, Newark, DE, 1990.

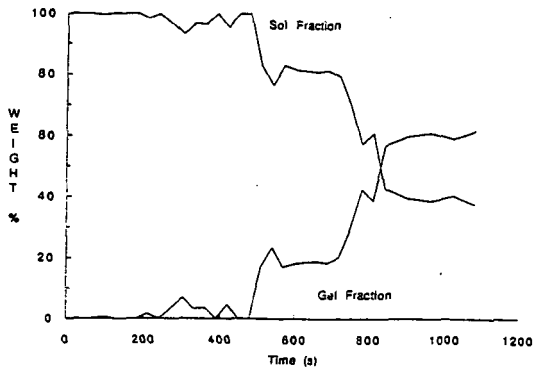

Figure 1. Temporal variation of gel and sol product fractions at 425°C from simulated poly(arylether sulfone) pyrolysis.

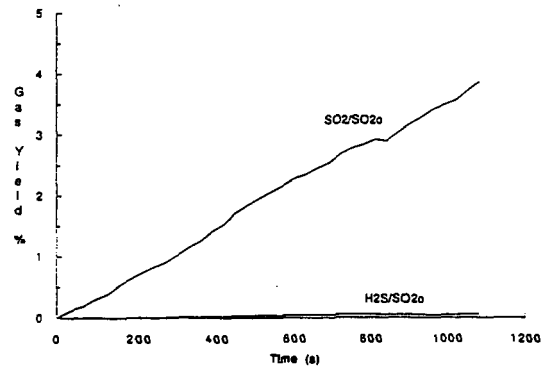

Figure 2. Temporal variation of sulfur-containing gas fraction at 425°C from simulated poly(arylether sulfone) pyrolysis.

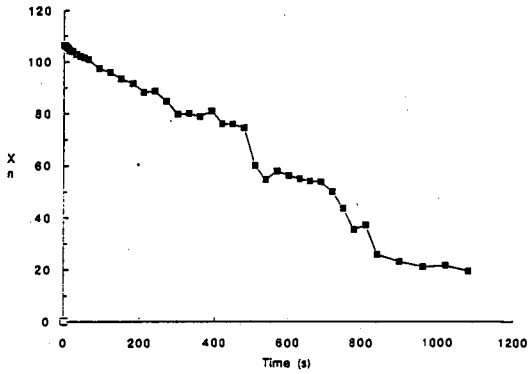

Figure 3. Temporal variation of number average degree of polymerization of sol fraction at 425°C from simulated poly(arylether sulfone) pyrolysis.

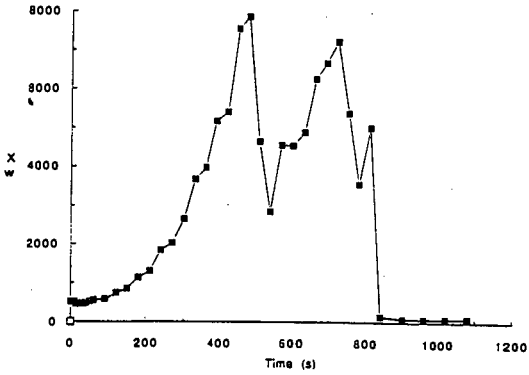

Figure 4. Temporal variation of weight average degree of polymerization of sol fraction at 425°C from simulated poly(arylether sulfone) pyrolysis.

PYROLYSIS OF PHENOL-FORMALDEHYDE RESIN: EXPERIMENTS AND MODELING

Michael A. Serio, Sylvie Charpenay, Rosemary Bassilakis, and Peter R. Solomon

Advanced Fuel Research, Inc.
87 Church Street
East Hartford, CT 06108

Keywords: Pyrolysis, Phenol-Formaldehyde Resin, Modeling

INTRODUCTION

Fires kill nearly 10,000 people each year in the U.S. and cause nearly 300,000 injuries and over 6 billion dollars in property damage (1). Consequently, there is a great need for additional research on fires and fire safety. While non-polymeric materials (e.g., cooking fat) are the main sources of ignition, natural and synthetic organic polymers are most frequently the materials which are primarily responsible for the propagation of fires (2). To describe the pyrolytic degradation of a burning polymer, one needs to know the chemical reactions and rates for the bridge breaking (depolymerization) and crosslinking (repolymerization) reactions. But these reactions typically occur within a crosslinked macromolecular network, so their effects in fragmenting the macromolecule must be treated statistically. In addition, the effects of heat and mass transport within a material undergoing phase changes (solid to liquid and gas) must also be included. While statistical methods have been applied to the polymerization processes (3,4), such models have not been as well developed for the degradation processes, particularly for charring polymers.

This study is based on two techniques, one theoretical and one experimental which have resulted from research during the past ten years by Advanced Fuel Research, Inc. (AFR) on the pyrolysis of coal, a natural polymer. This work has led to development of a macromolecular network model to describe the thermal decomposition of coal (5-10). To develop this model, we have determined the rates and mechanisms for depolymerization, crosslinking, and the formation of char, tar, and gases. These processes are imposed upon a sample macromolecular network constructed in a computer, and Monte Carlo (or Percolation Theory) methods are used to determine the molecular weight of the network fragments as the population of bonds and crosslinks changes. The model includes a model for viscosity (melting) based on the molecular weight distribution of the macromolecular fragments. In addition to predicting the molecular fragments, the evolution of gas species is predicted from the thermal decomposition of peripheral functional groups in the network. The combined model has been called the FG-DVC model, which stands for Functional Group - Depolymerization, Vaporization and Crosslinking model. The FG-DVC model has been validated using literature data and data obtained in our laboratory (8-10).

The work on coal pyrolysis has also led to the development of a new instrument called the TG-FTIR which integrates a thermogravimetric analyzer (TGA) with an FT-IR for enhanced gas analysis (11-13). The TG-FTIR system provides kinetic information on the weight loss and volatile products used for validation of the FG-DVC model.

The modeling (FG-DVC) and experimental (TG-FTIR) techniques were applied to pyrolysis of phenol-formaldehyde (P-F) resin, which is an example of a charring polymer. Currently, these types of polymers present the most difficulty as far as predicting their behavior in a fire. Charring polymers are also of increasing importance because they have inherently higher flame retardance properties than non-charring polymers. The thermal decomposition of P-F has been the subject of numerous literature studies because of its commercial importance, which also makes it a good candidate for development of new models and techniques (14-24). Finally, the behavior of P-F is similar to coal in many respects and it has been used as a model system for coal (25-29).

EXPERIMENTAL

Apparatus

Details of the TG-FTIR method appear elsewhere (11-13). The apparatus consists of a sample suspended from a balance in a gas stream within a furnace. As the sample is heated in a helium flow, the evolving volatile products are carried out of the furnace directly into a 5 cm diameter gas cell (heated to 150°C) for analysis by FT-IR. The FT-IR can obtain spectra every 0.2 s to determine quantitatively the evolution rate and composition of several hydrocarbon compounds. The system allows the sample to be heated on a pre-programmed temperature profile at rates between 3°C min^{-1} and 100°Cs^{-1} up to a temperature between 20 and 1000°C and held for a specified time. The system continuously monitors: 1) the time-dependent evolution of the gases (including specific identification of the individual species such as, CH_4, C_2H_6, C_2H_4, C_2H_2, C_3H_8, benzene, etc,; 2) the heavy liquid evolution rate and its infrared spectrum with identifiable bands from the functional groups; and 3) weight of the non-volatile material (residue). An analysis of C,H,N and S in the residue at the end of the pyrolysis experiment can be obtained by introducing oxygen to burn the residue and analyzing the combustion products.

Sample

Phenol-Formaldehyde (P-F) resins are products of the condensation of phenols with aldehydes (usually formaldehyde) and represent an important group of thermosetting resins. The synthesis procedure for P-F resins is illustrated in Fig. 1a, along with a representative structure. The structure used in the simulation of P-F behavior in the FG-DVC model is shown in Fig. 1b.

These resins are classified in two basic types: novolaks (produced with acid catalysts and an excess of phenol) and bakelites or resols (produced with basic catalysts and an excess of aldehyde). Novalaks are linear polymers with molecular weights of 1000-1500 amu. These are not initially crosslinked and are fusible and soluble. Conversely, bakelites have short chains and are highly crosslinked insoluble resins. An advantage to working with bakelites is that, by adjusting the ratio of phenol to formaldehyde, non-linear polymers with different degrees of crosslinking can be obtained.

The sample of phenol-formaldehyde resin used in the current study was a bakelite and was obtained from Professor Eric Suuberg of Brown University. It was synthesized using NH_4OH catalyst, with a formaldehyde-to-phenol ratio of 4.33. The curing procedure was done in three stages: a) 2 hours at 60°C in vacuum; b) 12 hours at 120°C in vacuum; c) 2 hours at 300°C in helium.

Analysis

The FG-DVC model inputs require information from elemental, FIMS, solvent swelling/extraction and TG-FTIR, as shown in Fig. 2. The P-F resin was subjected to elemental analysis at Huffman Laboratories (Golden, CO). The results on a daf basis were C: 76.6, H: 5.5, O: 17.8, N: 0.1.

A sample of the P-F resin was sent for analysis in the Field Ionization Mass Spectrometer (FIMS) apparatus at Stanford Research Institute (30). The Field Ionization induces little fragmentation and so provides a determination of the sample's molecular weight. The FIMS analysis is done by a programmed pyrolysis of the material into the inlet of the mass spectrometer (held at vacuum). The mass spectra are taken at regular intervals so that the evolution of individual compounds can be tracked as a function of temperature. The FIMS technique provides detailed insight into the tar formation (and indirectly the char formation) processes. The formation of tar is key to the prediction of polymer combustion properties since it impacts the ignition, soot formation, smoke formation, and char formation.

The sample of P-F resin was extracted with pyridine at the boiling point to obtain the amount and composition of the extract. A portion of the dried, extracted solids was also swelled in pyridine in order to determine the volumetric swelling ratio (VSR). This solvent swelling measurement was carried out according to the method of Green, Kovac and Larsen (31,32). The value of the VSR can be used in the FG-DVC model to determine the starting value of the molecular weight between

crosslinks. However, this requires an assumption of the monomer molecular weight. It is more convenient to use the pyridine extractables amount which is determined from the same experiment.

RESULTS

Pyrolysis experiments were performed on the P-F sample using the TG-FTIR apparatus (11-13) over a range of heating rates (3-100°C/min). Figure 3a illustrates the weight loss, the sum of the evolved products, and the temperature history for a 20 mg sample taken on a 30°C/min temperature excursion, first to 150°C to dry for four minutes and then to 900°C for pyrolysis.

During the excursion, infrared spectra are obtained once every 41 s. The spectra show absorption bands for CO, CO_2, CH_4, H_2O, SO_2, COS, C_2H_4, and NH_3. The spectra above 250°C also show aliphatic, aromatic, hydroxyl, carbonyl, and ether bands from tar. The evolution of gases derived from the IR absorbance spectra are obtained by a quantitative analysis program that employs a database of integration regions and calibration spectra for different compounds (11-13). Figure 3b through 3f illustrate the evolution rates and integrated amounts evolved for H_2O, tars, CO_2, CH_4, and CO respectively. Because the data are quantitative, the sum of the evolved products matches the weight loss as determined by the TGA balance.

Pyrolysis of phenol formaldehyde resin in the TG-FTIR apparatus led to the formation of tar, CO, CO_2, CH_4, and H_2O as illustrated in Fig. 3. The product mix and evolution profiles are consistent with previous studies on the thermal degradation of this material (14-24). CO evolved in two distinct peaks, one before tar evolution (450°C at 30°C/min), the other after tar evolution (620°C at 30°C/min). The CO_2 evolution rate peaked at approximately the same temperature as the first CO peak, while the CH_4 evolution rate was a maximum at roughly the same temperature as the second CO peak. Water evolution occurred at the same time as tar evolution for all heating rates. A composite species evolution plot from the TG-FTIR analysis of phenol formaldehyde at 30°C/min is shown in Fig. 4a.

The overall pyrolysis behavior of phenol formaldehyde is very similar to that of Wyodak subbituminous coal. The elemental compositions of these materials are similar although the bridging groups between the aromatic rings are different. A composite species evolution plot from the TG-FTIR analysis of Wyodak coal is shown in Fig. 4b. In both cases, there is a CO_2 peak prior to tar evolution, a CH_4 peak following tar evolution, and a water peak at the same temperature as tar. The amount of tar is also comparable: about 12% for phenol formaldehyde and 9% for Wyodak. The only significant difference between the gas evolution of the two samples is for CO, since all of the CO evolves after the tar peak for Wyodak while there is an early peak before tar evolution in the case of phenol formaldehyde. The similarity of the evolution profiles and the char yields for the two materials provides support for the idea of using a model developed for coal (FG-DVC) to describe a synthetic polymer (P-F). Of course, it is also true that the similarity in the product yields does not guarantee that the decomposition mechanisms are the same. However, the model has the flexibility to incorporate these different mechanisms, as discussed below.

MODELING

The FG-DVC model was originally developed based on a polymeric representative of coal which is aromatic clusters connected by weak (ethylene) bridges and which also include functional groups such as carboxyl or methoxy which promote crosslinking and/or lead to gas evolution. The depolymerization occurs by random, homolytic cleavage of the weak bridges (8-10).

Phenol-formaldehyde resin is also a charring polymer which decomposes by random degradation with crosslinking. The system does not produce many volatile products, and there is formation of char after complex crosslinking reactions. It is the nature of the depolymerization and crosslinking reactions which is different for P-F resin than for coal.

Model Implementation

The implementation of the FG-DVC model for a specific polymer system requires the specification of several parameters, some of which are constrained by the known polymer structure and some of

which are constrained by experimental characterization data. A flow diagram of the model inputs and outputs is given in Fig. 2. The basic idea is to validate the model using simple small scale experiments like TG-FTIR, FIMS, solvent swelling, and elemental analysis and then use the model to make predictions for conditions where experimental data are not readily available such as at high heating rates. This approach has been highly successful in using the FG-DVC model to make predictions for pyrolysis of coal under combustion conditions at high heating rates using a model that was validated using low heating rate TG-FTIR and fluidity data (33).

Network Polymers - First, the polymer network has be to defined. This requires specification of the following parameters: monomer units and subunits, the types of bridges and the fraction of breakable vs. unbreakable bridges, the number and type of peripheral groups, and number of initial crosslinks (unbreakable linkages at branch points in the polymer chains). Since synthetic polymers usually have a regular and repetitive structure, they can often be represented in the model by monomers (a monomer being the smallest repetitive unit) linked by a single type of bridge. Depending on their complexity, monomers can be described as being composed of submonomers of different types, which are linked together by either labile (breakable) or unbreakable bridges. The reason for including submonomers is to describe more accurately the structure.

In the case of polymer resins like phenol formaldehyde, the structure is not necessarily a unit which repeats over a short length scale as shown in Fig. 1a. Consequently, some average structures must be written (as shown in Fig. 1b). This is even more true in the case of coal where the repeating unit is purely a statistical quantity.

Once the monomer units and subunits have been established, the parameters of the network are then defined through the mass of monomers, submonomers, labile bridges, and unbreakable bridges. Once the polymer network has been specified, the next step is to specify the depolymerization reactions, crosslinking reactions, and gas forming reactions. This is done based on the known polymer structure and literature work.

Depolymerization Reactions - Phenol-formaldehyde is an example of a polymer constructed by joining aromatic units with labile (methylene) bridges. Usually, single atom bridges between aromatic rings are not very labile. However, the ortho situated hydroxyl group activates the decomposition of the methylene linkage due to a keto-enol tautomerism (34).

The depolymerization process, done by breaking labile bridges, can be performed with hydrogen abstraction from either other labile bridges, if those can give hydrogen, or other possible hydrogen donor species in the polymer, such as the aromatic rings. In the latter case, all the bridges can be broken, while in the former case, only part of them are actually broken. The choice of depolymerization process is based on the hydrogen availability in the polymer. Currently, the model does not include hydrogen transfer along the chain since this is not usually important for aromatic polymers. The weight of the evidence from the literature suggests that, for the depolymerization of phenol-formaldehyde, hydrogen donation occurs from other methylene bridges (14-24).

Crosslinking Reactions - In the case of charring polymers, an important reaction to model is the crosslinking of the polymer. In the version of the FG-DVC model used for coal, crosslinking reactions are related to gas evolution, in particular CO_2 and CH_4 (8,9,35). It seems obvious that, in the case of polymers, these gases might also be related to crosslinking events, along with other gases as well. As discussed above, phenol formaldehyde has a behavior very close to coal. The same types of gases evolve (CO_2, CH_4, CO, H_2O) and the total weight loss is comparable to coal's weight loss. However, the most probable crosslinking reaction in phenol formaldehyde involves H_2O evolution (16) as discussed below and in Ref. 36. The crosslinking efficiency, i.e., the number of crosslinks introduced per mole of gas evolved, is an adjustable parameter of the model.

In the case of phenol formaldehyde, one of the possible crosslinking reactions involves elimination of a labile bridge at the crosslink site.

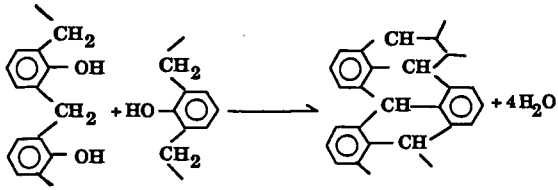

(Rxn 1)

In our nomenclature, we reserve the term crosslinks to refer to bonds which cannot be broken during the preliminary pyrolysis stages (< 600°C) such as C-C aryl linkages. For example, the methylene linkages between the phenolic groups in phenol-formaldehyde would not be considered crosslinks in our model because these can be broken at relatively low temperatures because of the activating mechanism of the ortho situated hydroxyl groups, discussed above. Conversely, the formation of an ether link by the reaction of two hydroxyls (discussed below) may act as a crosslink under primary pyrolysis conditions because the reaction also removes this activating mechanism.

The difference between crosslinks and unbreakable bonds in the model is as follows: crosslinks are unbreakable bonds which act a branch points (divergence of two chains) while unbreakable bonds are part of a linear chain. This distinction is made in Fig. 1b where examples of a crosslink (X.L.) and hardbond (H.B.) are shown.

Gas Evolution - For aromatic polymers, the gas evolution occurs from decomposition of peripheral groups including bridge structures. In the FG-DVC model, these groups are distributed based on the known polymer composition using a mixture of functional group sources (6,7). This is the "FG" part of the model. The specific mechanisms of gas evolution have not been input into the model with the same level of detail as the char and tar formation (treated in the "DVC" part of the model). It has been found that the absence of detailed gas formation mechanisms has not prevented us from accurately predicting gas formation from coal over a wide range of heating rates (0.05°C/s - 20,000°C-s) (9,33). It is expected the same will be true of phenol-formaldehyde, although we do not yet have the high heating rate data to verify this assumption.

Experimental Inputs - The next step in setting up the model is to use experimental data to further constrain the model. This is shown schematically in Fig. 2. For polymers, with a regular repeating structure, there are obviously no adjustments required to match the elemental analysis data. However, for polymers with an irregular repeating structure, like phenol formaldehyde, the peripheral groups and bridge structures are distributed statistically and must be in agreement with known structures based on FT-IR and elemental analysis data.

A second experimental input required for polymers which have an indefinite structure is the number of starting crosslinks. This can be based on either the volumetric swelling ratio or the pyridine extractables as discussed above.

Simulations of Phenol-Formaldehyde Pyrolysis

A literature review showed that several reactions involving water elimination might lead to the formation of crosslinks. The fact that we observe in the TG-FTIR analysis a water peak at 200-300°C (see Fig. 3b) (which is a temperature range too high for moisture) might indicate that crosslinking reactions have occurred during low temperature pyrolysis. Reaction 2 is a curing reaction which occurs at low temperature and forms water.

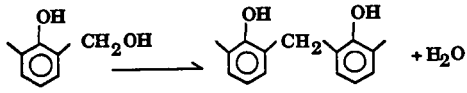

(Rxn 2)

However, a methylene bridge formed ortho to a hydroxyl group would not act as a crosslink under primary pyrolysis conditions. Reaction 1 (see above) is a possible pathway to produce crosslinks at low temperatures (16). Reaction 3 is also thought to occur at relatively low temperatures, although the extent of the reaction and its temperature range are subject to debate between researchers.

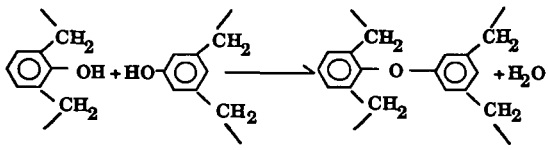

(Rxn 3)

An ether linkage formed in this manner could act as a crosslink under primary pyrolysis conditions.

Since several reactions can lead to the production of water, it is not likely that every water molecule evolved corresponds to a crosslink. Different test cases showed that a value of 0.5 for the crosslinking efficiency of H_2O seems to be the best choice. One of the crosslinking reactions (Reaction 1) takes place between the –OH of a phenol and a methylene bridge, thus removing a labile bridge. To take this into account, we also included in the model, for every new crosslink formed, a reaction transforming a labile bridge next to the crosslink into an unbreakable bridge. Since it was not known *a priori* if Reaction 1 is the important pathway for crosslinking, simulations were done with this reaction and also with Reaction 3 as the main crosslinking reaction.

The network parameters (amount of available hydrogen, initial crosslink density, and starting oligomer length) were chosen to match the experimental value of pyridine extractables (0.8%) and the amount of tar from TG-FTIR experiments (12%). Although we did not make any fluidity (inverse viscosity) measurements on phenol formaldehyde, the network parameters were input into the fluidity model and the predictions are consistent with the fact that no melting was observed during pyrolysis of this material at low heating rates.

Two sets of assumptions were used in the pyrolysis simulations of phenol-formaldehyde. These assumptions are summarized in Table 1 as Case 1 and Case 2.

TABLE 1

SUMMARY OF ASSUMPTIONS USED IN PHENOL-FORMALDEHYDE PYROLYSIS SIMULATIONS

	Number of Hard Bonds	Number of Initial Crosslinks	Crosslinking Reaction
Case 1	0	320	1
Case 2	600	320	3

For the first case, we considered that relatively few hard bonds were present in the original resin, since there is probably no condensation yet. A significant number of starting crosslinks was also necessary in order to have a 3-dimensional network, and also to limit vaporization of dimers, trimers, etc., since these are not present in the FIMS spectra (36). While there are no real crosslinks in the original phenol-formaldehyde structure (see Fig. 1a), these must be introduced during the curing process, perhaps by Reaction 1, since the curing is done up to relatively high temperatures (300°C). Having included the reaction transforming a labile bridge into unbreakable bridges when a crosslink is formed, we found that no initial hard bonds and approximately one branch point for every three monomers gave the best fit to the TG-FTIR data (see Figs. 5 and 6 and Table 1). The solid lines in Figs. 5 and 6 are the FG-DVC model predictions while the experimental data are represented as symbols connected by lines. Using an alternative crosslinking reaction (Reaction 3), more initial hard bonds (approximately one for every four bridges) were necessary, keeping the same crosslink density. This is Case 2 in Table 1. This rather high value of hard bonds (while we expect few original bonds) might indicate that there is a process of consumption of labile bridges in the polymer during curing or in the early stages of pyrolysis, since these would not be expected in the original structure. In both of these two cases, a narrow range in the network parameters was found to give the best fit. When either set of parameters was used in the model, the main features of the tar FIMS spectra were simulated (36).

The kinetic parameters for gases and tar were selected by fitting TG-FTIR evolution curves for different heating rates. The tar evolution was found to correspond to an activation energy of 51.4 kcal, which is very close to activation energies found in the case of coals (8-10). The overall rate is, however, lower than that for coals since the tar peak for phenol formaldehyde occurs at higher temperatures. A comparison of the product evolution data with the model predictions is given for two different heating rates in Figs. 5 and 6. Excellent agreement was obtained. Similar results were obtained for the Case 2 parameters. The gas predictions are not very sensitive to the choice of network parameters while the tar and char yields are sensitive. Case 1 is thought to be more realistic since it does not require the assumption of a large amount of starting hard bonds. Additional analysis of the cured P-F resin, such as by solid state C^{13}-NMR, would be required in order to definately rule out Case 2.

Once the model has been fully validated, it can be used to make predictions for a different range of network parameters or a different range of experimental conditions. An example of this is shown in Fig. 7 where the effect of changing the starting number of crosslinks on the predictions for weight loss, tar evolution rate, and tar molecular weight distributions (MWD) are shown. The model predicts the correct trend in the change in the tar molecular weight distribution, tar yield, and weight loss with increasing initial crosslink density based on the results that have been obtained for coal (35).

CONCLUSIONS

The main conclusions from this effort can be summarized as follows: 1) The TG-FTIR method can provide information on several aspects of polymer thermal decomposition behavior including kinetics and degradation mechanisms; 2) The FG-DVC model can be generalized to predict kinetics, product evolution, tar yields, and tar molecular weight distributions for phenol formaldehyde and other charring polymers over a wide range of conditions; 3) The key inputs required to model the decomposition of a charring polymer are the network parameters, depolymerization reactions, crosslinking reactions, and gas formation reactions; 4) The choice between two alternative crosslinking reactions may lead to a different choice of network parameters.

ACKNOWLEDGEMENTS

This work was supported by the National Science Foundation under Phase I SBIR Grant No. ISI-8961476. The authors also acknowledge helpful discussions with Professor Eric Suuberg of Brown University, who also provided the phenol-formaldehyde resin sample.

REFERENCES

1. Gann, R.G. and Dipert, R., "Polymer Flammability", Encyclopedia of Polymer Science and Engineering, John Wiley & Sons, NY, 1986.
2. Cullis, C.F. and Hirschler, M.M., The Combustion of Organic Polymers, Clarendon Press, Oxford, 1981.
3. Rodriguez, F.R., Principles of Polymer Systems, McGraw-Hill, New York, 1982.
4. Polymerization Kinetics and Technology, (N.A.J. Platzer, Ed.), American Chemical Socieyt, Washington, 1973.
5. Solomon, P.R., "New Approaches in Coal Chemistry", ACS Symposium Series **169**, American Chemical Society, Washington, DC, 1981, pp 61-71.
6. Solomon, P.R. and Hamblen, D.G., in Chemistry of Coal Conversion, (R.H. Schlosberg, Ed.), Plenum Press, NY, 1985, Chapter 5, pg. 121.
7. Serio, M.A., Hamblen, D.G., Markham, J.R., and Solomon, P.R., Energy & Fuels, **1**(2), 138, (1987).
8. Solomon, P.R., Hamblen, D.G., Carangelo, R.M., Serio, M.A., and Deshpande, G.V., Combustion and Flame, 71, 137, (1988).
9. Solomon, P.R., Hamblen, D.G., Carangelo, R.M., Serio, M.A., and Deshpande, G.V., Energy & Fuels, **2**, 405, (1988).
10. Solomon, P.R., Hamblen, D.G., and Yu, Z.Z., Fuel, **69**, 754, (1990).
11. Carangelo, R.M., Solomon, P.R. and Gerson, D.J., Fuel, **66**, 960 (1987).
12. Whelan, J.K., Solomon, P.R., Deshpande, G.V., and Carangelo, R.M., Energy and Fuel, **2**, 65, (1988).
13. Solomon, P.R., Serio, M.A., Carangelo, R.M., Bassilakis, R., Gravel, D., Baillargeon, M., Baudais, F., and Vail, G., Energy & Fuel, (1990).
14. Symposium on Phenolic Resins, Parts I and II; Rept. Org. Coatings and Plastic Chem., **26**, 85, (1966); and **27**, 84, (1967).
15. Monographs in Macromolecular Chemistry: Thermal Stability of Polymers, (R. Conley, Ed.), Marcel Dekker, Inc., New York, 1970, Volume 1.
16. Yamashita, Y. and Ouchi, K., Carbon, **19**, 89, (1981).
17. Honda, H. and Sanada, Y., Fuel, **36**, 403, (1957).
18. Shulman, G.P. and Lochte, H.W., J. Appl. Polymer Sci., **10**, 619, (1966).
19. Ouchi, K. and Honda, H., Fuel, **38**, 429, (1959).
20. Jackson, W.M. and Conley, R.T., J. Appl. Polymer Sci., **8**, 2163, (1964).
21. Conley, R.T. and Bieron, J.F., J. Appl. Polymer Sci., **7**, 103 and 171, (1963).
22. Conley, R.T., J. Appl. Polymer Sci., **9**, 1117, (1965).
23. Lochte, H.W., Strauss, E.L., and Conley, R.T., J. Appl. Polymer Sci., **9**, 2799, (1965).
24. Ouchi, K., Carbon, **4**, 59, (1966).
25. van Krevelen, D.W., Coal, Elsevier, Amsterdam, 1961.
26. Suuberg, E.M., Wojtowicz, M., and Calo, J., 22nd Symposium (Int) on Combustion, The Combustion Institute, 1988, pg. 79.
27. Suuberg, E.M., Calo, J.M., and Wojtowicz, M., ACS Div. of Fuel Chem. Preprints, **31**(3), 186, (1986).
28. Wojtowicz, M., Ph.D. Thesis, Brown University, (1988).
29. Wolfs, P.M., van Krevelen, D.W., and Waterman, H.I., Fuel, **39**, 25, (1960).
30. St. John, G.A., Butrill, Jr., S.E. and Anbar, M., ACS Symposium Series, **71**, p. 223, (1978).
31. Green, T.K., Kovac, J., and Larsen, J.W., Fuel, **63**, 935, (1984).
32. Green, T.K., Kovac, J., and Larsen, J.W., In Coal Structure, (R.A. Meyers, Ed.), Academic Press, NY, 1982.
33. Serio, M.A., Solomon, P.R., Charpenay, S., Yu, Z.Z., and Bassilakis, R., ACS Div of Fuel Chem. Preprints, **35**(3), 808, (1990).
34. van Krevelen, P.W., Chimia 1974, **28**, 504.
35. Solomon, P.R., Serio, M.A., Deshpande, G.V., and Kroo, E., Energy & Fuels, **4**(1), 42, (1990).
36. Serio, M.A., Charpenay, S., Bassilakis, R., and Solomon, P.R., "A Statistical Network Model for Polymer Degradation", Final Report under NSF Grant No. ISI-8961476, (October 1990).

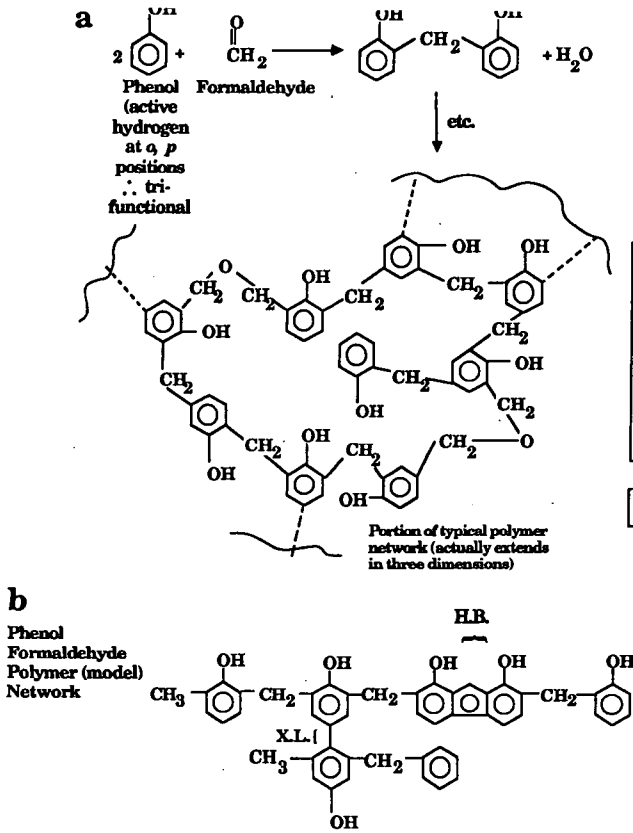

Figure 1. Phenol-Formaldehyde Structures.

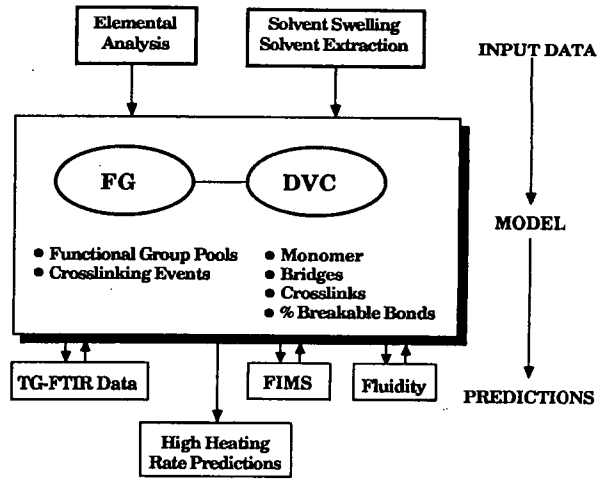

Figure 2. Structure of FG-DVC Model and Major Inputs and Outputs.

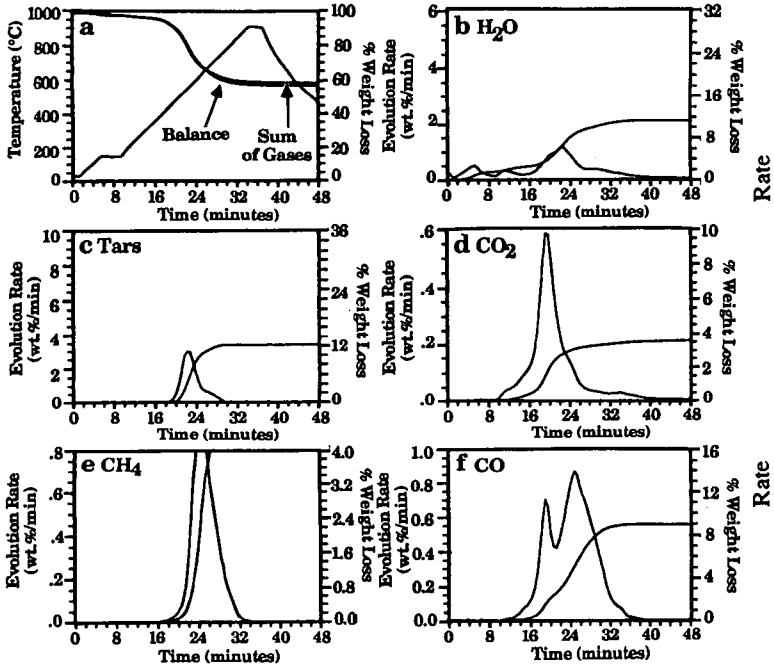

Figure 3. TG-FTIR Analysis of Phenol-Formaldehyde at 30°C/min.

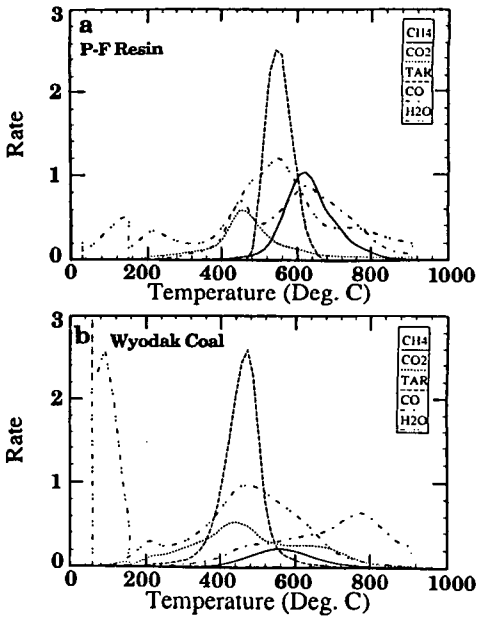

Figure 4. Composite TG-FTIR EvolutionPlots for a) Phenol-Formaldehyde Resin; b) Wyodak Subbituminous Coal.

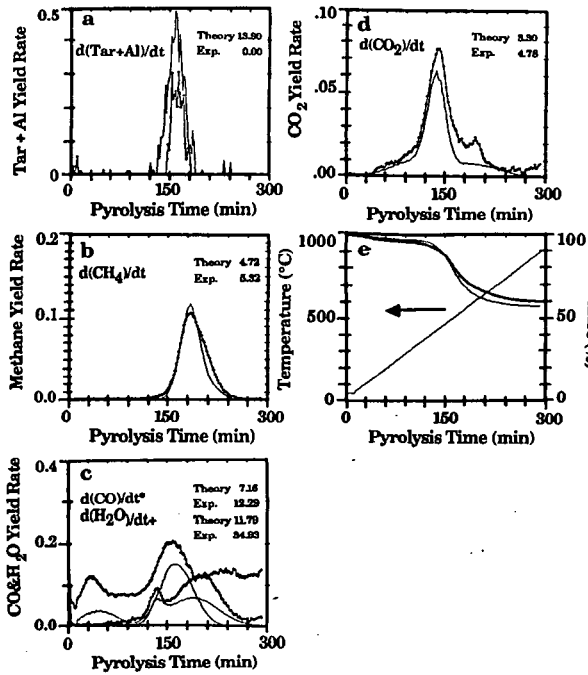

Figure 5. Comparison of FG-DVC Model Predictions (solid lines) with Pyrolysis Data (at 3°C/min) for Phenol-Formaldehyde Resin. Case 1.

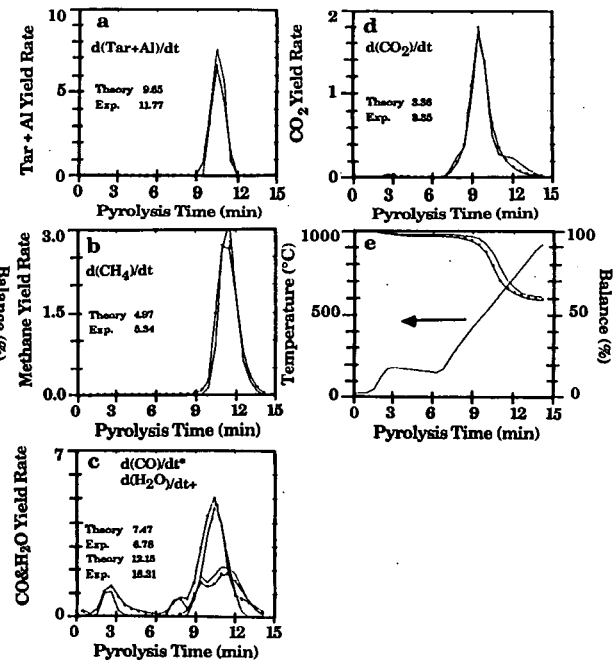

Figure 6. Comparison of FG-DVC Model Predictions (solid lines) with Pyrolysis Data (at 100°C/min) for Phenol-Formaldehyde Resin. Case 1.

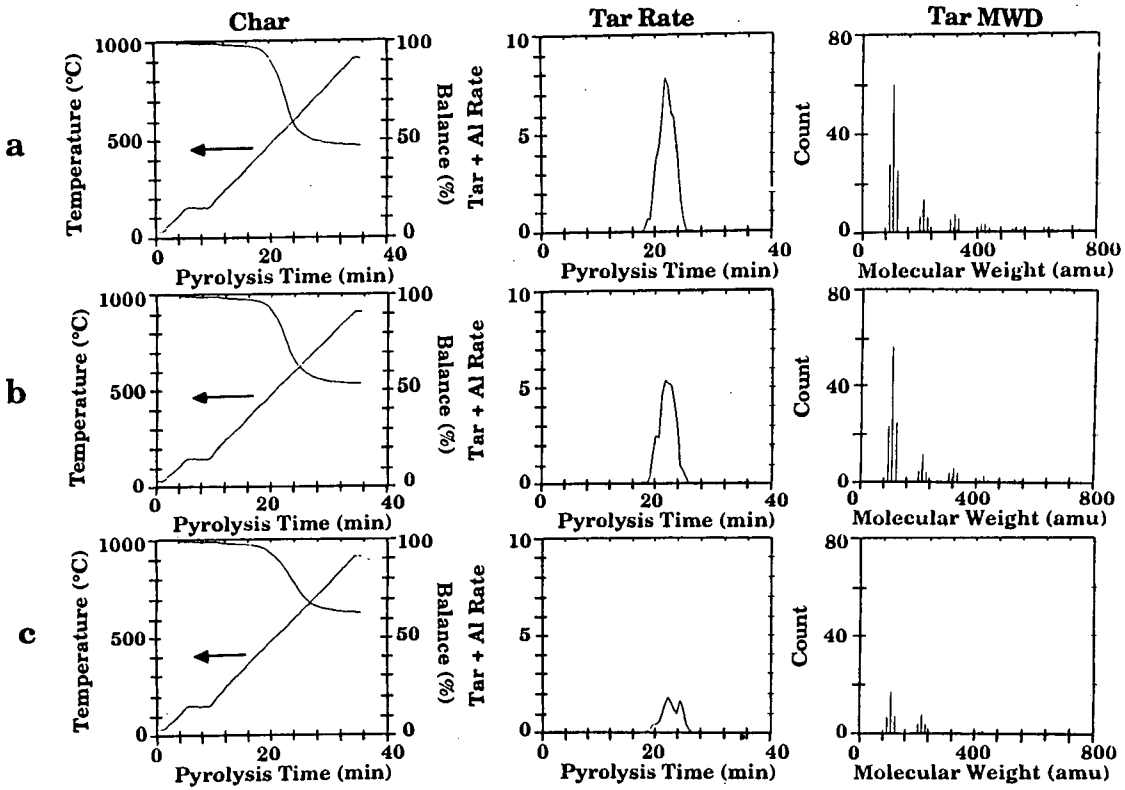

Figure 7. Simulation of Results for Weight Loss, Tar Evolution Rate and Tar Molecular Weight Distribution for Three Different Initial Crosslink Densities. a) 50 Crosslinks; b) 150 Crosslinks; c) 450 Crosslinks.

Thermolysis of 2,2-Diphenylpropane and 4-Cumyl Phenol

Concetta LaMarca, Cristian Libanati and Michael T. Klein*
Robert J. Cotter[1] and Stephen M. Andrews[1]

Center for Catalytic Science and Technology
Department of Chemical Engineering
University of Delaware
Newark, DE 19716

KEYWORDS: polymer, pyrolysis, model compounds.

ABSTRACT

The thermal reactivity of 2,2-diphenylpropane is relevant to the stability of a broad class of polymers which are made using bisphenol A. Consequently, the pyrolysis of 2,2-diphenyl propane and 4-cumyl phenol, its analog containing a hydroxy substituent, have been studied at 450 and 500°C. 2,2-DPP is observed to react to 1,1-diphenylethane, 1,1-diphenylethylene, toluene, ethylbenzene, 2-phenyl propene diphenylmethane, benzene and cumene. 4-Cumyl phenol reacts to an analogous spectrum of products, but at faster reaction rates indicating activation by the hydroxy substituent. A free-radical mechanism consistent with experimental results has been proposed herein together with the associated rate parameters for elementary steps.

INTRODUCTION

Polymer thermal stability is important for purposes of recycling and in regards to degradation during end-use applications and high temperature processing. A broad class of these polymers (e.g., polycarbonate, polysulfone, polyarylate, polyetherimide) are prepared using bisphenol A, and therefore the thermal reaction of materials containing this moiety are of interest.

This reactivity can be probed directly in experiments with the polymeric materials themselves. Theseexperiments can provide much relevant but system-specific information. A second, complementary approach is in experiments using pure component, model compounds, which provide a great deal of fundamental information about the reaction pathways, kinetics and mechanisms. This information can be used in the prediction of the reaction of polymeric materials beyond the range of experiments with the actual polymers.

In this work we follow the second tact to study the reactivity of materials containing the isopropylidene linkage. We present results of pyrolysis experiments of 2,2-diphenylpropane [2,2-DPP] and its hydroxy substituted analog, 4-cumyl phenol [4-CP].

The reaction pathways and kinetics of 2,2-diphenylpropane have not been thoroughly studied. Previous experimental work [1] indicates the bond homolysis activation energy as E_a=65.7 kcal/mol and $log_{10}A$=15.7. Pryor, Gleicher and Church [2] studied ring ozonation of 2,2-DPP at 25°C. Duty, Geier and Harwood [3] demonstrated resistance of 2,2-DDP to oxidation by dichromate when reacted in an aqueous solution at 250°C and 18 hrs. Schanne and Haenel [4] used potassium to cleave the phenyl ring to form benzene and 2-phenylpropane by what they propose to be a radical ion mechanism. Golden [5] irradiated 2,2-DPP at 1000 megarads using electron beam radiation. The reaction products were primarily methane and hydrogen, with little CO, CO_2 and hydrocarbon gases found.

Herein we extend this previous literature through more comprehensive study of the reaction pathways, kinetics and mechanisms for the pyrolysis of 2,2-diphenylpropane and 4-cumyl phenol.

EXPERIMENTAL SECTION

2,2-DPP and 4-cumyl phenol were pyrolysed at 450°C and 500°C for batch holding times of 2-120 min. Initial concentrations were nominally 60 mM.

[1] Amoco Performance Products, Inc., Research & Development Center, 4500 McGinnis Ferry Rd., Alpharetta, GA 30202-3944

Materials

2,2-DPP was obtained from Aldrich and subsequently distilled and collected at 113–117°C and 3 mm Hg. 4-Cumyl phenol was obtained from Aldrich and recrystallized before use. Dibenzyl ether, used as an external standard for GC analysis, was obtained from Aldrich. Gold band ampules (Wheaton) were used to fabricate batch reaction vessels.

Procedure

The reactors were loaded by weight with a typical charge of 25 mg of reactant. One reactor was prepared for each desired reaction time. The ampules were purged with argon to avoid oxidation and then immediately sealed using a propane/O_2 flame. These reactions were then immersed into a constant-temperature, fluidized sand bath (Techne) for the desired reaction time. The reaction was quenched by immersion in a cold, room-temperature fluidized sand bath. Reactors were checked for leaks by weighing both before and after reaction.

Reactant conversion and product yields were quantified by use of the external standard, dibenzyl ether, added to the reaction mixture after reaction. All materials were then recovered in methylene chloride. Analysis was performed by GC (Hewlett-Packard 5880) equipped with an FID to quantify yields and GC/MSD (Hewlett-Packard 5890 GC/H-P 5970 MSD) to identify products.

RESULTS AND DISCUSSION

2,2-Diphenylpropane pyrolysis at 450°C was at holding times ranging from 2.0–120.0 minutes; reaction at 500°C was for holding times ranging from 5–60 min. The detailed product spectrum, shown in Table 1 as product molar yields vs. time, includes benzene, toluene, ethylbenzene, styrene, cumene, 2-phenylpropene, 1,1-diphenylethane, 1,1-diphenylethene and diphenylmethane. At 450°C, a 32% conversion of 2,2-DPP was observed at 120 min, where the products in most significant yields were 1,1-diphenylethane and 1,1-diphenylethene, followed by benzene, toluene and ethyl benzene.

The Delplot technique [6] is a data analysis approach which reveals reaction path information allowing discrimination between primary, secondary and higher order products. For example, in a first-rank Delplot, product selectivity (yield/conversion) is examined as a function of conversion. In extrapolation to zero conversion, primary products have finite y-intercepts, while that for higher order products goes to zero. In a second-rank Delplot (yield/conversion^2 vs. conversion), primary products diverge as $\chi \rightarrow 0$, while secondary products have finite intercepts.

First-rank Delplots for 2,2-DPP pyrolysis at 450°C indicate that all products except diphenylmethane, toluene, ethyl benzene and styrene were clearly primary. Delplots for 2,2-DPP pyrolysis at 500°C suggest all products but diphenylmethane to be primary. This may indicate that at 500°C the intermediates that lead to toluene, ethyl benzene and styrene may be very short lived.

4-Cumyl phenol was pyrolysed at both 450 and 500°C to final holding times of 101 and 60 min, respectively. Table 2 summarizes the reaction products, namely benzene, toluene, ethyl benzene, cumene, phenol, 2-phenyl propene, methylpropyl benzene, 4-methyl phenol, 4-ethyl phenol, 4-hydroxy diphenylmethane, 4-hydroxy-(1,1-diphenylethane) and 4-hydroxy-(1,1-diphenylethene). These are analogous to the products observed from 2,2-DPP pyrolysis. 4-hydroxy diphenylethane and 4-hydroxy diphenylethene were observed in the highest yields, with relatively large amounts of phenol. The first-rank Delplots for 4-cumyl phenol pyrolysis at 500°C suggest most products to be primary with the exception of methylpropyl benzene, 4-ethyl phenol and hydroxydiphenylmethane.

The foregoing information suggests the 2,2-DPP and 4-CP pyrolysis pathways to be straightforward. Primary pyrolysis provides most of the products, with secondary reactions accounting for only diphenylmethane (for 2,2-DPP) and methylpropyl benzene, 4-ethyl phenol, and hydroxy diphenylmethane (for 4-CP). Pseudo-first-order rate constants for the reaction of both 2,2-DPP and 4-cumyl phenol to their primary products are shown in Table 3. The suggested Arrhenius parameters (two temperatures only) for primary 2,2-DPP pyrolysis are also listed in Table 3. 4-Cumyl phenol pyrolysis was much faster than that of 2,2-DPP. For example, for reaction at 500°C and 60 min, the 4-cumyl phenol conversion was 93%, whereas only 80% conversion was observed for 2,2-DPP.

A set of elementary steps consistent with the observed product spectra is shown in Figure 1. For 2,2-DPP, initiation by unimolecular decomposition can proceed through fission of two different bonds, leading to

the production of either methyl and diphenyl ethyl radicals (which subsequently become methane and 1,1-diphenylethane following hydrogen abstraction) or to phenyl and isopropyl benzene radicals (similarly leading to benzene and cumene). The former is expected to be more facile since the controlling bond dissociation energy is ~66 kcal/mol, 14 kcal/mol lower than that of ~80 kcal/mol for the latter. Propagation is by hydrogen abstraction by any radical from 2,2-DPP. The thus-derived 2,2-DPP radical has two β-scission pathways available. One leads to a methyl radical and diphenylethene and has a lower heat of reaction than the second, leading to a phenyl radical and 2-phenyl propene. A thermodynamically favorable phenyl shift can ultimately lead to toluene and ethyl benzene. Termination is by combination of any two radicals. An analogous set of steps could lead to the observed 4-CP products.

In summary, the structure and thus-derived thermochemical properties of 2,2-DPP and 4-CP control their pyrolysis activity. No evidence for a significant kinetic chain was found. The main products all appear to be primary and are explained nicely by elementary steps in strict accord with thermochemical estimates.

ACKNOWLEDGEMENT

The authors gratefully acknowledge financial support from Amoco Performance Products, Inc. We are also thankful for the laboratory assistance of Ken Crovetto and Wendy Rise.

REFERENCES

1. Robaugh, D. A. and S. E. Stein. "Stabilities of highly conjugated radicals from bond homolysis rates". *J. Am. Chem. Soc.*, **1986**, *108*, 3224–3229.

2. Pryor, W. A., G. J. Gleicher, and D. F. Church. "Relative reactivities of alkylbenzenes and related compounds toward ozone. The mechanism of ozonation at benzylic positions." *J. Org. Chem.*, **1984**, *49*, 2574–2578.

3. Duty, R. C., M. Geier and J. Harwood. "Precursors to aromatic units in coal." *Fuel*, **1985**, *64*, *March*, 421–423.

4. Schanne L. and M. W. Haenel. "Cleavage of carbon-carbon-bonds by solvated electrons." *Tetrahedron Letters*, **1979**, *44*, 4245–4248.

5. Golden, J. H. "Degradation of Polycarbonates II. Effect of radiation on model compounds." *Die Makromoleckulare Chemie*, **1963**, *66*, 73–81.

6. N. A. Bhore, M. T. Klein and K. B. Bischoff. "The Delplot technique: a new method for reaction pathway analysis." *Ind. Eng. Chem. Res.*, **1990**, *29*, 313–316.

Table 1 - Product Molar Yields for Pyrolysis of 2,2-Diphenylpropane
Reaction at 450°C

Time (min)	0.00	2.00	5.00	10.00	15.00	20.00	30.00	45.00	60.00	120.00
2,2-DPP	1.0000	0.9715	1.0157	0.9604	0.9932	0.9124	0.9106	0.8427	0.8121	0.6812
Benzene	0.0000	0.0005	0.0012	0.0047	0.0067	0.0079	0.0094	0.0102	0.0125	0.0130
Toluene	0.0000	0.0004	0.0006	0.0027	0.0067	0.0104	0.0160	0.0202	0.0253	0.0383
Ethylbenzene	0.0000	<0.0001	<0.0001	0.0018	0.0042	0.0067	0.0103	0.0132	0.0173	0.0245
Styrene	0.0000	<0.0001	<0.0001	0.0006	0.0012	0.0018	0.0026	0.0032	0.0043	0.0052
Cumene	0.0000	<0.0001	0.0008	0.0026	0.0033	0.0037	0.0043	0.0046	0.0056	0.0060
2-PhenylPropene	0.0000	0.0004	0.0010	0.0032	0.0044	0.0051	0.0057	0.0061	0.0080	0.0071
DiPEthane	0.0000	0.0002	0.0017	0.0068	0.0122	0.0175	0.0262	0.0367	0.0542	0.0931
DP Ethylene	0.0000	0.0003	0.0014	0.0063	0.0124	0.0191	0.0295	0.0419	0.0668	0.0990
DPM	0.0000	<0.0001	0.0002	0.0003	0.0007	0.0009	0.0015	0.0021	0.0030	0.0073

Reaction at 500°C

Time (min)	0.00	5.00	15.00	45.00	60.00
2,2-DPP	1.0000	0.8872	0.6547	0.3302	0.2020
Benzene	0.0000	0.0131	0.0185	0.0237	0.0278
Toluene	0.0000	0.0176	0.0419	0.0823	0.1067
Ethylbenzene	0.0000	0.0122	0.0238	0.0393	0.0445
Styrene	0.0000	0.0035	0.0069	0.0107	0.0115
Cumene	0.0000	0.0061	0.0070	0.0087	0.0093
2-PhenylPropene	0.0000	0.0098	0.0120	0.0116	0.0109
DiPhenylEthane	0.0000	0.0334	0.0983	0.2070	0.2487
DP Ethylene	0.0000	0.0403	0.1274	0.2359	0.2582
DPM	0.0000	0.0013	0.0083	0.0414	0.0730

Table 2 - Product Yields for Pyrolysis of Cumyl Phenol
Reaction at 450°C

time/min	0.00	2.00	5.00	10.00	20.00	47.58	60.00	101.02
Cumyl Phenol	1.0003	0.8909	0.8753	0.8217	0.7247	0.614	0.5636	0.4699
benzene	0.0157	0.0150	0.0154	0.0157	0.0164	0.0191	0.0193	0.0242
toluene	0.0004	0.0009	0.0020	0.0043	0.0086	0.0183	0.0219	0.0402
et. benzene	0.0000	0.0003	0.0013	0.0031	0.0061	0.0129	0.0155	0.0297
cumene	0.0000	0.0015	0.0038	0.0076	0.0122	0.0232	0.0279	0.0469
phenol	0.0000	0.0030	0.0059	0.0148	0.0211	0.038	0.0472	0.0834
2pp	0.0000	0.0062	0.0088	0.0163	0.0197	0.0251	0.0283	0.0369
4mp	0.0000	0.0003	0.0012	0.0030	0.0062	0.0127	0.0154	0.0272
4ep	0.0000	<0.0001	0.0008	0.0024	0.0055	0.0113	0.0132	0.0218
HDPM	0.0000	<0.0001	<0.0001	<0.0001	0.0007	0.0029	0.0049	0.0124
hdpethane	0.0000	0.0005	0.0044	0.0108	0.0214	0.0493	0.0681	0.1145
hdpethene	0.0000	0.0014	0.0063	0.0159	0.0329	0.0594	0.0707	0.0825

Reaction at 500°C

time/min	0.00	5.00	15.00	30.00	45.00	60.00
Cumyl Phenol	1.0000	0.8222	0.5018	0.2472	0.1570	0.0665
benzene	0.0000	0.0020	0.0043	0.0068	0.0092	0.0127
toluene	0.0000	0.0085	0.0226	0.0429	0.0574	0.0852
et. benzene	0.0000	0.0058	0.0148	0.0303	0.0448	0.0665
cumene	0.0000	0.0109	0.0235	0.0352	0.0572	0.0569
phenol	0.0000	0.0148	0.0407	0.0760	0.1380	0.1737
2pp	0.0000	0.0178	0.0315	0.0398	0.0565	0.0536
methpropbenz	0.0000	0.0021	0.0022	0.0028	0.0036	0.0038
4mp	0.0000	0.0062	0.0164	0.0307	0.0354	0.0512
hdpethane	0.0000	0.0329	0.0859	0.1400	0.1405	0.1390
hdpethene	0.0000	0.0621	0.1390	0.1614	0.1387	0.1380

Table 3: Reaction Pathway Parameters; 2,2-Diphenylpropane and 4-Cumyl Phenol

a) 2,2-Diphenylpropane

Reactant/Product	k_1(450°C) [/min]	k_1(500°C) [/min]	E_a [kcal/mol]	$\log_{10} A$
DPP	3.31E-03	2.61E-02	45.8	9.6
Benzene	1.86E-04	9.82E-04	37.0	9.2
Toluene	4.23E-04	3.33E-03	45.9	8.7
Ethyl Benzene	2.75E-04	1.53E-03	38.1	6.2
Styrene	6.94E-05	4.00E-04	38.9	5.8
Cumene	8.06E-05	6.16E-05		
2-Phenyl Propene	1.10E-04	4.21E-06		
1,1-DP Ethane	9.38E-04	8.02E-03	47.7	9.6
1,1-DP Ethene	1.04E-03	8.82E-03	47.5	9.6

a) 4-Cumyl Phenol

Reactant/Product	k_1(450°C) [/min]	k_1(500°C) [/min]	E_a [kcal/mol]	$\log_{10} A$
4-Cumyl Phenol		4.46E-02		
Benzene		1.07E-08		
Toluene		3.70E-03		
Ethyl Benzene		6.40E-04		
Cumene		2.98E-04		
Phenol		6.60E-03		
2-Phenyl Propene		2.82E-03		
4-Methyl Phenol		2.45E-03		
4-Hydroxy(1,1-DP Ethane)		6.24E-03		
4-Hydroxy(1,1-DP Ethene)		7.58E-03		

Figure 1
Elementary Steps for Reaction of 2, 2 - DPP

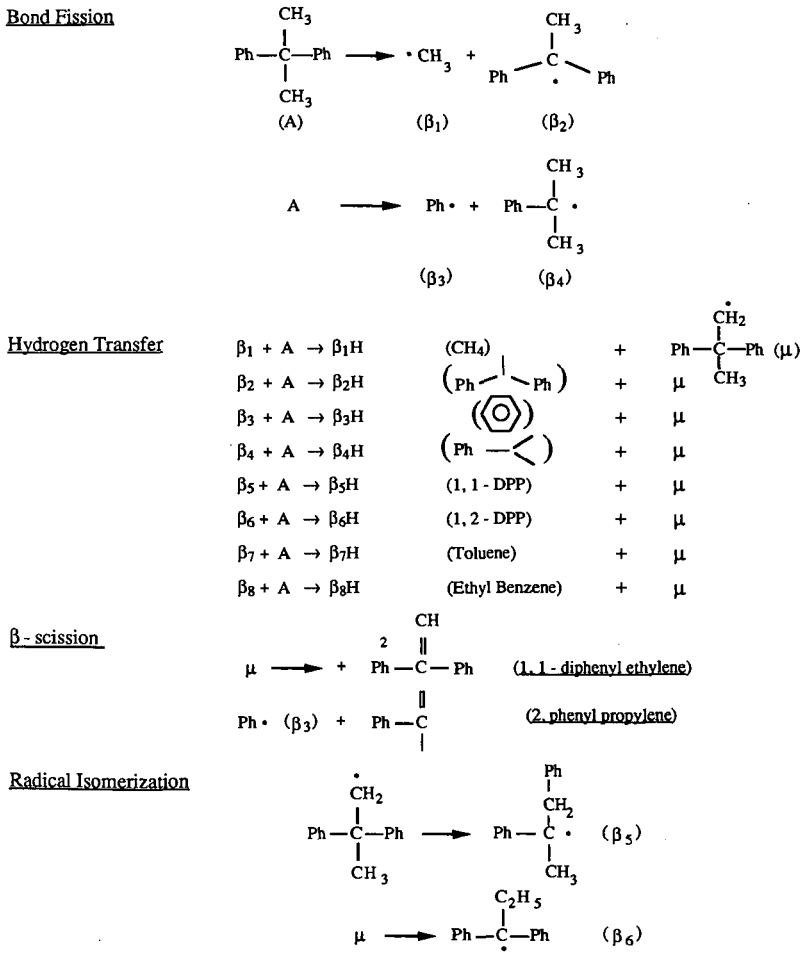

PYROLYSIS OF BIOMASS AND POLYMER MIXTURES - MUNICIPAL SOLID WASTE AS AN EXAMPLE

Wei-chuan Lai and Prof. Barbara Krieger-Brockett
Chemical Engineering, University of Washington
Benson Hall BF-10, Seattle, WA 98195.

Keywords: refuse-derived fuel, pyrolysis, heat transfer, composition and particle size effects

ABSTRACT

Incineration and thermal conversion of municipal solid waste are receiving considerable attention from both a political and scientific viewpoint. Polymers are present, both natural and manmade, representing about 80 weight % of the waste. Little quantitative reaction data is available and potential pollution problems have been identified when the polymeric mixtures contain chlorine and are reacted or incinerated at high temperature. The purpose of this work is to provide a quantitative basis for the engineering design of reactors to recover hydrocarbons from this waste. We have performed experiments under controlled conditions on a reasonably well-characterized "model" for municipal solid waste, that is, commercially available densified refuse-derived fuel (d-RDF), made by sorting, drying and compressing municipal solid waste. The resulting relatively uniform composition and density pellets have, however, low thermal conductivity, making the apparent reaction rate limited by the local heat transfer rate. This pyrolysis study employs single, "macro"-particle experiments where particle non-isothermality can be measured and its effect on product slate can be understood. A variety of polymeric substrates as well as commercial RDF have been heated under well-controlled conditions spanning those of industrial importance. The devolatilization behavior, such as time-temperature history and evolved gas composition, has been measured in detail. The results have been used to develop correlations applicable to reactor design and pollution control. Specialized statistical methods are used to quantify the contribution of a single mixture constituent to pyrolysis behavior. Conclusions from the experiments have aided in the development of a mathematical model of the devolatilization process and have increased our understanding of the role of reactant composition, as well as particle mass and heat transfer, during gasification and combustion.

INTRODUCTION

The ongoing work described in this preprint is a portion of a study (1) of the transport rates and chemical reaction behavior during thermal conversion of a particular form of muncipal solid waste (MSW), namely densified refuse-derived fuel (d-RDF). It is made commercially by removing recyclables and non-combustibles, drying and compressing the remaining mixture (manmade and natural polymers as well as other materials) into pellets of relatively uniform size and density (~1-2 cm diameter, 2-3 cm long cylinders, specific gravity between 1 and 2). The resulting material is considerably more compact, has approximately the heating value of coal, and can be economically transported to a central site for thermal conversion. It is envisaged that this central site could then be expected to have a larger, more advanced design thermal conversion process with potentially the flexibility to optimize certain products, and certainly the capability of pollution control and monitoring.

While some work has been performed on d-RDF and MSW (1-3), it remains to be determined what reaction conditions optimize particular products, what are the effects of pellet moisture, size and density on conversion rate and products, and in particular, what changes in the waste stream polymeric mixture result in desirable or undesirable pyrolysis products. Reactor design will require devolatilization kinetics data on the d-RDF constituents, and a knowledge of whether constituents co-react when confined to the interior of the relatively non-porous particle of d-RDF, or whether the constituents react independently. By studying the behavior of single particles as in other studies (4), we can direct the efforts in mathematical modeling of the pellet behavior, provide a basis for judging adequate kinetic models, and make suggestions regarding appropriate reactor configurations.

EXPERIMENTAL ASPECTS

The experimental apparatus consists of a single particle reactor which allows determination of particle temperature and gas evolution history, heat transfer rates, and total product analysis. It is described elsewhere (1,5). The d-RDF compositions studied span the range found in practice (Table 1) as interpreted by the standard deviation of the 10 composition studies available in the recent literature. To

understand the role of composition, laboratory-fabricated pellets as well as commercial pellets are studied under the well-controlled reaction conditions likely to occur in industrial practice (Table 2).

As in other studies where sample size must remain constant while composition is changed, in this study the weight fractions of waste constituents sum to unity, making the composition variables correlated and the interpretation of results ambiguous unless special experimental designs and biased regression methods are employed. Consider a 1 gram sample of say 4 equal concentration components (25% by weight). Its reaction behavior is to be compared to another 1 gram sample (so sample temperature history remains constant) with a different composition. In the second sample, it is desired to determine the pyrolysis product slate change when one of the constituents is reduced to say 10% by weight. Owing to the constant sample size, this change necessitates that one of the other constituents make up the remaining 15%. Changes in behavior cannot be unambiguously attributed to a reduction in the former, but rather to either a reduction in the former or increase in the latter constituent. This difficulty is lessened when one constituent predominates as in the case of paper-like components of MSW. In Table 1 it can be seen that components 1-4, 7, and perhaps 6 can be approximated by paper such as newsprint with a lignin content close to that of native wood . Daugherty et al. (6) have studied the stability of d-RDF with respect to biological degradation and long term integrity of the pellets. They found a well-behaved d-RDF pellet can be made when $Ca(OH)_2$ is used as a binder comprising approximately 1-8% by weight. The binder is similar to the inorganic material that accompanies the combustible fraction in actual MSW. For a number of reasons (1), we were able to justify reducing the composition classes in d-RDF to four: paper as exemplified by newsprint, plastics as equal fractions PVC and polyethylene, non-combustibles as exemplified by metal and glass, and inorganic substances as exemplified by binder. The ranges over which these four components were varied are shown in Table 2. The combination of compositions and reaction conditions actually run in our experimental program was a special mixture design (1,7), and ridge regression as well as other biased regression methods were used to calculate the effects of composition changes.

The procedure consists of heating the sample one-dimensionally with a constant radiative heat flux for a fixed pyrolysis time of 12 min. The constant heating time can be rationalized as analogous to the constant time-at-temperature (residence time) a particle experiences in a moving bed reactor. Particle size is varied as are initial particle moisture, composition, and the intensity of the heat flux, all in systematic combinations dictated by the experimental design (1,7). During the pyrolysis, time-temperature profiles are measured at several depths (Fig. 1) and gas evolution rate and composition are also measured as functions of time (Fig. 2). Hydrocarbons are measured as well though only carbon oxides and total gas yield are shown in Fig. 2. The overall pyrolysis product yields are measured as integrated batch yields as well; Table 3 reports typical yields of interest for this paper. In addition, though not the subject of this paper, tar composition is measured in detail as are char surface area and composition by FTIR. To narrow the focus, this paper will concentrate on the composition history of the gases since it is seen to be an indicator of the pyrolysis chemistry occuring in the large, non-uniform temperature particle. The gas composition is measured semi-continuously using a computer controlled automatic sampling valve and a gas chromatograph.

RESULTS

The d-RDF pellets were pyrolyzed and the time-temperature histories (at 2, 6 and 9 mm into the particle) and gas flux histories are shown in Figs. 1 and 2 respectively. A temperature plateau at about 100°C can be seen to occur at interior thermocouple locations owing to the constant temperature evaporation of water as the heating front passes. The gases are released (Fig. 2) with the peak in the rate controlled by the heating rate applied at the surface, as well as the size and moisture content of the particle. Using data similar to Fig. 2, this paper will present a limited discussion on the comparison of pyrolysis behavior between d-RDF samples with high and low fractions of plastics.

Direct comparisons will be presented in which the only difference between 2 experiments is the fraction of plastics (the remainder being made up by paper (newsprint)). In these, it is useful to *subtract* the yields, or subtract the gas flux histories and report the difference as a function of time. That is, the data analogous to Fig. 2 for an experiment with low fraction plastics are subtracted from the data resulting when a high fraction plastics pellet is pyrolyzed. The *fractional* difference provides perhaps more insight when concentrations are small as in our pyrolyses, and this is shown in Figs. 3 and 4 for carbon oxides and hydrocarbons respectively (the low plastics result is the reference or denominator). Thus Figs. 3 and 4 report fractional difference in gas composition as a function of pyrolysis (reaction) time for the cases of high and low plastics content in d-RDF. It is important to keep in mind the sample-to-

sample variation expected in such a heterogeneous reactant and we have studied this by replicate experiments. For replicates, the difference between measured gas concentrations expressed as a fraction of one of them is less than approximately two-fold over the entire time interval; thus fractional concentration variations greater than 3 in Figs. 3 and 4 represent probable composition effects in the pyrolysis behavior. It can be seen that the hydrocarbons, especially C_2H_4 and CH_4, appear to be sensitive to the concentration of plastics. This is to be expected judging from the thermal degradation products measured for polymers (8-16).

The time-dependent pyrolysis behavior is to likely represent data with a high degree of noise or uncertainty in them. A more robust measurement, though revealing less kinetic and reaction information, is the comparison of overall (time-integrated) yields from a plastics-rich compared to a plastics-poor sample of d-RDF. In Table 4 are presented three direct comparisons of overall yields, and as before, the pyrolysis component concentrations in the product gas are subtracted for the two cases, and the result expressed as a fractional difference. The three direct comparisons represent different values of other experimental conditions. It can be seen in Table 3 that even replicate d-RDF (laboratory fabricated) pyrolyses exhibit variations in measured product concentrations of about 20%. Thus only differences in overall yields exceeding 25-30% in columns 5,9, and 13 (Table 4) can be interpreted as actual composition effects attributable to the high plastics content. This high a difference is observed for all gases except CO_2, and in some cases such as ethylene, the difference is over a 200% increase in yield in the product.

DISCUSSION

The composition effects presented here are direct comparison experiments, that is, only one pair of compositions is varied at a time. Other data (1) indicate that the magnitude of these enhanced pyrolysis product yields is dependent in a complex way on all the other reaction condition variables, namely particle size, initial moisture, heating rate experienced, and in particular, on the amount of inorganic material (binder) present. It is interesting to note that the experimentation to date, and the regression of the results indicate that the d-RDF constituents can be assumed to react independently. Current work is focused on mathematical modeling of the independent reactions, prediction of the effect of such a high moisture content as is typical of MSW (Table 1) and prediction of the coupled processes of heat transfer and reaction rate in the non-isothermal RDF particle.

Comparison to Pyrolysis of Polymers

It is well known that thermal degradation of Poly(vinyl chloride) (PVC) releases HCl. Hydrogen Chloride generation begins at temperatures as low as 130°C. Up to 99% of the chlorine contained in PVC is lost as HCl, with very little vinyl chloride monomer formed. In inert atmospheres, and at temperatures ranging from 160 to 700°C, more than 75 pyrolysis degradation products have been identified and they included olefinic hydrocarbons, benzene, toluene, xylenes, ethylbenzenes, aliphatic, naphthalenes, and methylated species. Sometimes condensed aromatics such as biphenyl and anthracene were also identified (13). Although many products have been identified, the major products of PVC pyrolysis were hydrogen chloride gas and benzene. In some cases, chlorinated compounds were also identified at higher temperatures; for example, ethylene chloride at 400°C, chlorobenzene, di- and trichlorobenzenes at 500-700°C, and vinyl and ethyl chloride at 550°C (14). For these reasons, we believe that HCL should have been produced in our RDF pyrolyses.

Degradation of polyethylene (PE) under varying oxidative conditions (500 -800°C) has also long been carried out. The products identified consisting of olefin and n-hydrocarbon with chain lengths of 8 to 23 carbons, in addition to lower molecular weight species such as acetaldehyde, acrolein and benzene (15). It was found that when oxygen in the gas stream was reduced, the amount of carbon dioxide product decreased and hydrocarbon production increased (16). These findings are consistent with our RDF pyrolyses in that (recall no oxygen is present) few hydrocarbons and relatively more condensible volatiles are in the product slates, consistent with the degradation of plastic components. Our carbon dioxide concentration is greater than from pure plastic degradation, attributable to the cellulose decarboxylation from the paper fraction in RDF.

Since HCl is highly soluble in water, HCl gas produced from pyrolysis of PVC is believed to be trapped in the cold tar trap in the form of hydrochloric acid. The trap tar sample collected was analyzed for water and low molecular weight tar components such as Methanol, Acetaldehyde, Acetone, and Acetic acid, by GC using a Supelco 80/100 mesh Porapak Q column. Using the same column, the

response to HCl was calibrated. Calibration results show that the retention time of HCl is 0.71 minute and therefore does not interfere in a major way with any other peak, but that the Porapak Q column is not sensitive enough to detect HCl unless it has a concentration of at least 3.65×10^{-6} g/µl in our sample. Due to this low HCl sensitivity, we detected no HCl in all our pyrolysis product samples. The HCl analysis is currently in progress.

ACKNOWLEDGMENTS
The authors would like to acknowledge the financial support of the Department of Energy through the Solar Energy Research Institute, Contract No. XK-7-07224-1.

REFERENCES

1) Lai, Wei-chuan, Ph.D. thesis, Dept. of Chemical Engineering, U. of Washington, 1991.
2) Levie, Benjamin Eli, Ph.D. Thesis, "Pyrolysis of Refuse Derived Fuel Pellets", University of Colorado, Dept. of Chemical Engineering, 1988.
3) Agrawal, Ravindra K., F. Gandhi, and R. J. McCluskey, "Low-Pressure Pyrolysis of Newsprint: Product Formation", J. of Analytical and Applied Pyrolysis, 6 (1984), 325-338.
4) Russel, W.A., Saville, D., and Greene, M.I., "Model for Short Residence Time Hydropyrolysis of Single Coal Particles," 1979 AIChE J., 25 65.
5) Chan, W. C. Ricky, Marcia Kelbon and B. Krieger-Brockett, "Single-Particle Biomass Pyrolysis: Correlations of Reaction Products with Process Conditions", Ind. Eng. Chem. Res., 27, 2261-2275 (1988).
6) Daugherty, K. E., O. Ohlsson, A. Safa, and B. J. Venables, "Densified Refuse Derived Fuel as a Power Source", Proceedings of the American Power Conference, 45, pp 930-935, 1986.
7) Cornell, John A., Experiments with Mixtures (Designs, Models, and the Analysis of Mixture Data). Second Edition. N.Y.: John Wiley & Sons, Inc. (1990).
8) Hodgkin, J. H., M. N. Galbraith, and Y. K. Chong, "Combustion Products from Burning Polyethylene", J. of Macromol. Sci. - Chem., A17(1), 35-44 (1982).
9) Iida, Takeo, Motoharu Nakanishi, and Kunio Goto, "Investigations on Poly(vinyl Chloride). II. Pyrolysis of Chlorinated Polybutadienes as Model Compounds for Poly(vinyl Chloride)", J. of Polymer Science: Polymer Chemistry Edition, 13, 1381-1392 (1975).
10) Ishihara, Yumiko, Hidesaburo Nanbu, Tadashi Ikemura, and Tomoyuki Takesue, "Catalytic Decomposition of Polyethylene Using a Tubular Flow Reactor System", Fuel, 69, 978-984 (1990).
11) Khalturinskii, N. A., "High-Temperature Pyrolysis of Polymers", J. of Thermal Analysis, 32 (1987), 1675-1682.
12) Mallya, Narayani and James E. Helt, "Effects of Feedstock Components on Municipal Solid Waste Pyrolysis", in Research in Thermochemical Biomass Conversion, edited by A. V. Bridgwater and J. L. Kuester, pp113-126, New York: Elsevier Applied Science,1988.
13) Chang, E. P. and R. Salovey, "Pyrolysis of Poly(vinyl Chloride)", J. of Polymer Science: Polymer Chemistry Edition, 12, 2927-2941 (1974)
14) Lattimer, Robert P. and William J. Kroenke, "The Formation of Volatile Pyrolyzates from Poly(vinyl Chloride)", J. of Applied Polymer Science, 25, 101-110 (1980)
15) Hodgkin, J. H., M. N. Galbraith, and Y. K. Chong, "Combustion Products from Burning Polyethylene", J. of Macromol. Sci. - Chem., A17(1), 35-44 (1982).
16) Boettner, E. A. and Gwendolyn L. Ball, "Combustion Products of Plastics and Their Contribution to Incineration Problems", in Chemical Engineering Applications in Solid Waste Treatment. Edited by Guy E. Weismantel. AIChE Symposium Series, No. 122, Vol. 68 (1972).

Table 1

MSW Composition, wt % (Analyses from 10 studies)

MSW Fraction:	Average	standard deviation
1. Paper	40.1	6.6
2. Yard Waste	13.7	5.1
3. Food Waste	11.5	4.7
4. Wood	3.1	1.1
5. Plastics	4.9	3.4
6. Rubber & leather	1.9	0.9
7. Textiles	2.1	0.8
Subtotal	77.3	2.5
8. Metal	9.5	1.7
9. Glass	9.9	1.6
10. Misc. Inorganics	3.3	2.6
Total	100.0	
Moisture Content	25.6	3.1

Table 2

Experimental Conditions Studied

	Symbol	Range			
Process variables					Comments
Heat flux	q	12.6×10^{-4}	to	21.0×10^{-4}	W/m^2
Moisture content	MC	5.0%	to	30.0%	dry basis
Particle thickness	L	1.0	to	2.0	cm
Composition variables					
Paper	X_1	0.57	to	0.95	weight fraction
Plastics	X_2	0.00	to	0.20	weight fraction
Metal/Glass	X_3	0.05	to	0.15	weight fraction
Binder	X_4	0.00	to	0.08	weight fraction

Table 3

Replicate Runs: Reaction Conditions and Integrated Gas Yields over Pyrolysis Time

	Replicates:			fractional difference
	Run 24	Run 25	difference	of Run 24
X1(PAPER)	0.76	0.76	0	
X2(PLASTICS)	0.1	0.1	0	
X3(MET&GLASS)	0.1	0.1	0	
X4(Binder)	0.04	0.04	0	
Q(cal/cm2-s)	4	4	0	
MC(%)	17.5	17.5	0	
L(CM)	1.5	1.5	0	
GAS(%)2	5.473	4.454	1.0187	19.%
CO(%)2	1.746	1.313	0.4322	25.%
CO2(%)2	3.135	2.830	0.3044	10.%
CH4(%)2	0.245	0.183	0.0621	25.%
C2H2(%)2	0.012	0.010	0.0017	14.%
C2H4(%)2	0.058	0.050	0.0081	14.%
C2H6(%)2	0.053	0.068	-0.015	-29.%
			average:	19.0%

Table 4

Integrated Gas Yields over Pyrolysis Time for Comparison Experiments: High Versus Low Plastics Content

	Hi/lo plastics comparison for experiments with high binder, low metal/glass content, and 2 cm thick				Hi/lo plastics comparison for experiments with low binder, high metal/glass content, and 2 cm thick				Hi/lo plastics comparison for experiments with high binder, low metal/glass content, and 1 cm thick			
	Run 18	Run 51	18-51	18-51 /51	Run 33	Run 21	33-21	33-21 /21	Run 54	Run 55	54-55	54-55 /55
X1(PA)	0.71	0.82	-0.102		0.70	0.81	-0.102		0.71	0.82	-0.102	
X2(PL)	0.15	0.05	0.102		0.15	0.05	0.102		0.15	0.05	0.102	
X3(M&G)	0.07	0.07	0		0.13	0.13	0		0.07	0.07	0	
X4(BI)	0.06	0.06	0		0.02	0.02	0		0.06	0.06	0	
Q	5	5	0		5	5	0		5	5	0	
MC(%)	5	5	0		5	5	0		5	5	0	
L(CM)	2	2	0		2	2	0		1	1	0	
GAS(%)2	6.91	7.83	-0.92	-12.%	5.85	8.42	-2.58	-31.%	10.66	12.27	-1.60	-13.%
CO(%)2	1.62	1.88	-0.26	-14.%	1.62	2.61	-1.00	-38.%	2.36	2.92	-0.56	-19.%
CO2(%)2	4.63	5.56	-0.93	-17.%	3.36	5.12	-1.76	-34.%	7.69	8.74	-1.05	-12.%
CH4(%)2	0.31	0.21	0.09	45.%	0.20	0.36	-0.17	-46.%	0.32	0.41	-0.09	-21.%
C2H2(%)2	0.01	0.01	-0.002	-20.%	0.02	0.02	0.003	20.%	0.02	0.01	0.01	56.%
C2H4(%)2	0.16	0.05	0.11	238.%	0.05	0.10	-0.05	-52.%	0.09	0.09	-0.001	-1.%
C2H6(%)2	0.12	0.09	0.03	30.%	0.10	0.07	0.03	37.%	0.18	0.07	0.11	161.%

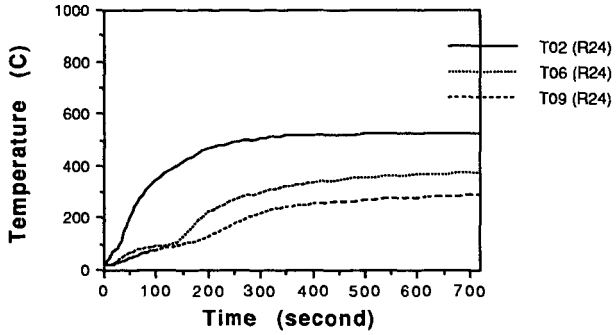

Fig. 1 - Time-Temperature Profiles at 3 different depths from the heated surface (average composition and reaction conditions, centerpoint of range studied, Run 24, conditions shown Table 3)

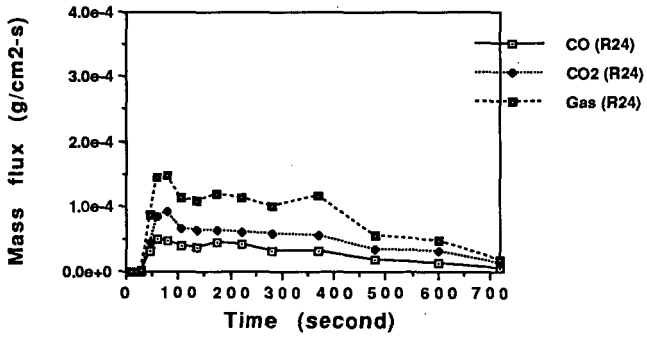

Fig. 2 - Gas Release Histories (Run 24) for Experimental Conditions shown in Table 3

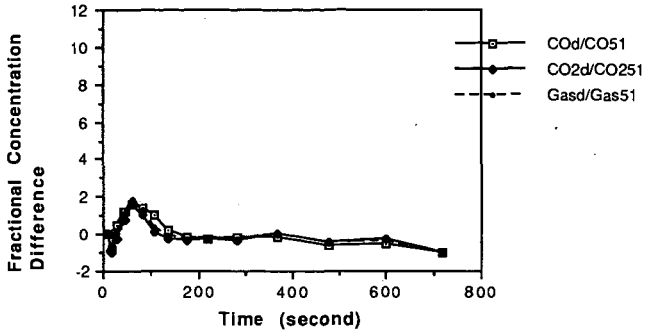

Fig. 3 - Difference in Carbon Oxide and Total Gas Concentration between two direct comparison Runs
(Runs 18 and 51) - Normalized by Concentrations in Run 51 (low plastics content)

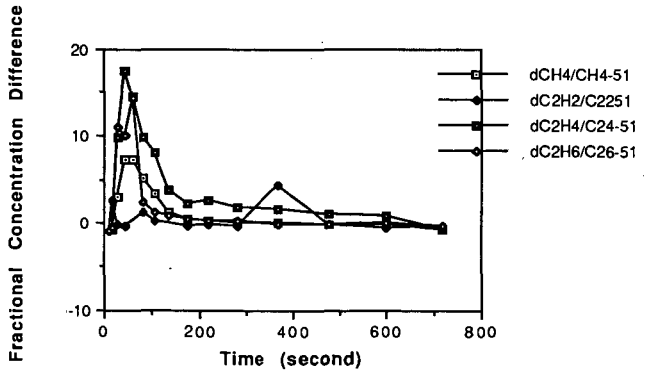

Fig. 4 - Difference in Hydrocarbon Gas Concentration between two direct comparison Runs
(Runs 18 and 51) - Normalized by Concentrations in Run 51 (low plastics content)

PY-GC-ION TRAP DETECTION OF SORGHUM GRAIN POLYPHENOLS (*syn.* VEGETABLE TANNINS): PRELIMINARY RESULTS

Guido C. Galletti
Centro di Studio per la Conservazione dei Foraggi - C.N.R.
via Filippo Re, 8
40126 Bologna, Italy

Keywords: pyrolysis-gas chromatography-ion trap detector mass spectrometry; polyphenol analysis; sorghum analysis.

ABSTRACT

Polyphenols (tannins) from sorghum grains with a high tannin content were analyzed by pyrolysis-gas chromatography-ion trap detector mass spectrometry (PY-GC-MS). Pyrolysis at 600 °C produced high relative percentages (around 50%) of catechol (1,2-dihydroxybenzene), and minor amounts of other phenolic compounds. Catechol was also the main fragment in the pyrogram of catechin (a monomeric unit of tannins). The absence of significant levels of catechol in the pyrogram of non-tannin polyphenols (such as lignin), and its relative lower abundance in that of low-tannin containing sorghum grains suggests the use of catechol as a remarkable characteristic fragment for quali- quantitative analysis of tannins by PY-GC-MS.

INTRODUCTION

Polyphenols (*syn.* vegetable tannins) can be divided into two classes, namely hydrolizable and condensed or non-hydrolizable tannins. The hydrolizable tannins are esters of mainly glucose with hydroxyphenolic acids such as gallic acid. The condensed tannins are polymers of flavanoid precursors such as catechin (scheme 1) (1).

Vegetable tannins influence the characteristics of many plant products - their taste, palatability, nutritional value, pharmacological and toxic effects, and their microbial decomposition - because of their ability to complex strongly with proteins, carbohydrates, nucleic acids, alkaloids and minerals (2,3,4).

Structure elucidation of monomeric and oligomeric (up to 5-6 units) procyanidins has been accomplished by ^{1}H- and ^{13}C-NMR (5), and Fast Atom Bombardment Mass Spectrometry (6). Classical methods for routine quantitative analysis have included colorimetric (7,8) and protein precipitation assays (9), but their validity has been questioned (10).

Tannins have been chromatographed by HPLC (11) and gel permeation (12). Gas chromatography (GC) is unfeasible due to their large molecular weight, polarity and thermal lability. However, molecules with these chemical features are in principle suitable to be degraded by pyrolysis (PY), an effective technique for the study of complex, non-volatile samples, which can be integrated with a gas chromatograph-mass spectrometer (PY-GC-MS) to provide a rapid analysis of the degradation products, and hence the characterization of the original sample.

This paper reports on the GC-MS analysis of the pyrolysis products of tannins isolated by gel permeation from sorghum grain, and of catechin as a reference compound. It is anticipated that these preliminary results indicate whether pyrolysis

can provide characteristic fragments of diagnostic significance for the recognition of the non-volatile tannins by gas chromatography without the need for off-line degradation and derivatization or mass spectrometry.

EXPERIMENTAL

Extraction and gel permeation.

A detailed procedure for tannin extraction and purification has been described elsewhere (12). Briefly, a 100-g sample of ground sorghum grain was defatted in Sohxlet with diethyl ether. The residue was transferred into a dark bottle and extracted overnight at +1 °C under rotary shaking with acetone (3x300 ml). The residue was extracted under the same conditions with methanol (3x300 ml). The methanolic extracts were combined and the solvent was distilled off under vacuum in a rotary evaporator (T: 35 °C). A 500-mg aliquot of this crude extract was suspended in methanol (7 mL) and the slurry was applied onto a column packed with Sephadex LH 20 (35x3 cm). The column was eluted at 2 mL/min (detection 340 nm) with 95% ethanol (800 mL) to remove some coloured non-phenolic substances, then with acetone/water (7/3, 640 mL) to collect the brown polyphenolic fraction retained at the top of the column. The acetone/water solvent was evaporated in rotary evaporator under reduced pressure (T: 40 °C). The tannin was dried over P_2O_5 and stored at - 25 °C until analysis.

Pyrolysis-gas chromatography-mass spectrometry (PY-GC-MS).

About 1 mg of tannin was pyrolyzed using a CDS Pyroprobe 100 equipped with a platinum coil probe and a quartz sample holder. Catechin was pyrolyzed by applying 10 µL of a methanolic solution (10 mg/mL) in the quartz tube. The pyrolyzer was interfaced with a GC-MS system consisting of a Varian 3400 gas chromatograph coupled to a Finnigan MAT Ion Trap Detector (ITD) model 800 mass spectrometer and operating under the following conditions: injector (split 1/120) at 220 °C; SPB-5 column (30 m x 0.32 mm i.d.) programmed from 50 to 300 °C at 10 °C/min (He: 1 mL/min); transfer line at 220 °C; mass spectra recorded at 70 eV under the usual ITD software release 4.0 conditions.

RESULTS AND DISCUSSION

Two sorghum grain commercial cultivars, i.e. Arval and Argence representative of high- and low tannin content, respectively, were used for the present work. According to the vanillin test (8), Arval tannin content was 5.30 (expressed as catechin equivalent percentage of original sample dry matter) and that of Argence was 0.10. Table 1 collects these figures, and the yields of crude extract and tannin after gel permeation expressed as percentage of original sample dry matter and crude extract, respectively.

The total ion chromatograms (TIC) of the Arval and Argence tannin fractions after pyrolysis at 600 °C are shown in figures 1 and 2, respectively. Table 2 collects the eight most abundant ions in the mass spectra of the main peaks. The identification proposed for most of the pyrolysis fragments is reported in table 3. The fragmentation under pyrolysis was similar for the two samples, but the quantitative analysis (relative percentages) was substantially different (table 3). Catechol (identified by both mass spectrometry and injection of pure standard) was the main fragment (55.4%) in the pyrogram of Arval tannin (fig. 1, peak no. 24), whereas it was only 4.58% in that of

Table 3. Relative percentage and proposed identification of the main pyrolysis peaks in the two sorghum tannins Arval and Argence.

#	Arval	Argence	Compound
1	9.00	14.15	carbon dioxide
2	trace	trace	unknown
3	0.82	-	acetone
4	5.28	6.88	unknown
5	6.47	17.40	propylacetate
6	5.95	-	3-methylfuran
7	0.56	4.75	2-furanol, tetrahydro-2,3-dimethyl
8	0.34	0.94	unknown
9	0.67	0.27	3-furaldehyde
10	0.94	1.42	pyridine
11	0.20	0.15	toluene
12	1.28	0.71	unknown
13	1.16	-	unknown
14	0.33	-	unknown
15	0.30	0.39	unknown
16	1.51	17.69	phenol
17	1.09	0.88	unknown
18	0.22	1.17	unknown
19	0.51	1.80	4-methylphenol
20	0.62	3.81	guaiacol
21	0.45	0.28	unknown
22	0.17	0.36	unknown
23	0.52	2.53	ethylphenol
24	55.4	4.58	catechol
25	0.10	7.06	2-ethenylphenol
26	7.25	1.89	dihydroxytoluene

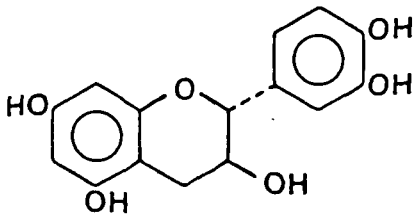

Scheme 1. Catechin (flavan-3-ol).

Table 1. Polyphenol estimation using the vanillin test (% of catechin equivalents (CE)), crude extract yield (% of original sample dry matter), and polyphenol yield (% of crude extract).

	CE	crude extract	polyphenol
Arval	5.30	2.40	43.0
Argence	0.10	1.81	3.4

Table 2. Eight-peak mass spectra of the pyrolysis fragments of Arval sorghum tannin.

#	scan	MW	m/z (%)							
1	142	44	44(100)	45(40)	43 (1)	-	-	-	-	-
2	147	-	43(100)	41(68)	42(38)	49(38)	45(36)	47(33)	48(30)	55(17)
3	151	58	58(100)	59(45)	42(44)	60(13)	44(12)	57(9)	40(7)	45(5)
4	155	-	43(100)	59(36)	42(13)	58(10)	41(4)	40(3)	44(3)	60(2)
5	169	102(0.2)	43(100)	61(25)	45(19)	42(15)	44(4)	41(1)	71(1)	59(1)
6	177	82	82(100)	53(91)	81(78)	50(43)	51(41)	52(18)	83(14)	54(12)
7	192	116	43(100)	75(12)	42(11)	57(7)	41(6)	44(6)	45(3)	40(2)
8	201	-	43(100)	45(58)	57(45)	74(34)	42(29)	73(27)	75(23)	41(22)
9	211	96	96(100)	95(94)	53(75)	51(56)	50(48)	43(39)	67(25)	52(22)
10	231	79	52(100)	79(91)	50(66)	43(62)	51(55)	80(37)	78(12)	53(11)
11	245	92	91(100)	92(50)	63(19)	65(18)	43(15)	41(11)	45(10)	50(10)
12	251	-	43(100)	85(25)	101(18)	100(14)	42(10)	45(4)	72(4)	44(3)
13	261	-	55(100)	43(60)	41(55)	83(48)	53(18)	42(17)	99(17)	98(13)
14	269	-	41(100)	55(76)	70(47)	43(36)	42(29)	69(25)	53(18)	56(12)
15	406	-	41(100)	53(53)	96(47)	42(44)	67(44)	55(38)	69(34)	81(34)
16	417	94	94(100)	66(65)	65(38)	63(23)	50(21)	40(17)	51(14)	53(12)
17	461	-	57(100)	41(99)	55(40)	43(39)	56(29)	70(27)	105(21)	83(20)
18	492	-	91(100)	45(83)	77(78)	128(72)	107(61)	108(61)	79(56)	69(50)
19	510	108	107(100)	108(85)	77(58)	79(50)	51(38)	50(31)	53(27)	63(23)
20	527	124	109(100)	81(99)	124(72)	53(54)	51(34)	52(33)	50(29)	63(14)
21	559	138	81(100)	43(40)	41(39)	54(30)	64(28)	42(25)	53(20)	138(10)
22	585	-	43(100)	55(30)	42(27)	107(15)	44(14)	51(13)	101(12)	69(12)
23	600	122	107(100)	77(43)	122(34)	41(22)	51(22)	53(17)	79(15)	50(14)
24	631	110	110(100)	63(38)	64(35)	53(30)	81(25)	51(18)	50(17)	82(17)
25	647	120	120(100)	91(97)	69(78)	41(48)	42(42)	57(23)	119(23)	73(22)
26	718	124	124(100)	78(75)	123(50)	51(42)	77(33)	67(20)	53(20)	106(18)

Argence tannin (fig. 2). In the latter, the main fragment was phenol (peak no. 17, 17.7%), which accounted for only 1.51% of Arval tannin TIC. Total phenolic content was also different in the pyrograms of the two tannins, i.e. 65.91% in Arval and 40.23% in Argence. The relative quantities of catechol were consistent with the results of the tannin colorimetric assay of the two sorghum cultivars reported in table 1, i.e. high percentage of catechol in Arval and low in Argence. In another work (13), it was also observed that catechol was present in non-significant amounts in the pyrogram of a non-tannin polyphenol such as lignin. The pyrolysis of catechin under the same conditions of tannins yielded catechol as the single degradation product (fig. 3). A black residue was observed in the quartz sample holder after pyrolysis, probably due to some polymerization reactions undergone by the other moiety of the molecule, which might explain the lack of other pyrolysis fragments. Increasing the temperature of pyrolysis up to 900 °C did not change the fragmentation. The reproducibility of triplicate pyrolysis of catechin was good (fig. 4).

CONCLUSION

PY-GC-MS analysis of condensed tannins containing catechin-like monomeric units shows catechol as main fragment. This compound is of diagnostic significance for condensed tannins not only because it is originated by a simple cleavage of one of its monomeric units, but also because it is peculiar of this class of polyphenols and not, for instance, of another class of polyphenols widespread in nature such as lignin, and because its formation under pyrolysis is quantitatively reproducible. Further studies are underway to screen a larger set of samples, to establish a quantitative correlation between the amount of catechin subjected to pyrolysis and the quantity of produced catechol, and to determine its range of linear response. If the preliminary results of the present work will be confirmed on a more quantitative basis, pyrolysis affords the prospect of a rapid and specific analysis of tannins by gas chromatography, a technique so far neglected for tannins, without the need of cumbersome sample preparation and derivatization.

REFERENCES

1. Haslam, E. (1966) Chemistry of Vegetable Tannins, Academic Press, London and New York.
2. Goldstein, J.L., Swain, T. (1963) Phytochemistry 2, 371.
3. Goldstein, J.L., Swain, T. (1965) 4, 185.
4. Bate-Smith, E.C., Swain, T. (1953) Chem. Ind. April 18, 377.
5. Gujer, R., Magnolato, D., Self, R. (1986) Phytochemistry 25, 1431.
6. Self, R., Eagles, J., Galletti, G.C., Mueller-Harvey, I., Hartley, R.D., Lea, A.G.H., Magnolato, D., Richli, U., Gujer, R., Haslam, E. (1986) Biomed. Environ. Mass Spectrom. 13, 449.
7. Price, M.L., Butler, L.G. (1977) J. Agric. Food Chem. 25, 1628.
8. Price, M.L., Van Scoyoc, S., Butler, L.G. (1978) J. Agric. Food Chem. 26, 1214.
9. Hagerman, A.E., Butler, L.G. (1980) J. Agric. Food Chem. 28, 947.
10. Maxson, E.D., Rooney, L.W. (1972) J. Cereal Chem. 49, 719.
11. Chiavari, G.C., Vitali, P., Galletti, G.C. (1987) J. Chromatogr. 392, 426.
12. Galletti, G.C., Self, R. (1986) Ann. Chim. (Rome) 76, 195.
13. Piccaglia, R., Galletti, G.C., Traldi, P. (1990) J. High Res. Chrom. 13, 52.

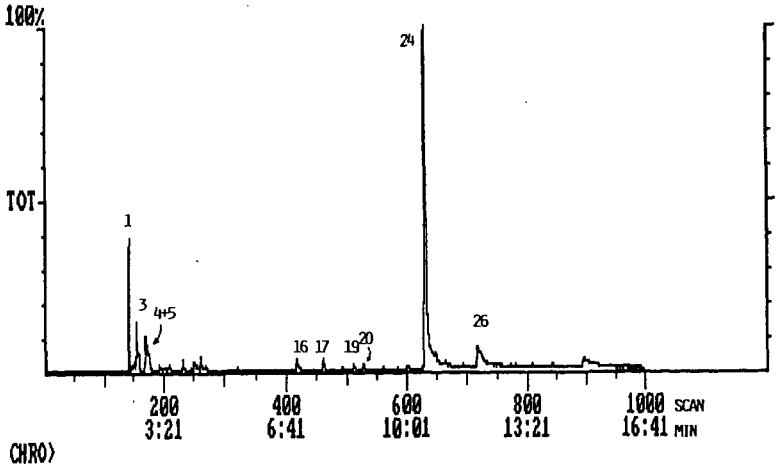

Fig. 1. Total ion chromatogram of Arval sorghum tannin after pyrolysis at 600 °C.

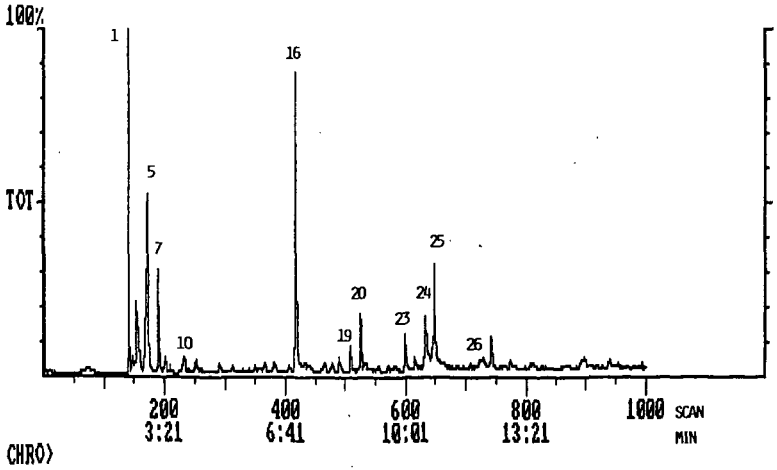

Fig. 2. Total ion chromatogram of Argence sorghum tannin after pyrolysis at 600 °C.

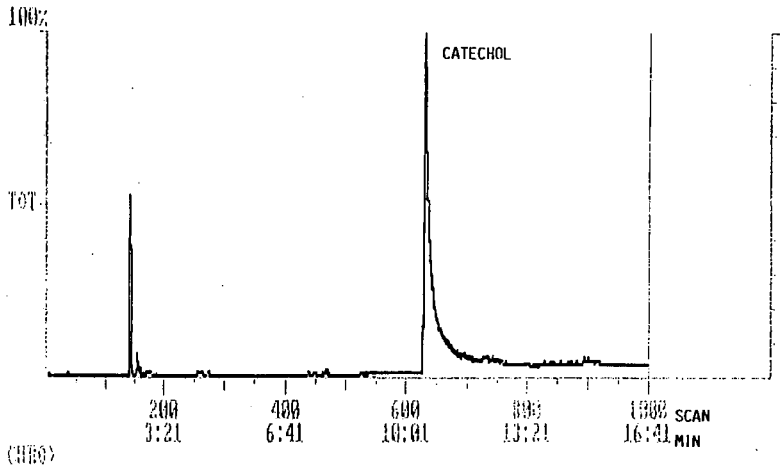

Fig. 3. Total ion chromatogram of catechin after pyrolysis at 600 °C.

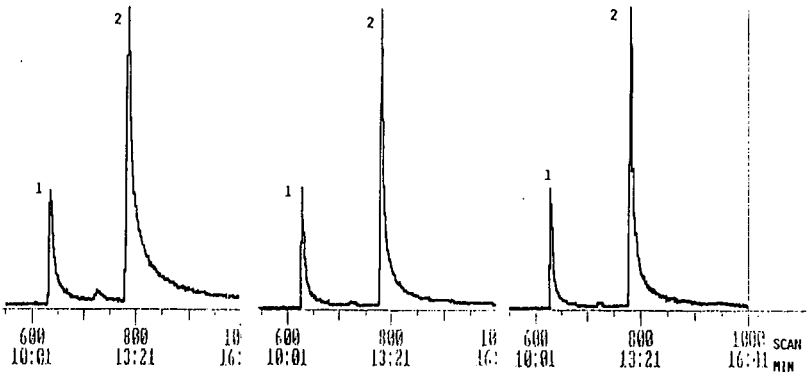

Fig. 4. Replicate pyrolysis of catechin under the same conditions of figure 1-3. (1) catechol, (2) p-hydroxybenzaldehyde which was added in view of its possible use as an internal standard in future quantitative experiments.

A NOVEL POLYPHENOL BIOPOLYMER ISOLATED FROM FOSSIL SEEDS: AN ALTERNATIVE SOURCE FOR (ALKYL)PHENOL MOIETIES IN COALS.

Pim F. van Bergen[*,#], Margaret E. Collinson[#], Jaap S. Sinninghe Damsté[*] and Jan W. de Leeuw[*].

[*]Organic Geochemistry Unit, Delft University of Technology,
De Vries van Heystplantsoen 2, 2628 RZ Delft, The Netherlands.

[#]Biosphere Sciences Division, King's College London,
Kensington Campus, Campden Hill Road, London, W8 7AH, UK.

Keywords: Polyphenol biopolymer, fossil seeds, selective preservation

INTRODUCTION

During the last years several papers have been published on the chemical composition of recognizable higher plant remains in sediments (*e.g.* spores, pollen[1], cuticles[2,3], bark[4,5], wood remains[6]). It is thought that these tissues have survived in the geological record because they are comprised of highly resistant biopolymers such as cutan[3], suberan[4] and lignin[6], whose chemical structures are only slightly modified during sediment diagenesis.

Within this context seeds have hardly been studied. To some extent this is remarkable since they are often produced in large amounts. Alternatively, if few seeds are produced they can be of large size. Extremes in this respect are orchids with produce over one million seeds per fruit per year (each weighing 5 μg) and the Seychelles coconut with a production of perhaps ten seeds in a lifetime weighing 20 kg each. Perhaps more important from a geochemical point of view, seeds possess protective envelopes derived from the integuments of the ovule. They comprise the seed coat and include the testa and tegmen at least one layer of which often becomes tough and sclerotic at biological maturity. The testa is a product of the outer integument whereas the tegmen is produced by the inner integument occuring inside the testa. On morphological features the tegmen is comparable to a cuticle. The protective layers represent only a few percent of the total biomass of the produced seed. However, in most cases it are only the seed coats that are found in the geological record, because the outer layers of seeds contain resistant compounds to protect the genetic material against physical and chemical processes such as temperature and humidity changes and bacterial and fungal attacks. Hence, seeds, and particularly their resistant layers, have a large potential to enter the geosphere and may become selectively enriched.

In this study outer and inner layers (testae and tegmens, respectively) of Late Eocene seeds of *Stratiotes* (water soldier) and *Sabrenia* (fossil water lily) were analyzed by means of flash pyrolysis-gas chromatography-mass spectrometry and flash pyrolysis-gas chromatography in order to test the above mentioned hypothesis. The testa of the studied seeds is a sclerotic layer, whereas the tegmen is a translucent tissue comparable to a cuticle. The *Sabrenia* seeds are obtained from the Brembridge Marls Member, Bouldnor Formation, Hamstead Ledge, Isle of Wight. The *Stratiotes* seeds are obtained from the Totland Bay Member, Headon Hill Formation, Hordle Cliff, Hampshire. In addition a comparison is made between the pyrolysate of the *Sabrenia* testae and the Beulah Zap lignite[7]. This coal sample was obtained from the Sentinel Butte Formation of the Fort Union Group (Upper Palaeocene), Mercer County, North Dakota.

EXPERIMENTAL

The fossil testae and tegmens were dissected by hand. The samples were ultrasonically extracted with methanol. The residues were dried in a vacuum stove at 30°C.

Curie-point pyrolysis-gas chromatography (PY-GC) analyses were performed with a Hewlett-Packard 5890 gas chromatograph using a FOM-3LX unit for pyrolysis. The samples were applied to a ferromagnetic wire. The Curie temperature was 610°C. The gas chromatograph, equipped with a cryogenic unit, was programmed from 0°C (5 min) to 320°C (20 min) at a rate of 3°C/min. Separation was achieved using a fused-silica capillary column (25m x 0.32mm) coated with CP Sil-5 (film thickness 0.4 μm). Helium was used as the carrier gas.

The Curie-point pyrolysis-gas chromatography-mass spectrometry (PY-GC-MS) analyses wre performed using the same equipment and conditions as described above for the PY-GC conneted with a VG 70S mass spectrometer operated at 70 eV with a mass range m/z 40-800 and a cycle time of 1.8 s.

RESULTS AND DISCUSSION

The pyrolysates of the fossil tegmens of both *Stratiotes* and *Sabrenia* seeds are dominated by series of *n*-alkanes and *n*-alk-1-enes. In addition, the pyrolysate of the *Sabrenia* tegmens shows the distinct presence of isoprenoids. Prist-1-ene is the most abundant compound. Since δ-tocopherol was also detected, this compound is thought to be the precursor of the observed isoprenoids[8]. The *n*-alk-1-enes and *n*-alkanes detected in pyrolysates of the tegmens are thought to be derived from a highly aliphatic biopolymer comparable to cutan[3].

On the contrary, the main compounds in the pyrolysate of the fossil testae of *Stratiotes* and *Sabrenia* are phenol and C_1 and C_2 alkylated phenols (Table 1). In addition, some methoxyphenols and benzenediols (mainly benzene-1,2-diols) are present. The abundance of these latter compounds is very low in the pyrolysate of the *Stratiotes* testae. The identification of these compounds was confirmed by comparison of mass spectra and relative retention times with those of authentic standards. The methoxyphenols present in these pyrolysates are not derived from lignin, since the distribution of these compounds in lignin pyrolysates is completely different[6]. The phenols and benzenediols detected are thought to be pyrolysis productes of a novel polyphenol biopolymer.

The seeds of *Stratiotes* as well as *Sabrina* are produced under or near the water surface. In these environments fungal activities are prominent. Since phenols are known to possess fungicidal properties[9], it is thought that the outer layer (testa) contains a polyphenol biopolymer as an additional protective shield for the genetic material. Hence, physical as well as chemical protection is conferred by the sclerotic testa.

As mentioned earlier the tegmen occurs inside the testa as a cuticle based on biological features. This similarity of tegmen and cuticle is supported by pyrolysis data since a highly aliphatic biopolymer comparable to cutan has been recognized as a constituent of tegmens.

The distribution patterns of the phenols and benzenediols in the pyrolysates of the testae are remarkably similar to those in the pyrolysate of the Beulah Zap lignite (Table 1; Fig. 1). This indicates that selective preservation of this novel biopolymer may be an alternative for the proposed demethoxylation of lignins[10] to explain the presence of phenol moieties in coals. Whether these phenol moieties in coal are derived from testae only remains to be seen, because this novel biopolymer may also occur in other tissues of water plants not yet investigated.

CONCLUSIONS

The two anatomically different seed layers of fossil *Stratiotes* and *Sabrenia*, tegmen and testa, respectively, show remarkable differences in chemical composition. The tegmens are mainly comprised of an aliphatic biopolymer comparable to cutan whereas the sclerotic testae contain a novel polyphenol biopolymer.

The highly similar distribution pattern of phenols and benzenediols observed in both pyrolysates of testae and lignites strongly indicates that selective preservation of the novel biopolymer may be an alternative for the proposed demethoxylation of lignins to explain the presence of phenol moieties in coals.

REFERENCES

1. Schenck, P.A., de Leeuw, J.W., Van Graas, G., Haverkamp, J. and Bouman, M. (1981), In: Organic Maturation Studies and Fossil Fuel Exploration 1981 (ed. J.Brooks), Academic Press, London. 225-237.
2. Nip, M., Tegelaar, E.W., Brinkhuis, H., de Leeuw, J.W., Schenck, P.A. and Holloway, P.J. (1986), Org.Geochem., 10: 769-778.
3. Tegelaar, E.W., de Leeuw, J.W., Largeau, C., Derenne, S., Schulten, H-R., Muller, R., Boon, J.J., Nip, M. and Sprenkels, J.C.M. (1989), J.Anal.Appl.Pyrolysis, 15: 29-54.
4. Tegelaar, E.W., Hollman, G., Van der Vegt, P., de Leeuw, J.W. and Holloway, P.J. (1990), In: Resistant biomacromolecules in morphologically characterized constituents of kerogen: a key to the relationship between biomass and fossil fuels (ed. E.W.Tegelaar). PhD thesis, University of Utrecht.
5. Wilson, M.A. and Hatcher, P.G. (1988), Org.Geochem., 12: 539-546.
6. Saiz-Jimenez, C. and de Leeuw, J.W. (1986), Org.Geochem., 10: 869-876.
7. Smith, K.L. and Smoot, L.D. (1990), Prog.Energy Combust.Sci. 16: 1-53.
8. Goossens, H., de Leeuw, J.W., Schenck, P.A. and Brassell, S.C. (1984), Nature, 312: 440-442.
9. Waller, G. (1987), Allelochemicals: Role in agriculture and forestry. Am.Chem.Soc.Symp.Series 330.
10. Senftle, J.T., Larter, S.R., Bromley, B.W. and Brown, J.W. (1986), Org.Geochem. 9: 345-350.

Table 1: Major identified peaks in pyrolysates of *Sabrenia* testae and the Beulah Zap lignite (Fig. 1)

1.	Phenol
2.	2-Methylphenol
3.	2-Methoxyphenol
4.	3-Methylphenol and 4-Methylphenol
5.	2,4-Dimethylphenol
6.	4-Ethylphenol
7.	4-Methyl-2-methoxyphenol
8.	Benzene-1,2-diol
9.	C_3-phenol
10.	4-ethyl-2-methoxyphenol
11.	4-methyl-benzene-1,2-diol

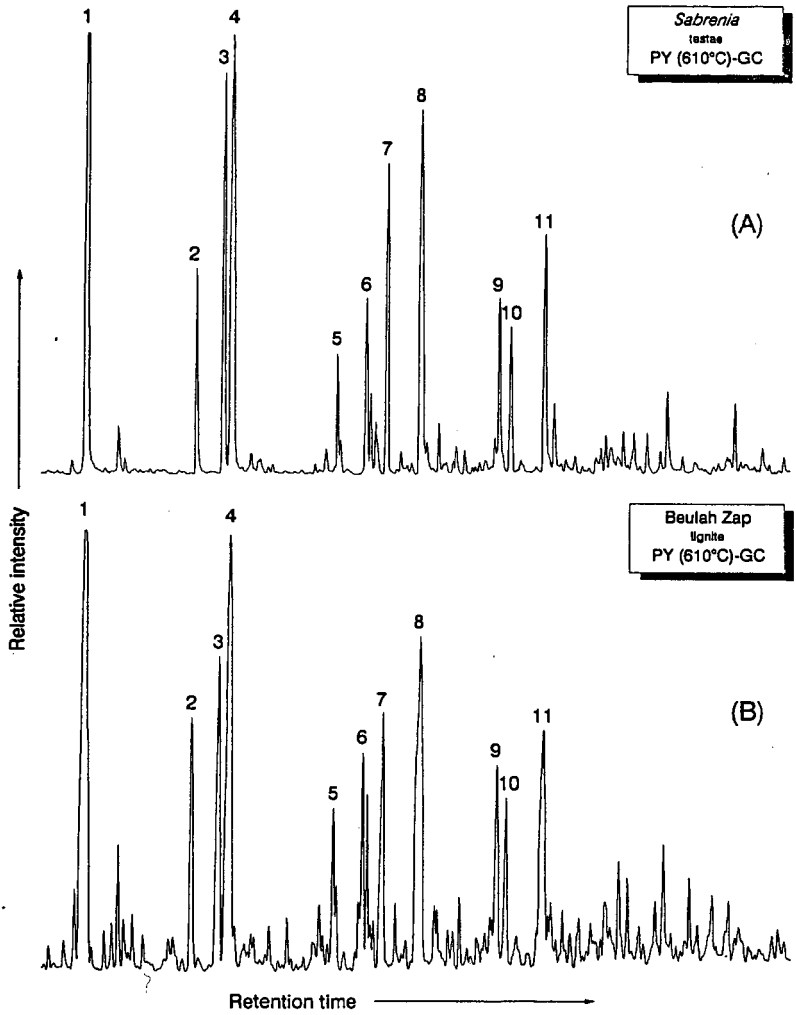

Fig. 1: Partial gas chromatogram of flash pyrolysates of *Sabrenia* testae (A) and the Beulah Zap lignite (B).

PYROLYSIS OF NATURAL RUBBER, WAXES AND RESINS WITH ZEOLITIC CATALYSTS.

Sara Gnecco, Ruby Cid, Victoria Caamano and Attila E. Pavlath*

Laboratorio de Recursos Renovables. Facultad de Ciencias, Universidad de Concepcion, Casilla 3-C, Concepcion-Chile and *Western Regional Research Center, U.S.D.A., 800 Buchanan St., Albany, C.A. 94710. U.S.A.

INTRODUCTION

In recent year there has been considerable interest in developing renewable resources, as alternatives to petroleum based substances. Oil and hydrocarbon producing plants, mostly growing in arid regions, are especially promising candidates to produce important chemical intermediates and fuels. (1-4).

In previous work (5,6), we have evaluated chemically the potential of some Chilean species growing in arid lands as hydrocarbon producing crops. Among the studied species, Euphorbia lactiflua, Euphorbia copiapina, Tessaria absinthioides and Bulnesia chilensis turned out to be promising sources of polyisoprene and/or n-paraffins. Their extracts are potential starting materials for fuels and/or chemicals through pyrolytic reactions. However, it is necessary to study the effect of various catalysts on the pyrolysis and identify the most promising ones, in order to utilize economically these plants.

Most of the work on the pyrolytic reactions of biomass were carried out with the carbohydrates. (8). There is very little known on the influence of catalysts, pretreatments and other reaction conditions on the compounds obtainable through the pyrolysis of the extracts from latex producing plants. It has been reported that mixtures of ethylene, propylene, toluene, xylenes, C_5 through C_{20} nonaromatics, and C_1 to C_4 alkanes can be obtained when these extracts are pyrolyzed in the presence of ZSM-5, a molecular shape-selective zeolitic catalyst developed by Mobil Oil Corporation (7).

It is difficult to taylor-make "a priori" a catalyst for all the types of reaction that take place in converting biomass extracts to valuable chemicals. However, we theorize that owing to their acidic and structural properties, such as larger pore size and central cavity size than those of

ZSM-5, thermostable zeolitic faujasites would be appropriate. Some bi-functional catalysts, e.g. Pt/faujasite, would be also good candidates to improve reduction of carbonyl groups and to diminish the formation of coke which deactivates the catalyst.

To assess the possibility of obtaining fuels, the main components of CH_2Cl_2 extracts from Chilean species,i.e.,polyisoprene, n-paraffins and resins, were pyrolyzed with various zeolitic catalysts, utilizing different heating rates and subtrate/catalyst (S/C) ratio. Conversion degree and best conditions of pyrolysis were estimated by means of thermo-gravimetry and differential scanning calorimetry.

EXPERIMENTAL

Extraction, fractionation and analysis.

Plant species were collected from the wild, in the North of Chile (III and IV Regions). Voucher specimens were kept at the University of Concepcion Herbarium (Conc.). Samples of latex from Euphorbia lactiflua were collected by tapping wild plants.

Dried milled samples were extracted in a Soxhlet apparatus with CH_2Cl_2 for 40 hours. After the evaporation of the solvent, the solids were again extracted using acetone to obtain acetone-soluble and acetone-insoluble fractions. Representative fractions were characterized by quantitative analysis, IR, ^1H and ^{13}C NMR spectroscopy, TLC and GC (5,6). Results are given in Table 1.

Isolation and Characterization of main components.

n-Paraffins.

Acetone-insoluble fractions were refluxed in a suspension of activated carbon, Johns-Manville cellite and hexane, filtered and dried to obtain the fractions of refined hydrocarbons which were analyzed by IR, ^1H NMR, ^{13}C NMR, and GC. (5).

NMR and IR spectra of refined hydrocarbons from different species revealed almost exclusively the presence of n-paraffins. The identification of hydrocarbons was carried out by the comparison of RRt data with those of authentic standards. The results revealed the presence of n-alkanes mixtures with chain lengths varying from n-nonadecane (n-C_{19}) to n-tritriacontane (n-C_{33}). In the mixture, n-heptaeicosane (n-C_{27}), n-

nonaeicosane (n-C_{29}) and n-hentriacontane (n-C_{31}) were the dominant alkane components.

Rubber

Fresh latex from E. lactiflua was mixed with C_2Cl_4. After removing the azeotrope, the solid was dried at 50°C for 12 hours. Dry latex was dissolved in CH_2Cl_2, then filtered, and the solution was added drop by drop to methanol. The precipitate was centrifuged, dried in a vacuum oven at 50°C for 2 hours and weighed. The yield was 8.05% in dry latex weight basis. The characterization was done by IR, NMR spectroscopy (^{13}C and ^{1}H) and TLC. All the data obtained agreed with those given in literature for cis-1,4-polyisoprene.

Resins

Resins isolated through succesive fractionation of dry latex from E. lactiflua and CH_2Cl_2 extract from C. odorifera were characterized by I.R., ^{13}C NMR and TLC with standards (5). The main components were: sterols (B-sitosterol-type), fatty alcohols (oley-type), fatty acids (oleic-type).

Preparation and Characterization of Catalysts

Series of HNaY, MNaY and M_1M_2NaY (M = Pt, Co, Mo) zeolites were prepared by impregnation or partial sodium exchange of a NaY zeolite faujasite-type (Linde, Si/A1 = 2.4) with NH_4^+ or suitable metalic ions. The degree of ionic exchange was determined by atomic absorption sodium analysis in the filtrate. Dehydration, deamination and dehydroxilation were carried out at 110°C, 250-420°C and 480-550° respectively. Reduction of PtNaY catalyst was carried out with H_2 at 520°C (9-10).

The crystallinity of the exchanged zeolites was determined by X-ray diffraction using the powder method (11). The specific areas of the prepared zeolites were determined by the absorption method of N_2. The analysis were performed in a volumetric BET conventional equipment at -196°C (12). The number of acid centers and their relative strengths were determined by a potentiometric method (13). Results are given in Table 2.

Thermogravimetric analysis.

C. odorifera n-paraffins, E. lactiflua polyisoprene and E. copiapina resins were selected as model substrates. The rate of weight loss, and the

weight of the residue of each substrate, catalyst, and mixtures S/C, were determined in a T.G.A. under N_2. A temperature range of 50-550°C and heating rates of 20, 40 and 80 degrees/min were used. The results for samples S/C = 1/1 (wt/wt) are given in Table 3. Percents of total weight loss (substrate + catalyst) were corrected and are given in percent of weight loss of the substrate.

DSC analysis

Calorimetric studies were carried out on a DSC-system, upon heating from 30 to 500°C at 80°C/min. The samples were sealed in aluminum pans with a pinhole on top for the escape of volatiles, which were flushed out of the reaction zone with a constant flow of N_2.

RESULTS AND DISCUSSION

According to the results of Table 3, as the heating rate increases, the T_{infl} also does. The T_{infl} is around 330 to 390°C and it is higher for the substrates without catalyst. The percent of weight loss at this point is from 37 to 64%, therefore it could be assumed that most of the pyrolytic products are formed around 400°C.

Results for samples S/C = 9/1 (wt/WT) are not given because were not reproducible. This may be due to the fact that it is very difficult to obtain homogeneous samples with this ratio, and a small error in the quantity of catalyst may cause a large error in the results.

In the DSC analysis, the pyrolysis of the mixtures S/C = 1:1 (wt/wt) could be separated into two large and broad peaks: one endothermic, with maxima around 200°C, the o ther, exothermic, with maxima around 430°C.

Below 300°C a minimal amount of volatile material is generated (Table 3), and the first range endothermic peak is probably due to melting and minor scissions. On the other hand, the second range temperature, exothermic peak, is located, within the experimental error, in the zone of maxima volatization rate (Table 3), therefore, an extensive decomposition seems to take place around 400°C.
The temperature of the maxima of the exotermic peak is lower for most of mixtures S/C than for the substrates without catalyst showing that they speed up the pyrolysis.

CONCLUSIONS

General conclusions emerging from the results are:

- The catalysts speed up the process of pyrolysis and enhances the percent of conversion of all substrates.
- The better conditions for the catalytic pyrolysis would be temperatures around 400°C and higher heating rate.
- Regarding the percentage of conversion (% wt final), the catalysts that seem to direct .more efficiently the pyrolysis of the extracts of hydrocarbon producing plants to mixtures with low C/H ratio, besides ZSM-5, were: Co(1)NaY, Mo(2)NaY and Co(1) Mo(0.5)NaY.

Continuing work.

The composition of pyrolytic volatile products and theirs combustion heats are being investigated to make the final conclusions about the most suitable pyrolytic conditions. Further results from these studies will be reported in the near future.

ACKNOWLEDGEMENTS.

The authors wish to thank to Research Office, University of Concepcion (DI 20.13.70), FONDECYT (Proj. 687/89) and Program in Science and Technology Cooperation, Agency for International Development (Grant DPE-5542-G-SS-8029-00) for financial support.

REFERENCES

1. M. Calvin, Science, **219**, 24 (1983).
2. G.E. Wickens, J.R. Gooding, D.V. Field Eds. "Plant for arid lands", London (1985).
3. M.E. Carr et. al. J.A.O.C.S., **62**, 136/ (1985).
4. E.A. Davis, J.L. Kuester, M.O. Bagby, Nature, **307**, 726 (1984).
5. S. Gnecco, J. Bartulin, C. Marticorena, A. Ramirez, Biomass **15**, 165-173 (1988).
6. S. Gnecco, J. Bartulin, C. Marticorena, J. Becerra, Phytochemistry, **28** (4) 1254-1256 (1989).
7. P.W. Weisz, W.O. Haag and P.G. Rodewald, Science, **206**, 57 (1979).
8. M.J. Antal, Advances in Solar Energy, American Solar Energy Society, Boulder, Colorado 1983, p. 61.
9. R. Cid, M.E. Konig, R. Arriagada, Applied Catalysis, **2**,189-194 (1982).
10. R. Cid, R. Arriagada, F. Orellana, J. Catal. **80**, 228-230, (1983).
11. R. Cid, R. Arriagada, F. Orellana, Bol. Soc. Chil. Quim. **30** (2), 63-67 (1985).
12. R. Cid, F. Orellana and A. Lopez-Agudo, Applied Catalysis **32**, 327-336 (1987).
13. R. Cid, G. Pecchi, Applied Catalysis, **14**, 15-21 (1985).

TABLE 1

YIELD, MOLAR RATIO C/H OF REPRESENTATIVE FRACTIONS AND POLYMERIC HYDROCARBON TYPE FROM SOME CHILEAN SPECIES.

SPECIES	CH_2Cl_2 EXTRACT		ACETONE-INSOLUBLE FRACTION		POLYMERIC HYDROCARBON TYPE[C]
	YIELD [A]	C/H RATIO[B]	YIELD[A]	C/H RATIO[B]	
E.LACTIFLUA	10.80	0.52	2.90	0.48	NR, WAXES
E.COPIAPINA	11.70	0.57	3.10	0.51	NR[D], WAXES
C.ODORIFERA	4.50	0.54	2.20	0.48	NR[D], WAXES
C.SALICIFOLIA	5.30	0.55	1.60	0.49	NR[D], WAXES
T.ABSINTHIOIDES	7.40	0.57	1.32	0.52	WAXES

A. Given as a percentage of plant dry weight; average value of extracts from 2-3 plant samples

B. C/H molar ratio calculated from quantitative analysis data

C. NR=natural rubber (cis-1,4-polyisoprene) identified by spectroscopic data

D. Traces.

TABLE 2. CHARACTERISTICS OF THE PREPARED ZEOLITES

DEGREE OF I.E. OR IMPREGNATION	SOLID DENOMINATION	CRYSTALLINITY %	S_{BET} (M^2G^{-1})	RELATIVE ACID STRENGTH
40% NH_4	H(40)-NAY	100	726	STRONG
64% NH_4	H(64)-NAY	100	713	STRONG
0.5 Wt % Pt	Pt (0.5)-NAY	100	680	WEAK
1Wt% Co(AS CO_3O_4	Co (1)-NAY	100	722	MODERATE
2Wt% Mo(AS MoO_3)	Mo (2) NAY	85	615	MODERATE
1Wt% Co ($ASCo_5O_4$)	Co (1) Mo (0.5)-NAY	90	710	MODERATE

I.E. =Ionic exchange

TABLE 3. THERMOGRAVIMETRIC ANALYSIS FOR MIXTURES S/C=1/1 wT/WT).

n	CATALYST	HEATING RATE (DEGREE/min.	$T_{INF.}$ (°C)	$\%W.L._{INF.}$	T_F (°C)	$\%WL._F.$
P	-	20	370	64.0	430	95.4
A	ZSM-5	20	350	50.6	480	91.0
R	H(40)NAY	20	320	51.8	460	93.5
A	H(64)NAY	20	330	46.6	450	92.5
F	Pt(0.5)NAY	20	315	23.9	450	68.7
F	Co(1)NAY	20	310	39.1	450	89.7
I	Mo(2)NAY	20	325	38.5	450	98.2
N	Co(1)Mo(0.5)NAY	20	320	41.8	450	94.8
S	-	40	390	55.2	480	85.9
	ZSM-5	40	360	46.2	480	84.4
	H(64)NAY	40	350	45.4	470	94.6
	Pt(0.5)NAY	40	330	24.5	460	61.8
	Co(1)NAY	40	330	37.6	450	90.8
	Mo(2)NAY	40	350	38.1	450	91.5
	Co(1)Mo(2)NAY	40	340	37.8	490	88.3
	-	80	420	53.0	490	82.9
	ZSM-5	80	390	40.0	470	89.7
	H(40)NAY	80	380	43.9	460	89.5
	H(64)NAY	80	360	46.7	480	92.2
	Mo(2)NAY	80	390	45.0	510	92.0
	-	20	350	46.1	450	82.1
R	ZSM-5	20	310	41.6	350	84.4
E	H(40)NAY	20	310	37.5	450	77.4
S	H(64)NAY	20	295	38.2	400	75.4
I	Pt(0.5)NAY	20	270	27.9	400	60.0
N	Co(1)NAY	20	300	36.9	450	75.0
S	Mo(2)NAY	20	320	48.4	450	98.4
	Co(1)Mo(0.5)NAY	20	300	43.7	400	83.6
	-	40	380	41.4	450	78.3
	ZSM-5	40	350	44.8	460	80.5
	H(40)NAY	40	330	40.9	420	81.8
	H(64)NAY	40	310	40.2	400	82.4
	Pt(0.5)NAY	40	300	34.8	450	77.0
	Co(1)NAY	40	300	43.9	450	95.2
	Mo(2)NAY	40	330	49.6	450	97.4
	Co(1)Mo(0.5)NAY	40	330	38.9	450	87.3

Continuation of TABLE 3.

CATALYST	HEATING RATE (DEGREE/min.	$T_{INF.}$ (°C)	%W. $L._{INF.}$	T_F (°C)	%WL. $_F$.
P -	20	390	42.9	460	82.9
O ZSM-5	20	385	50.0	450	91.5
L H(40)NAY	20	375	49.8	450	78.4
Y H(64)NAY	20	370	38.1	480	72.4
I Pt(0.5)NAY	20	400	36.6	470	57.4
S Co(1)NAY	20	350	31.5	450	91.9
O Mo(2)NAY	20	350	29.2	450	71.9
P Co(1)Mo(0.5)NAY	20	370	48.4	450	87.4
R					
E -	40	406	33.1	490	88.4
N ZSM-5	40	390	42.8	500	96.1
E H(40)NAY	40	390	47.3	470	88.6
H(64)NAY	40	370	40.3	480	80.8
Pt(0.5)NAY	40	340	25.3	500	75.0
Co(1)NAY	40	380	34.2	500	96.2
Mo(2)NAY	40	370	37.3	450	88.6
Co(1)MO(0.5)NAY	40	385	48.1	450	89.8
-	80	425	51.1	510	93.3
ZSM-5	80	400	46.6	500	97.7
H(40)NAY	80	390	42.5	460	86.0
H(64)NAY	80	400	39.2	480	79.4
Mo(2)NAY	80	410	45.0	510	82.1

$T_{INF.}$ = Temperature at inflection point

%WL INF. = % of weight loss at $T_{INF.}$

I_F = Temperature where no more weight loss occurs

$\%WL_F$ = % of weight loss at T_F.

ALKYLPYRROLES IN KEROGEN PYROLYSATES: EVIDENCE FOR ABUNDANT MACROMOLECULARLY-BOUND TETRAPYRROLE PIGMENTS

Jaap S. Sinninghe Damsté*, Timothy I. Eglinton*# and Jan W. de Leeuw*

*Delft University of Technology, Faculty of Chemical Engineering and Materials Science, Organic Geochemistry Unit, De Vries van Heystplantsoen 2, 2628 RZ Delft, The Netherlands.

#Fye Laboratory, Department of Chemistry, Woods Hole Oceanographic Institution, Woods Hole, MA 02543, U.S.A.

Keywords: alkylpyrroles, kerogen pyrolysates, macromolecularly-bound tetrapyrrole pigments

INTRODUCTION

Porphyrins and related compounds are well known biological markers often applied in geochemistry.[1,2] These tetrapyrrole pigments also occur in kerogen since upon off-line pyrolysis of kerogen DPEP-and ETIO-porphyrins are released.[3] Recently, Barakat and Yen reported that major amounts of 3-ethyl-4-methyl-1*H*-pyrrole-2,5-dione and, to a lesser extent, 3,4-dimethyl-1*H*-pyrrole-2,5-dione were formed upon controlled stepwise oxidation of a Monterey kerogen from the Santa Maria basin and Green River shale kerogen.[4] These compounds are thought to be derived from oxidation of entrapped ETIO-porphyrins.

Here we report the identification of C_1-C_6 alkylpyrroles as major pyrolysis products of a Miocene kerogen from the Monterey Formation (CA, USA) and provide evidence that they are derived from macromolecularly-bound tetrapyrrole structures. A more detailed and expanded account of this work will be presented elsewhere.[5]

SAMPLE

The kerogen sample studied is from an immature outcrop in the Santa Barbara basin of the Miocene Monterey Formation (CA, USA). Kerogen isolation was performed by HCl/HF treatment of the solvent-extracted sediment and yielded a kerogen isolate with the elemental composition: C, 60.31%; H, 6.45%; N, 3.55%; $S_{tot.}$, 9.81%; ash, 4.62%; O (by difference), 15.26%.

EXPERIMENTAL

Flash pyrolysis-gas chromatography-mass spectrometry (Py-GC-MS; 610°C, 10 s) was performed using a Curie point pyrolyser mounted on an Hewlett-Packard 5890 gas chromatograph equipped with a 25 m x 0.32 mm i.d. capillary column coated with CP Sil-5 (film thickness 0.45 μm). The gas chromatograph was connected with a VG-70s mass spectrometer operated at 70 eV with a cycle time of 1.8 s and a mass range m/z 50-800 at a resolution of 1000.

Flash pyrolysis-mass spectrometry (Py-MS) was performed using the FOM autoPYMS system. Pyrolysis (770°C) was performed *in vacuo* (180°C) and the products were transferred *via* an expansion chamber (200°C) to a Baltzers QMA 150/QMG 511 quadrupole mass spectrometer. The following MS conditions were employed: electron impact ionization, 15 eV; mass range, m/z 25-250; scan rate, 10 scans.s^{-1}.

RESULTS AND DISCUSSION

GC-MS of a flash pyrolysate of a kerogen isolated from an immature (R_o= *ca.* 0.30%) Monterey sediment revealed the abundance of a number pyrroles with alkyl side-chains containing 1-6 carbon atoms. Figure 1 shows a part of the total ion current and a summed mass chromatogram of m/z 80.07 + 81.08 +

94.08 + 95.09 + 108.10 + 109.11 + 122.11 + 123.12 + 136.13 + 137.13 + 150.14 + 151.14 of the flash pyrolysate, indicating the abundance of the C_1-C_6 alkylpyrroles. This was also evident from the Py-low voltage MS data (Figure 2) which show the abundance of m/z 81, 95, 109, 123 and 137, the molecular ions of the C_1-C_5 alkylpyrroles.

The alkylpyrrole composition in the flash pyrolysate is dominated by a small number of specific alkylpyrroles: 2,3,4-trimethylpyrrole, 3-ethyl-4-methylpyrrole, 2,3-dimethyl-4-ethylpyrrole, 2,4-dimethyl-3-ethylpyrrole and 3-ethyl-2,3,5-trimethylpyrrole (Table 1). Most of these compounds were identified by using authentic standards.

A similar alkylpyrrole composition was found to be present in the flash pyrolysate of the asphaltene fraction isolated from the bitumen of the same Monterey sediment sample. This lends further support to the hypothesis that asphaltenes can be thought of as small, "soluble" parts of kerogen.[6]

The very specific alkyl substitution pattern of the major alkylpyrroles (i.e. with an ethyl and a methyl group at position 3 and 4 and 0-2 methyl group(s) at the other positions) strongly suggest that they are derived from tetrapyrrole pigments (e.g. chlorophyll-*a*, bilirubin).

Therefore, the lininear tetrapyrrole bilirubin was flash pyrolysed under the same conditions as the kerogen sample. Indeed, C_1-C_6 alkylpyrroles were formed and their distribution is dominated by the same structural isomers as in case of the Monterey kerogen pyrolysate (Figure 3). Similar results were obtained for chlorophyll-*a* and protoporphyrin-IX dimethyl ester. These results are in good agreement with literature data.[7]

These results suggest that the Monterey kerogen contains significant amounts of macromolecularly-bound tetrapyrrole units. Quantitative pyrolysis of the kerogen and bilirubin using a polymer internal standard indicate that the kerogen on a weight for weight basis contains *ca.* 15% "bilirubin equivalents". This very high amount of tetrapyrrole pigments suggests either an abundant algal contribution to the sediment (probably related to upwelling conditions) or unique preservation characteristics associated with this deposit or a combination of both factors.

REFERENCES

1. Baker, E.W. and Louda, J.W. (1986), In: "Biological Markers in the Sedimentary Record", R.B. Johns (ed). Elsevier, Amsterdam. pp 125-225.

2. Filby, R.H. and Van Berkel, G.J. (1987), In: "Metal Complexes in Fossil Fuels", R.H. Filby and J.F. Branthaver (eds). ACS Symp. Ser. 344, ACS, Washington. pp 2-39.

3. Van Berkel, G.J. and Filby, R.H. (1987), In: "Metal Complexes in Fossil Fuels", R.H. Filby and J.F. Branthaver (eds). ACS Symp. Ser. 344, ACS, Washington. pp 110-134.

4. Barakat, A.O. and Yen, T.F. (1989), Energy Fuels, 3: 613-616.

5. Sinninghe Damsté, J.S., Eglinton, T.I. and de Leeuw, J.W. (1991), Geochim. Cosmochim. Acta (submitted).

6. Behar, F. and Pelet, R. (1985), J. Anal. Appl. Pyrol., 7: 121-135.

7. Whitten, D.G., Bentley, K.E. and Kuwada, D. (1966), J. Org.Chem. 31: 322-324.

TABLE 1. Alkylpyrroles identified in the pyrolysates.

peak number	compound(s)
1	C_1 alkylpyrroles
2	C_2 alkylpyrroles
3	C_3 alkylpyrroles
4	2,3,4-trimethylpyrrole
5	3-ethyl-4-methylpyrrole
6	2,3-dimethyl-4-ethylpyrrole
7	2,4-dimethyl-3-ethylpyrrole
8	3-ethyl-2,3,5-trimethylpyrrole

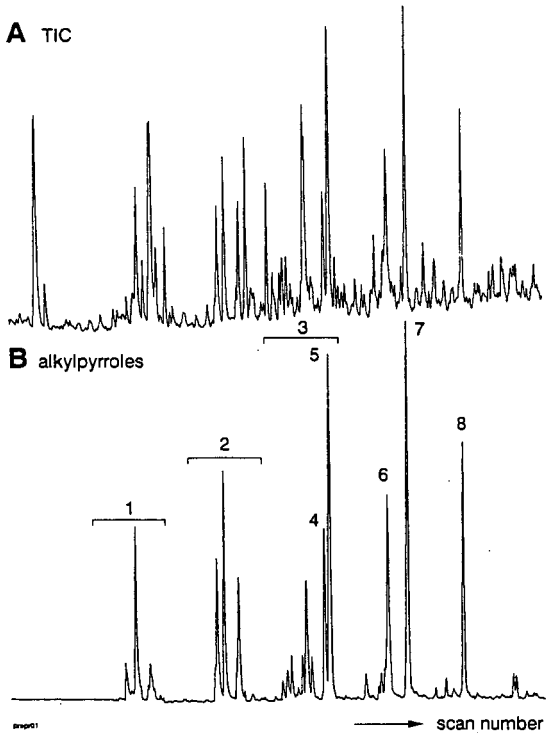

Figure 1. Partial Total Ion Current (TIC; A) of the flash pyrolysate (610°C) of the Monterey-25 kerogen and accurate mass chromatograms (mass window 0.01 amu) of m/z 80.07 + 81.08 + 94.08 + 95.09 + 108.10 + 109.11 + 122.11 + 123.12 + 136.13 + 137.13 + 150.14 + 151.14 showing the distributions of the C_1-C_6 alkylpyrroles (**B**). Peak numbers refer to alkylpyrroles listed in Table 1.

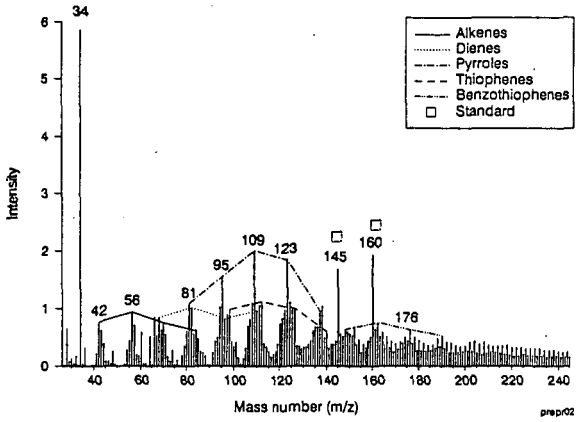

Figure 2. Py-MS spectra of Monterey-25 kerogen. For quantitation poly-4-*t*-butylstyrene was co-pyrolysed, which gives rise to its monomer, 4-*t*-butylstyrene (m/z 160, 145).

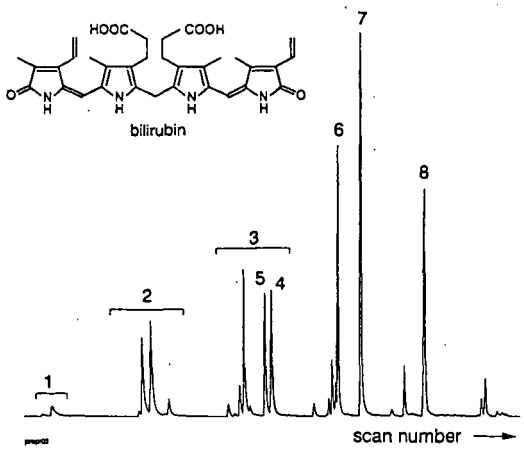

Figure 3. Accurate (mass window 0.01 amu) summed mass chromatograms of m/z 80.07 + 81.08 + 94.08 + 95.09 + 108.10 + 109.11 + 122.11 + 123.12 + 136.13 + 137.13 + 150.14 + 151.14 for the flash pyrolysate (610°C) of bilirubin. Peak numbers refer to alkylpyrroles listed in Table 1.

NEW APPROACHES TO THE STUDY OF CELLULOSE PYROLYSIS

R. J. Evans, F. A. Agblevor, H. L. Chum
Chemical Conversion Research Branch
Solar Energy Research Institute
Golden, Colorado 80401

J. B. Wooten, D. B. Chadwick and S. D. Baldwin
The Philip Morris Company
Richmond, Virginia 23261

KEY WORDS: Pyrolysis, Cellulose, Mass Spectrometry, Labeled Cellulose

INTRODUCTION

Cellulose pyrolysis presents some unique questions that include the effect of polymer secondary structure, (e.g., crystallinity), the intrinsic mechanism of pyrolysis by homolytic or heterolytic pathways, the role of alkali-metal catalysis, and the existence of major pathways, other than levoglucosan formation by "transglycosylation."[1-4] Most of the advances in the last five years have resulted from new analytical information. Piskorz et al.[5] and Richards[6] have published papers in recent years that describe hydroxyacetaldehyde formation as a major product and have speculated on the mechanism of this newly recognized, important product. These workers have used bench-scale pyrolysis units with physical collection of samples and employed chromatographic analysis of the products. Another approach is to perform pyrolysis with on-line analytical capability, either gas chromatography (Py-GC or Py-GC-MS) or mass spectrometry (Py-MS). Pouwels et al.[7] have recently reported a detailed analysis of cellulose pyrolysis products using Py-GC-MS analysis. The major disadvantage of the GC approach is the collection of products on the head of the column where thermal degradation or other reactions can occur for some of the pyrolyzate constituents. The advantages of Py-MS are complete product collection and time-resolved analysis, but ambiguities arise due to the nature of the ionization method and the detection of products with the same nominal mass. The typical approach is to use low-voltage, electron ionization (12-25 eV) to preserve the parent ions as much as possible.[8] When this approach is coupled with multivariate data analysis, it is often possible to deconvolute the major components among the products.[9]

We report here the implementation of several new tools for the study of cellulose pyrolysis using molecular beam mass spectrometry (MBMS).[10] The new tools for py-MBMS investigations include systematic catalytic additions to identify correlated products, tandem mass spectrometry for identifying the contribution of specific compounds to nominal masses, preliminary rate analysis techniques for time-resolved data, and the growth and purification of ^{13}C labeled cellulose using Acetobacter xylinum to be used in the study of cellulose pyrolysis.

EXPERIMENTAL

The MBMS and pyrolysis procedures have been previously described.[10] A sample (1- 30 mg) contained in a quartz holder or "boat" is inserted into flowing (13 l/min at reactor temperature), preheated (typically 500°C) helium carrier gas. The hot gases are expanded through an orifice on the apex of a sampling cone into a low pressure chamber. The pressure difference is sufficient for free-jet expansion, which quenches the products and allows light gases, high-molecular-weight compounds, and reactive products to be simultaneously sampled and analyzed. A molecular beam, collimated through a second expansion, enters an ion source, where approximately 20 eV electron impact ionization is used to form ions. The mass range of interest (typically 15-300 amu) is scanned each second throughout the time for complete pyrolysis product evolution. Data are processed by integrating the spectra over the time of pyrolysis (10 to 90 s, depending on the sample and gas temperature), and by subtracting the background. If time-resolved data analysis is to be performed, each individual spectrum in a pyrolysis experiment is background-corrected. Factor analysis was used to analyze the results, either on a set of spectra from

related pyrolysis experiments to determine common behavior, or on time-resolved data to deconvolute different groups of products. The techniques used for factor analysis have been adapted from the methods of Windig and Meuzelaar[8] that have been recently described by Windig.[11] The software package was the ISMA program[11] (Interactive Self-modeling Multivariate Analysis).

Avicel microcrystalline cellulose (FMC Corp., PH-102) was used throughout this work. Catalytic additions of salts were made by adding an appropriate amount of aqueous solution to just form a slurry and then allowing the material to dry completely in air at room temperature. Additions are reported as wt % cation relative to sample weight.

Cellulose was prepared with ^{13}C at the C-1 position by growing cultures of Acetobacter xylinum on media that included D-[1-^{13}C]-glucose. The cellulose sheets, or pelicles, were allowed to grow in media and then were thoroughly cleaned to remove other biopolymers and metal contamination. This cleaning procedure included autoclaving the pelicles in a solution of Alconox detergent followed by exhaustive washings in deionized water (resistivity = 10^7 ohm). The pelicles were analyzed by C-13 NMR and found to be free of non-cellulosic carbon signals. The level of $^{13}C_1$ enrichment was 14%.

RESULTS AND DISCUSSION

The pyrolysis of cellulose is shown in figs. 1 and 2 for samples treated with different levels of KOH to demonstrate the two major product groups known to form: anhydrosugars and hydroxyacetaldehyde and their related compounds. The sample treated with 0.001% K has a product slate dominated by levoglucosan as shown by the average spectrum in fig 1B. Levoglucosan ionization fragment ions contribute to the intensity at m/z 144, 98, 73, 70, 60, and 57. The evolution profiles for m/z 43 and 144 are shown in fig. 1A as key markers for the two major product groups. In most natural cellulosic material, the yield of levoglucosan is less than that obtained from pure, isolated cellulose, such as Avicel. The average spectrum and time-resolved profiles for the pyrolysis products from cellulose treated with 0.5% K is shown in fig. 2. Hydroxyacetaldehyde, at m/z 60, fragments in the ion source to give fragment ions at m/z 31 and 32 and acetyl compounds give a major fragment ion at m/z 43. These masses are good indicators for the other major product slate. These data support the hypothesis that the level of alkali metals determine the relative amounts of these two major cellulose pyrolysis products. This point will be further demonstrated below.

A major question in cellulose pyrolysis is the existence of other "product classes" in cellulose pyrolysis. The systematic addition of catalytic alkali metal salt has been used to simulate the range of product groups encountered in cellulosic biomass pyrolysis. Salts investigated include NaCl, NaOH, KOH, and K_2CO_3 at the 0.001 to 0.1 wt. % level. Multivariate analysis of the average pyrolysis spectra was used to deconvolute three main groups of products. These catalysts show different mechanistic effects at various levels of addition. The factor score plot, the mass variable loading projections, and the variance diagram are shown in fig. 3. The score plot reveals a systematic effect from the catalytic addition with two trends and three main product groups. The three product groups are controlled by the level of salt addition. The mass-variable axes projections (fig. 3B) show that the masses are fanned out, which indicate that most masses belong to more than one of the three groups. The variance diagram (fig. 3C), which provides visual insight into the weighted average of the mass vectors, shows the three main maxima that indicate the direction of the component axes. The pure mass method is used to determine the vector coordinates that best represent the major, independent, real chemical "components." Chemical components in this application means suites of products that have correlated abundances in the spectra and hence appear to be controlled by the same chemical pathways. In this data set, three components were determined as represented by the pure masses, m/z 31, 144, and 191. The mathematically derived spectra of these three resolved components are shown in figs. 4-6, along with the relative amounts of these components for each sample.

The component spectrum 1 (fig. 4B) shows the key fragment ions at m/z 31, 32 and 43 that are due to the aldehyde and related structures. The plot of the relative concentration of component 1 for each sample as a function of wt % cation shows a systematic trend with higher yields at higher levels of alkali

metal. Six biomass samples (pine, fir, beech, maple, wheat straw, and bagasse) were analyzed along with the treated cellulose and were projected into the factor-analyzed cellulose results. These samples are included in fig. 4-6 as a function of their analyzed alkali metal concentrations. The resolved spectrum of component 2 in fig. 5B matches levoglucosan and shows higher relative concentrations in the samples with low levels of alkali metals that decreases monotonically with increased alkali-metal concentration. The biomass samples fit within this curve. Recent work[5,6] has established that these two groups are the major products of cellulose pyrolysis, and our work shows that their relative amounts are controlled by alkali catalysis, which promotes the formation of the aldehydes at the expense of anhydrosugars. The results indicate a third product class that is also a function of alkali catalysis at low levels and that product group is shown in the component spectrum in fig. 6B. The peak at m/z 191 is of great interest since it is higher than the anhydrosugar weight of 162 and because it is an odd mass ion indicating either a protonated m/z 190 or a fragment ion of a higher mass, such as m/z 192. The peaks at m/z 173 and 163 and 145 are correlated with the intensity of m/z 191. The other major product is m/z 126, which could be 5-hydroxymethyl furfural, or hydroxybenzenes.[12] This will be discussed in relation to the CID of m/z 126. The peak at m/z 114 and fragment ion m/z 85 are common products from pentosan pyrolysis products and are thought to be due to a lactone.[10] The relative concentration of component three shows a maximum at intermediate levels of cation concentration and the biomass samples show good agreement with the trends for the cellulose samples. These results imply that the pyrolytic behavior in biomass samples can be largely explained by these three product groups and that the effect of alkali-metal catalysis is sufficient to explain the control of the pyrolysis of cellulose in these materials.

Time-resolved data analysis can be used to estimate the relative kinetic rates for these different classes. As an initial application of this idea, the two sets of time-resolved spectra for the pyrolysis of cellulose treated with .001 and .5% K (as KOH) (shown in figs. 1A and 2A) were combined in the same data set and subjected to factor analysis to deconvolute the major trends as a function of reaction time. Only two significant chemical components were derived by this process in contrast to the three from the alkali-metal experiment. There are two possible reasons for this: 1) the third pathway was not active because these samples are from the two extremes of the sample distribution in fig. 3A, or 2) the two sets of time-resolved spectra did not contain sufficient variation to allow independent expression of the intermediate product group. The masses associated with the third product slate are divided between the other two. The mathematically derived spectra of the two components are shown in fig. 7 and clearly represent aldehyde and anhydrosugar product groups.

Using the relative yields of these two components in each spectrum the data are analyzed by plotting three calculated values that represent tests for zero, first, and fractional order rate behavior.[13] The test for zero order is a plot of fractional conversion to products, expressed as

$$X_i = \left(\sum_{t=0}^{i} S_{ij}\right) / \left(\sum_{t=0}^{n} S_{nj}\right)$$

where S is the score for the j component (j=1 to 2, in this case) at time i, and n is the time for complete conversion. This can be subsequently converted to a first order test by plotting $-\ln(1-X_i)$ and as a fractional order test by plotting $(1-X_i)^{(1-n)}$, where n is the fractional order of reaction.[13] The slope of the line can be converted to the rate constant when these values are plotted versus time, and straight line behavior is observed. In these experiments, there is a nonisothermal period while the sample is heated to the reactor temperature. The initial portion of the time-resolved behavior is therefore ignored. This method should be considered a screening technique since there are several uncontrolled factors (e.g., temperature of reacting solid, mass transfer, etc.) that prevent the calculation of intrinsic chemical kinetics with certainty. However, this rapid analytical approach is a way of comparing samples that sheds light on the chemical processes and utilize data that in the past were ignored. The use of factor analysis to deconvolute chemically specific information from time-resolved data is an improvement over weight loss rate analysis. Plots of these calculated values versus time are shown in fig. 8 for the evolution of the aldehydes component from the 0.5% K-treated cellulose and the anhydrosugar component for the 0.001% K-treated cellulose. In both the 0.001% K and 0.5% K samples, a reaction order of .8 and a rate constants of 0.17(±.02) s^{-1} were calculated for the anhydrosugars. For the aldehydes, a reaction order of 0.4 and rates of 0.07 to 0.11 s^{-1} were obtained for the 0.001% and 0.5% samples, respectively. The

difference in rates for the aldehydes, if statistically significant, is not unreasonable if one assumes a more "zero-order nature" for the formation of hydroxyacetaldehyde, which is dependent on catalytic activity. The reproducibility of the reaction order for the two reactions under extremes of reaction is illustrative of the insight that this rate analysis of time-resolved data can provide.

Collision induced dissociation (CID) of selected ions has been used to deconvolute ambiguous peaks in pyrolysis-mass spectrometry of cellulose, such as m/z 60, 126, 144, and 162, which are known to be due to more than one product, and m/z 191, 163, and 145, which appear to have new significance in light of results reported above. The results are presented in table 1 for a variety of materials. The species at m/z 191 gives rise to fragments at m/z 173 and 163, due to a loss of 18 and 28, respectively. The series of daughter ions of m/z 191, at m/z 163, 145, and 127, resemble the dehydration series from the electron ionization fragment ions of levoglucosan at m/z 162, 144, and 126. This may imply that the parent of m/z 191 (m/z 192?) may be a derivative from an anhydrosugar. The peak at m/z 163 may be an electron ionization fragment of the same species that gives rise to m/z 191 and it also has daughter ions at m/z 145 and 127, but with a new daughter at m/z 85. Comparing m/z 162 from levoglucosan and cellulose indicates some dramatic differences with the cellulose ion giving rise to a daughter at m/z 73 that is not produced from levoglucosan. The parent at m/z 145 from cellulose pyrolysis is also different from the m/z 145 ion from levoglucosan, which again may be due to the m/z 145 being derived from the same species that gives rise to m/z 191. The daughters of m/z 144 are also more complicated from cellulose than levoglucosan. The model compounds at m/z 126 show relatively unique daughters for each (1,2,3-trihydroxybenzene - m/z 108; 1,3,5-trihydroxybenzene - m/z 85; 5-HMF - m/z 97; levoglucosenone - m/z 98). Untreated Avicel yields m/z 97 as a daughter of m/z 126, which indicates the 5-HMF and no hydroxybenzenes. The presence of salts lowers the overall daughter ion abundance from m/z 126, and the presence of m/z 108 would indicate the trihydroxybenzene in addition to 5-HMF. It is not generally recognized that the furfurals can arise from alkali metal catalysis, but these data support that hypothesis. The daughters of m/z 60 are also fairly unique for the model compounds and show that the daughters from treated cellulose can be resolved into the relative amounts of levoglucosan, hydroxyacetaldehyde, and acetic acid by the relative amounts of m/z 42, 32, and 45. Factor-analysis-based methods are being developed for deconvoluting CID spectra due to multiple products present at the nominal mass of interest.

Recent pyrolysis MBMS experiments of Acetobacter cellulose, grown on D-[1-^{13}C]-glucose media are reported here and this is a most exciting new tool for PY-MS studies of cellulose pyrolysis. The selectively enriched, labeled and unlabeled Acetobacter cellulose samples were prepared and purified by the same methods to remove potential metal ion contaminants and to insure that both samples could be compared. The regular and $^{13}C_1$ Acetobacter cellulose samples were pyrolyzed in triplicate at 520°C in flowing helium. The sample size was approximately 5 mg. Since m/z 145 and 127 are associated with another product group (that is alkali-catalyzed) in addition to being the isotope peaks of m/z 144 and 126, respectively, the enrichment effect can be masked by the differences between samples in the level of inorganic contamination. The ratio of m/z 126/144 is a sensitive indicator of the relative amounts of these different product groups. The data in table 2 show that the ratios of m/z 126/144 are 0.53 and 0.50 for the regular and enriched Acetobacter cellulose samples, respectively. This leads to the conclusion that there is no significant difference between the two samples in the relative amounts of the major pyrolysis product groups. Therefore, the differences in table 2 that are statistically significant are due to the isotope enrichment at the C_1 position. The average spectrum for the replicates of regular cellulose pyrolysis is indicative of anhydrosugar formation (there was a low abundance of m/z 43, which is a confirmation that these are clean samples). Therefore, isotope effects from this sample will only be relevant to part of the range of cellulose pyrolysis products. An analysis of variance (ANOVA) was performed for the triplicate runs for the two samples. The results are presented as the F-ratio, which is a statistical parameter used to estimate the probability of significant differences between two or more classes of replicated samples. For this experiment, an F-ratio of 7.71 indicates 95% confidence that the measured difference is significant and an F-ratio of 21.2 implies 99% confidence. The ions with an F-ratio greater than 3.5 are included in tables 2 and 3. The F-ratio test shows significant enrichment at m/z 144 with an F-ratio of 87 for m/z 145 and 69 for m/z 144. Since this ion is a six carbon product, which must contain C_1, this verifies that the enrichment can be detected for C_1 containing species. Simulation

data are included in the tables that assume 14% enrichment and the presence of C_1 in the products at every mass. Note that the peak intensities are very close for m/z 144 and 145 for the labeled Acetobacter average and those in the simulated enrichment. The products at m/z 126 also contain six carbon atoms and again the enrichment values for m/z 126 and 127 closely match the simulated values. Of the lower molecular weight products, only m/z 98 is significantly higher.

To force the distribution of pyrolysis products to the aldehyde product slate, samples of the Acetobacter cellulose were treated with 0.1% KOH and treated similarly to the samples described above. In this sample, m/z 126 shows significant enrichment, but no low-molecular-weight products are higher in the enriched cellulose. This indicates that the m/z 60 products that are present under these alkali-catalyzed conditions are not formed from the C_1 position in cellulose, and glycolaldehyde must come from the C2 to C6 positions. This work is continuing with labeled cellulose at other carbon positions.

In summary, the use of systematic catalytic additions to promote formation of product groups, the use of rate analysis of time-resolved data, and the use of CID for characterization, improves the application of Py-MS as a tool for studying the chemistry of cellulose pyrolysis. The most exciting new development is the use of ^{13}C-labeled cellulose that has specifically labeled positions and allows the source of each pyrolysis product to be traced to the exact position in the cellulose structure.

ACKNOWLEDGMENTS

The assistance of Carolyn Elam, David Gratson, Dingneng Wang, and Kuni Tatsumoto in experimental work, and of Willem Windig in discussions of multivariate analysis and use of the ISMA program is greatly appreciated.

REFERENCES

1. Antal, M. J., Jr. In Advances in Solar Energy; Boer, K. W.; Duffier, J. A., Eds.; Plenum: New York, 1885, vol.2, pp 175-728.

2. Shafizadeh, F. Applied Polymer Symposium 1975, 28, 153-174.

3. Kilzer, F. J.; Broido, A. Pyrodynamics 1965, 2, 151-163.

4. Golova,O. P. Russian Chemical Reviews, 1975, 44(8), 687-697.

5. Piskorz, J.; Radlein, D.; Scott, D. S. J. Anal. Appl. Pyrol. 1986, 9, 121-137.

6. Richards, G. N. Ibidem. 1987, 10, 251-255.

7. Pouwels, A. D.; Eikje, G. B.; Boon, J. J. Ibidem. 1989, 14, 237-280.

8. Meuzelaar, H. L. C.; Kistemaker, P. G. Anal. Chem. 1973, 45, 587-590.

9. Windig, W.; Meuzelaar, H. L. C. Ibidem. 1984, 56, 2297-2303.

10. Evans, R. J.; Milne, T. A. Energy Fuels 1987, 1, 123-137.

11. Windig, W.; Lippert, J. L.; Robbins M. J.; Kresinske, K. R.; Twist, J. P.; Snyder, A. P. Chemometrics and Intelligent Laboratory Systems, 1990, 9, 7-30.

12. Richards, G., N.; Shafizadeh, F.; Stevenson, T. T. Carbohydr. Res. 1983, 117, 322-327.

13. Carlson, L.; Feldthus, A.; Bo, P. J. Anal. Appl. Pyrol. 1989, 15, 373-381.

Table 1. Results of CID-MS on key masses from the pyrolysis of cellulose and selected model compounds. Conditions for CID were Argon collision gas and ion energies of approximately 20 eV. The intensities are relative to a parent ion intensity of 1000.

Parent	Material	Daughter Ions: m/z(intensity)
191	Avicel	127(168) 173(134) 145(113) 163(31)*
163	Avicel	145(112) 85(62) 127(36) 91(24)*
162	Avicel	73(44) 98(42) 144(42) 89(26)*
162	Levoglucosan	98(273) 116(114) 70(57) 106(52)
145	Avicel	85(77) 127(47) 99(34)* 73(31)*
145	Levoglucosan	73(223) 98(89)* 74(79)*
144	Avicel	72(92) 98(70) 73(57)*
144	Levoglucosan	73(144) 98(123)*
126	1,2,3-THB[1]	108(26) 80(26) 125(7)
126	1,3,5-THB[1]	85(20) 98(7) 125(7)
126	5-H-M-Furfural	97(486) 69(45) 125(11)
126	Levoglucosenone	98(281) 95(53) 80(48) 70(42) 97(41)
126	Avicel	97(121) 98(46) 80(41) 69(18) 81(11) 70(11)
126	cel+.05%Na2CO3	97(34) 80(21) 98(12) 108(12)*
126	cel+.5%K2CO3	98(20) 80(16) 97(14) 125(9)* 108(7)*
126	cel+.05%NaCl	97(59) 98(22) 80(13) 125(10) 108(7)*
126	Aceto. Cel#1	97(179) 98(45) 80(35) 69(33)
126	Aceto. Cel#2	97(109) 98(61) 69(25) 80(24) 70(16) 111(15)
60	Acetic Acid	45(533) 43(259) 42(48) 16(36) 15(12)
60	Hydroxyacetal.	32(1200) 31(873) 45(88) 43(35) 29(34) 42(32)
60	MeFormate	31(650) 32(477) 30(298) 29(75) 45(8) 15(6)
60	2-propanol	45(1700) 44(381) 31(202) 32(142) 43(80)
60	Levoglucosan	42(124) 31(60) 30(11)
60	Cel+.05%Na2CO3	42(108) 31(73) 32(32) 45(16) 43(9) 30(8)*

*These peaks have low signal-to-noise and their identification as daughters should be considered tentative.

[1]trihydroxybenzene

Table 2. Significant differences in the relative yields of pyrolysis products in regular ($I_{(m/z)R}$) and $^{13}C_1$-enriched ($I_{(m/z)E}$) Acetobacter xylinum cellulose. Each sample was run in triplicate and analysis of variance was performed to determine the degree of statistical significance (F-ratio, Level of Significance: 21.2, 1%; 12.2, 2.5%; 7.71,.5%). The difference between these values shows the effect of enrichment. Simulated values ($I_{(m/z)S}$) are presented as if each mass was enriched by 14% in $^{13}C_1$.

		Experimental			Simulated	
m/z	$I_{(m/z)R}$	$I_{(m/z)E}$	F-ratio	$(I_{(m/z)R}-I_{(m/z)E})$	$I_{m/z)S}$	$(I_{(m/z)R}-I_{(m/z)S})$
43	1.37	1.19	37.8	0.18	1.33	0.04
55	1.37	1.25	6.3	0.12	1.23	0.14
68	1.16	1.08	5.1	0.08	1.00	0.16
90	0.39	0.51	7.5	-0.11	0.48	-0.09
99	1.35	1.52	19.0	-0.16	2.38	-1.03
101	0.86	0.72	6.2	0.13	0.78	0.08
103	0.50	0.61	4.9	-0.11	0.57	-0.08
113	1.36	1.18	23.8	0.18	1.22	0.14
114	2.02	1.87	6.4	0.16	1.93	0.09
116	1.37	1.52	9.8	-0.15	1.41	-0.04
126	2.90	2.38	4.8	0.52	2.53	0.38
127	0.56	0.91	37.7	-0.35	0.89	-0.33
142	0.31	0.22	3.6	0.10	0.27	0.04
144	5.50	4.72	68.5	0.78	4.76	0.75
145	0.84	1.46	87.8	-0.62	1.49	-0.65
146	0.20	0.29	39.2	-0.09	0.29	-0.09
163	0.30	0.37	3.6	-0.07	0.30	0.00
167	0.22	0.15	4.1	0.07	0.20	0.02
192	0.16	0.23	22.0	-0.07	0.17	-0.01

Table 3. Significant differences in the relative yields of pyrolysis products in regular and $^{13}C_1$-enriched Acetobacter xylinum cellulose treated with 0.1% KOH. See Table 2 caption for details.

		Experimental			Simulated	
m/z	$I_{(m/z)R}$	$I_{(m/z)E}$	F-ratio	$(I_{(m/z)R}-I_{(m/z)E})$	$I_{m/z)S}$	$(I_{(m/z)R}-I_{(m/z)S})$
29	1.49	1.65	5.3	-0.16	1.50	-0.01
45	0.96	1.26	5.4	-0.30	1.44	-0.48
57	3.14	2.83	21.1	0.31	2.87	0.27
68	1.00	0.86	19.7	0.14	0.91	0.09
74	1.43	1.30	18.2	0.13	1.60	-0.17
85	2.52	2.36	19.0	0.16	2.43	0.09
97	1.80	1.60	6.0	0.19	1.71	0.08
98	3.58	3.32	18.1	0.25	3.33	0.25
126	3.35	2.60	11.8	0.74	2.93	0.41
127	0.59	0.95	34.4	-0.36	0.97	-0.39
142	0.26	0.21	41.7	0.04	0.24	0.02
144	0.80	0.48	20.5	0.32	0.71	0.09
145	0.43	0.33	5.3	0.10	0.48	-0.05
190	0.15	0.20	7.9	-0.06	0.14	0.01
191	0.14	0.17	120.	-0.04	0.14	-0.00

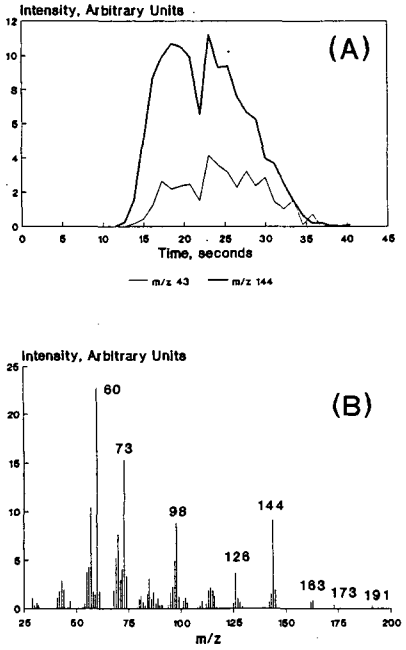

Fig. 1. The pyrolysis of Avicel cellulose treated with .001% K (as KOH) at 540 °C: (A) time-resolved evolution profile of m/z 43 and 144 (B) the average, background-corrected spectrum of pyrolysis products.

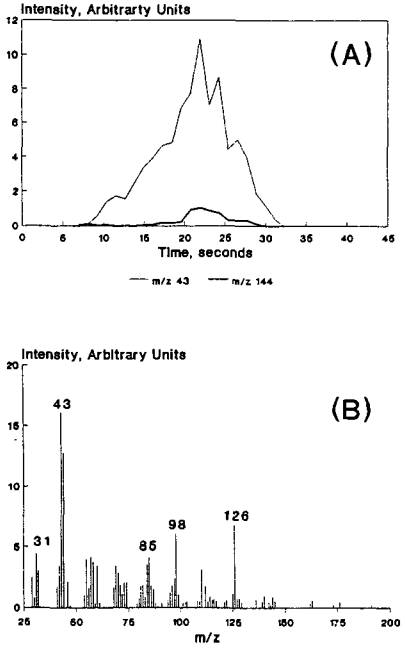

Fig. 2. The pyrolysis of Avicel cellulose treated with .5% K (as KOH) at 540 °C: (A) time-resolved evolution profile of m/z 43 and 144 (B) the average, background-corrected spectrum of pyrolysis products.

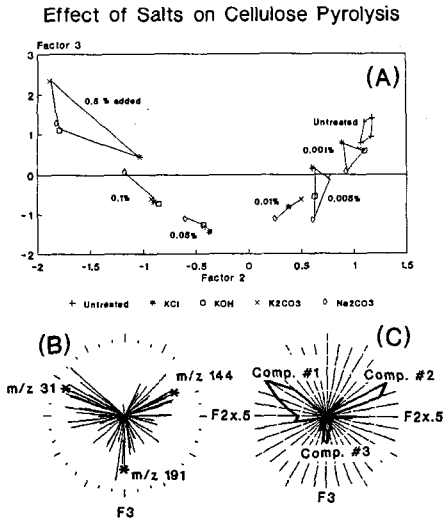

Fig. 3. The results of factor analysis of pyrolysis- mass spectra of avicel cellulose treated with different levels of salts: (A) plot of factor 2 score vs factor 3 score showing the two major trends in the data set; (B) mass variable loading projections showing underlying distribution of data set; and (C) the variance diagram, which is a weighted display of the mass axes projections and shows the maxima of clustering, which indicate the directions of component axes. The pure masses, which delineate component axis, are noted with asterisk in B.

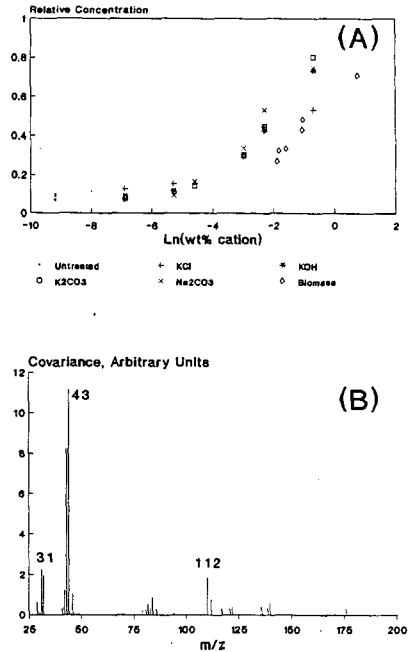

Fig. 4. The first component mathematically resolved from the data set in fig. 3 (pure mass m/z 31) showing its relative concentration in the samples (A) and the reconstructed spectrum (B).

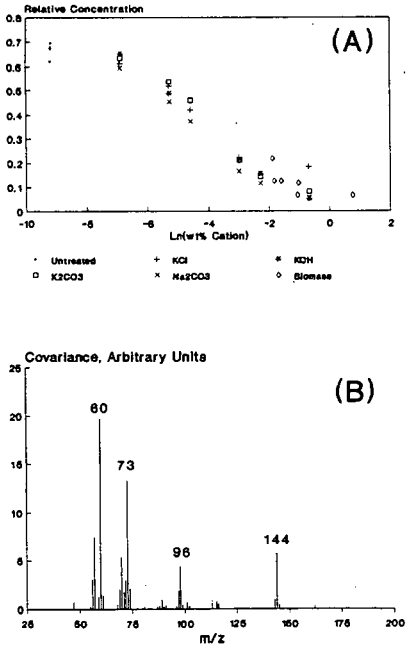

Fig. 5. The second component mathematically resolved from the data set in fig. 3 (pure mass m/z 144) showing its relative concentration in the samples (A) and the reconstructed spectrum (B).

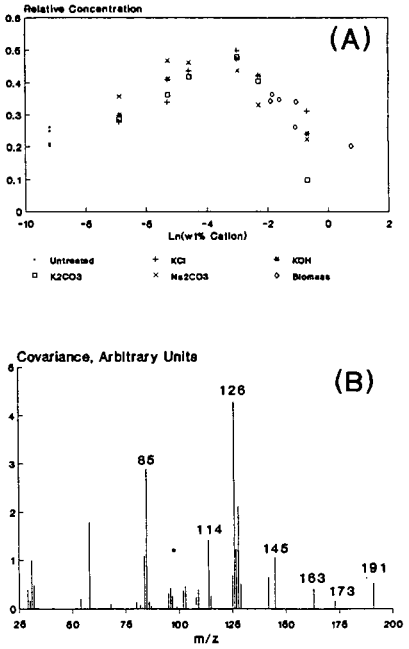

Fig. 6. The third component mathematically resolved from the data set in fig. 3 (pure mass m/z 191) showing its relative concentration in the samples (A) and the reconstructed spectrum (B).

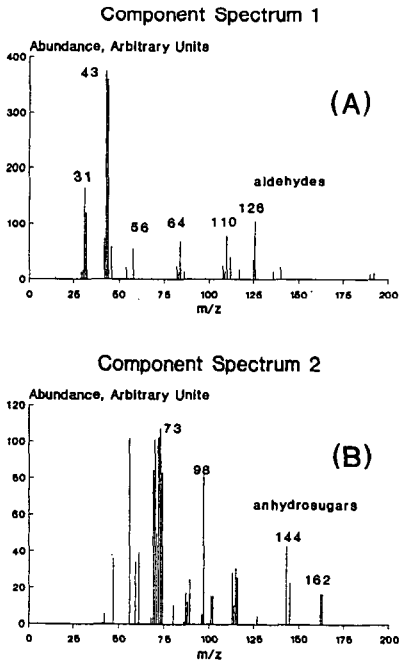

Fig. 7. The results of factor analysis on time resolved data for the .001% and .5% K-treated cellulose data sets, which were combined in one data set to deconvolute the major product slates: (A) component spectrum 1, which represents the aldehydes and (B) component spectrum 2, which represents the anhydrosugars.

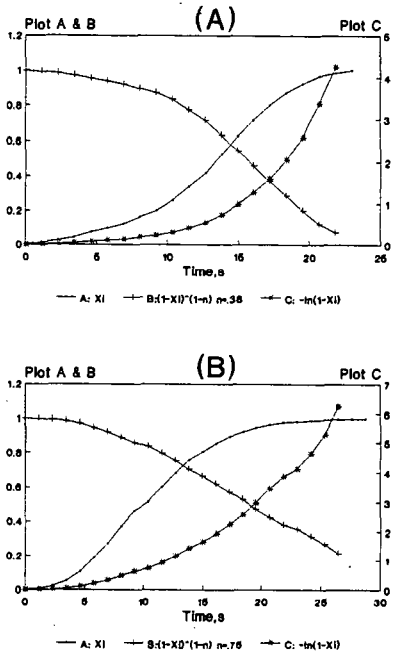

Fig. 8. Examples of the analysis of the rate of formation of the resolved components that are shown in fig. 7: (A) aldehydes from .5% K-treated cellulose and (B) anhydrosugars from .001% K-treated cellulose.

CHARACTERIZATION OF LIGNOCELLULOSIC MATERIALS AND MODEL COMPOUNDS BY COMBINED TG/(GC)/FTIR/MS

Jacek P. Dworzanski, Richard M. Buchanan, John N. Chapman
and Henk L.C. Meuzelaar
Center for Micro Analysis and Reaction Chemistry
The University of Utah, Salt Lake City, UT 84112

Key words: thermogravimetry, gas chromatography, mass spectrometry, infrared spectrometry, lignins, wood

INTRODUCTION

Thermal analytical methods have been widely used during the last two decades in the study of biomass thermochemical conversion processes [1-4]. Biomass, which represents a renewable energy resource, consists primarily of plant cells differentiated into characteristic tissues and organs. Lignins, hemicelluloses and cellulose, as the main components of the cell walls, were therefore extensively analyzed, especially from the point of view of their thermochemical reactivity, which is of basic importance for industrial processing of biomass [3].

All types of cellulose microfibrils are composed of linearly linked β-(1-->4)-D-glucopyranose units and differ only by the degree of polymerization. The remaining polysaccharides are known collectively as hemicelluloses and exhibit species related composition. These amorphous, complex heteropolymers characterized by a branched molecular structure exhibit a lower degree of polymerization than cellulose. Xylan is the predominant hemicellulose component of angiosperms ("hardwoods") whereas mannan forms the main hemicellulose of gymnosperms ("softwoods"). The third principal component of biomass, viz. lignin, is an irregular, high MW polymer formed by enzyme-initiated, free-radical polymerization of coniferyl alcohol (in hardwoods), coniferyl plus sinapyl alcohols (in softwoods), or coumaryl alcohol plus both above mentioned alcohols (in grasses) [5]. Lignins act as binding agents for the cellulose and hemicellulose fibers through a variety of linkages involving ether and carbon-carbon bonds of aromatic rings and propyl side chains.

Thermochemical conversion processes of lignocellulosic materials have been studied using mainly thermogravimetry (TG) [6] or flash pyrolysis (Py) followed by gas chromatographic (GC) separation and identification of the reaction products [1]. Modern analytical techniques based on coupled Py-GC/mass spectrometry (Py-GC/MS) [7] or direct Py-MS [2,8] as well as TG/MS or TG/infrared spectroscopy (TG/IR) [4] have proved to be especially useful for elucidating the relationships between biomass structure and pyrolysis/devolatilization mechanisms.

A novel TG/(GC)/FTIR/MS system developed at the University of Utah, Center for Micro Analysis and Reaction Chemistry [9] provides the opportunity for combining accurate weight loss measurements with precise information about composition and evolution rates of gaseous and liquid products as a function of temperature. In this paper, the usefulness of TG/FTIR/MS, TG/GC/MS and TG/GC/FTIR for thermochemical characterization of wood, lignins and cellulose will be discussed.

EXPERIMENTAL

The TG/FTIR/MS system consists of a Perkin Elmer model 7 Thermogravimetric Analyzer with high temperature furnace controlled by an IBM compatible PC and interfaced to a Hewlett-Packard GC/IRD/MSD system (GC - model 5890A, IRD - model 5965A and MSD - model 5971A) controlled by HP 9000 computers (Figure 1). As shown in Figure 1 a specially constructed, heated transfer line assembly allows direct coupling of the TG system to the GC injection port with the GC oven acting as a convenient heated coupling and flow distribution module. In order to make an efficient TG/GC interface, a 0.53 mm I.D. ("megabore") deactivated fused silica capillary column is used to transfer TG effluents to the GC oven. On the TG side this column protrudes several centimeters into a 1 mm i.d. quartz tube which, in turn, extends into the high temperature furnace to within 1 cm of the sample crucible. Both the outlet of the ceramic furnace tube and the quartz tube are vented by means of needle valves. The quartz tube may be also backflushed with helium to prevent air from entering the MSD vacuum system when the TG furnace is open or not yet purged. Inside the GC oven this capillary terminates with a splitter which provides 90 % of the total flow to the IRD and 10% to the MSD instrument. In order to enable GC separations of the TG effluent the capillary transfer line terminates within a specially designed repetitive vapor sampling inlet inside the GC oven. This inlet leads, in turn, to either (or both!) the IRD or MSD modules via a short (ca. 2 m) capillary column. The switching action of the repetitive sampling inlet causes diversion of the "protective" helium gas flow (see Figure 1) allowing only a short (1-2 sec long) burst of TG effluent to enter the column for further GC separation of the various components and subsequent spectroscopic (MS and/or IR) identification.

Samples A steam explosion lignin prepared from Yellow Poplar wood (Liridendron tulipifera) was isolated by extraction with sodium hydroxide followed by acid precipitation. This sample was donated by Professor Wolfgang Glasser of the Biobased Materials Center at Virginia Tech., in Blacksburg, VA. Douglas fir wood was air dried and analyzed as tiny particles obtained by scratching a piece of wood with a blade.

RESULTS AND DISCUSSION

Figure 2 summarizes some of the results obtained by TG/FTIR/MS analysis of steam explosion Yellow Poplar lignin. In Figures 2b and h the TG weight loss and the differential thermogravimetric (DTG) curves are presented at a heating rate of 15 C/min in helium atmosphere. These graphs reveal the onset of weight loss near 150 C, with a peak of maximum rate of weight loss at 350 C which follows two shoulders at 160 C and 230 C and preceeds a third around 420 C. Averaged mass spectra and infrared spectra of all products evolved during the course of the TG experiment are shown in Figures 2a and g, respectively. Inspection of the MS spectrum indicates the presence of components associated with the monomethoxy series: guaiacol {m/z 124 (M^+) and m/z 109 (M^+ - 15)}, 4-methylguaiacol {m/z 138 (M^+) and m/z 123 (M^+ - 15)}, 4-vinylguiacol {m/z 150 and m/z 135}, vanillin {m/z 152} and isoeugenol {m/z 164}. The components associated with the dimethoxy series are syringol {m/z 154 (M^+) and m/z 139 (M^+ - 15)}, 4-methylsyringol {m/z 168 and m/z 153}, 4-vinylsyringol {m/z 180}, syringaldehyde {m/z 182} and 4-(1-propenyl)-syringol {m/z 194}. These series of ions are typical for thermal degradation products obtained by pyrolysis of hardwoods or their lignin components [2]. In Figures 2e and f the comparative rates of evolution of guaiacol and syringol are shown as well as 4-methylguaiacol and 4-methylsyringol, respectively. The trace shown in Figure 2k demonstrates the profile of the components exhibiting characteristic alkyl-aryl ether

stretching vibration in the 1260-1290 cm^{-1} region, typical for mono- and di-methoxy phenols, e.g., building blocks of lignin. Our technique enables also the detection of minor contaminants in lignin samples and profiles of the ion m/z 114 (Figure 2d) as well as the trace at 1184 cm^{-1} (Figure 2j), characteristic for C-O stretching vibrations of lactones, strongly suggest the presence such struetures as 3-hydroxy-2-penteno-1,5-lactone (M.W. 114) a carbohydrate "marker" from thermal dissociation of xylanes [10] which may be utilized for quantification of hemicellulose residues in lignin preparations. The total ion current (Figure 2b - TIC) and total absorption (Figure 2h - TAP) profiles of the thermal breakdown products released during the TG experiment reveal substantial differences in shape compared to the recorded DTG curve. This is primarily due to the tuning of the MSD instrument for higher masses as well as due to the fact that a high percentage of the weight loss is caused by low molecular weight components (H_2O, CO, CO_2, MeOH) as demonstrated by the averaged IR spectrum shown in Figure 2g. Nevertheless, the rate of evolution profiles are virtually the same (compare curves in Figures 2c and i for CO_2), hence stronger responses for higher masses facilitate monitoring of high MW components.

Any ambiguities which inevitably arise in regard to the identity of particular components may, to a large extent, be overcome by GC preseparation of thermal dececomposition products. The TG/GC/MS/IR system is capable of separating major products, while still allowing characterization of the evolution profile for particular components, as illustrated in Figures 3 and 4. This enables inspection of selected spectra, providing the way for unequivocal identification and chemical interpretation of thermal processes occurring during the TG experiment. In the TG/GC/MS run of Douglas fir wood vapor samples were taken at 1 minute intervals, so profiles for each GC peak can be followed by identifying peaks with the same GC retention time. This task is greatly facilitated by the selection of characteristic ions at m/z 114, 98, 109 and m/z 138, as shown in Figures 3 b-e. The mass spectrum of the component eluting at 8.31 min is shown in Figure 3f and contrasted with a library spectrum of 3-hydroxy-2-penteno-1,5-lactone (Figure 3j), a typical thermal fragment of the pentose moieties. The mass spectrum of the component taken 11.21 min (Figure 3g) shows spectra of polyhexosc pyrolysis products, viz. furanone-2 (M.W. 84) and 5-methylfuranone-2 (M.W. 98) which are the products of depolymerization and further decomposition of cellulose [11]. For the temperature range 350-450 C profiles taken at m/z 109 and m/z 138 can be fully confirmed as representing guaiacol and methylguaiacol fragment and molecular ions, respectively, derived from lignin. This is clearly shown by comparison of the mass spectra taken at 11.53 min and 12.99 min with library spectra (Figure 3).

Results of the TG/GC/IR analysis of Douglas fir wood are reported in Figure 4. In Figure 4 a TG and DTG curves are contrasted with total absorption chromatogram (TAC) profiles recorded at 1 minute intervals each minute after "injection" of the TG vapors, wheras the averaged FTIR spectrum of all volatile components is shown in Figure 4b. This spectrum reflects the complex composition of the pyrolysis products and is dominated by gases with strong absorption coefficients, such as CO_2, CO and H_2O, thereby complicating individual band assignments and chemical interpretations concerning any additional minor components. In Figure 4c a detailed view of an expanded section of the chromatograms shown in Figure 4a is presented (8-24 mins) and the presence of numerous series of peaks is demonstrated. At 24 s retention time a set of chromatographic peaks exists which reach maximum intensity at 11 min. TG run time (265 C). The spectrum of this component contains a strong absorption band at 1184 cm^{-1}, the selected wavenumber chromatograms of which are shown in Figure 4d, indicating the presence of the C-O stretching vibrations of lactones. In addition to the profiles of these main components, showing the correspondence to the 3-hydroxy-2-penteno-1,5-

lactone from hemicelluloses, there are also two additional sets of peaks at retention time 7 s and maximum rate of evolution at 13 min. (295 C) as well as at 40 s and maximum evolution rate at 16 min. (340 C). The last profile clearly exhibits an evolution maximum that is coincident with a profile shown in Figure 4e. The components characterized by retention times approx. 30 s and strong absorption at 1810 cm-1, typical for carbonyl absorption of unsaturated lactones, confirm the presence of 2-furanones generated during the thermal breakdown of celllulose. Finally, the third major stage in the pyrolysis of wood is seen in the occurrence of components reaching peak evolution rates in the 17-18 min run time (355-370 C) range and decreasing relatively slowly afterwards. Strong absorption bands near 1500 cm^{-1} and just below 1300 cm^{-1} indicate the presence of phenol and aryl-alkyl ethers functionalities, as would be expected from the breakdown products of lignin. An infrared spectrum of such component taken at 42 s after sampling (marked with asterisk in Figure 4f) is shown in Figure 4g and is contrasted with a FTIR reference spectrum of guaiacol, presented in Figure 4h.

Characteristics of this technique combine precise temperature information and accurate weight loss with detailed MS and IR response profiles thereby providing detailed information about the mechanisms and kinetics of thermal degradation processes. Chemical interpretations of the components evolved during heating of lignocellulosic materials under a helium atmosphere are greatly facilitated by inspection of the infrared and mass spectra, if necessary after GC preseparation.

ACKNOWLEDGEMENTS

Financial support of the work reported here was provided by the Advanced Combustion Engineering Research Center (funded by NSF, the State of Utah, 23 industrial participants, and the U.S. DOE), as well as The Consortium for Fossil Fuel Liquefaction Science (UKRF-4-23576-90) and by Hewlett-Packard Corporation.

REFERENCES

1. Antal, M.J., Jr. In Boer, K.W.; Duffie, J.A., Eds., Advances in Solar Energy, ASES Publication, New York, **1985**, Vol 2, p. 175.
2. Evans, R.J.; Milne, T.A.; Soltys, M.N. J. Anal. Appl. Pyrol. **1986**, 9, 207.
3. Shafizadeh, F. J. Anal. Appl. Pyrol. **1982**, 3, 283.
4. DeGroot, W.F.; Pan, W-P.; Rahman, M.D.; Richards, G.N. J. Anal. Appl. Pyrol. **1988**, 13, 221.
5. Graham, R.G.; Bergougnou, M.A.; Overend, R.P. J. Anal. Appl. Pyrol. **1984**, 6, 95.
6. Shafizadeh, F.; McGinnis, G.D. Carbohydr. Res. **1971**, 16, 273.
7. Martin, F.; Saiz-Jimenez, C.; Gonzalez-Vila, F.J. Holzforschung, **1979**, 33, 210.
8. Windig, W.; Meuzelaar, H.L.C.; Shafizadeh, F.; Kelsey, R.G. J.Anal. Appl. Pyrol. **1984**, 6, 233.
9. Holbrook, K.M.; Buchanan, R.M.; Meuzelaar, H.L.C.; Proc. of the 38th ASMS Conf. on Mass Spectrometry and Allied Topics, Tucson, Arizona, June 3-8, **1990**, p. 900.
10. Evans, R.J.; Milne, T.A. Energy Fuels **1987**, 1, 123.
11. Pouwels, A.D.; Tom, A.; Eijkel, G.B.; Boon, J.J. J. Anal. Appl. Pyrol. **1987**, 11, 417.

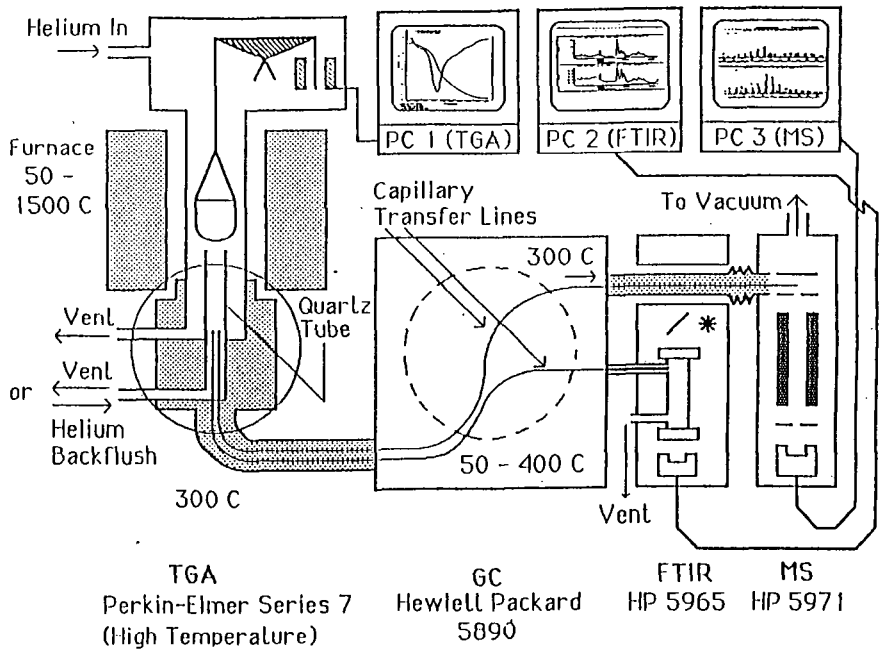

Figure 1. TG/GC/IR/MS instrument configuration.

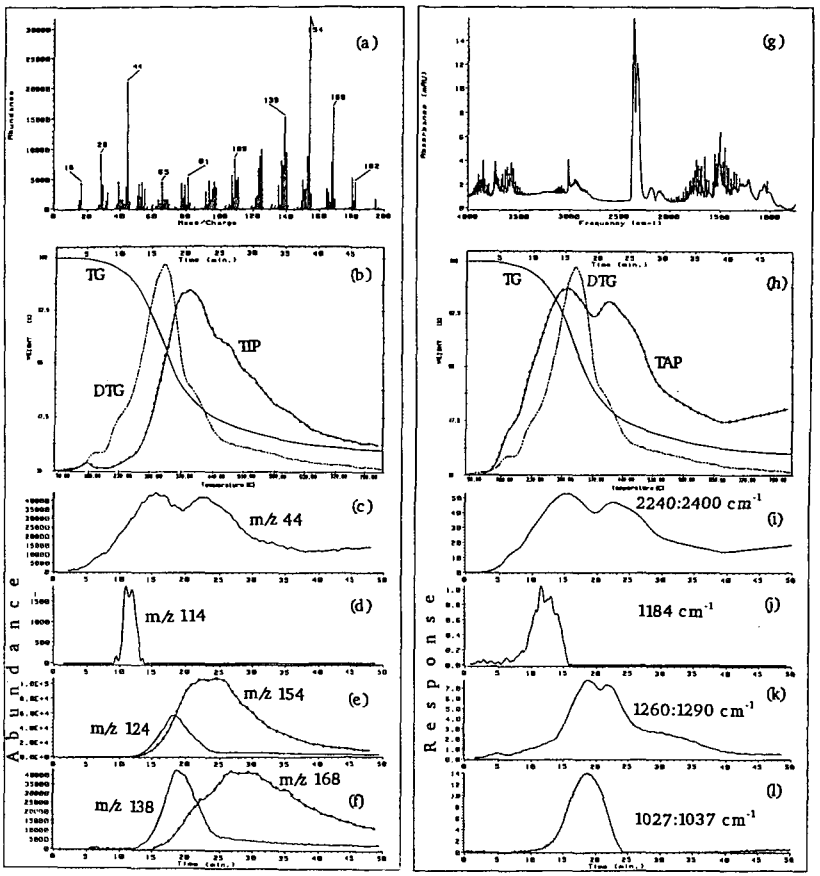

Figure 2. TG/FTIR/MS analysis of steam explosion lignin from Yellow Poplar wood: (a) the averaged MS spectrum of thermal degradation products; (b) TG, DTG and total ion profiles (TIP) of the degradation products; TG heating rate: 15 C/min; (c)-(f) selected ion profiles indicating the evolution of CO_2 (c); 3-hydroxy-2-penteno-1,5-lactone (d); guaiacol (m/z 124) and syringol (m/z 154) (e); 4-methylguaiacol (m/z 138) and 4-methylsyringol (m/z 168) (f);
(g) the averaged FTIR spectrum of thermal degradation products; (h) TG, DTG and the total absorption profiles (TAP) of the thermal degradation products; (i)-(l) selected wavenumber profiles indicating the evolution of CO_2 (i), lactones (j), alkyl-aryl ethers (k) and methanol (l).

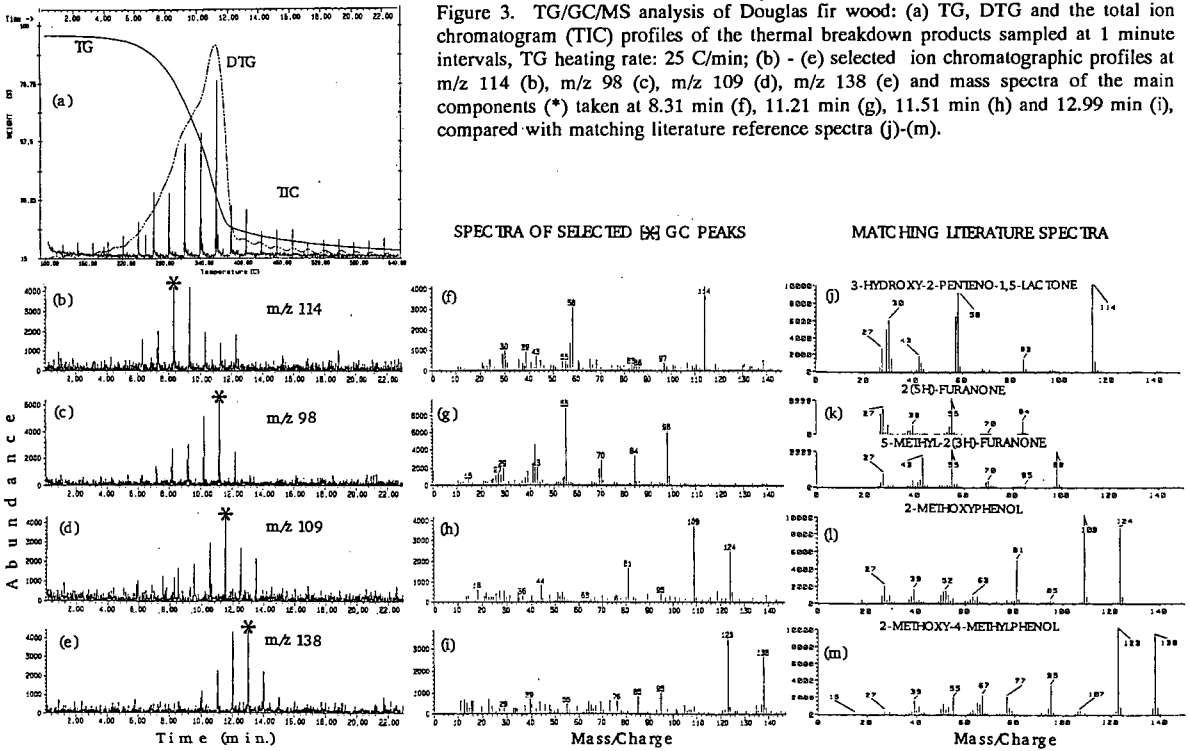

Figure 3. TG/GC/MS analysis of Douglas fir wood: (a) TG, DTG and the total ion chromatogram (TIC) profiles of the thermal breakdown products sampled at 1 minute intervals, TG heating rate: 25 C/min; (b) - (e) selected ion chromatographic profiles at m/z 114 (b), m/z 98 (c), m/z 109 (d), m/z 138 (e) and mass spectra of the main components (*) taken at 8.31 min (f), 11.21 min (g), 11.51 min (h) and 12.99 min (i), compared with matching literature reference spectra (j)-(m).

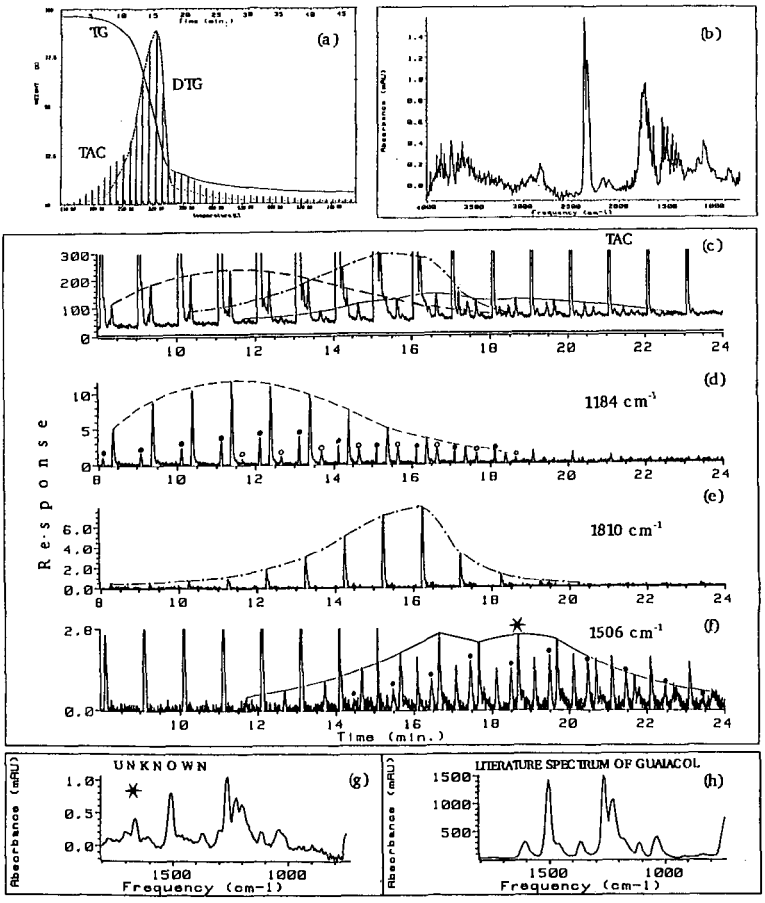

Figure 4. TG/GC/IR analysis of Douglas fir wood: (a) TG, DTG and the total absorption chromatogram (TAC) profiles of the thermal breakdown products sampled at 1 minute intervals, TG heating rate:15 C/min; (b) the averaged FTIR spectrum of all volatile degradation products; (c) the expanded section of the total absorption chromatogram shown in (a); degradation products from hemicellulose (- -), cellulose (---) and lignin (—); (d) - (f) selected wavenumber chromatographic profiles [(d) at 1184 cm^{-1} (lactones derived from hemicellulose), (e) at 1810 cm^{-1} (furanones derived from cellulose), (f) at 1506 cm^{-1} (phenols derived from lignin)]; (g) FTIR spectrum of the unknown component (*) taken at 18.70 min and corresponding to the phenols derived from lignins (---) compared with the reference spectrum of guaiacol (h).

LASER PYROLYSIS GAS CHROMATOGRAPHY/MASS SPECTROMETRY OF SINGLE SPHEROCARB PARTICLES IMPREGNATED WITH BITUMINOUS AND POLYMERIC SUBSTANCES

Waleed S. Maswadeh, Huaying Huai and Henk L.C. Meuzelaar
Center for Micro Analysis & Reaction Chemistry, University of Utah
214 EMRL, Salt Lake City, UT 84112

Keywords: coal devolatilization, laser pyrolysis, mass spectrometry

INTRODUCTION

A major bottleneck in the development of novel coal characterization methods, such as laser pyrolysis GC/MS, capable of analyzing individual coal particles, is the unavailability of suitable standard samples. Although carefully homogenized and characterized standard coals are now available through the Argonne National Laboratory Premium Coal Sample Program (ANL-PCSP) such "statistically homogeneous" coal powders are of limited value as reference materials for single particle analysis methods. Even if it would be feasible to prepare particles of closely similar chemical composition and size, e.g., by using highly concentrated coal maceral fractions and careful sieving, remaining variations in shape, density, porosity or thermal conductivity could still introduce an unacceptably high level of uncertainty for most optimization and calibration purposes.

In an attempt to find model coal char particles with well defined chemical [1,2] and physical properties, e.g., for the purpose of modeling char oxidation reactions, several authors have used Spherocarb® particles. Flagan et al [3] have even prepared spherical char particles spiked with mineral matter components in order to more closely mimic actual coal char particles. Although Spherocarb particles still show considerable variability with regard to size (rel. s.d. ~20% on a volume basis), other characteristics such as shape, density, porosity, thermal conductivity and chemical composition are assumed to be quite constant.

Unfortunately, Spherocarb particles are of little value for modeling coal devolatilization reactions due to their very low volatile matter yields. This prompted us to think of ways to increase volatile matter yields by introducing a variety of model compounds, ranging from low molecular weight, bitumen-like components to polymeric materials such as soluble lignins or resins. To the best of our knowledge this article represents the first reported use of bitumen and polymer impregnated Spherocarb particles for modeling devolatilization processes in individual coal particles.

EXPERIMENTAL

Bitumen-like low MW compounds, consisting of a mixture of alkylnaphthalenes prepared by open column LC subfractionization of a coal pyrolyzate, [4] with additional 1-3 ring alkylaromatics and hydroxyaromatics added in later were impregnated into a small batch of Spherocarb particles, in the 125-150 μm dia. size range from a 8 mg/ml solution in methanol, followed by evaporation of the solvent at room temperature. The average amount of bitumen adsorbed by each particle was estimated to be approx. 70 ng. Soluble polymeric materials, such as steam-exploded cottonwood lignin and fossil resin derived from Utah (Blind Canyon seam)

coal were impregnated from 8 mg/ml solutions in 2:1 methanol/dichloromethane and toluene, respectively. Assuming complete absorbtion of the polymers into the Spherocarb particles the maximum average amount of polymer per particle was estimated at 70 ng. Experiments with actual coal particles in the 100-150 μm size range, prepared by careful sieving, involved Illinois #6 coals from the ANL-PCSP program.

Laser pyrolysis gas chromatography/mass spectrometry (laser Py-GC/MS) experiments were performed with two different experimental configurations as shown in Figures 1a and 1b respectively. The first experimental set-up (Figure 1a) has been described before in more detail [5] and consists of an EDB (electrodynamic balance), a 50 W cw CO_2 laser and a Finnigan MAT ITMS system. The EDB type particle levitation cell was constructed in such a way as to provide line-of-sight access to the center of the cell for the two opposing CO_2 laser beams as well as for a stereo microscope and a two-color optical pyrometer. Typical cell operating parameters for levitating a 120 μm dia. Spherocarb particle are: ring electrode 3000 V (60 Hz ac), upper end cap +100 V dc, lower end-cap -100 V dc. A second, novel experimental set-up (Figure 1b) uses copper electron microscopy grids with 45 x 45 μm openings separated by 5 μm thick bars (78% open, see Figure 2) to support individual coal particles in a downward directed flow of air or inert gas in the center of two CO_2 laser beams crossing at a 37° angle. Since the grids are mounted directly against the mouth of the sampling inlet, yields of volatile products are maximized. Furthermore, introducing, positioning, stabilizing and retrieving individual particles is greatly simplified compared to the set-up in Figure 1a, while conductive heat losses may be assumed to be minimal in view of the light construction of the grid.

The cw CO_2 laser (Apollo 3050 OEM) is capable of electronic pulsed beam operation. The 8 mm dia. beam is split equally into 2 separate beams focussed at the center of the levitation cell or grid (beam waist ca. 400 μm, typical power densities 4-10 MW/m^2). A co-linear, parfocal HeNe laser beam permits positioning of the particle in the center of the CO_2 laser beam. Two IR detectors measure integrated pulse energy and time-resolved pulse energy, respectively.

Finally, a heated fused silica capillary GC column (2m x .18 mm DB5) equipped with a special air sampling inlet enables intermittent sampling of volatiles from the center of the levitation cell or grid into the ITMS vacuum system while providing a highly useful degree of GC separation. During a typical run the GC column is ballistically heated from 50 C to 200 C in approx. 2 minutes.

RESULTS AND DISCUSSION

The novel laser pyrolysis GC/MS configuration shown in Figure 1b, in which coal and Spherocarb particles are supported on ultralight electron microscopy grids (Figure 2), promotes efficient collection of volatile pyrolysis products. As shown in Figure 3, this results in high quality Py-GC/MS profiles of single coal particles. Nevertheless, due to the inherent heterogeneity of individual coal particles with regard to physical and chemical characteristics, marked differences in absolute and relative yields of pyrolysis products are observed during successive analyses of actual coal particles, e.g. for the purpose of kinetic studies, as shown in Figure 4.

This prompted us to use Spherocarb particles spiked with known quantities of low MW bitumen-like substances (Figures 5 and 6) or soluble polymeric substances, such as lignin (Figure 7) and fossil resin (Figure 8). Laser desorption studies of bitumen-like substances, composed of alkynaphthalenes and other 1-3 ring alkylaromatics (Figures 5 and 6), are relevant in view of the well known presence of significant quantities of thermally extractable bitumen in many low or medium rank coals [6]. As illustrated in Figure 5, kinetic studies of bitumen release rates from Spherocarb particles as a function of laser pulse length do indeed show a markedly constant relative abundance of major bitumen components.

Since the bulk of the coal components undergoing devolatilization reactions consists of nonvolatile, macromolecular compounds which undergo bond scission reactions in addition to the thermal desorption behavior exhibited by low MW, bitumen-like compounds, it is desirable to work with polymeric materials when modeling coal devolatilization processes. Ideally, one would like to introduce high MW coal components, e.g., obtained by solvent extraction of suitable coals into the Spherocarb particles. Unfortunately, it tends to be quite difficult to remove effective solvents such as pyridine from these extracts, let alone from a strongly adsorbing Spherocarb matrix. These considerations led us to focus on soluble model polymers rather than on high MW vitrinite components. Because of its chemical resemblance to vitrinite components in peats and low rank coals, we chose a soluble lignin. Secondly, we selected a fossil coal resin, which appears to be the only high MW coal component readily soluble in common organic solvents.

Both the lignin and the resin are known to depolymerize readily under typical pyrolysis conditions, thus producing mixtures of characteristic building blocks. As expected from a hardwood lignin [7] the cottonwood lignin sample produces both guaiacylic (e.g., m/z 124, 138, 152) and syringylic (e.g., m/z 154) building blocks (see Figure 7). Similarly, the Blind Canyon seam resin, known to consist primarily of polymeric sesquiterpenoids [8], produces a characteristic series of sesquiterpenoid building blocks as shown in Figure 8, ranging from cadinenes (m/z 204) through the partially aromatized calamenes (m/z 202) to the fully aromatized cadalene (m/z 198). It should be noted here that the resinite pyrolysis patterns shown in Figure 8 appear to be more simple than those obtained by conventional pyrolysis GC/MS techniques. Whether this is due to selective loss of less stable pyrolysis products in the Spherocarb particles or to differences in primary pyrolysis mechanisms at the much higher heating rates achieved by the CO_2 laser (10^4-10^5 K/sec) needs to be investigated further.

Although the experiments with polymer impregnated Spherocarb particles are still in a relatively early stage, the selected ion chromatograms in Figures 7 and 8 demonstrate that it is indeed possible to introduce readily detectable amounts of such polymers. Unknown at present, however, are the answers to the following fundamental questions:

(1) what is the maximum weight % of polymeric materials that can be introduced;
(2) how can the amount of polymeric material adsorbed into each Spherocarb be conveniently controlled and measured;
(3) to what extent does the Spherocarb matrix influence the devolatilization mechanisms and kinetics; and
(4) are polymer impregnated Spherocarb particles well enough defined to achieve the desired reduction in interparticle heterogeneity during devolatilization experiments?

The primary objective of several experiments currently underway in our laboratory is to find answers to the above questions.

CONCLUSIONS

The feasibility of producing bitumen and polymer impregnated Spherocarb particles for coal devolatilization modeling experiments has been established. Bitumen-impregnated Spherocarb particles show a markedly decreased level of interparticle heterogeneity compared to actual coal particles. Spherocarb particles impregnated with (soluble) polymeric materials produce readily detectable volatile products thought to represent characteristic building blocks produced by bond scission reactions. Although the "volatile matter enhanced" Spherocarb particle approach appears to offer promise for modeling coal devolatilization reactions, several fundamental questions regarding the quantitative and qualitative behavior of such systems remain to be answered before this approach can be recommended as a general tool for devolatilization studies in individual coal particles.

ACKNOWLEDGEMENTS

This work was sponsored by the Advanced Combustion Engineering Research Center. Funds for this Center are received from the National Science Foundation, the State of Utah, 23 industrial participants, and the U.S. Department of Energy.

REFERENCES

1. Spjut, R.E., Sarofim, A.F., Longwell, J.P., "Laser Heating and Particle Temperature Measurement in an Electrodynamic Balance," Langmuir, Vol. 1, #3, 1985.
2. Phuoc, T.X., Maloney, D.J., "Laser Pyrolysis of Single Coal Particles in An Electrodynamic Balance," 22nd Symp. (Intl.) on Combustion (The Combustion Institute), 1988, pp. 125-134.
3. Levendis, Y.A., Flagan, R.C., "Synthesis, Formation and Characterization of Micro Sized Glassy Carbon Spheres of Controlled Pore Structure", Carbon 27, 265-283, 1989.
4. Hoesterey, B.L., Windig, W., Meuzelaar, H.L.C., Eyring, E.M., Grant, D.M., Pugmire, R.J., "An Integrated Spectroscopic Approach to the Chemical Characterization of Pyrolysis Oils" in Pyrolysis Oils from Biomass: Producing, Analyzing and Upgrading, 1988, ACS Symp. Series 376, J. Soltes and T.A. Milne (eds.), pp. 189-202.
5. Maswadeh, W., Arnold, N.S., Meuzelaar, H.L.C., "Laser Pyrolysis-transfer Line Chromatography/Mass Spectrometry of Single, Levitated Coal Particles", ACS Preprints, Div. of Fuel Chem., Vol. 35(3), August 1990, pp. 713-720.
6. Yun, Y., Meuzelaar, H.L.C., "Simultaneous Thermogravimetric and Mass Spectrometric Observations on Vacuum Pyrolysis of Argonne PCSP Coals," ACS Preprints, Div. of Fuel Chem., Vol. 33, #3, Sept. 1988, pp. 75-84.
7. Saiz-Jimenex, C.S., Boon, J.J., Hedges, J.I., Hessels, J.K.C., deLeeuw, J.W., "Chemical Characterization of Recent and Buried Woods by Analytical Pyrolysis", J. Anal. Appl. Pyrol., 11 (1987) 437-450.
8. Meuzelaar, H.L.C., Huai, H., Lo, R., Dworzanski, J. "Chemical Composition and Origin of Fossil Resins from Utah Wasatch Plateau Coal", submitted to Fuels Processing Technology (1990).

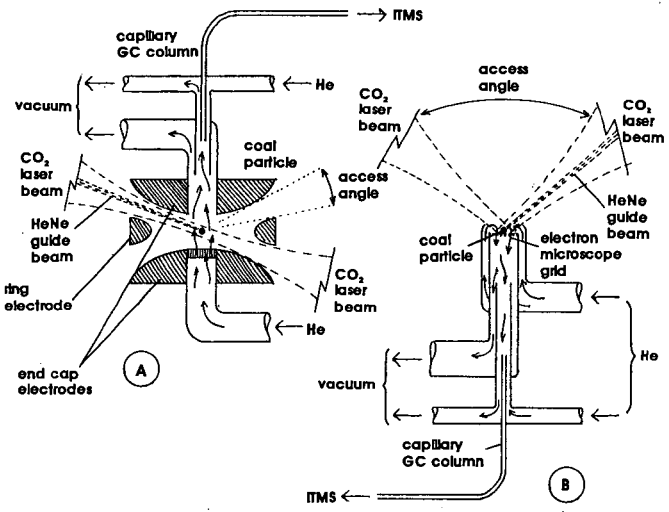

Figure 1. Laser Py-GC/MS configurations used: (a) electrodynamic balance (EDB) with opposing laser beams; (b) electron microscope grid with crossed laser beams. Note special sample inlet and capillary GC transfer line connection to ion trap mass spectrometer (ITMS).

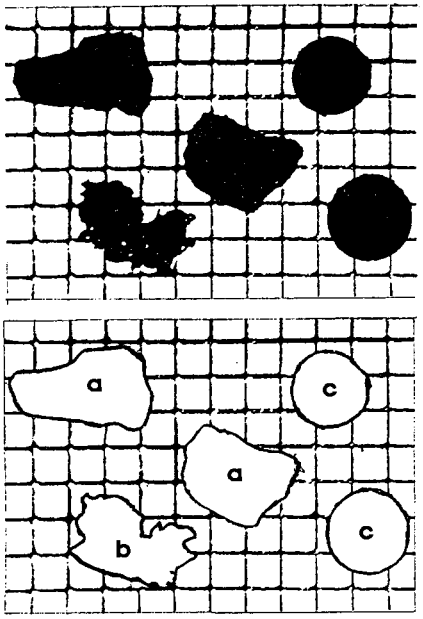

Figure 2. Microscopic view of coal and char particles on 400 mesh copper electron microscope grid; (a) fresh particles of Illinois #6 coal, (b) char particle, (c) Spherocarb particles. (a) and (c) were added later. Note degree of size and shape variation present.

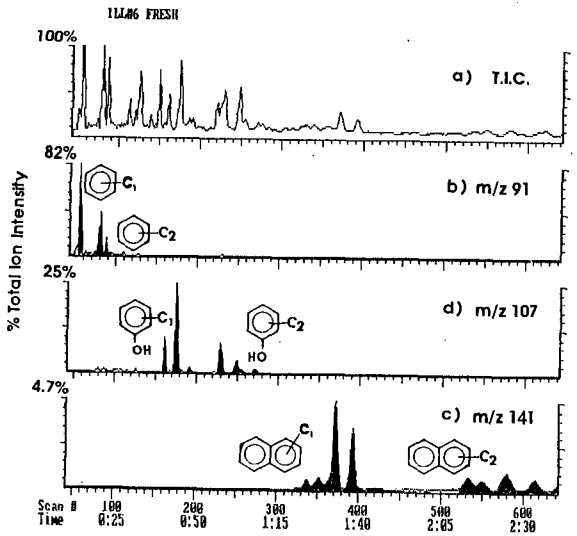

Figure 3. Laser Py-GC/MS profiles of single Illinois #6 coal particle obtained with system configuration shown in Figure 1b. Note good signal-to-noise ratio and useful degree of chromatographic separation. Highly similar patterns ean be obtained with the system configuration shown in Figure 1a as well as by conventional Curic-point Py-GC/MS.

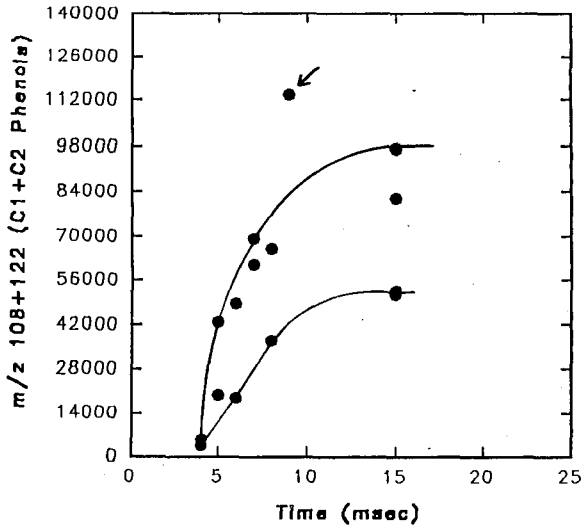

Figure 4. Relationship between laser pulse time and yield of specific pyrolysis products (C_1 and C_2 alkylphenols) during 14 consecutive laser Py-GC/MS runs on individual Illinois #6 coal particles. Note large variations in yield. Curves fitted to maximum and minimum values only. Arrow indicates outlier with anomalous GC/MS pattern. Experimental conditions as in Figure 1b.

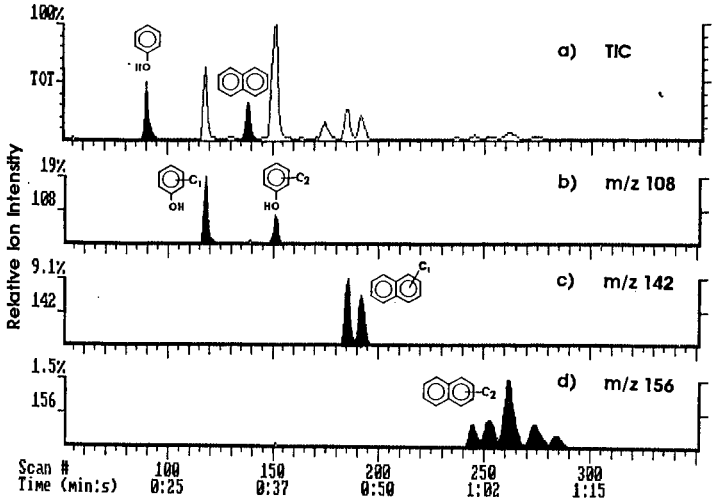

Figure 5. Laser desorption GC/MS profiles of a single Spherocarb particle impregnated with a mixture of bitumen-like compounds. Note separation of various alkylaromatic isomers. Experimental configuration as in Figure 1a.

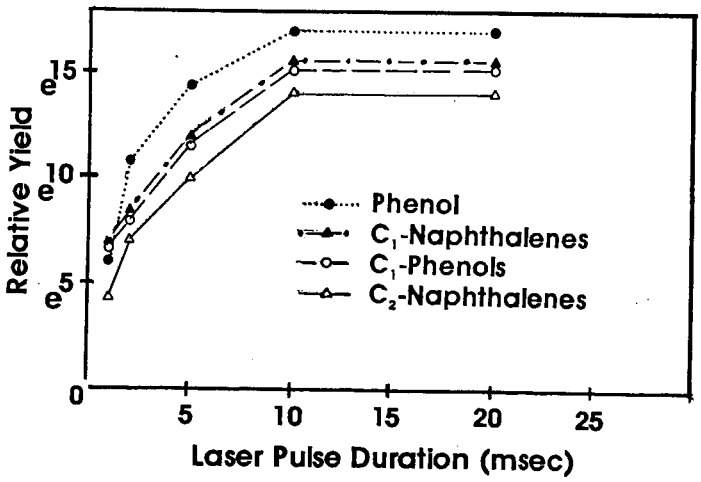

Figure 6. Relationship between laser pulse time and desorption yields of some of the model compounds shown in Figure 5. Each dot represents the average of 2 different laser desorption GC/MS analyses. Note closely similar relative abundances at all pulse durations, except for phenol.

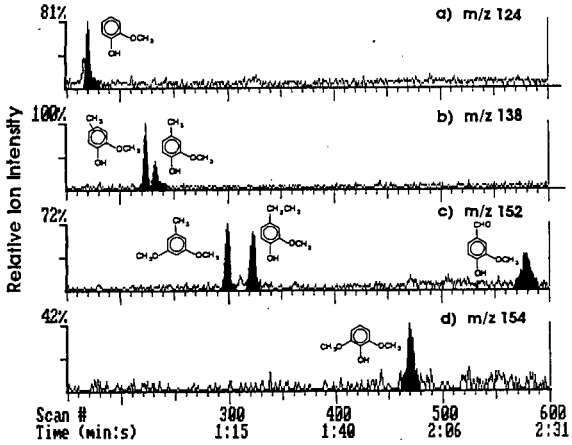

Figure 7. Selected ion chromatograms obtained by Laser Py-GC/MS analysis of a single, lignin impregnated Spherocarb particle. Note presence of characteristic hardwood lignin building blocks. Experimental conditions as in Figure 1b.

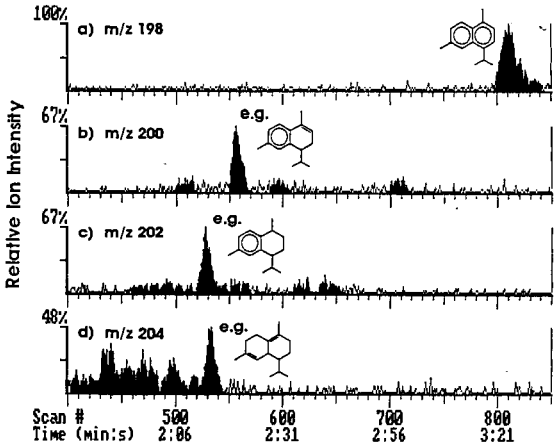

Figure 8. As Figure 5 but using a single, fossil resin impregnated Spherocarb particle. Note characteristic sesquiterpenoid building blocks. It should be noted here that a minor portion of the signals at m/z 198 (cadalene) and 202 (calamenes) represents low MW (monomeric) rather than polymeric components. Experimental conditions as in Figure 1b.

IDENTIFICATION OF CHEMICAL MARKERS FOR BACTERIA BY PYROLYSIS-TANDEM MASS SPECTROMETRY

Kent J. Voorhees and Stephan J. DeLuca
Department of Chemistry and Geochemistry
Colorado School of Mines
Golden, CO 80401

Keywords: Pyrolysis, Tandem Mass Spectrometry, and Bacteria

INTRODUCTION

There is a substantial body of literature concerning the identification of microorganisms by mass spectrometry (1-11), however, little has been done to identify bacteria in complex variable backgrounds. Several sample introduction and ionization methods have been used for mass-spectrometric analysis of bacteria. Sampling methods may be classified as either direct or indirect, depending on whether whole organisms or extracts are used in the analysis. Of the direct sampling methods, pyrolysis is the most frequently used, although recently FAB methods utilizing whole cells have been shown to be useful for identifying microorganisms (12-13). Pyrolysis has been used with direct introduction of pyrolysate to the ionizer (Py-MS, i.e., pyrolysis *in vacuo*) and also in conjunction with gas chromatography (Py-GCMS). Both electron ionization and chemical ionization have been used in Py-MS and Py-GCMS analyses.

The simplest and most rapid of these methods is direct Py-MS with electron ionization. The Py-mass spectra, however, are generally quite complex and do not easily lend themselves to chemical interpretation. On the other hand, Py-GCMS allows identification of the chemical components of cellular material, hence, specific biomarkers may be found (1,10,14). The presence of such compounds may be used to unambiguously identify target materials, even in complex backgrounds.

Tandem mass spectrometry adds a dimension to traditional Py-MS which permits identification of specific compounds in a pyrolysate (5,11). The purpose of the present research was to determine the feasibility of using Py-MS/MS to detect bacterial biomarkers in complex backgrounds of particulate material.

EXPERIMENTAL

Measurements were obtained with an Extrel Model EL-400 triple quadrupole mass spectrometer fitted with a Curie-point pyrolysis inlet (11). Daughter ion spectra were collected for m/z 79, 111, 117, 126, and 135. These ions were chosen based on our experience with the samples. The samples used are described in Table 1. All samples were suspended in methanol at about 1mg/ml. Approximately 10 μL of each suspension was applied to 610°C Curie-point wires, and the solvent evaporated under a stream of hot air.

Multivariate statistical analyses were carried out with the RESOLVE program (15). Each Py-MS spectrum was collected as a set of raw intensities. Prior to principal components analysis, the data were normalized to constant length. The results, displayed as Karhunen-Loeve (K-L) or principal components plots, show the distribution of the samples in the multivariate mass spectral space. Factor spectra for the components were also derived. Factor spectra show the correlations (positive and negative) of mass spectral peaks with directions in the principal component space.

RESULTS AND DISCUSSION

In previous experiments (unpublished), we found that the Py-MS patterns of bacteria could vary more within strains of a given species than between different species. For example, the intensities of m/z 52 and 79 varied drastically among strains of *B. subtilis* and *B. licheniformis*. Strains showing large m/z 79 and 52 peaks were sporulated, while other strains were vegetative cells. We postulated that the m/z 79 and 52 peaks were markers for sporulation. The daughter ion spectra of m/z 79 for the test samples (Figure 1) showed that m/z 52 is a strong daughter of m/z 79 for the bacteria, while samples such as fog oil and diesel smoke showed virtually no m/z 52 as a daughter of m/z 79.

The principal components plot shown in Figure 2a separates the *B.g.* spores and *B. subtilis* from the rest of the samples. The factor spectrum generated for principal component 2 (Figure 2b) shows peaks at m/z 52 and 79 positively correlated with the *B.g.* and *B. subtilis* samples, while peaks at m/z 51 and 77 are positively correlated with the remainder of the samples.

Sporulating bacteria produce large quantities of picolinic acid (2-pyridine-carboxylic acid) which forms the hardened "shell" of the spores. The EPA/NIH library spectrum (16) of picolinic acid (virtually identical to that of pyridine) shows large peaks at m/z 79 (i.e., pyridine molecular ion) and m/z 52. Because the mass spectra of pyridine and picolinic acid are so similar, it is not possible to determine which of these species is liberated upon pyrolysis. It is clear, however, that the presence of picolinic acid in the spores is responsible for the separation seen in the K-L plot.

The negative correlation of peak m/z 77 with the sporulated organisms indicates that this peak is more intense (relatively) in the other samples as is obvious by inspection of Figure 1. In order to determine the chemical species responsible for the peak at m/z 79 in samples other than sporulated bacteria, parent ion spectra of m/z 79 were collected. The parent ion spectrum of m/z 79 for diesel smoke is shown in Figure 3. This spectrum is quite complicated and it appears that at least three compound classes are present. The peak at m/z 94 appears to be due to alkylcyclodienyl hydrocarbons (e.g., methylcyclohexadiene). The m/z 105 peak may be due to alkyl benzaldehydes (e.g., 2,6 dimethylbenzaldehyde) and the series of peaks at m/z 107, 121, 135 and 149 are probably produced by a series of alkyl phenols. Although these identifications are tentative (based on a comparison of EPA/NIH library spectra with the parent and daughter spectra) each of the compound types listed above show a significant m/z 77 peak as well as an m/z 79

peak. It is clear that many compounds contribute to the peak at m/z 79, however, sporulated bacteria are easily identified by the presence of large quantities of picolinic acid, as reflected in the intense m/z 52 peak in the daughter spectrum of m/z 79.

Representative spectra of daughter ions of m/z 117 are illustrated in Figure 4. The major peaks appearing in these spectra are m/z 89, 80, 91, 115 and 117. The K-L plot in Figure 5a shows scores of the samples on the first two principal components. The fog oil, wood smoke, and diesel smoke samples are clearly separated from the other samples, all of which contain protein. The factor spectrum associated with this separation (Figure 5b) shows two distinctive patterns; one correlated with the fog oil and smokes shows large peaks at m/z 91 and 115 while the other pattern (negative direction) has strong peaks at m/z 89 and 90. The spectrum in the negative direction is that of indole, a known pyrolysis product of proteins containing the amino acid tryptophane. The peaks at m/z 91 and 115 are probably due to unsaturated alkyl aromatic compounds, for example, 2-methylbutenylbenzene. The daughter ion spectrum of m/z 117 appears to contain markers for the presence of protein in a sample.

We have observed that the base adenine (MW 135) is liberated by pyrolysis of DNA. It was postulated that adenine could be used as a marker for organisms since all living material contains nucleic acids. The daughter ion spectra in Figure 6 are representative of the sample set. The K-L plot in Figure 7a shows a distribution of samples in the Component 2 direction with wood smoke, fog oil, and diesel smoke at one extreme and *E. coli* and MS-2 coliphage at the other. The factor spectrum associated with Component 2 (Figure 7b) indicates the presence of adenine (m/z 108) in the negative direction, and a series of alkyl phenols (m/z 107, 93, 79, etc.) in the positive direction. The parent ion scan of m/z 135 for diesel smoke shows a homologous series of alkyl chain lengths (of an alkyl phenol) extending up to at least 290 amu (a C14 alkyl group).

The daughter ion spectrum of m/z 135 indicates the presence of nucleic acids by the appearance of an m/z 108 peak. This suggests that the daughter ion spectrum of m/z 135 may be used to determine the presence of living material (or recently living material) in an aerosol sample. This would provide a useful branch point for a decision tree; if adenine is not present, there is no bacterial threat.

Daughter ion spectra were also collected for m/z 111, 126, and 128. In each case there were clear separations of background materials (i.e., fog oil, diesel and wood smoke) from the targets (i.e., MS-2 coliphage, *E. coli, B.g.* spores, etc.). The factor spectra associated with these separations, however, were quite complex and could not be interpreted chemically with a high degree of confidence. For example, factor spectra for the daughters of m/z 126 showed correlations of peaks with fog oil that indicated the presence of unsaturated hydrocarbons (probably nonene). The spectra associated with other samples, however, could contain contributions from nucleic acids (thymine), proteins, and carbohydrates (methylhydroxypyranone).

CONCLUSIONS

The feasibility of using pyrolysis-tandem mass spectrometry to identify biomarkers in complex backgrounds has been demonstrated. Three markers for biological substances have been identified. Adenine, a marker for nucleic acids and hence all living material, is detected in the daughter ion spectrum of m/z 135. The presence of protein in a sample may be inferred from the daughter ion spectrum of m/z 117, which indicates the presence or absence of indole, a product of pyrolysis of proteins containing the amino acid tryptophane. Pyridine, from picolinic acid, is seen in the daughter ion spectrum of m/z 79. This is a marker for the presence of sporulated bacteria. These ions obviously do not solve the problem of identifying specific organisms in ambient samples. There are however hundreds more ions to be studied, and if biomarkers are present in the pyrolysates, Py-MS/MS has the capability of finding them.

REFERENCES

1. Fox, Alvin; Morgan, Stephen L.; Larsson, Lennart; and Odham, Goran; Eds.; Analytical Microbiology Methods. 1989 Plenum Press, NY.

2. Anhalt, John P. and Fenselau, Catherine, Anal. Chem. 1975, 47(2), 219-255.

3. Voorhees, Kent J.; Harrington, Peter B.; Street, Thomas E.; Hoffman, Stephen; Durfee, Steven L.; Bonelli, Joseph E. and Firnhaber, Cynthia S. from "Computer-Enhanced Analytical Spectroscopy, V. 2, H.L.C. Meuzelaar, Ed., 1990, 257-275.

4. Voorhees, Kent J.; Durfee, Steven L.; and Updegraff, David M., J. Microbiol. Meth. 1988, 8, 315-325.

5. Voorhees, Kent J.; Durfee, Steven L.; Holtzclaw, James R.; Enke, C.G.; and Bauer, Mark R., J. Anal. Appl. Pyrol., 1988, 14, 7-15.

6. Tas, A.C.; Van Der Greef, J.; DeWaart, J.; Bouwman, J.; and Teu Noever de Braw, M.D., J. Anal. Appl. Pyrol., 1985, 7, 249-255.

7. Tas, A.C.; DeWaart, J.; Bouwman, M.C.; Teu Noever de Braw, M.C.; and Van Der Greef, J. J. Anal. Appl. Pyrol., 1987, 11, 329-340.

8. Van der Greef, J.; Tas, A.C.; and Teu Noever de Brauw, M.C. Biomed. Env. Mass Spec., 1988, 16, 45-50.

9. Tas, A.C.; Bastiaanse, H.B.; Van Der Greef, J.; and Kerkenaar, A. J. Anal. Appl. Pyrol., 1989, 14, 309-321.

10. Morgan, Stephen L.; Fox, Alvin; and Gilbert, James. J. Microbiol. Meth., 1989, 9, 57-69.

11. DeLuca, Stephan; Sarver, Emory W.; Harrington, Peter de B.; and Voorhees, Kent J. Anal. Chem. 1990, 62, 1465-1472.

12. Heller, D.N.; Feuselau, C.; Cotter, R.J.; Demirev, P.; Olthoff, J.K.; Honovich, J.; Uy, M.; Tanaka, T. and Kishimoto, Y. Biochem. Biophys. Res. Comm., 1987, 142(1), 194-199.

13. Seid, Robert C., Jr.; Bone, William M.; and Phillips, Lawrence R. Anal. Biochem., 1986, 155, 168-176.

14. Holzer, G.; Bourne, T.F.; Bertsch, W. J. Chromatog. 1989, 468, 181-190.

15. Harrington, P. de B.; Street, T.E.; Voorhees, K.J.; Radicati di Brozolo, F.; Odom, R.W. Anal. Chem. 1989, 61, 715-719.

16. Heller, S.R. and Milne, G.W.A. EPA/NIH Mass Spectral Data Base, 1978, Nat. Stand. ref. data ser.; NSRDS-NBS 63.

ACKNOWLEDGMENT

The authors wish to thank Teledyne-CME and the U.S. Army CRDEC for their support of this project.

Table 1. Samples used in the study

Substance	Category
Fog oil	f
Wood smoke	w
Diesel smoke	d
Grass pollen (*Secale cerale*)	p
Dry Yeast	y
Aldolase	a
MS-2 coliphage	m
E. coli	e
B. subtilis (sporulated)	b
B. globigii spores (*B. subtilis var. niger*)	g

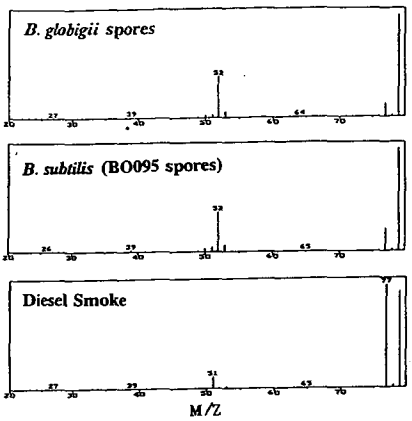

Figure 1. Selected daughter ion spectra for m/z 79.

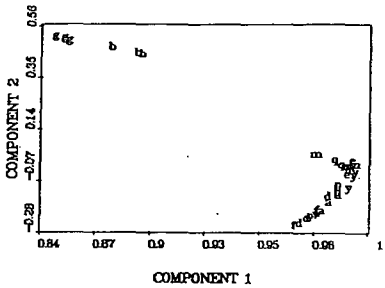

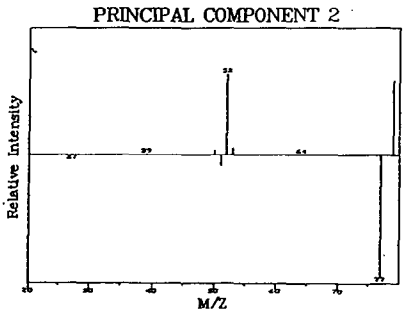

Figure 2. Principal components plot (a) and factor spectrum (b) for daughters of m/z 79.

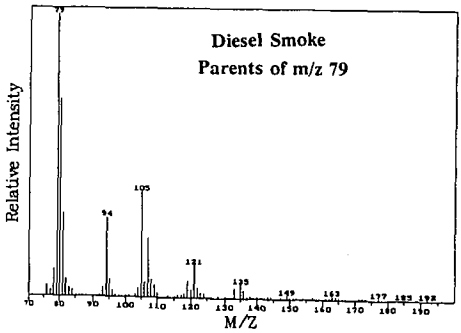

Figure 3. Parent ion spectrum of diesel smoke for m/z 79.

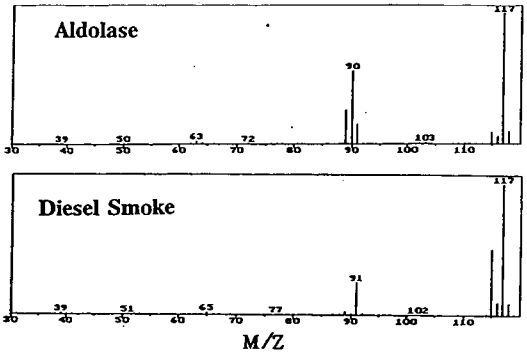

Figure 4. Selected daughter ion spectra for m/z 117

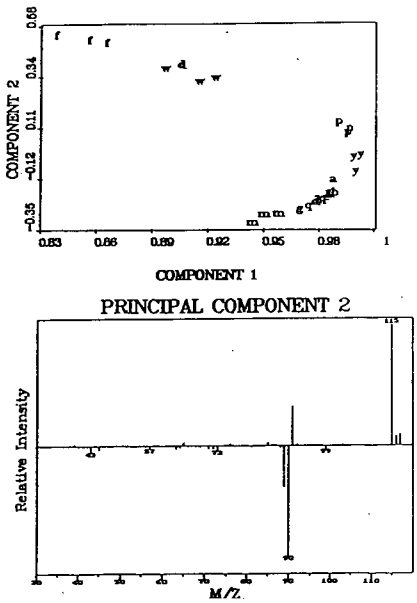

Figure 5. Principal components plot (a) and factor spectrum (b) for daughters of m/z 117.

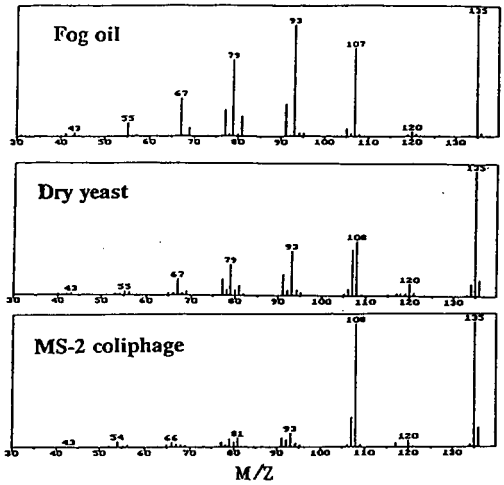

Figure 6. Selected daughter ion spectra for m/z 135.

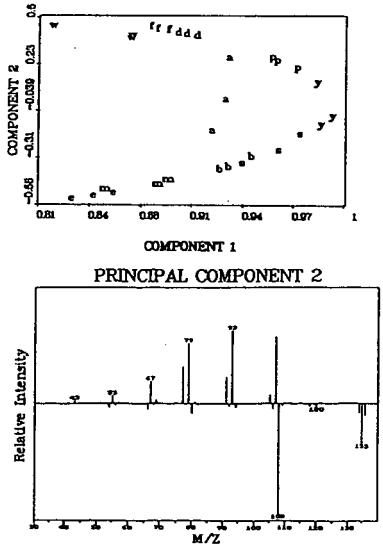

Figure 7. Principal components plot (a) and factor spectrum (b) for daughters of m/z 135

STABLE CARBON ISOTOPIC COMPOSITION OF INDIVIDUAL PRODUCTS FROM FLASH PYROLYSIS OF KEROGENS

By

Tim Eglinton[1], Brian D. Fry[2], Katherine H. Freeman[3] and J.M. Hayes[3]

[1]Dept. of Chemistry, Woods Hole Oceanographic Institution, Woods Hole, MA 02543
[2]Ecosystems Center, Marine Biological Laboratories, Woods Hole, MA 02543
[3]Biogeochemical Laboratories, Depts. of Geological Sciences and of Chemistry, Indiana University, Bloomington, IN 47405

Keywords: Kerogen, Flash Pyrolysis, Compound-specific Isotopic Analysis.

ABSTRACT

Recent analytical developments now allow determination of the stable carbon isotopic compositions of individual compounds eluting from a capillary gas chromatography column. This study describes compound-specific isotope measurements made on aliphatic hydrocarbon products from flash pyrolysis (800°C, 20s) of kerogens representing a range of depositional environments and ages. The carbon isotopic compositions of the major aliphatic pyrolysis products (*n*-hydrocarbons, acyclic isoprenoids and hopanoids), calibrated against those of deuterated *n*-alkane internal standards, were typically measurable to within ±0.5°/oo. The data show that for a given sample, *n*-alkenes and *n*-alkanes generally display rather similar values to one another irrespective of carbon number, suggesting a common (bio)polymeric origin. In several cases the average values also reflect the corresponding $\delta^{13}C$ TOC value, indicating that (for these samples) the *n*-hydrocarbons are derived from structurally important, or at least isotopically representative, components in the kerogen. Contrastingly, the isotope compositions of *n*-hydrocarbons varied substantially between samples (average values ranged from -33°/oo to -14°/oo). Differences in isotopic composition were also apparent between the compound classes studied (*e.g.* hopanoids were isotopically lighter than the *n*-hydrocarbons).

The data obtained allow new deductions to be made regarding the source(s) of the precursor components in the kerogen and their importance in dictating the overall $\delta^{13}C$ TOC value. This technique is particularly useful for samples which gives rise to pyrolysis products whose structures are not sufficiently diagnostic to distinguish between biological sources. In these instances, isotopic data in combination with structural information, may prove invaluable in resolving separate carbon sources.

INTRODUCTION

Determination of the sources and composition of kerogen - the insoluble organic matter which is preserved in sediments and is ultimately responsible for accumulations of oil and gas - is a major goal in organic geochemistry. Kerogens represent a composite of remnants from a wide variety of organisms (algae, bacteria, higher plants) derived from both terrestrial and marine sources and reflect these differing inputs in a number of ways.

Of the approaches used in organic geochemistry flash pyrolysis has become widely accepted as a technique which can provide important and useful information on the structure and composition of kerogen and related geomacromolecules. Much progress has been made in understanding the pyrolysis mechanisms involved and in establishing precursor-pyrolysis product relationships for wide range of biomacromolecules and associated biochemicals. Pyrolytic markers have been established for the major biochemical precursors such as lignins[1,2], aliphatic biopolymers[3], polysaccharides[4] *etc.* as well as materials of secondary origin such as sulfur-bound macromolecules[5-8]. From such relationships the potential exists to reconstruct the proportions of different precursor components from the various biological sources which together comprise the kerogen. However, for a large number of sedimentary situations (particularly in diagenetically altered samples) the structure of the products generated upon pyrolysis are not sufficiently diagnostic to resolve individual sources.

Natural variations in the abundance of stable carbon isotopes (as a result of fractionation effects related to atmospheric and dissolved CO_2 equilibria and uptake) potentially may be used to distinguish between carbon sources according to depositional environment[9] (*e.g.* freshwater *versus* marine) and trophic status[10] (*e.g.* aerobic photoautotrophs *versus* methanotrophs). Applications based on this premise are now well established and, typically, the isotopic composition of the gross kerogen is measured (*i.e.* $\delta^{13}C$ TOC) for these purposes. However, since kerogens are usually comprised of a wide variety of components derived from potentially separate sources, $\delta^{13}C$ TOC represents a composite value. In order to resolve these separate contributions, the isotopic compositions of each of the individual constituents must be determined.

It has been clear for some time, therefore, that isotopic analyses on a molecular level have the potential to provide much more detailed information. As a result of several analytical developments, it is now possible to obtain stable carbon isotopic compositions of individual compounds eluting from a GC[11-15]. Under conditions of optimal chromatography (*i.e.* baseline separation) and optimum sample size (individual peaks yielding 10^{-8} to 10^{-9} moles CO_2) a precision of $\pm 0.1^{o}/oo$ is currently attainable[14]. Previously the only practical alternative has been to isolate individual organic compounds using laborious fractionation and purification procedures so that they could be directly analyzed by isotope ratio mass spectrometry[16,17]. With this newly available technology for on-line determination of the carbon isotopic composition of individual components eluting from a gas chromatograph it is now feasible to determine the isotopic compositions of individual pyrolysis products.

The combination of pyrolysis with compound-specific isotope analysis therefore holds tremendous possibilities for identifying and quantifying contributions from the various sources according to both structure (biochemical origin) and isotopic composition, with the ability to de-couple marine input from terrigenous sources representing a particularly important application. This paper describes preliminary results from a study designed to assess the viability and utility of this approach for the characterization of kerogens according to organic matter sources and depositional environment.

EXPERIMENTAL

Six sediments representing a range of depositional environments (marine, estuarine, lacustrine) and ages (Recent to Carboniferous) were chosen for analysis. Selected details are provided in Table 1. Kerogens were isolated from the sediments using established HF/HCl procedures and solvent-extracted prior to analysis.

Off-line flash pyrolysis experiments were performed on the isolated kerogens using a CDS 120 pyrolyser. Samples (1-5mg) mounted in quartz tubes were pyrolyzed (800°C, 20s.) using a coil pyroprobe in a stream of helium carrier gas. Volatile products were swept from a heated zone (200°C) and trapped in a glass U-tube immersed in liquid N_2. At the end of the pyrolysis experiment the products were retrieved from the U-tube by dissolution in a dichloromethane/hexane (1:1) and transferred to vials. Purified aliphatic hydrocarbon fractions

were isolated from the pyrolyzates by liquid chromatography on short columns (10cm x 5mm) containing activated silica and alumina using hexane as eluant.

Compound identification was achieved by conventional Gas Chromatography-Mass Spectrometry (GC-MS) using a Carlo Erba 4160 GC interfaced to Finnigan 4500 quadrupole MS (EI 50eV).

Compound-specific isotope analysis of the purified pyrolysis products was performed by Gas Chromatography-Combustion-Isotope Ratio Mass Spectrometry (GC-C-IRMS). The instrument set-up consists of a HP 5890 GC linked *via* a combustion interface to a Finnigan Delta-S isotope MS. The interface consists of three major components: a micro-combustion reactor, a non-cryogenic water extractor and an open split interface. As organic compounds elute from the GC they are combusted to CO_2 and H_2O in the reactor. Subsequently water is removed prior to entry into the mass spectrometer. The entire system is controlled by Finnigan ISODAT software. The stable carbon isotopic compositions of components of interest were calibrated against those of deuterated *n*-alkane standards co-injected with the sample. The isotopic composition of the standards was previously determined by conventional sealed-tube combustion. All isotopic compositions are quoted relative to PDB.

The bulk kerogens were also combusted and analysed separately to provide $\delta^{13}C$ TOC values by conventional isotope mass spectrometry using a Finnigan Delta-S mass spectrometer.

RESULTS

Masses 44 ($^{12}C^{16}O^{16}O$), 45 ($^{13}C^{16}O^{16}O$) and 46 ($^{12}C^{16}O^{18}O$) are simultaneously monitored during the GC-C-IRMS run. The ratio of *m/z* 45/44 is used to determine the carbon isotopic composition of the compound. A correction is made for ^{18}O-containing CO_2 from the intensity of *m/z* 46. Figure 1 shows *m/z* 44 mass chromatograms from GC-C-IRMS analysis of two of the kerogens studied. Since each compound is combusted to CO_2 on exiting the GC, the *m/z* 44 trace is analogous to a conventional FID signal. An expanded portion of a chromatogram showing variations in the *m/z* 45/44 ion current ratio (in addition to the *m/z* 44 trace) is presented in Figure 2. Compounds enriched in ^{13}C elute slightly earlier than the corresponding ^{12}C equivalent, and thus each peak is manifested in the *m/z* 45/44 trace as an inflection, the ^{13}C-rich component constituting the leading edge of the peak. The ratio of the magnitude of excursions away from the baseline by the ^{13}C (+ve inflection) and ^{12}C (-ve inflection) component gives the isotopic composition.

Four types of hydrocarbons were typically observed to dominate the chromatograms: *n*-alkenes, *n*-alkanes, acyclic isoprenoid and hopanoid hydrocarbons. Average isotopic compositions for these compound classes determined in the manner described above (summed over the appropriate carbon number range) are listed in Table 1 the six kerogens. Results from replicate analyses suggest that most values may be considered accurate to within ±0.5°/∞, however, in the worst cases (*i.e.* for samples which display complex chromatograms, or for components which are incompletely resolved) the uncertainty may be ±1°/∞ or more. Marine kerogens typically proved more difficult to study than lacustrine samples because of the more complex pyrograms they generate. In Figure 3 the stable carbon isotopic compositions of these pyrolysis products are plotted with respect to carbon number for each of the kerogens. The data show that for a given sample the isotopic compositions of *n*-alkenes and *n*-alkanes are generally rather similar (*i.e.* irrespective of carbon number). This finding suggests a common origin, consistent with a (bio)polymeric source. The average values of these components also, in several cases, reflect the corresponding $\delta^{13}C$ TOC value (*e.g.* Green River, Westfield), suggesting that they are derived from structurally important, or at least isotopically representative, components in the kerogen. In instances where isotopic compositions of the pyrolysis products do not closely match the $\delta^{13}C$ TOC, then alternative components must be considered. Regarding this point it should be borne in mind that the present investigation has only dealt with aliphatic pyrolysis products. The isotopic

compositions of normal hydrocarbons in the Messel kerogen pyrolyzate showed the greatest difference compared to the $\delta^{13}C$ TOC value, being up to 10°/oo lighter. It has been proposed[18] that both the kerogen and the normal hydrocarbon pyrolysis products from this shale derive predominantly from the cell-wall material of the freshwater alga, *Tetraedron minimum*. Here, it is found that the hydrocarbon pyrolyzate is depleted in ^{13}C by *ca.* 5°/oo relative to the total organic carbon (Table 1). Accordingly, the kerogen must contain ^{13}C-enriched components that do not yield aliphatic hydrocarbons on pyrolysis. It is required either that the visually recognized cell-wall material is isotopically inhomogenous or that some additional component is present. The alkane/alkene δ values observed in this work are very similar to those of acyclic hydrocarbons in extracts of the Messel Shale[16,19].

The isotopic compositions of the various compound classes studied vary substantially from one sample to another. Average values for normal hydrocarbons range from *ca.* -33°/oo (Messel shale) to *ca.* -14°/oo (Westfield). With the exception of the Westfield kerogen, non-marine lacustrine samples (*i.e.* Messel and Green River kerogens) give lighter average isotope values than marine samples (Monterey, Peru, Spartina). The Westfield shale appears to represent a rather unusual and interesting case. The organic matter in the shale is almost exclusively comprised of the freshwater macroalga, *Botryococcus braunii*. The lack of isoprenoids in the pyrolyzate (Fig. 1) is also a characteristic feature of *B. braunii*-derived kerogens. Whilst the shale represents a freshwater lake deposit, the isotope values (both of the normal hydrocarbons and the TOC) are unusually heavy. This is likely to reflect low concentrations of dissolved CO_2 in the environment of carbon fixation. In such circumstances, many carbon-fixing organisms utilize special pathways (such as assimilation of HCO_3^-) for accumulation of inorganic carbon. Isotope effects associated with these largely irreversible processes are small in comparison to that of rubisco, and the resulting organic carbon is relatively enriched in ^{13}C.

Within-kerogen variations in isotopic composition are apparent between different compound classes generated from the samples studied. Isoprenoid hydrocarbons (when present) were found to vary significantly relative to the *n*-hydrocarbons (Fig. 1). In contrast, the hopanoids are in each case substantially lighter than both the TOC and *n*-hydrocarbons, with values as light as -50°/oo recorded for hopanoids in the Messel kerogen pyrolyzate. These latter values show good agreement with those reported by Freeman *et al.*[15] for hopanoids in solvent extracts of the same shale, indicating a bacterial (methanotrophic ?) contribution to the kerogen.

CONCLUSIONS

Whilst this study contrasts geochemically very different kerogens, the results demonstrate that isotopic compositions may be readily determined for individual pyrolysis products by GC-C-IRMS. The data allow several new deductions to be made regarding the source of these components and their importance in dictating the overall $\delta^{13}C$ TOC value of the kerogen. The approach holds much promise, therefore, for assessing the various sources of biological remnants comprising the kerogen, and also for interpreting the overall TOC value in terms of these separate contributions.

ACKNOWLEDGEMENTS

The isotope-ratio-monitoring GCMS facility at Indiana University has been established and maintained with support from Chevron Oil Field Research Corporation and from Finnigan MAT. We thank Dr. C.G. Johnson for operation of the conventional GC-MS system.

REFERENCES

1. Obst J.R. *J. Wood Chem. Technol.* 3, 377-397 (1983).
2. Saiz-Jimenez C. and de Leeuw J.W. *Org. Geochem.* 10, 869-876 (1986).
3. Tegelaar E.W., de Leeuw J.W., Largeau C., Derenne S., Schulten H.-R., Muller R., Boon J.J., Nip M. and Sprenkels J.C.M. *J. Anal. Appl. Pyrol.* 15, 29-54 (1989).
4. Helleur R.J. *J. Anal. Appl. Pyrol.* 11, 297-311 (1987).
5. Sinninghe Damsté J.S., Kock-van Dalen A.C., de Leeuw J.W. and Schenck P.A. *J. Chromatogr.* 435, 435-452 (1988).
6. Sinninghe Damsté J.S. Eglinton T.I., de Leeuw J.W. and Schenck P.A. *Geochim. Cosmochim. Acta* 53, 873-889 (1989).
7. Eglinton T.I., Sinninghe Damsté J.S., Kohnen M.E.L and de Leeuw J.W. *Fuel* 69, 1394-1404 (1990).
8. Eglinton T.I., Sinninghe Damsté J.S., Pool W., de Leeuw J.W., Eijkel G. and Boon J.J. *Geochim. Cosmochim. Acta* Submitted (1991)
9. Schoell M. *Advances in Petroleum Geochemistry, Volume 1.* (Eds J. Brooks and D.H. Welte) pp. 215-245. Academic Press, London (1984).
10. Fry B. and Sherr E. *Contributions to Marine Science* 27, 13-47 (1984).
11. Matthews D.E. and Hayes J.M. *Analyt. Chem.* 50, 1465-1473 (1978).
12. Vogler E.A., Meyers P.A. and Moore W.A. *Geochim. Cosmochim. Acta* 45, 2287-2293 (1981).
13. Gilmour I., Swart P.K. and Pillinger C.T. *Org. Geochem.* 6, 665-670 (1984).
14. Hayes J.M., Freeman K.H. and Popp B.N. *14th International Meeting on Organic Geochemistry* Abstract. (1989)
15. Freeman K.H., Hayes J.M., Trendel J.-M. and Albrecht P. *Nature* 343, 254-256 (1990).
16. Hayes J.H., Takigiku R., Ocampo R., Callot H.J. and Albrecht P. *Nature* 329, 48-51 (1987).
17. Boreham C.J., Fookes C.J.R., Popp B.N. and Hayes J.M. *Geochim. Cosmochim. Acta* 53, 2451-2455 (1989).
18. Goth K., de Leeuw J.W., Puttman W. and Tegelaar E.W. *Nature* 336, 759-761 (1988).
19. Freeman K.H. unpublished results.

Table 1. Stable Carbon Isotope Data for Kerogens

			$\delta^{13}C$ Value (‰)				
Kerogen	**Age**	**Env.**	**TOC***	**Σene[1]**	**Σane[2]**	**Σisop[3]**	**Σhop[4]**
Westfield, Scotland	Carb.	Lacustrine	-14.26	-14.71	-15.43	n.d.	-23.15
Messel, FRG	Eocene	Lacustrine	-27.69	-32.71	-33.13	-30.83	-45.47
Green River, UT, USA	Eocene	Lacustrine	-29.00	-28.99	-29.96	-31.27	-41.66
Peru, S. America	Contemp.	Marine	-20.47	-23.11	-23.82	-22.90	n.d.
Monterey, CA, USA	Miocene	Marine	-22.17	-23.95	-24.88	-24.64	n.d.
"Spartina", GA, USA	Contemp.	Estuarine	-18.54	-22.69	-23.30	-24.71	n.d.

*Determined by conventional sealed-tube combustion and MS.

[1]*n*-alkenes; [2]*n*-alkanes; [3]isoprenoids; [4]hopanoids.

n.d. = not detected

Figure 1. M/z 44 chromatograms from GC-C-IRMS of Westfield and Green River kerogen pyrolyzates (aliphatic hydrocarbon fractions).

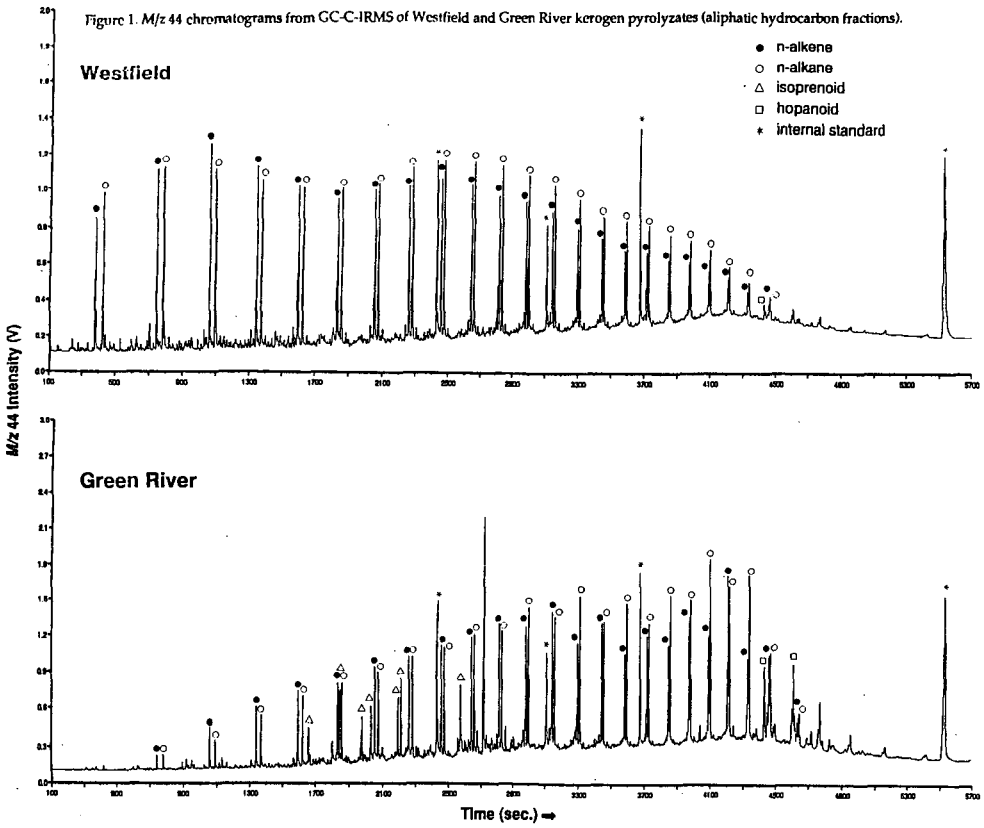

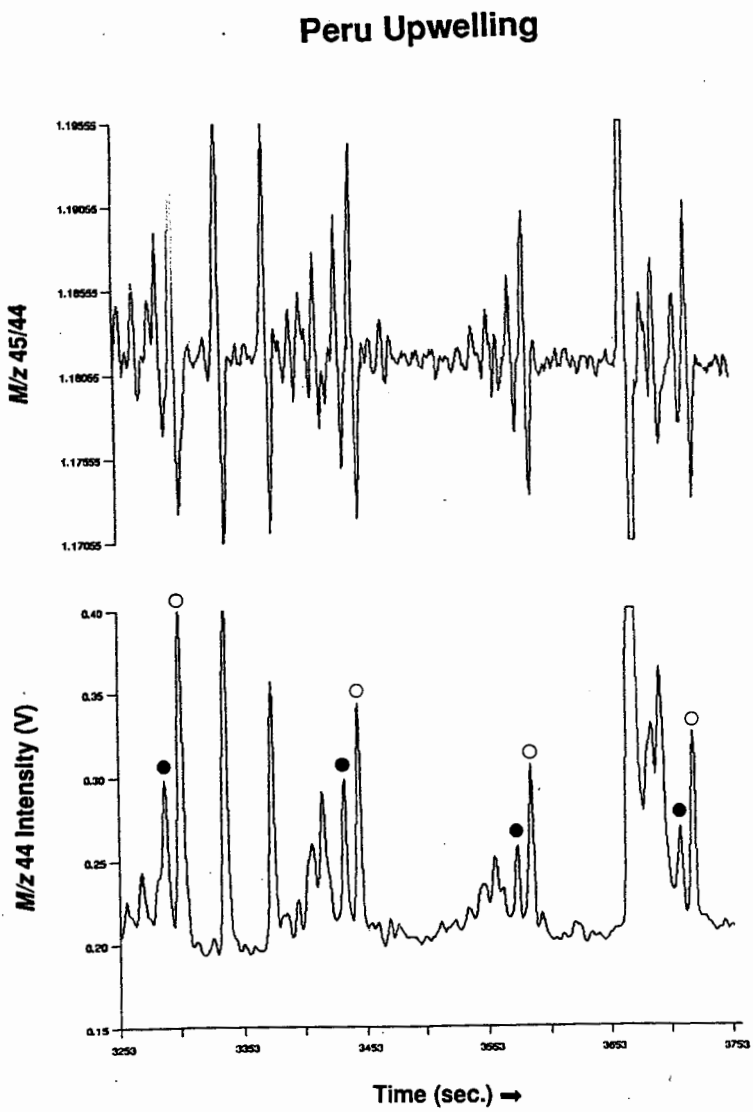

Figure 2. Partial chromatogram of *m/z* 45/44 ion current ratio (upper) and *m/z* 44 (lower) from GC-C-IRMS of Peru kerogen pyrolyzate (aliphatic hydrocarbon fraction). Open and closed circles represent *n*-alkanes and *n*-alkenes respectively.

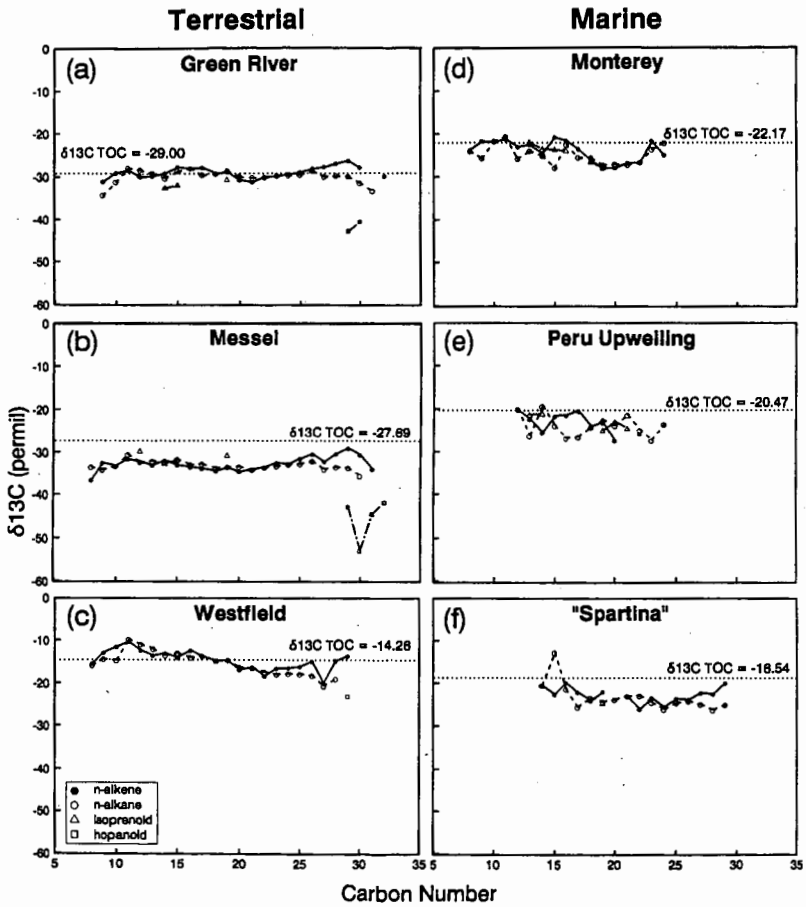

Figure 3. Plots of isotopic composition *versus* carbon number for different compound classes measured in the kerogen pyrolyzates.

IN SITU XAFS STUDIES OF SULFUR IN COAL DURING HIGH TEMPERATURE PYROLYSIS AND OXIDATION

M. Mehdi Taghiei, Frank E. Huggins, Naresh Shah and Gerald P. Huffman

233 Mining and Mineral Resources Bldg.
University of Kentucky
Lexington, KY 40506

Keywords: Sulfur, Pyrolysis, Oxidation, In situ XAFS.

Abstract:

In situ sulfur K-edge XAFS measurements have been performed on Illinois No. 6 and low rank Australian brown coals in order to study the behavior of sulfur forms in coal during pyrolysis and oxidation. The results show that under the relatively slow pyrolysis conditions employed, degradation of organic disulfide starts as low as 200°C while sulfide components degrade at temperatures around 300°C. Pyrrhotite was formed from pyrite during pyrolysis of Illinois No. 6 coal above 400°C. Results obtained during oxidation at temperatures up to 450°C are less well understood. Gradual formation of small amounts of sulfate occurs in both samples, while pyritic sulfur and organic sulfide decrease significantly, with most of the sulfur apparently leaving the sample as SO_2.

Introduction

It is well recognized that a full understanding of the behavior of all major forms of sulfur, both inorganic and organic, is essential for the solution of many of the significant research problems involving sulfur in coal. Until very recently, however, information about the different organic forms of sulfur in coal could not be obtained directly, but had to be based on indirect methods involving pyrolysis of the coal. Such pyrolysis techniques include the temperature-programmed reduction ("kinetogram") methods advanced by Attar[1], the flash pyrolysis ("pyroprobe") developed by Calkins[2,3], and a variety of pyrolysis/mass-spectroscopy and gas chromatographic/mass-spectroscopy techniques[4,5] that are usually performed on extracts and volatile fractions of the coal, rather than the bulk coal itself. Such pyrolysis methods have provided much useful information about sulfur in coal, but because they do not provide information on the sulfur remaining in the residue materials, the information obtained is not complete.

In the last two years, XAFS spectroscopy has been shown[6-9] to be a powerful method for the direct, nondestructive, quantitative determination of all major sulfur forms in coal. In this study, we report some preliminary results from the first *in situ* XAFS spectroscopic investigations of sulfur in coal under conditions of high temperature pyrolysis and oxidation. Emphasis has been given to the quantitative analysis of the various forms of sulfur produced during slow pyrolysis of coal in hydrogen and helium atmospheres as well as oxidation in a helium/oxygen mixture at temperatures up to 600°C.

Experimental

Thermal Analysis:

The coal samples used in this study were a bituminous Illinois No. 6 coal obtained from Argonne Premium Coal Sample Program Bank and a low rank Australian brown coal (Glencoe). The Illinois No. 6 coal contains 4.83 wt% sulfur of which 2.81 wt% is pyritic sulfur, while the Australian coal contains 5.1% organic sulfur and with very little pyritic sulfur (<0.2 wt%). Some model compounds, such as dibenzylsulfide and dibenzothiophene, have also been examined under similar oxidation conditions.

The X-ray reaction furnace used in this work is modified from the design of Sinfelt and Lytle[10]. A chromel-alumel thermocouple is imbedded in a stainless steel backing plate in contact with the sample cell. Temperatures were monitored with a digital voltmeter. Water flow through jackets in the furnace body helps to dissipate heat and prevent the mylar windows of the fluorescent detector from melting. Reactant gases were flowed through the samples which were packed into the cell.

XAFS spectra of samples were obtained while flowing a gas stream of helium or hydrogen in pyrolysis and mixture of 95% helium, 5% oxygen in oxidation at temperatures up to 600°C. Since each spectrum takes approximately 30 minutes to complete, these are considered slow pyrolysis and oxidation processes.

XAFS Analysis:

The XAFS measurements were performed at beam line X19-A at the National Synchrotron Light Source in Brookhaven National Laboratory. Experimental procedure are discussed elsewhere[6].

The least squares method for analysis of X-ray absorption near edge structure (XANES) of the sulfur K-edge spectra is based on the concept that the experimental spectrum can be modelled as the sum of an arctangent function representing the edge step and a number of absorption peaks which arise from 1s⇒3p electronic transitions of the major forms of sulfur in the coal. The shape of the absorption peaks is modelled as a function of energy by a combined 50:50 Lorentzian:Gaussian function. An example of least-squares curve fitting of the sulfur K-edge XANES spectrum of the Illinois No. 6 coal is shown in Figure 1. This spectrum is fit by one-step arctangent function representing the edge step, six peaks of 50% Gaussian - 50% Lorentzian shape representing three different forms of sulfur, both organic and inorganic, and several scattering resonance peaks[6].

To convert the measurement of relative peak areas to wt% sulfur in the different forms, the calibration method described elsewhere[8] was utilized. It has been observed that the 1s⇒3p transition probability increases with increasing sulfur valence. Therefore, calibration constants for converting XANES peak area percentages to sulfur weight percentages have been experimentally determined for the functional forms of sulfur that occur in coal[9]. For this work an additional calibration constant had to be determined for pyrrhotite, which was formed from the degradation of pyrite during pyrolysis. The error in the resulting sulfur percentages is approximately ±5 - 10%.

Results and Discussion

In situ sulfur XANES spectra obtained during pyrolysis of Illinois No.6 coal are shown in Figure 2. The effect of pyrolysis on different forms of sulfur in this coal as a function of temperature is illustrated in bar-graph form shown in Figure 3. It is evident that between 250°C and 600°C, the organic sulfide component decreases from 19% of total sulfur to about 10%. Simultaneously, pyrite begins to transform to pyrrhotite; this transformation continues as the temperature is raised and appears to be more or less completed at 600°C. No significant differences were observed between the pyrolysis in helium and that in hydrogen.

The results of *in situ* XANES measurements for pyrolysis of Australian (Glencoe) coal under H_2 and He atmospheres are shown in Figures 4 and 5, respectively. It is seen that disulfide compounds start to degrade at about 200°C while sulfide components decrease when the temperature reaches around 400°C. Growth of a peak with a negative valence state was observed as a function of temperature during the pyrolysis of Australian coal in both He and H_2 atmospheres. Since this coal contains virtually no iron (<0.05 wt%) the appearance of this peak may indicate the formation of organic compounds such as thioketones or similar functional groups during the course of experiments. A similar peak was observed during the thermal oxidation of a mixture of 50:50 wt% of dibenzothiophene and dibenzylsulfide.

The changes that occur in the sulfur forms of the Glencoe coal during oxidation under a mixture of 95% He-5% O_2 flowing gas are illustrated in bar-graph form in Figure 6. Decomposition of organic sulfide component occurs at the same temperature as for pyrolysis (above 400°C). The only significant changes during the oxidation of this coal are a gradual increase in the sulfate component and a decrease in the sulfide component. Since the Australian coal is one that contains no pyrite, the sulfate is believed to be either an organic sulfate or possibly $CaSO_4$. The latter could result from the reaction of SO_2 released from sulfide groups with carboxyl-bound calcium in the coal macerals. At the conclusion of the experiment, the sample contained 4.2 wt.% sulfur, indicating that about 1 wt.% of the sulfur had left the sample as SO_2 formed by oxidation of the organic sulfides.

Figure 7 shows the percentage of different sulfur forms in Illinois No. 6 coal under oxidation in a mixture of 95% helium - 5% oxygen. Pyrite was partially removed from this sample by centrifugation in carbon tetrachloride prior to the oxidation experiment. The initial sulfur content of the sample was 3.6 wt.%, with a pyritic sulfur content of approximately 1.6 wt.% according to the XANES results. The principal change during oxidation is a significant decrease in pyritic sulfur and a small, gradual increase in sulfate. It should be mentioned that the sample was heated to 500°C, but a spectrum was not obtained because of a loss of the X-ray beam at that temperature. The final bar graph obtained at room temperature therefore is from a sample that had experienced oxidation up to 500°C. Pyrite has disappeared and a small peak from elemental sulfur is observed. Since the final sulfur content of the sample was 1.7%, most of the pyritic sulfur leaves the sample as SO_2.

Conclusions

Based on the *in situ* XAFS measurements of the sulfur K-edge of the coal samples reported in this research, the following conclusions can be made:

- *In situ* XAFS high temperature measurements can provide insight into the behavior of sulfur compounds during thermal reactions.
- During pyrolysis, the degradation of disulfide starts to occur at about 200°C, while the organic sulfide decomposes at above 400°C. The conversion of pyrite to pyrrhotite in Illinois No. 6 coal was observed above 400°C.
- During oxidation of an Illinois No. 6 coal at temperatures up to 500°C, pyritic sulfur decreases markedly, while a small and gradual formation of sulfate is observed. A minor amount of elemental sulfur was also formed.
- During oxidation of a brown coal containing no pyrite at temperatures up to 450°C, organic sulfides decreased approximately 50% and a gradual increase of sulfate was observed.

References

(1) Attar A.; In Analytical Methods for Coal and Coal Products; Ed, Karr C.; Academic Press: New York, **1979**, 1.

(2) Calkins W. H.; Energy & Fuels; **1987**, 1, 59.

(3) Calkins W. H.; ACS, Div. Fuel Chem.; **1985**, 30(4), 450.

(4) Bakel A. J., Philp R. P., and Galves-Sinibaldi A.; Geochemistry of Sulfur in Fossil Fuels; Eds., Orr W. L. and White C. M.; ACS, **1989**, 429, 326.

(5) Boudou J. P.; Geochemistry of Sulfur in Fossil Fuels; Eds, Orr W. L. and White C. M.; ACS; **1989**, 429, 345.

(6) Huffman, G. P., Huggins F. E., Shah N., Mitra S., Pugmire R. J., Davis B. Lytle F. W., and Greegor R. B.; Energy & Fuels; **1989**, 3, 200.

(7) Gorbaty M. L., George G. N., and Kelemen S.R.; ACS, Div. Fuel Chem., Preprints; **1990**, 35(3), 779.

(8) Huffman G.P., Huggins F. E., Francis H. E., Mitra S., and Shah N.; Processing and Utilization of High-Sulfur Coal III, Elsevier; **1990**, 21.

(9) Huffman G. P., Mitra S., Huggins F. E., and Shah N.; (to be published) Energy & Fuels; **1991**.

(10) Sinfelt J. H., Via G. H., and Lytle F. W.; Chem. Phys.; **1982**, 76, 2779.

Acknowledgement

The authors acknowledge the Electrical Power Research Institute (EPRI) for supporting this research under EPRI contract No. RP-8803. We also are grateful to the U.S. Department of Energy for the use of synchrotron facilities at the National Synchrotron Light Source at Brookhaven National Laboratory.

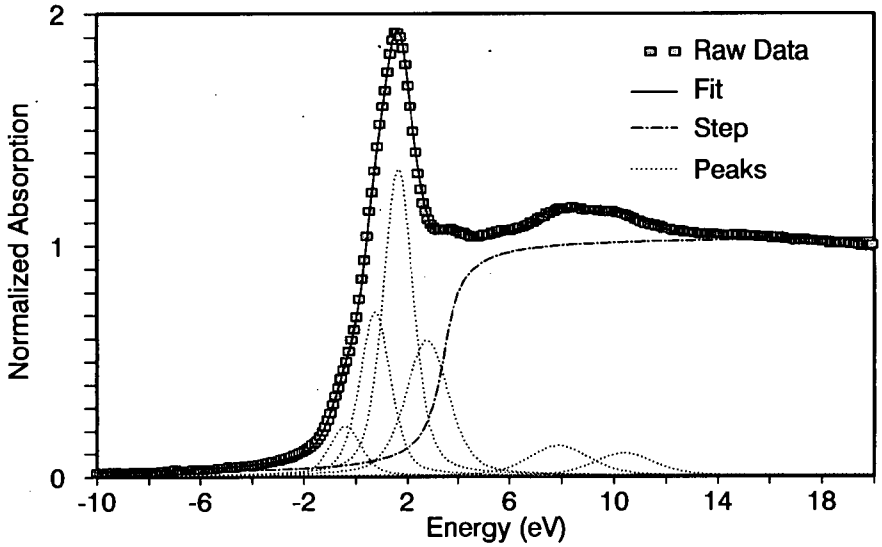

Figure 1. Example of least-squares fitting of the sulfur K-edge XANES spectrumof the Illinois No. 6 coal. The spectum is fit by one-step arctangent function and a number of peaks of 50% Gaussian - 50% Lorentzian shape.

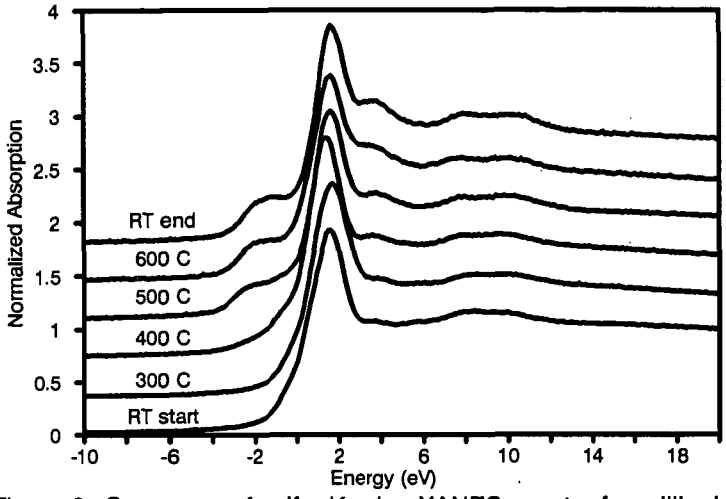

Figure 2. Sequence of sulfur K-edge XANES spectra from Illinois No. 6 at indicated temperatures during pyrolysis in helium.

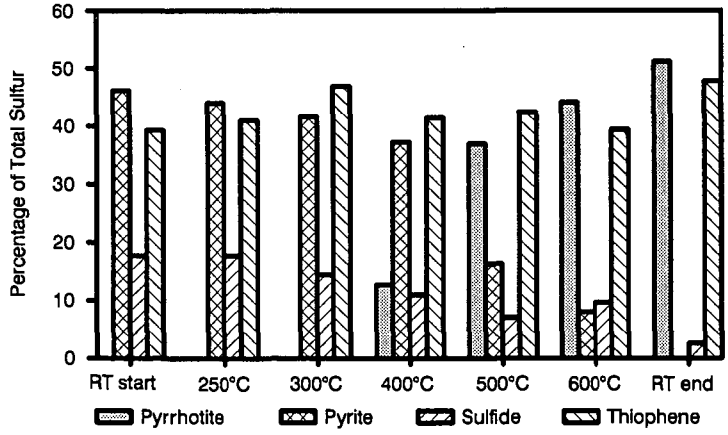

Figure 3. Percentage of different sulfur forms in Illinois No. 6 under pyrolysis in helium obtained by least-squares analysis of the XANES spectra shown in Figure 2.

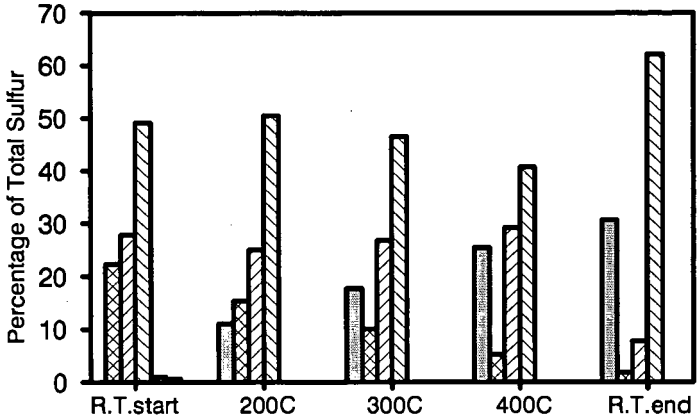

Figure 4. Percentage of different sulfur forms in Australian brown coal (Glencoe) under pyrolisis in hydrogen.

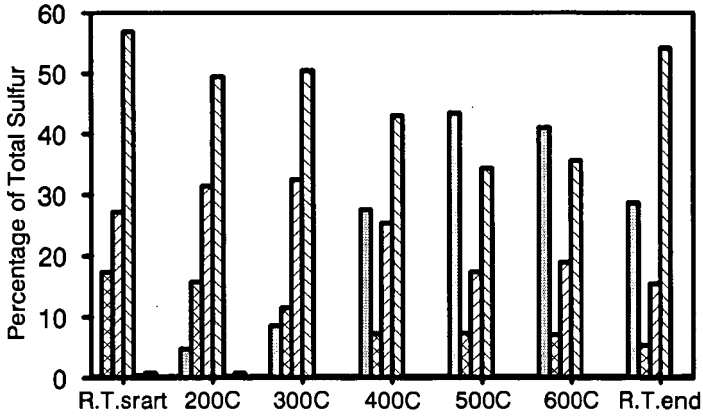

Figure 5. Percentage of different sulfur forms in Australian brown coal (Glencoe) under pyrolisis in helium.

See Text | Disulfide | Sulfide
Thiophene | Sulfone | Sulfate

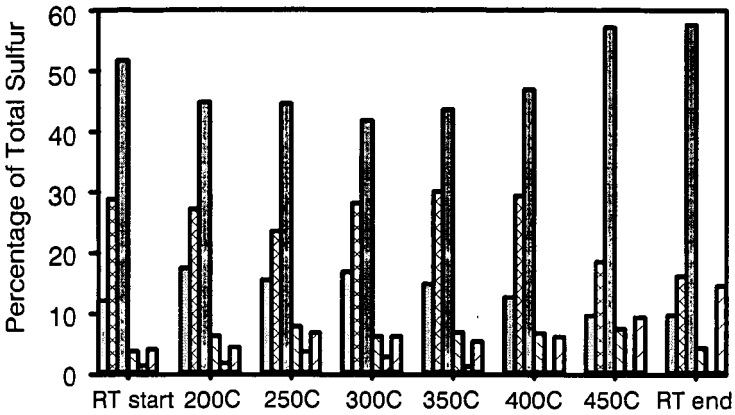

Figure 6. Percentage of different sulfur forms in Australian coal (Glencoe) under oxidation in 95% helium + 5% oxygen.

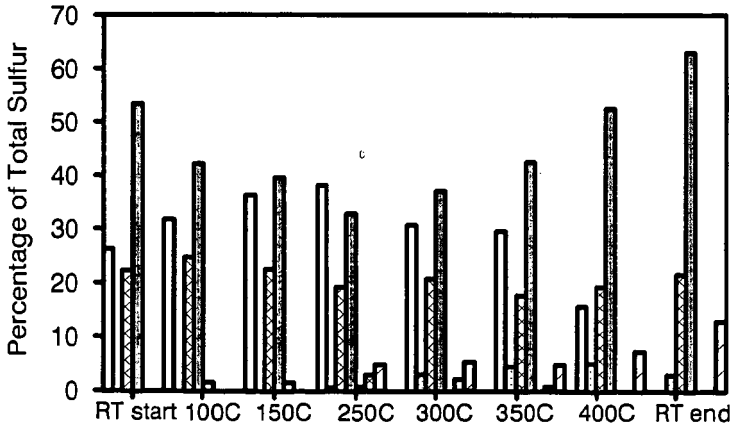

Figure 7. Percentage of different sulfur forms in Illinois No. 6 coal under oxidation in 95% helium + 5% oxygen.

Disulfide Pyrite Elemental Sulfure Sulfide
Thiophene Sulfoxide Sulfone Sulfate

STRUCTURE AND STRUCTURAL DIVERSITY IN RESINITES AS DETERMINED BY PYROLYSIS-GAS CHROMATOGRAPHY-MASS SPECTROMETRY

Ken B. Anderson and Randall E. Winans
Chemistry Division, Building 200
Argonne National Laboratory
9700 S. Cass Avenue
Argonne, IL, 60439.

Keywords: Resinite, Py-GC-MS, Classification

INTRODUCTION

A number of workers have reported data concerning the analysis of fossil resins,[1-7] (often referred to as "amber", but referred to herein by their correct general geologic name - resinite). It has become apparent from these data, that a number of chemically distinct forms of resinite exist in the geosphere. At present however, no convention exists for the differentiation of these chemically distinct materials. This problem of nomenclature is further compounded by a degree of ambiguity in the petrographic identification of resinites[8], and also by the inappropriate use of the term "resin" to describe certain petroleum and source rock components. As a result, the literature concerning the geochemistry of higher plant resins is somewhat confused.

General structural characteristics of a number of different resinites have been established by previous studies. Results of analyses carried out in our laboratory however, indicate that even within closely related samples, a significant degree of variability of composition exists, often as the result of differences in botanical origin and/or level of thermal maturity. We have therefore sought to develop a classification system for resinites, and to establish criteria by which individual resinites may be unambiguously classified.

In order to investigate the nature and extent of variability in resinite structure, we have sought to establish a broadly based resinite sample collection. The results of Pyrolysis-Gas Chromatography-Mass Spectrometric (Py-GC-MS), analyses of a number of different resinite samples from this collection, and the implications of these results to the nomenclature and classification of resinites, are described herein.

EXPERIMENTAL

Py-GC-MS analyses were carried out using an HP-5890 GC coupled with an HP-5970 MSD. Resinite samples (approx. 1 mg) were subjected to pyrolysis in the presence of excess tetramethylammonium hydroxide (TMAH) to effect in-situ methylation of acidic components,[9] using a C.D.S. "pyroprobe" coil type pyrolyzer. 60m DB-5 and DB-1701 columns were used to obtain adequate chromatographic separation of components.

RESULTS AND DISCUSSION

A thorough review of the literature, and the results of analysis of our own carefully screened suite of true resinite samples, suggests that three basic structural families of resinites predominate in the geosphere. A small number of less common forms are also known, but are usually restricted to a very small number of sites. The results of Py-GC-MS analyses of examples of each of these resinite classes, illustrated in Figure I, clearly reflect the compositional differences reported by previous authors. These data also demonstrate that Py-GC-MS is a useful technique for providing detailed information concerning the molecular composition of resinites, especially when used in conjunction with in-situ methylation procedures. As a consequence of these observations, (and parallel spectroscopic data) a preliminary classification system, outlined in Table I and described in detail below, has been developed to rationalize and clarify the nomenclature of resinites, and to enable

researchers to conveniently indicate the specific chemical nature of resinite samples with which their work may be concerned. A more comprehensive description and justification of this classification system will be reported elsewhere.

In addition to resins with structures related to the resinite structures described below, modern plant genre produce numerous other resins, with diverse structural characteristics and compositions. The apparent absence of these resins from geologic strata of significant age however, suggests that these resins are unable to survive diagenetic and/or catagenetic processes in a recognizable form, except perhaps in specialized, rare circumstances.

Class I resinites, which appear to be by far the predominant form of resinite in the geosphere, have been shown by a number of previous workers to be polyditerpenoid structures, based predominantly on the 14,15- polymerization products of labdatriene carboxylic acids, especially communic acid or zanzibaric acid (structures I-IV below).[1-5] Other mono and diterpenoids are often incorporated (or physically occluded) in the structure to a lesser extent. Whilst the results of our analyses concur with these reports, our data indicate that the specific composition of class I resinites, as assessed by Py-GC-MS, varies significantly between samples, and reflects both the botanical origin and maturity of the resinite.

Class I resinites, unlike class II and III resinites which appear to have specific botanical origins, appear to be derived from a number of paelobotanical sources (see Table I). Modern analogues of class I resinites are produced, often in large amounts, by a number botanical genre, including the: Araucariaceae, Taxodiaceae, Leguminoseae,[10] Cupressaceae,[11] and possibly others. This diversity of sources and often copious production probably accounts for the observed predominance of class I resinites in geologic samples.

Py-GC-MS data (illustrated in Figure II) and other results, suggest that class I resinites may usefully be further divided into divided into three sub-classes on the basis of molecular composition. Resinites based on polycommunic acid can and should be distinguished from those based on polyzanzibaric acid, and for some purposes it may also be useful to further divide communic acid based class I resinites into succinylated and non succinylated forms. A number of class I resinites, including "Baltic amber" (succinite), which together comprise probably the single largest source of resinite, incorporate succinic acid as a cross-linking agent between occasional communol units incorporated into a communic acid based polymeric structure. In other communic acid based class I resinites however, succinic acid is absent, suggesting a related but distinct origin for these materials. These finer sub-categories are useful for distinguishing related resinites of distinct botanical origins, and may also aid in establishing correlations between geographically dispersed samples of closely related structural character. Class I resinites may therefore be sub-divided according to the basic character of the polymeric structure as follows: I(a) Succinylated polycommunic acid; I(b) Non-succinylated polycommunic acid; and I(c) polyzanzibaric acid.

Notable features of the chromatograms illustrated in Figure II are: (i) Significant differences in the distributions of intact diterpenoids (eluting between 55 and 70 minutes in these chromatograms), which reflect the different botanical origins (and possibly also the thermal maturities) of the samples, and (ii) the presence of abundant dimethyl succinate in the pyrolysis products of the class Ia sample. This compound is not observed in the pyrolysis products of class Ib or Ic resinites. A more comprehensive analysis of these data will be presented elsewhere. Slight, but highly significant differences are also observed in the nature of the products eluting between 30 and 55 minutes in these chromatograms. These compounds are predominantly bicyclic carboxylic acids derived from the labdanoid ring system of the parent acids. Preliminary data suggest that differences in these products may be useful for distinguishing class Ia and Ib resinites from class Ic resinites in mature samples, in which no detectable intact diterpenoids remain.

Class II resinites have been shown to be based on polymers of sesquiterpenoid hydrocarbons related to cadinene (V).[6,12,13] Although less common overall than Class I resinites, Class II resinites are very abundant in several locations throughout the world, including the U.S. (specifically Utah) and S.E. Asia (where both modern and fossil deposits occur) and constitute a major resource of resinite. This class of resinite is known to be derived from trees of the Dipterocarpaceae, especially Shorea, modern resins of which, known as Damar, are still commercially exploited, and differ little in structural terms from Class II resinites. Class II resinites are very easily distinguished from Class I and III resinites by pyrolytic techniques (See for example Figures I) on the basis of the nature of the pyrolysis products, especially the absence of significant amounts of carboxylic acids. Spectroscopic data is also often definitive for the classification of resinites of this class.

Class III resinites, which are composed almost entirely of natural polystyrene (VI), are the least common of the three resinite classes defined in Table I, currently identified deposits being restricted to the Eastern US and (possibly) Germany[7,10]. These resinites are believed to be derived from the resins of Hammelidaceae, especially Liquidambar. Class III resinites are very easily recognized and classified on the basis of spectroscopic and/or pyrolytic data; the principle problem associated with recognition of these materials being confirmation of the provenance of the sample (ie: being sure that the sample is not synthetic polystyrene which has inadvertently been collected as fossil material).

Class II and III resinites are also distinct from Class I resinites in that resinites of these classes are soluble in organic solvents, and hence may be recovered and concentrated by extraction.

As indicated above, although all resinites of a given class share a number of common structural characteristics, the composition of volatile and volatilizable materials produced by pyrolysis varies considerably between samples. These differences reflect variations in the composition of the original resins, and also differences in the thermal maturity of the samples. These differences are particularly important in class I samples, due to the diversity in the botanical origins of these resinites, but are also likely to be important in other resinites.

In immature class I samples, such as those illustrated in Figure II, abundant, intact diterpenoids are released by volatilization and thermal depolymerization as a result of pyrolysis. These diterpenoids probably reflect the composition and nature of the original resin and hence are of considerable interest. With increasing thermal maturity however, the significance of these compounds decreases, and substituted unsaturated bicyclic carboxylic acids become increasingly predominant in the pyrolysis products. This probably reflects semi-random cross-linking, especially between olefins, and double bond migration to thermodynamically more stable isomers. This results in a thermally more stable polymeric structure, which is less able to thermally "unzip", and which therefore cleaves off naphthenic structures derived from the labdanoid ring system of the precursor, in this case communic acid. The low abundance of tricyclic products in the pyrolyzate of mature resinite samples suggests that cyclization reactions are not an important maturation process in resinites. At high levels of maturity aromatization and elimination of substituents also appear to be significant. This trend is demonstrated in Figure I, which illustrates Py-GC-MS data for a series of class Ib resinites obtained from New Zealand coals of known maturity. Similar trends are observed in other class I resinites.

CONCLUSIONS

Py-GC-MS is a useful technique for the rapid characterization of resinites, especially when used in conjunction with in-situ methylation procedures, which permit chromatographic analysis of acidic components without complex sample preparation.

Although significant diversity exists in resinite structures, the majority of resinites may be classified into one of three basic structural groups. Resinites from the largest and most important of these may be further subdivided on the basis of specific structural characteristics into three subclasses. Within these classes, details of specific composition may vary significantly between samples as a consequence of differences in botanical origin and/or level of maturation, but sufficient common structural characteristics exist within these classes to validate application of such a classification system.

ACKNOWLEDGMENTS

The authors wish to acknowledge Mr. J. Gregar of the Argonne National Laboratory for preparation of specialized glassware. We also wish to express our gratitude to Dr. P. Dunn, and Dr. F. Hueber of the National Museum of Natural History - Smithsonian Institute, Dr. D. Grimaldi of the American Museum of Natural History (ANMH), Dr G. Mustoe of Western Washington University, Dr T.V. Verheyen of the Coal Corporation of Victoria, Dr D. Paris of the New Jersey State Museum (NJSM), Dr A. Criddle of the Natural History Museum (London), Dr J. Crelling of the University of Southern Illinois, and Dr A. Clemmens of the Coal Research Association of New Zealand (Inc.) for generously providing resinites samples. Reference numbers given in figure captions refer to sample numbers of the organizations indicated. This work was performed under the auspices of the Office of Basic Energy Sciences, Division of Chemical Sciences, U.S. Department of Energy, under contract number W-31-109-ENG-38.

REFERENCES

1. (a) Gough, L.J.; Mills, J.S. *Nature* **1972**, *239*, 527-528.
   (b) Mills, J.S.; White, R.; Gough, L.J. *Chem. Geol.* **1984/85**, *47*, 15-39.

2. Cunningham, A.; Gay, I.D.; Oehlschlager, A.C.; Langenheim, J.H. *Phytochem.* **1983**, *22(4)*, 965-968.

3. (a) Thomas, B.R. *Acta Chem. Scand.* **1966**, *20(4)*, 1074-1081.
   (b) Thomas, B.R. In *Organic geochemistry - methods and results*; G. Eglinton and M.J.T. Murphy, Eds.; Springer-Verlag: New York, 1969; pp 599-618.

4. (a) Anderson, K.B.; Botto, R.E.; Dyrkacz, G.R.; Hayatsu, R.; Winans, R.E. *Preprint, Fuel Chemistry Div., ACS* **1989**, *34(3)*, 752-758.
   (b) Anderson, K.B.; Botto, R.E.; Dyrkacz, G.R.; Hayatsu, R.; Winans, R.E. *Fuel* **1990**, *69*, 934-935.

5. Beck, C.W. *Appl. Spec. Rev.* **1986**, *22(1)*, 57-110.

6. Van Aarssen, B.G.K.; Cox, H.C.; Hoogendoorn, P.; De leeuw J.W. *Geochim. Cosmochim. Acta* **1990**, *54*, 3021-3031

7. Grimaldi, D.; Beck, C.W.; Boon, J.J. *American Museum Novitates* **1989**, *2948*, 1-28.

8. Stach, E.; Mackowsky, M.-.T.h.; Teichmuller, M.; Teichmuller, R.; Taylor, G.H.; Chandra, D. In *Stach's Textbook of Coal Petrology*, 3rd edition; Gebruder Borntraeger: Berlin-Stuttgart, 1982; 535 p.

9. (a) Challinor, J.M. *J. Anal. Appl. Pyrol.* **1989**, *16*, 323-33.
   (b) Dworzanski, J.P.; Berwald, L.; Meuzelaar, H.L.C. *Appl. Environ. Microbiol.* **1990**, *56(6)*, 1717-24.

10. Langenheim, J.H. *American Scientist* **1990**, *78*, 16-24.

11. Mangoni, L.; Belardini, M. *Gazz. Chim. Ital.* **1964**, *94*, 1108-21.

12. Meuzelaar, H.L.C.; Huaying Huai; Lo, R; Dworzanski, J.P. *Preprint, S.M.E. Meeting, Salt Lake City, Utah*, February 1990.

13. Brackman, W.; Spaargaren, K.; Van Dongen, J.P.C.M.; Couperus, P.A.; Bakker, F. *Geochim. Cosmochim. Acta* **1984**, *48*, 2483-2487.

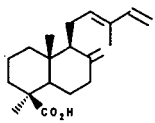

I

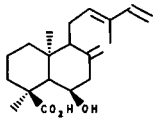

II

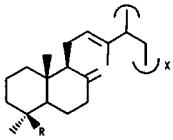

III

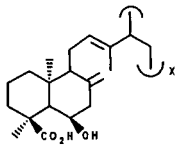

IV

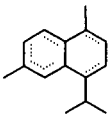

V

VI

Structures indicated in text: I - Communic acid (trans isomer). II - Zanzibaric acid (trans isomer). III - Basic polymeric structure of class Ia and Ib resinites. (i) R = COOH (polycommunic acid), (ii) R = CH_2OH (may be succinylated ie: CH_2O-CO-$(CH_2)_2$-CO-O-R': R'=H or communol unit of polymer.). IV - Basic polymeric structure of class Ic resinites, polyzanzibaric acid. V - Cadinene (dotted lines indicated double bond isomers). VI - styrene.

TABLE I.

Class I	
(a)	Basic structural character = polycommunic acid, partially copolymerized with communol. Significant incorporation of succinic acid, probably as a cross linking agent is characteristic. examples = Succinite (Baltic Amber)
(b)	Basic structural character = polycommunic acid, with varying degrees of copolymerization with communol. Succinic acid is absent. examples = New Zealand resinites, Victorian Brown Coal resinites.
(c)	Basic structural character = polyzanzibaric acid. Nearest equivalent modern resins: "Copal" esp. Pontianak, Kauri Resin, Manila Copal Brazil Copal, Congo Copal Most probable botanical affinity*: (i) Araucariaceae (esp. Agathis) (ii) Leguminosae (esp. Hymenaea) (iii) Cupressaceae, and possibly others.
Class II	Basic structural character = polymer of bicyclic sesquiterpenoid hydrocarbons, esp. cadinene, possibly with some triterpenoid component also present. examples = Utah resinites, (some) Indonesian resintes. Nearest equivalent modern resin: "Damar" Most probable botanical affinity*: Dipterocarpaceae (esp. Shorea)
Class III	Basic structural character = Polystyrene examples = (some) New Jersey resinites, Montana resinite Nearest equivalent modern resin: "Storax" (Sometimes = Styrax) Most probable botanical affinity*: Hammelidaceae (esp. liquidambar)

*Based on equivalent modern resins.

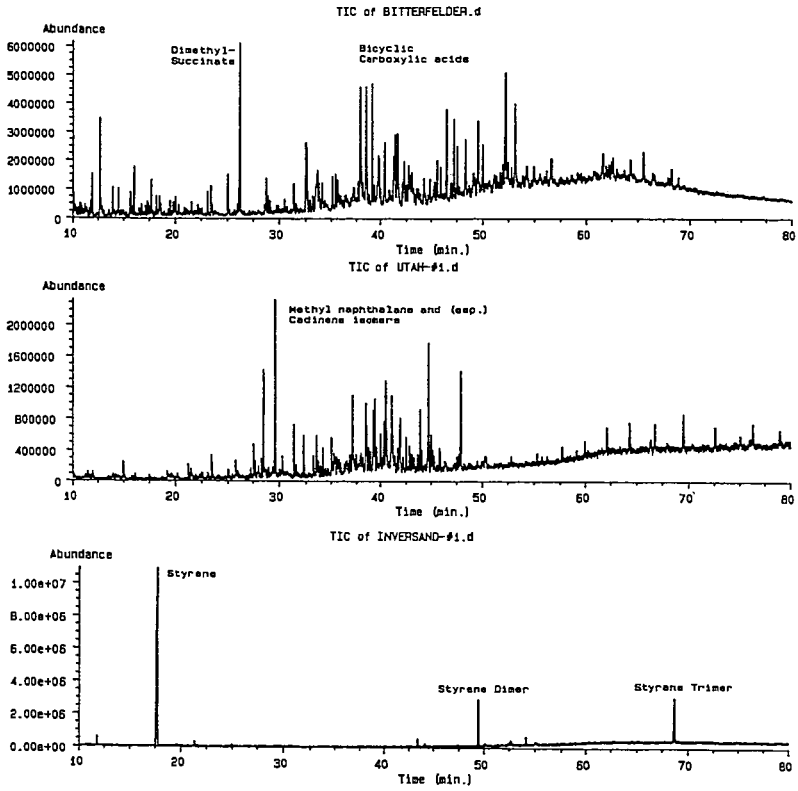

Figure I. Py-GC-MS data for typical examples of Class Ia, II and III resinites. Top: CLASS Ia - Bitterfelder resinite (Germany) [AMNH # B-3]. Centre: CLASS II - Blind Canyon resinite (Utah, U.S.A.). Bottom: CLASS III - Sayrville resinite (New Jersey, U.S.A.) [NJSM #14156]. $T_{pyrolisis}$=540 °C, Column = 60m DB-1701.

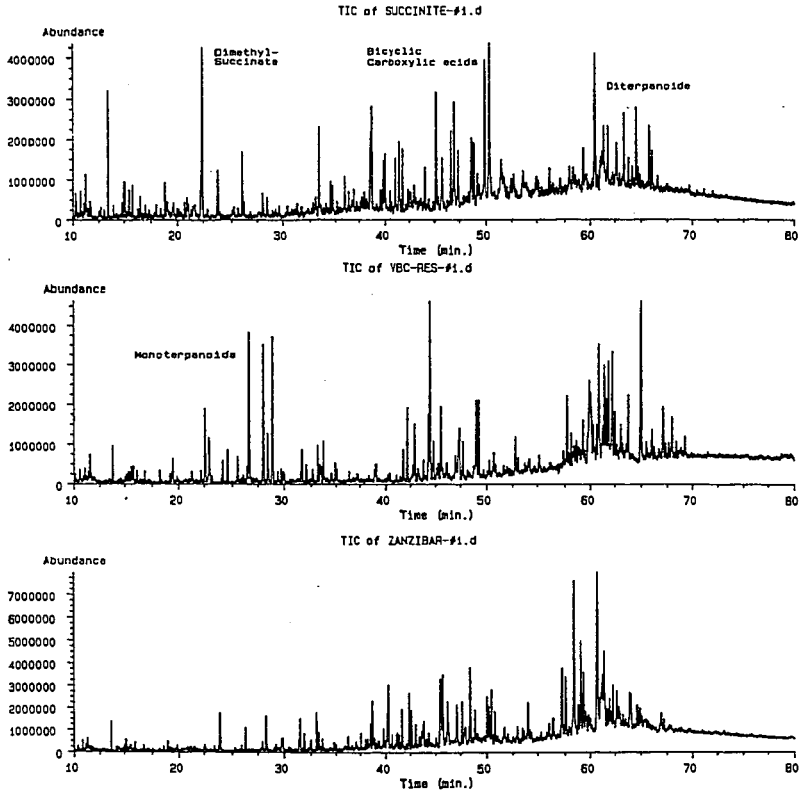

Figure II. Py-GC-MS data for class Ia, Ib, and Ic resinites. Top: Succinite, Baltic region, Eastern Europe [USNM #353431], Centre: Victorian Brown Coal resinite, Latrobe Valley, Victoria, Australia Bottom: Zanzibar resinite, Zanzibar, Africa [AMNH # H252]. $T_{pyrolisis}$=480 °C, Column = 60m DB-5.

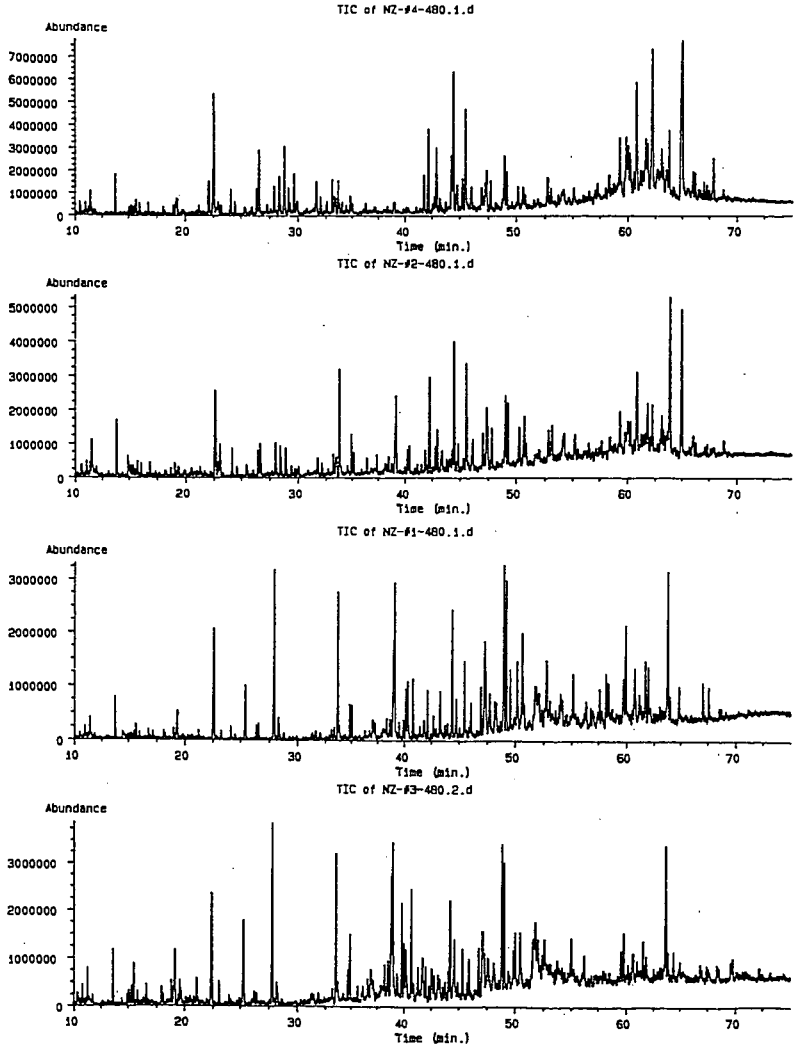

Figure III. Py-GC-MS data for New Zealand Class Ib resinites, showing changes in pyrolysis product distribution as a consequence of increasing thermal maturation. $T_{pyrolisis}$=480 °C, Column = 60m DB-5.222

STRUCTURAL ELUCIDATION OF POLYMERIC DITERPENOIDS IN FOSSIL GYMNOSPERM RESINS BY MEANS OF PYROLYSIS COMBINED WITH GC-MS.

Ben G.K. van Aarssen and Jan W. de Leeuw.

Delft University of Technology, Faculty of Chemical Technology and Materials' Science, Organic Geochemistry Unit, De Vries van Heystplantsoen 2, 2628 RZ Delft, The Netherlands

Keywords: fossil gymnosperm resins, polymeric diterpenoids, flash-pyrolysis-gas chromatography-mass spectrometry.

INTRODUCTION

Fossil resins originating from Gymnosperm trees have been the subject of several studies concerning the structure of their high molecular weight fractions [1-4]. Although such resins may be sourced from quite different plant families the structures of the macromolecular moieties have similar features. Formation of these substances is thought to occur *via* a light and/or oxygen induced polymerisation of diterpenoid monomers with a labdane carbon skeleton, such as communic acid [1]. Because the polymers are insoluble in common organic solvents, structural studies have been performed using techniques like IR [5], solid state NMR [3,6,7] and Py-MS [4,8]. In this study we show that Curie point pyrolysis-GC-MS and off-line pyrolysis GC-MS are useful methods to gain information on the structure of the polymeric fractions of fossil resins. For this purpose a fossil resin from the Fushun coal mine in China was analyzed.

EXPERIMENTAL

Curie-point pyrolysis-gas chromatography-flame ionisation detection (Py-GC-FID) analyses were performed with a Hewlett-Packard 5890 gas chromatograph using a FOM-3LX unit for pyrolysis. The samples were applied to a ferromagnetic wire with Curie temperatures of 770°C (Fe) or 358°C (Ni). The gas chromatograph, equipped with a cryogenic unit, was programmed from 0°C (5 min) to 320°C (20 min) at a rate of 3°C/min. Separation was achieved using a fused-silica capillary column (25m x 0.32mm) coated with CP Sil-5 (film thickness 0.4 μm). Helium was used as the carrier gas.

Curie-point pyrolysis-gas chromatography-mass spectrometry (Py-GC-MS) analyses were performed using the same equipment and conditions as described above for Py-GC-FID connected with a VG 70S mass spectrometer operated at 70 eV with a mass range m/z 40-800 and a cycle time of 1.8 s.

Extraction of the resin was achieved by thoroughly mixing the finely powdered resin ultrasonically several times with a variety of solvents like methanol, dichloromethane, ethylacetate and acetone. The combined extracts were methylated with diazomethane and analysed by GC-MS using the same equipment described for Py-GC-MS (CP Sil-5 column, film thickness 0.32 μm, temperature program from 70°C to 320°C (20 min) at a rate of 4°C/min).

For off-line pyrolysis-gas chromatography-mass spectrometry, an aliquot of the extracted resin was transferred into a quartz tube and heated under a constant flow of nitrogen (100 ml/min) at 425°C for 45 min. The released products were trapped in two flasks with pentane. The first was held at room temperature and the second at -20°C. The trapped pyrolysates were combined and analyzed by GC-MS as described above.

RESULTS AND DISCUSSION

Extraction of resins is often incomplete because of inclusion of soluble compounds in the insoluble macromolecular matrix. To differentiate between pyrolysis products and evaporated compounds the whole resin was analysed at both a Curie temperature of 770°C and of 358°C. At 358°C no pyrolysis takes place and only volatile compounds are analysed. The chromatograms of both analyses of the whole resin are shown in Figures 1a and 1b. The compounds released were tentatively identified by Py-GC-MS. The most abundant compound present in the mixture obtained at a Curie temperature of 770°C is a mono-unsaturated bicyclic C_{15}-carboxylic acid. The mass spectrum and suggested structure for this compound are shown in Figure 2a. Furthermore, a series of C_5, C_7 and C_8 unsaturated branched acyclic hydrocarbons is present.

Also very abundant are camphor and dehydroabietane. Comparison of the product mixtures obtained at a Curie temperature of 770°C (Fig. 1a) with that of the flash-evaporate (Fig. 1b) shows that both camphor and dehydroabietane are present as such in the resin. This is also true for the C_{15}-acid. However, at a Curie temperature of 770°C the latter compound is much more abundant, indicating that it is formed upon pyrolysis as well. This is also supported by the presence of a co-eluting similar compound with an additional double bond, which is absent in the flash-evaporate.

To concentrate on the products formed upon pyrolysis, and thus on the structure of the insoluble macromolecule, the resin was thoroughly extracted and the residue was pyrolysed at a Curie temperature of 770°C. The resulting chromatogram is shown in Figure 3a. Compounds like camphor and dehydroabietane are no longer present, showing that the extraction was successful. Flash evaporation at a Curie temperature of 358°C of the residue showed that virtually all the volatile compounds were extracted indeed. From the Py-GC analysis it is clear that the major pyrolysis products are the bicyclic C_{15}-acid, a similar bicyclic C_{14}-acid and the series of branched alkenes. Comparison of the chromatogram of the flash-evaporate (Fig. 1b) with that of the methylated extract (Fig. 3b) shows that many diterpenoid methyl esters with an abietane or pimarane carbon skeleton are present in the extract, but not in the evaporate. These C_{20}-compounds are probably present as free acids in the evaporate and hence not GC-amenable on the apolar column used. This is exemplified by the broadened peak reflecting the C_{15}-carboxylic acid in the evaporate. It should be noted that no bicyclic C_{20}-diterpenoids with labdane carbon skeletons could be detected in the pyrolysate nor in the extract. At the end of the chromatogram of the extract a broad hump is visible. Mass spectrometric analysis showed that this hump reflects several badly resolved dimeric diterpenoid acids, probably with labdane carbon skeletons. The mass spectrum of one of these compounds and a possible structure are shown in Figure 2b.

The chromatogram of the GC analysis of the methylated pyrolysate obtained by off-line pyrolysis of the extracted resin is shown in Figure 4. The pyrolysate obtained by off-line pyrolysis resembles the pyrolysate obtained by flash pyrolysis very well. The most abundant compounds are the mono- and di-unsaturated bicyclic C_{15} methyl esters. Again no bicyclic C_{20} diterpenoid methyl esters were detected.

The results shown indicate that the fossil resin consists of two fractions. A soluble low-molecular-weight fraction and an insoluble high-molecular-weight fraction. The distinction between these two fractions is however not clear-cut, as shown by the presence of dimeric diterpenoids in the extract. The flash-evaporate obtained at a Curie-temperature of 358°C can however not be taken as representative for the soluble fraction, because of the presence of non GC-amenable acids, which will do show up in the chromatogram. The high-molecular-weight fraction yields upon pyrolysis predominantly an unsaturated bicyclic C_{15}-carboxylic acid, which is probably the pyrolysis product of a polymeric diterpenoid. As shown in Scheme 1 a pyrolysis mechanism can be conceived starting from a polymeric structure as suggested in literature [1-4]. This mechanism can also explain the presence of unsaturated branched hydrocarbons in the pyrolysate. The acid is also found in the methylated extract as its methyl ester, indicating that some thermal breakdown of the polymer has already occurred in nature. On the other hand, volatile compounds like camphor are still included in the resin, indicating that the resin has not undergone severe diagenesis. No bicyclic C_{20}-compounds are formed upon pyrolysis of the polymer, as was shown by the off-line pyrolysis. Conclusions about the structure of the polymer in Gymnosperm resins based on the presence of diterpenoid monomers in pyrolysates should therefore be taken with care [4,8], because they are probably based on included, soluble and volatile compounds and not on pyrolysis products. Because no methyl esters of the C_{15}-pyrolysis products were detected in the flash pyrolysate, the polymer of the fossil resin used in this study must be built up of non-methylated monomers. The question recently discussed in the literature by several authors [7,8], as to whether or not Yallourn resinite polymer is methylated for a significant part, can therefore quickly be answered using the analytical methods described above.

CONCLUSIONS

The results described above support earlier conclusions about the structure of polymers present in fossil and recent gymnosperm resins. The resin studied contains a polymerized bicyclic diterpenoid, probably communic acid. Polymerization has occurred through the side chain, possibly *via* a 1,2 mechanism. The methods used in this work are relatively fast and simple and the results are complementary to those obtained by spectroscopic methods. Furthermore, they allow for further and more detailed studies of the basic structural units present in such polymers and the way they have polymerized by isolation and structural analysis of dimers and pyrolysis products. Such studies are now in progress.

REFERENCES

1. Carman R.M., Cowley D.E. and Marty R.A. (1970), Aust. J. Chem., 23: 1655-1665.
2. Mills J.S., White R. and Gough L.J. (1984/85), Chem. Geol., 47: 15-39.
3. Wilson M.A., Collin P.J., Vasallo A.M. and Russel N.J. (1986), Org. Geochem., 7: 161-168.
4. Anderson K.B., Botto R.E., Dyrkacz G.R., Hayatsu R. and Winans R.E. (1989), Am. Chem. Soc. Div. Fuel Chem. Prepr., 34(3): 752-758.
5. Beck C.W. (1986), Appl. Spectr. Rev., 22: 57-110.
6. Cunningham A., Gay I.D., Oehlschlager A.C. and Langenheim J.H. (1983), Phytochem., 22: 965-968.
7. Wilson M.A., Vasallo A.M., Liu Y.L. and Pang L.S.K., (1990), Fuel, 69: 931-933.
8. Anderson K.B., Botto R.E., Dyrkacz G.R., Hayatsu R. and Winans R.E. (1990), Fuel, 69: 934-936.

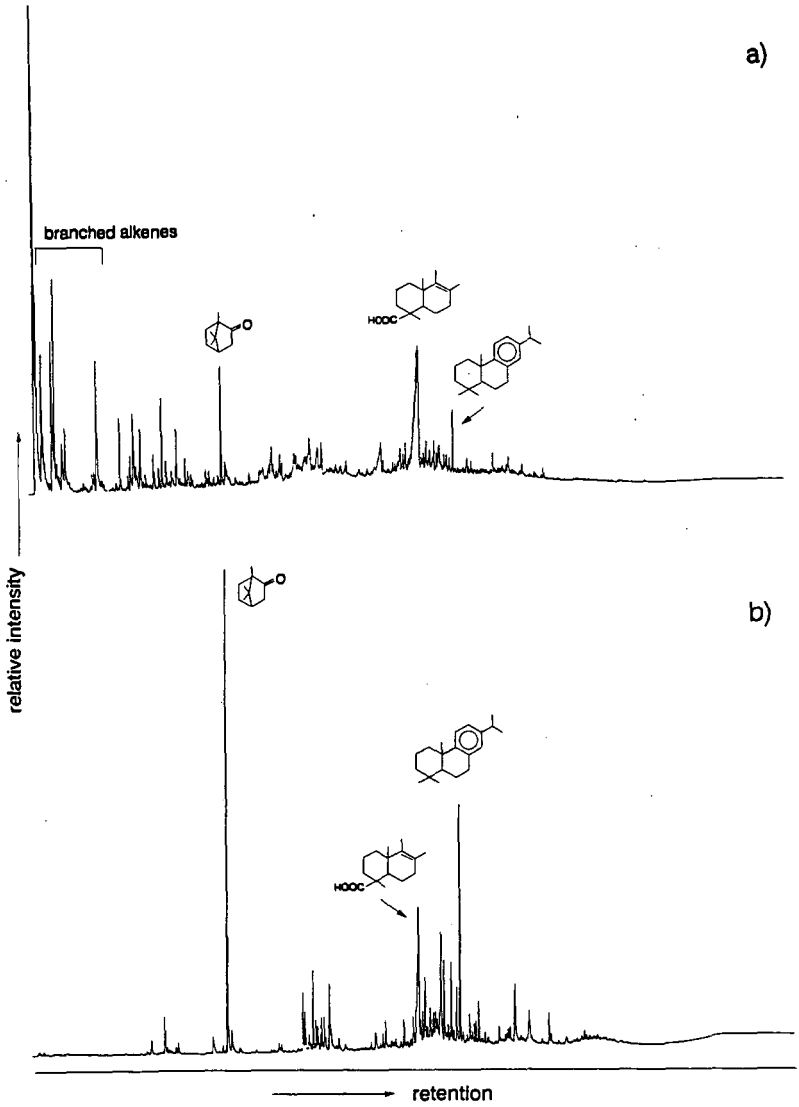

Fig. 1. Py-GC-FID traces of the whole fossil resin at Curie temperatures of a) 770°C and b) 358°C.

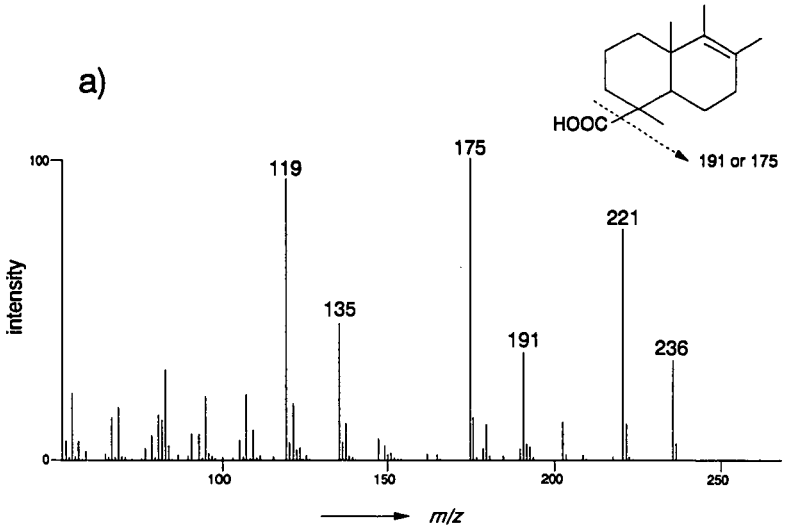

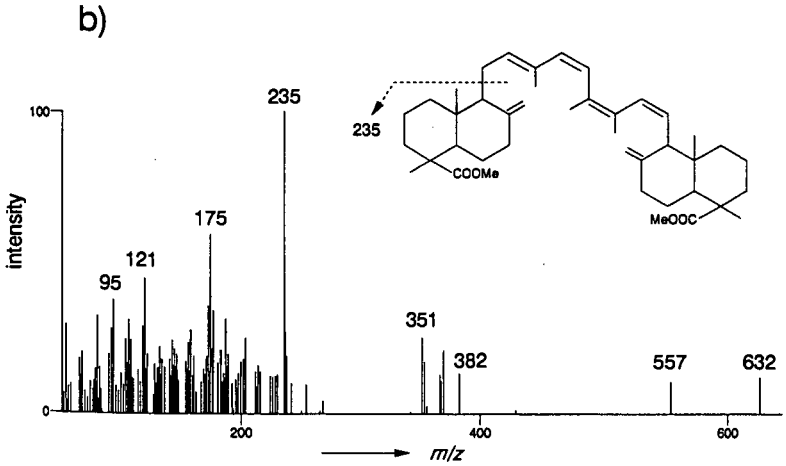

Fig. 2. Mass spectra of a) the major pyrolysis product of the fossil resin at a Curie temperature of 770°C and b) a diterpenoid dimer present in the resin extract.

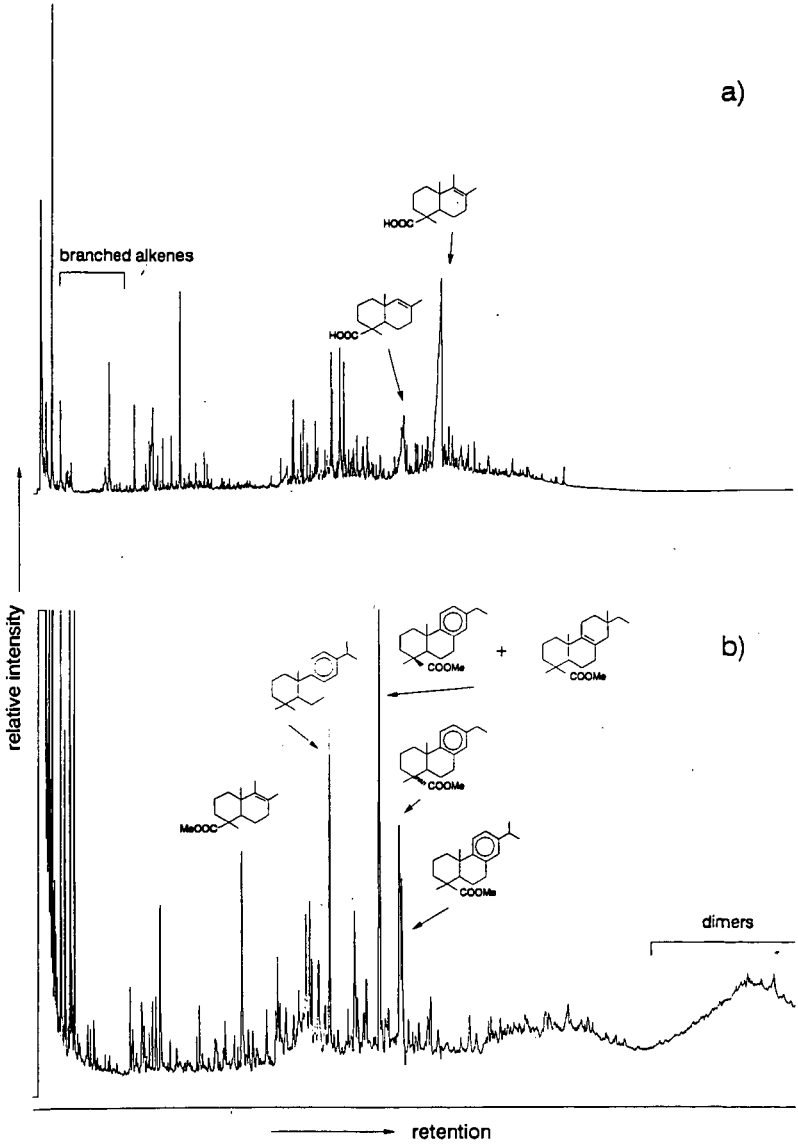

Fig. 3. a) Py-GC-FID trace of the extracted resin at a Curie temperature of 770°C. b) GC-FID trace of the methylated resin extract.

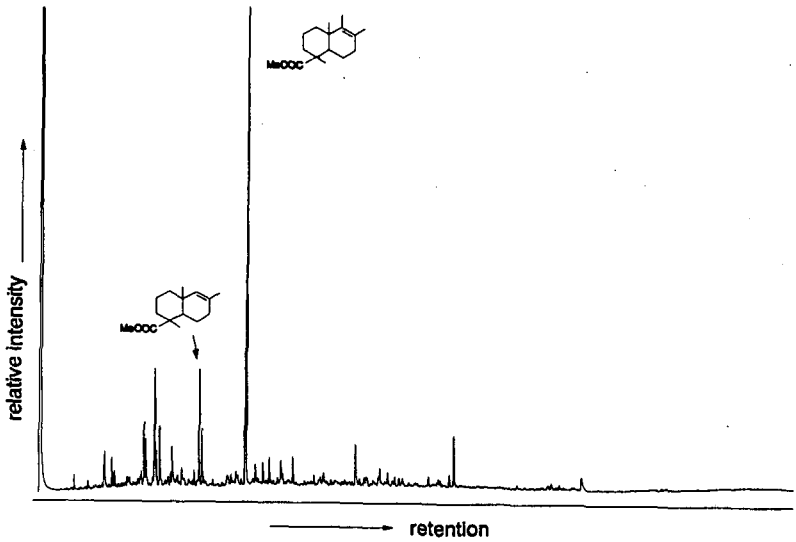

Fig. 4. GC-FID trace of the methylated pyrolysate obtained from the off-line pyrolysis of the extracted resin.

Scheme 1

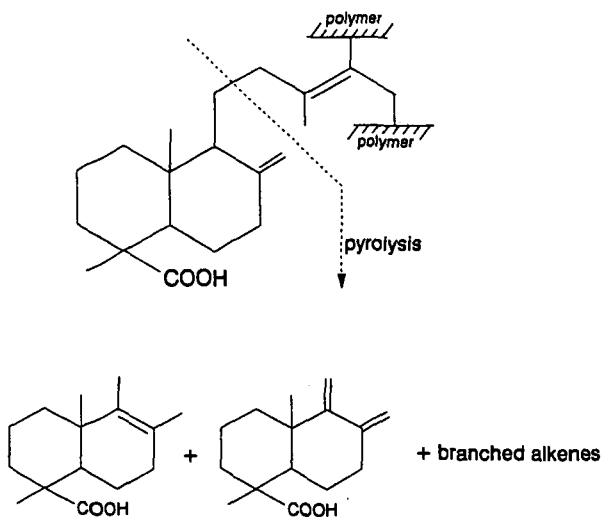

ANALYSIS OF PERU MARGIN SURFACE SEDIMENTS BY PY-MS

By

T.J. Eglinton[1], M.A. McCaffrey[1#], H. Huai[2] and H.L.C. Meuzelaar[2].

[1]Dept. of Chemistry, Woods Hole Oceanographic Institution, Woods Hole MA 02543.

[2]Center for Micro Analysis and Reaction Chemistry, EMRL, University of Utah, Salt Lake City, UT 84112.

Keywords: Peru Upwelling Sediments, Early Diagenesis, Pyrolysis-Mass Spectrometry

INTRODUCTION

In off-shore Peru high sedimentary organic carbon contents are a direct consequence of the extremely high primary productivity (*ca.* 1000g Carbon $m^{-2}.yr^{-1}$)[1] which, in turn, is supported by the upwelling of nutrient-rich waters near the coast. Diatoms represent the major phytoplankton type and give rise to sediments dominated by biogenic silica and planktonic organic matter. The remineralisation of this large flux of organic matter to the bottom waters and sediments results in oxygen depletion over large areas of the shelf which, in turn, promotes organic carbon preservation in the underlying sediments. Sulfide from sulfate reduction is prevalent in the bottom waters[2] and with a limited availability of iron (due to the dominant biogenic input coupled with a very low influx of detrital sediments) the excess sulfide is available for reaction with the organic matter. As a result high organic sulfur concentrations are found in the sediments[3].

The coastal Peru upwelling region is believed to be a modern analogue to the depositional environments of petroleum source rocks such as the Miocene Monterey Formation of the California Borderland[4]. Because organic matter alteration pathways in surface sediments ultimately influence kerogen type and eventual petroleum yield, there has been interest in characterizing surface sediments such as those off-shore Peru. Lipid[5-10], carotenoid[11] and amino acid[12] constituents as well as general biogeochemistry[1,13] have been studied previously. However, studies of the macromolecular components of the sediments have been less extensive[3,14].

This paper describes results from Py-MS analyses of sediment samples obtained from discrete intervals in a 1-meter core obtained from the upper continental shelf of the Peru Upwelling region. Factor and discriminant analysis of the Py-MS data revealed several distinct changes within this 1-meter section.

EXPERIMENTAL

Sample Recovery and preparation

Fifteen sediment samples obtained from a single *ca.* 1-meter box core were used for this study. The core ("SC3") was taken during a cruise of the R/V Moana Wave in 1987, and was retrieved from Station 4 (15°06.16'S, 75°42.09'W) at a water depth of 253m (within the prevailing oxygen minimum zone). Further information concerning the location and detailed geochemistry of these samples are provided elsewhere[15]. General geochemical descriptions of the samples are listed in Table 1.

Present address: Chevron Oil Field Research Company, Richmond CA 94802

Wet sediment samples were pre-extracted with isopropanol, followed by a methanol-chloroform mixture (to remove soluble lipid components) and subsequently air-dried prior to further analysis. Organic carbon and nitrogen measurements were made on de-carbonated sediment samples using a Perkin Elmer 2400 CHN analyzer.

Pyrolysis-Mass Spectrometry (Py-MS)

Similar experimental and mathematical procedures to those described by Metcalf *et al.*[16] were adopted for the present investigation. Briefly, dried samples were suspended in methanol (5 mg/ml) and approximately 75 µg of sediment was applied to each wire (Curie temperature, 610°C). Uniform sample coating was achieved by rotation of the wires during air-drying.

Py-MS was performed on an Extranuclear 5000-l quadrupole MS system described by Meuzelaar *et al.*[17]. Pyrolysis was started 30 s after introduction of the sample into the mass spectrometer. Py-MS conditions were as follows: temperature rise time 5s, total heating time 10s, electron energy 12 eV, mass range *m/z* 20-300, scanning rate 2000 amu/s, total number of scans acquired = 70. Each sample was analysed in triplicate.

Multivariate Statistical Analysis

Multivariate statistical analysis of the Py-MS spectra was performed using the SIGMA (System for Interactive Graphics-oriented Multivariate Analysis) program described by Windig and Meuzelaar [18].

The stored Py-MS data were firstly calibrated and normalized. Subsequently, factor analysis was performed, followed by discriminant analysis. Discriminant analysis was applied on the first seven factors (explaining 82% of the total variance, see Table 2) selected on the basis of Cattell "scree break" criterion[19]. As applied here, discriminant analysis involved an orthogonal rotation of factor space aimed at maximising outer/inner variance ratios. Outer variance is a measure of the differences between groups of spectra; inner variance is a measure of the internal variation within replicates as a consequence of experimental scatter or sample heterogeneity. The results are expressed in terms of discriminant scores which provide a quantitative measure of the differences, and in the form of numerically-extracted discriminant spectra[20], which give information about the mass intensity changes involved. The pyrolysis data are interpreted in terms of chemical "components" by means of the "variance diagram" (VARDIA) technique, a method developed for numerical analysis of unknown mixtures[21]. The basic principle is that the VARDIA plot shows how strong the correlated behavior of all mass variables is in all possible directions (in steps of 10°). Directions in the discriminant space which can be attributed to such chemical components are called "component axes".

RESULTS

Figure 1 shows averaged Py-MS spectra of samples from four intervals within the core. In general, the spectra are rather similar, being dominated by low mass ions and containing maxima at similar *m/z* values. Major series include ions those due to sulfur compounds such as H_2S (*m/z* 34), S_2 or SO_2 (*m/z* 64), HSSH (*m/z* 66), and S_4 (*m/z* 128), as well as sugar products (*e.g.* *m/z* 114, 126, 128, 144). Other mass peak patterns reflect contributions from aliphatic hydrocarbons and alkylaromatics (alkylphenols and alkylbenzenes).

Despite the similarity between the traces, factor and discriminant analysis allowed a number of distinctions to be made between the samples studied. Table 2. lists results from factor analysis of the data matrix including all samples and mass peaks. Slightly over 50% of the total variance is explained by the first factor, with the second and third factors accounting for a further 17% and 5% respectively.

The results from discriminant analysis of the data set are presented in Table 3 and Figure 2. Tighter clustering of the replicates and better separation between different samples is observed after discriminant

rotation than in the original score plots (not shown here). It is apparent that Discriminant function 1 (DF1) strongly reflects sediment depth, as clearly revealed by a cross-plot of these two parameters (Fig. 3). Fluctuations which are not directly related to depth are manifested in DF2 (non-depth-related variations are also evident in DF's 3 & 4, Fig. 2b). In addition, three or four "sub-groups" may be identified in Figure 2a (as indicated by the circles). The spectra shown in Figure 1 each correspond to one of these four groups.

In order to determine the chemical variations responsible for these fluctuations, variance diagrams were constructed in which the DF's are kept orthogonal to one another, but may be rotated (in 10° increments) so as to study axes which most clearly reflect differing "chemical components". This is shown in Figure 4(a) in DF1/DF2 space, in which three separate "components" may be identified. A fourth was identified in DF3 (Figure 4b). Mathematically-extracted "discriminant spectra", obtained for each of these chemical "components" from rotation within this framework are presented in Figure 5. Component "A" (DF1 & DF2, 10°) shows a typical pattern derived from sugar moieties. Component "B" (50°) shows strong influence from sulfur-derived compounds as well as some higher mass components (m/z 155, 159, 173 etc.). Component "C" (320°) contains, in addition to sulfur compounds, alkylaromatics including alkylbenzene and phenolic compounds. Component "D" from DF3 & DF4 (70°) contains mass peaks possibly characteristic for terpenoid component(s).

From these data we may conclude that the depth-related variation in "kerogen" reflected in DF1 is primarily the result of a decrease in sugar-containing components together with a corresponding increase in sulfur-containing and alkylaromatic components. The latter is consistent with current concepts concerning sulfur incorporation into organic matter during early diagenesis[22,23]. Other fluctuations independent of depth are presumably a consequence of variations in conditions at the time of deposition. The chemical components responsible for these latter variations are yet to be fully interpreted.

CONCLUSIONS

Py-MS in conjunction with multivariate statistical analysis of Peru margin sediments has allowed several insights to be made into the formation and transformation of macromolecular organic matter during early diagenesis. Distinctive depth-related changes in chemical composition were observed, including a loss of sugar-containing moieties and an increase in sulfur content. Features reflecting fluctuations due to other influences on organic matter composition were also detected. This study demonstrates the utility of this approach as a rapid method for providing information on macromolecular sedimentary organic matter composition.

ACKNOWLEDGEMENTS

Drs. J.W. Farrington and D. Repeta are thanked for making these valuable samples available.

REFERENCES

1. Reimers C.E. and Suess E. *Coastal Upwelling and its sediment record, Part B.* (eds. J. Theide and E. Suess). pp. 311-337. Plenum, New York (1983).
2. Fossing H. (1990) *Continental Shelf Research*. In press.
3. Patience R.L., Clayton C.J., Kearsley A.T., Rowland S.J., Bishop A.N., Rees A.W.G., Bibby K.G. and Hopper A.C. *Proceedings Scientific Results, Leg 112, Ocean Driling Program.* (Eds. E Suess, R von Huene *et al.*) pp. 135-153. ODP College Station, Texas (1990).

4. Soutar A., Johnson S.R. and Baumgartner T.R. *The Monterey Formation and related siliceous rocks of California.* pp. 123-147. SEPM Los Angeles (1981).
5. Volkman J.K., Farrington J.W., Gagosian R.B. and Wakeham S.G. *Advances in Organic Geochemistry, 1981* (eds M. Bjoroy *et al.*) pp. 228-240. Wiley and Sons (1983).
6. Wakeham S.G., Farrington J.W. and Gagosian R.B. *Org. Geochem.* **6**, 203-215 (1984).
7. Volkman J.K., Farrington J.W. and Gagosian R.B. *Org. Geochem.* **11**, 463-477 (1987).
8. Farrington J.W., Davis A.C., Sulanowski J., McCaffrey M.A., McCarthy M., Clifford C.H., Dickinson P. and Volkman J.K. *Org. Geochem.* **13**, 607-617 (1988).
9. McCaffrey M.A., Farrington J.W. and Repeta D.J. *Org. Geochem.* **14**, 61-68 (1989).
10. McCaffrey M.A, Farrington J.W. and Repeta D.J. *Geochim. Cosmochim. Acta* **54**, 1713-1724 (1990).
11. Repeta D.J. and Gagosian R.B. *Geochim. Cosmochim. Acta* **51**, 1001-1009 (1987).
12. Henrichs S.M., Farrington J.W. and Lee C. *Limnol. Oceanogr.* **29**, 20-34 (1984).
13. Henrichs S.M. and Farrington J.W. *Limnol. Oceanogr.* **29**, 1-19 (1984).
14. Whelan J.K., Kanyo Z., Tarafa M. and McCaffrey M.A. Pre-print (1990)
15. McCaffrey M.A. Ph.D. Thesis. MIT/WHOI, WHOI-90-29 (1990).
16. Metcalf G.S., Windig W., Hill G.R. and Meuzelaar H.L.C. *Int. J. Coal Geol.* **7**, 245-268 (1987).
17. Meuzelaar H.L.C., Haverkamp J. and Hileman F.D. *Pyrolysis Mass Spectrometry of Recent and Fossil Biomaterials; Compendium and Atlas.* Elsevier, Amsterdam 294 pp. (1982).
18. Windig W. and Meuzelaar H.L.C. *Proceedings of the 34th ASMS Conference.* Cincinnati, pp. 64-65. (1985).
19. Cattell R.B., *Multivariate Behavioral Research.* **1**, 245-276 (1966)
20. Windig W., Kistemaker P.G. and Haverkamp J. *J. Anal. Appl. Pyrol.* **3**, 199-212 (1981).
21. Windig W. and Meuzelaar H.L.C. *Anal. Chem.* **56**, 2297-2303 (1984)
22. Sinninghe Damsté J.S. Eglinton T.I., de Leeuw J.W. and Schenck P.A. *Geochim. Cosmochim. Acta* **53**, 873-889 (1989).
23. Sinninghe Damsté J.S., Rijpstra W.I.C., Kock-van Dalen A.C., de Leeuw J.W. and Schenck P.A. *Geochim. Cosmochim. Acta* **53**, 1343-1355 (1989).

Table 1 Geochemical Description of Samples of Peru Sediments from core SC3.

Sample #	Depth (cm)	TOC (%)	%N	Dry wt/wet wt.
1	4-5	11.10	1.26	0.0699
2	9-10	9.20	1.07	0.0640
3	16-17	9.17	1.17	0.0765
4	27-28	9.79	1.19	0.0831
5	30-31	11.02	1.26	0.1115
6	38-39	8.67	1.21	0.1381
7	42-43	8.19	1.03	0.0978
8	46-47	6.19	0.71	0.0859
9	55-56	7.67	0.88	0.1026
10	65-66	7.67	0.92	0.2415
11	70-71	6.81	0.77	0.1467
12	75-76	6.94	0.79	0.2610
13	77-78	7.61	0.87	0.2532
14	85-86	7.00	0.75	0.1717
15	94-96	7.09	0.77	0.1741

Table 2 Results from Factor analysis of normalized Py-MS data.

Factor	Eigen Val.	% Total Var.	% Cum. Var.
1	118.01	50.87	50.87
2	39.91	17.20	68.07
3	12.07	5.20	73.27
4	8.27	3.57	76.84
5	4.94	2.13	78.97
6	3.92	1.69	80.66
7	3.78	1.63	82.29

Table 3 Results from Discriminant analysis of Py-MS data.

Discr. Func.	Eigen Val.	% Outer Var.	% Total Var.	Canonical Corr.
1	40.30	61.88	17.10	0.988
2	11.57	17.77	4.92	0.959
3	7.79	11.96	9.55	0.941
4	3.84	5.89	38.16	0.891
5	1.16	1.77	4.31	0.732
6	0.29	0.45	5.70	0.475
7	0.18	0.27	2.55	0.388

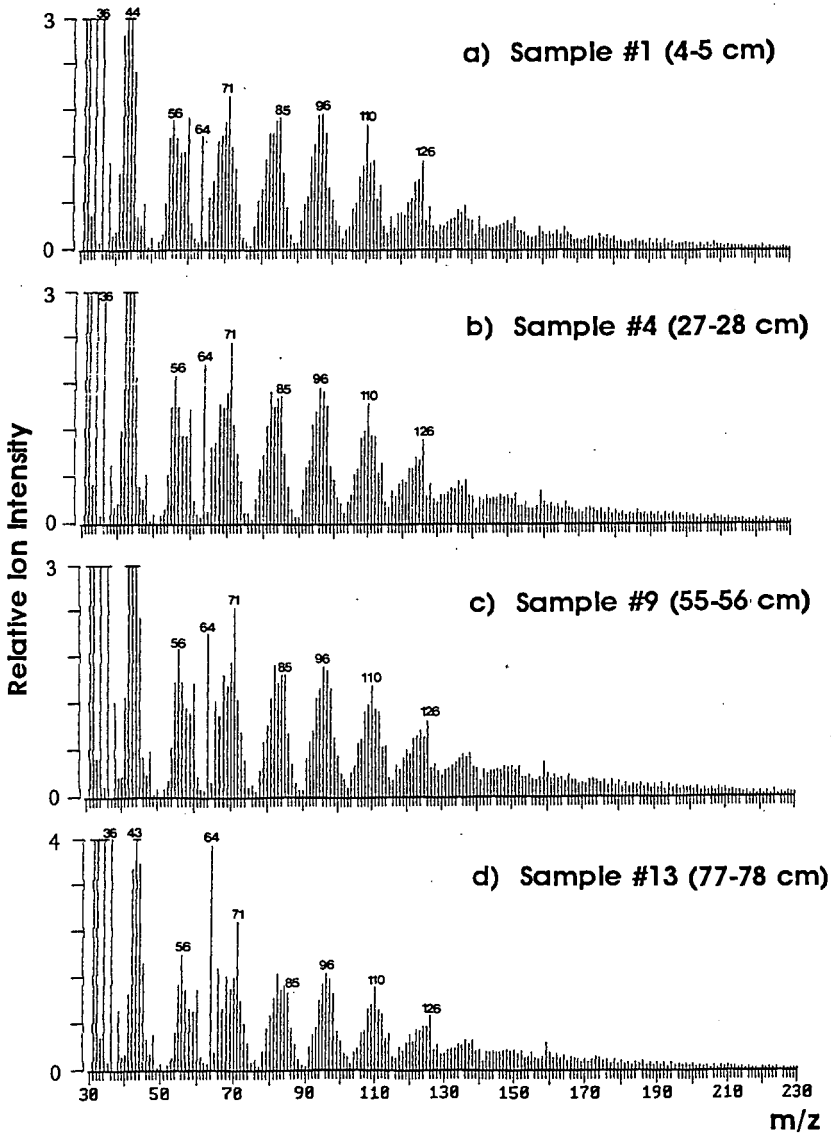

Figure 1. Averaged Py-MS spectra from triplicate analyses of four extracted Peru sediments from core SC3.

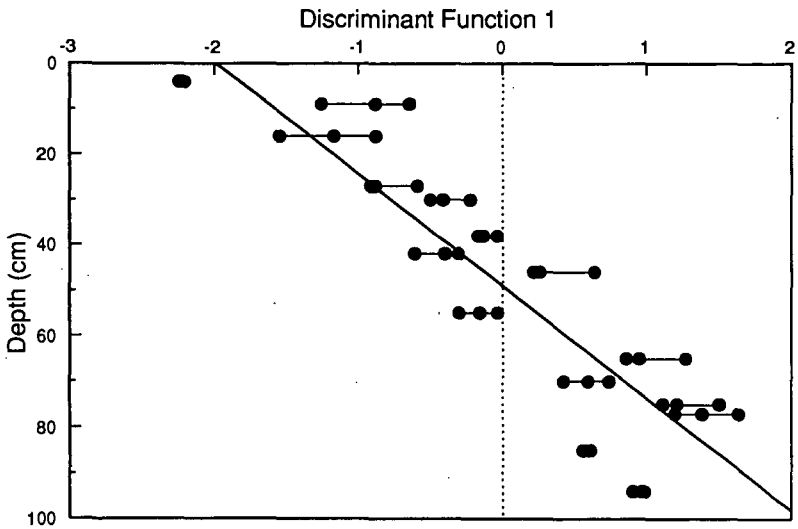

Figure 3. Plot of Discriminant Function 1 versus Depth (cm)

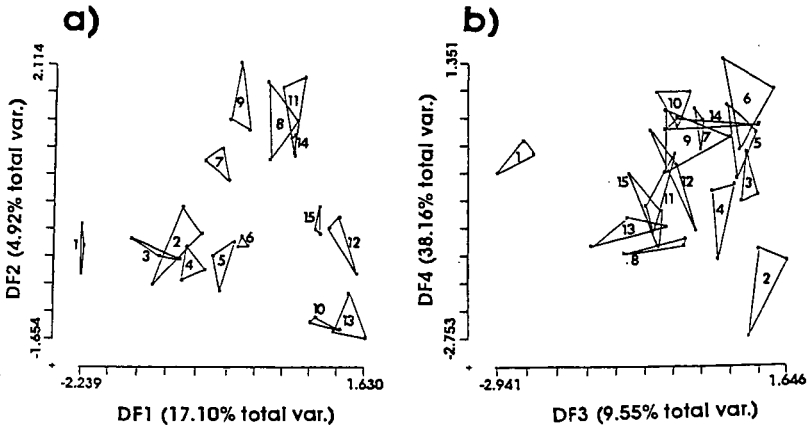

Figure 2. Score plot from Discriminant analysis of normalized Py-MS data:
(a) Discriminant Function 1 versus Discriminant Function 2;
(b) Discriminant Function 3 versus Discriminant Function 4.

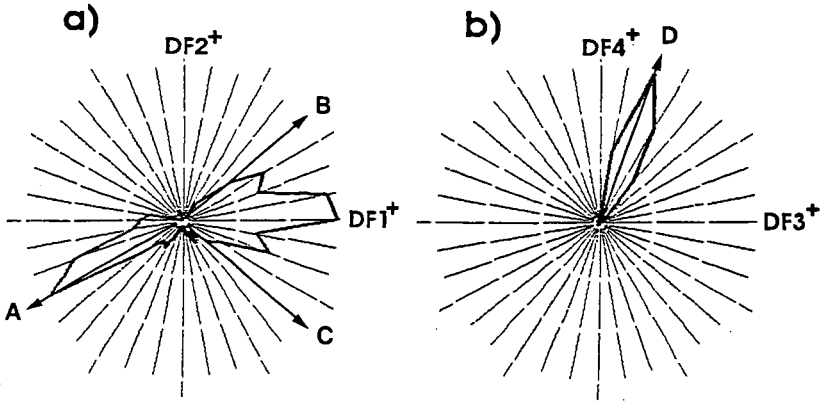

Figure 4. Variance diagram (VARDIA) showing presence of four discrete chemical component axes in the space spanned by discriminant functions 1 and 2 (a) and 3 and 4 (b).

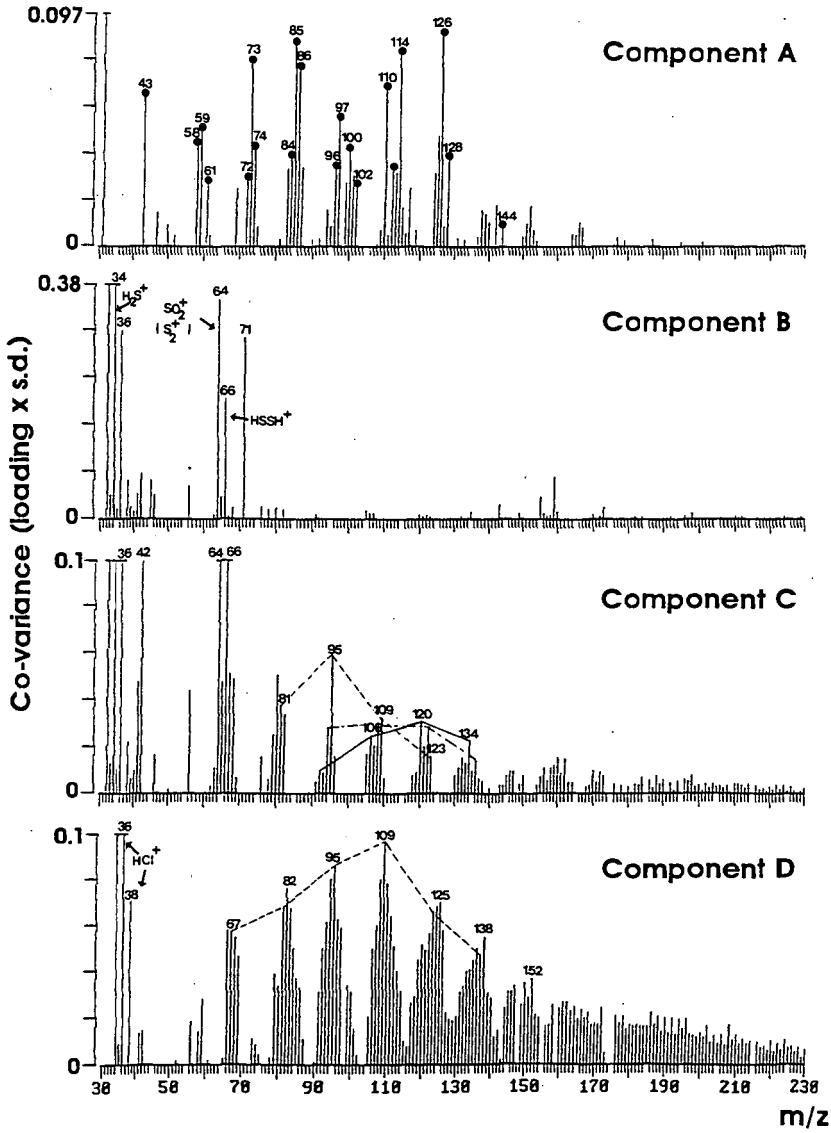

Figure 5. Mathematically-extracted "Discriminant Spectra" of Chemical Components A, B, C and D.

MECHANISMS OF HYDROCARBON FORMATION DURING FLASH PYROLYSIS OF KEROGEN

Walter A. Hartgers, Jaap S. Sinninghe Damsté and Jan W. de Leeuw

Organic Geochemistry Unit, Faculty of Chemical Technology and Materials' Science, Delft University of Technology, De Vries van Heystplantsoen 2, 2628 RZ Delft, The Netherlands.

Keywords: alkylbenzenes, fatty acids, sodium salts, aromatic carotenoids

INTRODUCTION

Geomacromolecules, which account for by far the greatest part of organic matter in sediments, are, due to their physical properties and complex structures, not easily accessible for common spectroscopic methods to eludicate their structure. Therefore, thermal and chemical degradation techniques are often applied to obtain structural information on these substances. Flash pyrolysis (Py) in combination with gas chromatography (GC) and mass spectrometry (MS) has proven to be a useful method of characterizing geomacromolecules (e.g. kerogen) at a molecular level.[1,2] Upon flash pyrolysis of kerogen mixtures of *n*-alkanes, *n*-alk-1-enes, saturated and aromatic (poly)cyclic hydrocarbons are commonly generated.

However, the mechanisms by which these compounds are formed are not completely known. This is surprising since a full understanding of the thermal degradation processes is essential for interpretation of the compound distributions with respect to the macromolecular structure. Therefore, we have flash pyrolysed silicon-bound hydrocarbons, which serve as model compounds for hydrocarbon moieties in kerogen.[3] Although these experiments gave some insight into the thermal degradation of hydrocarbon moieties, the major pyrolysis products were formed by processes involving the O-Si and Si-C bonds and are thus not really representative of hydrocarbon moieties in kerogen.

In this paper we report the C_0-C_4 alkylbenzene distributions in flash pyrolysates of two kerogens and flash pyrolysis experiments with new model compounds (sodium salts of fatty acids) aimed at the interpretation of the alkylbenzene distributions of the kerogen pyrolysates.

EXPERIMENTAL

Sediment samples were extracted and decarbonated (Paris Basin shale, G6-2-2[4]) or isolated (Womble shale[5]) and subsequently re-extracted with organic solvents.

Hexadecanoic acid and 12-hydroxy-octadecanoic acid are commercially available (Aldrich) and were converted to their corresponding sodium salts by adding a NaOH solution followed by evaporation of the water. 16-(4'-methylphenyl)hexadecanoic acid was synthesized by a Grignard reaction of 16-oxo-hexadecanoic acid, prepared by oxidation of 16-hydroxydecanoic acid (Aldrich), with 4-bromomagnesium-toluene and subsequent hydrogenolysis[6] of the formed alcohol using triethylsilane and $BF_3 \cdot$ etherate.

The samples were pressed onto ferromagnetic wires. These wires were inductively heated in 0.15 s to their Curie-temperature (610° or 770°C) at which they were held for 10 s. On line gas chromatography (GC) was performed using a Hewlett Packard HP-5890 gas chromatograph equipped with a cryogenic unit and programmed from 0°C (5 min) to 320°C (10 min) at a rate of 3°C/min. The pyrolysate was separated on a 25 m fused silica capillary column coated with chemically bound CP Sil-5 (0.32 mm I.D.; film thickness 0.45 μm).

Py-GC-MS was performed using the same pyrolysis and GC-conditions as mentioned above with a Hewlett Packard HP-5890 gas chromatograph directly coupled to the EI ion source of a VG-70s double focussing mass-spectrometer (mass range *m/z* 40-800; cycle time 1.8 s; ionisation energy 70 eV). C_0-C_4 alkylbenzenes were identified by comparison of relative retention time and mass spectral data with those of authentic standards.

RESULTS AND DISCUSSION

Alkylbenzenes in flash pyrolysates of kerogen

Alkylbenzenes are often important pyrolysis products of immature kerogens and coals. They are assumed to be formed *via* β-cleavage of alkylaromatic moieties in the kerogen structure.[1] The origin of these alkylaromatic units in kerogen is far from understood. Therefore, the C_0-C_4 alkylbenzene distributions of ca. 30 pyrolysates of immature kerogens from different geographical locations and of different types were examined to see whether these are biologically controlled.

Figure 1 shows the alkylbenzene distributions of the flash pyrolysates of two kerogens from the Toarcian Paris Basin and the Ordovician Womble Shale which both contain type II kerogens. Significant differences between the distribution patterns are observed. For example, the abundance of 1,2,3,4-tetramethylbenzene (compound 36, Table 1) in the Womble flash pyrolysate relative to that in the Paris Basin pyrolysate is noteworthy. The substitution pattern of this compound suggests that it is generated by β-cleavage of macromolecularly bound aromatic carotenoid structures. Five major aromatic carotenoids occurring in nature are: renieratene, isorenieratene, isorenierapurpurin, chlorobactene and okenone (figure 2).[7] They all possess 1-alkyl-2,3,4-trimethyl- and 2-alkyl-1,3,4-trimethylbenzene moieties, which are likely to generate 1,2,3,4-tetramethylbenzene upon flash pyrolysis.

Since these aromatic carotenoids are mainly biosynthesized by photosynthetic sulphur bacteria, it is suggested that these bacteria were important contributors to the organic matter of the Ordovician Womble shale. Because of the natural habitat of photosynthetic sulphur bacteria this, in turn, suggests that a part of the photic zone of the water column or sediment was anoxic.

This example shows that alkylbenzenes (and possibly other flash pyrolysis products) contain palaeoenvironmental information. However, to decode this information the mechanisms involved in the formation of these pyrolysis products (*e.g.* β-cleavage in case of alkylaromatic units) need to be known. The study of model compounds is, therefore, a prerequisite to fully understanding kerogen pyrolysis product distributions.

Flash pyrolysates of model compounds

The sodium salt of 16-(4'-methylphenyl)hexadecanoic acid was selected for study because unlike free fatty acids it will not evaporate off the wire without degradation and is, thus, a simple model compound for aromatic moieties in kerogen. It yields upon flash pyrolysis (figure 3A) a homologous series of 4-alkyltoluenes and 4-alkenyltoluenes with a chain length of up to 15 carbon atoms. The series of 4-alkenyltoluenes probably have their double bond in the ω-position. These compounds are supposed to be formed by simple homolytic C-C bond cleavage. 1,4-Dimethylbenzene which would be the favoured pyrolysis product resulting from β-cleavage of the aromatic moiety is also a major compound (figure 3A).

However, the presence of 4-methylstyrene as a major pyrolysis product is puzzling. ^{1}H NMR and TLC of the synthesized product indicated that it is not completely pure and contains a non-GC amenable impurity, which may be responsible for the formation of 4-methylstyrene upon pyrolysis. Alternatively, an uncommon rearrangement reaction of 16-(4'-methylphenyl)hexadecanoic acid sodium salt may also lead to the generation of this compound. Furthermore, the abundance of toluene and benzene in the pyrolysate is remarkable since the formation of these products requires the cleavage of a C-C bond α to the aromatic ring. Since this degradation pathway is deemed unlikely due to the relatively high bond strength, cyclisation and aromatization of the alkyl chain may be an alternative route to generate these products during flash pyrolysis.

To investigate this phenomenon in more detail, the sodium salts of hexadecanoic acid and 12-hydroxy-octadecanoic acid were also flash pyrolysed (figures 3B and 3C). Flash pyrolysis of hexadecanoic acid generates a series of *n*-alkanes and *n*-alk-1-enes up to C_{15} (figure 3B). The lack of hydrocarbons with more than 15 carbon atoms shows that recombination of two radicals is not an important process. The peaks eluting after heptadecane are identified as hexadecanal and hexadecanoic acid, which evaporate from the wire during flash pyrolysis. The results of this experiment are comparible to the flash pyrolysate of Silicon bound *n*-octadecane.[3] Benzene, toluene and other alkylbenzenes were not generated in detectable amounts,

indicating that cyclisation and aromatisation of the *n*-alkyl chain is not occurring during flash pyrolysis.

Surprisingly, flash pyrolysis of the sodium salt of 12-hydroxy-octadecanoic acid generates a homologous series of alkan-7-ones and alken-7-ones with the unsaturation in the ω-position as the major products. However, more important from our point of view, benzene, toluene and, to a lesser extent, other alkylbenzenes (*i.e.* 1-phenylalkanes, 2-alkyltoluenes) which can be formed by cyclisation and aromatisation of a linear chain are also important pyrolysis products. This indicates that if an alkyl moiety contains at least one functional group alkylbenzenes can be formed *via* cyclisation and aromatisation reactions during flash pyrolysis.

CONCLUSION

Alkylbenzene distributions in kerogen pyrolysates have a potential to give information on biological contributions and palaeoenvironmental conditions. However, much more work aimed at the understanding of the thermal processes responsible for their formation has to be performed before we can fully decode the information contained in pyrolysis product distributions. Experiments with model compounds are essential in this respect but our preliminary investigations are rather confusing and warrant further investigation.

REFERENCES

1. Larter, S.R. and Horsfield, B. (1991), In: "Organic Geochemistry", M.H. Engel and S.A. Macko (eds). Plenum Press, New York. In press.

2. Rullkötter, J. and Michaelis, W. (1990), Org. Geochem., 16: 829-852.

3. Hartgers, W.A., Sinninghe Damsté, J.S. and de Leeuw, J.W. (1991), J. Anal. Appl. Pyrol. In press.

4. Mackenzie, A.S., Patience, R.L., Maxwell, J.R., Vandenbroucke, M. and Durand, B. (1981), Geochim. Cosmochim. Acta, 45: 1709-1721.

5. Fowler, M.G. and Douglas, A.G. (1984), Org. Geochem., 6: 105-114.

6. Parnes, Z.N., Boelestova, G.I. and Kursanov, D.N. (1977), J. Org. Chem. USSR, 13: 434-436.

7. Liaaen-Jensen, S. (1978), In: "Photosynthetic Bacteria, R.K. Clayton and W.R. Sistrom (eds), Plenum Press, New York. pp 233-248.

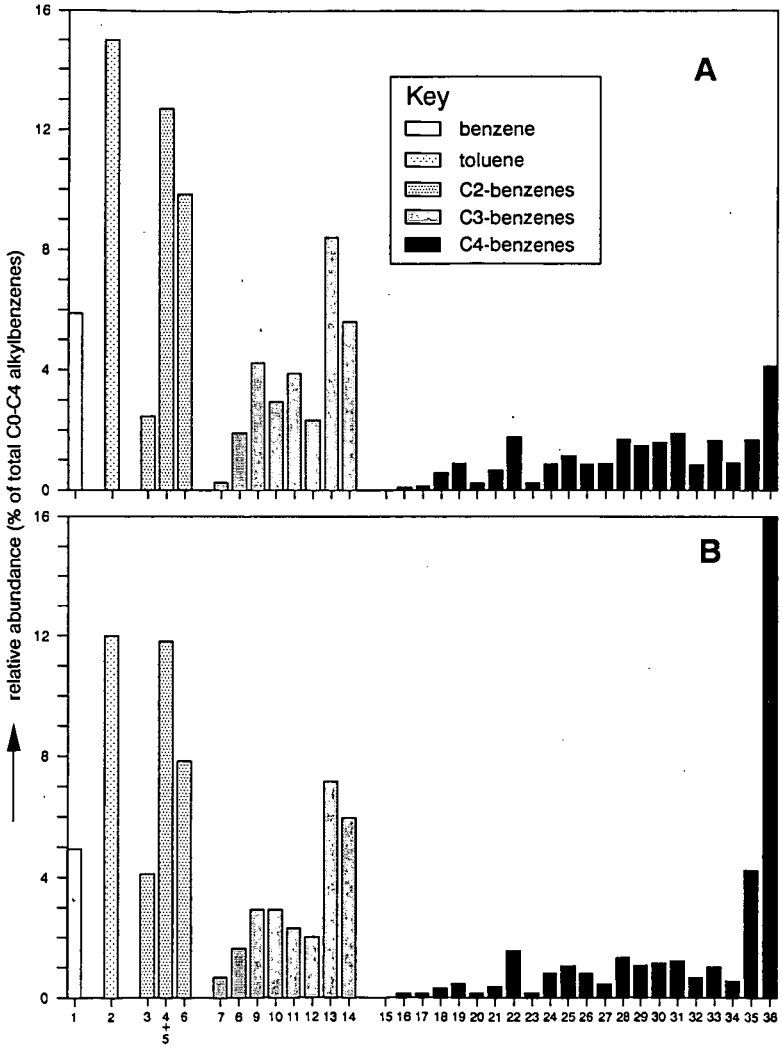

Figure 1. Bar plots showing the distribution of the C_0-C_4 alkylbenzenes in the flash pyrolysates of the kerogen of (A) Paris Basin G6-2-2 and (B) Womble shale. Numbers refer to compounds listed in Table I.

Table 1: Alkylbenzenes identified in kerogen pyrolysates.

1	benzene	20	1-isopropyl-2-methylbenzene
2	toluene	21	1,3-diethylbenzene
3	ethylbenzene	22	1-propyl-3-methylbenzene
4+5	1,3-/1,4-dimethylbenzene	23	1,4-diethylbenzene
6	1,2-dimethylbenzene	24	1-propyl-4-methylbenzene
7	iso-propylbenzene	25	n-butylbenzene
8	n-propylbenzene	26	1-ethyl-3,5-dimethylbenzene
9	1-ethyl-3-methylbenzene	27	1,2-diethylbenzene
10	1-ethyl-4-methylbenzene	28	1-propyl-2-methylbenzene
11	1-ethyl-2-methylbenzene	29	1-ethyl-2,5-dimethylbenzene
12	1,3,5-trimethylbenzene	30	1-ethyl-2,4-dimethylbenzene
13	1,2,4-trimethylbenzene	31	1-ethyl-3,4-dimethylbenzene
14	1,2,3-trimethylbenzene	32	1-ethyl-2,6-dimethylbenzene
15	t-butylbenzene	33	1-ethyl-2,3-dimethylbenzene
16	iso-butylbenzene	34	1,2,4,5-tetramethylbenzene
17	sec-butylbenzene	35	1,2,3,5-tetramethylbenzene
18	1-isopropyl-3-methylbenzene	36	1,2,3,4-tetramethylbenzene
19	1-isopropyl-4-methylbenzene		

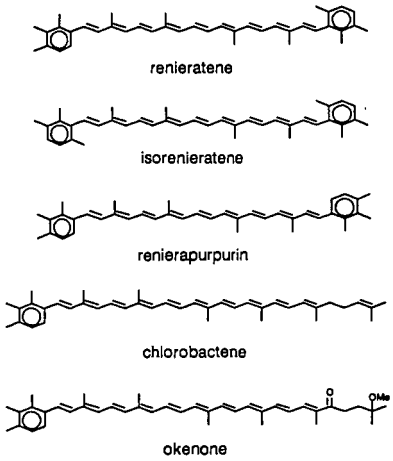

Figure 2. Chemical structures of some aromatic carotenoids.

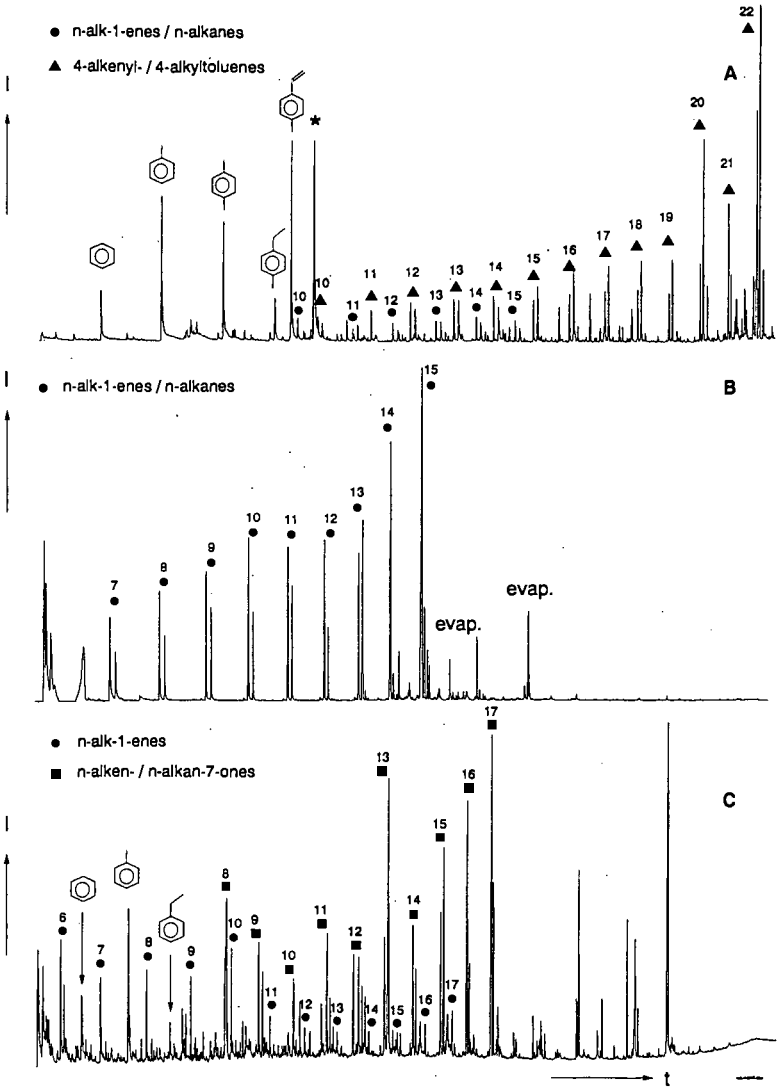

Figure 3. TIC (A, C) and GC (B) traces of the flash pyrolysates (770°C) of the sodium salts of (A) 16-(4'-methylphenyl)hexadecanoic acid, (B) hexadecanoic acid and (C) 12-hydroxy-octadecanoic acid. Numbers indicate total numbers of carbon atoms of compounds identified.

COAL PYROLYSIS: MEASUREMENTS AND MODELING OF PRODUCT EVOLUTION KINETICS AND CHAR PROPERTIES

Robert M. Carangelo, Michael A. Serio, Peter R. Solomon,
Sylvie Charpenay, Zhen-Zhong Yu, and Rosemary Bassilakis

Advanced Fuel Research, Inc.
87 Church Street
East Hartford, CT 06108

Keywords: Coal Pyrolysis, Kinetics, Reactivity

INTRODUCTION

Thermogravimetric analysis (TGA) has been employed in coal science to perform a number of characterizations including: proximate analysis,[1] kinetics of weight loss,[2] char reactivity,[3-6] and gas adsorption measurements.[7] A complementary technique, evolved product analysis, has been employed to study pyrolysis product distributions and kinetics,[8-11] functional group compositions,[10,12,13] and temperature programmed desorption.[14-15] We have developed a TG-FTIR instrument which combines TGA with evolved product analysis by Fourier Transform Infrared (FT-IR) spectroscopy. FT-IR analysis of evolved products has advantages over mass spectroscopy in allowing analysis of very heavy products, and over gas chromatography in speed.

The application of TG-FTIR to coal and petroleum source rock has recently been described.[16,17] To analyze coal, a sequence of drying, pyrolysis and combustion is employed to obtain: proximate analysis, volatiles composition, volatiles kinetics, and relative char reactivity. By using several different heating rates, kinetic rate constants have been obtained.[18,19] The purpose of this paper is to describe its application in characterizing the volatile evolution kinetics and char reactivities of the Argonne premium coal samples. The technique is being employed to obtain the kinetic and composition parameters for a recently developed general model of coal pyrolysis, called the FG-DVC model,[20] which stands for Functional Group - Depolymerization, Vaporization and Crosslinking model. This is a network model based on an assumed polymeric structure for coal and includes the processes of depolymerization and crosslinking and the formation of char, tar and gases. The reactivity parameters will be included in an extension of the model which is currently under development.

EXPERIMENTAL

<u>Apparatus</u> - A schematic of the TG-FTIR instrument is presented in Fig. 1. Its components are as follows: a DuPont 951 TGA; a hardware interface (including a furnace power supply); an Infrared Analysis 16 pass gas cell with transfer optics; a MICHELSON 110 FT-IR; (Resolution: 4 cm^{-1}, Detector: MCT). A helium sweep gas (250 cc/sec) is employed to bring evolved products from the TGA directly into the gas cell. A window purge of 700 cc/sec is employed at each end of the cell. The system is operated at atmospheric pressure. This instrument package is now available commercially as the "TG/plus" from Bomem, Inc.

The most difficult volatiles to analyze are the heavy decomposition products which condense at room temperature, such as tars from coal. In the TG/plus, the high conductivity helium sweep gas and the rapid cooling cause these products to form an aerosol which is fine enough to follow the gas through the analysis cell. The cell is connected without restrictions to the sample area. The aerosol is also fine enough that there is only a little scattering of the infrared beam and it is thus attenuated almost as though the tar was in the gas phase, as shown in Fig. 2. Based on the aerosol's Rayleigh scattering of infrared radiation, the diameter of the aerosol droplets is less than 1.0 μm.

<u>Procedure</u> - As an example of the analysis procedure, the pyrolysis and oxidation of a lignite is described. More detail can be found in Refs. 16 - 18. Figure 3a illustrates the weight loss from

this sample and the temperature history. A 35 mg sample of Zap lignite, loaded in the sample basket of the DuPont 951, is taken on a 30°C/min temperature excursion in the helium sweep gas, first to 150°C to dry for 240 sec, then at 30°C/min to 900°C for pyrolysis. Upon reaching 900°C, the sample is immediately cooled to 250°C over a twenty minute period. After cooling, a small flow of O_2 (0.3 cc/sec) is added to the helium sweep gas at the 57 minute mark and the temperature is ramped to 700°C at 30°C/min (or as high as 1000°C) for oxidation.

During this excursion, infrared spectra are obtained once every thirty seconds. As shown in Fig. 2, the spectra show absorption bands for CO, CO_2, CH_4, H_2O, SO_2, COS, C_2H_4, and NH_3. The spectra above 250°C also show aliphatic, aromatic, hydroxyl, carbonyl and ether bands from tar. The evolution of gases derived from the IR absorbance spectra are obtained by a quantitative analysis program which employs a database of integration regions and calibration spectra for different compounds [16-18]. The routine employs regions of each calibration spectrum which permit the best quantitation with the least interferences. The routine is fast enough to allow the product analysis to be displayed on the computer screen during the actual experiment.

Figure 3b illustrates the integral of the evolution curves to obtain cumulative evolved product amounts. Because the data are quantitative, the sum of these curves match the weight loss as determined by the TGA balance. Discrepancies occur in this match because of missing components such as H_2 which cannot be seen by IR. Also, when O_2 is introduced, the balance shows a net gain in weight due to O_2 chemisorption.

Reactivity Measurements - Initial char reactivity measurements were made using the isothermal measurement developed at Pennsylvania State University in which the time for 50% burnoff ($\tau_{0.5}$) was measured.[6] In our char characterization work, we had difficulty applying the isothermal technique to chars formed over a wide range of conditions. A temperature level selected for one char was inappropriate for another. The temperature was either too high for the rate to be chemically controlled or too low for the $\tau_{0.5}$ to be reached in a reasonable time period.

In order to overcome this difficulty, a non-isothermal technique was developed.[3-5] A Perkin-Elmer TGA 2 was initially used for this method. Recent measurements have been made using the TG-FTIR instrument discussed above and good agreement has been found between these two systems. The sample is heated in air at a rate of 30 K/min until a temperature of 900°C is reached. The TGA records the sample weight continuously and, at the end of the experiment, the weight and derivative are plotted.

The "critical" temperature (T_{cr}) at which the derivative of the fractional weight loss with respect to time reaches a value of 0.065 wt. fraction/min ≈ 0.001 wt. fraction/s was chosen as an index of reactivity to be compared with the $\tau_{0.5}$ values measured by the isothermal technique. The actual critical slope used is arbitrary. A value is chosen which is large enough to be unambiguously determined, but small enough so that reaction occurs in the chemically controlled regime. Values of ln $\tau_{0.5}$ were plotted against $1/T_{cr}$ and a good correlation was observed.[3]

Temperature Programmed Desorption - Temperature programmed desorption (TPD) has proved to be a valuable tool for characterization of surfaces of carbonaceous materials such as coal chars.[14,15] An example of the application of this technique to the characterization of chars from two coals is shown in Figure 4. This work was done in our TG-FTIR system described above by operation in a slightly different mode. The chars were prepared by programmed pyrolysis at 30° C/min to 1000° C, then cooled to 200° C, exposed to air for ten minutes, and then reheated to 1000° C. Samples which have a high oxidation reactivity have a larger increase in weight due to O_2 uptake and desorb CO_2 much more readily. In Figure 4, a comparison is made between a highly reactive char produced from a low rank (Zap lignite) coal (solid line) compared with a relatively unreactive char produced from a high rank (Pocahontas) coal (dashed line). The differences between these samples can be rapidly and easily assessed using this technique.

Samples - The coals analyzed were Argonne premium coal samples. The characterization of these samples has appeared elsewhere.[21]

RESULTS

Char Properties - The results from the application of the TG-FTIR instrument to measurements of T_{cr} and oxygen chemisorption capacity on the Argonne Premium coals are shown in Fig. 5. As expected, the values of T_{cr} decrease with decreasing rank which indicates that lower rank coals are more reactive. This variation in reactivity with rank is primarily due to mineral contributions to reactivity.[3-5] The measurements of oxygen chemisorption capacity (OCC), which are related to the active site concentration, are inversely related to T_{cr} and are also shown in Fig. 5. In our work, we have found that the value of T_{cr} is a more useful correlative parameter for reactivity than the OCC.[22]

Kinetics - The TG-FTIR system was used to conduct programmed pyrolysis experiments on the Argonne premium coals over a range of heating rates (3, 30, 50, 100°C/min).[18,19] When comparing the multi-peak evolution curves of a given specie in different coals, an interesting feature was observed. As the coal is increased in rank, the leading edges and the early peaks shift to higher temperatures while the trailing edges remain at the same temperature. An example of this is shown for water for five coals in Fig. 6.[23] From this figure it appears that this feature can be explained in the light of the geological aging process of coal formation. With increasing aging temperature and time, the maturation process gradually evolves the loosely bound functional groups and leaves the tightly bound groups intact. The FG-DVC model has been used to successfully simulate the shifts in the evolution curves as a function of rank.[23] This was done by extrapolating the kinetics determined in the TG-FTIR experiments at moderate heating rates (3-100°C/min) to geological conditions and assuming that the coals of increasing rank are the products from lower rank coals pyrolyzed under natural conditions at increased times and temperatures.

Relationships between Kinetic Rates of Different Volatile Species - It was also found that some pools in the different gas species have peak evolution rates at the same temperature and those peaks have the same shifts when the heating rate changes. The Utah Blind Canyon coal gives a good example as shown in Fig. 7. The TG-FTIR measurements indicate that the tar evolution, the CO_2-Loose, CO-Loose, and the H_2O-Loose pools all show very close peak temperatures at about 480° C for 30° C/min., at about 519° C for 100° C/min. and at about 430° C for 3° C/min. runs. This feature implies that these volatile pools can be fit with the same kinetic parameters. This may also imply that there is some common chemistry.

Model Predictions - The kinetic parameters for the functional group pools from the eight Argonne premium coals have been determined using a set of rules that were developed to allow a systematic method of establishing the rank variations (e.g., the frequency factors were fixed at values of less than 10^{15}/sec. and only the activation energies were allowed to vary with rank). The details will be provided in a future publication. A typical comparison of theory and TG-FTIR experiments is shown in Figs. 8 and 9 for two widely spaced heating rates. The agreement between the theory and experiment is generally quite good except for CO_2. For this specie, residual oxygen in the TG-FTIR causes some oxidation at the slowest heating rate and minerals contribute evolved CO_2 which is not modeled. CO also shows some differences in the predicted amplitude, while the agreement is good for water, weight-loss, CH_4, tar and H_2O. The kinetic parameters obtained from the TG-FTIR method extrapolate well to very low heating rates, as in natural maturation processes,[23] as well as to the high heating rates of importance in most coal gasification and combustion processes.[19]

CONCLUSIONS

The TG-FTIR instrument provides a simple, fast and reliable method for providing information on product evolution kinetics and char reactivity for coals and other polymeric materials. The information from this test has been used to provide validated kinetic and composition

parameters for a general model of coal pyrolysis, called the FG-DVC model. This model can make accurate predictions of both very low and very high heating rate pyrolysis events.

ACKNOWLEDGEMENTS

This work was supported under U.S. DOE Contract No. DE-AC21-86MC23075 through the Morgantown Energy Technology Center. Richard Johnson is the Project Manager.

REFERENCES

1. Ottaway, W.; *Fuel*, **1982**, *61*, 713.
2. Ciuryla, V.T.; Weimer, R.F.; Bivans, A.; and Motika, S.A.; *Fuel*, **1979**, *58*, 748.
3. Solomon, P.R.; Serio, M.A.; and Heninger, S.G.; *ACS Div. of Fuel Chem. Preprints*, **1986**, *31*, (3), 200.
4. Best, P.E.; Solomon, P.R.; Serio, M.A.; Suuberg, E.M.; Mott, W.R, Jr.; and Bassilakis, R.; *ACS Div. of Fuel Chem. Preprints*, **1987**, *32*, (4), 138.
5. Serio, M.A.; Solomon, P.R.; Bassilakis, R.; and Suuberg, E.M.; *ACS Div. of Fuel Chem. Preprints*, **1989**, *34*, (1), 9.
6. Mahajan, O.P., R. Yarzab, and P.L. Walker, Jr., Fuel, 57, 643, (1978).
7. Suuberg, E.M.; Calo, J.M.; and Wojtowicz, W.; *ACS Div. of Fuel Chem. Preprints*, **1986**, *31*, (3), 186.
8. Winans, R.E.; McBeth, R.L.; and Neill, P.H.; *ACS Div. of Fuel Chem. Preprints*, **1988**, *33*, (3), 85.
9. Chakravarty, T.; Windig, W.; Hill, G.R.; and Meuzelaar, H.L.C.; *Energy & Fuels*, **1988**, *2*, (4), 400.
10. Solomon, P.R. and Hamblen, D.G.; Finding Order in Coal Pyrolysis Kinetics, Topical Report submitted to U.S. Department of Energy under Contract No. DE-AC21-FE05122, (1983), also *Progress in Energy and Combustion Science*, **1983**, *9*, 323.
11. Burnham, A.K.; Oh, M.S.; Crawford, R.W.; and Samoun, A.M.; *Energy & Fuels*, **1989**, *3*, 42.
12. Attar, A. and Hendrickson, G.G.; *Coal Structure*, (R.A. Meyers, Ed.), Academic Press, NY, 1982; Chapter 5, p. 131.
13. LaCount, R.B.; Anderson, R.R.; Friedman, S.; and Blaustein, B.D.; *Fuel*, **1987**, *66*, 873.
14. Hall, P.J. and Calo, J.M.; *Energy & Fuels*, **1989**, *3*, 370.
15. Zhang, Z.G.; Kyotani, T.; and Tomita, A.; *Energy & Fuels*, **1989**, *3*, 566.
16. Carangelo, R.M.; Solomon, P.R.; and Gerson, D.G.; *Fuel*, **1987**, *66*, 960.
17. Whelan, J.K.; Solomon, P.R.; Deshpande, G.V.; and Carangelo, R.M.; *Energy and Fuels*, **1988**, *2*, 65.
18. Carangelo, R.M., Solomon, P.R., Bassilakis, R., Gravel, D., Baillargeon, M., Baudais, F., and Vail, G., Applications of TG-FTIR in the Analytical Lab, American Laboratory, p. 51, (1990).
19. Serio, M.A., Solomon, P.R., Charpenay, S., Yu, Z.Z., and Bassilakis, R., Kinetics of Volatile Product Evolution from the Argonne Premium Coals, ACS Div. of Fuel Chem. Preprints, 35, (3), 808, (1990).
20. Solomon, P.R.; Hamblen, D.G.; Carangelo, R.M.; Serio, M.A.; and Deshpande, G.V.; *Energy & Fuels*, **1988**, *2*, 405.
21. Vorres, K.S.; *"Users Handbook for the Argonne Premium Coal Sample Program"*, Supported by US DOE, Contract No. W-31-109-ENG-238 (1989).
22. Serio, M.A., Solomon, P.R., Yang, Y.P., and Suuberg, E.M., "The Use of TG-FTIR Analysis to Determine Char Combustion Properties", presented at the AIChE Annual Meeting, Chicago, Ill, (Nov. 11-16, 1990).
23. Solomon, P.R., Serio, M.A., Carangelo, R.M., Bassilakis, R., Yu, Z.Z., Charpenay, S., and Whelan, J., Analysis of Coal by TG-FTIR and Pyrolysis Modeling, presented at the Pyrolysis '90 Meeting in Holland, June 1990, to be published in Journal of Analytical and Applied Pyrolysis.

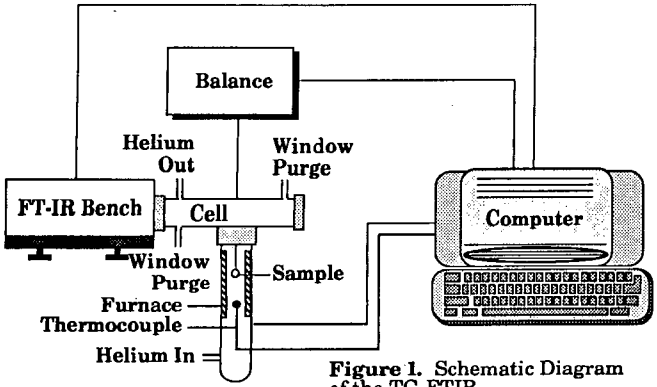

Figure 1. Schematic Diagram of the TG-FTIR.

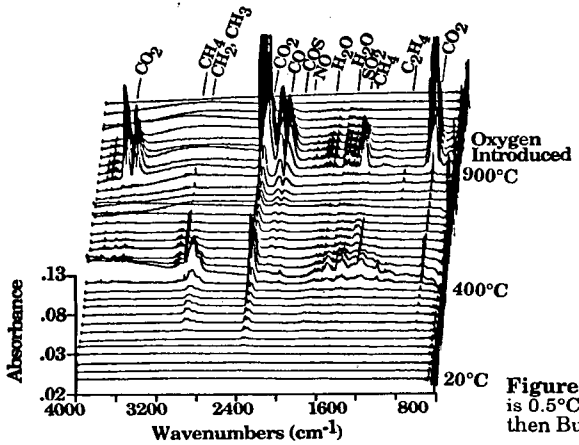

Figure 2. Spectra from TG-FTIR of Coal. Heating Rate is 0.5°C/s^{-1} from 20 to 900°C. The Remaining Char is then Burned at 700°C.

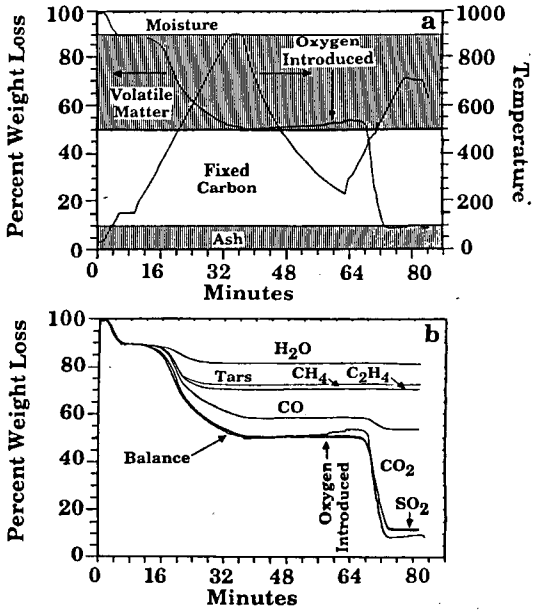

Figure 3. TG-FTIR Analysis of a Lignite. a) Temperature History and Weight Loss; b) Species Contributions to Weight Loss.

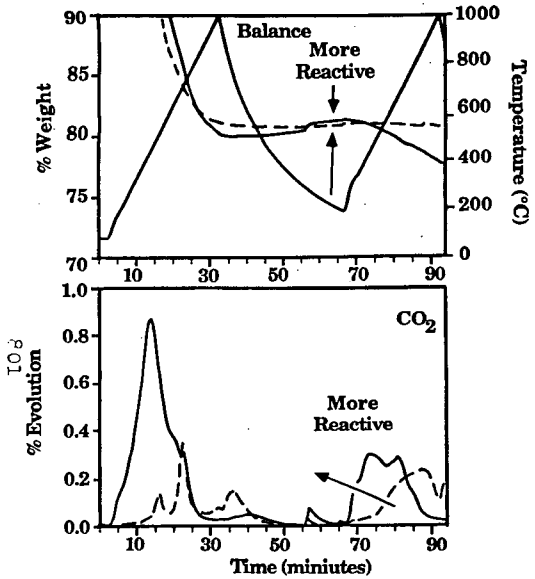

Figure 4. Temperature Programmed Desorption Curves for Pocahontas (---) and Zap Lignite (—).

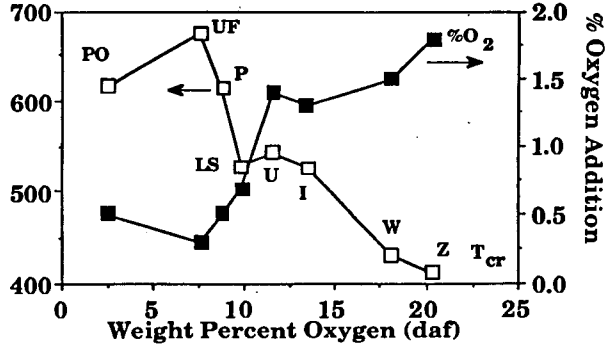

Figure 5. Rank Variation of T_{cr} and Oxygen Chemisorption Capacity (as-received basis).

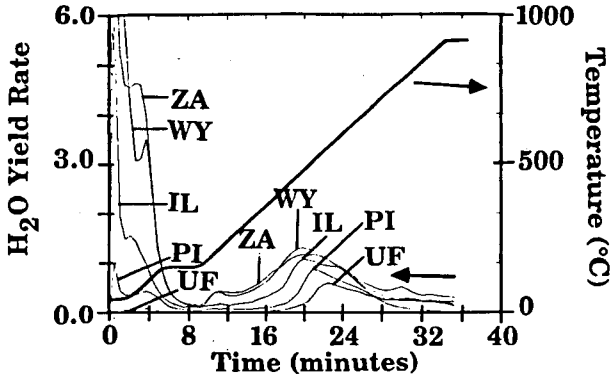

Figure 6. Evolution Curves for H_2O Measured in a TG/Plus for Five Coals from the Argonne Premium Samples Collected at 30°C/min (UF-Upper Freeport, PI-Pittsburgh, IL-Illinois, WY-Wyodak, ZA-Zap Lignite)

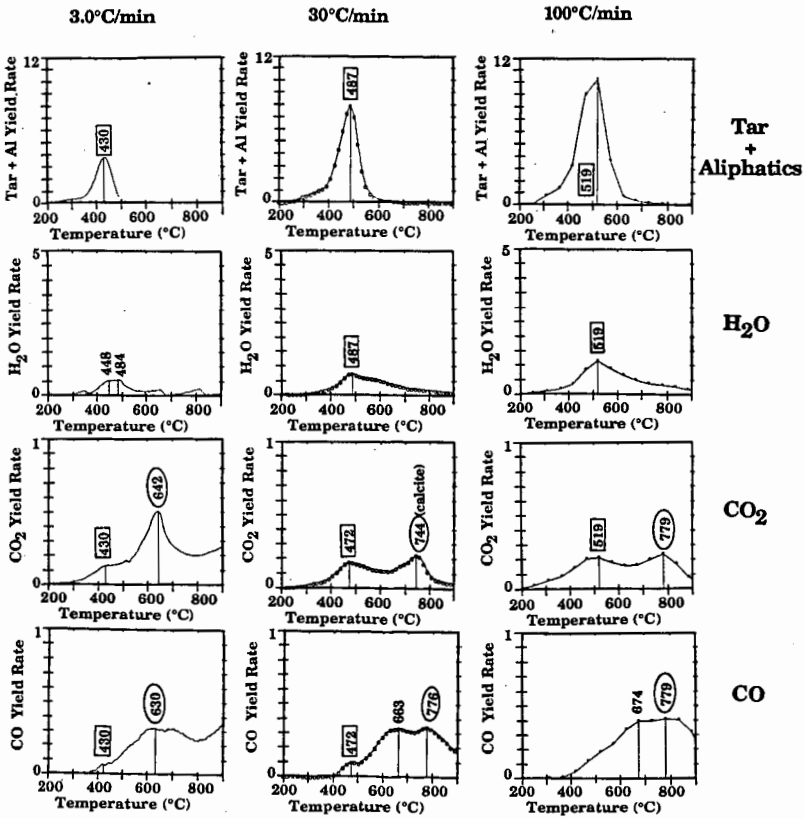

Figure 7. Evolution of Tar, H_2O, CO_2, and CO from Utah Blind Canyon Coal a Three Heating Rates.

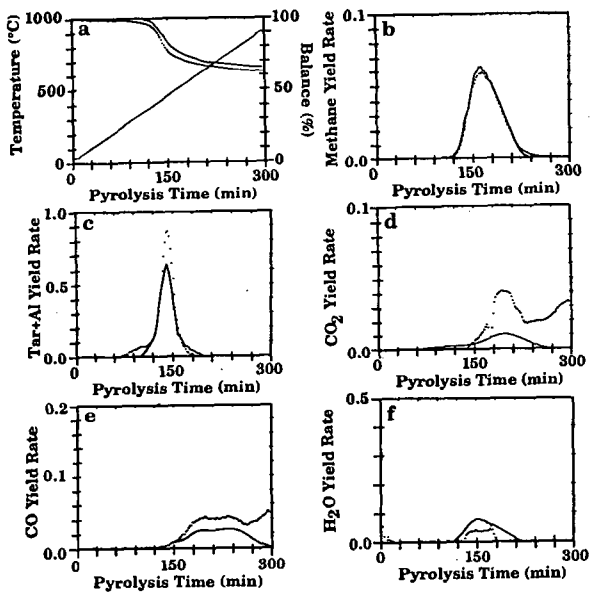

Figure 8. Data from TG-FTIR Heating Rates (···) and Predictions of FG-DVC Model for Pittsburgh No. 8 Bituminous Coal at 3°C/min. a) Weight Loss and Temperature; b) Methane; c) Tar + Aliphatic Gases; d) CO_2; e) CO; f) H_2O.

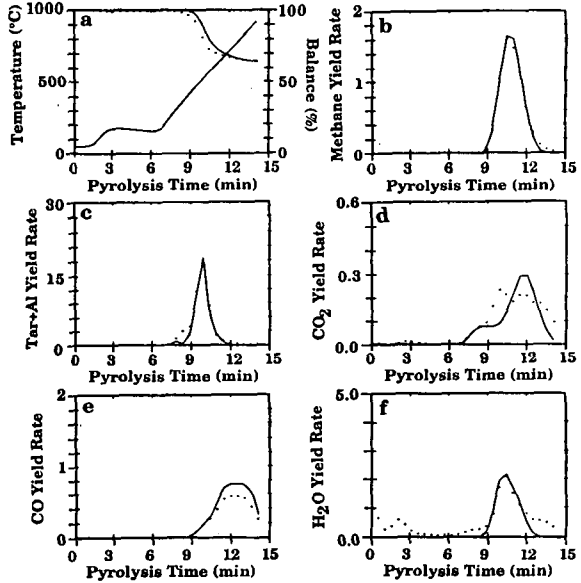

Figure 9. Data from TG-FTIR Heating Rates (··) and Predictions of FG-DVC Model for Pittsburgh No. 8 Bituminous Coal at 100°C/min. a) Weight Loss and Temperature; b) Methane; c) Tar + Aliphatic Gases; d) CO_2; e) CO; f) H_2O.

SURFACE MODIFICATION OF OXIDIZED COAL BY METHANOL VAPOR

McMahan L. Gray, Ralph W. Lai, and Arthur W. Wells

U.S. Dept. of Energy, P.O. Box 10940
Pittsburgh, PA 15236

Keywords: Coal Surface; Oxidation; Methylation

ABSTRACT

A bituminous coal was oxidized at 125°C for times varying from 0 to 48 hours and then chemically treated with a gaseous mixture of nitrogen, methanol, and an acid catalyst at 190°C for one hour. The differences between oxidized and methanol-treated coal surfaces were characterized by zeta potential, induction time, and contact angle measurements. Methanol-treated coals had more positive zeta potentials, lower induction times, and higher contact angles indicating a significant increase in the hydrophobicity of the treated coal surfaces. Using C13 labeled methanol for tracing the reaction products, NMR analysis indicated between 0.5 - 1.2 carbons are added per 1000 carbons of coal as a result of the treatment.

INTRODUCTION

In fine coal processing, the product quality depends largely on the surface properties of the feed coal. Processes that rely on surface properties of coal and its associated mineral matter include flotation [1-3], selective agglomeration [4-6], selective flocculation [7,8], and electrostatic separation [9,10]. The rheology of coal-water and coal-oil slurries is also dependent on the surface properties of the coal and its associated mineral matter [11-13]. Therefore, in handling or processing fine coals, we must understand the relationship between their surface properties and beneficiation response.

The hydrophobicity of the coal surface varies with rank, the extent of oxidation, and the nature and amount of inorganics. During mining, stockpiling, and processing of coal, oxidation of the coal occurs. Such oxidation can dramatically influence the wettability of the coal particles resulting in poor recoveries in surface-dependent coal beneficiation processes.

Both fresh and oxidized coals contain a variety of functional groups containing oxygen, nitrogen, and sulfur. Due to their abundance and polarity, oxygen containing functional groups contribute more to the chemical behavior of the coal surface than do those containing nitrogen and sulfur. Analyses of coals indicate that the major oxygen functional groups are phenols, ethers, and carbonyls [14-19]. The presence of polar oxygenate functional groups, such as phenols and carbonyl containing groups, is assumed to result in increased hydrophilicity of the coal surface.

Capping of polar oxygenate functional groups through methylation is expected to increase the hydrophobicity of the coal surfaces. A method for the methylation of coal surfaces has been reported [20]. This method consists of treating fine coal particles with a gaseous mixture of nitrogen, methanol vapor, and an acid catalyst (SO_2 or HCl) at temperatures of 150 -190°C for one hour. It is proposed that the polar coal hydroxyl groups (ROH) are converted to ethers, while the carboxylic groups (RCOOH), if present, are esterified. The following chemical reactions were proposed:

$$ROH + CH_3OH \xrightarrow[\text{Heat, } N_2]{\text{Acid Catalyst}} ROCH_3 + H_2O$$

Alcohols or Phenols — Methanol — Ethers — Water

and

$$RCOOH + CH_3OH \xrightarrow[\text{Heat, } N_2]{\text{Acid Catalyst}} RCOOCH_3 + H_2O$$

Carboxylic Acids — Methanol — Esters — Water

The resulting ethers and esters are less hydrophilic than the original phenolic and carboxylic groups and have less hydrogen bonding potential. After this treatment, the coal particle surface becomes more hydrophobic and should respond better in conventional beneficiation processes.

In this investigation, a Pittsburgh seam bituminous coal was air oxidized at 125°C for various times up to 48 hours, and some of these oxidized samples were treated with methanol as described above. The oxidized and methanol-treated coal surfaces were characterized by measurement of zeta potential, induction time, and contact angle. The determination of the degree of methylation was achieved by reacting the coal with C13 labeled methanol in the presence of an acid catalyst followed by NMR analysis of the incorporated C13 label. The goal of this investigation was to clarify the chemistry of this surface modification method.

EXPERIMENTAL PROCEDURES

Sample Preparation:

The ultimate analysis of the Pittsburgh seam bituminous coal is shown in Table 1. Both 100 X 325 mesh coal powders and 1cm x2cm x3cm coal chunks were examined. The powdered coals were prepared by passing a 1/4 inch X 0 size fraction through a jaw crusher followed by hammer milling to yield a 28 X 0 mesh sample. This coal sample was then dry screened to obtain the 100 X 325 mesh size fraction. The coal chunks were machined and wet ground to the desired size. One side of the chunk was polished with emery cloth and alumina powder to obtain a smooth surface. Both the powered coal samples and the coal chunks were stored under an argon atmosphere to reduce air oxidation.

Accelerated Oxidation:

The coal samples were placed in an oven at 125°C for 2, 4, 8, 24, and 48 hours. The bed thickness for the coal powders during this oven oxidation was approximately 1/8 inch. All of the oxidized coals were stored under argon after treatment.

Methanol Treatment:

As described by Attar [21], the oxidized coal samples were exposed to a gaseous mixture of nitrogen, methanol, and either SO_2 or anhydrous HCL at a temperature of 190°C for one hour. Twenty-gram samples of powered coal were poured into a fritted one-inch diameter VYCOR tube 18 inches long with glass wool on both sides to maintain the uniform solid core packing. The coal chunk was placed in the same

tube and the chunk was also centered using glass wool. The methanol saturated nitrogen gas flow during these runs was approximately 680 ml/min with 7.0 volume percent of the flow being the acid catalyst (SO_2 or HCl). After treatment, samples were cooled to room temperature and stored under argon.

Zeta Potential Measurements:

Zeta potentials of these oxidized and treated fine coals were measured using the PEN KEM LASER ZEE MODEL 501 instrument. Coal particles (0.30g) were placed in 100 ml of 10^{-3} M potassium nitrate solution and sonified for one minute. The proper pH was achieved by addition of dilute nitric acid or sodium hydroxide solutions and the zeta potentials were measured in the pH range of 2.0 - 11.0.

Induction Time Measurements:

The attachment of a particle to an air bubble is the requirement for successful flotation. This phenomenon involves the thinning and rupture of the wetting film between colliding bubble and particles. Induction time [22-23] is defined as the contact time required to thin the disjoining film between coal particle and air bubbles and establish a three-phase contact. This important parameter is closely related to flotation processes and is useful in determining flotation kinetics as well as in predicting flotation recoveries of fine coal particles.

Using accepted procedures [23] for obtaining consistent induction time measurements, one gram of fine coal particles was agitated in 100 ml of distilled water for two minutes. After the formation of a uniform coal slurry, approximately 20 ml was transferred into a rectangular optical PLEXIGLASS cell to form a bed of particles. The cell was placed on the moving stage of the microscope for measurements. Inside the cell, a microsyringe was used to form an air bubble 2mm in diameter at the tip of the glass tube and let stand for one minute to reach equilibrium before making contact with the particle bed. The contact time was gradually increased from short times to determine the minimum time for the particle to adhere to the surface of the bubble. The contact time was then preset and ten measurements were taken at different regions of the particle bed to yield the average induction time.

Contact Angle Measurements:

Contact angle has been widely used to evaluate the hydrophobic nature of coal, first by Brady and Gauger [24], who showed that the hydrophobicity varied with rank. Later, Horsely and Smith [25], Sun [26], and Aplan [27] have investigated in detail the relationship between the contact angle and rank and have related the contact angle to coal floatability.

The contact angles in this work were measured using the captive bubble method [28]. The polished coal chunks were mounted and placed into distilled water in a PLEXIGLASS cell. The air bubble was attached to the oxidized and treated coal surfaces by using a screw-type microsyringe equipped with an inverted 22 gauge needle. The air bubble was allowed to reach equilibrium for 20 minutes and the contact angle measurement was taken on both sides of the bubble by a Gartner Scientific goniometer at ten different areas over the polished surface.

Surface Treatment using C13 Labeled Methanol :

To obtain a better understanding of the proposed chemical reactions, C13 labeled methanol was reacted with coal particles to determine the degree of methylation. A 250 ml three-necked round bottom flask was charged with 700 mg of untreated Pittsburgh seam coal and then flushed with nitrogen. The flask was heated to 190°C with a heating mantle and was allowed to equilibrate (190 +/- 5°C). After equilibration, the pure nitrogen atmosphere was replaced with nitrogen containing 7 percent acid catalyst. The C13 labeled methanol from the Aldrich Chemical Co. (99 atom %) was added from a microsyringe, through a MININERT valve into a small suspended beaker for the saturation of the reaction atmosphere. To assure that saturation was achieved, the labeled methanol was added until droplets were observed condensing on the walls of the flask. The coal sample was exposed to this gaseous mixture for one hour. Following reaction, the flask was swept with nitrogen and cooled to room temperature. To assure that physically adsorbed reagents were removed, the treated coal samples were vacuum dried for 24 hours and stored under argon.

The methylated coal samples were analyzed by a Brucker CXP-100 nuclear magnetic resonance spectrometer. The spectra were acquired by spinning at the magic angle, using a cross-polarization contact time of 1.0 ms, 3.5 μm -90 degree pulse width and a 2.0 second recycle time. The spectrometer was operated at 25.18 MHz and the aromatic carbon resonance was assigned a chemical shift of 129 ppm.

RESULTS AND DISCUSSION

Air oxidation of the coal under either ambient temperature conditions or under accelerated conditions can result in the uptake of oxygen and the conversion of hydrocarbon constituents into oxygen containing functional groups [29-32].

Accelerated oxidation of the Pittsburgh seam coal indicates that at long exposure times there was a significant increase in the oxygen content determined by difference. The results of the oxidation of this coal are summarized in Table 2.

As expected, the oxygen content increased with the oxidation time. The apparent increase in the oxygen content shown in Table 2 is a measure of total oxidation and should not be interpreted directly as increase in oxygen functionality on particle surfaces. Increasing the number of polar groups on the coal surface is expected to cause the coal to become more hydrophilic. The increase in the hydrophilicity of the oxidized coals can be attributed to increased interfacial attractive forces between polar oxygenate functionality on the coal surface and liquid water.

The surface potential of particles in an aqueous solution can be determined by electrophoresis, in which electrophoretic mobilities (μ) are measured in an applied electric field. The zeta potential (ζ) for a particle in an aqueous solution can be calculated by the von Smoluchowski equation (1):

$$\zeta = \mu\eta/(\varepsilon_r\varepsilon_o)$$

where η is the viscosity of the aqueous solution, ε_r is its dielectric constant, and ε_o is the permittivity of free space.

Figure 1 shows the zeta potentials in aqueous solutions of pH 2 to 11 for fresh and oxidized coals. The negative potentials observed at high pH are assumed to result from the adsorption of hydroxyl ions and/or the deprotonation of acid sites, and the positive potentials observed at low pH result from the adsorption of hydrogen ions

on basic sites. Comparison of the zeta potentials between the fresh and oxidized Pittsburgh seam coals over the pH range of 2 to 11 reveals that the zeta potentials of the oxidized coal are approximately 30 mV more negative than the fresh coal in the entire pH range. Furthermore, the curve of the zeta potentials of the oxidized coal does not have an isoelectric point (point of zero charge) while the fresh coal has an isoelectric point at the pH of 5.0. Since these zeta potentials are measures of the average distribution of surface potential, it is apparent that the oxidized coal surfaces are dominated by acidic sites while the fresh coal has a mixture of basic and acidic sites. This increase in acidic sites on the oxidized coal surface is also supported by the observed increase in the oxygen content shown in Table 2. It is assumed that the presence of more oxygen containing functional groups (i.e., phenols or carboxylic acids) on the interface between the coal particle and the aqueous phase will cause the coal to be more hydrophilic.

Both the induction time and contact angle measurements in Figures 2 and 3 indicate that the coal surface becomes more hydrophilic with longer oxidation times. The fresh Pittsburgh seam coal had an induction time of 1350 microseconds. After 48 hours of oxidation, this value increased to 2200 microseconds. Fresh Pittsburgh seam coal had a contact angle of 45 degrees, which decreased to 21 degrees after 48 hours oxidation. The increase in induction time and the decrease in the contact angle indicate that a more hydrophilic surface results from oxidation.

Following oxidation, 20 gram samples of oxidized coal were treated with the gaseous mixture of nitrogen, methanol, and 7% sulfur dioxide at 190°C for one hour to investigate restoration of the hydrophilicity of the coal surface. In Figure 4, it is apparent that the zeta potentials of the methanol-treated oxidized coal powder show a significant increase of approximately 20 mV as a result of treatment. This suggests a reduction in the acidic sites of the treated coal surface indicating a higher level of hydrophobicity. Comparison of the treated coal (Figure 4) with the fresh coal (Figure 1) shows that the isoelectric point was only slightly lower (pH of 4.2 verses 5.0) for the treated coal, suggesting that the oxidized coal surface was restored to nearly its original hydrophobicity.

Consistent with the zeta potential changes observed, the methanol treatment also reduced the induction time and increased the contact angles of the oxidized coals. Both results, presented in Figures 2 and 3, indicate increasing hydrophobicity of the oxidized coal surface as a result of the treatment.

To determine the effectiveness of the acid catalyst, a comparison study was performed using C13 labeled methanol. Pittsburgh seam coal was reacted on a small scale, as described in the experimental section, with the C13 labeled methanol with and without acid catalyst (SO_2 or anhydrous HCl). These C13 labeled coal samples were then analyzed by NMR to determine the amount of methylation.

The spectra from the treated samples are shown in Figure S. The peak at 52 ppm indicates that methylation occurred; however, the labeled peak is enhanced by 100 fold due to the 99% C13 enrichment of the labeled methanol. The spectra indicate that the level of methylation was the highest when anhydrous HCl was used as the acid catalyst. The incorporation of the labeled methanol can be determined by the change in aromaticity during the treatment. The carbon aromaticity of the coal samples determined by the NMR analyses is summarized in Table 3.

The NMR results presented in Figure 5 and Table 3 can be used to estimate the degree of derivitization of the coal. The results are tabulated in the last column of

Table 3. The values are arrived at by assuming the chemistry is simple conversion of coal hydroxyl groups to methyl ethers:

$$\text{Coal-OH} + {}^{*}CH_3OH \longrightarrow \text{Coal-O-}{}^{*}CH_3 + H_2O$$

The uncertainty in measurements of f_a (aromaticity of the coal) is substantial, but the data indicates little if any influence of gaseous SO_2 as an acid catalyst for the above reaction. However, the presence of gaseous HCl appears to increase the incorporation of label into the coal. In all cases the amount of apparent methylation is small (0.5-1.2 carbons/1000 carbons of coal) when expressed in terms of total carbon in the sample. This could be misleading if the derivitization reaction is limited to the coal surface, because only a very small fraction of the total sample carbon is present as exposed carbon on the particle surface. Unfortunately, the CP C13 NMR is not surface selective and yields only a measure of derivitization relative to the total carbon in the sample. Other chemical reactions could also result in the incorporation of label into the product coal to produce esters or silylethers.

The similarity of the methoxy chemical shifts of product structures is such that we cannot rule out the possibility that these mechanisms of incorporation are minor contributors to the C13 intensity in Figure 5.

SUMMARY

Accelerated oxidation of the Pittsburgh seam coal resulted in a more hydrophilic surface, which was indicated by more negative zeta potentials, higher induction times, and lower contact angles. However, upon treatment of these oxidized coals with gaseous nitrogen, vaporized methanol, and 7 percent SO_2 at 190°C for one hour, the apparent original hydrophobicity of the coal was restored.

NMR analysis of the C13 labeled coal indicates that anhydrous HCL is a more effective methylation catalyst than SO_2 and confirms that the proposed methylation reactions do occur. The NMR results indicate little if any enhancement of methoxy incorporation when SO_2 treatment is compared with simple treatment with no acid catalyst in the methanol saturated nitrogen.

ACKNOWLEDGEMENTS

The authors would like to thank the following persons for their significant contribution to this paper.

Albert V. Lesutis for conducting experimental work.
Richard F. Sprecher and Paula Flenory for their assistance with NMR analyses.

Reference in this report to any specific commercial product, process, or service is to facilitate understanding and does not necessarily imply its endorsement or favoring by the United States Department of Energy.

REFERENCES

1. Brown, D.J., "Coal Flotation," Froth Flotation - 50th Anniversary Volume, Fuerstenau, D.W., ed., AIME, New York, pp. 518-538 (1962).
2. Zimmerman, R.E., "Froth Flotation," Coal Preparation, 3rd ed., Leonard, J.W. and Mitchell, D.R., eds., AIME, New York, pp. 10-66 - 10-90 (1968).

3. Baker, A.F., Miller K.J. and Deurbrouck, A.W., "Two-Stage Flotation Selectively Floats Pyrite from Coal," Coal Mining and Processing, pp. 44-46 and 56 (August 1973).
4. Mehrotra, V.P., Sastry, K.V.S. and Morey, B.W., "Review of Oil Agglomeration Techniques for Processing of Fine Coals," Int. J. Min. Proc., Vol. 11., pp. 175-201 (1983).
5. Keller, D.V., "The Otisca Process of Preparation and Dewatering of Fine Coal," Proceedings of the Consolidation and Dewatering of Fine Particles Conference, University of Alabama, pp. 152-71 (August 10-12, 1982).
6. Chiang, S.H. and Klinzing, G.E., "Process of Removing Mineral Matter from Coal," U.S. Patent Number 4,613,429 (September 23, 1986).
7. Attia, Y.A., Conkle, H.N. and Krishnan, S.V., "Selective Flocculation Coal Cleaning for Coal Slurring Preparation," in Proc. 6th Int. Symp. Coal Slurry Combust., pp. 582-97 (1984).
8. Attia, Y.A., "Cleaning and Desulfurization of Ultrafine Coal Suspensions by Selective Flocculation," Processing and Utilization of High Sulfur Coals, Attia, Y.A. ed., Elsevier (1985).
9. Inculet, I.I., "Electrostatic Mineral Separation," Research Studies Press, John Wiley and Sons, Inc., N.Y. (1984).
10. Advanced Energy Dynamics, Inc., "Dry Electrostatic Cleaning of Ohio Coals," Final Report, Grant No. 10-85-016, Ohio Coal Development Office of the Ohio Department of Development (March 1987).
11. Chiang, S.H. and Venkatadri, R. "Effect of Surface Property on Fine Particle Dewatering," Proc. 4th World Congress on Filtration, Ostend, Belgium (April 20-24, 1986).
12. Dinger, D.R., Funk, J.E. Jr., and Funk, J.E. Sr., "Rheology of a High Solids Coal Water Mixture: Co-Al," Proc. Fourth International Symposium on Coal Slurry Combustion, Orlando, FL., Pittsburgh Energy Technology Center, Pittsburgh, PA (1982).
13. Tsai, S.C. and Knell, E.W., "Rheology and Its Effects on Atomization of Coal Water Slurry," First Annual Pittsburgh Coal Conference, Pittsburgh, PA, September 17-21 (1984).
14. Rosenbaum, J.M., Ph.D. Thesis, U.C. Berkeley (1981).
15. Abdel-Baset, Z., Given, P.H. and Yarzab, R.F., Fuel Vol. 57, p. 95 (1978).
16. Teo, K.C., Finora, S. and Leja, J., Fuel Vol. 61, p. 71 (1982).
17. Schafer, H.N.S., Fuel Vol. 49, p. 271 (1970).
18. Lyengar, M.S. and Lahiri, A., Fuel 36 (3), p. 286 (1957).
19. Ruberto, R.G. and Cronauer, D.C., in: Organic Chemistry of Coal, (J.W. Larsen, ed.), ACS Symposium Series, 71, p. 50 (1978).
20. Attar, J., "Coal Demineralization and Depyritization Process," U.S. Patent 4,597,769 (1986).
21. Attar, J., "Coal Demineralization and Depyritization Process," U.S. Patent 4,597,769 (1986).
22. Sven-Nillson, I., "Effect of Contact Time Between Mineral and Gravitational Collosion Efficiencies for Single Collectors at Intermediate Reynolds Numbers," J.Colloid and Interface Sci., Vol 94, No. 2, pp. 328-335 (1934).
23. Eigeles, M.A. and Volova, M.L., "Kinetic Investigation of Effects of Contact Time Temperature and Surface Condition on the Adhesion of Bubbles to Mineral Surfaces," in Proc. 5th International Mineral Processing Congress, IMM, London, pp. 271-284 (1960).
24. Brady, G.A. and Gauger, A.W., "Properties of Coal Surfaces," Ind. Eng. Chem., Vol 32, p. 1599 (1940).
25. Horsley, R.M. and Smith, H.G., Fuel Vol. 30, p. 54 (1951).
26. Sun, S.C., Trans AIME, Vol. 199, p. 67 (1954).

27. Aplan, F.F., "Examining The Floatability of Western Coals," Geology, Mining, Extraction and the Environment, AIME, New York, NY, pp. 380 (1983).
28. Wark, I.W. and Cox, A.B., Trans. AIME, Vol 112, p. 189 (1934).
29. Bouwman, R., and Ivo L.C. Freriks, "Low Temperature Oxidation of a Bituminous Coal. Infrared Spectroscopic Study of Samples from a Coal Pile," Fuel, Vol. 59, pp. 315-322 (May 1980).
30. Rhoads, C.A., Senftle, J.T., Coleman, M.M., Davis, A. and Painter, P.C., "Further Studies of Coal Oxidation," Fuel, Vol. 62, pp. 1387-1392 (Dec. 1983).
31. Gethner, J.S., "Thermal and Oxidation Chemistry of Coal at Low Temperatures," Fuel Vol. 64, pp. 1443-1446 (Oct. 1985).
32. Huffman, G.P., Huggins, F.E., Dunmyre, G.R., Pignocco, A.J. and Lin, M.C., "Comparative Sensitivity of Various Analytical Techniques to the Low-Temperature Oxidation of Coal," Fuel, Vol. 64, , pp. 849-856 (June 1985).

TABLE 1: ULTIMATE ANALYSIS OF AS-RECEIVED PITTSBURGH SEAM COAL, GIVEN AS PERCENT BY WEIGHT

Moisture	1.3
Carbon	78.1
Hydrogen	4.9
Nitrogen	1.5
Sulfur	1.2
Ash	5.5
Oxygen (by difference)	8.1

TABLE 2 : OXIDATION OF PITTSBURGH SEAM COAL AT 125 C

TIME (HRS.)	OXYGEN CONTENT (Wt.%)*
0	8.1
4	8.5
8	8.5
24	9.9
48	10.8

* WEIGHT DIFFERENCE METHOD

TABLE 3 : EXPERIMENTAL RESULTS OF C13 LABELED METHANOL-TREATED COALS

COAL SAMPLE	AROMATICITY (+/- 0.02)	C13/1000 CARBONS
UNTREATED	0.71	----
NO ACID CATALYST *	0.68	0.5
7 % SO2 *	0.68	0.5
7 % HCL *	0.64	1.2

* ALL TREATMENTS PERFORMED IN THE PRESENCE OF C13 LABELED METHANOL AND NITROGEN AT 190°C FOR ONE HOUR

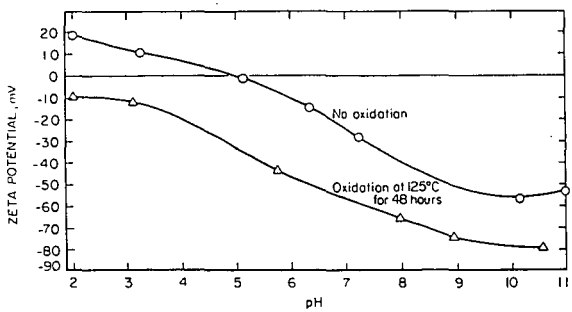

Figure 1. Effect of Oxidation on Zeta Potential of Pittsburgh Seam Coal.

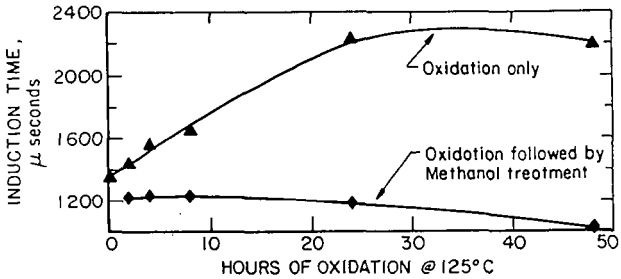

Figure 2. Effect of Oxidation and Methanol Treatment on Induction Time Measurements on Pittsburgh Seam Coal.

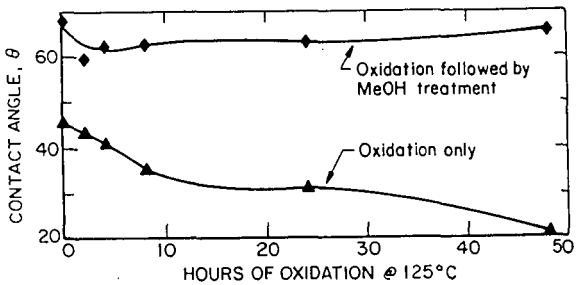

Figure 3. Effect of Methanol Treatment on the Contact Angles of Oxidized Pittsburgh Seam Coal.

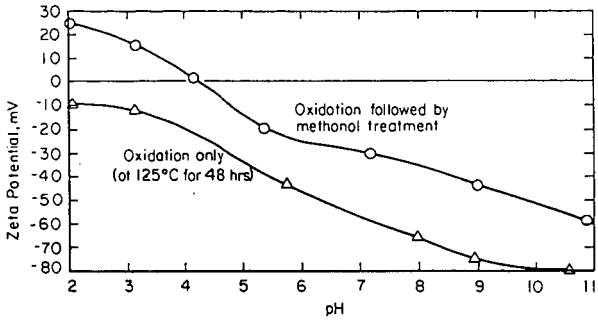

Figure 4. Effect of Methanol Treatment on Zeta Potential of Oxidized Pittsburgh Seam Coal.

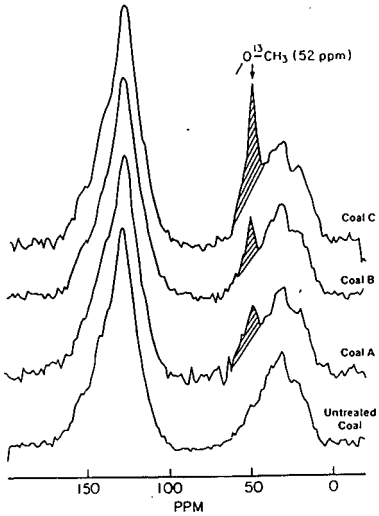

Figure 5. Comparison of Acid Catalysts for C^{13} Methanol-Treated Pittsburgh Seam Coal
Coal A - No Catalyst Presence
Coal B - 7% SO_2
Coal C - 7% Anhydrous HCL

GLASS TRANSITION TEMPERATURE OF MODIFIED COALS

Thomas K. Green, Wei-Ping Pan, Michael R. Clark
Department of Chemistry
Western Kentucky University
Bowling Green, KY 42101

Keywords: coal, glass transition, hydrogen bonding

INTRODUCTION

Coals are macromolecular solids (1). Although they are not polymers in the sense they possess a repeat unit, they do possess several properties typical of synthetic crosslinked macromolecular networks (2). The crosslinks are thought to be covalent in nature. Hydrogen bonds (3,4) and intermolecular polarization forces (5,6) can be important associative forces as well.

Coals behave as glassy materials at room temperature (2). In the glassy state, macromolecular motion is impeded and only short segmental motion of the polymer chain is possible. The glassy state of a material is characterized by its glass transition temperature, T_g, the temperature at which the polymer changes from a glass to a rubber. A rubber is characterized by significant macromolecular mobility compared to the glassy state. The practical utility of polymers and their different properties depend heavily on their glass transition temperatures. Thus, an important area of research is to understand how different molecular features affect the glass transition temperature.

This research is based on the premise that the glass transition temperature is a fundamental property of coals as well, and that it may have an important relation to several other coal properties. For example, the diffusivity of organic solvents in polymers increases by several orders of magnitude at the glass transition temperature (7). If the same concept can be applied to coal, the advantages of lowering the glass transition temperature of coal to enhance coal reactivity are obvious, particularly if the reaction is thought to be diffusion-controlled. Peppas _et al_. have demonstrated that coals swollen with pyridine exhibited lower glass transition temperatures than unswollen coals (8). In this research, we are primarily concerned with the impact of the network of hydrogen bonds in coals on their glass transition temperatures. Both differential scanning calorimetry (DSC) and thermomechanical analysis (TMA) were utilized to establish the importance of hydrogen bonding to T_g for two Argonne premium coals.

EXPERIMENTAL

Sample Preparation. Argonne premium Illinois and Wyodak coals were obtained in sealed ampoules from Argonne National Laboratory. Both coals were dried overnight under vacuum at 105°C. Analysis found: Illinois #6; C, 65.6%; H, 4.7%; N, 1.2%: Wyodak; C, 67.5%; H, 4.99%; N, 0.84%. The coals were alkylated according to the method of Liotta (3) using tetra-_n_-butylammonium hydroxide and the appropriate alkyl iodide in THF. One sample was exposed to THF

with no alkylating agent and is identified as the THF blank. Both elemental and IR analysis confirmed that alkylation had occurred.

Differential Scanning Calorimetry (DSC). The DuPont 910 DSC was used to measure the glass transition temperatures of the samples. Samples were heated from ambient to 600°C at a heating rate of 10°C/min. The system was purged with nitrogen at a rate of 100 mL/min to provide an inert atmosphere. Sample sizes of 5 mg or less were used. The DuPont 2000 Thermal Analysis System was used to analyze the data. Heat flow was plotted as a function of temperature. The glass transition temperature is indicated by a change in the baseline curve in a negative direction. The analysis package identified the inflection point of the change in the curve and this inflection was reported as T_g.

Thermal gravimetric analysis (TGA). The Shimadzu HT 50 TGA was used to monitor weight loss as a function of temperature. The samples were run under nitrogen at a flow rate of 100 mL/min and heated from ambient to 550°C at a heating rate of 10°C/min.

Thermomechanical Analysis (TMA). The DuPont 943 TMA was employed to assess the softening characteristics of the coals. The TMA uses a weighted probe that will penetrate the sample due to the softening which indicates the onset of the glass transition. Probe displacement is plotted as a function of temperature and the softening point is indicated by a negative probe displacement. The macroexpansion probe was used on the TMA. The coal samples were obtained in powdered form. Flat-bottom aluminum DSC pans were used to hold the samples. The coal powder was packed into the pans to a thickness of about 2-3 mm. Typical sample weights were about 20 mg. The pans were then placed in the TMA under a 100 g weight load. This was done to ensure that settling of the sample would be complete. Probe displacement was monitored as a function of time at ambient temperature to insure that the sample was well-packed into a pellet. A 10 g weight was then applied and the cell was purged with nitrogen at a rate of 300 mL/min to obtain an inert environment. The sample was heated at a rate of 10°C/min to a temperature just below the temperature of significant weight loss as indicated by the TG curves.

RESULTS

Elemental Analysis. The O-alkylated coals were analyzed for carbon, hydrogen, and nitrogen. The hydrogen/carbon ratios for the various coals were consistent with the addition of approximately 6 alkyl groups per 100 carbons for the Illinois #6 coal. For the Wyodak coal, elemental analysis indicated addition of approximately 8 methyl groups per 100 carbon. FT-IR analysis of the O-alkylated coals indicated reaction had occurred as evidenced by the increased C-H absorption at 2900 cm^{-1}, reduction of the O-H absorption at 3300-3600 cm^{-1}, and the appearance of an absorption at 1700 cm^{-1} which is attributable to the C=O of esters formed from carboxylic acids.

DSC Results. A typical DSC thermogram obtained using the dry, whole Illinois #6 coal is presented in Figure 1. Note that there

is an increasing negative heat flow into the sample relative to the aluminum oxide reference. The glass transition is identified by the slope shift that occurs near 300°C. Its onset temperature of 295°C was reported as T_g. These results are consistent with those of Peppas et al. for a coal of similar rank (8).

The results for both coals and their alkylated derivatives are summarized in Table I. For the Illinois #6 coals, all reported values are the average of at least five measurements, except for the THF blank (no alkylating agent), which is the average of only two measurements. For the Wyodak coals, only three measurements were made. The effect of O-methylation is to decrease T_g by 100°C for the Illinois #6 coal and 75°C for the Wyodak coal. The effect of the alkyl chain length is not significant for the Illinois #6 coal, although there is clear tread of decreasing T_g with increasing chain length. Exposure of the Illinois #6 coal to THF solvent results in a lower T_g by 50°C.

TG Results. The percent weight loss versus temperature curves for the Illinois #6 coals are presented in Figure 2. Weight loss for the dry, whole coal and the THF blank (no alkylating agent) is not significant until nearly 400°C, which is significantly above the reported T_g's for these coals. This result indicates that no major thermal degradation of the coal occurred before T_g, consistent with the results of Peppas et al (8).

Initial weight loss for the O-alkylated coals occurs at much lower temperatures than the whole coal. Approximately 5-10% of the weight loss occurs in the range of 200-350°C for these coals. An additional 15-25% weight loss occurs in the region of 350-550°C. These coals are clearly much more volatile than the whole coal, which is consistent with other studies (3). It appears that these coals are in a rubbery state, however, before any significant weight loss occurs, since their T_g's are all near 200°C as measured by DSC.

TMA Results. The whole and O-methylated coals were analyzed by TMA in order to assess their softening characteristics. The DSC results indicated that the O-methylated coal should soften at a much lower temperature than the whole coal. This expectation was confirmed. The results on the Illinois #6 coals are shown in Figure 3, where the probe displacement (dimensional change) is plotted against temperature. Note that the O-methylated coal softens at a much lower temperature than the whole coal. Similar results were obtained on the corresponding Wyodak coals.

DISCUSSION

The lowering of T_g by O-methylation of the coal is most probably attributed to the disruption of the hydrogen bond network known to exist in these coals. The hydrogen bonds serve as crosslinks between macromolecular chains and represent an important attractive force that should restrict chain mobility. That their disruption by O-alkylation lowers T_g of the coal is therefore not surprising. The effect of THF solvation on T_g is also substantial, although not as large as O-alkylation. This effect might attributed to a

partial disruption of the hydrogen bond network by THF, which is a known hydrogen bond acceptor. THF is also expected to swell the coal substantially. When the THF is removed, not all of the disrupted hydrogen bonds are expected to reform.

The length of the added alkyl group appears to have only a small effect on T_g, contrary to our expectations. We believed that the addition of longer alkyl groups might disrupt noncovalent interactions other than hydrogen bonding that might exist between the macromolecular chains, thereby lowering T_g even more. Either these interactions are not important or O-alkylation fails to disrupt them. In the future, we plan to examine the effects of C-alkylation (5) on the glass transition temperatures of coals to explore this aspect more fully.

REFERENCES

1. Green, T.; Kovac, J.; Brenner, D.; Larsen, J. W. in "Coal Structure," Meyer, R. A., Ed.; Academic Press, New York, 1982, p 199.

2. Treloar, L. R. G. "The Physics of Rubber Elasticity," Clarendon Press, Oxford, 1975.

3. Liotta, R.; Rose, K.; Hippo, E.; J. Org. Chem. 1981, 46, 277-283.

4. Larsen, J. W.; Green, T. K.; Kovac, J. J. Org. Chem. 1985, 50, 4729.

5. Miyahe, M.; Stock, L. M. Energy Fuels 1988, 2, 815.

6. Quinga, E. M. Y.; Larsen, J. W. Energy Fuels 1987, 1, 300-304.

7. Crank, J.; Park, S. J. "Diffusion in Polymers," Academic Press, London, 1968.

8. Lucht, L. M.; Larsen, J. M.; Peppas, N. A. Energy Fuels 1987, 1, 56-58.

Acknowledgements: We would like to acknowledge the generous support of Shimadzu Instruments for loan of the TGA HT 50 and DuPont Instruments for financial support for the TMA and DSC. M. Clark gratefully acknowledges the ACS Polymer Division for a Summer Research Fellowship.

TABLE I

Glass Transition Temperatures of Modified Coals

Coal	T_g, °C Illinois #6	Wyodak
Whole	300±5	276
THF Blank	247	---
O-Methylated	198±13	203
O-Butylated	185±7	---
O-Octylated	178±14	---

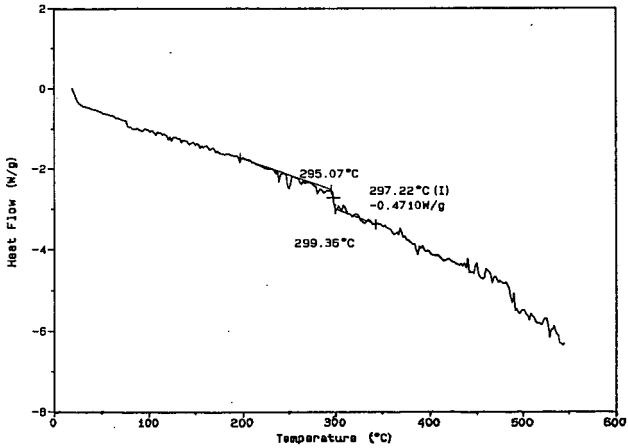

Figure 1. DSC Curve of Dry, Whole Illinois #6 Coal.

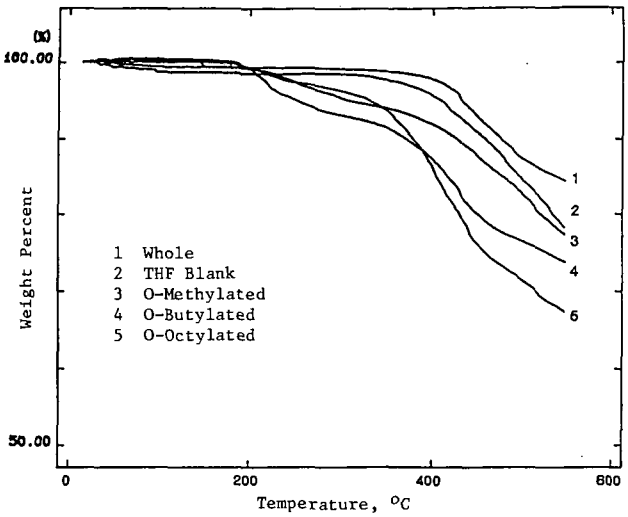

Figure 2. TGA Curves of Illinois #6 Coals.

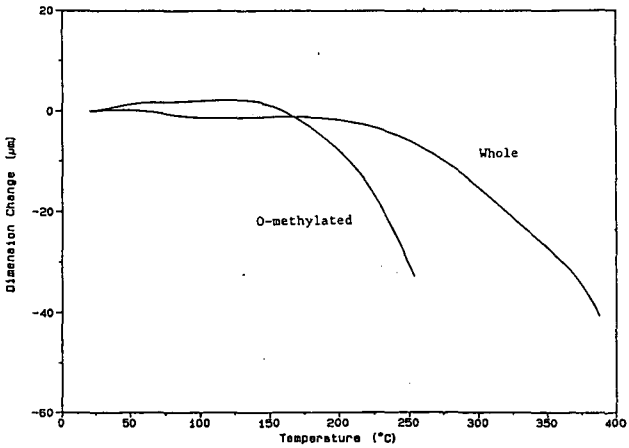

Figure 3. TMA Curves of Illinois #6 Coals

DISTRIBUTION OF ORGANIC SULFUR IN RAW AND SOLVENT EXTRACTED COALS

John T. Riley, Mingshe Zhu, D. Scott Coffey,
Sarah G. Sadler, Jeff M. Stidam, and Harold D. Graham, Jr.

Center for Coal Science
Department of Chemistry
Western Kentucky University
Bowling Green, KY 42101

Key words: organic sulfur, solvent extracted coals, bituminous coal

INTRODUCTION

The removal of organic sulfur from coal presents the most serious challenge in coal desulfurization. Before efficient chemical processes can be developed for the removal of organic sulfur, information on the nature and distribution of sulfur-containing organic compounds in coal is needed.

The general nature of the organosulfur constituents known to exist in coal and coal-derived products have been briefly reviewed (1-4). Most of the literature about organosulfur compounds in coal is qualitative in nature. It is generally accepted that the predominant organic sulfur species present in coal are aromatic groups containing thiophenic sulfur. However, the percentages of thiophenic sulfur in various types of coals are not known. The presence of sulfur containing functional groups such as thiols and sulfides in various coals is also accepted by most coal scientists. However, the percentages of these groups in the various types or ranks of coal are not known. The presence of disulfide groups (R-S-S-R') in some coals is not generally accepted by coal scientists, although there is evidence that such groups may be present in coals (5). The quantitative determination of the various organic sulfur groups present in different types of coal is an area of coal research that has not received the attention it deserves.

Most of the work on characterizing the organic sulfur compounds in coal has been concentrated on studies of the thiophenic compounds, which are the most stable of the organic species present in coal. The thiophenic sulfur compounds are also the most difficult organosulfur compounds to remove from coal. Evidence in the literature and from our own work indicates that as much as 45% of the organosulfur compounds in mid-rank coals is aliphatic in nature, and contains various sulfidic and thiolic groups (5-10). Attar and coworkers used thermokinetic analysis to determine the proportions of thiolic, thiophenolic, aliphatic sulfidic, aryl sulfidic, and thiophenic sulfur in five coals (2,3,6). These investigators estimated that 15-30% of the organic sulfur in coal is sulfidic, while 30-55% of the organic sulfur in lignite and 40-60% in bituminous coals is thiophenic. The remaining organic sulfur is assumed to be thiolic in nature. Yurovski used a classical approach to determine the types of organosulfur compounds in alcoholic solutions of phenol extracts of coal (5). In a study with a Russian coal Yurovski determined that about 48% of the organosulfur compounds in the coal were thiophenic in nature, while the remaining organosulfur compounds consisted of a mixture of thiols, sulfides, and maybe disulfides. George and Gorbaty used x-ray absorption near-edge structure (XANES) spectroscopy to study the distribution of sulfur groups in a Rasa lignite and an Illinois No. 6 bituminous coal (8-9). They concluded the lignite contained 30 ± 10% sulfidic and 70 ± 10% thiophenic sulfur (8), whereas the Illinois No. 6 coal contained 60 ± 10%

sulfidic and 40 ± 10% thiophenic sulfur (9). Huffman and coworkers used x-ray absorption fine structure (XAFS) spectroscopy to examine the structures of sulfur groups in several bituminous coals (10). They concluded that the organic sulfur compounds in bituminous coals were predominantly thiophenic in nature. The results for bituminous coals reported by Gorbaty and Huffman differ significantly.

Many of the difficulties encountered in the investigations of solid coals are reduced in the analysis of extracts and reaction products of the coals. Tetrahydrofuran, pyridine, and dimethylformamide are quite useful solvents for the extraction of coals. Buchanan reported the sequential extraction of pristine Illinois No. 6 coal, APCSP-3, with toluene, tetrahydrofuran, dimethylformamide, and pyridine provided an extract that contained 28% (by weight) of the coal and 29% of the organic sulfur (11). Calkins and coworkers used other solvents for selective sulfur extraction. He found that tetrahydrofuran was superior to acetonitrile, ethylenediamine, and pyridine for the extraction of organic sulfur compounds from a Pittsburgh No. 8 bituminous coal (12-13). Buchanan and coworkers reported that hot perchloroethylene extracts elemental sulfur, formed in the oxidation of pyrite, from bituminous coals (14). They also reported that no appreciable amount of organic sulfur was extracted by perchloroethylene.

There is a considerable amount of information in the literature to indicate that organic sulfur compounds can be preferentially extracted from bituminous coals. In this paper we are reporting the differences between the organic sulfur content in 25 bituminous coals and residues of these coals after extraction with tetrahydrofuran and dimethylformamide.

EXPERIMENTAL

Most of the coals used in the study are from the western Kentucky (Illinois Basin) coal field. A list of the seams and ranks of the 25 coals are given in Table 1. Coal 82071 is from the eastern Kentucky (Appalachian region) coal field and coal 82074 is from the Indiana Lower Block seam, which is also part of the Illinois Basin. The coals were collected for a USDOE-sponsored project conducted at Western Kentucky University and stored under nitrogen after preparation (15). Most of the coals are clean products collected at preparation plants with coals 82071, 82073, and 82074 being run-of-mine samples.

The coals were subjected to standard analysis by ASTM methods (16), or methods with equivalent or better precision, as follows: proximate analysis using the LECO MAC-400 moisture, volatile matter, and ash analyzer (ASTM D 5142); ultimate analysis using the LECO CHN-600 carbon, hydrogen, and nitrogen analyzer and the LECO SC-132 sulfur analyzer (ASTM D 4239). Analytical data for the raw coals are given in Table 1 and data for extracted coals are given in Tables 2 and 3. Organic sulfur was determined by the direct determination method developed in this laboratory (17).

Solvent extractions of the coals were carried out using standard Soxhlet extraction assemblies at the atmospheric reflux temperatures of the two solvents employed, N,N-dimethylformamide (DMF) and tetrahydrofuran (THF). Prior to extraction, -60 mesh (250 μm) samples of each coal were vacuum dried at 60°C for six hours. Ten gram samples of dried coal in cellulose Soxhlet thimbles were then extracted for periods of 20-24 hours. The extracted coals were then rinsed with refluxing methanol in the Soxhlet apparatus for 5-6 hours and vacuum dried at 150°C until the samples reached a constant weight (6-10 hours). The extracted samples used in this study were prepared by Lloyd and coworkers (15). The averages of the percent coal extracted in triplicate runs on the 25 coals by the two solvents are given in Table 4.

RESULTS AND DISCUSSION

As shown in Table 1, the coals used in the study are predominantly high volatile bituminous C (hvCb) coals. All except coals 82071 and 82074 are from the western Kentucky coal fields (Illinois Basin) and all except coals 82071, 82073, and 82074 are washed coals. The total sulfur in the raw coals ranged from 1.35% to 3.65%, as reported on a dry basis.

Extraction of coals with organic solvents such as DMF and THF remove organic matter with subsequent increases in the percent mineral matter in the coal residues. The data in Tables 2 and 3 show increases in the ash contents of the coal residues which are in proportion to the coal extracted by the solvents. The general decreases in carbon, hydrogen, and volatile matter percentages is consistent with this trend. A comparison of the dry oxygen values in Table 1 with those for the extracted coals in Tables 2 and 3 show general increases in oxygen upon extraction with the organic solvents. This is likely due to the enrichment of oxygen-containing mineral matter in the extracted coals.

The total sulfur values for the extracted coals increase from the enrichment of mineral matter (pyritic and sulfatic sulfur forms) in the residues, as can be seen by comparing the total sulfur values for the raw coals in Table 1 with those for the residues in Tables 2 and 3. The increases in total sulfur are greater for the DMF-extracted coals than those for the THF-extracted coals. This is to be expected since the total material extracted by DMF (mean percent extracted = 24.8%) is greater than that extracted by THF (mean percent extracted = 14.0%). When the organic sulfur values for the raw coals are compared to the organic sulfur values for the DMF- and THF-extracted coals, one can see that there is a reduction of the organic sulfur in the extracted coals. The last two columns in Table 4 illustrate the magnitude of the reduction in the organic sulfur values for the DMF- and THF-extracted coals, respectively. The mean difference between the organic sulfur in the raw coal and that in the DMF-extracted coals is 0.19% (absolute). This mean difference for the THF-extracted coals is 0.16%.

Using the mean organic sulfur values in the raw coals, the mean organic sulfur values in the DMF- and THF-extracted coals, and the extraction percentages, a mean value for the organic sulfur in the coal extracts can be calculated. The mean value for the organic sulfur (daf basis) in the 25 coals is 1.63%. The mean value for the organic sulfur (daf basis) in the DMF-extracted coals is 1.45% and for the THF-extracted coals is 1.47%. With a mean extraction percentage of 24.8% for DMF this means the calculated mean organic sulfur value in the DMF extracts of the 25 coals is 2.18%. Likewise, the mean extraction percentage of 14.0 for THF can be used to calculate a mean organic sulfur value of 2.61% in the THF extracts of the 25 coals. The calculated organic sulfur values in the extracts of the 25 coals represent a 33.7% enrichment of organic sulfur in the DMF extracts and a 60.1% enrichment of organic sulfur in the THF extracts.

The lower percentage enrichment of organic sulfur in the DMF extracts compared to that for the THF extracts is consistent with the observations of other researchers. DMF extracts a greater percentage of the coals (24.8%) than THF (14.0%). The first material extracted from coal is richer in sulfur, and possibly oxygen and nitrogen, than the material removed as the extraction proceeds (18).

The data in Tables 1-4 were plotted in various ways in attempts to identify any trends in the rate of extraction of organic sulfur from the 25 coals. The only apparent relationships found were weak correlations between the organic sulfur extracted by the solvents and some of the other sulfur values for the coals. Figure 1 does indicate that the rate of extraction of organic sulfur from the coals using THF as the solvent may be dependent on the daf organic sulfur in

the raw coals. The correlation coefficient for this line is a moderate 0.56. However, as shown in Figure 2, the regression line between the daf organic sulfur in raw coals and the amount of organic sulfur extracted from the coals by DMF does not indicate a similar trend and gives a very low correlation coefficient. Also, as indicated by the other regression line in Figure 2, there does not seem to be any relationship between the percent of coal extracted and the amount of organic sulfur extracted from the coals. The data for the extractions with THF also indicated no such relationship.

The data in Table 4 strongly indicates that organic sulfur is removed from the 25 coals by the two solvents and enriched in the extracts. The organosulfur compounds that are the most likely to be extracted by the solvents are aliphatic in nature. Attempts to show a correlation between the amount of organic sulfur removed and changes in carbon and hydrogen values that would be consistent with the extraction of aliphatic compounds were unsuccessful. Work with the extracts themselves is necessary to establish any such relationship. Future experiments to study extracts of the coals are planned.

CONCLUSIONS

In conclusion, it can be stated that the data presented here indicate that organic sulfur is often enriched in the DMF and THF extracts of bituminous coals. The amount of organic sulfur preferentially extracted by the two solvents is weakly related to the sulfur contents of the coals. The average enrichment of organic sulfur in the THF extracts of the coals was calculated to be about 60%, whereas that for the DMF extracts was about 34%. The average percent of coal extracted by the solvents was 14% for THF and about 25% for DMF. It is likely that the organosulfur constituents extracted by the two solvents are aliphatic in nature, but no such conclusions can be drawn from the data presented in this paper.

ACKNOWLEDGMENT

The authors wish to thank Drs. W.G. Lloyd and J.W. Reasoner for providing the extracted coal samples used in this work. We gratefully acknowledge financial support of this work through a grant from the Center for Research on Sulfur in Coal in Carterville, IL, and through the Robinson Professorship from the Ogden Foundation at Western Kentucky University.

REFERENCES

1. Stock, L.M.; Wolny, R.; Balkrichna, B.; Energy & Fuels, 1989, 3, 651-61.

2. Attar, A.; Corcoran, W.H.; Ind. Eng. Chem. Prod. Res. Dev., 1977, 16, 168-170.

3. Attar, A.; "Sulfur Groups in Coal and Their Determinations," Chap. 56 in Analytical Methods for Coal and Coke Products, Vol. III, Karr, C.K., Ed., Academic: New York, 1979.

4. White, C.M.; in Handbook of Polycylic Aromatic Hydrocarbons; Bjorseth, A.; Ed.; Marcel Dekker: New York, 1983, Chap. 13, 525-616.

5. Yurovskii, A.Z.: Sulfur in Coals, Published for the U.S. Department of the Interior, Bureau of Mines and the National Science Foundation, by the Indian National Scientific Documentation Centre, New Delhi, 1974, 56-62.

6. Attar, A.; Dupuis, F.; "Data on the Distribution of Organic Sulfur Functional Groups in Coals," in Coal Structure, Gorbaty, M.L., and Ouchi, D., Eds., Advances in Chemistry Series 192, American Chemical Society: Washington, D.C., 1981.

7. Riley, J.T., et al., "Removal of Aliphatic Sulfur and Chlorine Compounds from Coal," Technical Reports 1-3, Center for Research on Sulfur in Coal, Carterville, IL, 1990.

8. George, G.N.; Gorbaty, M.L.; J. Am. Chem. Soc., 1989, 111, 3182.

9. George, G.N.; Gorbaty, M.L.; Kelemen, S.R.; Prepr. Pap. - Am. Chem. Soc., Div. Fuel. Chem., 1989, 34(3), 738.

10. Huffman, G.P.; Huggins, F.E.; Mitra, S.; Shah, N.; Pugmire, R.J.; Davis, G.; Lytle, F.W.; Greegor, R.B.; Energy & Fuels, 1989, 3, 200.

11. Buchanan, D.H.; Osborne, K.R.; Warfel, L.C.; Wanping, M.; Lucas, D.; Energy & Fuels, 1988, 2, 163.

12. Calkins, W.H.; Energy & Fuels, 1987, 1, 59.

13. Calkins, W.H.; Prepr. Pap - Am. Chem. Soc., Div. Fuel Chem., 1985, 30(4), 450.

14. Buchanan, D.H.; Chanen, C.; Puharich, K.; Warfel, L.C.; Hackley, K.C.; Kruse, C.W.; "Organic Sulfur Removal from Illinois Coal," Final Tech. Rept., Center for Research On Sulfur in Coal, Carterville, IL, October, 1990.

15. Lloyd, W.G.; Reasoner, J.W.; Hower, J.C.; Yates, L.P.; Clark, C.P.; Davis, E.; Fitzpatrick, A.; Irefin, A.; Jiminez, A.; Jones, T.M.; Reagles, C.L.; Sturgeon, L.P.; Whitt, J.M.; Wild, G.D.; Predictors of Plasticity in Bituminous Coal," Final Rept., USDOE Contract No. DE-FG22-81PC40793, February, 1984.

16. Annual Book of ASTM Standards, Vol. 5.05, Amer. Soc. for Testing and Materials, Philadelphia, PA (published annually).

17. Riley, J.T.; Ruba, G.M.; Lee, C.C.; "Direct Determination of Total Organic Sulfur in Coal," in Geochemistry in Sulfur in Fossil Fuels, W.L. Orr and C.M. White, Eds., ACS Symposium Series No. 429, American Chemistry Society: Washington, D.C., 1990.

18. Buchanan, D.H.; Eastern Illinois University, Charleston, IL, private communication.

Table 1

Source and Characterization Data[A] for Coals Used in the Study

Coal No.	Seam	Apparent Rank[B]	Moisture	Vol. Matt.	Ash	C	H	N	Total Sulfur	O (by diff.)
82074	IN L. Bl.	hvCb	10.46	35.0	8.77	73.42	5.03	1.51	1.72	9.56
82049	Elm Lick	hvCb	6.95	35.6	5.48	78.42	5.29	2.03	1.89	6.89
82048	KY #9	hvCb	8.73	37.1	9.21	72.49	4.88	1.64	3.17	8.61
82050	Bancroft	hvBb	2.81	39.8	5.95	75.97	5.11	1.36	3.12	8.49
82077	KY #11	hvCb	7.77	37.2	8.05	74.06	5.07	1.60	3.37	7.84
82060	KY #9	hv8b	7.06	36.6	7.86	73.80	4.97	1.64	2.87	8.87
82056	KY #9	hvCb	7.11	36.5	8.19	76.12	4.98	1.67	3.05	5.99
82080	KY #11	hvCb	8.40	38.1	6.38	74.78	5.10	1.62	3.35	8.78
82071	Mason	hvAb	3.24	34.3	7.07	78.37	5.01	1.61	1.35	6.59
82066	KY #11/12	hvCb	8.13	36.9	9.39	72.75	4.88	1.36	3.10	8.51
82051	Bancroft	hvBb	3.08	38.9	6.43	75.26	5.06	1.31	2.73	9.21
82067	KY #9	hvBb	2.83	36.1	8.85	72.87	5.05	1.56	2.86	8.81
82076	KY #9/11	hvCb	7.56	37.4	8.76	70.81	5.07	1.46	3.65	10.25
82063	KY #9	hvCb	7.92	36.3	8.30	73.74	4.95	1.63	3.37	8.02
82061	KY #9	hvCb	6.77	36.3	10.77	70.87	4.82	1.43	3.43	8.69
82064	KY #9	hvCb	7.49	36.5	7.95	76.31	4.81	1.64	3.12	6.17
82073	KY #9	hvAb	2.81	36.0	8.23	75.06	5.10	1.70	3.56	6.35
82062	KY #9	hvCb	5.96	36.8	8.51	72.94	4.86	1.60	3.09	9.00
82057	KY #14	hvCb	7.56	32.7	21.13	61.03	4.39	1.23	3.33	8.89
82069	KY #6	hvAb	2.74	35.3	8.78	76.02	4.96	1.62	2.59	6.02
82058	KY #14	hvCb	5.59	33.6	17.73	64.12	4.47	1.05	3.27	9.35
82052	Bancroft	hvCb	3.09	39.5	6.80	75.47	5.00	1.15	3.06	8.52
82059	KY #9	hvBb	6.38	36.5	9.15	74.33	4.92	1.75	3.39	6.46
82047	KY #9	hvCb	11.56	37.3	10.97	71.29	4.94	1.59	3.43	7.78
82054	KY #9	hvCb	8.30	37.5	8.15	74.73	5.07	1.68	3.30	7.07

[A] Moisture is as-determined, other analytical values are on a dry basis. All values are percentage by weight.
[B] Apparent rank using as-determined moisture for calculation.

Table 2

Analytical Values[A] for DMF-Extracted Coals

Coal No.	Vol. Matt.	Ash	C	H	N	Total Sulfur	O (by diff.)
82074	33.0	10.28	72.44	4.62	1.72	1.74	9.19
82049	33.5	6.90	74.50	4.76	7.70	2.14	4.00
82048	34.1	11.92	67.26	4.52	1.83	3.68	10.80
82050	37.6	7.74	72.22	4.75	2.14	3.54	9.61
82077	33.7	10.17	71.40	4.52	1.64	3.57	8.69
82060	33.0	10.67	71.18	4.42	2.00	3.12	8.60
82056	34.9	10.34	70.60	4.80	2.41	3.13	8.72
82080	34.9	7.99	71.10	4.71	1.55	3.31	11.33
82071	30.8	9.41	74.64	4.64	2.12	1.52	7.68
82066	32.9	11.55	67.14	4.64	2.02	3.21	11.44
82051	35.7	7.86	69.04	4.89	2.06	2.94	13.21
82067	32.2	12.50	69.08	4.74	1.54	3.26	8.88
82076	33.7	10.69	68.91	4.64	1.75	3.60	10.41
82063	32.6	10.39	68.46	4.21	1.72	3.40	11.82
82061	33.3	13.82	65.50	4.47	1.95	3.68	10.59
82064	32.0	9.74	69.74	4.27	2.30	3.13	10.83
82073	31.6	12.36	70.90	4.49	1.37	4.24	6.83
82062	33.2	11.09	70.33	4.54	1.60	3.23	9.21
82057	30.1	26.64	56.12	3.87	1.65	3.56	8.16
82069	31.3	12.33	71.18	4.55	1.53	3.07	7.35
82058	31.0	23.46	56.53	4.16	1.61	3.55	10.70
82052	40.3	9.28	70.47	5.22	2.14	3.42	9.46
82059	33.4	11.96	69.01	4.39	1.98	3.91	8.75
82047	34.2	13.64	67.54	4.39	1.69	3.96	8.79
82054	35.9	10.39	69.40	4.73	1.83	3.55	10.09

[A] Analytical values are reported as percentage by weight on a dry basis.

Table 3

Analytical Values[A] for THF-Extracted Coals

Coal No.	Vol. Matt.	Ash	C	H	N	Total Sulfur	O (by diff.)
82074	28.4	7.95	72.09	4.79	1.39	1.42	12.36
82049	36.0	5.94	73.45	5.46	1.89	2.05	11.21
82048	36.6	10.47	68.62	5.07	1.51	3.41	10.92
82050	39.4	6.78	72.55	5.43	1.58	3.28	10.38
82077	34.5	8.89	71.94	4.71	1.33	3.60	9.53
82060	33.2	9.11	78.88	4.03	1.74	2.99	3.25
82056	35.2	9.56	70.27	5.17	2.10	3.22	9.68
82080	35.7	7.18	73.37	5.03	1.54	3.48	9.40
82071	32.4	7.70	77.11	5.20	1.90	1.47	6.62
82066	33.9	10.80	70.19	4.80	1.70	3.27	9.24
82051	39.7	7.14	71.66	5.52	1.78	3.13	10.77
82067	32.4	10.18	73.44	4.92	1.46	3.10	6.90
82076	34.5	9.84	71.23	5.00	1.66	3.82	8.45
82063	33.2	9.37	71.17	4.69	1.63	3.45	9.69
82061	33.7	12.25	69.93	4.68	1.72	3.69	7.73
82064	32.3	8.95	70.66	4.41	1.96	3.29	10.73
82073	32.7	9.85	73.86	4.91	1.47	3.89	6.02
82062	33.7	9.96	72.18	4.71	1.91	3.28	7.96
82057	31.2	23.53	60.67	4.16	1.44	3.48	6.72
82069	32.3	9.73	74.29	4.96	1.59	2.77	6.66
82058	33.1	19.59	60.76	4.45	5.78	3.34	6.08
82052	39.2	8.40	71.69	5.43	1.38	3.29	9.81
82059	30.6	9.68	66.89	3.13	1.71	3.37	15.25
82047	36.5	11.99	66.83	4.85	1.49	3.62	11.22
82054	36.0	9.50	70.27	5.18	1.95	3.56	9.54

[A] Analytical values are reported as percentage by weight on a dry basis.

Table 4

Extraction Percentages and Organic Sulfur Values for Extracted Coals

Coal No.	% Coal[A] Extracted-DMF	% Coal[A] Extracted-THF	Raw Coal Org. S[B]	DMF-Ext.[B] Coal Org. S	THF-Ext.[B] Coal Org. S	Raw - DMF-Ext. Org. Sulfur	Raw - THF-Ext. Org. Sulfur
82074	18.7	10.7	0.76	0.54	0.78	0.22	-0.02
82049	18.7	13.4	0.84	0.62	0.83	0.22	0.01
82048	22.5	12.0	1.66	1.76	1.64	-0.10	0.02
82050	22.7	14.6	0.85	0.86	0.82	-0.01	0.03
82077	24.1	14.2	1.93	1.75	1.89	0.18	0.04
82060	32.3	17.2	1.82	1.63	1.74	0.19	0.08
82056	22.1	13.4	1.62	1.21	1.52	0.41	0.10
82080	23.0	15.4	2.03	1.98	1.92	0.05	0.11
82071	27.3	11.0	1.00	0.64	0.89	0.36	0.11
82066	23.1	15.6	1.80	1.86	1.68	-0.06	0.12
82051	21.1	12.6	0.95	0.88	0.83	0.07	0.12
82067	31.9	16.3	1.75	1.63	1.62	0.12	0.13
82076	23.0	14.5	1.98	2.07	1.83	-0.09	0.15
82063	23.5	13.9	1.70	1.60	1.55	0.10	0.15
82061	23.4	13.3	1.95	1.80	1.77	0.15	0.18
82064	21.0	13.3	1.74	1.63	1.56	0.11	0.18
82073	34.2	16.3	1.88	1.81	1.69	0.07	0.19
82062	26.4	14.9	1.89	1.79	1.67	0.10	0.22
82057	24.6	13.3	1.66	1.08	1.42	0.58	0.24
82069	33.0	14.2	1.54	1.36	1.30	0.18	0.24
82058	24.6	12.7	1.85	1.25	1.57	0.60	0.28
82052	22.6	17.4	1.91	1.59	1.63	0.32	0.28
82059	28.4	15.3	1.98	1.29	1.66	0.69	0.32
82047	24.2	12.8	1.83	1.85	1.50	-0.02	0.33
82054	22.9	12.4	1.90	1.66	1.50	0.24	0.40

[A] Dry coal basis.
[B] Dry, ash-free basis.

Figure 1. Organic Sulfur in Raw Coal vs. Organic Sulfur Extracted by THF

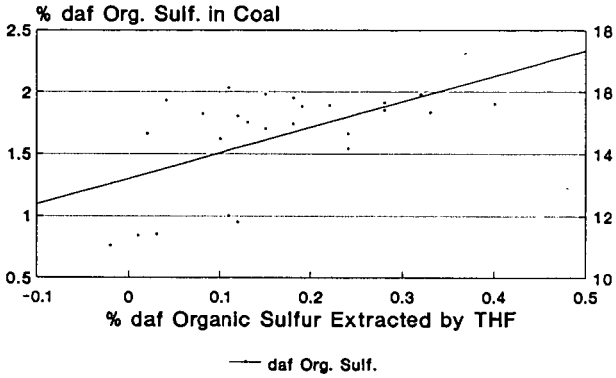

Figure 2. Organic Sulfur in Raw Coal vs. Organic Sulfur Extracted by DMF

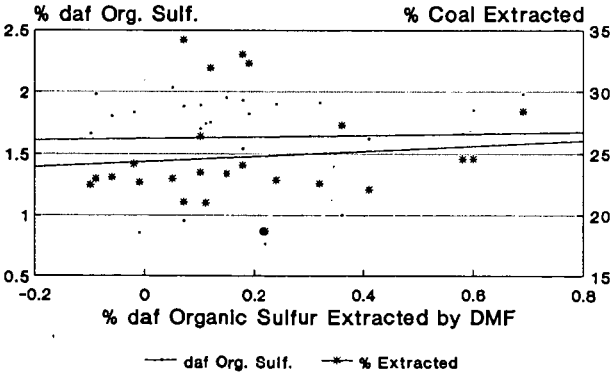

EVALUATION OF COMBINATION FUELS FOR FLUIDIZED BED COMBUSTORS BY THERMAL ANALYTICAL TECHNIQUES

Wei-Ping Pan, Mary Campbell, and John T. Riley,

Center for Coal Science
Department of Chemistry
Western Kentucky University
Bowling Green, KY 42101

Mingxu Zhang

Huainan Mining Institute
Huainan, Anhui, China

Key works: thermogravimetry, coal, municipal solid wastes, fluid bed combustion

ABSTRACT

The objective of this study is to find suitable combinations of coal fines, municipal solid waste (MSW), and limestone to produce fuel pellets for fluidized bed combustion systems. The coal fines, MSW (paper), and sorbent limestone were mixed in different combinations and the volatile matter and char contents of all mixtures, as well as the original materials, were evaluated by thermogravimetric analysis (TGA). Using different rates of heating and variable atmospheres, information was obtained that can be useful in predicting the combustion behavior and efficiency of the combination fuels. Optimum limestone content can be determined by selectively introducing CO_2 during the final stages of the combustion process to check for excess CaO. The use of combined techniques such as TGA, differential thermal analysis (DTA), and TGA-FTIR can be utilized to determine detailed information on the combustion and thermal properties of the combination fuels.

INTRODUCTION

More than 150 million tons of municipal solid waste (MSW), are generated in the United States each year. This excessive amount of generated waste, combined with decreases in landfill sites, causes serious environmental problems and forces the establishment of programs for reducing the volume of waste deposited in landfills.

Mass burning of unprocessed MSW and preparation/firing of refuse-derived fuel (RDF), are the two main methods currently being evaluated for waste-to-energy technologies (1,2). There are several methods used for the firing of RDF. The chief method employed in this study is fluidized bed combustion. Fluidized bed combustion systems are particularly suited to waste fuels because of their ability to burn low grade and variable fuels as well as absorb sulfur oxides through the use of sorbents.

Fluidized bed combustion systems have been constructed in the U.S., Europe, and Japan, for the burning of RDF alone or combinations of RDF and wood waste (3). However, there is little or no information available regarding RDF firing in the presence of coal in fluidized bed combustion systems, or co-firing of wood wastes with coal. There have been several studies conducted on the preparation of fuel

pellets using coal fines and limestone, which serves as a sorbent for sulfur oxides (4-6). This information was valuable in the evaluation of the combustion performance of fuel pellets prepared from coal fines, MSW or wood waste, and limestone sorbent.

The burning profiles of coal and RDF are quite different, but there is a high probability that blends of these two fuels, when co-fired under the right conditions, perform suitably as a boiler fuel. This conjecture forms the basis of the study reported in this paper.

In general, normal production of coal yields millions of tons of coal fines each year (about 20% of total yield). These fines, however, can not be sold because of handling problems. The cost of recovery of these fines is small compared to the mining of coal. Coal fines are an excellent source of an energy-rich fuel that can be blended with RDF to produce pellets suitable for use in fluidized bed combustion systems.

When coal contains high amounts of organic sulfur it is impossible to remove the sulfur using conventional physical cleaning methods. Fluidized bed combustion systems utilizing coal-limestone-fuel mixtures have the potential for resolving this limitation since limestone, which is abundant in nature, can be used as a sorbent for emitted SO_2.

SAMPLE PREPARATION AND RESULTS

Thermal Analysis of Raw Materials

The materials used for this study are coal fines (Illinois #6), Kentucky agricultural limestone, and newspaper. All samples were prepared and analyzed in Western Kentucky University's Coal and Fuel Characterization Lab. The three materials were studied by thermogravimetric analysis (TGA) to assess their thermal behavior. The TGA experimental conditions used were 10 mg sample size, air atmosphere with a flow of 50 mL/min, and a heating rate of 20°C/min. The instrument used was a Shimadzu HT 1500 TGA Thermogravimetric Analysis System.

Test results for the three materials are shown in Figure 1. The TG curve for coal depicts two weight loss stages, the first consisting of a 3.09% moisture loss followed by a second weight loss of 85.25% containing two overlapping DTG peaks. The first DTG peak is a result of the combustion of aliphatic materials in coal and the second is due to the combustion of the aromatic materials of coal. T_{Max1} and T_{Max2} occur at 417°C and 440°C, respectively.

Figure 1 also shows two decomposition stages for limestone. There is an initial moisture loss of 1.73% beginning at 397°C and a second weight loss of 40.95% beginning at 563°C. This is due to limestone being converted to CaO and CO_2 gas. R_{Max} (mg/min), was 0.76 at 817°C. Experimental conditions were identical to that used for coal.

Finally, Figure 1 represents three major weight loss stages for newspaper with the first being a moisture loss of 4.35%. The second weight loss of 88.57% represents the major decomposition of materials in newspaper and has an R_{Max} of 5.34 at 353°C. The overlapping peak is shown on the DTG curve and represents the decomposition of impure cellulosic materials with higher lignin content in the newspaper. The third and last weight loss phase of 5.91% is due to char gasification and has a small peak at 475°C. Experimental parameters were again identical to those used in the TG analysis of coal. It is evident from the TG curve that newspaper decomposes 150°C earlier than coal. Total weight losses of

coal, limestone, and newspaper (established on a moisture free basis), were 88%, 42.7%, and 98.8%, respectively.

Thermal Analysis of Coal-Limestone Mixtures

In order to decide upon an optimum amount of limestone for the combination fuels for the fluidized bed combustor, mixtures of coal and limestone were tested by TGA. Testing procedures preceding 800-850°C were identical to those previously examined. However, after 800°C or 850°C, temperatures were held constant for 5 minutes, the atmosphere was changed to CO_2 gas for 25 minutes, and a determination was then made as to the amount, if any, of weight gain that occurred (See Figure 2). If a weight gain did occur, this indicated that an excess of CaO was in the residue and was converted back to $CaCO_3$ when the CO_2 was added. If a weight gain did not occur, this indicated that all of the CaO reacted with the SO_2 to produce $CaSO_4$, leaving no excess CaO in the residue. This method was developed by R.F. Culmo and R. L. Fyans (7).

Next the optimum temperature at which the limestone completely decomposed needed to be determined. A 5% limestone, 95% coal mixture was used to obtain the suitable temperature values. The TG results show that there is no significant weight changes above 800°C. Therefore 800°C and 850°C were chosen for the isothermal temperature values for test runs.

Using the chosen optimum temperature values, the optimum limestone percentage needed to be determined. To accomplish this goal, different percentages of limestone (0,1,2,3,4,5, and 10%), were added to the coal. The results of these tests, as shown in Figure 3, indicate a suitable limestone percentage is between 1% and 3%. A plateau in the weight gain curve occurs between 1-3% and increases significantly with increased amounts of limestone (excess CaO). Thus, 2% limestone was chosen for the following study. It should be recognized that excess limestone will reduce the flame temperature in the fluidized bed combustion system and also increase the operational costs.

Considering that the heating rate is higher in fluidized bed combustors than that used in the experimental tests used thus far, higher heating rates for tests were chosen to observe the effect heating rates may have on the decomposition of the fuel mixtures. Heating rates of 20°C/min, 35°C/min, 40°C/min, and 50°C/min were chosen for additional experiments. These heating rates were used with 2%, 5%, and 10% limestone percentages. The TG results indicate the weight gain, due to absorbed SO_2, at different heating rates and limestone percentages was not significantly affected under these specific experimental conditions.

A determination of the change in weight loss during combustion as a function of varying coal-limestone mixtures was made. It was determined that the 2% limestone did not show any catalytic effect on the first thermodecomposition stage of coal. Similar results were obtained for the second thermodecomposition stage.

Finally, the effect of limestone on the thermal behavior of the mixture with respect to changes in the parameters T_{max} and R_{max} was determined. The TG results indicate that at heating rates of 20°C/min and increased limestone content, T_{Max1} and T_{Max2} shift to slightly higher temperatures. The TG curve also shows that R_{Max1} and R_{Max2} slightly decrease with increased limestone percentage. Both TG curves present the same results; higher limestone content may delay the decomposition and combustion slightly as T_{Max} increases and R_{Max} decreases.

Thermal Analysis of Combination Fuels

The combination fuels tested consist of coal, limestone, and newspaper (RDF), in varying percentages. According to the results of the preliminary

studies, it is believed that a 2% limestone content in the mixture is sufficient for absorbing the SO_2 emitted for the burning of the coal tested. The mixtures of coal, limestone, and newspaper are 90/2/8, 80/2/18, and 70/2/28, respectively.

The general TG curve of the combination fuel is shown in Figure 4. There were four thermodecomposition stages observed, excluding the moisture loss. The T_{Max} for each stage was 283, 384, 450, and 489°C. It is believed that the first and second stages are due to the decomposition of newspaper, with the first being mainly due to cellulosic materials and the second to lignin content. Previously, Figure 1 indicated that there was one overlapping DTG peak with T_{Max} = 352°C. In the case of the combination fuel, however, the overlapping peak noted in Figure 1 became two separate peaks, and the first peak occurred 70°C earlier than noted for the newspaper alone. This may be due to reduced sample particle size that occurred during the grinding and preparation of the combination fuel. The third and fourth decomposition stages are due to the thermodecomposition of coal. However, the third stage was enhanced by two possible factors: (1) additional char gasification from the newspaper and/or (2) catalyzation of the char gasification by the limestone. The results for T_{Max}, R_{Max} versus newspaper content are shown in Table 1.

To better understand and further verify the proposed mechanisms involved in the TG curve analysis, 50% coal/50% newspaper, 50% newspaper/50% limestone, and 50% coal/50% limestone test mixtures were also studied.

The TG and DTG curves of the 50% limestone/50% newspaper indicate three thermodecomposition stages with the first two peaks being due to the thermodecomposition of newspaper. The third peak was due to the decomposition of limestone. T_{Max} for peak one did not significantly change compared to that for 100% newspaper. R_{Max}, however, decreases by 20%. T_{Max} of peak two did not show any significant change. However the value of R_{Max} was five times greater than 100% newspaper. This might be due to the catalytic effect on char gasification. It is presently unknown why the third peak shifted 10°C earlier than 100% limestone; however, R_{Max} values were similar.

One may assume that the experimental values such as those listed in Table 2 may be used to predict the effects of varying amounts of limestone by utilizing known decomposition values for pure limestone and pure newspaper. However, in this case, there were significant differences between calculated (predicted) values and those obtained through experimentation. The first peak was retarded by the calcium, yielding lower weight loss values, and the second peak is influenced by a catalytic effect from the calcium. The third weight loss phase, however, was not effected because it was only due to the decomposition of limestone.

The TG results for 50% coal/50% limestone showed two thermodecomposition stages. The first peak, a combination of two overlapping peaks, shifted 20°C higher than that for 100% coal. Again, the third peak, due to the thermodecomposition of limestone, occurred 20°C lower than that for 100% limestone. Likewise, R_{Max} for peak one was reduced by 50% compared to that for 100% coal. The TG results of 50% coal/50% newspaper showed three thermodecomposition stages with the first peak being due to newspaper, the second peak due to coal, and the third peak due to char gasification combined with less combustible materials from coal.

From reactivity studies, it can be concluded at this point in the analysis that the addition of limestone retarded the decomposition of coal and newspaper in the early stages, and then promoted the char gasification in the later stages due to the catalytic effect of calcium.

Ongoing research with combinations of TGA-FTIR and DTA techniques will provide a better understanding of the overall decomposition and combustion processes for coal-RDF-limestone fuels.

ACKNOWLEDGMENTS

The authors are grateful to Shimadzu Scientific Instruments, Inc. for the loan of the HT 1500 TGA, to China's National Coal Corporation, and the International Scholar's Program at Western Kentucky University for a scholarship and support of Mingxu Zhang.

REFERENCES

1. McGowin, C.R.; Petrill, E.M.; Perna, M.A.; Rowley, D.R; "Fluidized Bed Combustion Testing of Coal/Refuse-Derived Fuel Mixtures," Babcock and Wilcox, Report from EPRI Project RP718-2 (1989).

2. Hickman, C.E.; Center for Electric Power, Tennessee Technological University, personal communication.

3. "Summary of Recent Literature Pertaining to the Incineration of Municipal Solid Wastes," prepared by the Center for Environmental Information, Inc., NYSEG contract No. 87-372 (August, 1988).

4. Conkle, H.N.; Dawson, W.J.; Rising, B.W.; "Reconstitution of Coal and Limestone for Use in Industrial Stoker Boilers," paper presented at the 18th Biennial Conference of the Institute of Briquetting and Agglomeration, Colorado Springs, CO (August, 1983).

5. Giammar, R.D.; Hopper, D.R.; Radhakrishnan, E.; Webb, P.R.; "Evaluation of Emission from Industrial Stoker Boilers," presented at AIChE meeting, Boston, MA (August, 1979).

6. Rising, B.W.; Conkle, H.N.; Dawson, W.J.; Litt, R.D.; "Advanced Development of a Coal/Limestone Fuel Pellet for Industrial Boilers," Contract No. 68-02-3189, Final Report from Battelle's Columbus Laboratories for the U.S. EPA (October, 1983).

7. Culmo, Q.R.F.; Fyans, R.L.; "Thermogravimetry as a Tool for Determining Combustion Efficiency and Calcium Utilization of a Fluidized Bed Combustion Furnace" in Compositional Analysis by Thermogravimetry, C.M. Earnst, Ed., ASTM STP997, American Society for Testing and Materials, Philadelphia, PA, 1988, pp. 245-55.

Table 1

T_{Max} and R_{Max} vs. Newspaper Content

	8% Newspaper	18% Newspaper	28% Newspaper
T_{Max1}	283	290	287
T_{Max2}	384	385	384
T_{Max3}	450	451	454
T_{Max4}	489	490	492
R_{Max1}	1.66	2.20	2.68
R_{Max2}	2.12	2.08	1.92
R_{Max3}	1.29	1.29	1.60
R_{Max4}	0.53	0.49	0.49

Table 2

Calculated Values for Weight Loss of 50% Newspaper/50% Limestone

Temp.°C	Tested Values %	Calculated Values Newspaper	Calculated Values Limestone	Difference %
150-381	37.05	42.12	0.015	-5.09
381-539	13.16	3.10	0.825	9.24
539-800	20.77	0.10	20.5	0.17
Total	71.04	49.4	22.1	-0.46

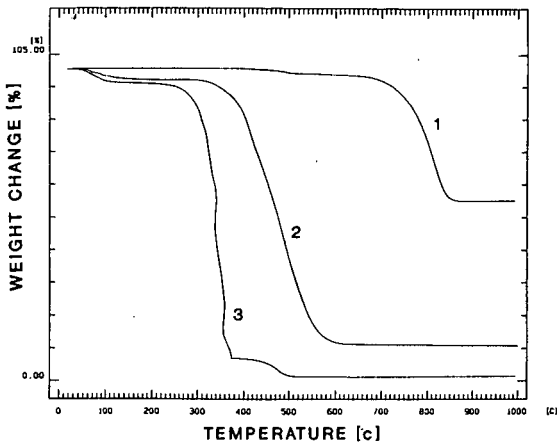

Figure 1. The TG Curves of three original samples
1-limestone; 2-coal; 3-newsprint;

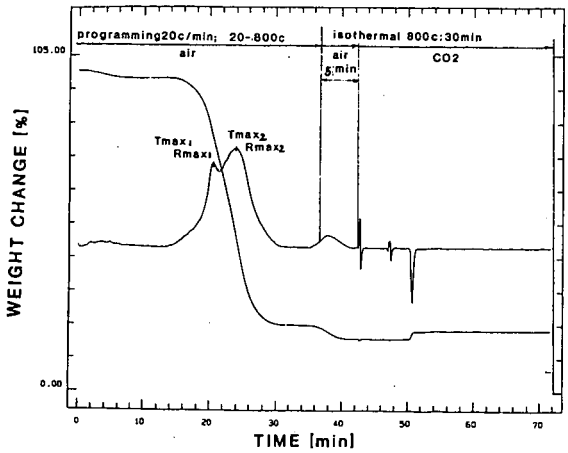

Figure 2. TGA analysis of coal/limestone mixtures

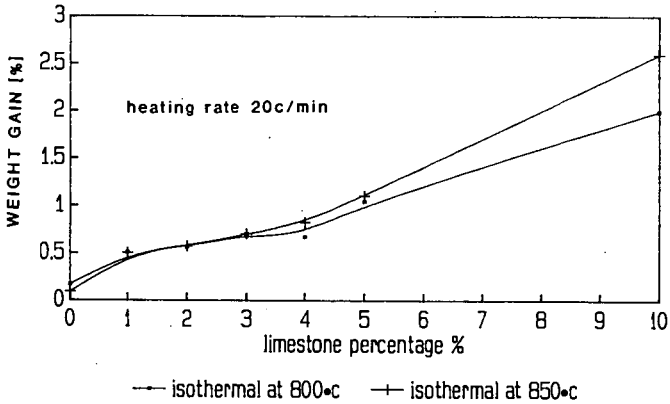

Figure 3. Weight gain vs. limestone percentage

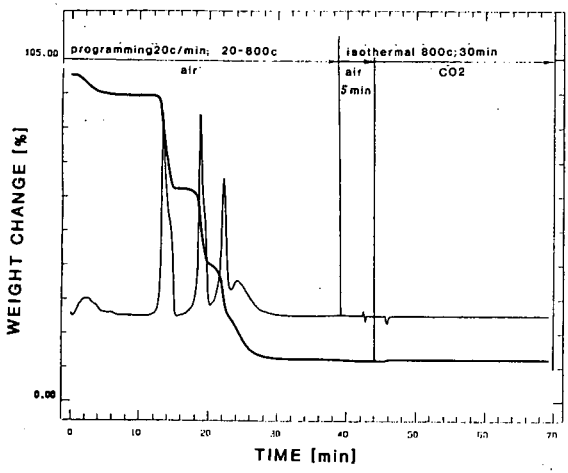

Figure 4. TGA analysis of combination fuels(C+L+N)

ARENECHROMIUM COMPLEXES IN COAL

Michael D. Ettinger and Leon M. Stock
University of Chicago, Department of Chemistry
Chicago, Illinois 60637

Keywords: Coal, Chromium, Hydrogenation.

Introduction

When an arene is coordinated to $Cr(CO)_3$, profound changes in its reactivity occur[1,2]. Ring and benzylic hydrogen atoms exhibit enhanced acidity, and typical arene reactions such as electrophilic aromatic substitutions are quenched. In contrast, the ring carbon atoms are activated toward attack by nucleophiles[1]. These changes in reactivity are manifestations of the forceful electron withdrawing nature of the $Cr(CO)_3$ component, and of the ability of this group to stabilize charged intermediates. In addition, arenechromium tricarbonyl complexes have been proven to be good catalysts in the hydrogenation of dienes[3]. While most simple complexes such as toluenechromium tricarbonyl require the use of high temperatures and dihydrogen pressures, arenechromium tricarbonyl complexes with napthalene, anthracene, and phenanthrene show remarkable activity under extremely mild conditions. Coal arenechromium tricarbonyl complexes may prove to be good internal hydrogenation catalysts for the hydrogenation of surrounding molecules.

Results and Discussion.

Experiments were carried out with a coal liquid in this exploratory investigation to avoid solubility problems inherent in the use of solid coals. The coal liquid used was distilled at approximately 850°C from run 250D at the Wilsonville pilot plant with Illinois No. 6 coal. In contrast to solid coals and heavy distillates, this material is soluble in all common organic solvents.

The first stage of research centered on the conversion of the aromatic hydrocarbons in the coal liquid into arenechromium tricarbonyl complexes. Reactions to form complexes with the coal liquid were carried out by a procedure for simple molecules in which the arene is refluxed in dioxane with chromium hexacarbonyl. However,this method required long reaction times and large excesses of chromium hexacarbonyl to achieve acceptable levels of complexation. To alleviate these problems, the use of an alternative reagent, triaminechromiumtricarbonyl, was investigated. This reagent is easy to synthesize[5], equation 1, and has been used

$$Cr(CO)_6 + KOH + EtOH + nBuOH \xrightarrow[\text{2) conc } NH_4OH, 25^oC, 2hrs]{\text{1) } 150^oC, 4hrs} (NH_3)_3Cr(CO)_3 \quad (1)$$

to obtain several organochromium complexes[6]. Reactions of the coal liquid with triaminechromiumtricarbonyl proved to be very successful. High yields of complexation with the coal liquid arene molecules were obtained. Indeed, the product was orange colored and crystalline in nature. The ^{13}C NMR spectrum of one such product is shown in Figure 1. The carbonyl resonance appears at 234 ppm and

the aromatic carbon resonances shift to 80-100 ppm as anticipated.

The second stage of the investigation centers on hydrogenation transfer chemistry of the coal liquid arenechromium tricarbonyl complexes. Studies have been carried out with simple arenechromium tricarbonyl complexes[1,7] as catalysts in the hydrogenation of methyl 2,4-hexadienoate in which the severity of reaction conditions varied from 150°C at 700 psi dihydrogen pressure for toluenechromium tricarbonyl to 27°C at 57 psi dihydrogen pressure for napthalenechromium tricarbonyl. The dramatic increase in activity of the polycyclic arenechromium tricarbonyl complexes is that there are two long Cr-C bonds with the bridgehead carbon atoms that have bond orders less than one[8]. Thus, the longer and weaker bonds should be more easily displaced by the incoming diene ligand in the rate determining step. This advantage is not realized in the case of the monocyclic arenechromium tricarbonyl complexes such as benzenechromium tricarbonyl where all of the Cr-C bonds have equal length with bond orders close to unity. The effect of solvent was also examined. Coordinating solvents such as tetrahydofuran or acetone increased the rate of the hydrogenation reaction presumably by facilitating the initial ligand substitution step.

Hydrogenation reactions were carried out under mild conditions in a glass microhydrogenation apparatus at pressures lower than 200 psi and temperatures less than 50°C using dideuterium gas. The use of dideuterium allows the reduction step to be detected by means of deuterium NMR. A hydrogenation reaction was carried out with napthalenechromium tricarbonyl to catalyze the hydrogenation of methyl 2,4-hexadienoate in the presence of small amount of coal liquid to test whether or not the coal liquid would poison the catalyst. This reaction, equation 2, proved to be successful with a

$$\underset{1.23M}{CH_3CHCHCHCHCO_2CH_3} + \underset{80.3 \times 10^{-3}M}{C_{10}H_8Cr(CO)_3} \xrightarrow[\substack{45^oC,1.5hr \\ 25mg\ Coal\ Liq}]{150psi\ D_2,Acetone} CH_3CHDCHCHDCO_2CH_3 \quad (2)$$

63% conversion of methyl 2,4-hexadienoate to methyl hex-3-enoate-2,5-d_2. It was evident that the presence of the coal liquid does nothing significant to inhibit the catalyst. The next set of experiments were carried out with the coal liquid arenechromium tricarbonyl complexed material. The coal liquid arenechromium tricarbonyl complexed material proved to be unsuccessful in catalyzing the hydrogenation of the surrounding molecules . In part, this could be due to the fact that all of the possible active sites for hydrogenation may of have been rendered unreactive by complexation with $Cr(CO)_3$. To test this line of reasoning, experiments were carried out on a mixture of the coal liquid arenechromium tricarbonyl complex and unreacted coal liquid as shown in equation 3. Analysis of the ^2H NMR spectrum of the coal liquid arenechromium tricarbonyl reaction product showed that no significant deuteration had taken place.

$$\underset{0.5g}{\text{Coal Liquid}} + \underset{0.5g}{\text{Coal Liquid-Arene-Cr(CO)}_3} \xrightarrow[45^oC,16hrs]{86psi\ D_2,\ 5ml\ Acetone} \text{N.R.} \quad (3)$$

In order to clearly test the catalytic activity of the coal liquid arenechromium tricarbonyl complex, experiments were carried out with methyl 2,4-hexadienoate as the substrate and the coal liquid arenechromium tricarbonyl complex as the catalyst as shown in equation 4. The ^2H NMR of the reaction product showed the coal liquid and unreacted methyl 2,4-hexadienoate indicating no reaction.

$$\underset{1.23M}{CH_3CHCHCHCHCO_2CH_3} + \underset{0.5g}{\text{Coal Liq-Arene-Cr(CO)}_3} \xrightarrow[45^oC,\ 1.5hrs]{150psi\ D_2,\ 2.5ml\ Acetone} \text{N.R.} \quad (4)$$

Although the activity of the coal liquid arenechromium tricarbonyl complex as a hydrogenation catalyst appears to be small for methyl 2,4-hexadienoate as well as for unreacted coal liquids under the mild conditions employed, it may well prove to be viable under moderately more severe conditions. In addition, the nature of the aromatic rings in this particular coal liquid may actually lead to very inactive coal liquid arenechromium tricarbonyl complexes. A slightly heavier distillate may contain more polycyclic aromatic hydrocarbons and yield more active complexes while still affording the conveniences provided by the use of a coal liquid.

In order to test the hypothesis that hydrogenation substrates do not exist in the coal liquid, a reaction was carried out with napthalenechromium tricarbonyl, an active catalyst, and unreacted coal liquid as the substrate, equation 5. A comparison of the ^2H

$$\underset{0.5g}{\text{Coal Liquid}} + \underset{7.72 \times 10^{-3}M}{C_{10}H_8\text{-Cr(CO)}_3} \xrightarrow[75^oC,\ 25\ hrs]{200psi\ D_2,\ Acetone} \text{Coal Liquid-D} \quad (5)$$

NMR spectra of the unreacted coal liquid before and after the reaction, Figure 2, shows that dideuterium addition has taken place. First, the relative aromatic deuterium content has decreased and the aliphatic deuterium content has increased. Second, the two major resonances of the unreacted coal liquid at approximately 1.54 ppm and 1.16 ppm are no longer the dominant resonances. Rather, the new dominant resonances in the reacted coal liquid are at approximately 2.27 ppm and 1.45 ppm. In addition, two other new signals have appeared at 3.57 ppm and 2.71 ppm. Thus, it can be concluded that hydrogenation of the coal liquid had occurred.

Conclusions

A synthetic method for the preparation of coal arene chromium tricarbonyl complexes has been established. The series of hydrogenation reactions with coal liquid arene chromium tricarbonyl complexes shows that there is nothing inherent in coal materials that poison the arenechromium tricarbonyl catalyst and that there are active sites in the coal liquid for hydrogenation. However, the actual arenechromium tricarbonyl complexes formed in the coal liquid are not active enough for extensive hydrogenation under the mild experimental conditions that we used. As mentioned before, monocyclic complexes require higher temperatures and pressures for hydrogenation than polycyclic complexes do. Research in this area is continuing to test the capacity of coal liquid arenechromium tricarbonyl complexes to catalyze dihydrogen addition.

Experimental.

The coal liquid was obtained through Amoco Research Center from the Wilsonville Pilot Plant, Run 250D. The ^{13}C NMR spectra were recorded on a General Electric GN 300 operating at 300MHz. The ^{2}H NMR spectra were recorded on a Varian XL 1000 operating at 400MHz. The ^{1}H NMR spectra were recorded on the University of Chicago 500MHz spectrometer. Tetrahydrofuran, dibutyl ether, and dioxane were freshly distilled from sodium benzophenone ketyl immediately before use. Hexane was shaken with sulfuric acid prior to use. All solvents were deoxygenated by means of standard freeze-pump-thaw methods. Potassium hydroxide, acetone, and chromium hexacarbonyl were used as received.

Triaminechromium tricarbonyl

Chromium hexacarbonyl (17.6g, 0.08mol), potassium hydroxide (32.0g), ethanol (80ml), n-butanol (80ml) and water (25ml) were placed in a flame dried three neck flask fitted with a stirrer and a reflux condenser. The reaction flask was placed in an oil bath which was warmed gradually to 150°C. Chromium hexacarbonyl, which sublimed initially, was washed out later by the solvent and no more sublimation took place. The reaction solution gradually turned red. After 4h at reflux, the mixture was collected, 150mL of concentrated aqueous ammonia solution was added and the mixture was slowly stirred for two hours. A yellow precipitate was collected on a a glass filter, washed with aqueous ammonia and ether.

Coal liquid arenechromium tricarbonyl

Triaminechromium tricarbonyl (4.68g, 0.025mol), coal liquid (5g), and dioxane (25mLs) were loaded into a 100 mL flask provided with a magnetic stirrer, and a reflux condenser. The solution was refluxed on an oil bath for 48 hrs. The reaction mixture was filtered through Celite in a glass filter and the flask and Celite were washed with ether. The product was purified over a column of silica gel with a 1:1:4 chloroform : dichloromethane : hexane.

Napthalenechromium tricarbonyl

Napthalenechromium tricarbonyl was prepared by a slightly modified procedure[10] to that described by Pauson[4]. A mixture of napthalene (5.3g, 0.042mol) and chromium hexacarbonyl (4.4g, 0.020mol) were refluxed in dibutyl ether (100 mL), hexane (10mL), and tetrahydrofuran (1mL) for 70 hrs. The heating bath was maintained at 160°C for 15 hrs and at 145°C for the remaining time. Solvent and excess napthalene were removed under vaccum and the product purified on a column of silica gel with a 1:1:4 chloroform : dichloromethane : hexane.

Hydrogenation reactions

Hydrogenation reactions were carried out on a 10mL micro hydrogenation apparatus. Typically, the reactants and dried, deoxygenated acetone were placed in the reactor and it was evacuated and flushed with dinitrogen three times, dideuterium three times and then brought up to the final dideuterium pressure at the desired temperature. After the reaction time, the mixture was filtered through Celite in a glass filter and concentrated under vaccum.

Acknowledgement. We are indebted to the Office of Fossil Energy of the U. S. Department of Energy for their support of this investigation.

References

1. Semmelheck, M. F. J. Organom. Chem. Library 1976, 1, 371.
2. Jaouen, G. in 'Transition Metal Organometallics in Organometallics in Organic Synthesis', Vol. 2, H. Alper (ed), Academic Press 1978.
3. Cais, M., Fraenkal, D., Weidenbaum, K. Coord. Chem. Rev. 1975, 16, 27.
4. Mahaffy, C. A., Pauson, P. L. Inorg. Synth. 1979, 19, 154.
5. Razuvaev, G. A., Artemov, A. N., Aladjin, A. A., Sirotkin, N. I. J. Organometal. Chem., 1976, 111, 131.
6. Moser, G. A., Rausch, M. D. Synth. React. Inorg. Met. -Org. Chem., 1955, 280, 255.
7. Cais, M., Rejoan, A. Inorg. Chim. Acta, 1970, 4, 509.
8. Muir, K. W., Ferguson, G., Sim, G. A. Inorg. Chem. 1966, 5, 1851.

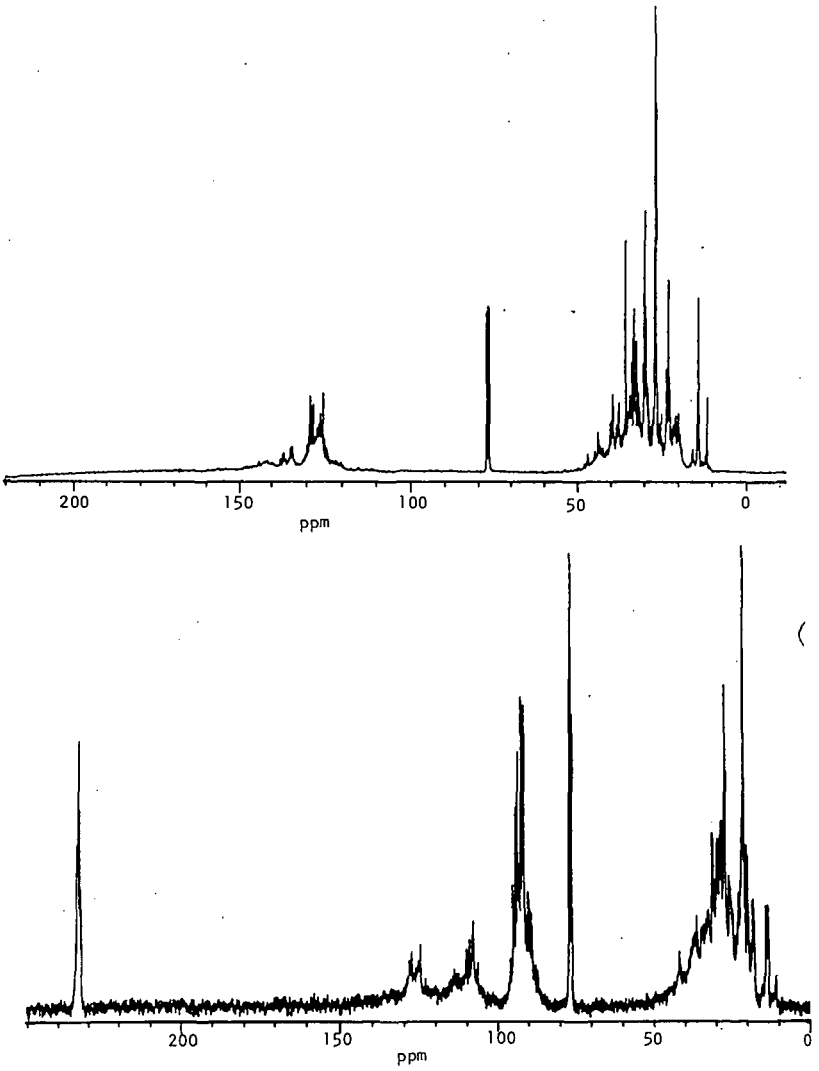

Figure 1. (a) ^{13}C NMR Spectrum Of Wilsonville Coal Liquids in $CHCl_3$.
(b) ^{13}C NMR Spectrum Of Coal Liquid Arene-$Cr(CO)_3$ in $CHCl_3$

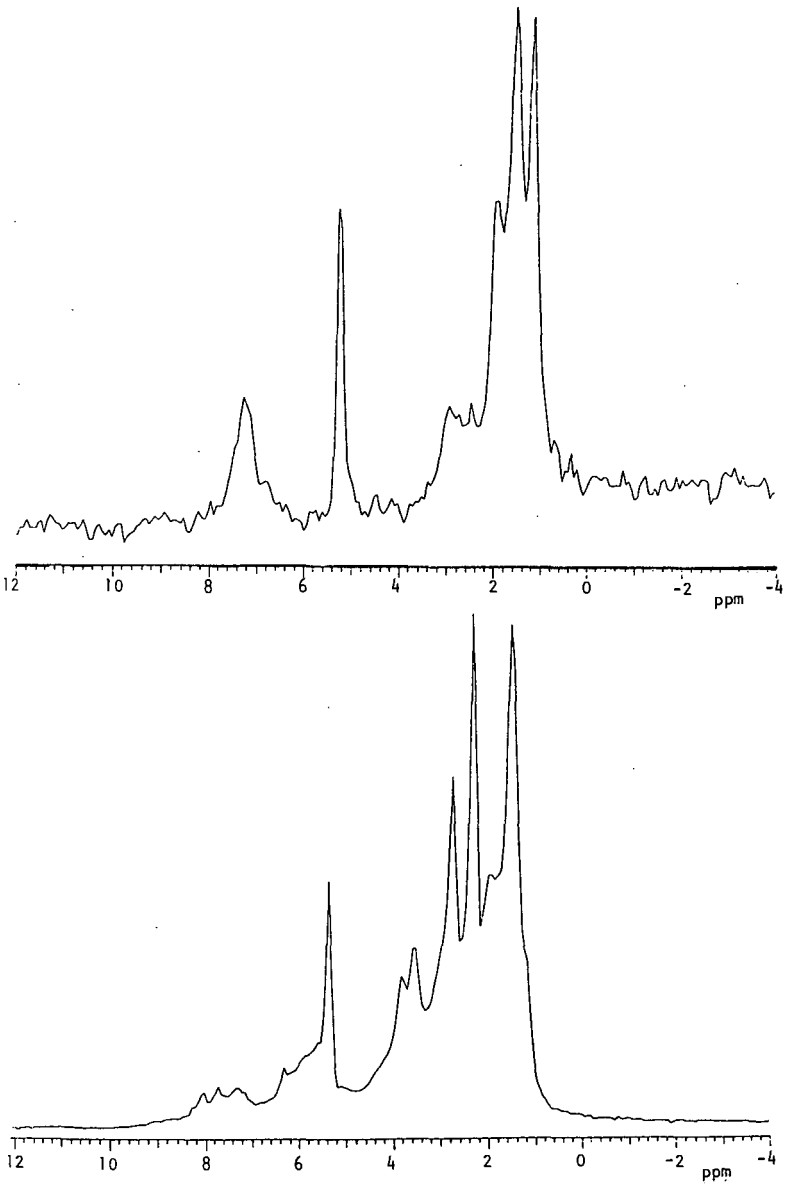

Figure 2. (a) ^2H NMR Spectrum of Unreacted Coal Liquid in CH_2Cl_2
(b) ^2H NMR Spectrum of Equation 6 Product in CH_2Cl_2.

SYNTHESIS AND CHARACTERIZATION OF PYRIDINE AND 2,6-DIPHENYL-PYRIDINE ETHERS

Leonard L. Matz
Independent
3061 Bishop Road
Appleton, NY 14008

Key words: Ethers; Pyridine Ethers; Synthesis of Ethers;

INTRODUCTION

Three novel pyridine ethers have been synthesized for extension of studies on coal systems[1]. Past studies have revealed that hydrogen bonding activates alkyl-aryl ethers toward cleavage by iodide ion in pyridine involving hydrogen bonding to coal[2]. Pyridine ethers have been synthesized *de novo* from 2,6-diphenyl-1,3,5-pentanetrione which had also been synthesized *de novo* from 1-phenyl-1,3-butanedione after formation of its mono-then di-anion and combination with methyl benzoate[3,4]. These reactions seem to provide good yields because of the driving force of the charged molecular species. Coal is now thought to be as elastomer in which strong internal hydrogen bonding gives it high glass transition temperatures. The same acidic hydrogen donors and basic hydrogen receptors that provide strong hydrogen bonds in the bulk structure populate the surface of coal powders[5]. As in experiments using 1,3-dimethylnapthalene and decalin[6], solvation properties of the pyridine ethers will be tested on coal fractions in contemplated experiments.

RESULTS

1,5-Diphenyl-1,3,5-pentanetrione The enolate carbanion of 1-phenyl-1,3-butanedione was obtained by proton extraction with sodium hydride in the aprotic solvent, 1,2-dimethoxy ethane (monoglyme). Condensation of this carbanion with methyl benzoate yielded the triketone, 1,5-diphenyl-1,3,5-pentanetrione. This aroylation apparently involves the di-anion of the β-diketone which is formed in a step-wise extraction of its α-hydrogens. The terminal α-hydrogen is not the first extracted from the β-diketone, but is only extracted after mono-anion formation and in the presence of methyl benzoate. The terminal α-hydrogen is, however, the site of reaction of the β-diketone with the carbonyl carbon of the ester. The methoxide group of the ester neutralized by the Na^+ counter ions, then leaves the condensation product. Exposure to air with its incipient moisture and neutralization of the reaction mixture with 6N HCl provide the protons for neutralization of the carbanions present and formation of the triketone.

This reaction occurs with a high degree of efficiency since 86.9% yields could be obtained (See Table 1).

Apparently once formed, the di-anion is quite reactive and the

reaction is evidently specific for the terminal carbon of the dianion. As expected, the symmetric triketone formed was soluble in diethyl ether, but its solubility varied considerably depending on the pH of the reaction mixture (Table 2)

These differences could be a reflection of minor changes in the structure of the triketone. Variation of the color, crystalline form and melting points of triketone which substantiate similar earlier observations are also suggestive of small variations in the structure of the triketone. Because of the H-bonding, various keto-enol tautomeric forms can be envisioned and as pH changes occur in the solvent all of these forms are undoubtedly present in the solution. At low pH values the triketone is probably found as a doubly H-bonded enolic structure (Formula 1), at intermediate pH values as a mono-H-bonded structure (Formula 2) and at high pH values as a keto form (Formula 3) with little H-bonding (Fig. 2).

2,6-Diphenyl-4(1H)-pyridinone This pyridinone was produced by the cyclization of the 1,5-diphenyl-1,3,5-pentanetrione with liquid ammonia. Because of the high pH of the reaction milieu, which causes the enolization of the ketone groups, the addition product is the primary amine-enol or dienol intermediate.

Cyclization by addition of the primary amine to the other terminal carbon of the pentanetrione chain then readily occurs. This di- or trienolic structure is then dehydrated to form the highly conjugated diphenylpyridine derivative with its quinoid-like pyridine ring.

The synthesized pyridinone possessed the literature values of the physical properties. In addition, the physical properties of the triketone and pyran were considerably different. These results suggest because of their interdependence that the structural parameters attributed to these isolates are consistent and reputable.

DISCUSSION

As expected the product, 1,5-diphenyl-1,3,5-pentanetrione, is formed with a high degree of efficiency (86.9% yields). Although the symmetric triketone was solyble in diethyl ether, variations of the pH of the reaction mixture produced slight variations in the structure of the triketone and therefore variation of the color, crystalline form and melting points of triketone products. Because of the H-bondong, various keto-enol tautomeric forms can be envisioned and as pH changes occur in the solvent all of these forms are undoubtedly present in the reaction mileaux.

The ultrastructure of coals is susceptible to study using small molecular weight organic molecules which are not susceptible to alteration by the interior of the coal pores. We have chosen to use the commonly accepted organic molecules which are very resistant to alteration insuch an organic mileaux- ethers. Theoretically these molecules can be used as molecular sieves to approximate the size of coal pores[7]. Unfortunately, the ethers which we have used have

proven to be unreasonable solvents since they react with the coal ultrastructure.

Another problem in interpretation occurs becasuse of the interaction of the pyridine ethers with the coal structure[8]. For example, the results of the study involving the use of 4-methylpyridine reported above.

SUMMARY

1-Hydrogen bonding is a significant interference in the synthesis of 2,6-diphenyl-1,3,5-pentanetrione, yet yields of 90+% prove this specific synthesis effective.

2-Because of the very prominant unsaturation of the products of this synthesis-the product compounds are very colorful.

3-These ethers cannot be considered innert and make interpretation of these results difficult.

EXPERIMENTAL

Melting points (uncorrected) were determined on a Thomas Hoover Capillary Melting Point Apparatus (Uni-melt) and observed at a rate of 2°C/min. 1H-NMR Spectra were measured on a Varian T-60 Nuclear Magnetic Resonance Spectrometer using tetramethylsilane (TMS) as an internal standard. The solvents used were either chloroform-d or acetone-d6. Infrared spectra were recorded on a Perkin-Elmer 337 grating Spectrophotometer with calibration peaks at 1601 and 907 cm^{-1}. Mass spectral analysis was conducted on a Dupont 21-490 Mass Spectrometer. TLC was performed on precoated Silica Gel 60F-254 plates (Merck, Darmstatd, 0.25 mm thickness).HPLC analysis was carried out on a Model 342 Gradient Liquid Chromatograph system, retention times and area measurements were recorded by a Shimadzu Chromatopac C-R1B. The column used for the HPLC was 4.6 mm x 25 cm CB reverse phase. Pre-injection clean up of HPLC samples included centrifugation in a Beckman Microfuge TM 11 at 11,000 rpm. Organic solids were dried under vacuum for at least 2 h over $CaSO_4$ before analysis.

Preparation Of 1,5-diphenyl-1,3,5-pentanetrione[3,4] Sodium hydride (36.99 g/1.54 moles in a 60% mineral oil dispersion) was added to 100 mls of dried 1,2-dimethyoxyethane under a blanket of anhydrous nitrogen. After stirring for 15 m at room temperature the glyme which contained mineral oil and suspended fines was removed, discarded and replaced at least three times to insure removal of the mineral oil after addition of 200-300 ml of glyme. The slurry was then heated to reflux and the 1-phenyl-1,3-butanedione (50.00 g/0.31 moles) in 150 mls of solvent was added dropwise (over 30-60 m) from an addition funnel. After 45 m from completion of the addition, a solution of methyl benzoate (50.32 g/0.37 moles) in 100 ml of glyme was added dropwise. The reaction mixture was then heated at reflux for 4-8 h. After equilibration with the atmosphere and cooling, the reaction mixture which was usually

thick and crusty, was resuspended with additional glyme, if necessary, stirred and adjusted to pH=6 with concentrated HCl. The glyme was then removed in a rotary evaporator. The tar-like residue was extracted with diethyl ether, and the yellow-brown ethereal solution was dried over anhydrous Na_2SO_4. After removal of most of the ether, the crude 1,5-diphenyl-1,3, 5-pentanetrione was recrystallized from the residue with 95% ethanol as yellow-brown crystals to give 47.33 g (57.7% Yd.):mp 107.0-109.0°C, (lit., 106-109°)[1]; NMR ($CDCl_3$): δ = 11.8-12.0 (d,1), 7.8-8.0 (m,6), 7.4-7.6 (m,7), 6.0 (s,1); IR (KBr): 3450, 3150,2950, 2880, 1630, 1590, 1500, 1400, 1300, 1290, 1170, 900, 780, 690 cm^{-1}: Mass Spectrum, m/e : 266, 105.

Preparation of 2,6-diphenyl-4(1H)-pyridinone[3] 1,5-diphenyl-1,3,5-pentanetrione (43.95 g/0.17 moles) was dissolved in 200 ml of anhydrous ethanol. Commercial anhydrous liquid ammonia was then bubbled through the mechanically stirred slurry until the solution became dark brown and the reaction mixture cooled to room temperature. The solution was then taken to dryness by heating in an open round bottom flask at 90-100°C until a brownish tar remained. This procedure was then repeated and slightly modified by the addition of 50 g of anhydrous Na_2SO_4 before the final evaporation. Recrystallization is accomplished directly from the residue with benzene. After drying 27.21 g (66.6% yield) of a white powder was isolated and identified as 2,6-diphenyl-4(1H)-pyridinone: mp 176-179°C (lit., 176-179°C[2]; NMR (CD_3COCD_3): δ = 8.0-8.3 (m, 7), 7.3-7.4 (m, 7), 7.2 (s, 1); IR (KBr): 3450, 3150, 3080, 2950, 2825, 1640, 1600, 1550, 1260, 975, 950, 780, 705, 555; Mass Spectrum (m/e): 247, 247.

Preparation of 4-methoxypyridine[7]. To 10 ml of dried methanol were added 1.7 g/0.074 moles of metallic sodium. After disappearance of the sodium and cessation of H_2 evolution, 5.00 g/0.033 moles of dried 4-chloropyridine hydrochloride (Aldrich) dissolved in 30 mls of dried methanol were added dropwise over 2 h. The reaction mixture was then heated at reflux for 7 days. TLC revealed only trace amounts of 4-chloropyridine and the 4-methoxypyridine (Yd.= 2.80 g/0.026 moles, 76.9%) was isolated by vacuum distillation: bp 152-154°C (=400 torr) or 41-45°C (0.7-0.8 mm) [lit., 95-96°C at 31 mm[5] or 190.5-191.0°C (738.3 mm)[4]]; NMR (CD_3COCD_3) δ: 8.4-8.6 (d. 4), 6.7-6.9 (d, 4), 3.8 (s, 1); IR (KBr): 3450, 3050,2990, 2960, 2860, 1600, 1460, 1440, 1295, 1220, 1035, 828, 820, 540, cm^{-1}; Mass Spect (m/e): 109.

Preparation of 4-phenoxypyridine[8]. Phenol (12.44 g/0.073 moles) was dissolved in dried toluene under a blanket of anhydrous nitrogen (Fig. 5). Metallic sodium (3.04 g/0.132 moles) was then slowly added to the stirred reaction mixture. After 1 h 4-chloropyridine-hydrochloride (6.61 g/0.044 moles) was slowly added through one side neck of the three neck flask. This caused formation of H_2 and care was taken to control the reaction. After addition of the hydrochloric acid salt, the reaction was heated at reflux for 10 days. At this time, TLC revealed only trace amounts

of remaining reactant. Work up involved[14] neutralization of the reaction mixture to pH=7 followed by steam distillation of the reaction mixture. The distillate was extracted with liberal quantities of diethyl ether, the ethereal extracts were dried with Na_2SO_4 and the diethyl ether partially removed in a rotary evaporator. Vacuum distillation of the remaining extract gave 3.2 g of 4-phenoxypyridine (35.1 % Yd.): bp 78-79 (50 ul) [lit., 134-136 (10 mu)[12]; NMR (CD_3Cl) δ: 8.2-8.4 (d, 2), 7.0-7.4 (m, 10), 6.8-7.0 (m, 6); IR(neat): 3007, 3005, 2950, 2850, 2730, 2620, 2500, 1595, 1500, 1270, 1220, 886, 760, 700, 532 cm^{-1}; Mass Spect (m/e): 206.

Preparation of 2,6-diphenyl-4-chloropyridine[12] 2,6-diphenyl-4(1H)-pyridinone (12.17 g/0.049 moles) and phosphorus pentachloride (30.75 g/0.993 moles) were mixed under nitrogen and moistened with dry phosphorus oxychloride (8 mls)(Fig. 5). While heating to 150°C for 2 h the liquid milieux progressed from a cloudy white to clear red appearance. The phosphorus oxychloride was then removed by distillation and the melt poured into cold water. After stirring the cooled suspension until the viscous reaction mixture became a flocculent precipitate, the precipitate was collected on a Buchler funnel. 10.50 g (86.3% Yd.) of 2,6-diphenyl-4-chloropyridine was recrystallized from the precipitate with 95% ethanol: mp 83-84°C (lit., 72)[10] ; NMR ($CDCl_3$) δ: 7.9-8.2 (m, 8), 7.6 (s, 1), 7.3-7.5 (m, 9) or NMR (CD_3COCD_3) δ: 8.0-8.4 (m, 8), 7.8 (s, 1), 7.4-7.6 (m, 9); IR (KBr): 3450, 3150, 1570, 1420, 1240, 865, 770, 735, 690 cm^{-1}; Mass Spect (m/e) 265, .

Preparation of 2,6-diphenyl-4-methoxypyridine[10] Metallic sodium (0.65 g/0.028 moles) was added slowly and carefully to 10 ml of dried methanol in a three neck reaction vessel(Fig. 5). After disappearance of the sodium and abatement of H_2 evolution , the solution was refluxed for 1 hr. After cooling, 2.15 g/0.094 moles of 2,6-diphenyl-4-chloropyridine dissolved in 15 mL of dried methanol was added to the reaction vessel. The temperature was again raised to reflux of the reaction mixture. After 6 days HPLC revealed that 50% of the 2,6-diphenylpyridine was 2,6-diphenyl-4-chloropyridine and 50% was 2,6-diphenyl-4-methoxy-pyridine. Therefore, 0.65 g/0.028 moles in 10 mL of dried methanol was again added to the reaction mixture. After refluxing for four more days, the reaction mixture was then poured into ice water and the aqueous solution extracted several times with diethyl ether. The ether extracts were then combined and concentrated to give 1.83 g/0.007 moles of impure 2,6-diphenyl-4-methylpyridine. Recrystallization was accomplished with absolute methanol giving 1.14 g/0.004 moles of 2,6-diphenyl-4-methoxypyridine (46.3 %Yd.): mp 79-80°C (lit., 79-80°C)[5]; NMR ($CDCL_3$) δ: 8.0-8.2 (m, 4), 7.3-7.6 (m, 8), 7.1 (s, 1), 3.8 (s, 1); IR (KBr): 3050, 2850, 2000, 1550, 1400, 1350, 1210, 1070, 1020, 895, 860, 835, 770, 690, 630 cm^{-1}; Mass Spect (m/e) 261.

REFERENCES

1.Mayo, F. R.; Buchanan, D. H.; Pavelka, L. A. *Prepr. Pap.-Am. Chem.Soc.,Div. Fuel Chem.* **1980**, *25(2)*,182. (b) Mayo, F. R.; Buchanan, D. H.; Pavelka, L. A.; Hirschon, A. S., manuscript submitted to *Fuel*.

2.Buchanan, D.H.; Takemura, N.; Sy, J. N. O. "Intramolecular Hydrogen Bonding Enhances the Rate of Nucleophilic Cleavage in Alkyl-Aryl Ethers" *J.Org.Chem.* **1986**, *51*, 4291-4294.

3.Light, R. J.; Hauser, C. R. "Aroylations of β-Diketones at the Terminal Methyl Groups to Form 1,3,5-Triketones. Cyclizations to 4-Pyrones and 4-Pyridones" *J.Org.Chem.* **1960**, *25*, 538-546.

4.Miles, M. L.; Haris, T. M.; Hauser, C. R. "Aroylations at the Methyl Group of Benzoylacetone and Related β-Diketones with Esters to Form 1,3,5-Triketones by Sodium Hydride. Other Terminal Condensations." *J.Org.Chem.* **1965**, *30*, 1007-1011.

5. Fowkes, F. M., Jones, K. L., Li, G., & Lloyd, T. B. Surface Chemistry of Coal by Flow Microcalorimetry. *Energy & Fuels* **1989**, *3*, 97-105.

6. Bockrath, B. C., Schroeder, K. T. & Smith, M. R. Investigation of Liquefaction Mechanisms with Molecular Probes. *Energy & Fuels* **1989**, *3*, 268-272.

7. Black, S. H. & Gerhardt, P. The Void Volume of Bacterial Spores. *J. Bacteriol.* **1960**, *59*, xx.

8. Sy, J. & Buchanan, D. H. *J. Org. Chem.* **198X**, *xxx*, xxx.

9.Renshaw, R. R.; Conn, R. C. "Quaternary Derivation of Pyridyl Ethers. Onium Compounds. XVI" *J.Am.Chem.Soc.* **1937**, *59*, 297-303.

10. Haake, P.; Miller, W. B.; Tysee, D. A. *J. Amer. Chem. Soc.* **1964**, *86*, 3577-xxxx.

11. Koenig, E.; Greiner, H. "Uber 4-Pyridyl-pyridinium-dichloride und das Synthese von γ-Derivaten des Pyridins." *Ber.* **1931**, *64*, 1056-.

12. Patrenko-Kritschenko, P.; Shottly, S. "Uber die Kondensation der Aceton-dicarbonsaureester mit Aldehyden vermittels Ammoniak und Aminen." *Chem.Ber.* **1909**. *42*, 2020-2025.

TABLE

Table 1. Physical Properties of Synthetically Prepared Precursors and Ethers

Table 2. Physical Properties of 1,5-Diphenyl-1,3,5-pentanetrione

a-Moles 1-diphenyl-1,3-butanedione:mole NaH:moles methyl formate
b-Solvent not dried immediately before synthesis
c-Only one crystallization, second was usually not fruitful

Figures

Name	Recrystallization Solvent	Color	Mp (Bp)	% Yd
1,5-Diphenyl-1,3,5-pentanetrione	95% Ethanol	Yellow	107-109	57.7
2,6-Diphenyl-4(1H)-pyridinone	Benzene	Cream	176-179	66.6
2,6-Diphenyl-4H-pyran-4-one	Ethanol-Water	White	137-139	79.8
2,6-Diphenyl-4-chloropyridine	95% Ethanol	White	83-84	86.3
2,6-Diphenyl-4-methoxypyridine	Methanol	White	79-80	46.3
4-Methoxypyridine	Distilled Water	Clear	41-45	
4-Phenoxypyridine	Distilled Water	Clear	78-79	

Preparations	Mole Ratio[a]	Solvent (Recrys.)	Color	%Yd.	mp
F-1A	1-3.3-1	95% EtOH	brown	58.6	106-108
P-2A	1-4.2-1.2	95% EtOH	lime-yellow	86.9	108-110
P-2B	1-4.2-1.2	95% EtOH	lime-yellow	86.9	108-110
P-21A	1-4-1.2	95% EtOH	lime-yellow	—[b]	107.5-110
P-21B	1-4-1.2	95% EtOH Hexane Cyclohexane	browns	—	113-122
P-29A	1-5-1.2	95% EtOH	brown	57.7	107-109
P-29A-A	1-5-1.2	95% EtOh Hexane Cyclohexane	brown	57.7	106-108
P-29B	1-5-1.2	95% EyOH	brown	57.7	107-109
P-II1-A	1-4-1	95% EtOH	brown	38.0[c]	105-108

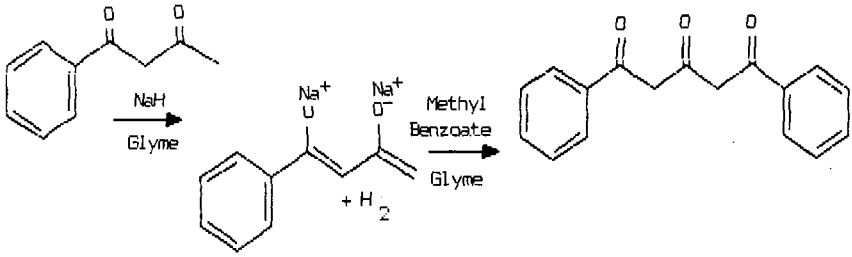

Fig. 1. Synthesis of 1,5-Diphenyl-1,3,5-pentanetrione

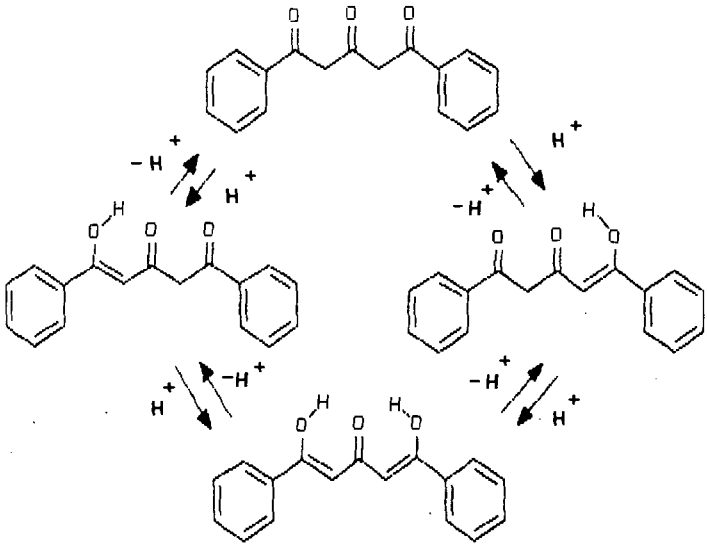

Fig. 2. Hydrogen Bonding of 2,6-Diphenyl-1,3,5-pentanetrione

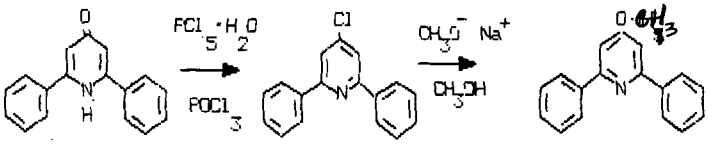

Fig. 3. Synthesis of 2,6-Diphenyl-4-methoxypyridine